

NUCLEAR GRAPHITE

R. E. NIGHTINGALE (ED.)

**ACADEMIC PRESS
1962**

ALCOIN LIBRARY

199668

ST. JOHN'S UNIVERSITY
COLLEGEVILLE, MINNESOTA

WITHDRAWN

NUCLEAR GRAPHITE

NUCLEAR GRAPHITE

Edited by

R. E. NIGHTINGALE

*Hanford Laboratories
General Electric Company*

Prepared under the auspices of the
Division of Technical Information
United States Atomic Energy Commission

ACADEMIC PRESS - 1962



New York and London

ALL RIGHTS RESERVED

COPYRIGHT ASSIGNED TO THE GENERAL MANAGER OF THE UNITED STATES ATOMIC ENERGY COMMISSION. ALL ROYALTIES FROM THE SALE OF THIS BOOK ACCRUE TO THE UNITED STATES GOVERNMENT. NO REPRODUCTION IN ANY FORM (PHOTOSTAT, MICROFILM, OR ANY OTHER MEANS) OF THIS BOOK, IN WHOLE OR IN PART (EXCEPT FOR BRIEF QUOTATION IN CRITICAL ARTICLES OR REVIEWS), MAY BE MADE WITHOUT WRITTEN AUTHORIZATION FROM THE PUBLISHERS.

ACADEMIC PRESS INC.
111 FIFTH AVENUE, NEW YORK 3, NEW YORK

United Kingdom Edition published by
ACADEMIC PRESS INC. (LONDON) LTD.
BERKELEY SQUARE HOUSE, LONDON W.1

Library of Congress Catalog Card Number 62-21148

PRINTED IN THE UNITED STATES OF AMERICA

TK
9668
NS

List of Contributors

- D. E. BAKER, *Hanford Laboratories, General Electric Company, Richland, Washington*
- J. C. BOKROS, *John Jay Hopkins Laboratory for Pure and Applied Science, General Atomic Division, General Dynamics Corporation, San Diego, California*
- T. J. CLARK, *Hanford Laboratories, General Electric Company, Richland, Washington*
- R. E. DAHL, *Hanford Laboratories, General Electric Company, Richland, Washington*
- J. M. DAVIDSON, *Hanford Laboratories, General Electric Company, Richland, Washington*
- D. R. DE HALAS, *Hanford Laboratories, General Electric Company, Richland, Washington*
- W. P. EATHERLY, *National Carbon Company, Parma, Ohio*
- J. C. FOX, *Hanford Laboratories, General Electric Company, Richland, Washington*
- J. L. JACKSON, *Hanford Laboratories, General Electric Company, Richland, Washington*
- L. H. JUEL, *Great Lakes Carbon Corporation, Niagara Falls, New York*
- J. KORETZKY, *Battelle Memorial Institute, Columbus, Ohio*
- H. H. W. LOSTY, *Research Laboratories, General Electric Company, Ltd., Wembley, England*
- R. A. MEYER, *John Jay Hopkins Laboratory for Pure and Applied Science, General Atomic Division, General Dynamics Corporation, San Diego, California*
- P. F. NICHOLS, *Hanford Laboratories, General Electric Company, Richland, Washington*
- R. E. NIGHTINGALE, *Hanford Laboratories, General Electric Company, Richland, Washington*
- E. L. PIPER, *National Carbon Company, Parma, Ohio*
- W. C. RILEY, *Battelle Memorial Institute, Columbus, Ohio*
- C. A. SWITZER, JR., *Great Lakes Carbon Corporation, Niagara Falls, New York*
- R. E. WOODLEY, *Hanford Laboratories, General Electric Company, Richland, Washington*
- E. M. WOODRUFF, *Hanford Laboratories, General Electric Company, Richland, Washington*
- H. H. YOSHIKAWA, *Hanford Laboratories, General Electric Company, Richland, Washington*

Preface

Contributions to the literature on nuclear graphite originate from many technical disciplines. The physicist is concerned with radiation effects and moderator physics; the chemist studies the gas-graphite kinetics, chemical reactions, and structure; and the nuclear engineer must be familiar with the properties of graphite and the changes that occur in the reactor environment. The boundaries between each of these fields are indistinct. Indeed, the mutual exchange of ideas resulting from engineers' and scientists' working as a team on the nuclear applications of graphite has contributed significantly to the present state of understanding. It is hoped that bringing together the literature on nuclear graphite within a single volume will stimulate this cooperative effort to continued growth and achievement.

The graphite technology that has developed since Acheson first described the manufacture of graphite in an electric furnace in 1896 was directly applicable in the early 1940's when the search began for an extremely pure graphite to serve as the neutron moderator in the first nuclear reactor. Thus it might be said that the technology of nuclear graphite is considerably more than 20 years old. However, the effects of radiation on graphite, which is a major concern of the modern literature, were unknown less than 20 years ago, and in this important respect the technology of nuclear graphite is a young field indeed. The first unclassified literature began to appear only six years ago following the First United Nations International Conference on the Peaceful Uses of Atomic Energy, held in Geneva in 1955. The bulk of the literature still exists in the form of government reports, many of which are not readily available. One of the objectives of this book has been to survey the literature and to provide a comprehensive, selected bibliography of useful references.

The volume of material existing in the field of nuclear graphite can best be appreciated from the fact that approximately 5000 government reports and journal publications were located and abstracted in the preparation of this book. The subject matter is current to January 1961; more recent material has been included wherever possible.

A book describing the manufacture, properties, and uses of a material such as graphite necessarily embraces a wide diversity of topics, and coherent organization posed a problem. Although some duplication was unavoidable, it has been minimized by the frequent use of cross references. A critical review of this volume will reveal variations in the depth and detail of subject treatment from chapter to chapter. To a large extent this reflects the varying extent of scientific understanding that currently exists

in the various topics. Some sections on new or particularly difficult topics are simply an empirical collation of observations, whereas other topics have been given a rather rigorous theoretical treatment.

An effort has been made to present the different views of controversial subjects. When one interpretation seemed clearly preferable, the authors have so indicated; in other cases, however, conflicting arguments or experimental observations could not be resolved on the basis of existing information, and the authors have reserved judgment.

This book is intended to serve as a reference for those concerned with the development and use of nuclear graphite. Its organization should also make it useful as a text to orient the newcomer to the field. The opening chapter discusses some of the historical aspects of nuclear graphite and develops the subject matter to the time when the first radiation effects were observed. Thereafter, the text follows this sequence: manufacture, properties, radiation effects, and reactor design. The chapters on manufacture, machining, structure, properties, and gas-graphite reactions contain a considerable amount of general information and should be most useful to engineers and scientists concerned with the broad field of graphite technology. The chapters on theory of radiation effects and irradiation techniques provide the background for subsequent chapters on radiation effects. The chapters devoted to metal-graphite compatibility and moderator design will be of special interest to the reactor design engineer.

The editor takes great pleasure in thanking the chapter authors for their willing help and cooperation in completing this task. All contributed generously of their own time without any remuneration in the belief that the result would serve a useful purpose. It was indeed a pleasure to work with the staff of General Electric's Technical Information Operation at Hanford; its excellent library and extensive files contributed in large measure to the preparation of this volume. Mr. B. B. Lane of this staff deserves special mention for his assistance in searching the literature, referencing, and indexing, and for his helpful editorial work on the manuscript.

The invaluable comments of many technical reviewers in the United States and the United Kingdom are also gratefully acknowledged. Many of their suggestions have been incorporated into the final manuscript. The final review and editing were conducted by members of the Division of Technical Information of the U. S. Atomic Energy Commission. It is a pleasure to acknowledge their valuable service.

R. E. NIGHTINGALE

July 1962

Contents

LIST OF CONTRIBUTORS

v

PREFACE

vii

CHAPTER ONE

Graphite in the Nuclear Industry

R. E. NIGHTINGALE

1-1 Early Use of Nuclear Graphite	1
1-2 Current Applications	6
1-3 Future Applications	16
References	17

CHAPTER TWO

Manufacture

W. P. EATHERLY and E. L. PIPER

2-1 Raw Materials	22
2-2 Forming	32
2-3 Baking	37
2-4 Impregnation	40
2-5 Graphitization	42
2-6 Purification	45
2-7 New Techniques	48
References	50

CHAPTER THREE

Machining Practice

C. A. SWITZER, JR., and L. H. JUEL

3-1 General Machining Techniques	53
3-2 Requirements in the Nuclear Industry	56
3-3 Equipment and Methods in the Nuclear Industry	58
3-4 Cementing Techniques	62
References	65

CHAPTER FOUR

Nuclear Properties

P. F. NICHOLS and E. M. WOODRUFF

4-1 Nuclear Requirements for Moderator Graphite	67
4-2 Graphite-moderator Physics	68
4-3 Nuclear Purity	74
References	84

CHAPTER FIVE

Structure

R. E. NIGHTINGALE

5-1	Structural Units and Nomenclature	87
5-2	Crystal Structure	89
5-3	Forces Within Crystallites	90
5-4	X-ray Diffraction by Polycrystalline Graphite	91
5-5	Lattice Dimensions	92
5-6	Lattice Distortions and Dimensions of Crystallites	96
5-7	Pore Structure	99
5-8	Grain Structure	104
5-9	Structural Changes During Graphitization	108
	References	113

CHAPTER SIX

Physical Properties

R. E. NIGHTINGALE, H. H. YOSHIKAWA, and H. H. W. LOSTY

6-1	Thermodynamic Properties	117
6-2	Thermal Properties	120
6-3	Electronic Band Structure	129
6-4	Electronic Properties	132
6-5	Chemical Properties	142
6-6	Mechanical Properties	147
6-7	Density	161
6-8	Surface Properties	166
6-9	Permeability	176
6-10	Material Designations of Electrographites	186
	References	186

CHAPTER SEVEN

Theory of Radiation Effects in Graphite

D. R. DE HALAS

7-1	Interaction of Radiation with a Solid	195
7-2	Displacement of Atoms in Graphite by Knock-on Atoms	200
7-3	Creation of Displacements in Graphite by Neutrons	215
7-4	Atomic Displacement Rates in Graphite in a Nuclear Reactor	218
7-5	Reactor Radiation Dosage Units	223
7-6	Nature of Radiation-induced Defects in Graphite	232
7-7	Glossary of Symbols	234
	References	236

CHAPTER EIGHT

Irradiation Techniques

D. E. BAKER and J. M. DAVIDSON

8-1	Low-temperature Irradiations	239
8-2	Room-temperature Irradiations	241

8-3	High-temperature Irradiations	244
8-4	Controlled-atmosphere Irradiations	248
8-5	Reactor-graphite Monitoring Methods	255
	References	257

CHAPTER NINE

Radiation-induced Structural and Dimensional Changes

R. E. NIGHTINGALE, H. H. YOSHIKAWA, and E. M. WOODRUFF

9-1	Radiation Effects on Crystal Structure	259
9-2	Radiation Effects on Macrostructure	273
9-3	Dimensional Changes Near Room Temperature	276
9-4	Dimensional Changes at Elevated Temperatures	283
9-5	Dimensional Changes in Moderator Structures	288
	References	290

CHAPTER TEN

Radiation Effects on Electrical and Thermal Properties

R. E. NIGHTINGALE

10-1	Electrical Resistance	295
10-2	Magnetoresistance	299
10-3	Hall Coefficient	299
10-4	Thermoelectric Power	300
10-5	Magnetic Properties	302
10-6	Thermal Conductivity	304
10-7	Specific Heat	309
	References	310

CHAPTER ELEVEN

Radiation Effects on Mechanical Properties

H. H. W. LOSTY

11-1	Single Crystals	313
11-2	Elastic Moduli of Nuclear Graphites	313
11-3	Strength	316
11-4	Irradiation Under Stress	318
11-5	Hardness and Machinability	321
11-6	Coefficient of Friction	321
11-7	Mechanical-property Changes in Graphite-moderator Stacks	322
	References	323

CHAPTER TWELVE

Stored Energy

R. E. NIGHTINGALE

12-1	Definition and Origin	325
12-2	Total Stored Energy	326
12-3	Measurement of Stored-energy Release Curves	331

12-4	Release Curves in Irradiated Graphite	336
12-5	Theory of Energy Storage	343
12-6	Relation of Stored Energy to Other Radiation-induced Property Changes	345
12-7	Reactor Safety and Operational Aspects of Stored Energy	347
	References	351

CHAPTER THIRTEEN

Annealing Radiation Effects

R. E. NIGHTINGALE

13-1	Introduction	355
13-2	Analysis of Annealing Experiments	355
13-3	Thermal Annealing	363
13-4	Radiation Annealing	376
13-5	Glossary of Symbols	383
	References	384

CHAPTER FOURTEEN

Gas-Graphite Systems

T. J. CLARK, R. E. WOODLEY, and D. R. DE HALAS

14-1	Survey of Gas-Graphite Systems	387
14-2	Carbon Dioxide-Graphite System	397
14-3	Oxygen-Graphite System	412
14-4	Steam-Graphite System	418
14-5	Hydrogen-Graphite System	421
14-6	Other Gases	427
14-7	Inhibitors and Protective Coatings	429
	References	437

CHAPTER FIFTEEN

Graphite-Metal and Graphite-Molten-salt Systems

R. A. MEYER and J. C. BOKROS

15-1	Liquid Metals	445
15-2	Compatibility of Solid Metals and Graphite	452
15-3	Compatibility of Molten Salts and Graphite	459
	References	461

CHAPTER SIXTEEN

Graphite-matrix Fuels

W. C. RILEY and J. KORETZKY

16-1	Advanced Fuel-element Concepts	465
16-2	Graphite as a Fuel Matrix	465
16-3	Fuel-Graphite Geometries	466
16-4	Fuel-element Fabrication	467
16-5	Effect of Fuel Loading and Particle Size on Physical Properties	472

CONTENTS

xiii

16-6	Radiation Effects in Fueled Graphite	473
16-7	Fission-product Release from Fueled Graphite .	477
16-8	Future Research Effort	479
	References	480

CHAPTER SEVENTEEN

Graphite Moderator Design

J. C. FOX

17-1	Advantages and Limitations of Graphite as a Structural Moderator .	483
17-2	Structural Design Considerations	484
17-3	Reactor Moderator Designs and Operating Experience	489
	References	521
AUTHOR INDEX		525
SUBJECT INDEX		534

Graphite in the Nuclear Industry

R. E. NIGHTINGALE†

1-1 Early Use of Nuclear Graphite

1-1.1 FIRST NUCLEAR REACTOR

When the group of scientists led by Enrico Fermi decided in 1942 to attempt to produce a self-sustaining nuclear chain reaction, they chose graphite as the moderator because it was the only suitable material available at that time. The first pile, CP-1, was constructed on a squash court under the West Stands of Stagg Field at the University of Chicago. Earlier Fermi and his collaborators had assembled the first exponential graphite-uranium structures at Columbia University for the purpose of determining the multiplication factor (k), the ratio of the number of neutrons in any one generation to the number of corresponding neutrons in the previous generation. If k could be made greater than 1, then a nuclear chain reaction could be produced. The first exponential pile, an 8-ft cube, was assembled from graphite blocks and contained about 7 tons of uranium oxide in iron containers; it was completed in July 1941. By the fall of that year, the multiplication factor (k_{∞}) for an infinite lattice of this type was known to be about 0.87. Although it was agreed that this could be increased if purer graphite and uranium could be produced, it was still not known whether k_{∞} could be made greater than 1.

In the spring of 1942, the work on experimental piles under Fermi was transferred to the University of Chicago. The first pile¹ constructed there of U_3O_8 and AGX graphite‡ yielded a k_{∞} of 0.944. Several lattice structures using different lots of graphite and uranium were used in the assembly of a number of experimental piles. Experiments on 29 of these are mentioned in early reports.² In July 1942 A. H. Compton estimated that a k_{∞} of 1.04 to 1.05 could be obtained in a pile of highly purified graphite and uranium oxide if the air were removed to reduce neutron absorption. A value of k_{∞} greater than 1 (actually 1.007) was obtained experimentally for the first time for Experimental Pile 9.

Enough data were collected and enough pure materials soon became available to make possible an attempt to produce a self-sustaining nuclear

† Hanford Laboratories, General Electric Company, Richland, Wash.

‡ AGX graphite was made from petroleum coke and coal-tar pitch by the National Carbon Company, using one pitch impregnation. It was graphitized by the Acheson process.

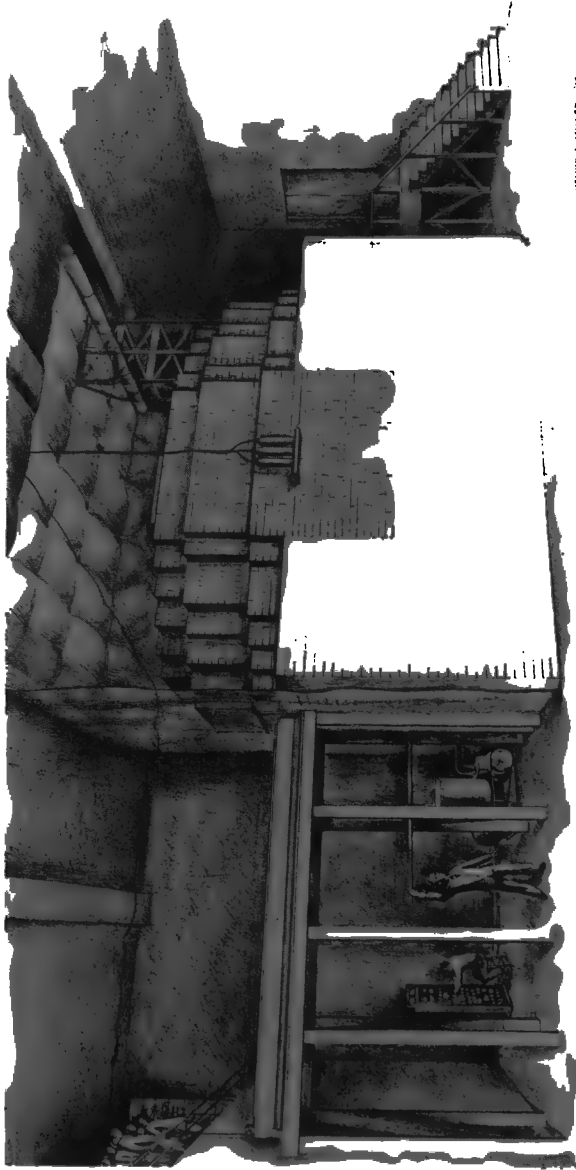


FIG. 1.1 The first nuclear reactor, CP-1, constructed under the West Stands of Stagg Field, University of Chicago. (Courtesy of Argonne National Laboratory.)

reaction, and the assembly of a pile was begun in October 1942. By this time the certainty of producing a chain reaction in an infinitely large system had virtually been established.³ The values of k_{∞} were estimated at 1.04 and 1.07 for uranium oxide-graphite and uranium-graphite piles, respectively, with an accuracy sufficient to make a chain reaction in an infinite system almost certain. The immediate questions remaining were: Could a self-sustaining reaction be produced in a structure of practical size? Would it be thermally stable, or would the reaction rate increase dangerously with temperature? Would it be controllable? The answer to all these questions, although not known with certainty, was believed to be "yes."

The production of the first nuclear chain reaction in CP-1 on Dec. 2, 1942, was, of course, a major milestone in the eventual utilization of nuclear energy for economic production of power. In his monthly report of the Physics Division of the Metallurgical Project, Fermi described this historic event very simply:⁴

Experimental Production of a Chain Reaction. The activity of the Physics Division in the past month has been devoted primarily to the experimental production of a divergent chain reaction. The chain reacting structure has been completed on December 2 and has been in operation since then in a satisfactory way. A program of tests on the operating conditions of the chain reacting unit and experiments for the investigation of the various radiations inside and outside the pile is in progress. The results will be reported as soon as possible.

The metal lattice at the center of CP-1 and two other major lattices making up most of the volume had been studied separately in Exponential Piles 18, 27, and 29. Because only a relatively small amount of metal (about 6 tons) was available and because several types of graphite of different purity were used, the pile was assembled in an approximately spherical shape with the purest materials in the center. The pile was supported on a wooden structure, with the lowest point of the graphite resting on the floor. No concrete or other heavy shielding was provided. The pile was surrounded by a tent of rubberized balloon fabric so that neutron-absorbing air might be evacuated. To complete the 26-ft-diameter sphere as planned would have required about 75 layers of the $4\frac{1}{8}$ -in. graphite bricks. Criticality was achieved at layer 57 without evacuating the air, and assembly of the sphere was discontinued about one layer above the critical dimensions (Fig. 1.1).

CP-1 was operated for several days at about 0.5 watt. It was found that not only was precise control accomplished by manual regulation of the cadmium strips, but also stable automatic control was possible. On December 12 a high-intensity test was carried out at about 200 watts, and measurements were made of the radiation intensities in and around the pile. Because of the danger of radiation at higher power, CP-1 was dismantled early in 1943 and reconstructed from the same materials at what is now the Argonne

National Laboratory. The addition of concrete shielding to the reconstructed pile, designated CP-2, allowed an increase in power to about 100 kw.

It is interesting to note that according to Fursov's work in Germany led to the conclusion that graphite could not be used with natural uranium to produce a nuclear chain reaction and no further effort was made to build such a pile. Calculations by physicists in the U.S.S.R. indicated that criticality could be achieved with 25 to 50 tons of uranium and a few hundred tons of graphite, and they proceeded to test this experimentally. Their experience was quite similar to that in the United States. Assembly of the pile with a spherical core and a 7.87-in. graphite-uranium lattice was started. The corners were eventually partially filled, and the pile became critical with 54 layers. Initial tests were at 10 watts, with a few short runs at several kilowatts. A negative reactivity temperature coefficient was found.

1-1.2 GRAPHITE IN CP-1

By the time a divergent nuclear chain reaction had been produced, information had already been gathered on the nuclear purity of several graphites by testing in special "sigma (σ) piles." These were constructed to measure the thermal-neutron-capture cross section of several grades of graphite available at that time. Accurate determination of the nuclear capture cross section of the graphite was necessary for two reasons: (1) if there were too much absorption in the graphite, a chain reaction would be impossible or might require that the dimensions of the pile be impractically large and (2) since the effect of absorption on reactivity is proportional to the square of the neutron density, the use of low-cross-section material near the center would reduce the size of the structure. For these reasons cross sections were measured on each grade of graphite used in CP-1, with the results shown in Table 1.1.

Table 1.1 — GRAPHITE² IN CP-1

Designation	Source	Amount, tons	Average thermal absorption cross section, mb
AGOT	National Carbon Company	255	4.97
Speer	Speer Carbon Co.	72.5	5.51
US	United States Graphite Co.	16	6.38
AGX	National Carbon Company	30	6.68
AGX	National Carbon Company	12 (Control-rod support pier)	
Speer	Speer Carbon Company		
		385.5	

The assembly of σ piles was a sensitive method capable of differentiating between the purest of the graphites then available. The graphite used in CP-1 was less pure than that now commercially available, but, because

methods of determining absorption cross sections have been changed and improved since these early measurements, these values are not precisely comparable to values quoted for graphites today (Sec. 4-3).

1-1.3 WIGNER EFFECT

During 1943 the Theoretical Physics Group of the Metallurgical Project, led by E. P. Wigner, was busy developing the information necessary to construct a large plutonium-producing pile. At that time the effect of intense heavy-particle radiation on pile materials was relatively unknown. In the same monthly report⁴ in which the nuclear chain reaction was reported, Wigner first called attention to the possible effects of fast particles on solids. He suggested that fast particles would act as projectiles and displace atoms from equilibrium lattice sites. Early calculations⁶ indicated that one 2-Mev neutron produced in fission would possess enough energy to displace about 2000 carbon atoms. The displacement of atoms from lattice sites by momentum transfer (which was soon to be confirmed experimentally) has become known as the "Wigner effect." The possible effects on strength, thermal conductivity, and dimensions of the graphite aroused much concern. The early investigators were faced with a problem that has arisen many times since in radiation-damage studies, i.e., that of attempting to learn or somehow predict what radiation-induced property changes will occur during the lifetime of a new higher flux reactor.

When construction was started on the first power-producing reactors (the X-10 Reactor in early 1943 and the first Hanford reactor in mid-1943), the only fast-neutron sources then available, i.e., the cyclotrons at Washington University and at the University of California, were wholly inadequate for a satisfactory prediction of what might happen to the graphite in a nuclear reactor. Cyclotron irradiations of several months were estimated to be equivalent in damaging effects to approximately one day in a Hanford reactor.⁷ Based upon the first radiation results from the X-10 Reactor in the spring of 1944 and the assumptions necessary at that time,⁸ it was stated: "W (Hanford Pile) could operate at least nine days without failure." Thus, by mid-1944 when it became apparent that there were no radiation sources of sufficient intensity to be used in predicting property changes of the graphite in the Hanford reactors beyond a few days operation, plans were made to construct several water-cooled test holes in the Hanford reactors so that changes in properties might be determined at frequent intervals.

The displacement of carbon atoms by fast neutrons was expected to produce changes in most of the properties of graphite, including a decrease in thermal and electrical conductivity, changes in dimensions and strength, and a storage of internal energy (Szilard complication). The possibility was suggested that the graphite bars might fuse together from the opening and closing of valence bonds at the surfaces of the bars.⁹ This question could not be dismissed lightly since calculations showed that during operation of the

Hanford reactors enough energy would be produced in the graphite to open all chemical bonds at least once. Even the possibility that the bars might break into small pieces could not be ruled out.

The radiation-damage studies that began with the start of the X-10 and Hanford reactors are the subject of several later chapters of this book. It will be seen that, although such catastrophic behavior as fusion or crumbling of graphite bars has never been observed, large changes in several properties do result from exposure to nuclear radiation, and these must be considered in the design of graphite-moderated reactors. Although much effort has been directed toward characterizing and understanding these complicated effects, many important unanswered questions have been revealed as new and more exacting moderator requirements are established for advanced reactor systems. Furthermore, since the properties of graphite may be varied greatly during manufacture, the development of graphites with improved properties for special applications is an active and fruitful field.

1-2 Current Applications

1-2.1 REACTOR MODERATOR

Although the properties of graphite make it suitable for many nuclear applications (moderator, reflector, fuel-channel sleeve, thermal column, fuel matrix, and control-rod material), by far the greatest use has been as a moderator and reflector. Nuclear graphite with an absorption cross section for thermal neutrons as low as 3.5 to 3.8 mb can now be manufactured in quantity at relatively low cost. Furthermore, graphite is strong enough to serve as a structural component, eliminating the necessity of employing metals with their higher cross sections. Although graphite is compatible with most reactor materials up to high temperatures, it must be protected from hot oxidizing gases.

Most serious engineering problems in the use of graphite as a moderator have resulted from radiation-damage effects: expansion at low temperature in the Hanford and Brookhaven graphite reactors; accumulation of stored energy in the Windscale, BEPO, and X-10 reactors; and hazards from possible uncontrolled burning in air-cooled reactors. These problems have arisen in the reflector graphite to much lesser degree because of the greatly reduced fast-neutron flux in the reflector. Problems in the use of graphite in the new high-temperature reactors will include oxidation and radiation-induced contraction of the moderator stack.

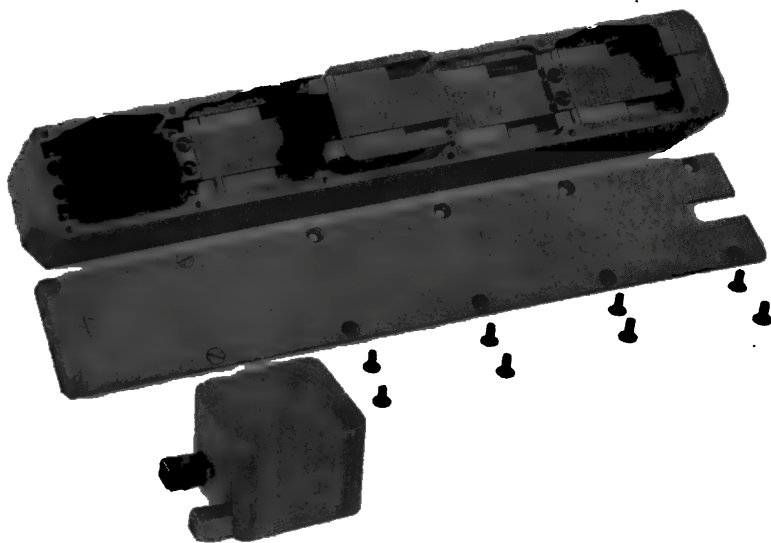
1-2.2 FUEL MATRIX AND OTHER APPLICATIONS

The development of fuel materials capable of producing high specific powers has been necessary to increase the efficiency and lower the capital costs of power reactors. Higher specific powers result in increased fuel

temperatures. Higher temperatures, in turn, have led to the development of high-temperature ceramic fuel materials such as the uranium oxides and carbides, which can be used alone or dispersed in a high-temperature ceramic matrix. Although the irradiation behavior of fueled graphite materials has not yet been thoroughly tested, the high-temperature strength, stability, and thermal conductivity of graphite make it a good matrix-material candidate (Chap. 16).

Graphite is used in a number of other special applications in the nuclear energy industry. In the reactor core boronated graphite is sometimes used as a high-temperature control-rod material. Recent designs for gas-cooled reactors employ graphite sleeves that support the fuel elements and channel the coolant.

Graphite is useful as a container for reactor irradiation experiments. Since it does not become highly radioactive, it can be handled with a minimum of shielding following irradiation. Furthermore, graphite possesses the high-temperature strength, stability, and chemical compatibility necessary in many experimental applications. Intricate parts can be machined to close tolerances. Figure 1.2 illustrates an application where a high-tempera-



high-temperature metal such as stainless steel would have made post-irradiation discharge and handling much more difficult.

1-2.3 COST OF NUCLEAR GRAPHITE

The cost of nuclear graphite varies widely, depending on purity, size, shape, and specific properties required. Currently the unmachined nuclear grade with an absorption cross section of approximately 4.3 mb costs \$1000 to \$1200 per ton in the United States in several-hundred-ton quantities. Machining adds an additional \$500 to \$1000 per ton. The purest material with a cross section of approximately 3.8 mb requires special processing, which adds approximately \$200 to \$400 per ton to the total cost. Thus the cost of 2000 tons of fabricated graphite for the core and reflector of a large reactor is several million dollars.

1-2.4 GRAPHITE-MODERATED REACTORS IN OPERATION AND PLANNED

The graphite-moderated reactors in operation, under construction, or definitely planned are listed in Table 1.2. A few low-power training and educational reactors have been omitted. Where operating characteristics have changed since design or initial operation, the current (January 1962) characteristics are given.

The amount of graphite used in the moderator and reflector of each reactor has been taken from published data or estimated from design information. The quantities are given in short tons (2000 lb). For more detailed information on the graphite grades, see Table 6.23.

Knowledge of the conditions under which graphite moderators have been used (temperature, flux, gas atmosphere, etc.), combined with a knowledge of the behavior of graphite, serves as a good index to problems that have been encountered in the reactors. In the first reactors and until recent years when enriched uranium came into more general use, heavy emphasis was placed on obtaining the purest graphite possible. In the United States the Hanford, the X-10, and Brookhaven Research reactors were designed to operate on natural-uranium fuel. The first British reactors, at both Windscale and Calder Hall, and the French reactors G1, G2, and G3 were designed for natural uranium. Today the optimum nuclear purity of the graphite is largely a question of economics since enrichment can be added at some increase in fuel costs to compensate for neutron capture. Designs of recent gas-cooled reactors, e.g., the Experimental Gas Cooled Reactor (EGCR) at Oak Ridge, and the Advanced Gas Cooled Reactor (AGR) at Windscale in England, call for a certain amount of enrichment so that neutron-absorbing metals can be used in the core. In the latest high-temperature gas-cooled reactor designs (HTGC, HTGR, and AVK Kraftwerk), graphite moderator is incorporated as a diluent for the fissile and fertile material in the fuel elements.

The rate of damage accumulation, as evidenced by a decrease in thermal

Table 1.2 — GRAPHITE MODERATED REACTORS

Reactor	Location	Date first critical	Reactor heat output, kw	Tons of graphite	Type of graphite in moderator	Gas atmosphere around graphite	Coolant and temperature	Ref.
<u>Research and Test Reactors</u>								
CP-1 (Chicago Pile)	Chicago, Ill.	December 1942 (dismantled 1943)	<0.2	385 mod. and refl.	AGOT plus some less pure grades	Air	No coolant, graphite at room temp.	2
CP-2 (Argonne Pile)	ANL, Lemont, Ill.	March 1943 (dismantled 1954)	0.2 to 2.0	472 mod. and refl.	Same as CP-1	Air	See CP-1	10
X-10 (Oak Ridge Graphite Reactor)	ORNL, Oak Ridge, Tenn.	November 1943	3500	400 mod. 274 refl.		Air	Air: inlet, atmospheric temp.; outlet, 80 to 140°C; max. graphite temp., 145°C	11
HTR (Hanford 305 Test Reactor)	Hanford Works, Richland, Wash.	February 1944	0.03 to 0.60	100 mod. 190 refl.	Gulf-Toledo grade G	Air	No coolant, graphite near room temp.	12
First Soviet graphite pile	Moscow, U. S. S. R.	1947	To several kilowatts	Several hundred		Air	No coolant	13,14
GLEEP (Graphite Low Energy Experimental Pile)	AERE, Harwell, Eng.	August 1947	100	565 mod. and refl.		Air	Air	15
BEPO (British Experimental Pile Zero)	AERE, Harwell, Eng.	July 1948	6500	310 mod. 540 refl.		Air	Air: inlet, atmospheric temp.; outlet, 80°C; max. graphite temp., 110°C	16-18

Table 1.2 (Continued)

Reactor	Location	Date first critical	Reactor heat output, kw	Tons of graphite	Type of graphite in moderator	Gas atmosphere around graphite	Coolant and temperature	Ref.
<u>Research and Test Reactors (Continued)</u>								
BGRR (Brookhaven Graphite Research Reactor)	BNL, Upton, L. I., N. Y.	August 1950	20,000	375 mod. 375 refl.	Principally AGOT in mod. AGHT in ref.	Air	Air: inlet, 50°C; outlet, 225°C	19
RPT (Reactor for Physical and Technical Investigation)	Moscow, U.S.S.R.	April 1952	15,000 to 20,000	33.5 mod. (?)	Density: 1.8 g/cm ³	He	Water: inlet, 29 to 30°C; outlet, 55 to 65°C; graphite temp. at peak power, 470°C	14, 15, 20, 21
IR (Experimental Uranium Graphite Isotope Reactor)	U.S.S.R.	1952	50,000	140 mod. (?)	Density: 1.65 g/cm ³	N ₂	H ₂ O: outlet, 90°C; max. graphite temp., 400-500°C	22
SR-305 (Savannah River Test Pile 305)	Aiken, S. C.	September 1952	0.025	135 mod. 125 refl.	CSGDF mod. CSO refl.	He	No coolant; graphite at 25°C	23, 24
APS (Atomic Power Station)	Obninsk, U.S.S.R.	May 1954	30,000	5 mod. 50 refl.	Density: 1.65 g/cm ³	Initially He, later N ₂	H ₂ O: inlet, 190°C, outlet, 280°C; max. graphite temp., 800°C	17, 25-27
PCTR (Physical Constants Test Reactor)	Hanford Works, Richland, Wash.	October 1955	0.1	20 mod. and refl.	Speer gas purified	Air	No coolant; graphite at room temp.	12
TTR (Thermal Test Reactor)	Hanford Works, Richland, Wash.	March 1951 at KAPL; August 1956 at Hanford	0.1	8 mod. and refl.	KC and CS	Air	No coolant; graphite at room temp.	12

Table 1.2 (Continued)

Reactor	Location	Date first critical	Reactor heat output, kw	Tons of graphite	Type of graphite in moderator	Gas atmosphere around graphite	Coolant and temperature	Ref.
<u>Research and Test Reactors (Continued)</u>								
BR-1 (Belgian Reactor-1)	Mol, Belg.	May 1956	4000	140 mod. 350 refl.	Central zone: grade A, density: 1.72 g/cm ³ ; outer zone: grade B, density: 1.65 g/cm ³	Air	Air: inlet, 60°C; outlet, 68°C; max. graphite temp., 90°C	28
SRE (Sodium Reactor Experiment)	Santa Susana, Calif.	April 1957	21,000	13 mod. 29 refl.	TSP	Graphite canned in zirconium; He blanket	Sodium: inlet, 285°C; outlet, 510°C	24, 27, 29, 30
TREAT (Transient Test Reactor Facility)	NRTS, Idaho	January 1959	10 ⁶ kw-sec bursts	Graphite in fuel matrix is moderator; 35 refl.	Graphite - UO ₂ fuel matrix	Canned in Zircaloy	Air: inlet, atmospheric temp.; outlet, inlet plus 100°C	24, 31
Zenith	Winfrith, Dorset, Eng.	December 1959	0.1	26 refl.		N ₂	Externally heated N ₂ : inlet, 400°C; outlet, 950°C; max. graphite temp., 800°C	34, 35
AGR (Advanced Gas Cooled Reactor)	Seascale, Cumberland, Eng.	1962	100,000	265 mod. and refl.		CO ₂	CO ₂ : inlet, 250-325°C; outlet, 500-575°C	27, 32, 33
UHTREX (Ultra-high Temperature Reactor Experiment), formerly Turret	LASL, Los Alamos, N. Mex.	1962	3000	4.63 mod.	Nuclear grade, density: 1.7 g/cm ³	He	He: inlet, 870°C; outlet, 1315°C	36, 37
EGCR (Experimental Gas Cooled Reactor)	ORNL, Oak Ridge, Tenn.	1962	85,000	67 mod. 90 refl.	Nuclear grade with needle coke	He	He: inlet, 265°C; outlet, 565°C	38

Table 1.2 (Continued)

Reactor	Location	Date first critical	Reactor heat output, kw	Tons of graphite	Type of graphite in moderator	Gas atmosphere around graphite	Coolant and temperature	Ref.
<u>Research and Test Reactors (Continued)</u>								
Dragon Reactor	Winfrith, Dorset, Eng.	1963	20,000	2.4 mod.	Graphite matrix fuel and low-permeability graphite fuel sleeves	He	He: inlet, 350°C; outlet, 750°C av. and 926°C max.; max. graphite temp. inside fuel box, 1700°C	39, 40
HTGR (High Temperature Gas Cooled Reactor)	Peach Bottom, Pa.	1964	115,000	21.5 mod. including fuel matrix; 52.5 refl.	Low-permeability type	He	He: inlet, 350°C, outlet, 750°C	41, 42
AVK Kraftwerk (Pebble Bed Reactor)	Juelich, W. Germany	1963	48,000		Graphite matrix fuel pebbles	He	He: inlet, 200°C, outlet, 850°C	43-45
MSRE (Molten Salt Reactor Experiment)	ORNL, Oak Ridge, Tenn.	1963	10,000			None: molten salt in direct contact with graphite	Molten salt fluorides of Li ⁷ , Be, Zr, Th, and U at 660°C	
<u>Production and Power Reactors</u>								
Hanford production reactors (8)	Hanford Works, Richland, Wash.	September 1944 to April 1955		First 6 reactors: 1200 mod. 600 refl.; last 2 1700 mod. 1000 refl.	Mostly F purified in mod.	CO ₂ and He	H ₂ O: inlet, 5 to 20°C	
Windscale reactors (2)	Seascale, Cumberland, Eng.	July 1950 and 1951 (shut down 1957)	160,000			Air	Air: inlet, atmospheric temp.; outlet, 200°C	46

Table 1.2 (Continued)

Reactor	Location	Date first critical	Reactor heat output, kw	Production and Power Reactors (Continued)			Gas atmosphere around graphite	Coolant and temperature	Ref.
				Tons of graphite	Type of graphite in moderator				
G1 French production reactor	Marcoule, Fr.	January 1956	38,000	1320 mod. 210 refl.			Air	Air: inlet, atmospheric temp.; outlet, 220°C	27, 47-49
Calder Hall reactors (4)	Seascale, Cumberland, Eng.	May 1956 to December 1958	220,000	730 mod. 550 refl.	PGA mod. PGB refl.		CO ₂	CO ₂ : inlet, 135°C; outlet, 333°C	16, 27, 50-54
Siberian power-station reactors (6)	Troitsk, U.S.S.R.	First reactor 1958	100,000 kw (e)					H ₂ O: inlet (?); outlet, 180-220°C	16
G2 & G3 French reactors	Marcoule, Fr.	G2: July 1958 G3: March 1959	205,000	700 mod. 500 refl.	Pechiney, nuclear grade, density 1.7 g/cm ³		CO ₂	CO ₂ : inlet, 80 and 150°C; outlet, 305 and 354°C	24, 27, 55-57
Chapel Cross reactors (4)	Chapel Cross, Annan, Dumfriesshire, Eng.	November 1958 to December 1959	220,000	730 mod. 550 refl.	PGA mod. PGB refl.		CO ₂	CO ₂ : inlet, 135°C; outlet, 330°C	24, 27
EDF 1 (Electricite de France-1)	Chinon, Fr.	1962	300,000	960 mod. 364 refl.	Pechiney, nuclear grade, density: 1.67 g/cm ³		CO ₂	CO ₂ : inlet, 140°C; outlet, 355°C	27, 58
EDF 2 (Electricite de France-2)	Chinon, Fr.	1963	785,000		Same as EDF 1		CO ₂	CO ₂ : inlet, 195°C; outlet, 365°C; max. graphite temp., 450°C	27, 58
Volga Reactor	Ulyanovsk region, U. S. S. R.	1960-1961	50,000 kw (e)					Na: max. temp., 540°C	14

Table 1.2 (Continued)

Reactor	Location	Date first critical	Reactor heat output, kw	Tons of graphite	Type of graphite in moderator	Gas atmosphere around graphite	Coolant and temperature	Ref.
Urals power-station reactors (2)	Beloyarsk, U. S. S. R.	1962	Production and Power Reactors (Continued)					16, 59
			285,000	820 mod. (?)	Density: 1.65 g/cm ³	N ₂	Boiling water and superheated steam: max. graphite temp. , 660 °C (boiling-water region), 725 °C (steam region)	
Berkeley reactors (2)	Berkeley, Gloucestershire, Eng.	1961-1962	555,000	1500 mod. 850 refl.	PGA mod. PGB refl.	CO ₂	CO ₂ ; inlet, 160 °C; max. graphite temp. , 375 °C	27, 60, 61
Bradwell reactors (2)	Bradwell-on-Sea, Essex, Eng.	1961-1962	530,000	1350 mod. 800 refl.	Moderator, density: 1.75 g/cm ³ ; reflector: Welland PGB	CO ₂	CO ₂ ; inlet, 180 °C; outlet, 390 °C; max. graphite temp. , 396 °C	27, 62, 63
Hunterston reactors (2)	Hunterston, Ayrshire, Scot.	1964	569,000	1340 mod. 905 refl.	PGA mod. PGB refl.	CO ₂	CO ₂ ; inlet, 204 °C; outlet, 390 °C; max. graphite temp. , 465 °C	24, 27, 64
Hinkley Point reactors (2)	Hinkley Point, Bridgewater, Somerset, Eng.	1963	980,000	2730 mod. 690 refl.	PGA mod.	CO ₂	CO ₂ ; inlet, 180 °C; outlet, 375 °C; max. graphite temp. , 385 °C	27, 65
Latina reactor	Latina, It.	1962	705,000	1475 mod.	PGA mod.	CO ₂	CO ₂ ; inlet, 180 °C; outlet, 390 °C	66
Hallam Nuclear Power Facility (sodium-graphite)	Hallam, Neb.	1962	256,000	83 mod. 80 refl.	Mold grade (extruded)	Graphite canned in 304 stainless steel; He blanket	Na: inlet, 320 °C; outlet, 508 °C; av. graphite temp. , 490 °C	24, 67

Table 1.2 (Continued)

Reactor	Location	Date first critical	Reactor heat output, kw	Tons of graphite	Type of graphite in moderator	Gas atmosphere around graphite	Coolant and temperature	Ref.
Production and Power Reactors (Continued)								
NPR (N Production Reactor)	Hanford Works, Richland, Wash.	1963		800 Mod. 1000 refl.	TSX mod. AGOT-LS refl.	Inert	Pressurized H ₂ O	
Japanese Gas Cooled Reactor	Tokai Mura, Japan	1962	585,000	1090 mod.		CO ₂	CO ₂ : inlet, 203°C; outlet, 398°C	68, 72
Trawsfynydd reactors (2)	Trawsfynydd, North Wales	1963	870,000	2130 mod. and refl.	PGA mod.	CO ₂	CO ₂ : inlet, 200°C; outlet, 399°C	69
Dungeness reactors (2)	Kent, Eng.	1964-1965	835,000	2140 mod. and refl.	PGA mod.	CO ₂	CO ₂ : inlet, 250°C; outlet, 410°C	70
Sizewell reactors (2)	Suffolk, Eng.	1964	950,000	2500 mod. and refl.	PGA mod.	CO ₂	CO ₂ : inlet, 214°C; outlet, 410°C	71

conductivity, growth, and build-up of stored energy, is greatly reduced as the temperature is increased, and above 300°C it is so low that it can almost be neglected in the reactor design. The extent to which radiation-induced property changes will occur can be judged to some degree from the information in Table 1.2 on the power generated per ton of graphite and by the coolant temperature. Although graphite temperatures may vary considerably throughout the core and are not generally stated in a list of operating characteristics, the maximum and minimum temperatures can be estimated from a knowledge of the lattice geometry, power generation, and coolant temperatures. Where they are available, inlet and outlet coolant temperatures are listed in Table 1.2. For gas-cooled reactors graphite temperatures will generally be 0 to 50°C higher than the coolant temperatures.

1-3 Future Applications

New methods of converting nuclear energy into useful power, such as very high temperature reactor cores, controlled fusion, direct heat-to-electrical energy conversion, and nuclear rocket propulsion, will involve temperatures in the range of 1500 to 3000°C and higher. Unless improved high-temperature materials are developed, the capability of these systems will be seriously limited. It is safe to assume that graphite and graphite-based materials will find increasingly important uses in these fields.

The extent to which graphite will be used in high-temperature gas-cooled reactor cores will depend largely on the degree to which permeability can be reduced and oxidation resistance improved. Direct conversion of fission heat to electricity has already been accomplished, but greatly increased efficiencies are needed for use in central power stations. Fuel elements operating at temperatures of 2000°C or higher may be required to produce the large temperature differential needed for efficient direct conversion in thermionic cells. Graphite matrix materials and other ceramic systems are certain to be given serious consideration.

Recent aeronautical and space applications require a material that will endure high heat fluxes, high surface temperatures, and a high flow of a corroding gas. [In nose cones for reentry missiles, for example, surface temperatures rise very rapidly, resulting in severe thermal shock. Graphite-based materials, because of their outstanding high-temperature strength, high sublimation temperature, and excellent thermal-shock resistance, are being developed for this purpose.] The thermal properties of graphite and its low neutron-capture cross section also suggest it as a leading candidate for high-temperature moderators in nuclear-propulsion reactors. For this use, however, improved resistance to attack by oxygen, carbon dioxide, and hydrogen is also needed.

New methods of fabrication are being developed by which it is possible to make graphite in various forms and shapes. For example, a graphite fabric⁷³ with a wide variety of weaves can be produced with a room-

temperature tensile strength of 15,000 psi. This increases to 30,000 psi at 2500°C. Possible uses of this new material include: filters for high-temperature nonoxidizing gases and corrosive fluids; additives to plastics and ceramics and to glass cloth to make them electrically or thermally conductive; packing in nose cones; and fire-resistant screens.

References

1. S. K. Allison, *The First Intermediate Pile at the University of Chicago*, USAEC Report CP-69, University of Chicago.
2. E. Fermi, Experimental Production of a Divergent Chain Reaction, *Am. J. Phys.*, **20**: 536-558 (1952).
3. E. Fermi, *Possibility of a Chain Reaction*, USAEC Report CP-383, University of Chicago, Nov. 26, 1942.
4. E. Fermi, *Report for Month Ending December 15, 1942, Physics Division*, USAEC Report CP-387, University of Chicago, December 1942.
5. V. S. Fursov, Work of the U.S.S.R. Academy of Sciences on Uranium-Graphite Reactors, in *Conference of the Academy of Sciences of the U.S.S.R. on the Peaceful Uses of Atomic Energy, July 1-5, 1955*, pp. 15-38, Publishing House of the Academy of Sciences of the U.S.S.R., Moscow, 1955.
6. F. Seitz, On the Disordering of Solids by Action of Fast Massive Particles, *Discussions Faraday Soc.*, **5**: 271-282 (1949).
7. *Laboratory Council. Information Session*, USAEC Report CS-484, University of Chicago, Feb. 22, 1943.
8. M. Burton and J. Franck, *Graphite Tests of W*, USAEC Report DuH-3736 (MUC-MB-206), University of Chicago, Apr. 29, 1944.
9. T. J. Neubert et al., *Neutron-Induced Discomposition of Graphite. I. Fundamentals*, USAEC Report ANL-5472, Argonne National Laboratory, January 1956.
10. H. E. Metcalf, *A Brief General Description of the Argonne Uranium-Graphite Pile (CP-2)*, USAEC Report CP-2459, University of Chicago.
11. M. C. Wittels, Evaluation of the ORNL Graphite Reactor, in *US/UK Graphite Conference Held at St. Giles Court, London, December 16-18, 1957*, pp. 64-81, USAEC Report TID-7565 (Pt. 1), 1957.
12. A. Fowler, Hanford Laboratories, General Electric Company, personal communication, December 1959.
13. A.E.I. Research Reactor, *Nuclear Eng.*, **1**: 14 (1956).
14. Survey of Soviet Reactors (Status According to Published Reports up to September 15, 1958), *Jaderna Energie*, **5**: 92-101 (1959); translation in Canadian Report AECL-1011, Chalk River, May 1960.
15. Reactors: World Report, *Nuclear Power*, **4**(33): 113-120 (1959).
16. H. S. Isbin, Catalog of Nuclear Reactors, in *Proceedings of the Second United Nations International Conference on the Peaceful Uses of Atomic Energy, Geneva, 1958*, Vol. 8, pp. 561-584, United Nations, New York, 1959.
17. H. Etherington (Ed.), *Nuclear Engineering Handbook*, pp. 13-123 to 13-159, McGraw-Hill Book Company, Inc., New York, 1958.
18. The World's Reactors, No. 1 BEPO—British Experimental Pile, *Nuclear Eng.*, **1**: insert opposite p. 14 (1956).
19. R. W. Powell et al., Control of Radiation Effects in a Graphite Reactor Structure, in *Proceedings of the Second United Nations International Conference on the Peaceful Uses of Atomic Energy, Geneva, 1958*, Vol. 7, pp. 282-294, United Nations, New York, 1959.
20. G. N. Kruzhilin, Reactor for Physical and Technical Investigations, in *Proceedings*

- of the First United Nations International Conference on the Peaceful Uses of Atomic Energy, Geneva, 1955, Vol. 2, pp. 435-448, United Nations, New York, 1956.
21. V. V. Goncharov et al., Some New and Rebuilt Thermal Research Reactors, in *Proceedings of the Second United Nations International Conference on the Peaceful Uses of Atomic Energy, Geneva, 1958*, Vol. 10, pp. 321-367, United Nations, New York, 1959.
 22. B. B. Brohovich et al., Disassembly of an Experimental Uranium-Graphite Isotope Reactor after Four Years of Operation, in *Proceedings of the Second United Nations International Conference on the Peaceful Uses of Atomic Energy, Geneva, 1958*, Vol. 7, pp. 241-249, United Nations, New York, 1959.
 23. R. C. Axtmann et al., *Initial Operation of the Standard Pile*, USAEC Report DP-32, E. I. du Pont de Nemours & Co., Inc., December 1953.
 24. *Nuclear Reactor Plant Data: Vol. 1, Power Reactors; Vol. 2, Research and Test Methods*, American Society of Mechanical Engineers, New York, 1959.
 25. D. I. Blokhintsev and N. A. Nikolaev, The First Atomic Power Station of the U.S.S.R. and the Prospects of Atomic Power Development in *Proceedings of the First United Nations International Conference on the Peaceful Uses of Atomic Energy, Geneva, 1955*, Vol. 3, pp. 35-55, United Nations, New York, 1956.
 26. N. A. Dollezhal et al., Operating Experience with the First Atomic Power Station in the U.S.S.R. and Its Use Under Boiling Conditions, in *Proceedings of the Second United Nations International Conference on the Peaceful Uses of Atomic Energy, Geneva, 1958*, Vol. 8, pp. 86-99, United Nations, New York, 1959.
 27. *Directory of Nuclear Reactors, Vol. 1, Power Reactors*, International Atomic Energy Agency, Vienna, 1959.
 28. G. Stiennon, Part I. The BR-1 Pile, Description and Use, in *Proceedings of the Second United Nations International Conference on the Peaceful Uses of Atomic Energy, Geneva, 1958*, Vol. 10, pp. 424-431, United Nations, New York, 1959.
 29. *Proceedings of the SRE-OMRE Forum Held at Los Angeles, California, November 8 and 9, 1956*, USAEC Report TID-7525, Atomics International, Jan. 15, 1957.
 30. W. E. Parkins, The Sodium Reactor Experiment, in *Proceedings of the First United Nations International Conference on the Peaceful Uses of Atomic Energy, Geneva, 1955*, Vol. 3, pp. 295-321, United Nations, New York, 1956.
 31. G. A. Freund et al., TREAT, a Pulsed Graphite-Moderated Reactor for Kinetic Experiments, in *Proceedings of the Second United Nations International Conference on the Peaceful Uses of Atomic Energy, Geneva, 1958*, Vol. 10, pp. 461-475, United Nations, New York, 1959.
 32. AEE Winfrith Heath, *Nuclear Power*, 4(33): 90-91 (1959).
 33. R. V. Moore et al., Advances in the Design of Gas Cooled, Graphite Moderated Reactors, in *Proceedings of the Second United Nations International Conference on the Peaceful Uses of Atomic Energy, Geneva, 1958*, Vol. 9, pp. 104-114, United Nations, New York, 1959.
 34. G. Gunnill and G. H. Kinchin, Zenith, *Nuclear Eng.*, 4: 368-393 (1959).
 35. K. J. Mitchell and R. A. Geary, The High Temperature Zero Energy Reactor "Zenith" in *Proceedings of the Second United Nations International Conference on the Peaceful Uses of Atomic Energy, Geneva, 1958*, Vol. 9, pp. 310-315, United Nations, New York, 1959.
 36. R. P. Hammond and J. P. Cody (Eds.), *A Preliminary Study of the Turret Experiment—An Operating Test of Unclad Fuel at High Temperature*, USAEC Report LA-2303, Los Alamos Scientific Laboratory, March 1959.
 37. R. P. Hammond et al., Turret—A Test of Unclad Fuel, *Nucleonics*, 17(12): 106-109 (1959).
 38. W. F. Banks, EGCR—Descendant of Calder Hall, *Nuclear Eng.*, 6: 28-32 (1961).

39. L. R. Shepherd et al., The Possibilities of Achieving High Temperatures in a Gas Cooled Reactor, in *Proceedings of the Second United Nations International Conference on the Peaceful Uses of Atomic Energy, Geneva, 1958*, Vol. 9, pp. 289-305, United Nations, New York, 1959.
40. DRAGON—General Description, *Nuclear Eng.*, **5**: 209-315 and insert facing p. 308 (1960).
41. Fifty-one Utilities Back Alternative to AEC-JCAE Gas Reactor, *Nucleonics*, **16**(12): 17-19 (1958).
42. P. Fortescue et al., HTGR—Underlying Principles and Design, *Nucleonics*, **18**(1): 86-90 (1960).
43. World Reactor Chart, *Nuclear Power*, **5**(45): facing p. 86 (1960).
44. German Pebble-Bed Unit Using Off-Shelf Equipment, *Nucleonics*, **17**(10): 26 (1959).
45. R. Schulten, A 15-Mw High-temperature Pebble-bed Reactor, in *Proceedings of the Second United Nations International Conference on the Peaceful Uses of Atomic Energy, Geneva, 1958*, Vol. 9, pp. 306-309, United Nations, New York, 1959.
46. *Euratom Data Booklet*, p. 42, European Atomic Energy Community, Brussels, Belgium.
47. Reactor G1 at Marcoule, *Nuclear Eng.*, **3**: 258 and insert (1959).
48. M. de Rouville et al., Experience Obtained During Two Year's Operation of the Reactor G1, in *Proceedings of the Second United Nations International Conference on the Peaceful Uses of Atomic Energy, Geneva, 1958*, Vol. 8, pp. 18-22, United Nations, New York, 1959.
49. P. Chambadal and M. Pascal, Recovery of the Energy Produced in Air Cooled Graphite Reactor G1, in *Proceedings of the First United Nations International Conference on the Peaceful Uses of Atomic Energy, Geneva, 1955*, Vol. 3, pp. 81-83, United Nations, New York, 1956.
50. Engineering Features of Calder Hall, *Nuclear Eng.*, **1**: 155 (1956).
51. Calder Hall, *Nuclear Eng.*, **1**: 266-303 and insert facing p. 276 (1956).
52. Calder Hall, The B.N.E.C. Symposium Papers, *Nuclear Eng.*, **1**: 383-390 and insert (1956).
53. H. G. Davey et al., Operating Experience at Calder Hall, in *Proceedings of the Second United Nations International Conference on the Peaceful Uses of Atomic Energy, Geneva, 1958*, Vol. 8, pp. 10-17, United Nations, New York, 1959.
54. J. B. W. Cunningham, Current Re-designs of Calder Hall, in *Proceedings of the Second United Nations International Conference on the Peaceful Uses of Atomic Energy, Geneva, 1958*, Vol. 8, pp. 416-423, United Nations, New York, 1959.
55. Report from Marcoule, *Nuclear Power*, **2**(17): 356-361 (1957).
56. *France Atome*, Description of Reactors G2 and G3, in *Proceedings of the Second United Nations International Conference on the Peaceful Uses of Atomic Energy, Geneva, 1958*, Vol. 8, pp. 334-355, United Nations, New York, 1959.
57. The Marcoule Reactor G2, *Nuclear Eng.*, **4**: 435-437 (1959).
58. M. Roux and M. Bienvenu, The Chinon Nuclear Power Plant EDF 1 and EDF 2, in *Proceedings of the Second United Nations International Conference on the Peaceful Uses of Atomic Energy, Geneva, 1958*, Vol. 8, pp. 356-379, United Nations, New York, 1959.
59. N. A. Dollezhal et al., Uranium-Graphite Reactor with Superheated High Pressure Steam, in *Proceedings of the Second United Nations International Conference on the Peaceful Uses of Atomic Energy, Geneva, 1958*, Vol. 8, pp. 398-414, United Nations, New York, 1959.
60. Berkeley Nuclear Power Station, *Nuclear Eng.*, **2**: 96-102 (1957).
61. S. A. Ghalib and J. R. M. Southwood, The Berkeley Power Station, in *Proceedings*

- of the Second United Nations International Conference on the Peaceful Uses of Atomic Energy, Geneva, 1958, Vol. 8, pp. 463-478, United Nations, New York, 1959.
62. R. D. Vaughan, Bradwell-On-Sea Nuclear Power Station, *Nuclear Eng.*, **2**: 140-145 (1957).
63. R. D. Vaughan and E. Anderson, The Bradwell Power Station, in *Proceedings of the Second United Nations International Conference on the Peaceful Uses of Atomic Energy, Geneva, 1958*, Vol. 8, pp. 450-462, United Nations, New York, 1959.
64. R. N. Millar, The Hunterston Power Station, in *Proceedings of the Second United Nations International Conference on the Peaceful Uses of Atomic Energy, Geneva, 1958*, Vol. 8, pp. 424-433, United Nations, New York, 1959.
65. Hinkley Point, *Nuclear Eng.*, **3**: 286 and facing insert (1958).
66. Latina, *Nuclear Eng.*, **4**: 329-342 and insert (1959).
67. R. L. Olson et al., The Sodium Graphite Reactor Power Plant for CPPD, in *Proceedings of the Second United Nations International Conference on the Peaceful Uses of Atomic Energy, Geneva, 1958*, Vol. 9, pp. 161-179, United Nations, New York, 1959.
68. Japan's First Nuclear Power Station, *Nuclear Power*, **5**(47): 104-118 and insert facing p. 118 (1960).
69. Trawsfynydd, *Nuclear Eng.*, **6**: 12-23 (1961).
70. *Applied Atomics*, No. 251, p. 1, July 20, 1960.
71. Sizewell-Contract Placed for Seventh "Commercial" Station, *Nuclear Eng.*, **6**: 7 (1961).
72. R. W. Bailey and J. L. Head, Earthquake-Resistant Core for Tokai-Mura, *Nuclear Eng.*, **6**: 25-27 (1961).
73. Fiber Stretches Graphite Use; Graphite Cloth, *Chem. Eng.*, **66**: 70 (May 4, 1959).

Manufacture

W. P. EATHERLY and E. L. PIPER†

Most electrographites are produced from a petroleum-coke filler and a coal-tar-pitch binder. Nuclear grades of electrographites are produced by modifications of conventional manufacturing methods, with special care being taken to exclude impurities that have significant neutron-absorption cross sections. The processing steps in the manufacture of a conventional nuclear graphite are summarized in Fig. 2.1. Various purification techniques,

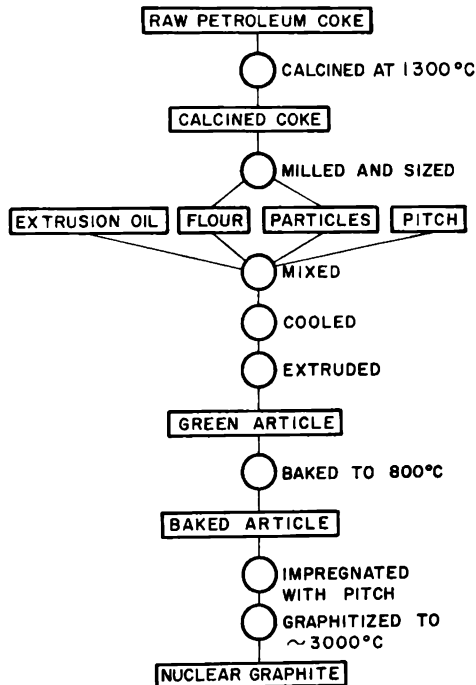


Fig. 2.1 Flow diagram showing the materials and processes used in the manufacture of nuclear graphite.

derived chiefly from similar processes employed in the production of spectrographic-arc carbons, have been introduced into the manufacture of nuclear-grade graphite to achieve purities that may exceed 99.999 per cent carbon.

† National Carbon Company, Parma, Ohio.

In this chapter the manufacture of electrographites will be discussed in some detail. Newer fabrication techniques, including pressure baking, gas decomposition (pyrolytic carbon), and hot working, are now finding application in the nuclear field. Information on many of these techniques, however, is restricted by proprietary and military considerations, and hence they can be described only in general terms.

2-1 Raw Materials

2-1.1 PETROLEUM COKE

All commercially produced carbons are composed of a carbonaceous filler material bonded by a carbonized binder, usually coal-tar pitch. The most commonly used filler materials are petroleum coke, metallurgical coke, anthracite, and lampblack. Of these, the most easily graphitized material is petroleum coke; i.e., when heated to a temperature of 2800 to 3000°C the carbon from petroleum coke achieves a higher degree of crystallinity[†] than that of other materials. For this reason almost all commercial graphites are made from a petroleum-coke base filler. Other easily graphitized cokes can be prepared from certain aromatic hydrocarbons, but economic considerations prevent their use in any commercial practice involving tonnage quantities.

(a) *Cracking.* Petroleum coke is a by-product in the refining of petroleum crude; today it is largely obtained by the cracking of a heavy refinery oil. This process produces gasoline, other light fractions, and coke. The cracking principle is employed by the petroleum industry to increase the yield of gasoline from crude beyond that which is possible by simple atmospheric or vacuum distillation. The cracking process decomposes the larger hydrocarbon molecules in the crude oil into the desired lighter fractions. The most stable of these are removed as cracked gasoline, and the more reactive components polymerize to form a heavy fuel oil or coke. The two techniques that are used commercially to break down the crudes are thermal and catalytic cracking.

The range of charge stocks that can be processed in thermal crackers is quite wide; the feed materials may be crudes or distillate fractions. After these charge stocks have been fractionated, the relatively heavy oils are fed under pressure through heated coils, where they attain the temperatures necessary for cracking ($\sim 500^{\circ}\text{C}$). The hot oils are then fed to a reaction chamber, where the cracking process takes place at a pressure of about 500 psi. A minimum of coke is formed. A flash chamber, in which the lighter fractions are vaporized, usually follows the reaction chamber. This arrange-

[†] The degree of crystallinity of a polycrystalline graphite refers to the degree to which the structure approaches that of a perfect crystal. A highly crystalline graphite has a high thermal and electrical conductivity, a small *c* spacing, and a large crystallite size (see Chaps. 5 and 6).

ment permits close control of the properties of the residual fuel oil, which may be sold as fuel oil or processed further to asphalt or coke.

Catalytic cracking is replacing thermal cracking because it produces higher octane gasoline. About two-thirds of the present cracking capacity in the United States is catalytic;¹ no new thermal-cracking units are being built. The catalytic process depends on the fact that the reactivity of the molecules in the gas-oil feed stock is increased in the presence of an active catalyst, usually an aluminum silicate. The mechanism of catalysis is not well understood, but the most generally accepted theory² is that the chemical bonds of the adsorbed hydrocarbons are weakened by interaction with the catalyst; this weakening allows them to deform and thereby assists in the formation of aromatics and isoparaffins. This mechanism can be contrasted with that of thermal cracking, which is primarily a dehydrogenation with the subsequent formation of olefins. The charge stock to a catalytic cracker may range from naphtha to reduced crudes, but it is normally a gas oil charged with some recycled material. The charge is forced into a stream of hot catalyst, vaporized, and passed into a reaction chamber, where the cracking takes place in a fluidized bed. In the reaction any catalyst carried over is inactivated by a coating of coke. After separation in a cyclone, the catalyst is returned to a regenerator, where the accompanying coke is removed by combustion and the catalyst is reactivated for further use. The cracked materials are fed to a fractionator and separated by boiling; the heaviest components (the slurry or fuel oils) are then ready for coking.

(b) *Coking.* The primary incentive for the production of coke is the additional yield of gas, gasoline, and gas oil obtained. Coking is essentially a thermal-cracking process, but it is carried out under more severe conditions. The coking unit may be charged with the heavy fractions described above or with atmospheric- or vacuum-reduced crudes and asphalts.

Coking may be achieved by any one of three different processes: batch, fluid, or delayed. Batch coking in stills has been superseded by delayed and fluid coking. Fluid coking is carried out in a fluidized bed of heated coke particles which seed the formation of a new coke. A portion of the particles is continuously removed. The coke made by this process is difficult to graphitize and displays poor crystallinity after heating to graphitizing temperatures. It is therefore not used for the preparation of commercial graphites but is used primarily as a source of fuel.

Practically all the petroleum cokes used in the manufacture of electrographite are prepared by the delayed coking process. In this process the heated feed stocks are first passed into a fractionator, where the light fractions are flashed off. The heavy residuum is then fed through pipe furnaces, where the temperature is raised to 480 to 500°C; this is sufficient to effect further cracking of the stock. The heated stock is then passed to an insulated drum at a velocity such that coking in the transfer lines is avoided. The residence time in the drum is long enough for the coke to form and

settle. Since the sensible heat in the charge stock is sufficient to produce the cracking reaction, no external heat is necessary. The temperature in the drum ranges from 400 to 450°C, and the pressure ranges from 10 to 70 psig. The overhead products (gas, gasoline, and gas oil) are removed from the top of the coker, passed through a fractionator, and then stored or processed further. The heavier materials can be recycled through the pipe furnaces to the coking drum. Usually, each coking unit is provided with two coke drums so that, while one is on stream, the other can be emptied and preheated for a subsequent run. Coke is removed from the drums by high-pressure water jets and is then loaded on railroad cars for shipment to the calciner.

(c) *Properties of Raw Coke.* The coking operation is all-important from the standpoint of graphite manufacture because it is at this point that the ultimate graphitizability of the coke is established. The graphitizability, in turn, is of major importance in determining the properties of the graphite made from the coke. The domains of carbon atoms that are destined upon further heat-treatment to become graphite crystallites are fixed in the coking operation by the polymerization of hydrocarbons into large polycyclic aromatic molecules. These are then aligned during the last stages of fluidity to form the embryonic crystals. An X-ray diffraction pattern of coke as it leaves the coker shows only one strong line,³ that arising from diffraction between layer planes in the distorted crystallites. This line indicates that the average distance between layers is about 3.45 Å. Upon further heat-treatment of the coke, this line becomes the (002) line of the graphite lattice. A weaker second line, the (110), can also be observed, which indicates⁴ that the number of benzene rings associated with the average layer plane is between 5 and 15. At this stage of development, the crystallites show no three-dimensional order, but the lamellar order is sufficient to cause alignment of adjacent crystals to varying degrees, depending on the charge stocks, on the quantities of recycled material used, and on the temperatures and pressures reached in the refining and coking processes. The effects on the properties of this planar alignment and of the growth and improved ordering with subsequent heat-treatment are discussed in Chaps. 5 and 6.

The fixed carbon† in coke from a delayed coker ranges from 85 to 90 per cent, and the volatile content ranges from 7 to 16 per cent, with a typical value of 11 per cent.⁵ Table 2.1 gives some values for ash and selected impurities in a typical raw (uncalcined) petroleum coke.

(d) *Calcination.* The first step in the preparation of raw coke for the manufacture of graphite is a heat-treatment at temperatures up to 1400°C to remove the volatile hydrocarbons and to effect a shrinkage of the filler material before it is incorporated in the formed article. This operation is called calcination and is performed either at the refinery or at the carbon

† The fixed carbon is the carbon remaining after heating to 1000°C.

plant. One type calciner is basically an inclined steel tube lined with brick and measuring approximately 150 ft in length by 8 ft in diameter. It is fired internally at the low end with oil or natural gas. As the volatiles are liberated from the coke, they ignite and provide an appreciable portion of the thermal energy required to maintain the calcining temperature. The inclined tube is rotated slowly to advance the coke to the low end in

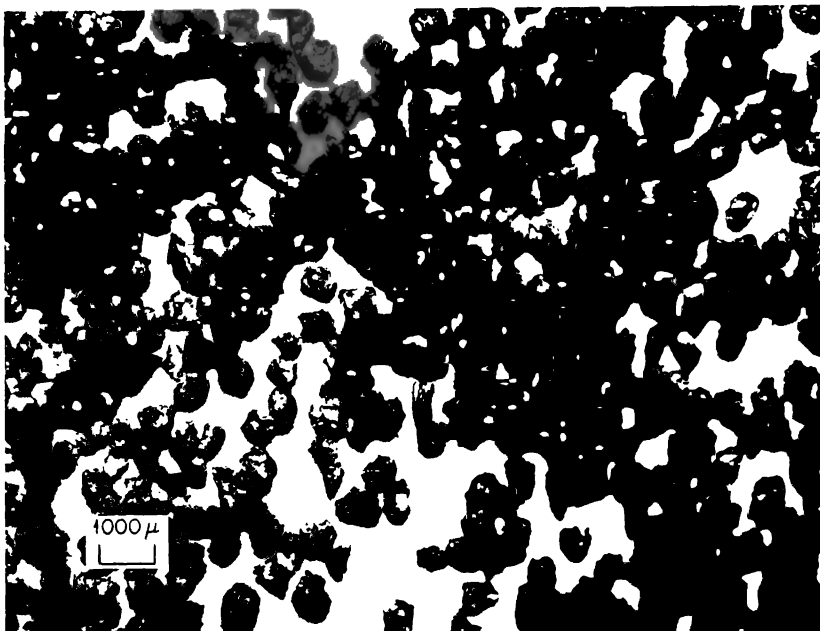
Table 2.1 — IMPURITIES IN RAW PETROLEUM COKE

Impurity	Range	Typical value
Total ash impurity, %	0.05 to 0.3	0.1
Sulfur, %	0.1 to 2.0	0.8
Vanadium, ppm	3 to 500	15
Boron, ppm	0.1 to 0.3	0.1
Nitrogen, %	0.1 to 1.4	1.0
Hydrogen, %	3 to 4.5	4.0

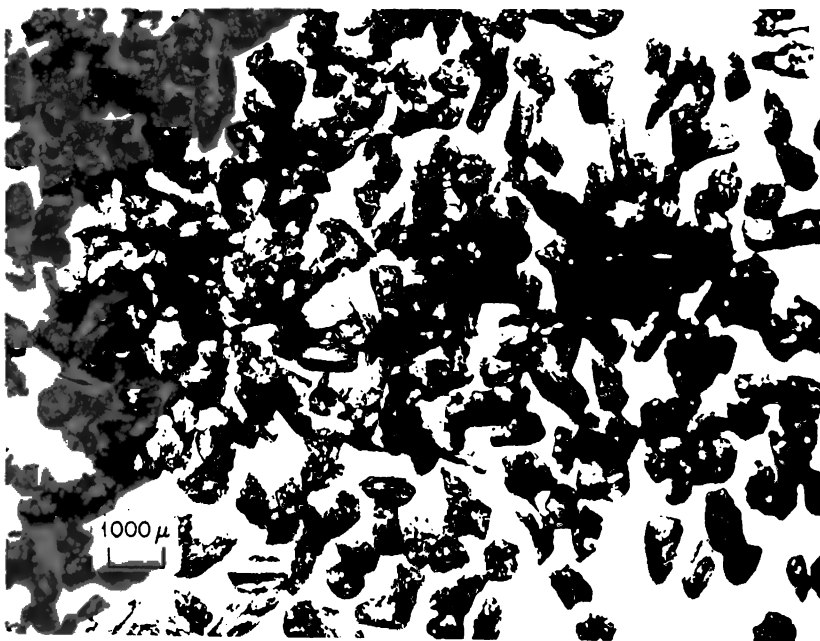
approximately 2 hr, the output being approximately 10 tons of coke per hour. After discharge from the calciner, the coke is cooled to temperatures below 200°C, either by a water spray controlled so that it cools without leaving the coke wet or by passage through water-cooled rotating ducts. The coke is now ready for crushing and sizing.

About 25 per cent of the weight of the raw coke is lost during calcination. This results from loss of the water that was picked up when the coke was hydraulically removed from the coker, the evolution of volatile matter in the coke, and dusting losses. An appreciable volume shrinkage accompanies this loss of weight and is the second important reason for the calcining step. If raw coke is formed with pitch into a carbon shape that is subsequently baked, the shrinkage of the filler coke may be sufficient to break the pitch-coke bonds and result in an extremely weak or cracked structure. Similarly, the evolution of excessive volatile matter, which must escape through a relatively impermeable mass during the early stages of the baking operation, exerts disruptive forces leading to the same end result. The calcining operation is therefore usually considered essential in the manufacture of graphite.

Calcination is a continuation of the cracking process. The "overhead fractions" in this case include light tars and such gases as hydrogen, carbon dioxide, carbon monoxide, and methane. When these materials are removed from the edges of the larger aromatic arrays in the coke, carbon bonds are disrupted. Upon re-forming they cause further polymerization and cross linking, as evidenced by the increased mechanical strength of the coke following calcination. X-ray diffraction studies of cokes heat-treated at temperatures intermediate between the raw and calcined states show clearly that the crystalline order is first reduced and then improved by the forces exerted by two opposing mechanisms: violent evolution of volatiles and



(A)



(B)

FIG. 2.2 Representative coke particles. (A) Texas-Lockport. (B) Kendall.

thermal recrystallization. Three-dimensional order is not yet present in the crystallites of calcined coke, but the average number of benzene rings associated with each layer plane of carbon atoms has increased over that present in the raw coke, as evidenced by the intensification of the (110) line. The reduced breadth of the half-peak intensity of the (002) line shows that the number and parallelism of the layer planes associated with each crystal are increased.

(e) *Crushing and Sizing.* Coke from the calciner is fed through a 1-in.-mesh screen, and the oversize material is passed through a crusher, normally of the two-roller variety. The coke is then screened to obtain a series of graded sizes of calcined particles ranging in diameter from a fraction of a millimeter to a centimeter. The material finer than about 0.5 mm is charged into a mill, where it is crushed further into the "flour" component, consisting of coke grains whose diameters range from 2 to 300 μ . Approximately half the coke flour remains on a 200-mesh screen. The coke particles and flour are then placed in storage bins to await the mixing operation.

(f) *Properties of Calcined Coke.* A casual examination of the sized particles of calcined cokes originating from two refineries using different feed stocks or cracking conditions may reveal a marked difference in the shapes of the particles. This difference arises from variations in the degree of alignment of the rudimentary crystals in the raw coke and determines the manner in which the calcined material fractures. A high degree of crystal alignment causes the material to fracture into flake- or needle-shaped particles, whereas particles of the less-ordered material are more clearly cubical or spherical in shape. Figure 2.2 shows particles of coke made by two different refineries and illustrates the differences in particle shape brought about by differences in refinery practices and in charge stocks employed.⁶ The Texas-Lockport coke is from the Lockport, Ill., refinery of the Texas Oil Company and was produced in a delayed coker from reduced Mid-Continent crudes. The Kendall coke was produced at the Bradford, Pa., refinery of the Kendall Refining Co., in a Dubbs coking unit from distillates of Pennsylvania crude.⁷ The longer spindle-shaped particles of the Kendall coke are softer (more easily graphitized) than the cube-shaped particles of Texas coke. Spindle-shaped coke is therefore the most desirable type of filler material for the manufacture of electrographites since it has a high degree of crystallinity. The elongated particle shape causes the anisotropic properties of the crystal to be reflected in highly anisotropic properties of the graphite body. This relation will be further discussed in Secs. 2-2.2 and 2-2.3 in connection with the forming operation.

The differences in crystallinity in these cokes are reflected not only by their particle shape, but also by their kerosene densities (Sec. 6-7.1), which are generally higher for the more crystalline cokes. The kerosene density of Kendall coke after calcination is 2.11 g/cm³; that of Texas coke

is 2.04 g/cm³. These may be compared with the density of a perfect graphite crystal of 2.26 g/cm³.

The hydrogen content of calcined coke is about 0.1 per cent, but the exact value varies markedly with the calcining temperature. For example, the hydrogen content⁸ of coke heated to 1000°C is approximately 0.4 per cent; this decreases to 0.05 per cent after heat-treatment at 1500°C. Table 2.2 lists the ranges and typical values of some metallic impurities in calcined

Table 2.2 — METALLIC IMPURITIES IN CALCINED PETROLEUM COKE

Impurity	Usual range	Typical value
Total ash impurity, %	0.1 to 0.5	0.15
Silicon, ppm	30 to 300	50
Iron, ppm	30 to 1500	40
Vanadium, ppm	3 to 500	15
Titanium, ppm	1 to 20	10
Aluminum, ppm	15 to 300	30
Manganese, ppm	5 to 50	10
Nickel, ppm	25 to 100	40
Calcium, ppm	15 to 250	20
Magnesium, ppm	5 to 50	10
Boron, ppm	0.1 to 0.3	0.1

cokes. These values vary markedly from one coke to another and depend on the charge stock used in the manufacture of the coke.

2-1.2 COAL-TAR PITCH

The search for a material having suitable properties as a binder for the petroleum-coke filler leads quickly to the choice of coal-tar pitch, the heavy residue derived from the distillation of coal tar from by-product coke ovens. The availability of this relatively inexpensive material in tonnage quantities has made possible the rapid growth of the carbon industry.

One of the important requirements of a binder for electrographite is that it be a thermoplastic material, being solid at room temperature and fluid at higher temperatures. This property allows thorough mixing of the filler with the binder, facilitates the forming of the filler-binder mixture, and permits storage and handling of the formed articles at room temperature without adverse effects on the shape of the product. The coal-tar pitch commonly used as a binder in graphite production should have a softening point of approximately 100°C so that mixing and forming can be accomplished in convenient steam-heated equipment. Handling of the formed articles is facilitated by the high viscosity of the pitch (of the order of 10⁹ poises) at room temperature.

A second requirement of the binder is that it have a high carbon content and that a major portion of this carbon be deposited as bonding coke by some economically feasible process. Here again, coal-tar pitch is ideal in

that its carbon content is approximately 93 per cent and the percentage of the pitch remaining after heating to 1000°C is about 55 per cent.

A third requirement of a carbonaceous binder is that its specific gravity be as high as possible, thereby effecting the deposition of the greatest number of carbon atoms in and around the filler coke particles. The room-temperature specific gravity of coal-tar pitch is about 1.30 g/cm³, well above that of any other binder. The low specific gravities of such materials as petroleum pitches, asphalts, and resins usually result in low graphite densities when these materials are used as binders, and there is an attendant drop in such properties as strength and conductivity.

Coal-tar pitch is thus remarkably well suited as a binder material for the manufacture of graphite. It will be in good supply as long as metallurgical coke is used as a reducing agent in the production of steel. Regarding its 93 per cent carbon content, pitch has been described⁹ as a form of "liquid carbon" which, through the addition of 7 per cent of alloying constituent, has a softening point of 100°C as contrasted with a sublimation point of 3800°C for the pure carbon.

(a) *Source of Coal Tar.* Metallurgical coke, the chief reducing agent employed by the steel industries in the blast-furnace reduction of iron ore, is prepared by the destructive distillation of bituminous coal in by-product coke ovens. These ovens are of varied designs, but all consist essentially of three brick compartments, the coking chambers, the heating chambers, and the regenerative chambers.¹⁰ In the Koppers oven the coking chambers are rectangular compartments 12 to 22 in. wide by 6 to 14 ft high by 30 to 42 ft long arranged in batteries of 10 to 100. Each of these compartments is separated by a heating chamber in which the combustion of fuel gas generates the heat necessary to distill the coal. Air for combustion is preheated in brick regenerative checkerwork chambers located beneath the battery of ovens. The chambers are arranged in pairs so that while one chamber is being heated by hot exhaust gases the other chamber is giving up its heat to the incoming air.

As the coal reaches a temperature of approximately 400°C, it passes through a plastic stage, during which time it may either expand or contract, depending on the source and rank of the coal. Coals charged into a by-product coke oven are blended to produce a contracting mixture to prevent excessive pressures on the oven walls. The shrinking coals are higher in volatile content, and, as the temperature is increased, these volatiles are removed through ducts at the top of the oven. The remaining coal resolidifies at approximately 500°C into a cellular structure, typical of metallurgical coke. Heating is continued for a total of about 20 hr, when the final temperature of carbonization is reached. The hot volatiles given off between 600 and 700°C are passed through primary coolers, where spraying with flushing liquor lowers the temperature to 150 to 200°C and condenses the coal tar. The gases are pumped off for separation and further processing.

Although the coal tar so produced varies markedly depending on the source of the coal and the conditions in the coke oven, it consists generally of a high percentage of aromatic hydrocarbons, some oxygenated compounds, and a relatively low concentration of paraffinic materials. In addition to pitch, the tars also contain tar acids (phenols), naphthalene, creosote oils, and tar bases (pyridine bases). These are removed by fractional distillation and chemical separation in the process of coal-tar refining.

(b) *Distillation of Coal Tar.* Coal tar can be distilled by either a batch or a continuous process. In the batch process, which is used primarily in Europe, the distillation takes place in horizontal or vertical pots with concave bottoms, usually operated under a partial vacuum. These stills can be fired externally or internally by the circulation of hot combustion gases through pipes passing through the tar. In the United States some kind of continuous method is the most popular for distilling coal tar. In a typical operation the tar, at a temperature of about 60°C, is fed into a tube still, which consists of a labyrinth of pipes in a gas-fired enclosure. The temperature is increased to approximately 200°C in pipes in a low-temperature region of the still. Water and light oils are removed in a dehydration column. The remaining material is cycled to the high-temperature region of the tube still, where it reaches a temperature of nearly 400°C. It is then flashed into a fractionating column, which separates the distillate into a light oil (crude naphtha), a medium oil (carbolic oil), and a heavy creosote. The residue at the bottom of the fractionator is coal-tar pitch. This is pumped through a heat exchanger, in which the raw tar is heated, to storage. The softening point of the pitch can be controlled by regulating the rate of flow of tar through the tube still or by controlling the temperature of the hot coil in the still.

(c) *Properties of Coal-tar Pitch.* The properties of coal-tar pitches may vary widely and, indeed, are adjusted to suit the application for which they are intended. The present discussion will be limited to the chemical and physical properties of pitches used as binders in the manufacture of electrographite.

The chemical nature of pitch has been and is currently the object of considerable study that involves the separation of the pitch into fractions that are soluble and insoluble in certain solvents. The subsequent division into additional fractions is carried out by further solvent extraction, vacuum distillation, molecular distillation, thermal diffusion, or chromatography. The compounds so isolated can then be analyzed either chemically or by infrared or ultraviolet spectroscopy. This type investigation has led to the identification of about 50 polycyclic aromatic compounds and 50 heterocyclic compounds containing nitrogen, oxygen, or sulfur.¹¹ Estimates of the total number of compounds in pitch range into the thousands. Although a categorical statement of the composition of coal-tar pitch is therefore impossible, the carbon-to-hydrogen ratio for pitch indicates that it is

composed of highly aromatic compounds. The constituents isolated by this study confirm this observation. The average molecular weight^{12,13} of the benzene-soluble fraction, which represents 70 per cent of the pitch, is 300. An average molecular weight of 600 has been obtained by osmotic technique on sample representing 93 per cent of the pitch.¹⁴ The highly aromatic nature of pitch is a property that makes this material particularly well suited as a binder in electrographite; i.e., it is more graphitizable than any other substance commercially feasible in this application.

Approximately 30 per cent of a typical binder pitch is insoluble in benzene, whereas the fraction insoluble in quinoline ranges from 9 to 16 per cent, with an average of 11 per cent. That fraction of pitch which is insoluble in quinoline is commonly referred to as the "solid phase." It consists of particles of carbon generally smaller than $10\ \mu$ in diameter and has a density of about $1.6\ \text{g/cm}^3$. A chemical analysis of the solid phase¹⁵ agrees remarkably well with that for the whole pitch (Table 2.3), except that the hydrogen content is only 2.6 per cent, or approximately two-thirds that found in the whole pitch.

Table 2.3 — CHEMICAL CONSTITUENTS IN COAL-TAR-PITCH BINDERS

Total ash impurity, %	0.03 to 0.3
Carbon, %	92 to 93
Hydrogen, %	4.2 to 4.5
Nitrogen, %	0.6
Oxygen, %	1.1
Carbon/hydrogen ratio (atomic)	1.0 to 2.0
	1.70 to 1.85

The boron and vanadium levels in coal-tar pitch vary with the source of the coal and with the technique used in preparing the pitch. Typical levels found in binder pitch are 0.7 ppm for boron and 7 ppm for vanadium. If the pitch is prepared from a cracked distillate and is to be used in nuclear-grade graphite, the boron level may decrease to 0.2 ppm and the vanadium to 2 ppm. The use of special pitches that are low in boron and heavy-metal constituents as binders in nuclear graphite is no longer an all-important consideration with the improved methods of graphite purification currently employed (see Sec. 2-4.2).

The physical properties of a typical binder pitch are listed in Table 2.4. One of the most interesting of these properties is the rapid decrease in viscosity with temperature; a variation of 11 orders of magnitude has been observed¹⁶ in the interval from 0 to 180°C . Pitch behaves as a Newtonian fluid; thus the viscosity is independent of the stress applied and varies only with temperature. The softening point is empirically determined since pitch does not undergo a phase change until it cokes and therefore does not have a sharp melting point.

The coking value of pitch is very important because it is the quantity of infusible carbon remaining as bond between the filler coke particles. It is measured by heating the weighed pitch sample slowly in a nonoxidizing atmosphere to a temperature above that at which it cokes. The residue,

Table 2.4 — PHYSICAL PROPERTIES OF COAL-TAR-PITCH BINDERS

Softening point ¹⁷ (cube in air), °C	100
Specific gravity at 25°C, g/cm ³	1.30
Volume coefficient of thermal expansion (25 to 200°C), per °C	4.5×10^{-4}
Thermal conductivity ¹⁸ at 25°C, cal/(sec)(cm)(°C)	$\sim 32 \times 10^{-6}$
Viscosity:	
At 25°C, poises	2×10^9
At 100°C, poises	5500
At 170°C, poises	3 to 4
Surface tension at 200°C, dynes/cm	55
Coking value after heating to 1000°C, %	55

expressed as a percentage of the initial sample weight, is defined as the coking value. This property is variable and has been indexed by several empirical tests. The 55 per cent coking value shown in Table 2.4 most nearly approaches that actually achieved in carbon manufacture.

2-2 Forming

2-2.1 MIXING

(a) *Mix Formulation.* In a typical nuclear-grade graphite, the filler component is composed of both particles and flour, the particles ranging in size from 0.4 to 0.8 mm. The flour component, about half of which passes through a 200-mesh screen, comprises approximately three-fourths of the particle-flour blend. The quantity of pitch binder used varies only within narrow limits when the forming is done by extrusion and is always in the neighborhood of 30 parts by weight of binder per 100 parts of filler. If the binder level is too low, excessive forming pressures must be exerted, and this results in abnormal expansion and attendant cracking of the formed material as it leaves the die. If the binder level is too high, the evolution of additional volatiles during the baking operation gives rise to a structurally poor product with inferior properties. Thus the quantity of binder must be maintained at a precise level for the extrusion process, which is the most commonly used forming technique in the carbon industry. When the carbon product is to be molded, the pitch level can be varied over a wider range of values without deleterious effects on the structure of the product.

(b) *Additives*. A frequently employed technique for increasing the bulk density of artificial graphite is that of adding furnace blacks or extremely fine ($<10\ \mu$) coke particles to the coke-pitch mixture, thereby filling voids that would otherwise exist between the larger particles (see also Sec. 6-7.2). Several experimental studies have been made of the effect of thermal blacks on density.^{19, 20} One investigator reported an increase in graphite density from 1.46 to 1.67 g/cm³ with the addition of 10 per cent furnace black (Thermax) to the mixture. Unless the application for which the graphite is intended specifically demands exceptional densities, the practice of including extremely fine carbonaceous materials in the mix is to be avoided because the difficulties in processing such mixtures through the baking stage mount rapidly as the permeability of the formed article decreases. Most nuclear-grade graphites produced in tonnage quantities are therefore made without the addition of these micron-sized filler materials.

The addition of a lubricating oil to the mix is a common practice when extrusion is the forming method employed. The oil serves to reduce the friction between the surface of the die and the mix, thereby reducing the quantity of pitch otherwise necessary for reasonable rates of extrusion. An oil is selected which is insoluble in the highly aromatic coal-tar pitch and is obtained as a distillate from a paraffinic derivative of petroleum. The quantity of oil used is approximately 3 wt.% of the filler material. The oil has no coking value and therefore does not remain as carbon in the final product as does the pitch binder.

(c) *Mixing Conditions*. The primary function of the mixing operation is to effect a uniform distribution of the pitch in the petroleum-coke filler materials. Ideally, each filler particle should be coated with a film of pitch. One method of facilitating a good distribution of the binder is to raise the temperature of the mixture to the point where the viscosity of the pitch is reduced to a level that allows it to flow freely around the petroleum coke. This temperature is normally in the range from 165 to 170°C, where, as indicated in Table 2.4, the viscosity of the binder is of the order of a few poises. Good distribution, as well as faster heating, is facilitated by charging only pitch particles less than 1 in. in size. The mixing is done commercially in steam-heated mixers of various designs. A common mixer consists of a cylindrical steam-heated housing within which the mixing is performed by paddles. The mixing time must be sufficient to allow the poorly conducting pitch and filler materials to heat thoroughly and to allow complete working of the pitch around the filler particles. Following the mixing operation, the mixture is cooled in rotating cylinders to permit handling prior to forming.

2-2.2 EXTRUSION

(a) *Equipment and Operation*. The most commonly used method of forming coke-pitch mixes is by extrusion through a die. This technique is a

semicontinuous process and is therefore more economical than the batch process of molding. Basically, an extrusion press consists of a horizontal cylinder, or "mud chamber," which contains the coke-pitch mixture, and a piston, usually hydraulically powered, which forces the mixture through a die mounted at one end of the cylinder. In the case of auger extrusion, the mix is fed continuously by a rotating screw. In another design the charge cylinder and die assembly are mounted on trunnions, which allow the cylinder to be tilted to a vertical position to receive the mix from the coolers. Once the mix has been charged into the cylinder, a ram compacts it. The ram can be raised to allow further charging and compacting until the cylinder is filled. It is then tilted back to the horizontal position for extrusion.

In the large extrusion press shown in Fig. 2.3, the cylinder-die assembly remains horizontal. The mix is introduced into the cylinder in the form of cylindrical compacts formed in a separate molding operation. During the extrusion operation the mix temperature is maintained slightly above the

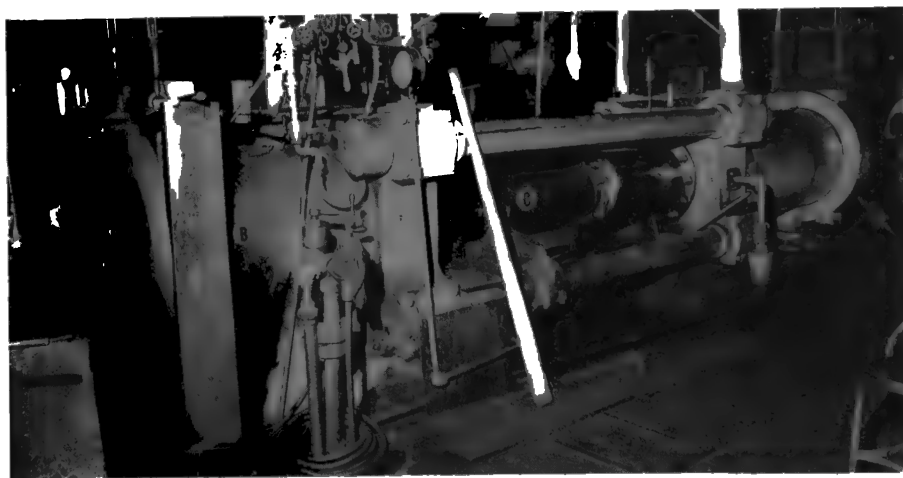


FIG. 2.3 A large extrusion press used in the production of nuclear graphite. (A) Extrusion die. (B) Steam-jacketed charge cylinder. (C) Extrusion ram.

softening point of the pitch by steam-heating the mix cylinder. Although the exact pressure required to extrude the mix depends upon the cross-sectional area and shape of the die, it is of the order of several tons per square inch. As the piece leaves the die, its surface is contacted by a marking wheel, which rolls on identifying information. When the piece has been extruded to the desired length, a cutoff blade separates the piece at the die. The piece is then moved by a conveyor belt to a cooling station. At this stage the formed article will have an apparent density between 1.65 and 1.75 g/cm³.

If the extruded article is rectangular in cross section, it is extruded onto

a steel table, where it is allowed to air-cool to room temperature before being moved to a storage area prior to baking. If the extruded article is round, the piece is allowed to roll down a steel platform into a tank of water at room temperature, where it is cooled quickly to prevent slumping and distortion in the "green" state. These pieces are then hoisted by a cylindrical clam onto pallets and stored prior to baking.

(b) *Particle Orientation.* During the extrusion operation the filler coke particles are aligned with their long dimensions parallel to the direction of extrusion, thereby giving rise to the anisotropy common to almost all grades of graphite (see also Sec. 5-8.2). This anisotropy originates, in turn, from the predominant orientation of the crystallite layer planes parallel to the long particle dimension. Thus the relative values of a given property measured parallel and perpendicular to the direction of extrusion will have a relation similar to those values measured parallel and perpendicular to the layer planes of the single crystal. The degree of anisotropy is influenced both by the source of coke, which determines the preponderant shape of the particles, and by the size of the particles. In general, anisotropy in extruded graphites is reduced as the particle size of the filler coke is increased. This effect arises from the fact that the particles tend to interrupt flow lines in the mix during the forming process, thereby reducing the alignment that would otherwise occur in an all-flour mix.

The effects both of the type coke and of the size of the particle on the anisotropy of the graphitized material are illustrated by values of the coefficients of thermal expansion shown in Table 2.5. As discussed previ-

Table 2.5 — EFFECT OF PARTICLE SIZE AND COKE TYPE ON ANISOTROPIC BEHAVIOR OF COEFFICIENT OF THERMAL EXPANSION IN EXTRUDED GRAPHITES

Coke type	Particle size	Coefficient of mean thermal expansion (25 to 100 °C) x 10 ⁶ per °C		
			⊥	Ratio (⊥)/()
Kendall	All flour	0.6	2.2	3.7
	Flour plus 1/2-in. particles	1.6	2.5	1.6
Texas-Lockport	All flour	1.9	3.3	1.7
	Flour plus 1/2-in. particles	2.2	2.4	1.1

ously, Kendall coke particles are more elongated and needlelike than the cubical or round particles of Texas-Lockport coke. Accordingly, the ratio of the expansion coefficient measured across the grain (⊥) to that measured with the grain (||) is higher for a graphite made from Kendall coke than for a Texas-coke graphite having the same grain size. The table also shows

that when $\frac{1}{2}$ -in. particles of either coke are included in the mix the anisotropy of the resulting graphites is reduced. The degree of anisotropy is reduced as the grain size is increased.

Other physical properties are affected similarly by alignment of particles in the extrusion process. Thermal and electrical conductivities of extruded graphites are greater when measured in the direction of extrusion. Strength and Young's modulus are higher when measured parallel to the direction of extrusion than when measured perpendicular to it; and, again, anisotropy is reduced as the filler particle size is increased. Graphites made from elongated needletype cokes have higher thermal and electrical conductivities and lower strength and Young's modulus than similar graphites prepared from more isotropic cokes.

2-2.3 MOLDING

(a) *Equipment and Operation.* Molding is the oldest technique by which carbonaceous materials are formed. It consists basically in compressing the filler-binder mixture in an enclosure of the desired shape fitted at one or both ends with moving plungers. Many variations of this process are in current use.

For production of small articles, such as electrographitic brushes, graphite seal rings, etc., the green mix is milled after it has cooled. In this way uniform charging and leveling of the mold are facilitated. At high binder levels, which can approach 50 wt.% of the filler material, the molding is carried out at room temperature and at pressures of the order of 10 tons/sq in. The product so formed is sufficiently permeable to permit the escape of binder volatiles during the bake without a disruption of the structure. If, however, the molding is done at elevated temperatures where the binder is more fluid, the quantity of binder must be reduced to prevent cracking of the piece during the baking operation. This critical binder content varies with the fineness of the filler material and the molding conditions.

When large carbon shapes are to be molded, a commonly used technique is jar molding. The heated mix is vibrated as it is charged into the mold; when the mold has been filled, a heavy weight is placed on the mix and it is vibrated again. This method makes possible the molding of shapes that are long compared with their diameters. This is not possible by conventional molding techniques owing to the loss of molding force by side-wall friction. Thus carbon cylinders 60 in. in diameter and 72 in. in length, having green densities of approximately 1.7 g/cm³, are jar molded routinely. The heated mix is fed slowly into a steam-heated mold in which the jarring operation takes place. The jarring action effects uniform compaction of the mix and is continued until no further reduction in volume occurs. The piece is then cooled in place gradually by passing first warm water and then cooler water through the mold.

(b) *Particle Orientation*. In the molding operation the elongated particles of filler coke align themselves with their long dimensions normal to the molding direction and oriented randomly about it (see Fig. 5.14). Thus in the graphitized state a molded article will exhibit higher thermal and electrical conductivities, higher Young's modulus, and higher strength in the two directions normal to the molding force. The method used to form a sample of graphite can, therefore, be determined uniquely by a measurement of any of these properties in three mutually perpendicular directions. Two values will be nearly alike and different from the third. If the two like values are higher than the third, the piece was molded; if they are lower, it was extruded. When thermal expansion is the property measured, the situation is reversed since expansion is always greater when measured across the grain of the graphite. Anisotropy in molded graphites is generally less than that found in extruded materials.

2-3 Baking

2-3.1 FUNCTION OF THE BAKING OPERATION

The formed green carbon body at this stage consists of a calcined petroleum-coke filler bonded by coal-tar pitch, which softens at a temperature of about 100°C. It is the function of the baking operation to convert the pitch from a thermoplastic material to an infusible solid while at the same time maintaining the shape of the formed body. This operation is by far the most critical in the manufacture of electrographite for several reasons. As the green carbon reaches a temperature of 200 to 300°C, it loses its mechanical strength and must be supported by a permeable pack that will maintain the shape of the body and vent the volatiles. As previously mentioned, these volatiles, generated by the pyrolysis of the pitch, must escape through a relatively impermeable mass without disrupting the structure. Since the volume of these gases is sizable, representing some 10 to 12 per cent of the weight of the article, the heating rate during volatilization, which persists to a temperature of approximately 500°C, must be retarded.

When the binder pyrolyzes, large quantities of hydrogen are evolved, allowing polymerization and cross linking to proceed within the binder and between the binder and filler materials. As the carbon body reaches the final baking temperature of 800 to 1000°C, this cross-linking process causes the carbon to become extremely hard and brittle. Simultaneously, a volume shrinkage of about 5 per cent occurs, giving rise to internal stresses that are sometimes great enough to crack the carbon body. In general, the shrinkage is directly proportional to the quantity of binder present and is therefore a function of the proportion of binder used in the mix and also of the coking value of the binder. Thus the large chemical and physical changes that occur in the coal-tar pitch as it pyrolyzes to

form bridges between the filler particles make the baking an extremely critical operation.

2-3.2 BAKING FURNACE

The baking of carbonaceous materials is carried out in gas-fired furnaces lined with ceramic-brick walls. The walls contain flues through which the hot gases circulate. These furnaces are of varied designs, but the basic construction is that shown in Fig. 2.4. For this particular furnace the air-

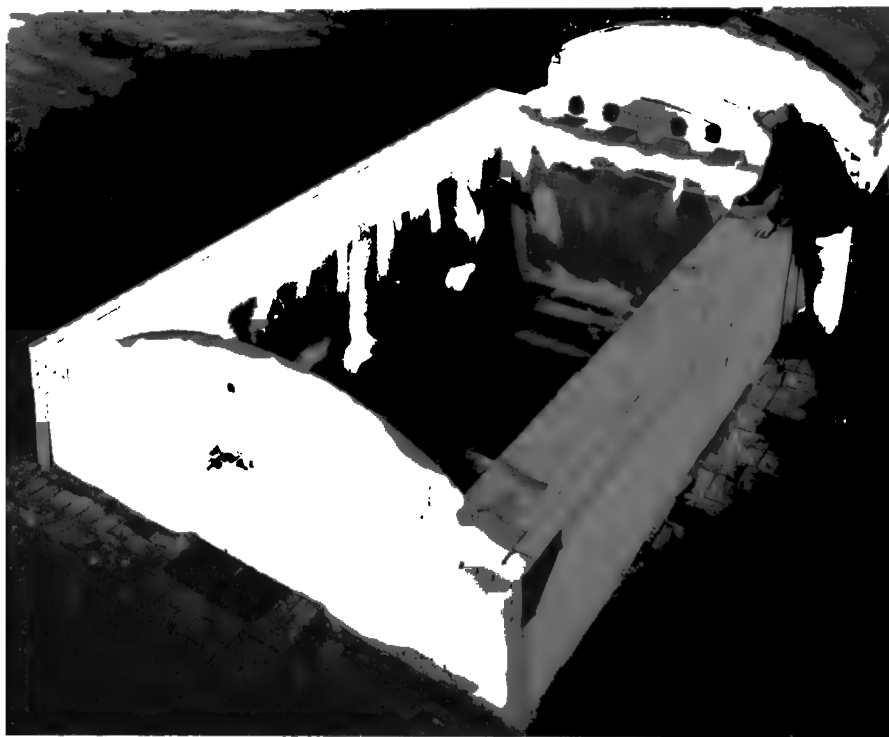


FIG. 2.4 A gas-fired furnace capable of baking to 1000°C.

natural gas mixture is introduced through four ducts at one end of the furnace and is ignited, heating the top of the charge and pack directly. The hot gases then flow downward through vertical flues at either end of the furnace and enter horizontal flues in the side walls and bottom. This permits heat to enter the pack from all six sides of the furnace. After passing through the flues in the furnace walls, the gases are fed through an underground duct to a stack that is common to a battery of furnaces. For improved thermal insulation the baking furnaces are normally constructed so that all, or part of, the furnace is beneath ground level. A cover consisting of a curved cast-steel framework supporting keyed ceramic brick

is placed over the packed furnace by an overhead crane, and the joint is mortared shut prior to each bake.

The method by which a baking furnace is packed varies widely, depending on the size and composition of the carbon article to be baked and on the design of the baking furnace. Generally speaking, two methods of packing are employed. By one of these methods, known as "bulk packing," the green carbon articles are surrounded by packing material; thus the furnace is solidly filled with the charge stock and pack. The second method employs steel cans, known as "saggers," in which the carbon stock is packed. In both cases the packing material is normally a mixture of sand and calcined coke. The packing material is sized to provide the necessary gas permeability in the pack while at the same time yielding a free-flowing mix that will facilitate the handling of the materials.

Because of the large mass and low thermal conductivity of a bulk-packed furnace, the time required for a baking cycle is approximately twice that for a sagger furnace. In a typical bulk furnace containing 4- by 4- by 50-in. bars being processed as nuclear-grade carbon, the total firing time is about three weeks. An additional two weeks is required for cooling and unpacking. The time cycle may be as long as two months in the larger furnaces. When a furnace is packed with saggers, the hot combustion gases impinge directly on the sagger walls, and heat is passed quickly through the relatively small quantities of packing material to the charge. As a result the final baking temperature is reached in approximately two weeks. An additional week or 10 days is needed for cooling. The faster cycle possible in sagger baking cannot be tolerated, however, by some carbon compositions without the development of structural flaws that arise primarily from the high rate of gas evolution.

Following a "soaking" period of one to two days, during which time the temperatures within the furnace become more nearly uniform, the fuel gas is shut off, and the furnace is allowed to cool. The cooling rate must be slow enough to prevent cracking of the brittle baked carbon due to thermal shock, and three to four days must sometimes elapse before the unloading operation begins. The used packing materials are fed through crushers to pulverize the lumps formed by the condensation of binder volatiles in the pack. This material is then screened and fed to silos, where it is cooled prior to being reused. Some of the packing material adheres to the baked stock; it is removed by wire brushes before the stock is packed in graphitizing furnaces.

2-3.3 PROPERTIES OF BAKED CARBON

The physical properties of baked carbons vary widely, depending on the final baking temperature, the degree of crystallinity of the coke, and the particle-to-flour ratio employed in the mix formulation. Table 2.6 lists a few properties that are typical of baked carbons of the type being

processed as nuclear grades. At this stage of the process, the carbon is brittle and extremely difficult to machine, having a Rockwell hardness on the S scale of about 100. Because of their low thermal conductivity, high coefficient of expansion, and high elastic modulus, baked carbons are susceptible to thermal shock.

Table 2.6 — TYPICAL ROOM-TEMPERATURE PHYSICAL PROPERTIES OF FINE-GRAINED BAKED CARBONS

Bulk density, g/cm ³	1.54 to 1.58
Electrical resistivity (ll), $\mu\text{ohm-cm}$	4000 to 6000
Thermal conductivity (ll), cal/(sec)(cm)(°C)	0.008 to 0.012
Flexural strength (ll), psi	4500 to 5000
Elastic modulus (ll), psi	2.7×10^6
Coefficient of thermal expansion (25-100°C) (ll) per °C	2.0 to 2.2×10^{-6}
Porosity, %	26

The chemical properties of baked carbon are subject to large variations and are therefore not scrutinized as closely in the intermediate product as they are in the raw materials and in the finished graphite. Properties of the baked article such as ash content and sulfur and boron levels hinge on the source of petroleum coke. Oxidation rates for baked carbon are usually greater than those for graphite owing to poorer crystallinity and to the catalytic effects of the ash.

2-4 Impregnation

2-4.1 PURPOSE

As indicated in Table 2.6, the porosity of baked carbon is approximately 25 per cent. It is the function of the impregnation operation to reduce the porosity and thereby increase the bulk density of the resulting graphite. For this purpose the carbon is impregnated with a fluid that, upon subsequent pyrolysis in a rebaking or graphitizing operation, will deposit secondary carbon in the voids. Because of its high coking value and availability in large quantities, coal-tar pitch is universally used as a commercial impregnant. The properties of a typical impregnating pitch differ somewhat from those of a binder pitch in that some of the heavier fractions normally present in a binder pitch are missing. In a typical impregnating pitch, the atomic ratio of carbon to hydrogen is about 1.65. Approximately 15 per cent of an impregnating pitch is insoluble in benzene, and the quinoline insoluble fraction is usually below 5 per cent. The specific gravity of these pitches at room temperature is approximately 1.25 g/cm³, and the softening point is approximately 100°C.

2-4.2 PITCH IMPREGNATION

Pitch impregnation is performed in a large autoclave such as that shown in Fig. 2.5. The baked stock is first loaded into band-steel baskets, which are placed inside a split cylindrical shell. Prior to being placed in the autoclave, the stock is lowered into a heating chamber, shown at the extreme right of Fig. 2.5, where the temperature is raised to above 200°C by the circulation of electrically heated air. Both the preheater and the autoclave are located below ground level to reduce heat losses. The purpose



FIG. 2.5 A vacuum-pressure autoclave for pitch impregnation. (A) Preheating chamber. (B) Cylindrical shell containing the baskets of baked stock. (C) Autoclave.

of the preheating step is to raise the temperature of the stock sufficiently above the softening point of the pitch so that its penetration is not retarded owing to chilling by the stock. Once the stock has been so heated, the shell and its contents are transferred to the autoclave, which is then sealed and partially evacuated to remove some of the air from the pores of the carbon. The autoclave is then filled with molten pitch from a tank above ground level. When the stock has been submerged in pitch, air pressure above the surface of the pitch is increased and held for a period of time dependent upon the cross section of the stock. In the case of 4- by 4-in. bars, a pressure of the order of 100 psi is maintained for several hours.

Following impregnation the pitch is forced pneumatically back into the tank from which it was supplied, and the steel shell containing the basket of stock is removed from the autoclave. Normally, the cooling operation is expedited by spraying the stock with water while it is still in the basket. Selected samples of the impregnated material are weighed to determine the quantity of pitch picked up, which normally falls somewhat below 20 per cent. At this point the stock is ready to be charged into a graphitizing furnace.

2-5 Graphitization

2-5.1 PURPOSE

The gas-baked carbon still contains some residual hydrogen. It is difficult to describe the material as possessing any true crystal structure since both long-range order and internal perfection, although latent, are not yet developed. X-ray patterns show only a very broad and displaced (0 0 2) line and no evidence of in-plane reflections. Nevertheless, the ultimate crystal orientation and size are inherent in the raw materials. It is the purpose of graphitization to effect this crystal growth and to perfect the internal order (see Sec. 5-9).

By the time the temperature reaches 1500°C, most of the hydrogen has been evolved, and the material is almost completely carbon except for some metallic impurities. From this temperature to about 2500°C, the dominant process is crystal growth, with the internal crystal structure still imperfect. Above 2500°C continued minor crystal growth occurs, but the major effects are diffusion and annealing of crystallite imperfections. This latter process continues at a measurable rate even at the sublimation temperature of the graphite.

The static properties of the graphite crystal are largely attained within the 2000 to 2500°C range. At these temperatures the Hall coefficient and magnetic susceptibility, for example, have attained their final values. Transport properties continue to improve, both the electrical and thermal conductivities increasing up to 3000°C. More-sensitive transport properties, such as the magnetoresistance, show significant changes even above 3000°C. However, very little change occurs in the room-temperature mechanical properties on heating above 2500°C.

2-5.2 THE ACHESON FURNACE

An electric furnace capable of producing temperatures approaching 3000°C was first developed by E. G. Acheson²¹ in 1895. The loading of such a furnace is shown in Fig. 2.6. The basic structure consists of a horizontal bed of fire-brick tiles laid over concrete piers. At each end of the bed is a concrete head through which graphite electrodes project into the furnace pack. The baked bars are stacked transversely in the furnace and the



FIG. 2.6 A large Acheson furnace being loaded prior to a graphitization run.

intervening spaces are then filled with granular coke. The coke pack is sized to afford the correct resistance for electrical heating since, particularly in the terminal stages of graphitization, most of the resistance heating arises from this pack. The sides of the furnace are built up by removable concrete

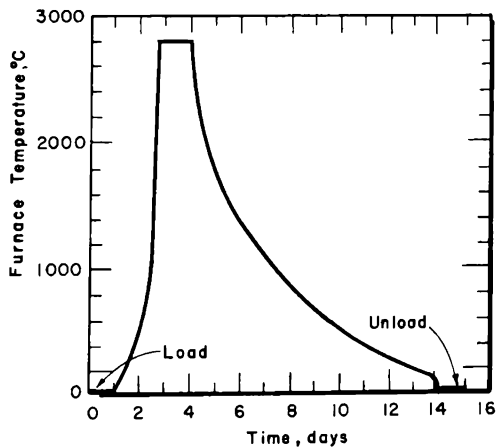


FIG. 2.7 A typical time vs. temperature cycle for a large graphitizing furnace.

blocks, and the pack is then surrounded by finely ground silicon carbide, coke, and sand to provide thermal insulation.

Power is supplied to the furnace at rates between 600 and 4000 kw, depending on the size of the furnace, the type of graphitizing charge, and the stage of the heating cycle. The integrated energy to effect graphitization ranges from 1.6 to 3.0 kw-hr per pound of finished graphite, the latter figure applying to nuclear grades. A peak temperature of 2600 to 3000°C is attained, depending again on the grade of graphite being produced. As indicated in Fig. 2.7, 3 to 4 days are required to heat the stock and about 10 days are required to cool the stock to temperatures at which it can be exposed to air.

2-5.3 PROPERTIES OF NUCLEAR GRAPHITE

The remarks made previously concerning the variation in properties of baked carbons apply to a lesser degree to graphitized materials. The raw materials influence to some extent the physical properties of the finished graphite, and the mode of fabrication also plays a profound role in determining these properties. It is precisely the interplay of these factors which makes it possible to vary production techniques to obtain a desired set of physical properties. Thus nuclear graphites have commonly been produced with the end objectives of high purity, high thermal conductivity, and, in so far as possible, maximum resistance to radiation damage. It should be emphasized that specialized grades aimed at high density, minimum gas content, high strength, low permeability, or other specific requirements may sacrifice other properties to attain these ends.

As a consequence it is not possible to give a generalized set of properties for all nuclear graphites; each application represents to some degree a unique problem. With increased sophistication of reactor design, the specialization of graphite grades to a particular end use is proceeding rapidly.

Some typical properties for a moderator graphite produced by the conventional techniques as described in the preceding sections are listed in Table 2.7. Standard deviations are also given to illustrate the degree of reproducibility attained in normal processing. These values are typical of a relatively fine-grained extruded material of approximately 4- by 4-in. cross section. Because the degree of orientation depends not only on fabrication techniques and raw material, but also on the geometry of the finished piece, the physical properties will vary as the size and shape are altered. In the case of moderator graphites, bulk density and purity are usually used as control properties, although strength, thermal conductivity, and thermal expansion are usually monitored for unusual fluctuations.

Certain other properties, although of less interest to the design engineer, are of considerable help in understanding the structure and radiation resistance of nuclear graphites. The magnetic susceptibility indicates the

Table 2.7 — ROOM-TEMPERATURE PROPERTIES[†]
OF A TYPICAL NUCLEAR GRAPHITE^{2,2a}

	Value	Standard deviation
Bulk density, g/cm ³	1.70	0.02
Electrical resistivity, $\mu\text{ohm-cm}$:		
to grain	734	59
⊥ to grain	940	111
Thermal conductivity, cal/(sec)(cm)(°C):		
to grain	0.543	
⊥ to grain	0.330	
Tensile strength, psi:		
to grain	1440	254
⊥ to grain	1260	308
Compressive strength, psi:		
to grain	5990	638
⊥ to grain	5960	918
Flexural strength, psi:		
to grain	2400	506
⊥ to grain	1970	509
Young's modulus, psi:		
to grain	1.49×10^6	0.14×10^6
⊥ to grain	1.11×10^6	0.09×10^6
Coefficient of thermal expansion, per °C:		
to grain	2.22×10^{-6}	0.39×10^{-6}
⊥ to grain	3.77×10^{-6}	0.42×10^{-6}
Permeability, Darcy units:		
to grain	0.115	
⊥ to grain	0.098	

[†] See text for significance of these values.

degree of crystallinity and is a good measure of orientation. Analysis of X-ray line shapes and spacings is utilized to measure perfection of the crystal structure, degree of graphitization, and orientation. The galvanomagnetic coefficients and thermoelectric effects yield data on internal crystal perfections and radiation-induced imperfections and on the role of chemical impurities. These properties are discussed in more detail in subsequent chapters.

2-6 Purification

Three generalized methods have been developed for producing graphite to the high purity required for plutonium-producing or thermal breeding reactors.²³ Each has been brought to an advanced degree of development by groups working essentially independently and geographically removed from each other. The methods are:

1. Utilization of extremely pure raw materials, or alternatively, the purification of the raw materials. This approach is exemplified by the British Pile Grade A (PGA) graphite.
2. Thermal purification of a formed graphite. In this method graphitization is conducted at a sufficiently high temperature to cause impurities to diffuse out of the graphite. National Carbon AGOT, Speer Nuclear-2 and Great Lakes R-1 are typical of this type material.
3. Chemical purification by the use of halogens. This can be achieved by direct use of a halide-containing gas in the "F process" and its variants or by the use of halide salts as developed by the French.

Each of the methods has its advantages and disadvantages. The first is generally restrictive as to choice of raw materials. The second is relatively inexpensive but only incompletely removes the impurities. The third approach produces the purest graphites but at some labor and expense. Obviously the three techniques can be used conjunctively, and, in fact, careful control of raw materials and handling techniques is required in any case.

2-6.1 THERMAL PURIFICATION

Most graphites produced for nonnuclear use are subjected to temperatures in the range from 2200 to 2800°C. The graphitizing furnaces are packed with metallurgical coke granules, which serve as resistor elements. It has long been recognized that heating to higher temperatures in a more carefully controlled environment would produce a purer graphite. With the construction of the first reactor during World War II, this technique of thermal purification was quickly utilized to produce nuclear-quality material. The furnace is packed with petroleum coke rather than with a less pure metallurgical coke, the effective cross sectional area of the furnace is reduced to obtain a higher resistance, and the heating cycle is lengthened. Peak temperatures attained are in the range 2800 to 3000°C, and these temperatures are held for one to two days.

Generally speaking, all low-boiling-point impurities are removed by graphitization; impurities that remain are those which form carbides or are soluble in graphite. Such impurities are extremely stable, often far beyond their vaporization temperatures, since they will frequently be found at imperfections within the graphite crystals. For example, vanadium carbide has a melting point in excess of 2800°C; boron carbide melts at 2350°C but also forms a substitutional impurity in the graphite lattice which is extremely stable.²⁴ Despite the fact that during thermal purification impurity atoms must diffuse out of the graphite, it has been found quite simple to purify large cross sections in this way. Material up to 20- by 20-in. has been produced in commercial quantities.

Table 2.8 — REPRESENTATIVE IMPURITY LEVELS OF THREE CLASSES OF GRAPHITES

Impurity	Impurity level, ppm		
	Unpurified	Thermally purified	Chemically purified
Total ash	1600	540	5
Silicon	94	46	<1
Iron	310	10	<2
Vanadium	30	25	<0.2
Titanium	34	11	1
Aluminum	40	2.5	0.1
Calcium	320	147	1.4
Boron	0.5	0.4	0.06
Sulfur	175	19	10

The chemical analysis of a normally graphitized material and of its thermally and chemically purified counterparts is given in Table 2.8.

2-6.2 CHEMICAL PURIFICATION

The ability of halides to penetrate both bulk graphite and graphite crystals, react with impurities, and remove them as volatile halide salts has long been recognized and employed to produce spectroscopic-grade electrodes for chemical analysis. As the requirements for nuclear material became more stringent, these techniques were perfected to produce material of larger cross section in large quantities.²⁵⁻²⁷

The technique utilized most widely in the United States has been purification by Freon-12 or chlorine,²⁴ although several other gases,²⁸ including sulfur hexafluoride, carbon tetrafluoride, and carbon tetrachloride have also been tested. The method of gas handling may be best visualized by reference to Fig. 2.8. The gas is carried to the furnace through the side headers and is introduced into the working area by transverse tubes terminating in the region B. The excess gas and the reaction products are carried to the top of the furnace through area C and are finally collected in fume hoods and scrubbed before release to the atmosphere.

The normal sequence of operation is to admit chlorine gas as the temperature of the furnace rises above about 1000°C, shift to Freon at temperatures of the order of 2000°C, and flush the furnace with nitrogen or inert gas during the cooling portion of the cycle. The last step is necessary to remove residual chlorine gas from the porous graphite. The Freon is employed to obtain fluorine, but almost equivalent results are obtained with chlorine. The only definite advantage in the use of fluorine is its ability to remove boron.

Data are given in Table 2.8 for a purified grade of nuclear graphite. The purity attained depends partially on the permeability and cross-sectional area of the graphite piece since gas must diffuse into the material

and the impurities must diffuse out. The data given in Table 2.8 apply to 4- by 4-in. cross sections.

The technique of using solid halide salts is not too dissimilar to the gas purification method. The complex system for the introduction of gases is replaced by a layer of a suitable salt, usually sodium fluoride, above and

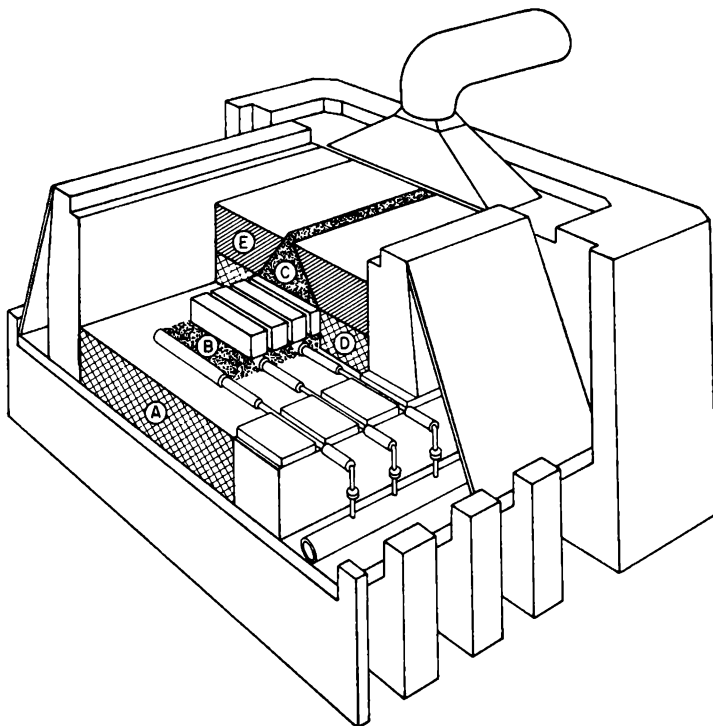


FIG. 2.8 Cutaway view of a gas purification furnace. The areas A, D, and E consist of petroleum-coke flour and particles sized to provide a low permeability pack. Areas B and C consist of coarse particles through which gases may readily pass. (From Odening and Bowman, *Industrial Carbon and Graphite*, Ref. 24.)

below the resistor coke beds and about 8 in. from the graphitizing material. The spacing is gauged to permit volatilization of the salt when the graphites attain temperatures of 2000°C . This method of purification produces materials comparable to those purified with gases.^{29, 30}

2-7 New Techniques

A number of new techniques and raw materials are being developed which, either collectively or individually, promise to revolutionize the properties and applications of graphite. Since most of these new processes are still under development or are just entering the commercial market, descriptive information is sparse. However, many of these new methods of manufacture have or will find important applications in nuclear tech-

nology, and a brief mention of these techniques will serve to indicate the nature and direction of future developments.

The most important modification in raw materials is the use of plastics and similar polymers as binders and impregnants. These materials permit comparatively rapid firing with much better control of physical properties and dimensions. Through a variation in the degree of aromaticity of the binder, finished materials can be produced with properties that range from those of a carbon to those of a crystalline graphite without changing the processing temperature. The wide range of viscosities, surface tensions, and different behaviors during pyrolysis have enabled the fabricator to match the impregnant to the microstructure of the base material. These polymeric impregnants have made possible the development of almost totally impermeable graphites. A more revolutionary approach is the direct use of cellulose to produce both impermeable³¹ and fibrous graphite.

The existence of various materials that catalyze the pyrolytic and crystallizing processes has long been known, but only recently have these been used in large-scale production. In particular, the addition of small quantities of metals or metallic carbides that dissolve and reprecipitate carbon increases the density of graphite.

It has been demonstrated³² that considerable attention to the control of atmosphere in the forming, baking, and graphitizing operations produces materials with minor but significant improvements in properties. The major gains, however, are in the uniformity of the product and in the predictability of the physical properties.

Two new methods of fabrication have recently entered the commercial stage, the first³³ involves forming and baking a carbon article under mechanical pressure. The heat is generated by passing electrical current directly through the carbonaceous raw materials until carbonization is complete. The method is extremely fast and produces a material with superior strength and density. The second³⁴ is a hot-working process, which produces a reorientation and recrystallization of the carbon. By this technique a graphite is produced which combines many of the best features of ordinary polycrystalline and pyrolytic graphites.

In summary, the recent techniques have made possible entirely new types of artificial graphite with physical properties of a revolutionary nature. Bulk densities in excess of 2.1 g/cm^3 can be produced by several means. Permeabilities have been reduced by a factor of 10^{12} and more. Tensile strengths are approaching 10,000 psi in large bulk graphites, with concomitant decreases in high-temperature creep. Reproducible thermal expansion coefficients can now be obtained with values ranging from less than 1×10^{-6} to 15×10^{-6} per $^{\circ}\text{C}$. These improvements reflect the impact of present-day technology on an industry that for many years was concerned almost exclusively with the production of current-carrying electrodes.

References

1. Cracking, *Petrol. Refiner*, **37**: 231-250 (September 1958).
2. A. N. Sachanen, *Conversion of Petroleum*, p. 31, 2nd ed., Reinhold Publishing Corporation, New York, 1948.
3. H. S. Pattin, National Carbon Company, unpublished data, May 1951.
4. H. J. Riley, The Carbonization Process, *Gas World*, **107**, No. 2774, Coking Section, 118-124 (Oct. 2, 1937).
5. L. M. Currie et al., The Production and Properties of Graphite for Reactors, in *Proceedings of the First United Nations International Conference on the Peaceful Uses of Atomic Energy, Geneva, 1955*, Vol. 8, pp. 451-473, United Nations, New York, 1956.
6. M. R. Hatfield, National Carbon Company, unpublished data, October 1938.
7. F. J. Healy et al., Dubbs Unit at Kendall Makes Record During Ninety-Eight Day Run, *Oil Gas J.*, **33**: 14 (Mar. 21, 1935).
8. C. V. Mitchell, National Carbon Company, unpublished data, February 1956.
9. V. C. Hamister, National Carbon Company, unpublished data, August 1954.
10. I. McI. Camp, *The Making, Shaping, and Treating of Steel*, 7th ed., United States Steel Corporation, Pittsburgh, 1957.
11. O. Kruber et al., Compounds Proved to be Present in Coal Tar, *Erdöl. u. Kohle*, **8**: 637-643 (1955).
12. H. G. Franck, The Real Nature of Coal-Tar Pitch, *Brennstoff-Chem.*, **36**: 12-20 (1955).
13. T. Edstrom, National Carbon Company, unpublished data, May 1959.
14. L. J. Wood and G. Phillips, Constitution and Structure of Coal-Tar Pitch, *J. Appl. Chem.*, **5**: 326-338 (1955).
15. H. Mallison, Distribution of Coal Tar and Pitch, *Bitumen, Teere, Asphalte, Peches*, **1**: 313-317 (1950).
16. E. L. Piper and V. C. Hamister, National Carbon Company, unpublished data, August 1959.
17. *Methods of Testing Coal Tar Products*, Barrett Division, Allied Chemical and Dye Corp., New York, 1942.
18. D. McNeil and L. J. Wood, Use of Coal-Tar Pitch as an Electrode Binder, in *Industrial Carbon and Graphite: Papers Read at the Conference Held in London, Sept. 24-26, 1957*, pp. 162-172, Society of Chemical Industry, London, 1958.
19. W. A. Hedden et al., *Experimental Carbons and Graphites for Irradiation Studies*, USAEC Report BMI-962, Oct. 26, 1954.
20. S. W. Bradstreet, *Graphite Technology*, Progress Reports 7 and 8, April 1 to June 1 and June 1 to August 1, 1958, Armour Research Foundation.
21. *A Pathfinder—Discovery, Invention, and Industry*, The Press Scrap Book, New York, 1910.
22. *Industrial Graphite Engineering Handbook*, Union Carbide Corporation, 1959.
23. P. M. Harris, *Purification of Graphite—Bibliography 1926-1955*, British Report AERE-Inf/Bib-109, October 1956.
24. C. A. Odening and J. C. Bowman, Recent Developments in Gas Purification of Graphite, in *Industrial Carbon and Graphite: Papers Read at the Conference Held in London, Sept. 24-26, 1957*, pp. 537-543, Society of Chemical Industry, London, 1958.
25. G. T. Sermon, *Purification of Graphite. Part I*, USAEC Report AECD-3912, United Carbon Products Co., June 16, 1948.
26. L. Brooks and G. T. Sermon, *Final Report. Part II. Technical*, USAEC Report AECD-3913, United Carbon Products Co., May 1949.

27. J. M. West, *Purification of Graphite*, USAEC Report HW-12780(Rev.), Mar. 21, 1949.
28. L. H. Juel, *Modifications of the F Process—Final Report*, USAEC Report AECD-3758.
29. P. Legendre et al., The Production of Nuclear Graphite in France, in *Proceedings of the First United Nations International Conference on the Peaceful Uses of Atomic Energy, Geneva, 1955*, Vol. 8, pp. 474–477, United Nations, New York, 1956.
30. A. Legendre et al., General Study on Nuclear Graphites Produced in France, in *Proceedings of the Second United Nations International Conference on the Peaceful Uses of Atomic Energy, Geneva, 1958*, Vol. 4, pp. 243–256, Geneva, 1959.
31. U. S. Patent application, Serial No. 676,435, 1957.
32. M. S. T. Price and F. W. Yeats, The Harwell Experimental Graphite Plant, in *Industrial Carbon and Graphite: Papers Read at the Conference Held in London, Sept. 24–26, 1957*, pp. 111–124, Society of Chemical Industry, London, 1958.
33. J. D. Hedges, *Formed Carbonaceous Articles, e.g., Electrodes*, British Patent 794,989, 1959.
34. New High Density Graphite Looks Good for Rocket Nozzles, *Materials in Design Eng.*, **52**: 13 (November 1960).

Machining Practice

C. A. SWITZER, JR.,† and L. H. JUEL†

3-1 General Machining Techniques

The machinability of graphite, or the resistance to cutting, depends not only upon hardness, but also upon properties not usually associated with hardness (see also Sec. 6-6.10). Electrographite, although abrasive, is a free cutting and readily machinable material as compared to steel. Lubricants or cutting fluids are neither required nor normally used, eliminating, in the case of pure nuclear graphite, the addition of a potential contaminant.

In the machining of graphite, the action of the cutting tool can be compared to the action of the tool on steel or ductile metals, on which considerable experience and data are available. Unlike steel, from which chips are removed by plastic flow of uniform cross section made up of very thin slip elements, graphite is crushed or fractured by the tool. The graphite chip is thus granular in form, and the surface is pitted when particles are torn from the matrix. This pitted appearance of the surface is largely dependent upon the grain size of the graphite and the depth of the cut taken.

Graphite can be turned, sawed, milled, bored, planed, drilled, shaped, ground, tapped, reamed, honed, and lapped. Although either woodworking or metal-working machines can be used in the machining of graphite, standard commercially manufactured metal-working machines are normally preferred because of their inherent accuracy, versatility, and automatic features.

Since a large fraction of the chips produced in the machining of graphite is in the form of extremely fine grains, high-efficiency cyclones or bag type dust collectors are required to collect the removed material. The removal of cutting dust is necessary because the indexing surfaces must be clean to maintain dimensional tolerances.

3-1.1 GRADES OF FINISHES

Graphite has a variable, nonhomogeneous structure made up of graphitized petroleum-coke particles and graphitized binder. It usually contains about 25 vol.% of fairly uniformly distributed fine pores (Sec. 5-7). The finish of graphite is largely dependent upon the structure of the parent stock and upon the feed and speed of cutting. In a machining operation the tool removes particles by a combination of crushing, shearing, and tearing

† Great Lakes Carbon Corp., Niagara Falls, N. Y.

actions. The maximum particle size of the original mix formula used in the manufacture of graphite has a decided effect upon the finished appearance of the machined surfaces, the surfaces of fine-grained graphites being less porous than those of coarser grained mixes with equal machining parameters.

The cutting tool makes numerous irregularities in the form of minute ridges and valleys on the machined surface. The magnitude, form, and spacing of these irregularities determine the degree of surface roughness. In the United States finishes on graphite are normally specified as root-mean-square (rms) average values. Finishes of the order of 63 to 240 μ in. can be readily attained. Somewhat finer finishes can be obtained if care is exercised in the machining operation. However, it becomes increasingly difficult to measure fine finishes as the particle size of the graphite increases.

Table 3.1 gives the finishes, as measured by visual metal scales of roughness, which can be expected in common machining operations.

Table 3.1 – SURFACE FINISHES ON MACHINED GRAPHITE

Operation	Finish, μin.
Band sawing	5000 to 1000
Diamond inserted circular sawing	250 to 500
Turning, boring, drilling, planing, shaping, milling	63 to 250
Grinding	32 to 125
Reaming	32 to 63

Any of the commercially available equipment can be used for testing the surface quality, with varying degrees of reliability; however, the method of visual comparison with sets of standard finish surfaces is normally employed. These commercially available scales are divided into gradations of average roughness expressed in terms of microinches. For a given rms value, the spacing and form of the irregularities will vary, depending upon the type of cutting tool used.

3-1.2 TOOLS

In the cutting of graphite, the tool material, as well as its geometric shape, has a bearing on the performance and life of the tool. New high-speed steel, ceramic-inserted, and carbide-inserted tools are used in machining operations, depending to a large degree upon individual preference and the particular operation. Tungsten-chromium-vanadium steel of T-1 or T-2 designation is currently popular in form cutters because it provides good wear resistance. The resistance to wear of carbide cutters is greater than that of high-speed tool steel, but the cost of such cutters is greater. In general, the choice of tool material is dependent upon the number of pieces to be machined and the required tolerances. In the machining of steel, tools often fail by heating (with resultant decrease in hardness) or by

spalling and crumbling of the cutting edge due to overstressing. These problems are not normally encountered with graphite. Failure, regardless of the tool material, is primarily due to wear on the cutting edge caused by the abrasiveness of the graphite.

In general, tools used in the machining of graphite are standard metal-cutting tools with minor variations. Tools and cutters are ground with a relief angle of from 15 to 20°. The back-rake angle is not critical in the appearance of the finished surface or the tool life. Most cutters have 0° rake, although small negative angles and positive rake angles up to 10° are used, depending more on individual preference than on a measurable advantage. The life of cutting tools between sharpenings is shorter on graphite than on steel. Excellent surface finishes can be obtained with a chip load (effective depth of cut per tooth) of from 0.0005 to 0.005 in. In single-point tools a rounded nose yields a finer finish, because of the reduced chip load at the trailing cutting edge, than does a pointed tool with the same feed and speed. The finer the load, the finer the finish.

Graphite can be machined to an excellent surface finish by grinding. However, even a soft-grade wheel, or one in which the abrasive grain can be easily dislodged, is too hard to sharpen itself automatically, and thus such wheels require dressing. During normal metal machining, as a wheel becomes dull, the increased friction tears the dull grains from the bond, and allows new points to come into action. Graphite, however, is too soft to allow self-sharpening of any presently available commercial grinding wheel.

3-1.3 SPEEDS AND FEEDS

The desired surface appearance dictates the feed and speed of the machines. As was stated previously, particles are torn from their bond leaving a pitted surface. The finer the cut or feed, the less the tearing of particles. A surface of good appearance, which is normally acceptable for nuclear graphite, is obtained by milling with a tool tip speed of approximately 1000 ft/min, a feed of 30 in./min, and a cut of $\frac{3}{32}$ in. Normally the feed on side mills is increased to approximately 100 in./min for the same tip speed and depth of cut as used on the end mills. Climb milling is employed where close tolerances are required since this reduces end chipping and inaccuracies associated with arbor deflection. Tolerances of ± 2 mils can be maintained on a production basis using the above cutting constants. Frequently closer tolerances are required, and these can be achieved by selecting proper machines and by giving special attention to machine setup and fixture design. Care must be exercised in indexing and clamping the stock during machining to assure that the stock is properly supported but unrestrained.

Graphite moderator blocks can be rough cut to length with standard metal-cutting band saws or, where size permits, with carbide-tip circular

saws. For operation at 3000 ft/min, a blade 0.035 in. thick with a 0.065-in. set and from 2 to 6 teeth per inch represents average band-saw requirements. Variations in blade specifications and machining speeds from this average can be made as dictated by the desired surface finish, tolerances, and stock size.

3-1.4 DUST COLLECTION

Since chips from the machining operation are granular, the most practical way to remove them is by pneumatic conveyance. An air velocity of approximately 4500 ft/min in the mains is adequate to convey the material. Hoppers connected to pneumatic mains below the cutting operation are normally used to collect the larger particles, which drop by gravity. The superfines, which do not readily settle, are collected by exhaust hoods with a static pressure of approximately 4 in. of water. The mains are constructed of 14-gauge sheet metal, and the elbows, hoods, and bends are constructed of 10-gauge material to reduce the maintenance of the piping necessitated by the abrasiveness of the material. Where bag type collectors are used, a classifier section is required because of the high dust load being conveyed. The hood design is usually a standard type similar to that used for fume collection.

Because graphite is abrasive, it is essential that wearing parts of all equipment be kept free from the graphite dust if excessive wear and maintenance are to be minimized.

3-2 Requirements in the Nuclear Industry

3-2.1 SIZES AND SHAPES

Since the machining requirements for each reactor differ considerably from each other, it is important that machining equipment be versatile. However, the equipment must also be accurate enough to maintain tolerances of 1 mil or less for the various machining operations. In most cases flexibility has been achieved by providing roller conveyors or other mechanisms for transferring material between machining stations. An example of a complex machined component for a research reactor is shown in Fig. 3.1.

3-2.2 CONTAMINATION CONTROL

Special factors are involved in the production and machining of nuclear graphite. Of primary concern is the possibility that the graphite might become contaminated, thereby increasing the capture cross section of the moderator. Care must be exercised that under no circumstances do water; lubricating oils and greases; nonferrous metals such as copper, brass, lead, cadmium, nickel, etc., come into contact with the graphite. The use of sealed bearings and oil-mist spray methods in the machining equipment is

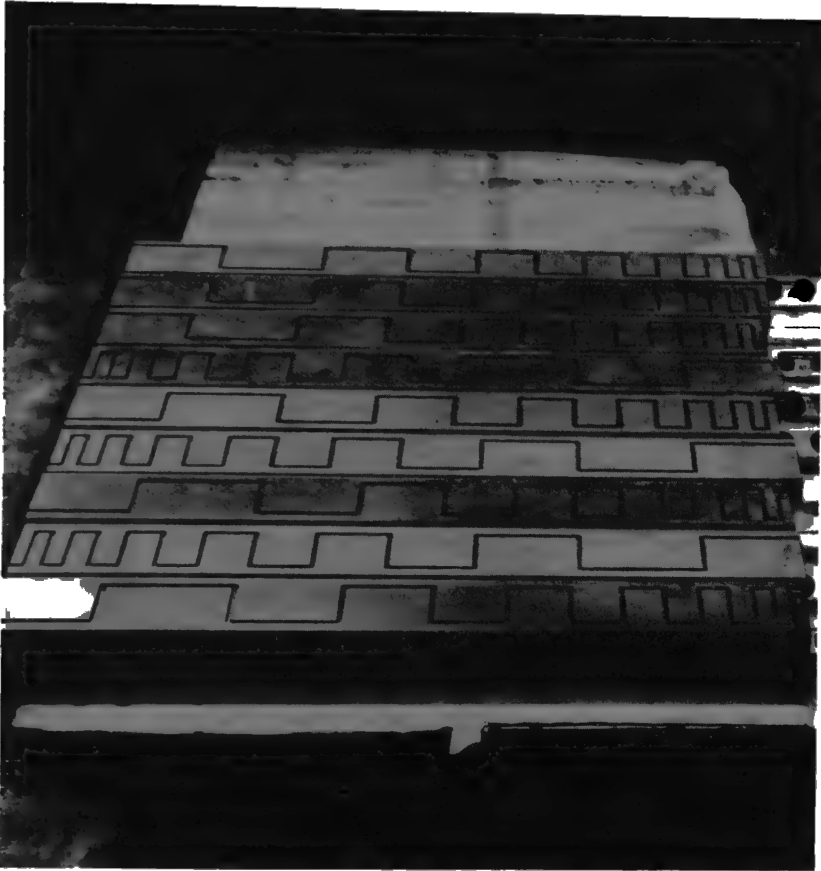


FIG. 3.1 Graphite stringers for a thermal column. These stringers are part of a gas-cooled thermal column for a research reactor. Tolerances were held to ± 5 mils on dimensions and $\pm 0.25^\circ$ on angles.

essential. Operators should wear special protective coveralls, gloves, caps, and shoes. Control must be exercised over the laundering of this clothing to ensure that boron compounds and other contaminants are not used. The arrangement of the machining facilities should be such that personnel are required to change into special clothing before entering and to remove it when leaving the clean machining area. Smoking and chewing of gum should not be permitted, and no food should be brought into the shop area. Neither soap nor cleansing agents containing boron should be allowed in the area. Provisions should be made so that in the handling of large quantities of raw and machined blocks, transport vehicles can be loaded and unloaded under clean conditions.

In machining areas a highly efficient dust-removal system is essential. It is advantageous to have the machining area under a slight positive pressure to prevent the entrance of dust-laden air through doorways and ventilators.

3-2.3 MOCK-UP AND ZONING

The mock-up or trial stacking of finished graphite moderator blocks provides a final check on any errors or omissions in the bill of material, drafting, or machining. The mock-up should be set up on an extremely level floor in an area protected from contamination. The blocks, stacked by hand in the designed pattern, should be marked as to position in the stack, i.e., layer number, row number, and position in row. Final assembled inspection ensures that blocks are in their proper place and that the cumulative stack height and alignment are as designed. The blocks are removed in reverse order, palletized in a manner to afford rapid and orderly assembly, wrapped, and marked on the wrapping to ensure ease and a minimum of confusion during actual erection. Speed in the installation of the moderator in the reactor shell is desirable to reduce the possibility of contamination.

3-3 Equipment and Methods in the Nuclear Industry

3-3.1 HANFORD

Figure 3.2 shows the equipment layout used in the machining of graphite for the two most recent Hanford reactors. For these reactors it was necessary to machine a large number (150,000 to 200,000) of individual blocks approximately 4 by 4 in. in cross section and up to 50 in. long. Because of the large number of blocks required and the similarity of many of the details, production-line machining proved to be the most economical method of fabrication.

Production machining at Hanford was accomplished through the use of separate machining lines for different block types.^{1,2} Tube blocks were machined to their required cross section and bored to size in the preshop areas. This supplied the material blanks for the machining lines in the fabrication shop. The fabrication shop contained production lines to complete the necessary details (machining to length, counterboring, cutting keyways, etc.) on each block. An inspection station was set up following each machine and at the end of each line.

Trunnion blocks were fabricated in line 1, where they were drilled, faced, and bored and their sides were milled. Tube blocks were cut to length, chamfered, counterbored, faced, and drilled on line 2. Line 3 consisted of equipment for the fabrication of keys and special shapes. Solid bars were finished on lines 4 and 5, which were set up to perform similar operations. Machining of the tube entry blocks was performed on line 6. However, similar machines were used in the various lines for performing the same or similar operations. The blocks were cut to length using De Walt crosscut or Do-All saws, cornered, chamfered on hydraulic push broaches of varying sizes, milled and squared to length, shaped with opposed ExCello hydraulic feed heads, and drilled with ExCello heads or a special deep-hole drill. The

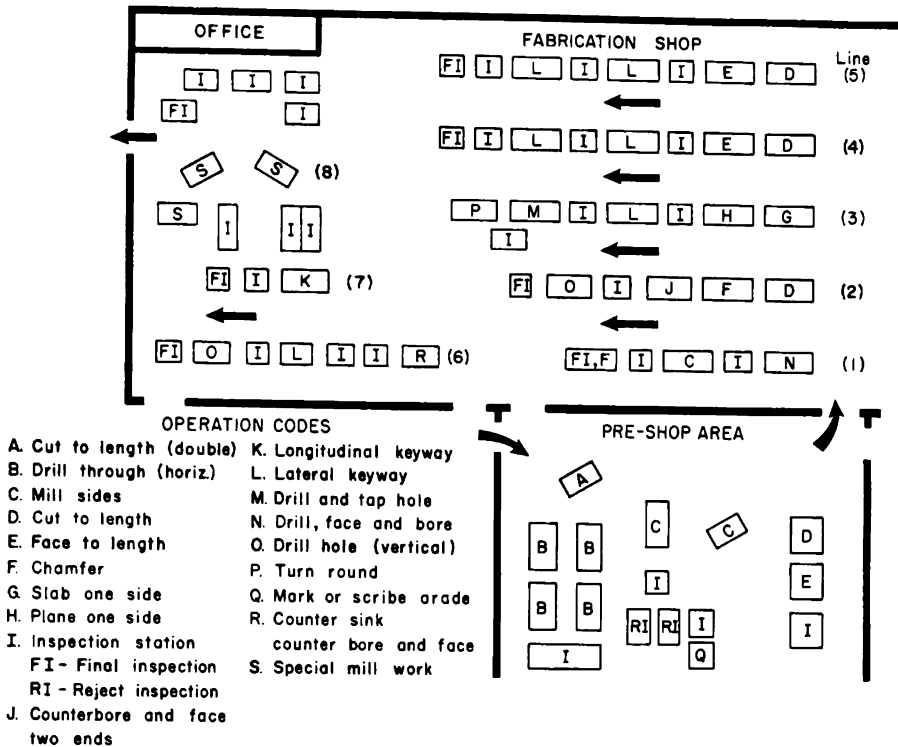


FIG. 3.2 Schematic diagram of the graphite machining facilities at the Hanford Atomic Products Operation, General Electric Company. Arrows indicate the direction of flow of material. Areas at the ends and between lines are used to bank material in process.¹

blocks were squared in cross section by Sunstrand duplex mills with special indexing and clamping fixtures. Keyways were cut with Sunstrand traveling head mills and Sunstrand simplex straddle mills. An Oliver wood planer and Do-All band saw were used for machining plates to thickness. In all operations carbide blades and/or inset-teeth cutters were normally used. Standard lathes were used for special turning operations, and standard milling machines were employed for special details not requiring a production-line setup.

3-3.2 BROOKHAVEN

Machining for the Brookhaven Research Reactor (BGR) was performed at BNL in an existing gymnasium building.³ The machining was divided into two major programs, a primary and a secondary program running concurrently. The primary program included all machining necessary to produce the nominal dimensions from the raw stock. The secondary operations included all subsequent machining performed on the primary squared stock.

In general, the primary machining program included the rough cutoff

of the stock by means of a Do-All saw, slitting of the raw stock to $4\frac{1}{4}$ - by $4\frac{1}{4}$ -in. pieces on a similar machine, squaring of the nominal 4- by 40-in. stock on a simplex Milwaukee milling machine, and end turning on the 5H vertical Milwaukee milling machine. The production rate realized on the Brookhaven machining was fifty 40- by 20- by 63-in. slabs per hour, including normal breakage on the cutoff operation. The slitting operation had a rate of 135 slit $4\frac{1}{4}$ - by $4\frac{1}{4}$ -in. pieces per hour. A two-step operation running concurrently was set up to straddle mill the blocks to 4.000 ± 0.001 in. Four 1- by 14-in. side mills machined two blocks at a pass.

The secondary program included all subsequent operations on the primary block and consisted primarily in cutting keyways, channels, end tapers, radii, etc. All fixtures and cutters for the secondary program were designed to produce the desired cut in a single pass. Model 2K and 5H vertical Milwaukee milling machines were used in machining keyways; radius cutters of the duplex type mill performed the channel machining operation. Keyways were cut at a rate of 60 per hour with a tolerance of ± 1 mil. Tapered trimming of block ends to a multiple of 1.5° was accomplished at a rate of 20 long blocks and 35 short blocks per hour.

The tolerances that can be achieved by these methods of machining can best be demonstrated by reference to the BGRR. In the assembly of this reactor prior to lay-up, check lines were scribed around the perimeter of the inside steel shield plate of the pile at 4-ft elevation intervals. The elevation at each 4-ft level and the cumulative levels were accurate to within 7 to 10 mils. The greatest deviation in width of any layer across 74 joints was less than 100 mils. These two measurements showed that an average machining tolerance of less than 1 mil could be achieved in squaring. Gap keyway locations were held well within 1 mil, as evidenced by the measured gap width of less than 20 mils in 25 ft (74 layers).

Inspection of machined pieces required the use of height gauges, dial indicators, and air gauges and/or special gauges for various operations. For the BGRR 10 per cent process inspection was carried out for each primary and secondary operation, and 100 per cent final inspection was carried out for the finished blocks.

3-3.3 UNITED KINGDOM GAS-COOLED REACTORS

The entire output of nuclear-grade graphite manufactured in the United Kingdom is sold through the United Kingdom Atomic Energy Authority. At the present time this output is machined at five major establishments. Because of different reactor designs, the machining operations vary; but, in general, all the shops follow similar production techniques.

Figure 3.3 shows the production line of A. Reyrolle & Company, Ltd., located adjacent to the Anglo Great Lakes factory at Newburn Haugh. Reyrolle has machined components on behalf of the Nuclear Power Plant Company for the Bradwell and Latina Reactors.



FIG. 3.3 The main production line of A. Reyrolle & Company, Ltd. View shows the automatic brick-transfer line and the station where the first two parallel sides of the bricks are milled. (From *Nuclear Engineering*, Ref. 4.)

The moderator-block transfer line comprises five machines connected by gravity roller conveyors and air-operated lifts.⁴ All machines on the line are interlocked so that the entire operation can be controlled from one station, with fixture clamps, etc., controlled by limit switches. These 8- by 8-in. cross-section blocks are initially trimmed with a circular saw.

The sides of the blocks are machined as they pass through duplex milling machines, the blocks being rotated 90° automatically while being transferred between the two machines. The stock is swung up into a fixture for boring by a vertical boring machine. Following boring the stock is transferred to two duplex mills for end machining of shiplap joints.

The boring machines, operating at a spindle speed of approximately 420 rpm, have a feed of 30 in./min with a 4 in. fly cutter. The duplex end mills, operating with a tip speed on the cutters of approximately 1000 ft/min, produce a satisfactory finish with a $\frac{3}{32}$ -in. cut and a feed of 30 in./min.

Cutters of 10 in. diameter with a 20° relief and a 10° positive rake are used in this operation. A feed of 100 in./min is used on the side mills, with a chip load of 0.005 in. and a tip speed of approximately 1000 ft/min. Normal tolerances on all machined blocks are held to within ± 2 mils.

3-4 Cementing Techniques

Intricate shapes or individual members of unusually large size are frequently required by the designer, and direct machining from a monolithic blank becomes both impractical and uneconomical. Through the use of suitable cementing and "welding" techniques, such components can be fabricated from less complicated or smaller elements, which in themselves are readily machined. The actual welding of small graphite elements of the simplest geometry has been reported, but the conditions required are such that the process cannot yet be considered as a practical method for fabricating carbon and graphite materials.

3-4.1 JOINTS

In general, the types of joints used in the fabrication of carbon and graphite are similar to those common to the fabrication of metal or wood. Threaded, pinned, tapered, butted, tongue-and-groove, and collar-and-sleeve joints, or modifications and combinations thereof, have all been used in a variety of applications. For the most part the proper cementing of two plane surfaces provides a joint that will be serviceable in most nuclear applications.

3-4.2 CEMENTS

Commercially available cements for bonding carbon and graphite may be of organic, inorganic, or metallic composition. Since most metallic elements and inorganic compounds are objectionable in nuclear applications,

only those cements of an organic or carbonaceous nature are considered here.

Carbonaceous cements are basically composed of a liquid and a filler. The filler usually consists of a carbon or carbonaceous powder, the fineness of which will depend upon the thickness of the joint to be made. The liquid may be any one or a combination of a variety of organic substances used either alone or in an appropriate solvent. Aqueous solutions of carbohydrates such as sugar, dextrin, and molasses; mixtures and solutions of hydrocarbons such as coal tar and its derivatives; and thermosetting resins such as those of the phenol-formaldehyde, furfuryl alcohol, and epoxy types have all been used in cement formulations. The ratio of liquid to filler is usually adjusted so that the cement will have a trowelable consistency.

Resin-base cements, because of their higher strength and inherent advantage of curing or hardening at low temperatures, have enjoyed widest acceptance. Specific additives and accelerators are frequently employed to impart special workability and hardening characteristics. These cements are often referred to as "single-package" and "two-package" cements, depending upon the shelf life or working life of the cement after mixing of the various components. The two-package cements generally require mixing of two components just prior to use, whereas single-package cements are compounded by the supplier and can be stored for periods of several months or more at ambient temperatures.

3-4.3 FACTORS INVOLVED IN JOINT PREPARATION

The physical properties and structural characteristics of the carbon and/or graphite elements to be cemented together are important considerations in the preparation of successful joints. This is especially true in those instances where the fabricated system is destined for service at elevated temperatures. In such cases the compatibility of the thermal-expansion coefficients of the joining components must be considered in relation to their respective strengths and moduli of elasticity. As a corollary, the grain orientations in the respective members must be taken into account since grain orientation is the underlying factor responsible for the anisotropy of electrographites.

Porosity is another important factor. As the porosity of the mating surfaces increases, it becomes desirable to saturate these surfaces with the liquid component of the resin, or alternatively, to use a cement with a high liquid-to-filler ratio.

Two important criteria for developing high-strength joints are the joint thickness and uniformity. In general, the strength of a cemented joint increases with decreasing joint thickness. For maximum strength the mating surfaces should be machined as flat and uniform as possible. Ground, milled, or planed surfaces give more reproducible joints of high strength, although carefully band-sawed surfaces can produce a strong joint.

3-4.4 TECHNIQUES

The techniques to be described for the cementing of graphites and carbons pertain to resin-base cements. However, the principles are generally applicable to all types of cements.

Before cement is applied, the machined surfaces are carefully cleaned to remove any machining dust or contamination. The cement is then applied to both mating surfaces, preferably by means of a notched trowel to control the thickness of the cement layer. Where possible, joints of 5 to 20 mils thickness are recommended. When the joint is closed, the trowel ridges are kept parallel to avoid the entrapment of air. The cemented assembly is held together at low pressures (of the order of 2 to 3 psi). Higher pressures are unnecessary and may even be detrimental.

Curing of the cement is a critical operation. Curing rates that are too high result in a frothy cement structure of low strength. Depending upon the particular curing characteristics of the liquid resin or the resin-accelerator system employed, curing may be effected generally between room temperature and about 150°C. For curing thermosetting resins rates of temperature rise of the order of 10°C per hour have been used successfully, although faster rates are possible where the areas to be joined are small. Care must be exercised in avoiding any relative movement of the joined material during curing. The cured assembly may then be heated to about 900°C in a protective atmosphere to carbonize the cement, or, if desired, the cement may be graphitized.

3-4.5 PROPERTIES OF CEMENTED JOINTS

High strengths in cemented joints are realized primarily through the use of resin-base cements in very thin joints (0.003 to 0.010 in.). With the techniques described cemented joints with a modulus of rupture of about 2000 psi are consistently attainable even after carbonization of the cement. When the cement is heated to graphitizing temperatures, the strength is decreased by about 10 to 30 per cent. Where thicker joints of the order of $\frac{1}{16}$ to $\frac{1}{8}$ in. are employed, a modulus of rupture of 800 to 1000 psi is typical after carbonization.

The electrical and thermal conductivity of a cemented joint are functions of the cement composition, the joint thickness, and the temperature to which the joint has been heated. The electrical resistivity of resin-base carbonaceous cements is quite high in the cured state, but after carbonization to 900°C it may drop to the order of 60×10^{-4} ohm-cm, and after graphitization to 2800°C, to 10 to 12×10^{-4} ohm-cm. The corresponding thermal conductivities tend to follow the order-of-magnitude changes typical for carbon and graphite products.

The permeability of a cemented joint varies over a wide range. Standard

impregnation techniques can be employed to reduce the permeability of a cemented assembly.

The cement in the joint of a fabricated component of carbon or graphite is susceptible to oxidation at elevated temperature. The rate of oxidation is a function of the maximum temperature that the cement experiences in the fabrication process. In applications where oxidation resistance is of prime importance and where it is economically feasible to heat the cement to graphitizing temperatures, the oxidation resistance of the cement can be enhanced so as to approach closely that of the parent stock. For many applications, however, oxidation, per se, is not an important factor and simple curing of the resin-base cement is sufficient. For certain nuclear applications it is necessary to employ intermediate heat-treatment temperatures to reduce the hydrogen and oxygen levels of the cement while maintaining high strengths.

Irradiation testing of cemented joints has begun as a result of the increasing interest in the use of cemented components in reactor cores. Few results have been reported to date. If any difficulties such as loss of strength are encountered, they will most likely occur with ungraphitized cements at the graphite-carbon boundary.

High-strength joints with areas greater than 2000 sq in. have been consistently produced. If certain factors mentioned above are taken into consideration, there appears to be no reason why even larger areas cannot be successfully joined.

It is apparent that each application of the cementing technique must be considered in light of the particular requirements and conditions to be met. These factors will then dictate the choice of cement and technique most suitable for achieving the desired results.

References

1. C. E. Love et al., *Inspection Manual. Production Machining of Graphite Moderator*, USAEC Report HW-59347, Hanford Atomic Products Operation, Mar. 16, 1959.
2. H. P. Oaks, Hanford Laboratories, General Electric Company, unpublished data, May 1957.
3. C. R. Binner et al., *Machining of Graphite for Brookhaven Reactor*, USAEC Report HKF-2, H. K. Ferguson Company, June 1, 1949.
4. Graphite Machining, *Nuclear Eng.*, 4: 206-215 (1959).

Nuclear Properties

P. F. NICHOLS† and E. M. WOODRUFF†

4-1 Nuclear Requirements for Moderator Graphite

There are two very basic nuclear requirements for moderator graphite, or, for that matter, any moderator material. First, it must be effective in slowing fast neutrons down to thermal energies, and, second, it must have a small cross section for neutron absorption. The slowing down of neutrons results principally from energy transfer during elastic collisions between the neutrons and the moderator atoms. For a material to be an efficient moderator, the collision rate per unit volume must be relatively high. The collision rate is proportional to the number of moderator nuclei per unit volume, and for this reason the density of moderator graphite should not be too low if the volume of the reactor core is to be minimized.

The graphite should absorb as few neutrons as possible during the moderating process because neutrons absorbed in any reactor component other than the fuel (parasitic absorption) are lost from the chain reaction. The typical impurities occurring in graphite have a greater propensity for absorbing neutrons than do the carbon atoms. It is, therefore, desirable to have the graphite as free as possible from such impurities.

It is of interest to consider the relative importance of high-purity graphite for thermal natural-uranium reactors and for thermal enriched-uranium reactors. For natural-uranium reactors a low neutron-absorption rate in the moderator is especially important. Such reactors must be very large to have any excess reactivity available at all, and a loss of excess reactivity as a result of a high rate of absorption in the moderator is especially undesirable. Excessive absorption in the graphite also causes nonproductive consumption of U^{235} atoms, thereby decreasing plutonium formation.

Neutron absorption in the moderator is basically undesirable in enriched-uranium reactors for the same reasons that it is undesirable in natural-uranium reactors. The decrease in the excess reactivity resulting from absorption in the moderator is not as critical a problem, however, because it is possible to gain excess reactivity by increasing the enrichment of the fuel. If the enrichment is increased in lieu of further purification, the formation of plutonium is decreased because there is competition for

† Hanford Laboratories, General Electric Company, Richland, Wash.

neutrons by absorption in U^{235} as well as in the impurities. The loss in plutonium production amounts to about 2.5 per cent for each 0.05 per cent of added enrichment.¹ Thus whether to increase the purity of the graphite or to increase the degree of enrichment becomes a question of economics.

4-2 Graphite-moderator Physics

The material in this section introduces the basic concepts of moderator physics and shows how they apply to graphite. For more detail the reader is referred to textbooks on reactor physics.^{2,3}

4-2.1 REACTOR-PHYSICS CONCEPTS

Very simply, the neutron cycle in a reactor consists of:

1. Absorption of slow neutrons by fuel.
2. Production of a new generation of fast neutrons from fission in the fuel.
3. Slowing down (moderation) of fission neutrons.
4. Leakage of neutrons and parasitic absorption of neutrons at all stages of the cycle.
5. Absorption by fuel of the new generation of slow neutrons.

In an infinitely large array of reactor cells,[†] the ratio of the number of neutrons in any stage of this cycle in one generation to the number of neutrons in the same stage of the previous generation is the infinite multiplication factor, k_{∞} . It should be noted that the above definition includes parasitic absorption but not the effects of neutron leakage; no leakage would occur in an infinitely large reactor. Analytically k_{∞} is given by

$$k_{\infty} = \eta \epsilon p f \quad (4.1)$$

where η is the number of fast neutrons resulting from the absorption of a neutron in the fuel, p is the probability that a neutron will escape resonance capture (for example in U^{238} resonances) while slowing down, ϵ is the fast-neutron multiplication factor, and f is the thermal utilization (the fraction of thermal neutrons absorbed in the fuel instead of in other cell components).

In a reactor of finite size, leakage of both fast and slow neutrons occurs. If P_f and P_s are defined as the fast and slow nonleakage probabilities, the following expresses the effective multiplication factor:

$$k_{eff} = k_{\infty} P_f P_s \quad (4.2)$$

For a reactor that is just critical,

$$k_{eff} = 1 \quad (4.3)$$

[†] A cell is a fuel column and its associated moderator.

One approximation to the critical equation, known as the "age-diffusion theory approximation," which assumes a continuous slowing-down process, is

$$\frac{k_{\infty}e^{-B^2\tau}}{(1 + B^2L^2)} = 1 \quad (4.4)$$

where L^2 is the thermal diffusion area, τ is the slowing-down area or age to thermal energies, and B^2 is the buckling. By definition

$$\tau = \frac{1}{6} \overline{r_s^2} \quad (4.5)$$

and

$$L^2 = \frac{1}{6} \overline{r_d^2} \quad (4.6)$$

where $\overline{r_s^2}$ and $\overline{r_d^2}$ are, respectively, the mean square distance a neutron travels in the reactor lattice while it is slowing down from fission to thermal energies and the mean square distance a neutron travels while it remains in the lattice as a thermal neutron. For a critical reactor the fast and slow nonleakage probabilities in Eq. 4.2 can be identified with the quantities in Eq. 4.4 in the following manner

$$P_f = e^{-B^2\tau} \quad (4.7)$$

$$P_s = 1/(1 + B^2L^2) \quad (4.8)$$

It is clear from Eq. 4.2 that k_{eff} depends not only upon k_{∞} , but also upon L^2 and τ , which, in turn, are dependent upon the properties of the moderator. The diffusion area in the moderator only is given by

$$L_m^2 = \frac{1}{3} \Sigma_{tr} \Sigma_a \quad (4.9)$$

where Σ_{tr} is the macroscopic transport cross section and Σ_a is the macroscopic absorption cross section. They are average values for the thermal-energy region. The age in a nonabsorbing moderator is given by

$$\tau_m(E_{th}) = \int_{E_{th}}^{E_f} \frac{1}{3\xi\Sigma_s\Sigma_{tr}} \frac{dE}{E} \quad (4.10)$$

where E_f is the initial energy of a fission neutron, E_{th} is the thermal-neutron energy, Σ_s is the macroscopic scattering cross section, and ξ is the average logarithmic energy decrement for each neutron collision in the moderator. If the reactor consists solely of fuel and moderator, the diffusion area in the entire lattice is approximated by

$$L^2 \approx L_m^2(1 - f) \quad (4.11)$$

where f is the thermal utilization. The age for the entire lattice is approximately the same for the moderator, i.e.,

$$\tau \approx \tau_m \quad (4.12)$$

if no sizable void fractions exist.

Of the important moderator parameters in Eqs. 4.9 and 4.10, the cross sections must be measured; the value of ξ can be calculated by a consideration of the moderating process.

4-2.2 MODERATOR PHYSICS

Now that some of the basic equations have been given and the terms have been defined, let us consider a simplified form of the process by which fast neutrons are slowed down by a moderator. Some refinement of this simplified discussion will be given in Sec. 4.2.4. The following assumptions, which are approximately true, shall be made:

1. The neutron loses energy in elastic collisions with the moderator nuclei.
2. The moderator nuclei are initially at rest in the laboratory system of coordinates.
3. The scattering of neutrons by the moderator nuclei is spherically symmetric in the center-of-mass system of coordinates.

If the laws of conservation of energy and momentum are applied to the system described above, an expression can be obtained for E_2 , the kinetic energy of a neutron in the laboratory system after collision, in terms of E_1 , the kinetic energy in the laboratory system before collision, and the scattering angle θ in the center-of-mass coordinate system. The result is

$$E_2 = E_1 \left\{ 1 + \frac{\alpha}{2} [(\cos \theta) - 1] \right\} \quad (4.13)$$

where α is given in terms of the atomic weight, A , of the scattering nucleus by

$$\alpha = \frac{4A}{(A + 1)^2} \quad (4.14)$$

From Eq. 4.13 it is apparent that in a glancing collision ($\theta = 0$) no energy is transferred and $E_2 = E_1$. The maximum amount of energy is transferred in a head-on collision ($\theta = 180^\circ$), and for carbon this energy transfer is 28.4 per cent. Since all values of θ are equally probable for spherically symmetrical scattering, the average energy transferred is just one-half this or 14.2 per cent. It should be noted that the fractional energy loss and ξ are independent of the initial energy.

If spherically symmetrical scattering is assumed, it is possible to obtain an expression for ξ . In the center-of-mass system, the probability that a neutron with an initial energy E_1 will have an energy after collision in the interval between E_2 and $E_2 + dE_2$ is

$$p(E_2) dE_2 = \frac{-dE_2}{\alpha E_1} \quad (4.15)$$

The average logarithmic energy change per collision, ξ , is

$$\xi = \overline{\ln \frac{E_1}{E_2}} = \int_{E_1}^{\alpha E_1} \left(\ln \frac{E_1}{E_2} \right) p(E_2) dE_2 \quad (4.16)$$

where the limits of integration are the maximum and minimum energies possible after collision. After the integration has been performed, this becomes

$$\xi = 1 + \frac{(A-1)^2}{2A} \ln \frac{A-1}{A+1} \quad (4.17a)$$

$$\approx \frac{2}{A + 2/3} \quad (\text{for large } A) \quad (4.17b)$$

Equations 4.17a and 4.17b agree to within 0.2 per cent for carbon.

4-2.3 MODERATOR PARAMETERS

There are several combinations of the moderator parameters ξ , Σ_a , and Σ_s , which are commonly used to compare the moderating characteristics of various substances. These are listed for the common moderators in Table 4.1.

Table 4.1 — MODERATOR PROPERTIES[†]

Moderator	ξ	$\xi \Sigma_s, \text{cm}^{-1}$	$\xi \Sigma_s / \Sigma_a$	$\rho, \text{g/cm}^3$
Graphite	0.158	0.063	200	1.65
Be	0.206	0.16	150	1.84
BeO	0.17	0.11	180	2.80
H ₂ O	0.93	1.5	70	1.00
D ₂ O(99.75 %)	0.51	0.18	21,000	1.10

[†] The values in this table, except those for graphite, have been taken from Ref. 4. The slowing-down power and moderating ratio for graphite have been recalculated on the basis of σ_a (2200 meters/sec) = 3.80 mb. (Ref. 5) and $\rho = 1.65 \text{ g/cm}^3$.

Two of the quantities in Table 4.1 are sometimes used as figures of merit of a particular substance as a moderator; these are discussed below:

1. The slowing down power, $\xi \Sigma_s$, is an index of the ability of a moderator to slow down neutrons. However, since this parameter is independent of the absorbing properties of a material, it is not a good representation of the usefulness of a particular material as a moderator. Boron, for example, has a high value of $\xi \Sigma_s$ but would be useless as a moderator material because of its high absorption cross section.

2. The moderating ratio, defined by $\xi \Sigma_s / \Sigma_a$, is a better index of the merit

of a particular material as a moderator. A shortcoming of the moderating ratio is that it is independent of density. For example, helium has a high value for the moderating ratio, but it would be a poor moderator because it has such a low density at normal pressures and temperatures. Perhaps the best specification for a moderator is that both moderating ratio and density be relatively high.

4-2.4 DETAILED MODERATION PROCESS IN GRAPHITE

Complications arise in the simplified discussion of neutron moderation of the previous sections when neutrons have high energies (several million electron volts) or when they approach thermal energies ($\sim 1/40$ ev). For high-energy neutrons the scattering is not necessarily spherically symmetric in the center-of-mass system because of the existence of several d-wave (neutron angular momentum quantum number $l = 2$) scattering resonances above 2 Mev which scatter anisotropically.⁶ The resulting preferential forward scattering reduces the average energy loss in a collision and increases the distances neutrons travel from their original source during the moderation process. However, this anisotropic scattering actually has only a small effect on the moderation of neutrons by graphite because most of the scattering involves neutrons with an energy of less than 2 Mev.

Excited states⁷ in the C^{12} nucleus at 4.43 Mev and 7.65 Mev result in some high-energy inelastic scattering[†] by graphite. This effect is also small and is less important in a graphite-uranium reactor than inelastic scattering by uranium. Inelastic scattering can occur in carbon only at energies in excess of the energies of the bulk of the fission neutrons; this is not the case with uranium.

In the low-energy region, the assumption that the carbon atoms are at rest in the laboratory system is invalid. They are, instead, in thermal motion, and, as a neutron slows down to near-thermal energies, it may gain energy from a carbon nucleus instead of losing energy to it. The neutrons reach an equilibrium distribution that is nearly Maxwellian in graphite.

4-2.5 NEUTRON TEMPERATURE

The true thermal-neutron distribution² can be approximated by a Maxwellian distribution characterized by a most-probable neutron temperature T_n . Neutron temperatures are determined experimentally either from detailed spectrum measurements⁸ or from measurements of reaction rates with absorbers of known cross section.⁹

The neutron temperature differs in general from the moderator temperature, even if the neutron distribution has reached the steady-state

[†] Inelastic scattering is a process in which some of the collision energy is absorbed internally in the scattering nucleus.

distribution. This is due to some absorption of the neutrons during thermalization, which prevents the neutrons from reaching an actual thermal equilibrium in the moderator. The work of Coveyou et al.,¹⁰ which is discussed in a review article by Cohen,¹¹ is of interest. Coveyou et al. calculated the energy distribution of neutrons moderated by free atoms of several atomic weights. They made least-squares fits of Maxwellian distributions to their calculated distributions and obtained the relation

$$\frac{T_n}{T_m} = 1 + 0.46\Delta \quad (4.18)$$

between the neutron temperature and moderator temperature, where $\Delta = 4\Sigma_a(kT_m)/\xi\Sigma_s$. Measured values of the neutron temperature^{9, 12-14} obtained with either of the two techniques listed above do not agree very well with each other or with the theoretical result. Some of the experimental results are higher than the theoretical value and some are lower.

The behavior of the neutron distribution in regions of different temperatures in a reactor is also of interest. If the neutron distribution has reached equilibrium in a region of temperature T_1 , neutrons passing from that region into another of temperature T_2 will eventually become part of the characteristic distribution of the new region. The process by which equilibrium is reached in the new surroundings is sometimes referred to as "rethermalization."

Some experimental work on neutron rethermalization in graphite has recently been undertaken.¹⁵ The spatial dependence of the absorption rate of a $1/\nu$ neutron absorber was studied in the vicinity of a temperature discontinuity. An analysis of these data provides temperature-dependent transfer cross sections (rethermalization cross sections) which are applicable to a group-diffusion treatment of the problem.

4-2.6 TEMPERATURE DEPENDENCE OF THE NEUTRON-ABSORPTION CROSS SECTION AND DIFFUSION LENGTH

The microscopic absorption cross section (σ_a) is inversely proportional to the relative velocity of approach of the neutron and the absorbing carbon nucleus.¹⁶ The relative velocity is approximately proportional to the square root of the neutron temperature (T_n). As the moderator temperature increases, so does the neutron temperature, although the two are not equal.

The variation of the diffusion length, L , is slightly more complex. From Eq. 4.9

$$L_m^2 = \frac{1}{3} \Sigma_{tr} \Sigma_a$$

In addition to the square-root temperature dependence of σ_a and a slight temperature dependence of σ_{tr} , both Σ_{tr} and Σ_a are temperature dependent because they are proportional to the graphite density, which changes with

temperature. If the temperature dependence of σ_{tr} is ignored, the temperature coefficient of L^2 is

$$\frac{1}{L^2} \frac{dL^2}{dT} = 2\beta + \frac{1}{2T_n} \quad (4.19)$$

where β is the coefficient of volume expansion for graphite. The second term in Eq. 4.19 is considerably larger than the first for all normal graphite-reactor temperatures. This result agrees well with the experimental temperature dependence of L^2 measured by Lloyd.¹⁷

The temperature dependence of L affects the reactivity of a reactor because it causes a change in the slow-leakage probability.

4-3 Nuclear Purity

Extremely small concentrations of certain impurities in graphite have an appreciable effect on the neutron-absorption cross section. In addition, small amounts of adsorbed water and nitrogen in the pores of the graphite have some poisoning effect. The effect of these impurities on the *moderating* properties, however, is usually negligible. For example, 0.015 wt.% of adsorbed water increases the slowing-down power about 1 per cent. As seen from Fig. 6.16, the amount of water adsorbed on graphite is in the range of 0.01 wt.% or less, except when the relative saturation pressure approaches the value of 0.9.

Although some measure of the poisoning effect of impurities can be determined by careful chemical analysis, it has become standard practice to measure the net effect of all impurities by a single test that measures the reactivity effect directly. One of two methods is normally employed: the danger-coefficient method or the pile-oscillator method.

4-3.1 DANGER-COEFFICIENT METHOD

Most danger-coefficient measurements on graphite⁹ (often called "delta in-hours" or "DIH measurements") have been performed in the Hanford 305 Test Reactor (HTR) shown in Fig. 4.1. Measurements are compared to a standard graphite bar about 4 by 4 by 48 in. placed at the center of a removable graphite stringer. The stringer is inserted into the center of the chain reactor, and the control rods are adjusted until the reactor is, in principle, exactly critical. The standard is then replaced by a test bar of the same size. The difference in reactivity in units of in-hours between the standard and test bars (DIH) is measured from either the rising or the falling period and is taken as a measure of the nuclear purity. In practice DIH values are obtained with the use of calibrated control rods as well as period measurements; the principle is the same. The DIH results from differences in both moderating and absorption characteristics between the standard and test bars. The assumption is made that the difference in moderating characteristics is caused only by a difference in the total number

of carbon atoms present in the two bars. An experimentally determined density coefficient of reactivity is used to correct the measured DIH values to a common density so that differences in DIH reflect only differences in absorption characteristics.

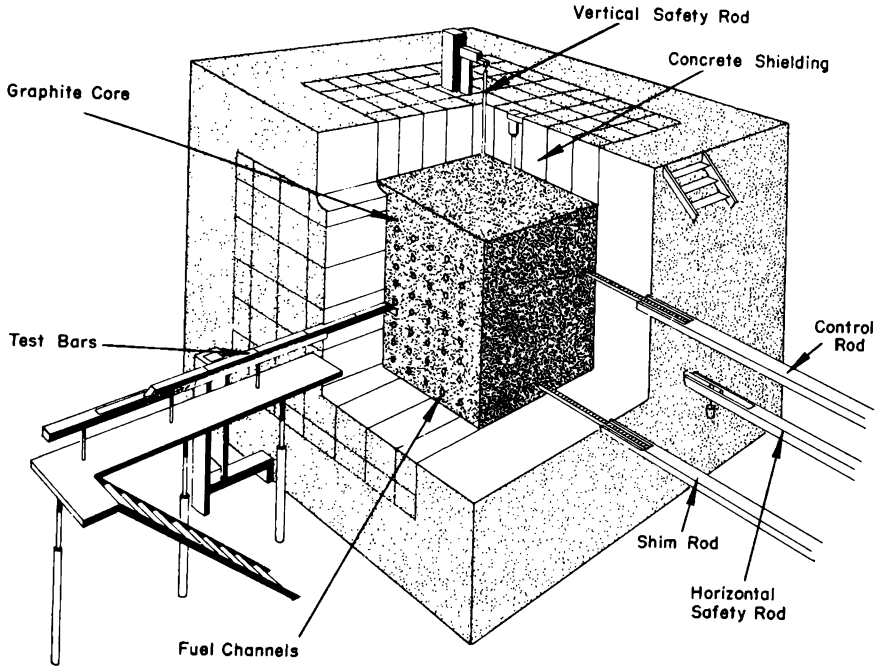


FIG. 4.1 Cutaway view of the Hanford 305 Test Reactor (HTR) showing removable graphite test stringer and control rods. Reactivity measurements and materials testing are performed in this facility.

It is possible to relate changes in DIH values to changes in σ_a by calibrating the reactor. This is done by the addition of a known quantity of an absorber at the sample position. In order to obtain an absolute value of the absorption cross section per carbon atom, one must measure the cross section of the standard bar in some other manner because it is difficult to eliminate the effects of sample moderation on the reactivity of the HTR. This calibration has been done⁵ for the HTR, and the relation between DIH values and the average absorption cross section per carbon atom for thermal neutrons (2200 meters/sec) in millibarn units is:

$$\sigma_a(2200 \text{ meters/sec}) = 4.47 \pm 0.04 - (0.733 \text{ DIH} \pm 0.03) \quad (4.20)$$

4-3.2 OTHER REACTOR METHODS

The pile-oscillator technique¹⁸ depends upon the change in reactivity that occurs when a sample of an absorber is rapidly oscillated between

two points in a reactor. The resulting oscillation in the reactor power, either locally or over the entire reactor, is measured as a function of time. The amplitude of the oscillation is proportional to the neutron-absorption rate in the sample. It is thus possible to measure the absorption cross section of a sample relative to that of a known absorber.

It is possible in some cases to detect a phase difference between the signals that result from the absorption and scattering characteristics of the sample and, in this way, to separate the effects.

One advantage of the pile-oscillator method over the danger-coefficient method is that the consequence of rapid random atmospheric changes on the reactivity has much less effect on the experimental result. A second advantage is that a smaller sample can be used effectively.

Another method that can be used to obtain an absorption cross section for graphite is a diffusion-length measurement of a graphite stack. A value of Σ_a can be obtained from Eq. 4.9 if Σ_{tr} is known. It is also possible, in principle, to detect trace amounts of some contaminants by irradiating graphite with neutrons and observing the radioactivity of the contaminants either with or without chemical separation. Up to the present time, these methods have not been applied to graphite to any great degree.

4-3.3 COMPARISON OF REACTOR METHODS

A comparison of the danger-coefficient and pile-oscillator methods and standards has recently been completed on American, British, and French graphites.⁵ The absorption cross sections determined in the HTR, the British GLEEP, and the French ZOE are listed in Table 4.2. The measurements in GLEEP were made by the danger-coefficient method. The absolute cross-section scale is based upon a series of diffusion-length experiments performed at Harwell on graphite blocks and measured in GLEEP. The error of ± 0.30 mb arises from the error in diffusion-length measurements. The pile-oscillator method was used in ZOE. The error of ± 0.15 mb includes all systematic errors.

Each lot of graphite listed in Table 4.2 consisted of from four to eight bars. The French values for lot VI were obtained by measuring in ZOE pieces cut from the ends of the bars before they were sent to Hanford. As a general rule, extremities of bars are somewhat less pure than the central part.¹⁹ On the average this difference amounts to 0.05 mb for the French bars. However, this does not provide the complete explanation for the differences in the French and American scales as deduced from the measurements in Table 4.2.

Because the purpose of these measurements was to compare experimental methods and standards, the graphites tested are not necessarily typical of the general purity level of French, British, and American graphites. The significant information is the rather good agreement of the tests made at the three laboratories on the same lots of graphite.

Table 4.2 — COMPARISON OF HTR, GLEEP, AND ZOE GRAPHITE ABSORPTION-CROSS-SECTION MEASUREMENTS⁵

Graphite lot	Cross section, mb		
	HTR	GLEEP	ZOE
I (American)	3.51 ± 0.06	3.63 ± 0.30	
II (American)	3.65 ± 0.06	3.75 ± 0.30	
III (American)	3.54 ± 0.06		3.65 ± 0.15
IV (British)	3.67 ± 0.06	3.76 ± 0.30	
V (British)	3.93 ± 0.06	4.12 ± 0.30	
VI (French)	3.53 ± 0.06		3.80 ± 0.15

4-3.4 NUCLEAR PURITY BY CHEMICAL ANALYSIS

Direct measurement of nuclear purity requires a neutron source, which is often not available. It is possible to estimate the purity of graphite from a knowledge of the concentrations and cross sections of the impurities. Although the absorption cross sections estimated in this way are not as accurate as those determined by methods described in the previous section, the chemical method has proven very helpful in identifying and minimizing the concentration of high-cross-section impurities during manufacture. Unlike the reactor methods, which do not identify the impurities or their concentrations, the chemical method provides a means of determining the effect of each processing step and each raw material on the nuclear purity.

A knowledge of the concentration of each impurity is also necessary before an estimate can be made of the rate at which the impurities will be removed by neutron absorption during the operation of the reactor. This rate is a function not only of the concentration and cross section of the impurities initially present, but also of the cross sections and half lives of their nuclear-reaction products.

A method of describing the neutron-absorption properties of impure carbon has been suggested by Strocchi et al.²⁰ The microscopic absorption cross section for graphite (σ_a) in terms of the cross sections for pure carbon (σ_c) and the cross sections of the impurities (σ_i) is given by

$$\sigma_a = \frac{M_c N (\sigma_c / A_c) + 10^{-6} N M_c \left[\sum_i C_i (\sigma_i / A_i) \right]}{M_c N / A_c} \quad (4.21)$$

where C_i is the concentration of the i th impurity in parts per million by weight of carbon, M_c is the mass of carbon, A_c and A_i are the atomic weights of carbon and the impurity, respectively, and N is the Avogadro number. This reduces to

$$\sigma_a = \sigma_c + 10^{-6} A_c \left[\sum_i C_i (\sigma_i / A_i) \right] \quad (4.22)$$

Table 4.3 — THERMAL-NEUTRON-ABSORPTION CROSS SECTION
AND GRAPHITE POISONING FACTOR FOR THE FIRST EIGHTY-THREE
ELEMENTS OF THE PERIODIC TABLE

Atomic number	Element	σ_a at 2200 meters/sec, barns	Atomic wt.	ℓ , ppm ⁻¹
1	H	0.332	1.0080	0.116
1	D	0.00046	2.0150	0.000080
2	He	0	4.003	0
3	Li	71	6.940	3.61
4	Be	0.010	9.013	0.00039
5	B	755	10.82	24.7
6	C	0.0034	12.011	
7	N	1.88	14.008	0.0474
8	O	<0.0002	16.000	<0.0000044
9	F	<0.010	19.00	<0.00019
10	Ne	<2.8	20.183	<0.049
11	Na	0.505	22.991	0.00776
12	Mg	0.069	24.32	0.00100
13	Al	0.230	26.98	0.00301
14	Si	0.16	28.09	0.0020
15	P	0.20	30.975	0.0023
16	S	0.52	32.066	0.0057
17	Cl	33.8	35.457	0.337
18	A	0.66	39.944	0.0058
19	K	2.07	39.100	0.0187
20	Ca	0.44	40.08	0.0039
21	Sc	24.0	44.96	0.189
22	Ti	5.8	47.90	0.043
23	V	5.0	50.95	0.035
24	Cr	3.1	52.01	0.021
25	Mn	13.2	54.94	0.0849
26	Fe	2.62	55.85	0.0166
27	Co	38.0	58.94	0.228
28	Ni	4.6	58.71	0.028
29	Cu	3.85	63.54	0.0214
30	Zn	1.10	65.38	0.00594
31	Ga	2.80	69.72	0.0142
32	Ge	2.45	72.60	0.0119
33	As	4.3	74.91	0.020
34	Se	12.3	78.96	0.0550
35	Br	6.7	79.916	0.030
36	Kr	31	83.8	0.13
37	Rb	0.73	85.48	0.0030
38	Sr	1.21	87.63	0.00487
39	Y	1.31	88.92	0.00520
40	Zr	0.185	91.22	0.000716
41	Nb	1.16	92.91	0.0044
42	Mo	2.70	95.95	0.0099
43	Tc	22	98.939	0.079
44	Ru	2.56	101.1	0.00894
45	Rh	149	102.91	0.511

Table 4.3 (Continued)

Atomic number	Element	σ_a at 2200 meters/sec, barns	Atomic wt.	f , ppm ⁻¹
46	Pd	8.0	106.7	0.026
47	Ag	63	107.880	0.21
48	Cd	2450	112.41	7.699
49	In	191	114.82	0.588
50	Sn	0.625	118.70	0.0019
51	Sb	5.7	121.76	0.016
52	Te	4.7	127.61	0.013
53	I	7.0	126.91	0.019
54	Xe	35	131.30	0.094
55	Cs	28	132.91	0.0744
56	Ba	1.2	137.36	0.00308
57	La	8.9	138.92	0.023
58	Ce	0.73	140.13	0.0018
59	Pr	11.3	140.92	0.0283
60	Nd	46	144.27	0.11
61	Pm			
62	Sm	5600	150.35	13.16
63	Eu	4300	152.0	9.99
64	Gd	46000	157.26	103.33
65	Tb	46	158.93	0.102
66	Dy	950	162.51	2.065
67	Ho	65	164.94	0.14
68	Er	173	167.27	0.365
69	Tm	118	168.94	0.247
70	Yb	37	173.04	0.076
71	Lu	112	174.99	0.226
72	Hf	105	178.58	0.207
73	Ta	21	180.95	0.041
74	W	19.2	183.86	0.0369
75	Re	86	186.22	0.16
76	Os	15.3	190.2	0.0284
77	Ir	440	192.2	0.809
78	Pt	8.8	195.09	0.015
79	Au	98.8	197.0	0.177
80	Hg	380	200.61	0.669
81	Tl	3.4	204.39	0.0059
82	Pb	0.170	207.21	0.000280
83	Bi	0.034	209.00	0.000057

The effect of individual impurities on the absorption properties is evaluated by defining a poisoning factor (f_i) for each impurity

$$f_i = 10^{-4} \frac{\sigma_i/A_i}{\sigma_c/A_c} \quad (4.23)$$

The factor f_i is actually the percentage of increase in the absorption cross section of carbon resulting from 1 ppm of the impurity element.

When f_i is substituted in Eq. 4.22, σ_a becomes

$$\sigma_a = \sigma_c \left[1 + 0.01 \left(\sum_i C_i f_i \right) \right] \quad (4.24)$$

The value of σ_c to be used in Eqs. 4.23 and 4.24 has not been established. Strocchi²⁰ used the value of $\sigma_c = 3.2$ mb to calculate the poisoning factors. Although the most recent value recommended by Hughes et al.²¹ is 3.73 ± 0.07 mb, this would appear to be high. A value of 3.4 ± 0.3 listed in an earlier report²² seems more probable and therefore has been used in tabulating the poisoning factors for the first 83 elements of the periodic table (Table 4.3).

The precision of the measurement of σ_a by Eq. 4.24 is determined by the completeness of the chemical analysis and the precision of the individual determinations of the various elements. The contribution of each impurity to the uncertainty in σ_a is $0.01 \sigma_c f_i \Delta C_i$, where ΔC_i is the uncertainty in C_i . For each $f_i \Delta C_i$ to be of the same order of magnitude, greater analytical accuracy (smaller ΔC_i) is required for elements with large f_i . In other words, the accuracy required in the analysis of an impurity is inversely proportional to the poisoning factor of that impurity.

Many elements with low poisoning factors at the concentration levels normally found in nuclear graphites contribute less to σ_a than the uncertainty in σ_a resulting from the limits of precision attainable on elements such as boron and certain rare earths with high poisoning factors. This is illustrated for a hypothetical graphite with an ignited-ash concentration of 300 ppm and an uncertainty in the boron determination of 0.1 ppm. The uncertainty in the boron determination results in an uncertainty in σ_a of 0.084 mb. In this case the contribution of silicon is comparatively insignificant, even if all the ignited ash is considered to be silica, since 300 ppm of silica would increase σ_a by only 0.0095 mb.

4-3.5 IMPURITIES IN NUCLEAR GRAPHITES

Elements that may contribute significantly to an increase in σ_a because of their high cross sections or high concentration in graphite include the following (see also Table 2.8):

Hydrogen. Hydrocarbons in the raw materials contribute traces of hydrogen that vary with the heat-treatment temperature and activity of the graphite surface. In material graphitized to 3000°C, the hydrogen content is probably below 50 ppm, which corresponds to a contribution of less than 0.22 mb to σ_a . Inadvertent contact with water or exposure to a humid atmosphere will result in an additional amount of hydrogen impurity as adsorbed water (Sec. 6-8.3).

Boron. The high absorption cross section of boron and the difficulty with which it is removed during purification make it the most important factor in determining the purity of nuclear graphite. Control of the boron content extends from the raw materials to the packing materials used in baking and

graphitizing furnaces, and even to the soaps used in laundering clothing worn by those in the machine shop. The boron concentration of thermally purified graphite is approximately 0.5 ppm; at this concentration boron contributes 0.42 mb to σ_a .

Nitrogen. Nitrogen is present in the gas contained in the pores of graphite. For a material with a bulk density of ρ_B , the contribution to σ_a based on the assumption that all pores are filled with air at standard conditions takes the form²³

$$(\Delta\sigma_a)_N \approx 1.466 \left(\frac{1}{\rho_B} - \frac{1}{2.25} \right) \text{mb} \quad (4.25)$$

For a graphite with $\rho_B = 1.7 \text{ g/cm}^3$, the contribution to σ_a is 0.215 mb.

Chlorine. Chlorine is present in some gas-purified graphites. Radiometric determinations by West²⁴ on graphites from various sources indicated the presence of 0.6 to 35 ppm of chlorine, corresponding to a contribution to σ_a of from 0.007 to 0.39 mb.

Titanium and Vanadium. These elements can usually be neglected in gas-purified graphites. In thermally purified graphites with an ignited-ash weight in excess of 50 ppm, they become important. In thermally purified graphite titanium and vanadium vary from 10 to 20 and 8 to 140 ppm, respectively,²⁰ with corresponding contributions to σ_a of 0.015 to 0.029 mb and 0.0095 to 0.167 mb.

Rare Earths. Accurate determinations for the rare-earth elements cannot presently be obtained with normal analytical methods. Gadolinium, with a cross section of 46,000 barns, as well as some of the other rare earths, requires analyses based on radioactivation for successful determination.²⁵⁻²⁹ Such analyses are expensive and time consuming and are not amenable to routine control. The uncertainty in the concentration of the rare earths presents a serious defect in the evaluation of the nuclear purity of graphite by the chemical method. However, removal of the rare earths through halogenation at high temperature permits use of the chemical method for gas-purified graphites with a greater degree of confidence. The concentrations of europium and samarium in the best gas-purified graphites have been found to be only about 1 per cent of those in typical unpurified materials.²⁹

4-3.6 APPLICATION OF THE CHEMICAL METHOD

A comparison of the results of the chemical method and the reactor method for a gas-purified and a thermally purified graphite is illustrated in Table 4.4. First, the DIH was measured in the HTR, and then chemical analyses were performed. No rare-earth determinations were included. In each case the HTR measurements were made on two bars, only one of which was later sampled for chemical analysis.

The cross sections determined from chemical analysis and those from

the DIH agree quite well in this case. Unfortunately a complete chemical analysis and the DIH have not been obtained on a sufficient number of samples to establish whether agreement within the indicated uncertainties is fortuitous.

As indicated in the previous section, limitations of the chemical method are inherent in the accuracy and completeness of the determination. Many

Table 4.4 — COMPARISON OF CHEMICAL AND REACTOR METHODS OF DETERMINING σ_a FOR TWO GRAPHITES [†]

Reactor Method				
Sample	DIH	σ_a (from Eq. 4.20), mb		
SP7B	1.108	3.65 \pm 0.05		
SP24B	0.265	4.27 \pm 0.05		
Chemical Method				
Impurity	Concentration, ppm		$C_i f_i$	
	SP7B	SP24B	SP7B	SP24B
Al	2.0	1.0	0.0060	0.0030
Ca	5.0	11.0	0.0190	0.0418
B	0.02	0.7	0.4940	17.2900
Fe	3.0	2.9	0.0498	0.0481
V	0.25	9.3	0.0088	0.3255
Ti	0.5	4.2	0.0215	0.1806
Si	6.0	10.0	0.0120	0.0200
S	13.0	4.0	0.0741	0.0228
			$\Sigma C_i f_i =$ 0.6852	17.9318
σ_a (from chemical analysis and Eq. 4.24), mb			3.42 \pm 0.30 [†]	4.01 \pm 0.35
σ_a (with contribution from nitrogen), mb			3.68 \pm 0.30	4.21 \pm 0.35

[†] The graphites were manufactured by and chemical analyses were performed by the Speer Carbon Co., Niagara Falls, N. Y. See Table 6.23 for a description of these samples.

[‡] Uncertainties in values from chemical analysis are only those derived from the uncertainty of σ_a .

new or improved methods of analysis have been developed as a result of these limitations.²⁴⁻³⁵ Variations in graphite purity with position in a graphitizing or purifying furnace have been noted.³⁶ The nature of these variations in a particular process must be determined before a routine sampling plan can be established. Because of further inhomogeneity of impurities in individual bars, the best correlation between chemical and reactor methods is obtained if the sampling for the chemical method is done after the entire test bar is reduced to a granular powder and thoroughly

blended.³⁷ Some prefer to reduce the bar to fines by drilling. The chemical method is, then, a destructive test; bars tested by the reactor methods, however, can be utilized in reactor construction.

Effective solution of problems in controlling the purity of nuclear graphite often requires the utilization of several methods of analysis. The use of chemical, radioactivation, and reactor methods is illustrated in the following case which occurred early in 1948 when the first gas-purified or "finished" heats were being tested. At that time the letter *F* was added to the graphite identification system to denote finished graphite, and the expression "F process" became common terminology. DIH values of the first two heats (CSF-1 and 2) from the Morganton, N. C., plant, operated at that time by National Carbon Company, averaged $+0.50$ and $+0.30$, respectively. These values were somewhat disappointing since earlier trial runs at Bay City, Mich., where the process was developed³⁸ had resulted in DIH values as high as $+0.90$. The gas distribution was observed to be poor in heat CSF-1 but satisfactory in CSF-2.

Bars from heat CSF-1 contained from 10 to 60 ppm of ash, whereas bars from CSF-2 contained only 2 ppm of ash. The analytical results at first appeared to be inconsistent with DIH values since low ash values as in CSF-2 were normally associated with much higher DIH values than $+0.30$. Further tests, revealing the distribution of impurities in the furnaces, led to the conclusion that the purifying chlorine gas was suspect. If some of the chlorine remained in the graphite bars, its high absorption cross section (33,800 mb) could account for low DIH values on bars with low ash content. It was decided to analyze for chlorine content by measuring the induced radioactivity. Samples from bars for which DIH had been determined and a standard of high-purity graphite to which a known amount of calcium chloride had been added were irradiated. The induced radioactivity was measured as a function of time to determine whether any Cl^{38} activity with a 37.3-min half life was present. After several days the longer half lives were identified, and the activity with a 37.3-min half life was separated by graphical analysis. Absorption measurements of the beta energy were in agreement with literature values for Cl^{38} , and, from the strength of the activity, the concentration of chlorine was calculated. It was clear that most of the difference between DIH and previous analytical results had been due to the presence of undetected chlorine. The difficulties with residual chlorine were eventually eliminated by discontinuing the addition of chlorine to the purifying furnace at a higher temperature to allow the chlorine to escape before the furnace had cooled.

From this example it is clear that normal analytical techniques are not always sufficient to permit a useful estimate of the absorption cross section of graphite, particularly in instances where high-cross-section impurities are not detected.

References

1. C. A. Mansius, Irradiation Processing Department, General Electric Company, personal communication, 1960.
2. A. M. Weinberg and E. P. Wigner, *The Physical Theory of Neutron Chain Reactors*, The University of Chicago Press, Chicago, Ill., 1958.
3. S. Glasstone and M. C. Edlund, *The Elements of Nuclear Reactor Theory*, D. Van Nostrand Co., Inc., Princeton, N. J., 1952.
4. S. Glasstone, *Principles of Nuclear Reactor Engineering*, p. 486, D. Van Nostrand Co., Inc., Princeton, N. J., 1955.
5. P. F. Nichols, Absorption Cross Section of Graphite, *Nuclear Sci. and Eng.*, **7**: 395-399 (1960).
6. J. E. Wills, Jr., et al., Scattering of Fast Neutrons from C^{12} and F^{19} , *Phys. Rev.*, **109**: 891-897 (1958).
7. F. Ajzenberg and T. Lauritsen, Energy Levels of Light Nuclei. V. *Rev. Mod. Phys.*, **27**: 77-166 (1955).
8. W. H. Zinn, Diffraction of Neutrons by a Single Crystal, *Phys. Rev.*, **71**: 752-757 (1947).
9. H. L. Anderson et al., Method for Measuring Neutron-absorption Cross Sections by the Effect on the Reactivity of a Chain-reacting Pile, *Phys. Rev.*, **72**: 16-23 (1947).
10. R. R. Coveyou et al., Effect of Moderator Temperature Upon Neutron Flux In Infinite, Capturing Medium, *J. Nuclear Energy*, **2**: 153-167 (1956).
11. E. R. Cohen, A Survey of Neutron Thermalization Theory, in *Proceedings of the First United Nations International Conference on the Peaceful Uses of Atomic Energy, Geneva, 1955*, Vol. 5, pp. 405-416, United Nations, New York, 1956.
12. G. B. Gavin, Determination of the Neutron Temperature at the Center of the Thermal Test Reactor, *Nuclear Sci. and Eng.*, **2**: 1-13 (1957).
13. M. Küchle, Neutron Temperature Measurements in Graphite, *Nuclear Sci. and Eng.*, **2**: 87-95 (1957).
14. G. M. Branch, *Neutron Temperature Measurements in Graphite and in a Uranium-Graphite Reactor*, USAEC Report MDDC-747, 1946.
15. R. A. Bennett and R. E. Heineman, Neutron Rethermalization Cross Section Measurements in Graphite, *Nuclear Sci. and Eng.*, **8**: 294-299 (1960).
16. A. M. Weinberg and E. P. Wigner, *The Physical Theory of Neutron Chain Reactors*, p. 488, The University of Chicago Press, Chicago, Ill., 1958.
17. R. C. Lloyd et al., Variation of Graphite Diffusion Length with Temperature, *Nuclear Sci. and Eng.*, **4**: 690-697 (1958).
18. A. M. Weinberg and H. C. Schweinler, Theory of Oscillating Absorber in a Chain Reactor, *Phys. Rev.*, **74**: 851-863 (1948).
19. H. Hering, Commissariat à l'Énergie Atomique, Centre d'Études Nucléaires, Saclay, France, personal communication, 1959.
20. P. M. Strocchi et al., L'analisi chimica nel controllo di qualità della grafite nucleare, *Energia nucleare (Milan)*, **5**: 815-823 (1958); translated in British Report IGIS-90 (RD/C), 1960.
21. D. J. Hughes et al., *Neutron Cross Sections*, USAEC Report BNL-325 (Suppl. 1), Brookhaven National Laboratory, Jan. 1, 1960.
22. D. J. Hughes and R. B. Schwartz, *Neutron Cross Sections*, USAEC Report BNL-325 (2nd ed.), Brookhaven National Laboratory, July 1, 1958.
23. P. F. Nichols, Absorption Cross Section of Graphite, *Nuclear Sci. and Eng.*, **7**: 395-399 (1960).

24. J. M. West, *Purification of Graphite*, USAEC Report HW-12780 (Rev.), Hanford Works, Mar. 21, 1949.
25. L. R. Bunney et al., Radiochemical Procedure for Individual Rare Earths, *Nucleonics*, **15**(2): 81-83 (1957).
26. G. I. Born et al., The Solution of Certain Analytical Problems in the Rare Earths by Radioactive Analysis, *Trudy Komissii Anal. Khim. Akad. Nauk. SSSR. Inst. Geokim. i Anal. Khim.*, **7**: 104-118 (1956).
27. A. M. Ross, *The Identification and Determination of Trace Amounts of Rare Earths in Graphite by Neutron Activation*, USAEC Report HW-14337, Hanford Works, Sept. 1, 1949.
28. G. E. Boyd et al., *Graphite Purity Research Program*, USAEC Report CC-976, University of Chicago, Dec. 22, 1943.
29. G. E. Boyd, *The Analysis of Graphite*, USAEC Report TID-5244, Apr. 17, 1946.
30. W. H. Johnston, *Graphite Program*, USAEC Report DuH-10641, E. I. Du Pont de Nemours & Co., July 15, 1943. (Classified)
31. P. W. Leppa and R. F. Markel, *F Process Final Report*, USAEC Report AECD-3759, Great Lakes Carbon Corp., Mar. 15, 1951.
32. R. E. Tate, *Report on Graphite*, Report NEPA-275, Fairchild Engine and Airplane Corp., Aug. 7, 1947. (Classified)
33. H. Hering, *Contrôle de Pureté du Graphite et de l'eau Lourde*, French Report CEA-1094, February 1959.
34. D. M. Robertson, *An Analytical Method for Sulphur in Nuclear Reactor Graphite*, USAEC Report HW-65522, Hanford Atomic Products Operation, June 6, 1960.
35. R. Ko, *Spectrographic Determination of Impurities in Nuclear Grade Graphite*, USAEC Report HW-66219, Hanford Atomic Products Operation, July 26, 1960.
36. W. C. Riley and A. M. Corners, *Effect of Process Variables on Graphite Purity*, USAEC Report HW-32497, Hanford Atomic Products Operation, July 20, 1954.
37. V. L. Redding, *Report on Graphite Testing for DR Pile*, USAEC Report HW-13118, Hanford Works, Mar. 29, 1949. (Classified)
38. L. Brooks, *Graphite Purification*, U. S. Patent No. 2,734,800, Feb. 14, 1956.

Structure

R. E. NIGHTINGALE†

The allotropic forms of crystalline carbon, diamond, and graphite occur in nature and can be synthesized. The crystalline form of diamond is face-centered cubic. Each atom is surrounded by four nearest neighbors at the corners of a regular tetrahedron. The smallest interatomic distance is 1.54 Å, which corresponds very closely to that found in aliphatic hydrocarbons. In fact, the diamond crystal represents the ultimate structure in a three-dimensional aliphatic carbon polymer. The crystal density of diamond (3.53 g/cm³) is somewhat higher than that of graphite (2.26 g/cm³). The three-dimensional system of strong C—C bonds produces the hardest material known.

In striking contrast to diamond, graphite is a soft electrically conducting material and, at ordinary temperatures and pressures, is thermodynamically slightly more stable. Graphites with a wide range of crystalline development can be manufactured. Those carbons in which the graphitic structure is not completely developed or in which the graphitic structure is limited to volumes on the order of a few thousand cubic angstroms are usually referred to as "amorphous carbons." Those in which the crystallites have been more highly ordered by heat-treatment at 2500 to 3000°C are referred to as "graphites."

5-1 Structural Units and Nomenclature

The nomenclature used in describing the structure of carbons has not been standardized; thus it is not uncommon to find a given term used in several ways in the graphite literature. Several terms that will be used in this and subsequent chapters to describe the structural units are defined below; some of these are illustrated in Fig. 5.1.

Crystallite (or crystal): Unit of the structure in which atoms are arranged in a characteristic, periodic array. The crystallite may contain small distortions due to structural defects (vacancies, interstitial atoms, impurities, dislocations, twinning, etc.). Crystals are impermeable to gases at ordinary temperatures.

Crystallite size: Apparent average size of crystallites as measured by X-ray

† Hanford Laboratories, General Electric Company, Richland, Wash.

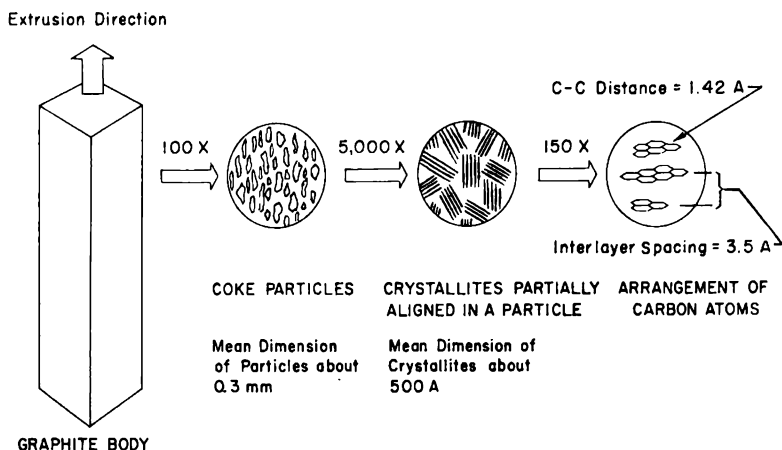


FIG. 5.1 The substructures of polycrystalline graphite. (From Davidson and Losty, *Mechanical Properties of Non-Metallic Materials*, Interscience Publishers, Inc., Ref. 1.)

diffraction methods, which assume cylindrical shape. (See Sec. 5-5 for discussion of physical significance.)

Coke particle (or grain): Discrete coke particles comprising the base aggregate in the green-mix formulation. Sizes vary over wide range (<0.074 to 6 mm). Smallest particles (<0.074 mm) are referred to as "flour." Anisotropy and shape are dependent upon the nature of the coke.

Graphitized particle (or grain): The graphitized coke particle. In the graphitized body it is infused with and surrounded by unaligned binder carbon. The graphitized particle contains regions in which the crystallites may be highly aligned.

Pores: The voids between crystallites, particles, and disorganized carbon. They may range in size from 10 Å or more to many microns. Closed pores are inaccessible to fluids.

Body: The formed piece. Properties of the graphite body are referred to as bulk or macroscopic properties.

Electrographite: Polycrystalline graphite usually manufactured from a petroleum-coke binder and graphitized in Acheson electric furnaces. Often referred to as "artificial graphite."

Nuclear graphite: A special grade of electrographite used (or of potential use) as a reactor core or reflector material. Raw materials and manufacturing processes are chosen to give desirable purity and structural characteristics.

To completely characterize the smallest unit, the perfect crystal (or crystallite), one must locate the atoms in the space lattice and describe the forces between atoms. In addition, since all graphites of industrial importance are composed of crystals of limited size containing imperfections of various types, the crystal size and perfection must be considered.

The average dimensions of relatively perfect crystallites in polycrystalline electrographites are of the order of 500 Å; however, they may vary in size from very small units of approximately 20 to 50 Å to several thousand angstroms.

The crystallites themselves are interconnected in varying degrees by chemical bonds and by weaker long-range forces. The packing of crystallites and of binder and filler phases is never perfect; there is always a system of pores. Although in the strictest sense the pore structure pertains not to the graphite but to the voids in the structure, the number and size of the pores are determined by the way the crystallites are packed and by the nature of the bonding between the filler and binder phases. Thus a knowledge of the size distribution of pores is helpful in characterizing the structure of graphite on a somewhat larger scale than the crystal structure.

On an even larger scale, the particles, disordered regions, and larger voids of the graphite body can be observed with the optical and electron microscopes. A description of the structure will be developed in subsequent sections of this chapter in terms of the structural units defined above: crystallites, particles, and pores.

5-2 Crystal Structure

The hexagonal crystal structure of graphite, as first proposed by J. D. Bernal² in 1924, is shown in Fig. 5.2. The two most important structural

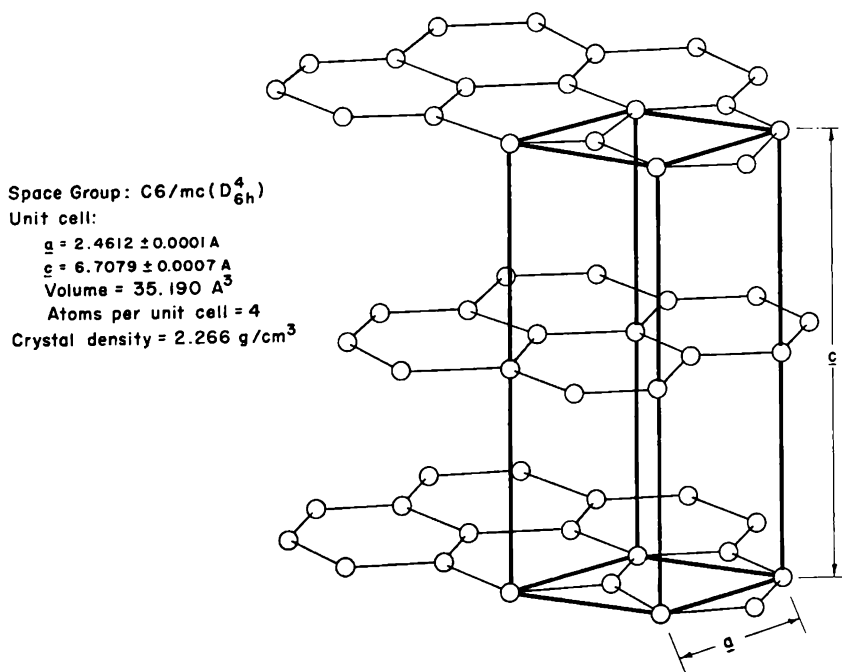


FIG. 5.2 Crystal structure of graphite.

features that give graphite many of its unique properties are: (1) the system of strong chemical bonds forming large sheets of hexagonal rings in which the electrons are quite mobile and (2) the large spacing between carbon layer planes. The extended ring structure is a logical one if the formation of graphite is considered to proceed by the growth of larger and larger molecules of the condensed benzene-ring system. Within the planes the C—C bond lengths are all equal (1.42 Å) and are close to the C—C bond length (1.39 Å) found in benzene.

The stacking of layer planes in the hexagonal structure is ABAB . . . ; i.e., layers in which every atom has an atom directly above it are separated by one layer. The occurrence of extra lines on X-ray powder photographs suggests that about 5 per cent of the graphite has a second type of stacking, i.e., ABCABC . . . for which the unit cell is rhombohedral.³ The relation between the hexagonal and rhombohedral forms of graphite is similar to the relation between the hexagonal and cubic close packing of spheres. When related to a normal hexagonal *c* axis, the rhombohedral unit cell has a height of $3/2 c$, giving rise to the extra X-ray lines.

5-3 Forces Within Crystallites

It is clear from both the crystal structure and the properties of graphite that the forces operating between atoms in a layer plane are due to strong chemical bonds, whereas those forces operating between the layer planes themselves are weak. The chemical forces between atoms can be described in terms of the hybridization of atomic orbitals.⁴ In diamond and saturated hydrocarbons four sp^3 hybrid orbitals are formed from the excited state of carbon, $1s^2 2s 2p_x 2p_y 2p_z$, by the combination of one *s* orbital and the three *p* orbitals. In the lowest energy state of such a combination, all bonds are equal and extend toward the corners of a regular tetrahedron. Each bond is effectively localized, thereby leaving few electrons free to move throughout the structure. This results in a very low electrical conductivity. The directional nature of the bonds produces an open structure with each atom occupying a relatively large volume. This open structure, which is possible only when directional forces are operative, is evidence that the bonds are molecular in character, as distinct from those found in ionic or metallic crystals.

The graphite structure is due to a second type of combination of the atomic orbitals of carbon called trigonal, or sp^2 , hybridization. One of the original *p* orbitals is left unchanged and three hybrid orbitals are formed by combination of the $2s$, $2p_x$, and $2p_y$ atomic orbitals. The lowest energy state of this combination gives three equivalent bond orbitals directed in a plane at angles of 120° . The third unused *p* orbital forms a π bond perpendicular to the planar system of sp^2 bonds. The nature of the π bond is such that the electrons are quite mobile in any given layer plane. In this sense graphite resembles a two-dimensional metal, a fact that is more fruitfully

exploited in terms of the electronic band structure of graphite (Sec. 6-3). The X-ray diffraction intensities of graphite indicate that the electron cloud around the carbon nucleus is slightly flattened, as might be expected if the electron density is concentrated in the plane of the carbon layers (Sec. 9-1.6). Because the bonding electrons are all used in forming C—C bonds within the carbon layers, the layers themselves are held together only by weak van der Waals forces. The bond strengths within the layer planes are approximately 150 kcal/gram atom (i.e., an average C—C bond strength of 100 kcal/mole), whereas the interlayer binding energy is estimated⁵ to be only 1.3 kcal/gram atom. This low binding energy is responsible for the compressive properties of graphite and the ease with which the planes can be separated by interstitial atoms. In fact, as will be seen in Chap. 6, most of the properties of graphite, i.e., semimetallic character, expansion, heat stability, strength, chemical reactivity, color, softness, and anisotropy, can be understood, at least in a qualitative way, from a knowledge of the types of forces operating between atoms.

5-4 X-ray Diffraction by Polycrystalline Graphite

The crystal symmetry and unit cell dimensions of graphite are derived from analysis of X-ray diffraction lines. It is also possible to obtain information from X-ray diffraction on the crystallite thickness and radius, the degree of preferred orientation, and the existence of stacking defects. Because X-ray studies have contributed so much to the understanding of radiation effects in graphite, it will be useful at this point to review briefly the fundamentals of X-ray diffraction as applied to graphite. Only those topics that may be helpful in guiding nonspecialists around confusing points or pitfalls in the use of X-ray data will be discussed. Several corrections must be made to the X-ray data from poorly crystallized carbons to obtain physically meaningful results.⁶ Because these corrections are not necessary for nuclear graphites, which are usually quite well crystallized, they will not be considered further. A standard text on X-ray diffraction should be consulted for more details on methods and interpretation.

Since two indexing systems have been used in describing the planes of hexagonal crystals, some confusion concerning the designation of crystallographic planes in graphite may have arisen for those who, although not X-ray diffraction specialists, have found it necessary to acquire some understanding of the basic principles and nomenclature.

The Miller indices utilize three numbers, h , k , and l , to define the crystal planes.[†] They are applicable to all crystal systems. The Bravais-Miller index system, employing four numbers, h , k , i , l , is applicable only to

[†] The Miller indices of a plane, h , k , and l , are the reciprocals of the intercepts of the plane on the axes in terms of the unit distances, a , b , and c , between lattice points. These distances become a , a , c in the particular instance of a hexagonal structure (Figs. 5.2 and 5.3).

hexagonal crystals. The additional index, i , is derived from a third coordinate axis lying in the plane x - y and making an angle of 120° with the positive y axis. The four Bravais-Miller indices are not independent,⁷ being related by the equation $h + k + i = 0$. Since the h , k , and l indices are the

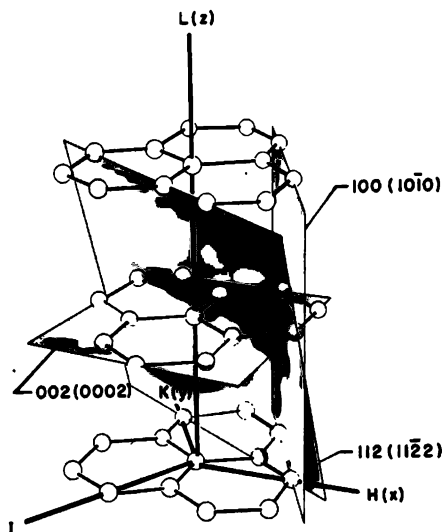


FIG. 5.3 Some prominent planes in the graphite crystal illustrating the Miller and Bravais-Miller indexing systems.

same in both systems, the Miller indices can be obtained from the Bravais-Miller indices by simply dropping the third index, i . Several planes in the hexagonal structure of graphite are shown in Fig. 5.3 to illustrate the relation of the two systems.

5-5 Lattice Dimensions

5-5.1 REFLECTIONS FROM CRYSTAL PLANES

The crystal planes, especially those with a high density of atoms, act as reflecting layers for X rays. It is particularly informative to study the reflection of X rays with wave lengths of the same order of magnitude as the interplanar distances. The condition for reinforcement of the X rays diffracted by the layers is given by the Bragg equation

$$n\lambda = 2d \sin \theta \quad (5.1)$$

where n is equal to the order of reflection, λ is the X-ray wave length, d is the interplanar spacing, and θ is the glancing angle that the incident and diffracted beams form with the plane. The interplanar spacings, which can be related to a and c , are calculated from the angles where diffraction maxima occur. Figure 5.4 shows the microphotometer records of diffraction photographs for a highly graphitic material and a less graphitic material.

In addition to differences in the positions of maxima, which result from slightly different interplanar spacings, it is apparent that lines from the highly crystallized sample are narrower.

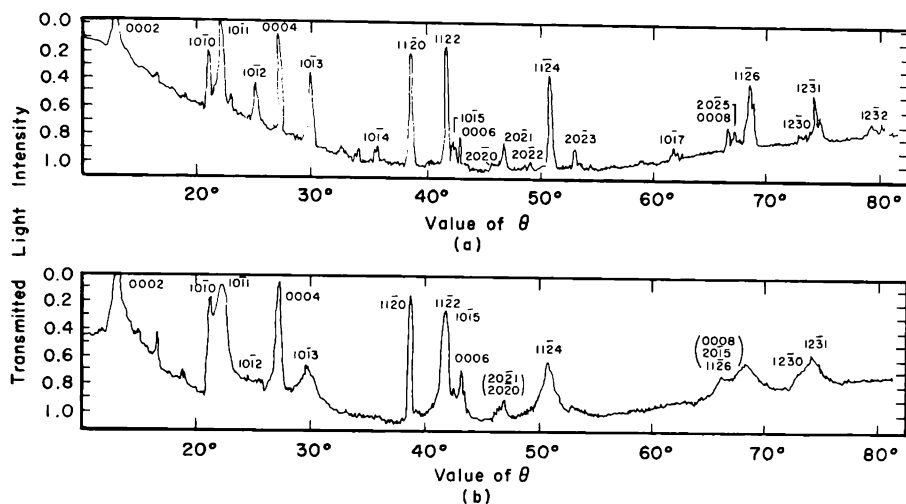


FIG. 5.4 X-ray diffraction lines of two graphites. (a) Highly graphitic material. (b) Less graphitic material.⁸

It is possible, if special precautions are taken, to measure the lattice dimensions of graphite very accurately. Such studies have revealed relatively large differences in the c dimension of various graphites and considerably smaller, though significant, differences in the a dimension.[†] Naturally occurring graphite flakes normally have a smaller c dimension, a slightly larger a dimension, and narrower diffraction lines than electrographites and are therefore considered to be structurally more perfect. The difference is not great for highly crystallized electrographites, however, and in fact Bacon¹⁰ has found in precise measurements of the unit cell dimensions that, of those specimens studied, the most perfect was a manufactured one, having a slightly smaller c dimension than a natural specimen.

5-5.2 LATTICE DIMENSIONS OF NUCLEAR GRAPHITES

Significant differences in the lattice dimensions among polycrystalline graphites are often observed, and detectable differences are always found within a given grade and even within a single bar. Table 5.1 illustrates the differences found in several grades of graphites. The lattice dimension, a , was measured from the (1 1 0) reflection of solid samples after penetration corrections had been made.¹¹ Thin powders, which gave sufficiently intense (0 0 2) reflections, were used to measure c . The table shows that the

[†] The apparent variations in a have been attributed⁹ to differences in stacking disorder, which can give rise to false values of a measured on the (h k 0) reflections.

graphitic structure is most highly developed in the natural flake material and only slightly developed in the calcined coke. KC graphite was manufactured from Kendall coke, a needle type that graphitizes to a high degree at 2800°C (Sec. 2-1.1). The Cleves coke from which CSF was manufactured

Table 5.1 — TYPICAL CRYSTALLITE PROPERTIES OF GRAPHITIC MATERIALS[†]

Material [‡]	$c, \text{\AA}$	$a, \text{\AA}$	$L_c, \text{\AA}$	$L_a, \text{\AA}$
Natural flake	6.719	2.464	940	3100
KC	6.718 ± 0.004	2.463	570 ± 70	1300 ± 400
French S-1 (Pechiney)	6.724	2.464	760	550
CSF	6.728 ± 0.006	2.462	510 ± 27	1650 ± 400
PGA-A201 (British)	6.728	2.464	435	600
PGA-L201 (British)	6.727	2.464	435	400
TSGBF	6.746 ± 0.006	2.462	390 ± 38	900 ± 190
Korite	6.793	2.452	59	220
Calcined Texas coke	6.953		27	
Thermax carbon black	7.165		16	

[†] Standard errors are indicated where a sufficient number of samples have been measured.

[‡] See Table 6.23 for a description of these materials.

[§] L_a is the average layer diameter of the crystallites, and L_c is the average thickness (see Sec. 5-6.1).

graphitizes to a lesser degree. The British and French materials were graphitized at approximately 2800°C. TSGBF was incompletely graphitized at the lower temperature of 2450°C. Korite graphite, although graphitized at 2570°C, was made from a poorly graphitizing Korite coke and therefore

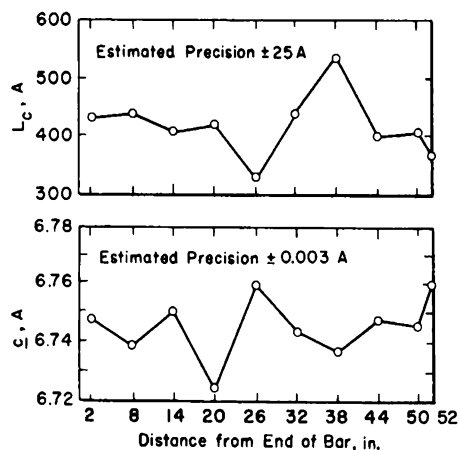


FIG. 5.5 Variations in crystallite properties along the central axis of a Speer gas-purified bar.

did not produce a good graphitic structure. A carbon black and a calcined petroleum coke are included for comparison.

The variation of crystal parameters along the length of the central axis of a Speer gas-purified bar is illustrated in Fig. 5.5. The unmachined bar, which had been extruded in a $4\frac{3}{8}$ -in. square cross section 48 in. long, was selected at random from a production lot. Small amounts of powder were removed along the center of the bar to measure the c spacing and crystallite

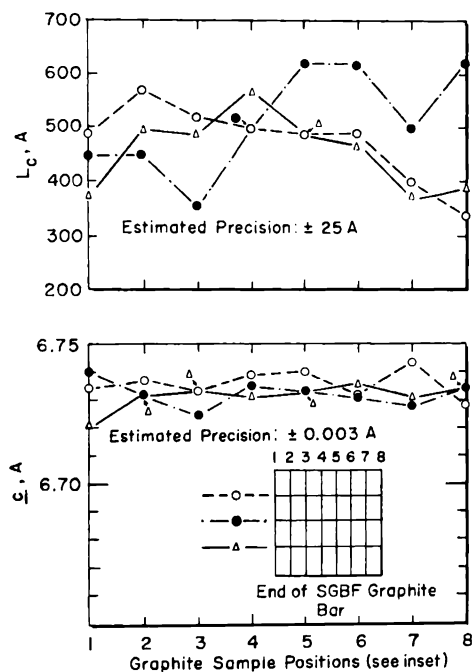


FIG. 5.6 Variations of crystallite properties transverse to the extrusion axis of a Speer gas-purified bar.

size (see Sec. 5-6). Differences are also found transverse to the extrusion axis, as shown in Fig. 5.6. Variations in c of ± 0.015 Å along and across the bar result from slight differences in raw materials and processing conditions and illustrate the need for care in selecting and measuring samples to be used in the study of radiation effects.

5-5.3 THERMAL EXPANSION OF CRYSTALS

The thermal expansion of crystals along the c axis has been measured in several laboratories.¹²⁻¹⁴ The change in interlayer spacing with temperature is shown in Fig. 5.7. Between 0 and 800°C the average coefficient of thermal expansion $[(1/c)(\Delta c/\Delta T)]$ is 28.3×10^{-6} per °C. Since a temperature variation of 1°C results in a change in c of about 0.0002 Å, it is sometimes necessary in very precise work to make corrections to a reference

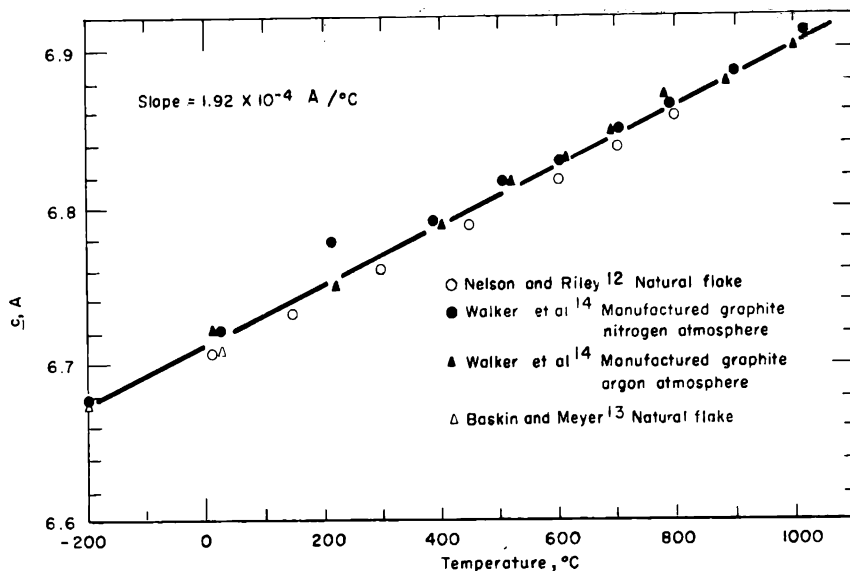


FIG. 5.7 Change in interlayer spacing with temperature.

temperature. The interlayer spacing of graphite exhibits the same temperature dependence in a nitrogen, argon, oxygen, or carbon dioxide atmosphere.

Changes in the a unit cell dimension with temperature are much smaller.¹² The thermal-expansion coefficient is -1.5×10^{-6} per $^\circ\text{C}$ over the range from 0 to 150°C and $+0.9 \times 10^{-6}$ per $^\circ\text{C}$ from 600 to 800°C .

5-6 Lattice Distortions and Dimensions of Crystallites

5-6.1 LINE BROADENING

Studies of the broadening of X-ray diffraction lines have contributed materially toward an understanding of the structural development of polycrystalline graphite and the changes in structure resulting from reactor irradiation. The breadth of diffraction lines is influenced by a number of factors which can be grouped into two classes: instrumental broadening and intrinsic crystallite broadening. The former is due to absorption in the sample, to the use of a nonmonochromatic X-ray source, to the finite size of the receiving slit, and to several geometrical factors whose magnitudes depend upon the equipment and techniques employed. Intrinsic crystallite broadening is due to short-range lattice distortions and to the limited size of the crystallites. Because the measured line broadening is always due to a combination of these two factors, it is necessary to correct for the instrumental broadening to determine the intrinsic broadening characteristic of a given material.

The apparent crystallite size (L) is related to the breadth of the diffraction line by the Scherrer equation

$$L = \frac{K\lambda}{\beta \cos \theta} \quad (5.2)$$

where K is a shape factor approximately equal to 1. The intrinsic breadth, β , must be carefully distinguished from the experimentally measured breadth, B †. The mean layer diameter (measured in the a direction), L_a , is usually determined from the (1 1 0) line, whereas the average thickness (measured in the c direction), L_c , is most commonly measured from the (0 0 2) line. Although the validity of this equation has been verified by a number of investigators, its usefulness in giving physically meaningful information is limited by three major uncertainties: the accuracy with which β can be deduced from B ; the separation of crystallite size and lattice-distortion broadening; and the uncertainty in the value of K . The effects of each of these on crystallite-size measurements in carbons will be considered separately.

5-6.2 DETERMINATION OF β

The most powerful technique for determining the pure diffraction profile of a line, from which β can be measured directly, involves a Fourier analysis of the experimental line profile. However, the Fourier method is time consuming and requires the use of high-speed computing equipment for practical application. A much quicker and generally satisfactory method has been developed by Jones¹⁵ in which the line profile is assumed to have a certain shape. A material whose line breadth is due entirely to instrumental broadening, such as sodium chloride or a highly crystalline natural flake graphite, is used as a standard to determine the contribution of the instrumental broadening to B .

5-6.3 SEPARATION OF SIZE AND DISTORTION BROADENING

In theory it is possible to estimate the relative proportion of crystallite size and lattice-distortion broadening from several orders of reflection since β is a different function of θ for the two cases. If broadening were due entirely to the finite crystallite size, then, from Eq. 5.2, β should be proportional to $\lambda \sec \theta$. If broadening were due to lattice strains, the interplanar spacing would change slightly from the perfect lattice, causing a shift in θ . Application of Eq. 5.1 shows that in this case β is proportional to $\tan \theta$ and independent of λ . The separation of crystallite-size and lattice-distortion effects from the functional dependence of β on θ has not yet been pursued

† The measured breadth, B , is obtained from the experimental line profile by measuring the angular breadth of the line in units of (2θ) degrees at half maximum intensity or by determining an integral line breadth, $\int I(2\theta) d\theta / I_{\max}$. The former method is most easily applied; however, the latter has been recommended by some investigators as being more accurate.

through systematic studies of a wide variety of carbons. It is likely, however, that only in well-developed graphites does broadening from lattice distortion become appreciable. In published values of the crystallite size of unirradiated graphite, it is generally assumed that strain broadening can be neglected, and β is substituted directly into Eq. 5.2 to obtain L . Although L is often calculated in the same way for irradiated graphite, it is likely that much of the line broadening in this case is due to lattice distortion, and L loses much of its physical significance. The separation of size and distortion broadening also becomes much more difficult since the intensities of higher order reflections decrease rapidly with neutron dose (Sec. 9-1.1).

5-6.4 SCHERRER SHAPE FACTOR

The shape factor, K , in Eq. 5.2 can have a range of values depending upon a number of factors. In calculations of L_c from the (0 0 2) line, a value of approximately 1.0 is recommended.⁷ For random layer structures where only two-dimensional lattice reflections of the type (h k) are observed, Warren¹⁶ has shown that a value of $K = 1.84$ should be used to calculate the layer diameter, L_a . Polycrystalline graphites lie somewhere between an oriented three-dimensional and a completely random two-dimensional structure, and thus the value used to calculate L_a will have a value between 1.0 and 1.84. Akamatu et al.¹⁷ have preferred to use an averaging method based upon the relative intensities of the (1 1 2) and (1 1 0) lines or upon the fraction of randomly disoriented layers. Unfortunately the value chosen for K is not always stated with published values of L .

5-6.5 CRYSTALLITE SIZE

It will be concluded from the foregoing that, although the average crystallite size may be a very useful property in characterizing and understanding the structure of graphite, there are currently a number of theoretical and practical barriers to obtaining absolute values. Klug and Alexander⁷ state that with most materials the accuracy of crystallite-size measurements does not exceed 25 to 50 per cent. Fortunately a relative crystallite size is almost as useful as an absolute value, and it is possible to obtain relative values of L that are self-consistent and accurate enough to have some physical significance.

The crystallite dimensions, L_c and L_a , of several moderator graphites are given in Table 5.1. Typical variations within a bar are shown in Figs. 5.5 and 5.6. Integral breadths were calculated from measured line profiles and corrected for instrumental broadening by the Jones method.¹⁵ A value of $K = 1$ was used for the shape factor in the Scherrer equation except in calculating L_a for the poorly crystallized Korite. In this case the random layer value of $K = 1.84$ was used since this probably gives a physically more realistic value. It will be noted that the more highly crystalline

graphites with low c values in general also have larger values of L . As will be seen in Chap. 9, there is a direct correlation between the crystallinity of graphites and their dimensional stability in a reactor.

Hedden et al.^{18,19} have conducted a systematic study of the crystallite properties of a number of experimental carbons and graphites prepared for irradiation studies from a variety of raw materials, including petroleum and pitch cokes, carbon blacks, and cokes made from phenolic resins and cane sugar. Because all test specimens were measured in the same laboratory, the results are directly comparable. A wide range of crystallite properties was obtained by the variations in raw materials and graphitizing temperature.

The mechanical grinding^{8,20} of both natural and manufactured graphites deforms the crystallites and eventually converts them to a structure that is randomly oriented about the c axis (turbostratic structure). The L_c and L_a values are markedly reduced and the interlayer spacing is increased by

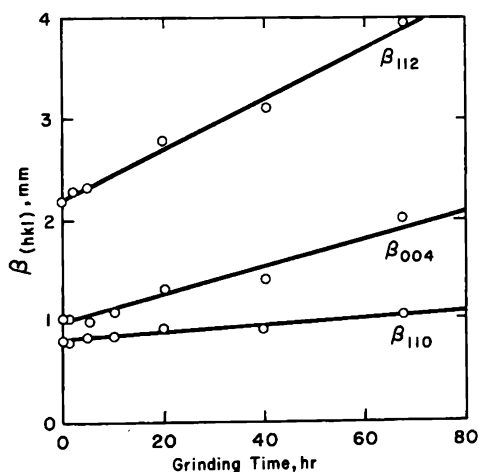


FIG. 5.8 Changes in X-ray line breadths of a polycrystalline graphite as a result of grinding.⁸

such treatment. The increase in line breadths as a function of grinding time (Fig. 5.8) is evidence of an increase in randomness of layer orientation and decrease in crystallite size. The fraction of rhombohedral graphite in a highly crystalline material is also increased during the grinding, as indicated by an increase in the intensity of the $(1\ 0\ \bar{1}\frac{2}{3})$ line.

5-7 Pore Structure

Pore structure refers to the number and size of pores and to the interconnections between them which result from the packing of crystallites, particles, and disorganized carbon. A number of experimental methods (X-ray small-angle scattering, electron microscopy, gas adsorption-desorp-

tion, and mercury porosimetry) have been used to study the pore structure. Considering the fact that several different physical principles are employed in each of these methods, a fairly consistent picture of the pore structure has emerged.

5-7.1 X-RAY SCATTERING

In principle the scattering of X rays at low angles (within about 2° of the undeviated beam) is capable of giving information on the existence and size of very small pores. Warren²¹ has measured the small-angle scattering from unirradiated and irradiated graphite. Definite conclusions could not be drawn on the effects of irradiation since changes were small on the samples studied. However, changes in intensity with orientation of both unirradiated and irradiated samples suggested that small disk-shaped cavities were present with dimensions several times greater in the a direction than in the c direction.

5-7.2 GAS ADSORPTION-DESORPTION ISOTHERMS

The size distribution of pores in the range 20 to 300 Å has been measured from gas adsorption-desorption isotherms by the Barrett, Joyner, and Halenda²² (BJH) method. Nitrogen or argon gas at liquid-nitrogen temperature is usually employed. Figure 5.9 is a typical pore-size curve for

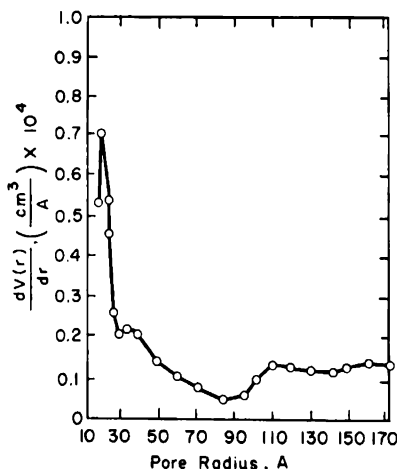


FIG. 5.9 Pore-size distribution curve for KC graphite. (From Spalaris, *Journal of Physical Chemistry*, Ref. 23.)

solid KC graphite showing the change in differential accessible volume [$dV(r)/dr$] with pore radius (r). Variations in the exact shape of the curves are common in petroleum-coke graphites, but most show the sharp peak at about 20 Å and possess a system of micropores out to 300 Å, the size limit in these studies. The surface area can be calculated from pore-

size curves and usually agrees to within 5 per cent with the BET† method (Sec. 6-8.2). Because the pores are not cylindrical (as assumed in the BJH theory²²) but are bounded by irregularly shaped crystallites, the term "pore radius" has no exact physical significance except a statistical one as indicated by the equation

$$r = \sqrt{A/\pi} \quad (5.3)$$

where A is the average cross sectional area of some irregular pore shape. Pulverizing the graphite greatly increases the number of pores and the surface area accessible to gases. The shape and intensity of pore-size curves change with irradiation and oxidation (Secs. 9-2 and 14-2.4).

5-7.3 INACCESSIBLE PORES

A somewhat different approach to micropore structure has been taken by Loch and Austin.²⁴ They define the percentage of inaccessible micropore volume as $100 (1 - \rho_a/\rho_t)$, where ρ_a is the density measured by the displacement of helium or by sink-float measurements in a bromoform-benzene-carbon tetrachloride mixture and ρ_t is the theoretical (or X-ray) density. Micropores so defined are inaccessible to the measuring fluid, and so the pore openings, although not necessarily the pores themselves, will be smaller than those measured by the gas adsorption-desorption method. Loch and Austin observed a general decrease in inaccessible micropore volume with increasing crystallite size for graphites prepared from a variety of raw materials and graphitized to 2570°C. This suggests that the pores are located between adjacent crystallites. Further evidence²⁴ for this is found in the relation between the inaccessible micropore volume and the crystallite size for several density fractions of a petroleum-asphalt graphite (Carbon 36 of Fig. 5.10). The micropore volume decreases continuously as the crystallite size increases. The crystallite size and micropore volumes of all density fractions of the phenolic-resin graphite (Carbon 46) were nearly the same; so the relation could not be adequately tested for this material.

Grinding to a particle size of 70μ produces significant increases in the helium densities. Since helium should penetrate openings as small as 5 Å, this indicates that subdivision and mechanical deformation open some pores that are completely inaccessible to helium before grinding. Using their data on average crystallite size and assuming a very simplified model of the micropore structure, Loch and Austin calculate the average spacing between adjoining crystallites to be in the range 3 to 8 Å. Dimensions of this magnitude are compatible with the idea that the micropores are inaccessible to liquids and relatively inaccessible to helium.

† A method developed by Brunauer, Emmett, and Teller which uses the surface of gaseous molecules to determine the total surface area present in a nonhomogeneous body.

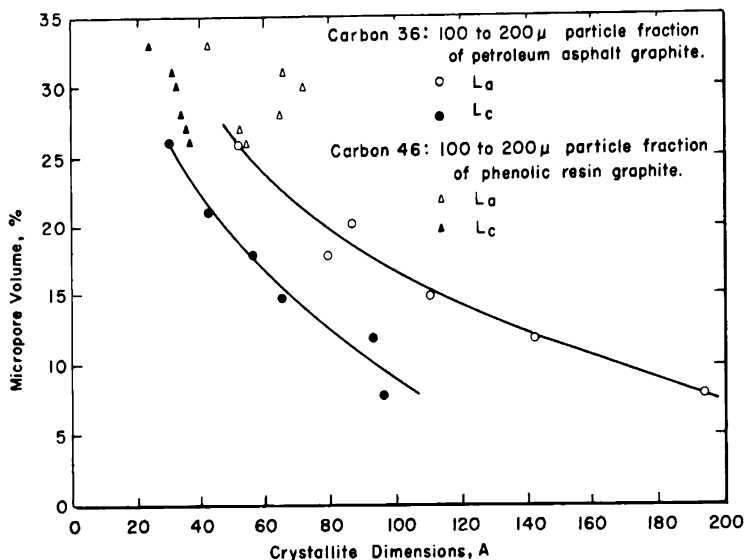


FIG. 5.10 The change in micropore volume with crystalline dimensions for sink-float density fractions.²⁴

5-7.4 MERCURY POROSIMETRY

Densities measured from the displacement of liquids and gases give information regarding the pores that are inaccessible to the measuring fluid in the 10-A range, and gas-adsorption techniques give information on the size and distribution of pores accessible to gases in the range 20 to 300 A. Mercury porosimetry²⁵ can be used to study the distribution and size of pores in the range 350 to 100,000 A. In this method mercury is forced into the pores under pressure, the capillary radius of the pores being related to the pressure by

$$r = \frac{2\gamma \cos \theta}{p} \quad (5.4)$$

where γ ($= 480$ dynes/cm) is the surface tension of mercury, θ ($= 140^\circ$) is the contact angle between mercury and graphite, and p is the applied pressure. Changes in the apparent volume of the mercury can then be attributed to the accessible volume $V(r)$ reached through pores of minimum radius, r . Because of the highly irregular nature of pores in a graphite body, the pore radius so defined is statistical in nature. In general, the pores have a relatively large cross section but are accessible through a small opening. Such a geometry is indicated from photomicroscopy and by the fact that in porosimetry measurements virtually none (less than 5 per cent) of the mercury is released from the sample when the pressure is relieved.²⁶

The quantity of most interest, the differential accessible volume $[dV(r)/dr]$ is shown as a function of r in Fig. 5.11 for AGOT and two

newer base materials fabricated by pressure baking. Pores in the size range shown are undoubtedly due to voids between grains. The difference in size distribution between the three materials illustrates the kind of control possible over the structure of the particles. Impregnation of the R-0013 and R-0018 base materials greatly reduces the number of pores in the 10,000- to 50,000-A range and shifts the peak to about 5000 A. The pore structure of the unimpregnated base stock is important in the achievement of low-permeability graphites.

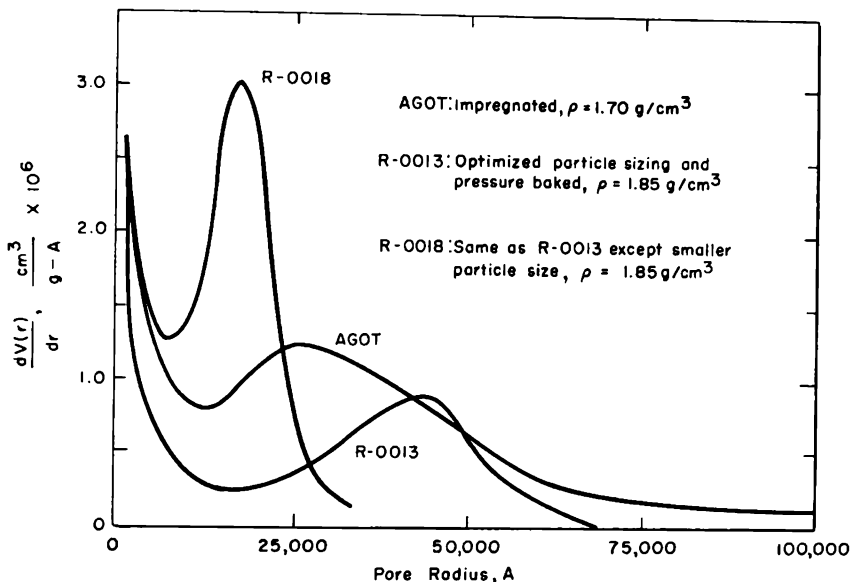


Fig. 5.11 Porosimetry of base graphites.²⁶

It is of interest to compare the total accessible pore volume in the range 15 to 170 Å to that in the range 2000 to 100,000 Å. The pore structures of CSF and AGOT are similar enough to allow a valid comparison. From the areas under the curves of Figs. 5.9 and 5.11, the total pore volumes accessible from 15 to 170 Å and from 2000 to 100,000 Å are 0.0021 cm³/g and 0.68 cm³/g, respectively. Thus, although the total large-pore volume is 320 times the small-pore volume, the average large-pore volume per angstrom [i.e., the average $dV(r)/dr$] is only about one-half that of the small pores.

Mercury porosimetry²⁷ has been extended to very high applied pressures (30,000 psi) to measure pores as small as 33 Å. Porosimetry measurements of pore distribution on bone-char adsorbents agreed well with those made by gas adsorption. Since the two methods are based upon different principles and techniques, this constitutes a good confirmation of some of the assumptions upon which the theories are based. Mercury-porosimetry measurements can be made rapidly; however, the apparatus needed to investigate small pores by this method is expensive and bulky because of the high

pressures required. It has been suggested²⁷ that the most efficient equipment for measuring the complete pore spectrum (20 to 100,000 Å) is a mercury porosimeter capable of exerting 500 to 1000 psi and a gas-adsorption apparatus for pores less than 300 Å.

If the porosimetry method is employed with samples to be irradiated in reactors, special care must be taken to remove the last traces of mercury so that the samples will not become so radioactive as to be impractical to handle.

5-8 Grain Structure

5-8.1 OPTICAL AND ELECTRON MICROSCOPY

The grain structure of graphites can be observed directly over a wide range of magnifications by optical and electron microscopy. The key to obtaining informative photomicrographs representative of the undisturbed surface lies in the metallographic techniques employed in polishing and etching. In contrast to metals, carbon bodies are porous, brittle materials composed of regions that differ widely in hardness. Normal metallographic operations tend to break down the fragile cellular wall structure of graphite and thus destroy much of the original structure. By vacuum impregnation with a penetrating resin, it has been possible to fill the voids and strengthen the wall structure so that polishing can be accomplished without seriously altering structural details.²⁸

Careful etching by a potassium dichromate-phosphoric acid solution²⁹ or slow oxidation in air has been employed in some cases to develop the structural details further. Cathodic etching of polished surfaces, which depends upon the differences in the binding energy of atoms in areas of different crystallographic orientation, has also been successfully employed.^{30,31}

Pincus and Gendron³² have reported recently on the use of sensitive-tint illumination for the microscopic examination of brush carbons. They state that the colors from graphitic carbons, in contrast to heat-treated carbon blacks, undergo a change from red to green and back to red as the microscope stage is rotated through 180° and that calcined cokes show a color change but in more moderate hues. Although the different orientations of reflecting surfaces can also be observed with ordinary polarized-light illumination, the sensitive-tint method makes the differences more distinct.

The grain structure of a needle-coke graphite³³ is illustrated in the sensitive-tint photomicrographs shown in Plate I (see also Sec. 2-1.1 and Fig. 2.2). The aligned (and presumably more graphitic) regions change from red to blue when the microscope stage is rotated 90°. Aligned areas composed of one color are several hundred times larger than the relatively perfect crystallites, and therefore the small misorientations of crystallites are not revealed by optical microscopy. The pores have been filled with an epoxy resin and, being nontextured purple areas that do not change color

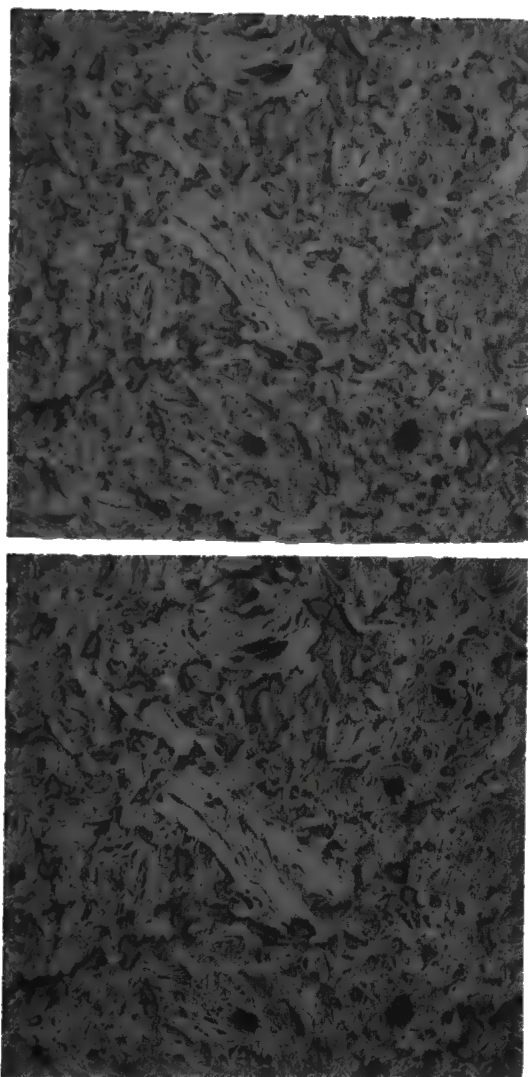


PLATE I The grain structure of a needle-coke graphite, GL-10, by sensitive-tint illumination. The microscope stage was rotated 90° between the top and bottom photomicrographs. Magnification, $40\times$. (Courtesy of T. J. Clark, Hanford Laboratories, General Electric Company.)

when the stage is rotated, are easily identified. The color of poorly aligned carbon regions also changes very little. It is not possible to identify with certainty carbon added as pitch binder or pitch impregnant. Striking differences in the grain structure of fine-grained low-permeability and pyrolytic materials can also be observed by optical microscopy techniques.

The practical limit of magnification with present optical techniques is about $500\times$. Electron microscopy has been employed to obtain magnifications of $50,000\times$ or higher (capable of resolving structural details of about

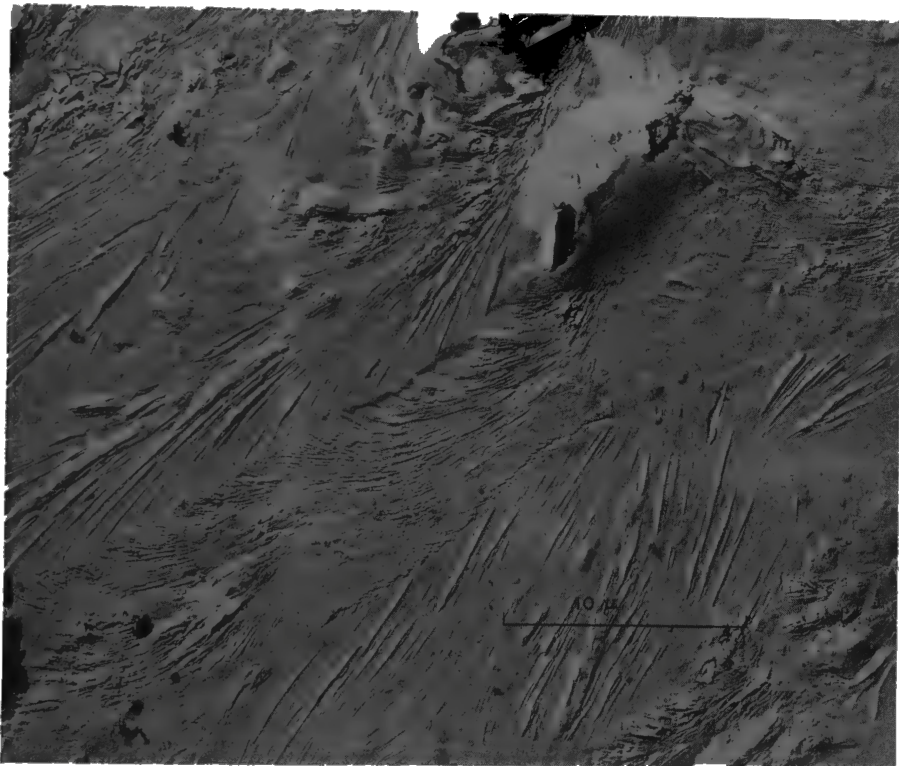


FIG. 5.12 Electron photomicrograph of CSF graphite. (Courtesy of E. M. Woodruff, Hanford Laboratories, General Electric Company.)

100 A). An electron photomicrograph of a CSF graphite at relatively low magnification is shown in Fig. 5.12. The graphite surface was first polished and cathodically etched. A cellulose acetate replica was prepared, shadowed with palladium at 30° , then coated with carbon. Finally the acetate was dissolved away, leaving a shadowed carbon replica of the original surface. The light regions in Fig. 5.12 result from shadows cast by protrusions on the film replica (depressions in the sample surface). The detailed texture of several highly aligned regions 5 to $10\ \mu$ thick is revealed. These regions are smaller than the areas on Plate I, which appear as single red or blue colors approximately 10 to $100\ \mu$ wide.

5-8.2 PREFERRED ORIENTATION

The grains in electrographites are preferentially oriented with respect to the direction of extrusion or molding. This orientation causes the macroscopic properties of a formed graphite body to be anisotropic because the internal lamellar structure of the crystallites themselves is also anisotropic. The degree of anisotropy depends upon the perfection of crystallites, extent of alignment of crystallites within a grain, shape of the grains, alignment of grains, and the nature of the binder-filler bonding.

A quantitative description of preferred orientation is difficult. The most complete and accurate description of crystallite orientation is given by pole figures⁷ in which the relative orientation of different crystallites is

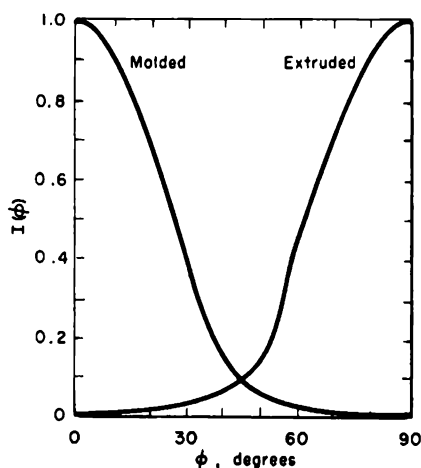


FIG. 5.13 Orientation function for well-oriented graphites. (From Bacon, *Journal of Applied Chemistry*, Ref. 34.)

shown by the stereographic projection of X-ray intensity data. This method is very time consuming, however, and has not been widely applied to polycrystalline graphite. Furthermore, the use of pole figures in determining the effects of crystal orientation on properties has not been explored.

A method that offers some hope of being more useful in relating orientation to physical properties has been suggested by Bacon.³⁴ From a single X-ray photograph, an orientation function, $I(\phi)$, can be obtained which is proportional to the density of the (0 0 2) planes parallel to the extrusion (or molding) direction. Here ϕ is the angle between the normal to the (0 0 2) planes and the extrusion or molding direction. Figure 5.13 shows a curve obtained by this method for a well-oriented graphite. In the case of molded materials, layer planes tend to lie parallel to the two equivalent directions (perpendicular to the molding force) and perpendicular to the third direction (Fig. 5.14). Thus the $I(\phi)$ vs. ϕ curve is a maximum at

$\phi = 0^\circ$ and decreases to a very low value at 90° . In extruded stock planes are preferentially oriented parallel to the extrusion direction and perpendicular to the other two directions. Alignment is greatest near the surfaces of the extrusion or molding die.

Those bulk properties (thermal expansion, electrical and thermal conductivity, and radiation-induced dimensional changes), which depend

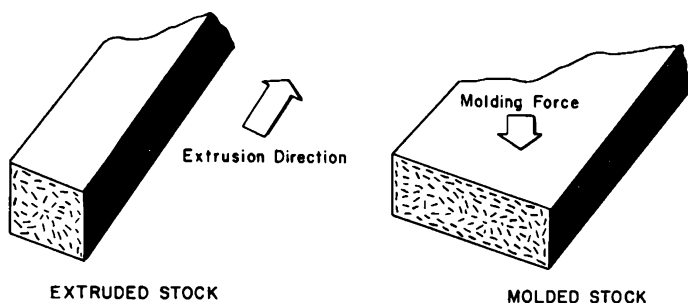


Fig. 5.14 Schematic representation of preferred grain orientation.

strongly on the perfection of the crystallites, are strongly anisotropic in oriented graphite. Since $I(\phi)$ relates only to the orientation of the crystallites, it gives no information about the intercrystalline pores and their effect on the macroscopic properties. One would really like to know the relation between preferred crystallite orientation [i.e., $I(\phi)$ vs. ϕ curve] and the macroscopic properties measured in a given direction. In practice this relation is complicated since the number, distribution, and shape of voids preclude a one-to-one correspondence between crystallite effects and macroscopic effects. For example, for a void-free graphite and with random crystallite orientation, the volume coefficient of thermal expansion (γ_v) is

$$\gamma_v = \gamma_c + 2\gamma_a \simeq 30 \times 10^{-6} \text{ per } ^\circ\text{C} \quad (5.5)$$

where γ_c and γ_a are, respectively, the coefficients of thermal expansion normal and parallel to the layer planes in the crystallite. Actually, because some expansion is absorbed in the voids, a bulk volume coefficient of thermal expansion in the range 5×10^{-6} to 15×10^{-6} per $^\circ\text{C}$ is measured (see Sec. 6-2.4). Other properties are also dependent to various degrees upon effects at crystal and grain boundaries.

Although some of the basic processes by which preferred orientation is produced during the manufacture of graphite have been identified, knowledge in this area is far from complete. Among the variables that must be considered are the size and shape of the extruded or molded bar, the size and shape of coke particles, the ratio of filler to binder, the viscosity and amount of binder, the forming temperature, the design of the die or mold, and the reduction in area of the body during forming.

Preferred orientation will be considered further when physical proper-

ties and radiation effects are discussed in subsequent chapters. It will be seen that the anisotropy of graphite is a disadvantage in some applications. However, it is almost always possible to minimize the anisotropy effects or, in special applications, to actually take advantage of them.

5-9 Structural Changes During Graphitization

A knowledge of the structural changes occurring during the graphitization of carbons has helped substantially in understanding the large differences observed in graphites prepared from different materials or by different processes. Moreover, since radiation effects are so strongly dependent upon structural properties, a better knowledge of the mechanism of graphitization has also suggested methods by which raw materials or processing variables can be changed to produce a graphite with improved resistance to radiation. Radiation effects are more easily understood by analogy with the graphitization process since in some ways radiation damage at low temperatures is analogous to "degraphitization" (Sec. 9-1).

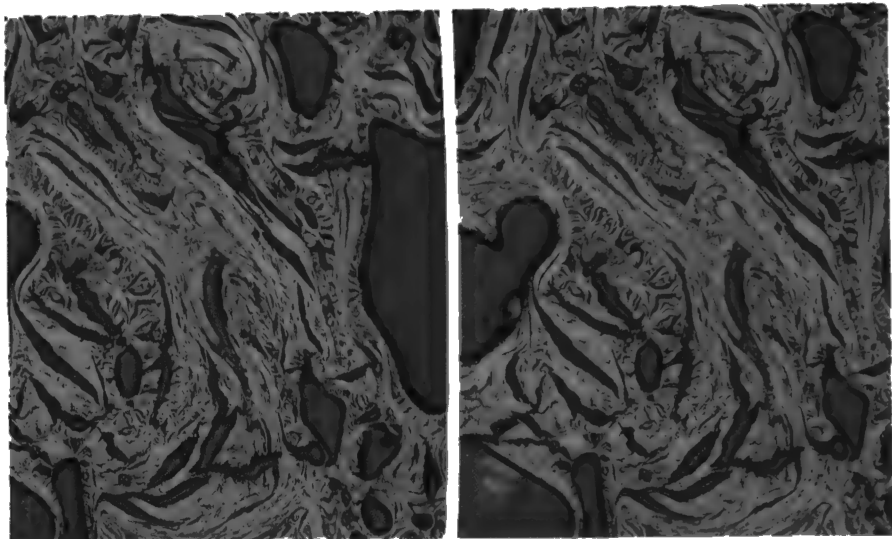
Much has been published on graphitization processes in carbon blacks, coal-tar pitches, petroleum asphalts, phenolic resins, sugar, and pure organic compounds. Much less has been published on the structural changes of filler-binder systems, which are more complex and less amenable to fundamental structural studies. Although structural changes occurring in the single-phase systems are used in subsequent sections to describe the general graphitization process, the exact properties of the material are determined also by the amount and type of binder, pitch impregnation, and special additives.

5-9.1 GRAPHITIZATION OF PETROLEUM COKES

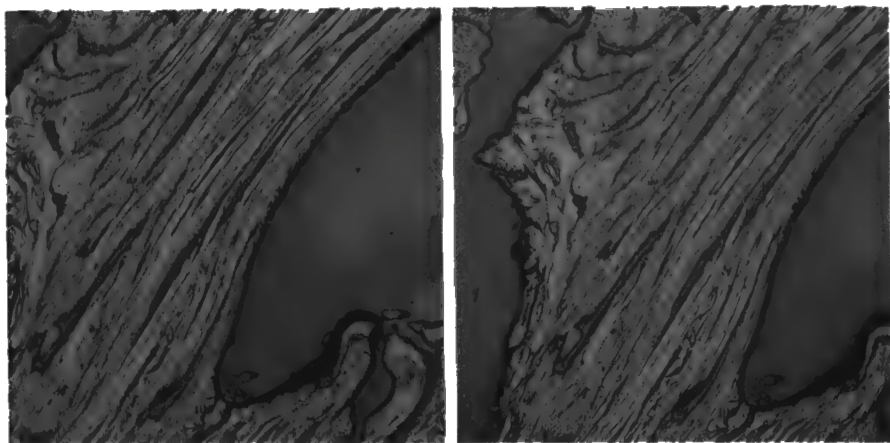
Three important experimental observations need to be accounted for in describing the graphitization process: (1) As chars, carbon blacks, or cokes are heated, crystallite development proceeds slowly at first and then increases very rapidly in the range 1800 to 2000°C. (2) The crystallite size is determined principally by the highest temperature of heat-treatment and is less dependent on the length of time the material is held at a given temperature. (3) The degree of graphitization† is markedly dependent upon the nature of the original carbon.

Petroleum cokes show remarkable flow patterns within the particles. This is caused by the evolution of gases during the coking process and is aided by thermal motion of the viscous mass. Large platelike aromatic molecules are aligned parallel to the flow by shear stresses. Upon solidification the raw coke has a textured, partially aligned structure. During cal-

† The term "degree of graphitization" and equivalent expressions are commonly used in the graphite literature. They are usually synonymous with "degree of crystallinity" (see Sec. 2-1.1). A "highly graphitic" carbon is one whose crystallite properties (a , c , L_a , L_c , etc.) approach those of the perfect crystal.



a



b

PLATE II Texture of petroleum cokes. (a) Calcined Cleves coke. Microscope stage rotated 90° between the two photomicrographs. (b) Calcined Continental coke. Microscope stage rotated 90° between the two photomicrographs. Magnification, $40\times$. (Courtesy of T. J. Clark, Hanford Laboratories, General Electric Company.)

cination the aligned structure is preserved, although fissures develop and enlarge as volatile hydrocarbons are lost. The resulting structure is shown in the sensitive-tint photomicrographs of Plate II. The Cleves coke has been used extensively as the filler for nuclear graphites. It is typical of the nonneedle cokes. The pores, which have been filled with resin, appear as irregular nontextured areas. Some aligned regions extending over small distances can be identified.

The Continental-coke specimen† (part b, Plate II) is an extreme example of a highly aligned needlelike coke. The pores are larger than conventional cokes and are somewhat elongated. The cracks are generally parallel to the flow structure. When subdivided the Continental coke yields

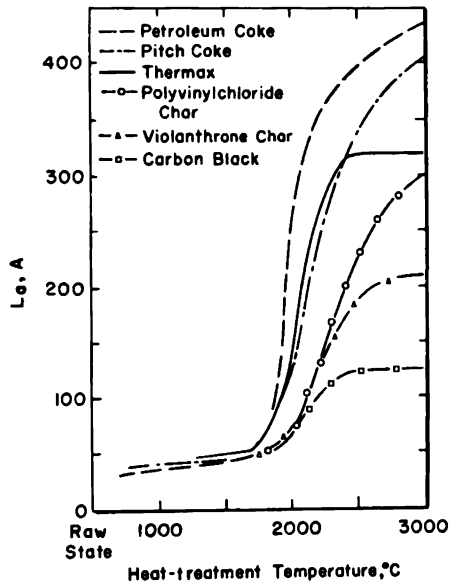


FIG. 5.15 Changes in the layer diameter of carbons with heat-treatment temperature. (From Akamatu and Kuroda, *Proceedings of the Fourth Conference on Carbon*, Pergamon Press, Ref. 36.)

longer and more splintery particles than the Cleves coke. In general, each coke particle has a characteristic eccentricity that is important in determining the anisotropy of the final graphite.³⁵ Further subdivision of the coke particles down to sizes corresponding to the highly aligned regions results in a higher degree of anisotropy of the coke particles.

Upon heating above the calcination temperature (1000 to 1300°C) development of graphitic structure continues,³⁶ slowly at first, and then quite rapidly as the temperature approaches 1800 to 2000°C (Fig. 5.15). The layer diameter of all carbons increases rapidly in the 1800 to 2000°C

† Lake Charles Continental coke supplied by the National Carbon Company.

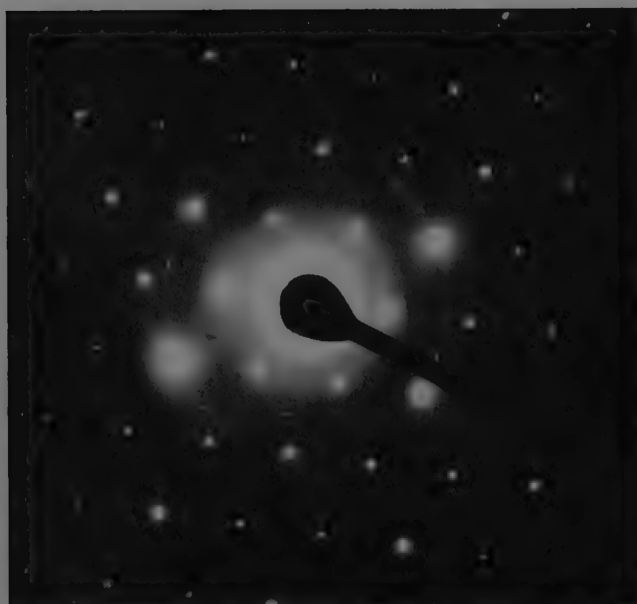
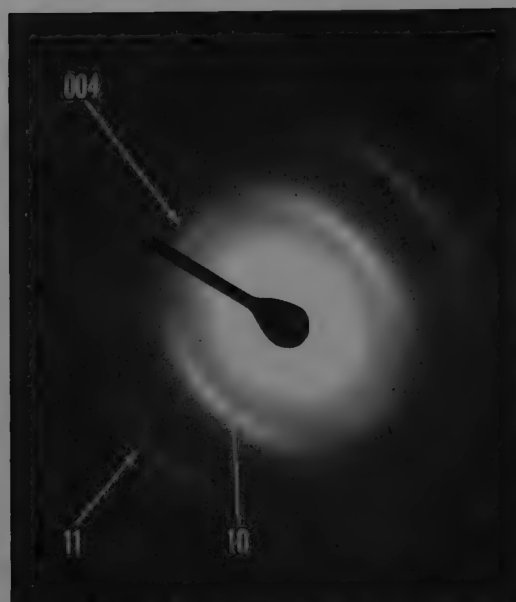


FIG. 5.16 Electron diffraction patterns of a petroleum-coke particle. (a) Raw coke. (b) Heated to 3000°C. (From Akamatu and Kuroda, *Proceedings of the Fourth Conference on Carbon*, Pergamon Press, Ref. 36.)

range, but the limit of crystallite perfection depends upon the type of carbon.†

The increase in crystalline development is also shown in electron diffraction photographs (Fig. 5.16). Diffuse (002), (004), (10), and (11) lines are partially developed, even in the raw coke. The (002) and (004) lines are absent in patterns taken with the incident electron beam normal to the flaky particle, indicating that the crystallites are aligned with the *c* axis normal to the surface, even at this early stage of crystalline development. Upon further heating the diffraction pattern becomes sharper until after heat-treatment at 3000°C the three-dimensional graphite lattice is highly developed. The grain is then composed of well-aligned minute crystallites.

The strong dependence of the crystallinity on the substructure of the starting coke indicates that vapor-phase condensation is not a likely mechanism for crystallization since such a process should be nearly independent of the coke structure. The mechanism that is generally favored involves the displacement and rearrangement of crystal planes and small groups of planes relative to one another. The extent to which this may occur depends strongly upon (1) the relative orientation of the crystallites and (2) the extent of cross linking existing at the time that thermal activation is sufficient to allow rearrangement. The more nearly two crystallites are aligned with their basal planes parallel, the easier it will be for them to rearrange and coalesce. Good alignment leads to a large crystallite without mass transfer or the work required to break strong chemical bonds. Those crystallites that are poorly aligned or strongly cross linked will not coalesce even at 3000°C. Hence the ultimate size of the crystalline regions is determined very early in the coking process. Those carbons with large regions of alignment form a highly graphitic product, whereas those with small regions of alignment form only small graphitic regions and resist further graphitization at all temperatures below the melting point.

5-9.2 GRAPHITIZATION OF CARBON BLACKS

Some graphitization occurs even in materials such as carbon blacks, which are often considered nongraphitizing. However, the graphitic regions are limited by the small regions of alignment and probably also by a more highly aliphatic structure. Changes in the internal structure of Thermax with an average particle size of 3000 Å were studied by Kmetko³⁷ and later by Akamatu and Kuroda³⁸. Little change is observed in electron photomicrographs until about 1500°C, when fine contrasts began to appear. As the heat-treatment temperature increases, these contrasts become dark striations that run from the periphery into the particle. Above 2500°C they develop into dark patterns whose bases coincide with the edges of the

† For the value of the Scherrer shape factor used in this work, see Ref. 17.

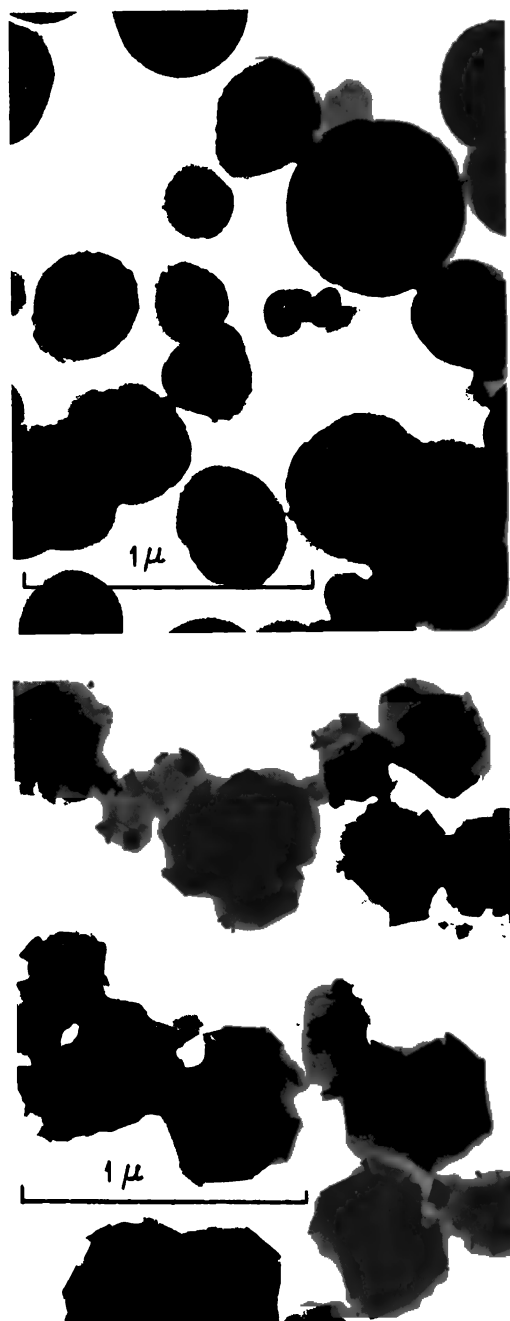


FIG. 5.17 Electron photomicrographs of Thermax. (a) Untreated. (b) Heat-treated to 3000°C. (From Akamatu and Kuroda, *Proceedings of the Fourth Conference on Carbon*, Pergamon Press, Ref. 36.)

polygonal outlines of the particle (Fig. 5.17). These patterns are presumably produced by diffraction effects, perhaps (0 0 2) reflections of the graphitic structure, and not by differences in thickness. Thus, even in carbon blacks, minute crystals imbedded in a matrix of disorganized carbon are oriented with basal planes parallel to the surface. Rearrangement occurs at high temperatures, producing a particle with greater preferred orientation along the surface. Toward the center the angles between the crystallites become too great to allow much rearrangement to occur.

5-9.3 COKE-GRAPHITE STRUCTURAL RELATIONS

The above discussion and other evidence by several investigators^{19, 36-38} point to the importance of the preorientation of the carbons in determining the final crystallite size. In view of the fact that radiation effects are strongly dependent upon the structural properties of the graphite, the following question becomes very important: "How can the coking process be controlled or varied to achieve desired structural characteristics in the final graphite?" Although some of the factors that distinguish graphitizing carbons from nongraphitizing carbons have been identified,³⁸ in general, little has been published on this subject. Commercial exploitation of coke-graphite structural relations is severely limited by the fact that standard petroleum cokes are by-products of the petroleum industry. An exception to this is the development of needlelike cokes in recent years,³³ giving evidence that the relation of initial coke structure to graphite properties has been recognized for a number of years. Certainly the need for graphites with special properties for use in the atomic energy, missile, and other industries will encourage further efforts in controlling the coking process to obtain desirable properties in the coke.

References

1. H. W. Davidson and H. H. W. Losty, Elastic and Plastic Properties of Carbon and Graphite, in *Mechanical Properties of Non-Metallic Brittle Materials*, London Conference of the National Coal Board, 1958, pp. 219-238, Interscience Publishers, Inc., New York, 1958.
2. J. D. Bernal, The Structure of Graphite, *Proc. Roy. Soc.*, **A106**: 749-773 (1924).
3. A. J. C. Wilson, Ed., *Structure Reports*, Vol. 11, p. 200, N. V. A. Oosthoek's Uitgevers Mij, Utrecht, 1947-1948.
4. C. A. Coulson, *Valence*, Clarendon Press, Oxford, 1952.
5. L. A. Girifalco and R. A. Lad, Energy of Cohesion, Compressibility and the Potential Energy Functions of the Graphite System, *J. Chem. Phys.*, **25**: 693-697 (1956).
6. R. E. Franklin, The Structure of Graphitic Carbons, *Acta Cryst.*, **4**: 253-261 (1951).
7. H. P. Klug and L. E. Alexander, *X-ray Diffraction Procedures for Polycrystalline and Amorphous Materials*, John Wiley & Sons, Inc., New York, 1954.
8. G. E. Bacon, *Crystallographic Studies of Graphites*, British Report AERE-MR-2702, 1958.

9. G. E. Bacon and R. E. Franklin, The a Dimension of Graphite, *Acta Cryst.*, **4**: 561-562 (1951).
10. G. E. Bacon, The Interlayer Spacing of Graphite, *Acta Cryst.*, **4**: 558-561 (1951).
11. A. J. C. Wilson, Geiger Counter X-ray Spectrometer—Influence of Size and Absorption Coefficient of Specimen on Position and Shape of Powder Diffraction Maxima, *J. Sci. Instr.*, **27**: 321-325 (1950).
12. J. B. Nelson and D. P. Riley, The Thermal Expansion of Graphite From 15°C to 800°C. Part I. Experimental, *Proc. Phys. Soc. London*, **57**: 477-486 (1945).
13. Y. Baskin and L. Meyer, Lattice Constants of Graphite at Low Temperatures, *Phys. Rev.*, **100**: 544 (1955).
14. P. L. Walker, Jr., et al., X-ray Diffraction Studies of a Graphitized Carbon—Changes in Interlayer Spacing and Binding Energy with Temperature, *Ind. Eng. Chem.*, **45**: 1711-1715 (1953).
15. F. W. Jones, The Measurement of Particle Size by the X-ray Method, *Proc. Roy. Soc. London*, **A166**: 16-43 (1938).
16. B. E. Warren, X-ray Diffraction in Random Layer Lattices, *Phys. Rev.*, **59**: 693-698 (1941).
17. H. Akamatu et al., Studies on Graphitization. I. Changes of Crystallinity, Diamagnetic Susceptibility and Electrical Conductivity in the Process of Graphitization, *Bull. Chem. Soc. Japan*, **29**: 574-581 (1956).
18. W. A. Hedden et al., *Experimental Carbons and Graphites for Irradiation Studies*, USAEC Report BMI-962, Battelle Memorial Institute, Oct. 26, 1954.
19. A. E. Austin and W. A. Hedden, Graphitization Processes in Cokes and Carbon Blacks, *Ind. Eng. Chem.*, **46**: 1520-1524 (1954).
20. P. L. Walker, Jr., and S. B. Seeley, Fine Grinding of Ceylon Natural Graphite, in *Proceedings of the Third Conference on Carbon Held at the University of Buffalo*, pp. 481-494, Pergamon Press, New York, 1959.
21. B. E. Warren and D. R. Chipman, *Small Angle X-ray Scattering Study of Radiation Damage in Graphite*, USAEC Report KAPL-1204, Massachusetts Institute of Technology, Oct. 1, 1954.
22. E. P. Barrett et al., The Determination of Pore Volume and Area Distributions in Porous Substances. I. Computations from Nitrogen Isotherms, *J. Am. Chem. Soc.*, **73**: 373-380 (1951).
23. C. N. Spalaris, The Micropore Structure of Artificial Graphite, *J. Phys. Chem.*, **60**: 1480-1483 (1956).
24. L. D. Loch and A. E. Austin, Fine Pore Structure—Crystallite Size Relationships in Carbons, in *Proceedings of the First and Second Conferences on Carbon Held at the University of Buffalo*, pp. 65-73, Waverly Press, Inc., Baltimore, Md., 1956.
25. H. L. Ritter and L. C. Drake, Pore-Size Distribution in Porous Materials—Pressure Porosimeter and Determination of Complete Macropore-Size Distributions, *Ind. Eng. Chem., Anal. Ed.*, **17**: 782-786 (1945).
26. W. P. Eatherly et al., Physical Properties of Graphite Materials for Special Nuclear Applications, in *Proceedings of the Second United Nations International Conference on the Peaceful Uses of Atomic Energy, Geneva, 1958*, Vol. 7, pp. 389-401, United Nations, New York, 1959.
27. L. G. Joyner et al., The Determination of Pore Volume and Area Distributions in Porous Substances. II. Comparison Between Nitrogen Isotherm and Mercury Porosimeter Methods, *J. Am. Chem. Soc.*, **73**: 3155-3158 (1951).
28. S. W. Martin and F. L. Shea, Jr., Microstructures of Carbon Products, *Ind. Eng. Chem.*, **50**: 41-46 (1958).
29. A. Tarpinian and G. E. Gazza, *A Technique for the Microstructural Examination of Polycrystalline Graphites*, Report WAL-TR-132.5/1, Watertown Arsenal Laboratory, February, 1959.

30. T. K. Bierlein et al., Etching of Refractories and Cermets by Ion Bombardment, *J. Am. Ceram. Soc.*, **41**: 196-200 (1958).
31. R. L. Hales and E. M. Woodruff, Technique for Microscopic Studies of Graphite, in *Proceedings of the Fifth Conference on Carbon Held at Pennsylvania State University*, Pergamon Press, New York (in press).
32. I. Pincus and N. J. Gendron, Microscopy and Structures of Brush Carbons, in *Proceedings of the Fourth Conference on Carbon Held at the University of Buffalo*, pp. 687-701, Pergamon Press, New York, 1960.
33. F. L. Shea, Jr., *Production of Coke from Petroleum Hydrocarbons*, U. S. Patent 2,775,549, Great Lakes Carbon Corp., Dec. 25, 1956.
34. G. E. Bacon, A Method for Determining the Degree of Orientation of Graphite, *J. Appl. Chem. (London)*, **6**: 477-481 (1956).
35. L. M. Currie et al., The Production and Properties of Graphite for Reactors, in *Proceedings of the First International Conference on the Peaceful Uses of Atomic Energy, Geneva, 1955*, Vol. 8, pp. 451-473, United Nations, New York, 1956.
36. H. Akamatu and H. Kuroda, On the Substructure and Crystallite Growth in Carbon, in *Proceedings of the Fourth Conference on Carbons Held at the University of Buffalo*, pp. 355-369, Pergamon Press, New York, 1960.
37. E. A. Kmetko, The Structure and Graphitization of Fine Coke Particles and of Thermal Carbon Blacks, in *Proceedings of the First and Second Conferences on Carbon Held at the University of Buffalo*, pp. 21-30, Waverly Press Inc., Baltimore, Md., 1956.
38. R. E. Franklin, Crystallite Growth in Graphitizing and Non-Graphitizing Carbons, *Proc. Roy. Soc. London*, **A209**: 196-218 (1951).

Physical Properties

R. E. NIGHTINGALE,[†] H. H. YOSHIKAWA,[†] and H. H. W. LOSTY[‡]

6-1 Thermodynamic Properties

6-1.1 PHASE DIAGRAM OF CARBON

The very high melting point and sublimation temperature of carbon make the determination of the phase diagram a formidable problem. The four phases commonly attributed to carbon are graphite, diamond, liquid, and gas (Fig. 6.1). Such familiar materials as charcoal and carbon black are not equilibrium phases and therefore do not appear on the phase diagram.

The phase boundary between diamond and graphite is reported³ to occur at 20,000 atm at 0°K and to extend upward to about 150,000 atm near 3800°K. As seen in the diagram, the vapor pressure becomes appreciable near 3600°K. The exact position of the triple point is still subject to question since the accuracy of such experiments is low. The most recent experimental determination² of the triple point of carbon indicated a pressure of 100 atm and a temperature of $3900 \pm 50^\circ\text{K}$. A second triple point occurs at the intersection of the diamond-graphite-liquid curves. It has been estimated³ that this point is in the vicinity of 4100°K and 200,000 atm.

Carbon exists only as a gas or liquid above 4000°K. By extension of the gas-liquid line, a critical point has been predicted¹ at 7000°K and 11,600 atm. The critical-point temperature was calculated from the average ratio of critical temperature to triple-point temperature for a number of elements. The pressure at the critical point was calculated by analogy with water, ammonia, chlorine, and mercury. Therefore, the estimate may be inaccurate.

The phase diagram indicates that the melting point of graphite is about 4000°K. It is nearly independent of the pressure above the minimum 100 atm necessary for the existence of the liquid phase. The melting-point curve is still subject to some doubt since experimental difficulties prevent the accurate determination of the onset of melting. The heat of fusion is not known precisely but is predicted⁴ to be 10 kcal/gram atom.

The sublimation temperature of graphite at which the partial pressure

[†] Hanford Laboratories, General Electric Company, Richland, Wash.

[‡] Research Laboratories, General Electric Co., Ltd., Wembley, England.

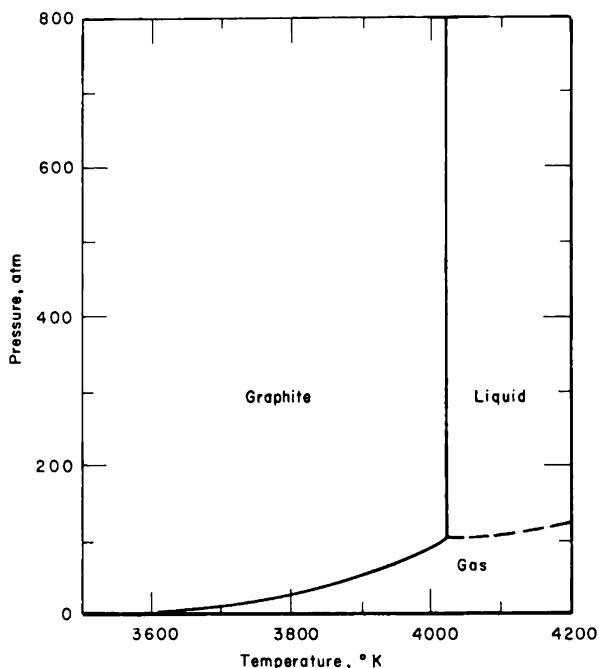


FIG. 6.1 The phase diagram of carbon. The triple point occurs at 100 atm and 4100°K, and the sublimation point occurs near 3620°K. Determinations were made by observations of a carbon arc.¹⁻³

of the gas phase is equal to 1 atm is reported² to be $3620 \pm 10^\circ\text{K}$. The heat of sublimation is subject to some doubt because of the uncertainty in the composition of the molecular species present in the vapor. However, the heats of sublimation of graphite to the various gaseous species (ΔH_0°) are much more precisely known and are listed in Table 6.1. Theoretical calcu-

Table 6.1 — HEAT OF SUBLIMATION OF GRAPHITE TO CARBON VAPOR⁵

Molecular species	ΔH_0° , kcal/mole
C	169.58
C ₂	195.8
C ₃	188.1
C ₄	229.5
C ₅	232.5

lations predict that large molecular species, C₅ and C₇, must be present to account for the observed rate of sublimation.⁴ The existence of such species has been confirmed by mass spectrometric analysis of the carbon vapor.⁵

6-1.2 SPECIFIC HEAT

The specific heat (C_p) of graphite can be described by a quadratic function of temperature from 13 to 50°K. Above 50°K C_p increases approxi-

mately linearly with temperature, and at room temperature C_p is about 2 cal/mole/°C. The linear increase extends to approximately 600°K (see Fig. 12.6). Near 800°K a pronounced curvature occurs, and C_p increases more slowly with increasing temperature. At approximately 2000°K C_p attains the value 6 cal/mole/°C characteristic of all monatomic solids at high temperature. Above 2000°K C_p increases slowly with temperature except for a sudden rise above 3300°K. This sudden rise is probably associated with a rapid increase in the number of vacancies. Such an increase near the melting or sublimation temperature is predicted and has been observed in several metals.⁶

The specific heat in the range 1 to 20°K has recently been the object of intensive theoretical and experimental investigations.⁷⁻¹⁰ At these low temperatures a crystallite-size effect is noted; the specific heat is larger in graphites composed of small crystallites. Figure 6.2 illustrates the marked

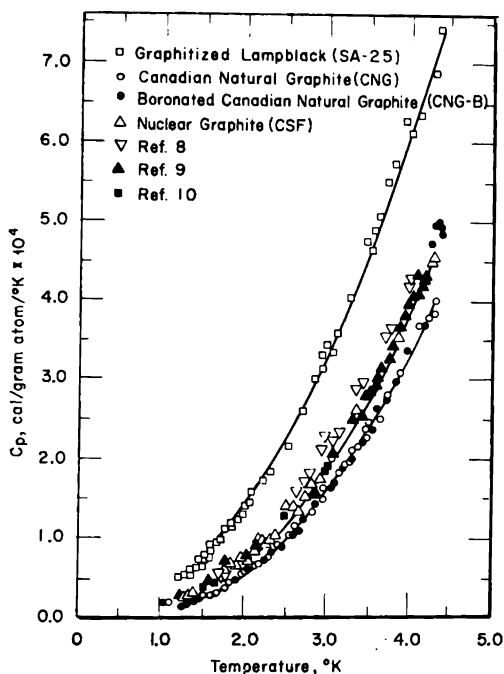


FIG. 6.2 The low-temperature specific heat of graphite. (From Desorbo and Nichols, *Physics and Chemistry of Solids*, Ref. 7.)

difference in behavior of various graphites at low temperatures and, in addition, indicates the good agreement in specific-heat measurements among the several investigators. The material CNG is a Canadian natural flake graphite having a high degree of crystalline perfection; CNG-B is the same material doped with boron to greatly reduce the free-electron concentration (see Table 6.23). The specific heats of CNG and CNG-B are identical at low temperature. Since it has been shown¹¹ by thermal-conductivity meas-

urements that boron doping does not change the lattice vibrational spectrum in the liquid-helium temperature range, it may be concluded that the free-electron concentration has little effect on the specific heat. Thus, although some contribution to the specific heat is expected from the free electrons, the magnitude must be small in comparison with the lattice contribution. Because the electron concentration is not a major factor, the difference in specific heat between natural flake graphite and the poorly graphitized carbon, SA-25, must be due to structural differences.

One interpretation¹² of the specific-heat curves ascribes the excess heat capacity of poorly graphitized material to a change in the magnitude of the modulus for interplanar shear. A more recent interpretation¹³ ascribes the excess heat capacity to a boundary effect which is proportional to the specific free surfaces of crystallites in the graphite. In this analysis a contribution from free electrons is assumed, and the final form for the specific heat in the limit of very low temperatures ($<15^\circ\text{K}$) is given by

$$C_p = \alpha T + \beta T^2 + \gamma T^3 \quad (6.1)$$

where α , β , and γ are constants. The linear term is the electronic contribution, and the value of α is obtained from calculations of the free-electron and hole concentrations based on the band theory. The second term is the component that depends on the particle size. The term in T^3 is the limiting low-temperature lattice contribution.¹⁴

6-1.3 THERMODYNAMIC FUNCTIONS

The thermodynamic functions of graphite at low temperature have been derived¹⁵ from the specific heat. The values are given in Table 6.2. The usual symbols for standard enthalpy (H°), entropy (S°), and free energy (F°) are used. Subscripts refer to the absolute temperature to which the values apply. Table 6.3 gives the values above room temperature.

6-2 Thermal Properties

6-2.1 THEORY OF THERMAL CONDUCTIVITY

Since graphite is a metallic type conductor of electricity, it might be anticipated that the electrons and holes that are responsible for the conduction of electricity would also transport heat. However, all evidence indicates that heat is transferred by lattice vibrations (phonons) rather than by electrons or holes. For example, in graphite the Weidemann-Franz ratio (R_{WF}) defined by

$$R_{WF} = \frac{k\rho}{T} \quad (6.2)$$

where k is the thermal conductivity, T is the absolute temperature, and ρ is the electrical resistivity, is much larger than in metals. For electronic

Table 6.2 — THERMODYNAMIC PROPERTIES OF GRAPHITE AT LOW TEMPERATURES BASED
ON THE SMOOTH CURVE OF SPECIFIC HEAT¹⁶

$T, ^\circ\text{K}$	$C_p,$ cal/mole/ $^\circ\text{K}$	$H_T^\circ - H_0^\circ,$ cal/mole	$(H_T^\circ - H_0^\circ)/T,$ cal/mole/ $^\circ\text{K}$	$S^\circ,$ cal/mole/ $^\circ\text{K}$	$-(F_T^\circ - H_0^\circ)/T,$ cal/mole/ $^\circ\text{K}$
13	0.0080	0.0421	0.0032	0.0041	0.0009
15	0.0102	0.0592	0.0039	0.0056	0.0017
25	0.0300	0.2478	0.0099	0.0154	0.0055
50	0.1210	2.0226	0.0404	0.0629	0.0225
75	0.2501	6.5963	0.0879	0.1346	0.0467
100	0.3963	14.674	0.1468	0.2275	0.0807
125	0.5723	26.714	0.2137	0.3346	0.1209
150	0.7718	43.456	0.2897	0.4563	0.1666
175	0.9804	65.339	0.3733	0.5925	0.2192
200	1.180	92.460	0.4623	0.7384	0.2761
225	1.461	124.895	0.5551	0.8916	0.3365
250	1.629	162.846	0.6514	1.0510	0.3995
275	1.843	206.232	0.7500	1.2157	0.4658
298.16	2.038	251.183	0.8424	1.3718	0.5294
300	2.053	254.946	0.8498	1.3846	0.5348

Table 6.3 — THERMODYNAMIC PROPERTIES OF GRAPHITE
ABOVE ROOM TEMPERATURE^{16, 17}

$$(H_{298}^{\circ} - H_0^{\circ} = 251 \text{ cal/mole})$$

$T, ^{\circ}\text{K}$	$C_P,$ cal/mole/ $^{\circ}\text{K}$	$H_T^{\circ} - H_{298}^{\circ},$ cal/mole	$S_T^{\circ},$ cal/mole/ $^{\circ}\text{K}$	$-(F_T^{\circ} - H_{298}^{\circ})/T,$ cal/mole/ $^{\circ}\text{K}$
298	2.07	0	1.37	1.37
300	2.08	4	1.38	1.37
400	2.85	251	2.09	1.47
500	3.50	569	2.80	1.67
600	4.03	947	3.49	1.92
700	4.43	1370	4.14	2.19
800	4.75	1830	4.75	2.47
900	4.98	2318	5.33	2.76
1000	5.14	2823	5.86	3.04
1100	5.27	3344	6.35	3.31
1200	5.42	3874	6.82	3.60
1300	5.57	4428	7.26	3.86
1400	5.67	4990	7.67	4.11
1500	5.76	5562	8.07	4.37
1600	5.83	6142	8.44	4.61
1700	5.90	6728	8.80	4.85
1800	5.95	7320	9.14	5.08
1900	6.00	7918	9.46	5.30
2000	6.05	8520	9.77	5.51
2100	6.10	9133	10.07	5.73
2200	6.14	9745	10.35	5.93
2300	6.18	10360	10.63	6.13
2400	6.22	10980	10.89	6.32
2500	6.26	11600	11.14	6.50
2600	6.30	12230	11.39	6.69
2700	6.33	12860	11.63	6.87
2800	6.36	13500	11.86	7.04
2900	6.39	14140	12.08	7.21
3000	6.42	14780	12.30	7.38
3500	7.46	18100	13.30	8.13

conductors of heat, the value of R_{WF} is predicted from theory to be a universal constant equal to 2.45 ohm-watts/deg². In most metals the observed value is between 2 and 3. However, in both single-crystal and polycrystalline graphite, the observed value of R_{WF} is 10 to 100 times larger.¹⁸ In addition, it has been found that drastic changes in the charge-carrier population produced by boron doping of graphite has only a slight effect on the thermal conductivity.¹¹ These facts imply that electronic conduction is not the primary mode of heat transfer in graphite.

Although the Weidemann-Franz ratio in graphite is not equal to the value predicted for a metal, it has been found empirically that the ratio of the electrical to thermal conductivity is a constant for almost all electrographites heat-treated above about 2600°C. If k is expressed in calories

per second per centimeter per degree centigrade and ρ is expressed in ohm-centimeters, the empirical relation

$$k = \frac{0.00031}{\rho} \quad (6.3)$$

is reported¹⁹ to be accurate for a number of graphites to ± 5 per cent for room-temperature measurements. It should be emphasized that this relation holds only for material heat-treated to 2600°C or more since the value of the ratio k/ρ varies with heat-treatment temperature up to about 2600°C and is constant only above that temperature. This relation becomes less accurate as the measuring temperature exceeds room temperature.

The conduction of heat in nonmetallic materials occurs by lattice vibrations (phonon conduction). It is characteristic of such processes that as the temperature is reduced the thermal conductivity becomes a function of the crystallite size. Scattering of phonons at the crystal boundaries limits the mean free path for the phonons. The thermal conductivity is given approximately by

$$k = \frac{1}{3} C_p \lambda v \quad (6.4)$$

where C_p is the specific heat, λ is the phonon mean free path, and v is the phonon velocity. At low temperatures, where phonon-phonon scattering can be neglected, k should be directly proportional to the specific heat. If this proportionality is assumed and if the phonons are assumed to travel with the velocity of sound, the mean crystallite size can be computed for any given graphite. The results²⁰ of such computations are in fair agreement with crystallite sizes calculated from measurements of the X-ray line broadening (see also Sec. 10-6.1).

At very low temperatures (10 to 20°K), the thermal conductivity of polycrystalline graphite decreases more rapidly with temperature than the specific heat.²¹ This has been explained as follows:¹⁸ It is assumed that the crystallites are bonded by an amorphous carbon layer. The specific heat of the amorphous carbon is expected to vary as T^3 , in common with most solids, whereas the specific heat of graphite crystallites having a predominantly two-dimensional structure is known⁷ to vary as $T^{2.4}$ between 10 and 20°K. Therefore the thermal conductivity of the amorphous carbon decreases more rapidly than the thermal conductivity of the crystallites as the temperature decreases. At sufficiently low temperatures the thermal conductivity of the graphite is determined by the thermal conductivity of the amorphous regions and therefore displays a T^3 dependence. However, the total specific heat of the graphite has a $T^{2.4}$ dependence because the crystallites determine the specific heat.

For well-crystallized graphites the thermal conductivity is a maximum near room temperature. This maximum occurs at a lower temperature in graphites with large crystallites and becomes very broad and is displaced

to high temperatures in graphites composed of small crystals (see Fig. 10.10). This behavior is predicted from Eq. 6.4 and is discussed further in Sec. 10-6.1.

6-2.2 THERMAL CONDUCTIVITIES OF GRAPHITE

In common with other properties, the thermal conductivity of single crystals of graphite is highly anisotropic. At room temperature the ratio of k measured transverse to the $[0\ 0\ l]$ direction to that measured parallel to the $[0\ 0\ l]$ direction is about 5. This anisotropy in the crystallites is reflected in the anisotropy of polycrystalline graphites. For most nuclear graphites the thermal conductivity measured parallel to the grain [$k(\parallel)$] ranges from 0.3 to 0.6 cal/(sec)(cm)(°C). The thermal conductivity measured perpendicular to the grain [$k(\perp)$] is somewhat lower. A value for the ratio $k(\parallel)/k(\perp) = 2$ is common, but the exact value depends upon the degree of orientation.

6-2.3 MEASUREMENT OF THERMAL CONDUCTIVITY

The determination of k below about 500°C can be accomplished most conveniently by measuring the heat transmitted by a sample in which a temperature gradient is maintained. This method is satisfactory up to temperatures where radiative heat losses become appreciable. Above 500°C radiative losses make accurate measurements difficult. The few measurements that have been reported suggest that k decreases approximately as $1/T$ (see Fig. 10.11).

Above 1000°C k decreases more slowly with increasing temperature.²² At these temperatures conductivity measurements are usually calculated from the radiative losses required to establish a given temperature gradient in the graphite specimen.

In one type apparatus²² the radial temperature distribution in a tube is measured pyrometrically on the surface and in holes drilled in the side of the tube. Radiant heat losses from the cylinder are calculated from the surface temperature.

6-2.4 THERMAL EXPANSION

The coefficient of thermal expansion (CTE) of different polycrystalline graphites near room temperature ranges from 2×10^{-6} to 6×10^{-6} per °C transverse to the extrusion direction and 0.5×10^{-6} to 5×10^{-6} per °C parallel to the extrusion direction. Thus the volume coefficient is much smaller than that of single crystals (Sec. 5-5.3).

The expansion of graphite is not a linear function of temperature. It is customary, however, to speak of an average coefficient of thermal expansion that is just the thermal dilatation divided by the temperature change. It has been found¹⁹ empirically that the average CTE (\parallel) or CTE (\perp) meas-

ured over one range of temperature can be extrapolated to a higher temperature by the addition of a term that depends upon the higher temperature. Table 6.4 gives the term to be added to the CTE measured over the range 20 to 100°C. The values apply to a wide range of polycrystalline graphites with an accuracy of $\pm 0.2 \times 10^{-6}$ per °C.

Table 6.4 — FACTORS FOR CALCULATION OF MEAN
COEFFICIENT OF THERMAL EXPANSION¹⁹

Final extrapolated temperature, °C	Term to be added to CTE determined over temperature range 20 to 100°C, per 10^7 °C
100	0
200	2.0
300	4.0
400	6.0
500	7.7
600	9.2
700	10.4
800	11.4
900	12.3
1000	13.2
1500	17.2
2000	21.2
2500	25.2

An exhaustive study^{23,24} of the effect of processing variables on the thermal expansion of graphite showed that even with a given set of raw materials the volume and linear thermal expansion of polycrystalline graphite varied by as much as 60 per cent. Small coke particle size and pitch impregnation were some of the variations that increased the volumetric CTE.

The effect of calcination temperature of the base-coke aggregate was tested²³ by determining the CTE of graphites that were made from Texas coke calcined between 400 and 2100°C. In both the parallel and transverse directions, a maximum in the CTE occurs for calcination temperatures between 400 and 800°C. The transverse CTE is independent of calcination temperature above 1200°C. In the parallel direction a minimum in the CTE occurs near a calcination temperature of 1200°C, and the CTE increases by about 25 per cent for graphite made from coke calcined at 2100°C.

The maximum processing temperature also affects the CTE. Figure 6.3 shows the variation in CTE (||) as a function of maximum heat-treatment temperature for a coke-base mix. The CTE is sensitive to the heat-treatment temperature,²³ particularly below 700°C. However, even at higher temperatures the CTE varies significantly with final graphitization temperature. Material prepared from coke that has not been calcined appears to have a higher CTE.

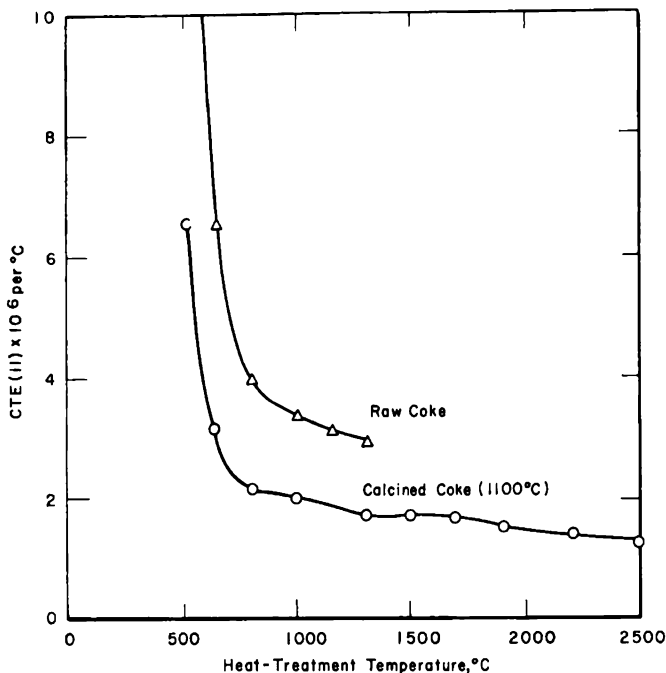


FIG. 6.3 The average coefficient of thermal expansion measured between 0 and 500 $^{\circ}\text{C}$ parallel to the direction of extrusion. The mix was prepared from Kendall coke.²³

6-2.5 THERMAL SHOCK

During rapid cooling of a body, the outer layers, which are at a lower temperature than the interior, contract more rapidly than the interior. As a result, tensile stresses develop at the surface, and compressive stresses, in the interior. A similar stress distribution can be generated when the body is heated rapidly from within. In the case of sudden heating of the body from the exterior, the exterior experiences a compressive stress, and the interior, a tensile stress. Generally, it is experimentally more convenient to quench heated samples than to heat samples rapidly. Hence rapid cooling is commonly used as a test of thermal-shock resistance.

When a heated body is suddenly quenched, the magnitude of the thermal gradient at the surface depends on the thermal conductivity of the body. For a given thermal gradient, the thermal strains depend on the magnitude of the coefficient of thermal expansion. A low value for the elastic modulus yields a lower thermal stress for a given thermal strain. Finally, a high tensile strength enables the material to withstand the thermal stress. Thus, the thermal-shock resistance for sudden cooling is high in a material that has a low coefficient of thermal expansion (α), a high thermal conductivity (k), a high tensile strength (S), and a low modulus of elasticity (E). Values of the figure of merit $KS/\alpha E$ for graphite and a number of other materials are given in Table 6.5. Graphite clearly outranks other high-temperature

refractory materials in thermal-shock resistance on the basis of this figure of merit. As a dramatic example of shock resistance, graphite specimens have been heated to 1650°C and quenched in water without damage.¹⁹

Table 6.5 — RELATIVE THERMAL-SHOCK RESISTANCE²⁵

Material	$kS/\alpha E$, cal/cm/sec
Graphite (grade AUF)	574
Titanium carbide	3.45
Beryllium oxide	1.21
Zircon	0.445
Magnesium oxide	0.122 to 0.349
Stabilized zirconia	0.065

6-2.6 SELF-DIFFUSION IN GRAPHITE

In the general theory of diffusive processes, the diffusion coefficient, D , is given by

$$D = A\lambda^2\nu \exp \left[\frac{\Delta S - (E/T)}{R} \right] \quad (6.5)$$

where A = a constant determined by the lattice geometry and the particular type of diffusive process

λ = a characteristic length having a value on the order of the lattice constant

ν = the lattice frequency

ΔS = the entropy change associated with the diffusion process

E = the activation energy for the formation and motion of the mobile unit

R = the gas constant

T = the absolute temperature

If the temperature-independent parameters are lumped into a constant, B , Eq. 6.5 reduces to

$$D = Be^{-E/RT} \quad (6.6)$$

Both experimental and theoretical investigations have concentrated on the determination of the activation energy, E .

Several possible mechanisms have been proposed for self-diffusion in graphite, and the activation energies have been calculated for the most likely mechanisms.^{26,27} Since exact interaction potentials are not known, estimates were made from the relation between the energy and length of the C—C bond in several carbon-based materials. These materials ranged from diamond with a C—C spacing of 1.54 Å and an energy† of 81 kcal/

† The bond energies for diamond and acetylene quoted in Ref. 26 were based on a heat of sublimation for graphite of 110 kcal/mole. The bond energies given here are based on the more recent value of 170 kcal/mole.

mole to acetylene with a $C\equiv C$ bond spacing of 1.20 Å and an energy of 192 kcal/mole. The bond-angle energy was estimated from the behavior of polymeric systems. The energy of formation of a vacancy was estimated from the heat of sublimation, and the energy of formation of an interstitial was estimated from a van der Waals attractive potential and an exponential repulsive potential. Using the value 170 kcal/mole for the heat of sublimation, Kanter²⁷ concluded that the atomic interchange mechanism with an activation energy of 113 kcal/mole was most probable for diffusion in graphite.

The activation energy for volume diffusion has been measured²⁸ from the uptake of C^{14} atoms in flakes of natural graphite heated in an atmosphere of $C^{14}O$. An activation energy of 163 ± 12 kcal/mole was obtained; at 2350°C the diffusion coefficient was 10^{-12} cm²/sec. Compared to the calculated value of 113 kcal/mole the observed activation energy is rather high; however, the accuracy of the calculated value is not high. An interstitial mechanism for self-diffusion appears to be excluded by the experimental results, but as yet there is no direct experimental evidence to allow a choice between the vacancy and the direct-interchange mechanism for self-diffusion.²⁷

In common with most other properties, diffusion in graphite is believed to be extremely anisotropic. The loose bonding between layers compared to the bonding within the layers leads to the expectation that the rate of diffusion along the layer planes would be much greater than across the planes. However, there is as yet no direct experimental proof of such an anisotropy.

Within metals it has been noted that regions of disorder, such as grain boundaries, dislocations, and uncrystallized regions, exhibit higher diffusion rates than the crystalline regions. Although perfect single crystals of graphite have no disordered regions, polycrystalline graphites do contain disordered regions through which diffusion may occur. Partially graphitized materials, binder-coke junctions, and dislocations are regions where the diffusion mechanism may differ from that for a perfect crystal. Thus it is necessary to separate the diffusion through the crystallized regions from the total diffusion before comparing theoretical predictions with experimental results.

The experimental determination of diffusion in polycrystalline graphite has been accomplished by measuring the depth of penetration of C^{14} atoms deposited on the surface.²⁹ An effective diffusion constant of $D = 1.2 \times 10^{-9}$ cm²/sec was measured at 2370°C. This value, which includes both volume and boundary diffusion, is about three orders of magnitude larger than the value obtained in natural flake graphite at 2350°C. Undoubtedly part of this large difference is due to the much larger volume of disordered regions in polycrystalline graphite.

6-3 Electronic Band Structure

The electronic band structure of graphite has received a great deal of attention from theoretical and experimental investigators in recent years.³⁰ Throughout the theoretical investigations the symmetry properties of the Bernal structure of graphite (Sec. 5-2) have played a major role since wave functions are constructed using group theoretical analyses based on the geometry of the lattice. Initially, the theoretical treatments were based on a two-dimensional model that neglected interlayer interactions. This is a fair approximation, and the results from such an analysis were used in more refined calculations that included the interlayer interactions. The more exact form of the band structure is in terms of interaction parameters that cannot be evaluated directly inasmuch as the appropriate wave functions and interaction potentials are not known.

The Brillouin zone is defined in the momentum space of the electrons. The momentum states included within a zone correspond to the allowed energy states of the band model. The nominal energy limit of the filled electron states is the Fermi level. Because the relation between energy and momentum is quite complex in most solids, the Fermi level may not coincide with the boundaries of the Brillouin zones. A detailed examination of the regions near the Fermi levels yields information on the possible momentum states that could give rise to free electrons within a solid. The presence or absence of free electrons determines whether the material in question displays a metallic, semiconductive, or nonmetallic character.

The form of the Brillouin zone for the Bernal structure of graphite is a hexagonal pill box with the top and bottom planes corresponding to wave vectors in the graphite planes and with the vertical edges parallel to the wave vectors in the c direction. The rhombohedral modification of graphite yields an entirely different zone, and as a result the band structure is different from that for the Bernal structure.³¹ The effect on the band structure of an admixture of the rhombohedral modification in a crystal with predominantly Bernal structure is not known.

Since the $1s$ electrons are well localized and are considered part of the ion core, only the $2s$ and $2p$ electrons of the isolated atom participate in the formation of the band structure in graphite. In the two-dimensional approximation, molecular orbital theory can be used to construct wave functions, which are designated as even states (π states) or odd states (σ states).

The lower σ bands are filled with electrons. The lower π band, which is normally filled, is the valence band; the upper π band, which is normally empty, is the conduction band. It is found that the σ bands are well separated in energy but that the π bands are degenerate in energy in the two-dimensional model.³² This degeneracy, which is solely due to crystal symmetry, leads to the incorrect prediction of a completely metallic character

for graphite. Therefore the calculations must be refined by taking into account the three-dimensional nature of the graphite lattice.

In the three-dimensional calculations, the degeneracy is modified. The three-dimensional calculations are most detailed in those regions where overlap or near overlap of the valence and conduction bands may occur. Near overlap is characteristic of an intrinsic semiconductor since thermal energies are then sufficient to excite electrons from the valence band into the conduction band. When overlap occurs, free electrons are present in the conduction band, and holes are created in the valence band at all temperatures. The occurrence of overlap depends principally upon the strength of the interlayer interaction. The form of these interactions has been computed by a perturbation technique to extend the detailed picture of the band structure into the overlap regions.³³

6-3.1 OVERLAP BAND MODELS

The character of the band structure is controlled by the magnitude of the interactions between atoms in the lattice. Two species of atoms are distinguished: *A* atoms, which lie directly above atoms in the adjacent planes, and *B* atoms, which lie directly above the centers of hexagons formed in the adjacent planes. In the generally accepted notation,³⁴ the intralayer interaction energy between *A* and *B* atoms is γ_0 . The interaction energy between *A* atoms on adjacent layer planes is γ_1 , and the interaction energy between *B* atoms on next nearest layers is γ_2 . The interaction energy between *A* and *B* atoms on adjacent layers, γ_3 , largely cancels owing to phase relations. Another quantity, Δ , is related to the energy difference between *A* and *B* atoms caused by the nonequivalence in the configurations of their nearest-neighbor atoms.

In one model of the band structure,³⁵⁻³⁷ the following set of parameters has been found to yield a consistent interpretation of almost all experimental observations of electronic properties in graphite:³⁸

$$\begin{array}{ll} \gamma_0 = 3.0 \text{ ev} & \gamma_2 = 0.016 \text{ ev} \\ \gamma_1 = 0.35 \text{ ev} & \Delta = 0.022 \text{ ev} \end{array}$$

These values are fixed by fitting the observed electronic properties, i.e., Hall effect, magnetoresistance, and de Haas-van Alphen effect, with formulas derived theoretically for the overlap model. With this set of constants, the branches of the valence and conduction band overlap, and this leads to the presence of free electrons and holes. Additional features can be seen in the band structure shown in Fig. 6.4, which was developed from this set of parameters.

An alternative model has been proposed in which the large diamagnetism of graphite is explained³⁹ on the basis of extreme degeneracy in the bands arising from a very small value for γ_1 of about 0.005 ev. Although the source of the free electrons and holes that are observed in graphite is unex-

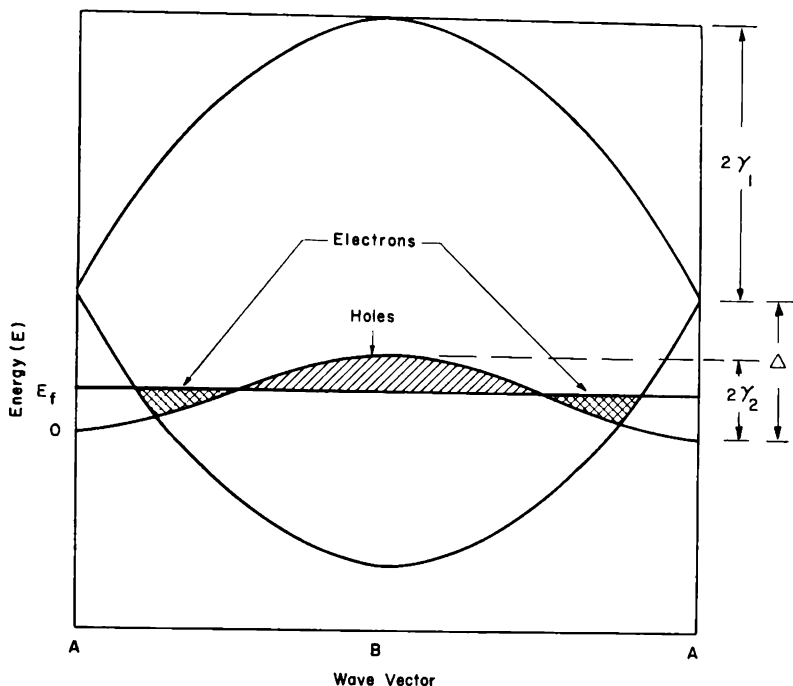


FIG. 6.4 The energy band structure along the edge of the Brillouin zone. E_f is the Fermi level. The presence of both free electrons and holes is indicated. (From Haering and Mrozowski, *Progress in Semiconductors*, Vol. 5, Heywood & Company, Ltd., Ref. 30.)

plained, this model is capable of yielding results consistent with a number of experimental observations.

6-3.2 ELECTRONIC BAND STRUCTURE OF POLYCRYSTALLINE GRAPHITE

The knowledge of the band structure in polycrystalline graphite is based upon the band structure derived for single crystals. Some insight into the band structure of polycrystalline graphite can be gained⁴⁰ from the changes in electronic properties of carbons with heat-treatment temperature (H_T).

For carbons with $H_T < 500^\circ\text{C}$, there is a large energy gap between the valence and conduction bands. However, the Fermi level lies deep within the valence band, giving rise to a concentration of free electrons as indicated by the negative value for the Hall coefficient. Although there is a large carrier concentration, the electrical conductivity is low since the effective mass of the carrier is high. In addition to the large effective mass, the larger number of crystallite boundaries, a necessary consequence of the small crystallite size, reduces the bulk conductivity.

With increasing H_T , the energy band separation decreases, and, in addition, the Fermi level rises. At $H_T \simeq 1750^\circ\text{C}$ the sign of the predominant charge carrier changes from negative to positive. This change in sign is

reflected by the change in the sign of the Hall coefficient and of the thermoelectric power. The maximum in the positive charge-carrier concentration occurs at $H_T \simeq 1900^\circ\text{C}$.

For $H_T > 1900^\circ\text{C}$ the number of negative carriers increases until, at $H_T = 2300^\circ\text{C}$, the Hall coefficient changes sign once again, indicating a predominance of negative charge carriers. For $H_T > 2300^\circ\text{C}$ the charge-carrier concentrations are approximately constant, but their mobilities continue to increase.

Overlap of the valence and conduction band takes place at $H_T \simeq 2600^\circ\text{C}$. Because of this overlap both negative and positive charge carriers are present. Thus the band structure of fully graphitized polycrystalline graphite is substantially the same as that of single crystals. This similarity suggests that the crystallite size of graphitized polycrystalline material is sufficiently large that surface and boundary effects do not strongly perturb the band structure.

6-4 Electronic Properties

The electronic band structure obtained theoretically is dependent upon experimental determinations of various electronic properties for the detailed configuration of the energy bands. Because graphite has a relatively small number of carriers, it possesses some of the properties of both a metal and semiconductor. There are, therefore, a variety of electronic properties that help to characterize the band structure.

6-4.1 MAGNETIC SUSCEPTIBILITY

The magnetic susceptibility (χ) of a substance is obtained from the ratio of the induced magnetic moment to the applied field. If χ is negative, the substance is diamagnetic and is repelled from the strongest part of an inhomogeneous magnetic field. Pure crystalline graphite has a very large anisotropic diamagnetic susceptibility; $\chi = -21.5 \times 10^{-6}$ emu/g in the a direction⁴¹ and -0.5×10^{-6} emu/g along the c axis.⁴²

Recent calculations of the susceptibility of graphite based on the three-dimensional overlap band model³⁸ yield excellent agreement with experimental results. Best agreement with experiment is obtained with values of the band parameter nearly equal to the values obtained from the de Haas-van Alphen effect. For the parameters that significantly affect the value of the diamagnetism, the values are $\gamma_0 = 2.8 \pm 0.1$ eV, $\gamma_1 = 0.27$ eV, and $\Delta = 0.025$ eV.

The diamagnetic susceptibility is highly dependent on the crystallite size in the a direction in carbons and polycrystalline graphite. For a variety of carbons,⁴³ there is an abrupt increase in χ at $H_T = 1500^\circ\text{C}$, which levels off above 2300°C . The large increase in χ occurs in the crystallite-size range from 75 to 150 Å. Doping with bisulfate ions⁴⁴ reduces χ for graphites with a crystallite size larger than 150 Å and produces a maximum in χ at $H_T =$

2200°C. This reduction in the value of χ is expected since the bisulfate ion introduces excess holes into the π band. However, the maximum in χ has not been explained, although it has been conjectured that the presence of bisulfate atoms may perturb the band structure. In view of the behavior of χ during graphitization, it is expected that upon irradiation χ would decrease as the lattice becomes more disordered. Such a decrease has been observed (Fig. 10.6).

6-4.2 DE HAAS-VAN ALPHEN EFFECT

The magnetic susceptibility of graphite is a function of the strength of the applied field (H). If the susceptibility is plotted against $1/H$, the variations in the susceptibility are periodic. This periodic variation in susceptibility is known as the de Haas-van Alphen effect. The presence of this effect results from the variation in the free-electron population as a function of the applied magnetic field.

The number of different kinds of carriers, their density, and their mobility are obtained from the amplitude and periods of the de Haas-van Alphen effect. In graphite crystals strong evidence^{45,46} is found for two periods, implying the existence of two charge carriers. Less firm indications of two additional periods have been found,^{47,48} which, if confirmed, would bring the total number of charge carriers to four.

6-4.3 HALL EFFECT

In a magnetic field a force is exerted on a moving charged particle which is perpendicular to the direction of motion. The force is given by the vector product of the magnetic field and the velocity of the particle. This same force is exerted on current carriers in electrical conductors when a magnetic field is applied. This force is counterbalanced by the generation of an electric field proportional to the vector product of the electric current (\mathbf{I}) and the magnetic field (\mathbf{H}). The potential difference across the conductor is known as the Hall voltage (E_H), and the Hall coefficient (R) is defined by

$$R = \frac{E_H}{\mathbf{I} \times \mathbf{H}} \quad (6.7)$$

For a multicarrier semiconductor the formula for the Hall constant⁴⁹ is given by

$$R = K \frac{n_h \mu_h^2 - n_e \mu_e^2}{(n_h \mu_h + n_e \mu_e)^2} \quad (6.8)$$

where K = a constant

n_h = the density of holes

μ_h = the mobility of holes

n_e = the density of electrons

μ_e = the mobility of electrons

In single-crystal graphite R exhibits an alternation in sign as a function of H . This alternation in sign, in conjunction with the values of the mobility of the majority carriers obtained from other experiments, is additional evidence of both free electrons and holes. Recent measurements⁴⁶ of the Hall effect at low magnetic fields and low temperature indicate the presence of minority carriers possessing substantially higher mobilities than the majority carriers.

In polycrystalline graphite R is constant for temperatures above 77°K and for fields greater than 2 kilogauss.⁴⁹ This high-temperature high-field value is usually the one quoted as the Hall coefficient for polycrystalline graphite. As seen in Table 6.6, fully graphitized petroleum-coke-based graphites display a negative R , indicating a preponderance of negative charge carriers. However, lampblack heat-treated to 3000°C displays a positive R , indicating that the sign of the predominant charge carrier is positive. It is concluded that the degree of crystallinity in lampblack-based materials with $H_T = 3000^\circ\text{C}$ is typically that of graphitizable carbons that have been treated to a much lower temperature.

Table 6.6 — HALL COEFFICIENTS OF CARBONS AND GRAPHITES⁵⁰

Material	Heat-treatment temperature (H_T), °C	Hall coefficient (R) at 300 °K, cm ³ /coulomb
Raw petroleum coke		-0.021
Petroleum-coke graphite (CSF)	2800	-0.06
Petroleum-coke graphite (AGX)	2600	-0.051
Petroleum-coke graphite (ECA)	3000	-0.049
Lampblack (SA-25)	3000	+0.014
Natural-graphite compact (pitch bonded)	3000	-0.038

The sign of the Hall coefficient in nuclear-grade graphites changes from negative to positive when subjected to reactor radiation (Sec. 10-3).

6-4.4 MAGNETORESISTANCE

The magnetoresistance is the change in the electrical resistance which results when a magnetic field is applied. It depends upon the transport properties of the charge carriers. The magnetoresistance has been used to derive values for the band parameters in the overlap model of graphite.

The variation in magnetoresistance with the direction of the applied magnetic field has also been used to determine the degree of anisotropy of the Fermi surface. A measure of the anisotropy of the Fermi surface is the ratio of the cross-sectional areas of the surfaces parallel and perpendicular to the edges of the Brillouin zone. The ratio obtained from the magneto-

resistance is about 12 to 1, which is in substantial agreement with semi-theoretical predictions.⁵¹

The magnetoresistance in polycrystalline materials is much less than in single crystals.⁴⁹ In Table 6.7 are found the values of the ratio $\Delta\rho/\rho$, where $\Delta\rho$ is the increase in electrical resistance upon application of a magnetic field and ρ is the initial resistance. In common with the Hall coefficient, the magnetoresistance is a function of both the temperature and the magnetic field. An $H^{1.74}$ dependence on the magnetic-field strength is observed between 77 and 290°K in polycrystalline graphite. An identical magnetic-field dependence occurs in single crystals at 290°K.

Table 6.7 — MAGNETORESISTANCE IN GRAPHITES AT 2140 GAUSS

Material	Heat-treatment temperature, °C	Magnetoresistance ratio				Reference
		300°K	195°K	77°K	4.2°K	
Petroleum-coke graphite	2600	0.0016	0.0020	0.0039		49
Petroleum-coke graphite (AGOT)	2800	0.0046				50
Petroleum-coke graphite (C-15)	3000	0.013				50
Single crystal		0.093		2.24	259	50

Part of the temperature dependence for single crystals can be related to the increase in ρ with increase in temperature. Thus, as the temperature increases, the same absolute magnetoresistance ($\Delta\rho$) would give rise to a smaller magnetoresistance ratio.

The low value of magnetoresistance ratio for polycrystalline graphites is due to several factors. The scattering of charge carriers at imperfections reduces the mean free path; carriers are also trapped at imperfections. Both effects reduce $\Delta\rho$ and hence the magnetoresistance ratio. The presence of crystalline imperfections and boundaries increases ρ , which also causes the magnetoresistance ratio to be lower in polycrystalline graphite than in single crystals. This explanation probably also accounts for the decrease in magnetoresistance ratio that has been observed when imperfections are introduced by neutron irradiation (Sec. 10-2).

At low temperatures identical periodicities for a given magnetic field are observed in the magnitude of magnetic susceptibility, magnetoresistance, and Hall effect. Since these electronic properties at low temperature are dependent on the density of states at the Fermi level, the identical periodicity in the three effects is not unexpected. However, the phase difference in the position of the maxima in the susceptibility, magnetoresistance, and Hall effect remains unexplained.

6-4.5 CYCLOTRON RESONANCE

A free charged particle moving perpendicular to a fixed magnetic field spirals with a frequency independent of the speed of the particle. If scattering processes do not interfere, electrons in metals also spiral when a magnetic field is applied. This process, known as "cyclotron resonance," is manifested by an increase in absorption of microwave radiation of the proper frequency. In practice the microwave frequency is kept fixed, and the magnetic field is varied.

Cyclotron resonance absorption has been observed in graphite at 24,000 and 72,000 Mc/sec. At the two frequencies the absorption effects obey the cyclotron-resonance relations, thereby confirming the identification of the absorption as cyclotron resonance.⁵² The results of these experiments have been interpreted on the basis of a three-dimensional electron band model for graphite. A continuous distribution of the effective masses is found for both carriers. If m_0 is the rest mass of a free electron,⁵³ the mass of one of the carriers ranges from 0 to 0.054 m_0 and of the other from 0.054 to 0.066 m_0 . From results of Hall measurements, the lighter carriers have been identified as electrons and the heavier carriers as holes.

6-4.6 ELECTRON-SPIN RESONANCE

Electron-spin resonance in graphite is predicted by the overlap model of the electronic band structure.⁵⁴ The shape of the resonance line corresponds to that predicted theoretically⁵⁵ for mobile charge carriers. In addition, the linear temperature dependence of the resonance-line intensity is in accord with predictions of the band models of the temperature dependence of the spin paramagnetism. Finally, the absolute intensity is in agreement with theoretical calculations, and hence the electron-spin resonance is ascribed to the presence of mobile charge carriers.⁵⁶

The anisotropy of the resonance with orientation of the applied magnetic field in the plane of the c axis of the graphite crystal is very pronounced. Since the magnitude of this anisotropy decreases rapidly with increasing temperature and is almost eliminated upon doping the graphite with 0.037 per cent boron, the anisotropy is very sensitive to changes in the Fermi level.⁵⁶

Electron-spin resonance has been measured in irradiated and in unirradiated polycrystalline graphite.^{57, 58} In the unirradiated graphite the spin density is as large as 10^{-4} centers per atom. It has been proposed that the increase to 10^{-3} centers per atom caused by neutron irradiation is associated with single displaced atoms in irradiated graphite.⁵⁸ If this identification is correct, it follows that there are two sources of spin resonance: one due to traps at interstitials and the other due to mobile charge carriers as previously described.

The information on charge carriers derived from various measurements of the electronic properties of single-crystal graphite is summarized in Table 6.8. The majority carriers, both electrons and holes, are most im-

Table 6.8 — PROPERTIES OF CHARGE CARRIERS IN SINGLE-CRYSTAL GRAPHITE⁴⁸

Type of carrier	Effective mass	Number/atom	Mobility, cm ² /volt/sec
Electron	0.036 m_0	3.4×10^{-5}	1.6×10^4
Hole	0.070 m_0	2.5×10^{-5}	1.5×10^4
Minority electron		10^{-9}	4×10^4
Minority hole		10^{-9}	150×10^4

m_0 = free-electron mass.

portant in determining the electronic properties of graphite because they far outnumber the minority carriers. Only at low temperatures are the minority carriers of any significance.

6-4.7 THEORY OF ELECTRICAL RESISTIVITY

The electrical resistivity (ρ) of a metal is given by

$$\frac{1}{\rho} = e \sum_i^N \mu_i n_i \quad (6.9)$$

where μ_i is the mobility of the i th carrier, n_i is the concentration of the i th carrier, N is the number of different charge carriers, and e is the electronic charge. Although the concentration of charge carriers in graphite is only on the order of 10^{-5} per atom, the mobilities are quite large ($\sim 10^4$ cm²/volt/sec). As a result the resistivity is comparable to many metals. The extreme anisotropy of the lattice introduces the further effect that the resistivity across the layer planes is about two orders of magnitude larger than along the planes.

In the band theory this fact is partly explainable on the basis of the concentration of the mobile charge carriers at the edges of the hexagonal Brillouin zone. At these regions the electrons all have momentum vectors predominantly in the a directions. Thus electron transport in the a directions is large compared to that in the c direction. In addition, there is an extreme difference in the curvature of the electron-energy band surfaces. The curvature in the direction of the momentum vector along the c axis is much less than the curvature in the a directions. Since the effective masses are inversely proportional to the curvature of the bands, the effective mass is smaller in the a directions than in the c direction.

6-4.8 ELECTRICAL RESISTIVITY OF SINGLE CRYSTALS

Owing to the small size and the platelet shape of single crystals of graphite, measurements are most conveniently made in the a direction along the graphite planes. At room temperature the lowest value recorded⁵⁹ for the electrical resistivity, ρ_a , of large, very pure, almost perfect single crystals is 0.040×10^{-3} ohm-cm. Direct measurements of the c axis resistivity (ρ_c) give a value of 5×10^{-3} ohm-cm. The resistivity in the c direction at 300°K, inferred from measurements⁶⁰ of the shape of the spin resonance line of single crystals, gives $\rho_c = 3.1 \times 10^{-3}$ ohm-cm.

From 4°K, the lowest temperature at which measurements have been made, ρ_a increases with increasing temperature. The increase is linear with temperature between 15 and 80°K. The value of ρ_c also increases with temperature almost to room temperature, where it goes through a maximum and thereafter decreases. This general temperature dependence is expected in single crystals with few crystal imperfections because scattering of electrons by interactions with lattice vibrations is the controlling factor. At liquid-helium temperatures the only resistance is that due to residual impurities. As the temperature increases, the amplitude of the lattice vibrations increases, and this increases the resistivity.

That the temperature dependence of resistivity is due to scattering by lattice vibrations is confirmed by measurements on irradiated graphite. The increase in resistivity in irradiated material is due to radiation-induced imperfections whose scattering power is not strongly temperature dependent. The resistivity of irradiated crystals⁶¹ actually increases slightly as the temperature is lowered to 4°K.

6-4.9 ELECTRICAL RESISTIVITY OF POLYCRYSTALLINE GRAPHITE

The electrical resistivity of polycrystalline material is greater than that of single crystals owing to several factors. The length of the conduction path along the low-conductivity a direction is longer because the orientation of the crystallites is not perfect; partially graphitized and less perfect regions of high resistance are interspersed within and between the well-crystallized grains; the presence of a large number of intercrystalline boundaries also serves to increase the resistivity by increasing the scattering of the charge carriers; and, finally, the existence of pores restricts the cross-sectional area for conduction to a fraction of the area otherwise available. All these factors increase the electrical resistivity of polycrystalline graphites to values substantially above those of single crystals.

Table 6.9 gives electrical resistivities at room temperature for a range of graphites. Typical values are on the order of 10^{-3} ohm-cm, with a pronounced anisotropy relative to the extrusion axis. The importance of starting materials is emphasized by the fact that the resistivity of graphite made from lampblack is about five times the resistivity of graphite made

from petroleum coke. Differences are also noted in graphites prepared from different petroleum cokes.

In common with other physical properties, the electrical resistivity of electrographite is highly dependent upon the starting materials and upon

Table 6.9 — ELECTRICAL RESISTIVITIES OF TYPICAL GRAPHITES¹⁹

	$\rho(I)$, 10^3 ohm-cm	$\rho(II)$, 10^3 ohm-cm
Lampblack-base graphite (molded)	5.1	4.6
Petroleum-coke graphite (molded)	1.3	1.0
Petroleum-coke graphite (extruded)	1.6	0.9

the processing of these materials. The maximum heat-treatment temperature is one of the most important factors in determining the electrical resistance of the carbon (Fig. 6.5). The coke calcination temperature also effects the resistivity of the graphite.

The electrical resistivities of graphites prepared from natural flake graphite and from calcined petroleum coke are almost equal; they are on

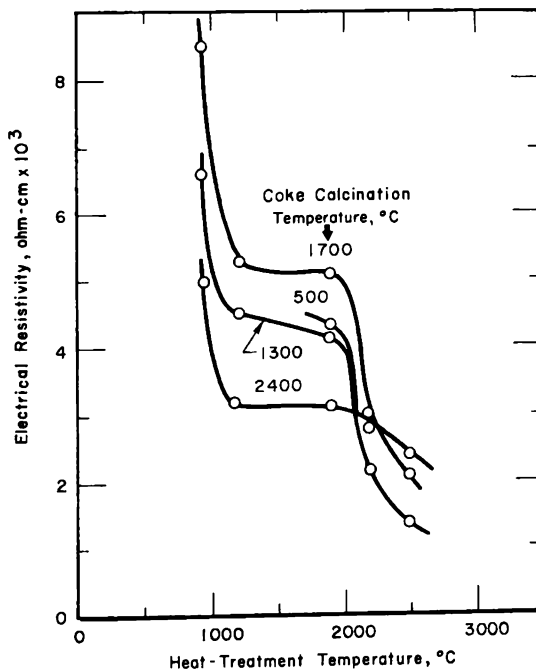


FIG. 6.5 The electrical resistivity of carbons made from petroleum-coke and coal-tar pitch. Except for the coke calcination temperature, the samples were prepared by the same process. (From Okada and Ikegawa, *Journal of Applied Physics*, Ref. 62.)

the order of 25 times greater than that of natural single crystals.⁶³ The large difference in the resistivities of single crystals and polycrystalline bodies prepared from natural flakes and a binder demonstrates the importance of the binder and of the interparticle junctions in determining the resistivity of polycrystalline graphite.

As the temperature of metals and single crystals of graphite is increased, the increase in scattering by lattice vibrations overrides the increase in the number of charge carriers. The temperature coefficient of electrical resistivity is therefore positive. However, the resistivity of polycrystalline graphite decreases with increasing temperature from room temperature to about 500°C. Hence the effect of scattering by lattice vibrations is more than offset by other factors. It has been shown qualitatively that, if the Fermi level is displaced from its level at absolute zero by the presence of impurity or surface states, a negative temperature gradient for the resistivity would result.⁵⁹

Some success in explaining the temperature dependence of the resistivity is achieved⁶³ if the mean free path of the charge carriers (L) is expressed as

$$\frac{1}{L} = \frac{1}{L_a} + \frac{1}{L_b} \quad (6.10)$$

where L_b is a mean free path determined by thermally induced scattering and L_a is the average crystallite size in the $[h k 0]$ direction as determined by X-ray methods. The value of L_b decreases with temperature, whereas L_a is independent of temperature. At low temperature the mobility of the charge carriers is determined mainly by L_a ; at higher temperatures the determining factor is L_b .

If the resistivity in the a crystal direction is given by

$$\rho = F(T) \left(\frac{1}{L_a} + \frac{1}{L_b} \right) \quad (6.11)$$

$1/L_b$ is found to depend on the square of the temperature, and $F(T)$, which is related to the number of available charge carriers, is inversely proportional to the temperature. The temperature dependence of the resistivity can then be expressed as

$$\rho = G \left(cT + \frac{1}{L_a T} \right) \quad (6.12)$$

Differentiation of this expression yields a maximum resistivity at a temperature

$$T_m = (cL_a)^{-1/2} \quad (6.13)$$

In Fig. 6.6 $L_a^{-1/2}$ is plotted against T_m . The confirmation of Eq. 6.13 is quite satisfactory.

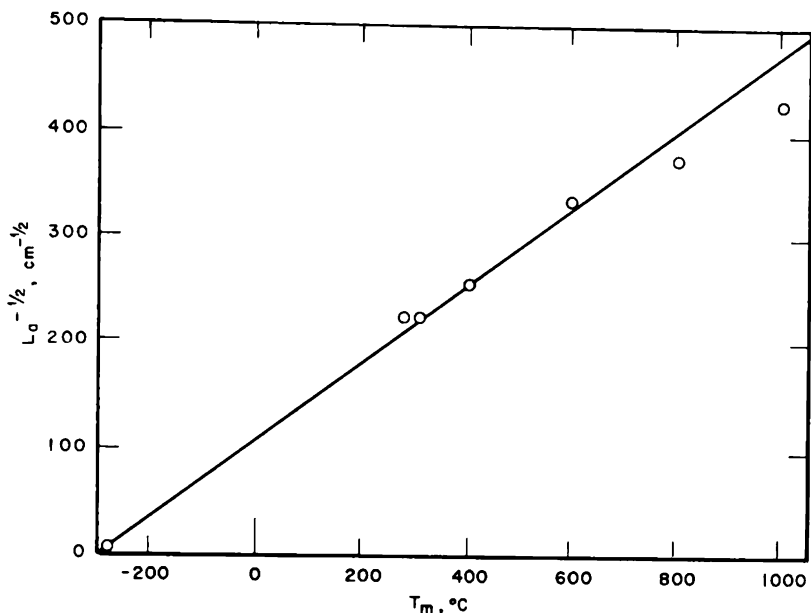


FIG. 6.6 The relation between crystallite size (L_a), as determined from X-ray line broadening, and temperature of minimum resistivity (T_m). (From Mason, *Industrial Carbon and Graphite*, Ref. 63.)

6-4.10 THERMOELECTRIC EFFECT

Unlike the process in metals, heat is conducted in graphite primarily by lattice vibrations. Thus the theories of thermoelectric power that are applicable to metals do not apply directly to graphite. The absolute thermoelectric power in single crystals of graphite is unique in one respect; it is positive in the c direction and negative in the a direction.⁶⁴ This has been interpreted to mean that in the c direction electrical conduction occurs predominantly by electrons. The magnitude of the absolute thermoelectric effect at room temperature in perfect single crystals is approximately $-5 \mu\text{V}/^\circ\text{C}$ in the a direction and $6 \mu\text{V}/^\circ\text{C}$ in the c direction. If impurities or defects are introduced either by doping or by reducing the crystallite size, the thermoelectric power tends to more positive values. In the direction of the a axis, there is an excellent correlation between the electrical resistivity and the thermoelectric power. The thermoelectric power changes from negative to positive as the electrical resistivity increases to above 10^{-4} ohm-cm.

Because of the presence of many imperfections, the thermoelectric power at room temperature is positive in polycrystalline graphite except in the most highly oriented materials (see Fig. 10.5). However, there is an anisotropy in the values with respect to orientation relative to the extrusion axis. The thermoelectric power generally increases with temperature, although exceptions to this have been reported for nongraphitized carbon.⁴⁰

As with electrical resistivity, the thermoelectric power is highly depend-

ent on the processing temperature. For both hard and soft carbons, the room-temperature thermoelectric power reaches a maximum at a processing temperature of 2000°C. It is interesting that the crossover from negative to positive values occurs at about 1700°C. This is approximately the temperature at which the Hall coefficient changes sign. For this reason it is believed that this dependence of the thermoelectric power on processing temperature is determined by the sign and density of the charge carriers. Thus in well-graphitized material an excess of negative charge carriers is indicated.

6-4.11 MISCELLANEOUS ELECTRONIC PROPERTIES

A variety of other experimental data is available which yields general information about the band structure. Photoelectric emission from a variety of graphites indicates that the density of states is relatively low at the Fermi level but increases by severalfold about 1 ev below the Fermi level.⁶⁵ The characteristic energy loss at 7.5 ev of electrons passing through graphite has been tentatively identified with the collective excitation of π electrons.⁶⁶ If this value is used for the characteristic energy loss, an analysis yields a value of 0.32 ev for γ_1 , the interaction energy between A atoms on adjacent layers. A value of 0.14 ev obtained⁵⁹ from infrared absorption in graphite does not agree well with the value of γ_1 derived from other measurements.

6-5 Chemical Properties

Graphite, although generally considered to be chemically inert, does react with many substances under certain conditions. These reactions can be classified as oxidation, carbide formation, or lamellar-compound formation. Reactions with metals, metal oxides, and oxidizing acids and the formation of lamellar compounds are discussed in the sections to follow. Those reactions of greater engineering importance are discussed in more detail in subsequent chapters. Gas reactions are discussed in Chap. 14; the compatibility of metals and fused salts with graphite in Chap. 15; and reactions with fissionable materials, in Chap. 16.

6-5.1 REACTION WITH METALS

Most metals react with graphite at high temperature to form carbides (Table 6.10). The temperature at which a noticeable reaction first occurs varies widely with the particle size of the reactants. Finely dispersed powders react more rapidly at a given temperature than two massive bodies in contact. In this respect it is necessary to distinguish between the chemical reactivity of metals with graphite and their compatibility in a given engineering application. Some metals that react at a significant rate when intimately mixed with graphite may still be compatible if a diffusion-limiting carbide interface is formed. Unfortunately the conditions appli-

Table 6.10 — REACTIONS WITH METALS

Element	Temperature, °C	Product or effect	Reference
Al	800	Al_4C_3 ; reaction rapid at 1400 °C	67
B	1600	B_4C ; commercial preparation carried out at 2400 °C	68
Be	900	Be_2C in vacuum or helium	69
Bi		See Sec. 15-1.1	
Co	218	Co_3C ; Co_3C is metastable; Co_2C is unstable	69
Cs		C_8Cs and other lamellar compounds; occurs with liquid or vapor at a few millimeters pressure	70
Cu	1010	No attack when copper-graphite surfaces contacted for 250 hr (see also Sec. 15-2.1)	71
Fe	600 to 800	Fe_3C	68
Hf	2000	HfC	69
K		C_8K and other lamellar compounds; occurs at temperatures where vapor pressure is a few millimeters of mercury	70
Li	500	Li_2C_2 after long periods; intermediate compounds formed after short times	72
Mg	1100	No attack near melting point	73
Mo	700	Mo_2C ; MoC forms at >1200 °C	74
	1200	Mo_2C (see also Sec. 15-2.1)	69
Na	400	C_{64}Na lamellar compound; reaction slow (see also Sec. 15-1.3)	70
	400	No reaction after carefully degassing to exclude O_2	75
	>450	Na_2C_2	69, 70
Nb	>870	NbC and Nb_2C formed in helium by surface-to-surface contact; some intergranular penetration (see Sec. 15-2.1)	74
Ni	1310	No stable carbides formed; solubility of carbon in Ni is 0.65 wt. % (see Sec. 15-2.1)	76

Table 6.10 (Continued)

Element	Temperature, °C	Product or effect	Reference
Pb	1090	No attack after 24 hr by Pb in Pb-Bi eutectic	77
Pu	1050	PuC from Pu turnings and graphite in vacuum; Pu ₂ C ₃ forms with excess carbon; PuC ₂ exists above 1750°C	78
Rb		C ₈ Rb and other lamellar compounds; occurs at temperatures where vapor pressure is a few millimeters of mercury	70
Si	1150	β -SiC	68
Sn		See Sec. 15-1.4	
Ta	1600	Ta ₂ C in H ₂	69
	2200	TaC (see Sec. 15-2.1)	69
Th	2100	ThC; ThC ₂ in vacuum	69
U	1150	UC; 0.005-cm interface layer in 200 hr	79
	1400	UC and trace of UC ₂ ; 0.07-cm interface layer in 200 hr (see also Sec. 15-1.4)	79
W	1400	W ₂ C and WC in H ₂	69
	1500	Carbide; surface-to-surface contact for 8 min (see Sec. 15-2.1)	80
Zr		See Sec. 15-2.1	

cable to the reaction of a metal with graphite are often not well described. This accounts for some of the results summarized in Table 6.10 which are ill-defined or seemingly contradictory.

The reaction temperatures listed in Table 6.10 are those given in the references. In some cases these correspond to temperatures at which a noticeable reaction first occurs when the graphite and metal are in contact for a few hours. Usually, however, the rate as a function of temperature has not been fully explored, and therefore the reaction may occur at a somewhat lower temperature. With the exception of potassium, rubidium, cesium, and possibly sodium, the reaction products are carbides. Most carbides are stable, although some hydrolyze in moist air. No stable carbides have been reported for a few of the elements.

6-5.2 REACTIONS WITH METAL OXIDES

Graphite reduces the metal oxides to the metals or, with an excess of graphite, to the carbides (Table 6.11). Carbon monoxide is evolved. When

the reaction is carried out in vacuum, the equilibrium for the reaction



is shifted to the right. Reduction to the carbide is usually, although not always, given by the equation

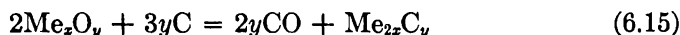


Table 6.11 — REACTIONS WITH METAL OXIDES

Oxide	Temperature, °C		Remarks	References
B ₂ O ₃	1200	†		81
V ₂ O ₅	438	†		82
	650			81
Fe ₂ O ₃	485			82
TiO ₂	930		Particle size of reactants was < 100 mesh	83
	1100	†		81
SiO ₂	1250	†		81
Al ₂ O ₃	1350	†		81
	1280		Al ₄ C ₃ formed	83
	1307 to 1450		Reaction follows parabolic rate law with activation energy of 310 kcal/mole CO	84
BeO	960		Be ₂ C formed	68
	1315	†		81
	2300		2-min surface-to-surface contact	80
ZrO ₂	1300	†		81
	1600		4-min surface-to-surface contact	80
UO ₂	800	†		81
	1320		12% weight lost in 1 hr for -325 mesh UO ₂ and graphite flour	85
	1650 to 2130		Reaction at interface follows parabolic rate law (see also Sec. 16-4.5)	86
MgO	1350	†		81
	1800		8-min surface-to-surface contact	80
ThO ₂	1380	†		81
	1427			87
	2000		4-min surface-to-surface contact	80
PuO ₂	850		Partial reduction	78
	1300		PuC or Pu ₂ C ₃	78

† Finely powdered oxide and graphite mixed in stoichiometric proportion based on reduction to the metal with evolution of carbon monoxide.

6-5.3 LAMELLAR COMPOUNDS

Many materials react with graphite to form lamellar compounds (also called interstitial and intercalation compounds). They are formed with a large number of salts, a few oxides, fluorine, chlorine, bromine, potassium, rubidium, and cesium. Several comprehensive reviews^{70, 88, 89} have recently appeared in which more than 50 different substances that form lamellar compounds are listed. Their preparation usually consists in exposing graphite to the liquid reactant for several hours or to the vapor in a closed system at temperatures where the vapor pressure is at least several millimeters of mercury. About 10 substances have been reported which form lamellar compounds only in an electrolytic cell.

Lamellar compounds are formed by attack at the edge of the carbon layers and diffusion of the reactant between the layer planes. X-ray diffraction studies show that the reactant is present in planar layers, one molecule thick, and separated by several graphitic carbon layers. The ratio of the average number of carbon layers to the number of reactant layers can be varied continuously by varying the concentration or vapor pressure of the reactant. The lamellar compounds C_8K , C_8Rb , C_8Cs , C_8Br , and C_8Cl are among the most concentrated ones known. Most other lamellar compounds are more dilute.

Lamellar compounds are usually better electrical conductors than graphite. It seems very likely that electron transfer between graphite and the reactant occurs during the formation of all lamellar compounds. The halides $C_n^+X^- \cdot 3X_2$, are examples of *p* type lamellar compounds in which electrons have been transferred from the graphite. The well-known potassium compounds of approximate composition $C_n^+K^+ \cdot 4K$ are *n* type.

Lamellar compounds have been used extensively in the study of the graphitization process,^{44, 90, 91} as an analytical method⁹² for estimating the extent of graphitization and as a method of estimating the rate of production of electron traps in irradiated graphite⁹³ (see Sec. 10-4).

6-5.4 MISCELLANEOUS REACTIONS

Graphitic oxide (also called graphitic acid) is formed when graphite is oxidized by strong HNO_3 – H_2SO_4 solutions.^{70, 88} The product does not have a fixed composition and always contains some hydrogen. The carbon-to-oxygen ratios are never less than 2 and may be as high as 3.5 to 4 for incompletely oxidized preparations. In the formation of graphitic oxide, the carbon layer planes are expanded from 3.5 to 6.2 Å. Although the structure has not been determined with certainty, it is likely that the layer carbon atoms are puckered. The carbon interlayer distance increases continuously to 11 Å when graphitic oxide is exposed to water.

Carbons form a wide variety of surface complexes with oxygen and oxygen-containing compounds.⁹⁴ In general, they have no well-defined

chemical composition, although some are quite stable and difficult to remove from the surface. The stability and quantity of complexes formed by any given sample are affected by its surface area, particle size, porosity, impurity content, and degree of graphitization. Since nuclear graphites have a much less active surface than the carbon blacks, they form fewer and less stable surface complexes. Nevertheless, the complexes formed with oxidizing gases play an important role in the oxidation of graphite (Chap. 14).

Graphite reacts with alkali hydroxides under extreme conditions. A solution of 50 per cent potassium hydroxide at 350°C attacks graphite.⁹⁵ No reaction occurs when the alkali hydroxide is melted in graphite, although at higher temperatures reaction occurs and hydrogen is formed.⁹⁶ The threshold temperature⁹⁷ for reaction with sodium hydroxide is about 750°C.

6-6 Mechanical Properties

The elastic constants of the dilatation of a graphite single crystal can be calculated from a knowledge of the thermal-expansion coefficients, the compressibility, and the specific heat. This calculation was first carried out by Riley,⁹⁸ and the results are given in Table 6.12. However, Riley inadvertently used Basset's⁹⁹ value of 44.9×10^{-13} cm²/dyne for the compressibility and appears to have been unaware that a value of 30×10^{-13} cm²/dyne had already been used to calculate the specific heat at constant pressure. The second column of figures therefore represents the values recalculated on a common basis of 30×10^{-13} cm²/dyne.

Table 6.12 — ELASTIC CONSTANTS OF SINGLE-CRYSTAL GRAPHITE

	Riley's ⁹⁸ value, 10 ¹³ cm ² /dyne	Recalculated, 10 ¹³ cm ² /dyne
S_{11} and S_{12}	1.8	1.20
S_{13}	-4.3	-2.85
S_{33}	58.5	38.84

The deflection characteristics have been determined on large natural graphite flakes loaded as cantilevers with the neutral axis in the basal plane (Fig. 6.7). When the load is removed, the flakes exhibit a small recovery and a large permanent set.

When a natural graphite flake is sheared,¹⁰¹ the proportion of rhombohedral stacking (Sec. 5-2) in the crystal increases. The rhombohedral structure anneals back to the normal hexagonal structure when the crystal is heated to 1300°C.

Little more is known about the mechanical properties of single crystals. Even if more precise information were available, it is doubtful that it would be directly applicable to the polycrystalline two-phase material with

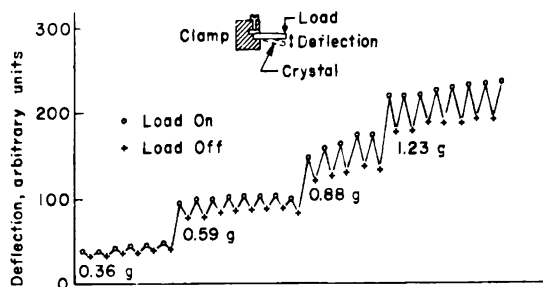


FIG. 6.7 Load-deflection characteristics of a cantilever made from a natural graphite crystal. (From Simmons, *Proceedings of the Third Conference on Carbon Held at the University of Buffalo*, Pergamon Press, Ref. 100.)

which this book is primarily concerned. The mechanical properties of polycrystalline graphites, about which much more is known, are discussed in the following paragraphs.

6-6.1 COMPRESSION

(a) *Elastic Modulus*. The stress-strain diagram (Fig. 6.8) for almost all polycrystalline graphites loaded in compression is markedly nonlinear and exhibits a large permanent set when the load is removed. The second loading curve is reproducible up to the previous maximum stress. The elastic

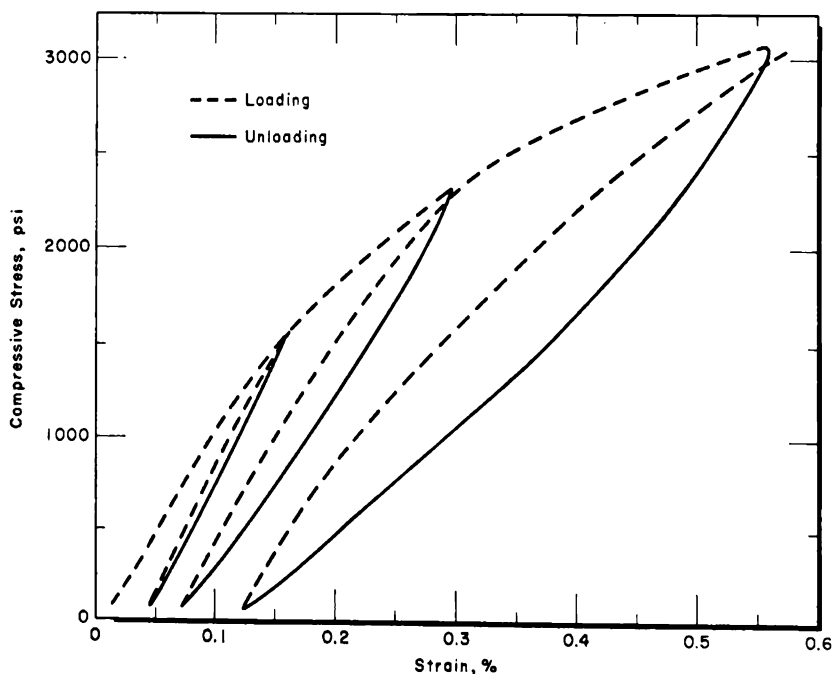


FIG. 6.8 A typical compressive stress-strain diagram for the nuclear graphite, PGA. Stress was applied parallel to the axis of extrusion.

modulus (defined as the slope of the line through the strains at zero and maximum stress for the second loading curve) decreases as the maximum load increases.

A detailed study of the behavior of one type of French nuclear graphite in compression has been reported by Arragon and Berthier.¹⁰² The modulus decreased by a factor of 2 from zero load to the breaking load, and the permanent set reached about 25 per cent of the total deformation. The modulus, permanent set, and total deformation were markedly anisotropic, with the maximum modulus and minimum permanent set in the direction of extrusion. The compressive stress to failure was not anisotropic. This behavior was attributed to residual stresses frozen into the graphite during manufacture. It has subsequently¹⁰³ been pointed out that because the deformation of the specimen was measured from the separation of the platens of the hydraulic press applying the load, the large permanent set observed may be due to crushing of the loading faces of the specimens. The permanent sets of samples measured in tension were much smaller.¹⁰³ Since, however, the breaking strain of graphite is in the range of 0.0 to 0.3 per cent in tension and 1.0 to 4.0 per cent in compression, permanent sets smaller by an order of magnitude are expected.

Experiments in compression have been carried out by measuring the strain with a Lamb type extensometer.¹⁰⁴ The permanent set was determined from the length of the test specimen (3.81 cm) to a precision of approximately 0.00025 cm with an optical comparator before and after stressing. The permanent sets obtained by this method agree to a high precision with the method employed by Arragon and Berthier.¹⁰²

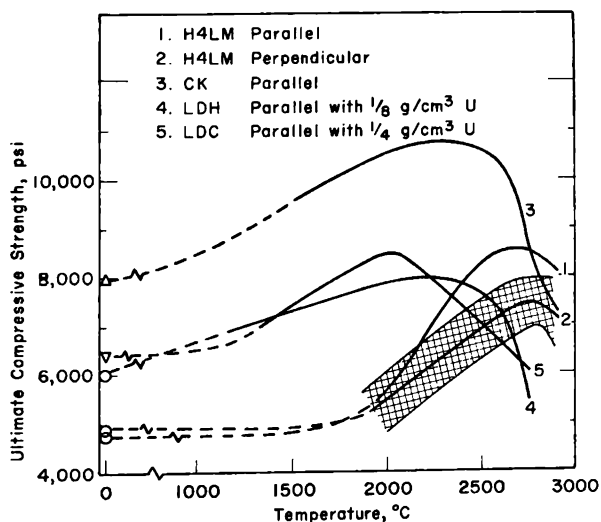


FIG. 6.9 The ultimate compressive strength of graphite as a function of temperature. The crosshatched band indicates the uncertainty in measurement of compressive strength on a single piece of H4LM graphite.¹⁰⁷

Table 6.13 — COMPRESSIVE STRENGTHS OF A NUMBER OF GRAPHITES AT ROOM TEMPERATURE

Grade	Manufacturer	Density, g/cm ³	Ultimate compressive strength, psi		Ref.
			With grain (II)	Across grain (I)	
PGA	British Acheson Electrodes, Ltd.	1.74	4650	5020	105
R-0013	National Carbon Company	1.85	7500	7500	106
R-0018	National Carbon Company	1.85	8700	8700	106
ATJ	National Carbon Company	1.73	8400	8500	106
R-0025	National Carbon Company	1.90	8600	8500	106
R-0020	National Carbon Company	1.90	9100	9000	106
ATL-82	National Carbon Company	1.88	9700	9700	106
MH4LM-90	Great Lakes Carbon Corp.	1.90	6650	6250	106
CCN	National Carbon Company	1.92	7500	6500	106
AJL-82	National Carbon Company	1.88	6500	6200	106
Graph-i-tite G	Graphite Specialties Corp.	1.88	7400	8500	106
Graph-i-tite A	Graphite Specialties Corp.	1.93	8500	9000	106
R-4	Graphite Specialties Corp.	1.98	6900	7200	106
AGOT	National Carbon Company	1.70	6000	6000	106
H4LM	Great Lakes Carbon Corp.	1.72	4800	4900	107
CK	Los Alamos Scientific Laboratory	1.71	8000		107
CS	National Carbon Company	1.68	5990 6850	5960 6430	19 19

Few other measurements of the elastic modulus in compression have been published. Values of 10.33×10^5 and 4.97×10^5 psi have been reported¹⁰⁵ for British A grade (PGA) measured parallel and perpendicular to the extrusion axis, respectively; however, the stress range over which these values were determined is not reported.

(b) *Compressive Strength.* The ultimate compressive strength is perhaps the simplest mechanical property of graphite to measure, and results for a wide range of materials have been published.^{102, 105-107} The values, which range from 4000 to 10,000 psi, are not strongly dependent on the direction of applied force. Typical results are given in Table 6.13.

The ultimate compressive strength of graphite increases as the test temperature increases and reaches a maximum between 2000 and 2500°C. The results shown in Fig. 6.9 are typical of the behavior of polycrystalline materials.

6-6.2 TENSION

(a) *Elastic Modulus.* The stress-strain diagram (Fig. 6.10) for polycrystalline graphite in tension is similar to that for compression. Since the breaking strain is low for this method of loading, the change in modulus with ultimate stress is small. The maximum permanent set is of the order of 20 per cent of the breaking strain. Behavior of this type has also been reported by other investigators.¹⁰⁸

The elastic modulus in tension over two cycles of loading has been

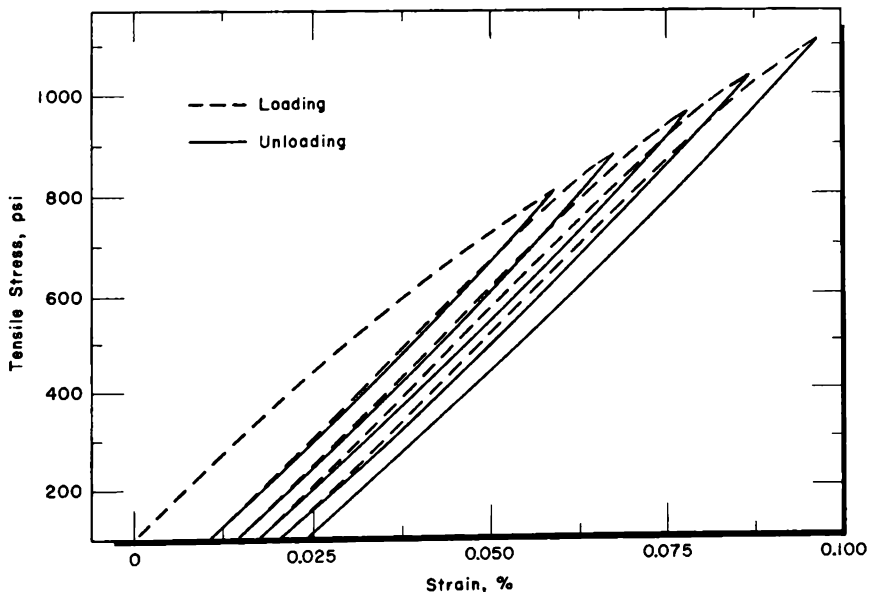


FIG. 6.10 A typical tensile stress-strain diagram for the nuclear graphite, PGA. Stress was applied parallel to the axis of extrusion.

determined by employing strain gauges, and the results have been compared with similar measurements in compression.¹⁰³ The experiments were carried out over a small range of strain (0.1 per cent in tension and 0.05 per cent in compression). There was no significant difference in the two moduli for two types of electrographite and one type of carbon. In contrast to this, the tensile moduli of PGA are reported¹⁰⁵ to be 16.3×10^5 and 8.12×10^5 psi in the two directions, compared with 10.33×10^5 and 4.97×10^5 psi for compression. If the compressive modulus had been determined near the ultimate stress, these values would then be low, and it is possible that no real contradiction exists.

(b) *Tensile Strength.* The tensile testing of brittle solids, e.g., materials with low breaking strains, presents many formidable problems. The shape of a test piece must be such that failure occurs in pure tension within the gauge length. Test pieces of the type used in testing ductile metals usually fail at the sharp radius at the end of the gauge length or at the shoulder for the collet. Test pieces of the type used for cast metals are usually more satisfactory. These have threaded ends to fit the jaws and are provided with an entry to the gauge length of shallow radius. An additional difficulty arises with most nuclear graphites because they are of relatively coarse texture, and a size effect may be observed if the gauge diameter is small.

An alternative method of measuring the tensile strength of brittle solids makes use of the fact that a disk compressed along one diameter will fail in tension along this diameter. In a series of tests on coal,¹⁰⁹ this method was shown to be more reliable than the conventional bend technique; the method has also been applied recently to graphite.¹¹⁰ An alternative approach is to test the specimen in the form of a long cylinder with a small ratio of wall thickness to diameter. The cylinder can be burst hydraulically, and the hoop stress at failure can be calculated. The cylinder end can readily be closed with an epoxy resin.

Few experimental results on the tensile strength of graphite have been published. It is reported¹⁰⁸ that the tensile strength determined by a direct tension test is about 0.47 to 0.68 of that obtained by flexure; no details are given of the type or size of specimen used for the tests. Malmstrom¹¹¹ reported high tensile strengths for a number of graphites, although more recent data¹⁹ suggest that these values may not be typical for the grades tested. It must be observed that Malmstrom's specimens were of the recommended design and that the values given are of the same order of magnitude as the flexural strengths. The ratio of tensile to flexural strengths is reported¹⁰⁵ to be 0.86 for PGA graphite. Hence it is not clear that a distinction between tensile and flexural tests exists. The disagreement may be due to the difficulties in performing tensile tests. It is clear, however, that the tensile strength will not exceed about half the compressive strength for common nuclear grades.

The tensile strength of graphite, like the compressive strength, increases

with temperature and reaches a maximum between 2000 and 2500°C. The maximum increase in the room-temperature strength ranges from 56 to 184 per cent for a variety of grades (Table 6.14). The breaking strain for ECA graphite, calculated from the tensile strength and dynamic Young's modulus, remains constant at 0.37 ± 0.01 per cent over the temperature range 0 to 2000°C.

Table 6.14 — EFFECT OF TEMPERATURE ON THE TENSILE STRENGTH OF A NUMBER OF GRAPHITES

Type of graphite	Density, g/cm ³	Tensile strength, psi						Ref.
		Room temperature		2500°C		Increase, %		
		(II)	(I)	(II)	(I)	(II)	(I)	
AGX	1.58	2200		3900		78		111
C-18	1.60	2500		5200		108		111
CEQ	1.55	3200		5000		56		111
ECA	1.67	3500		6900		97		111
EBP	1.76	3100		6300		103		111
Speer-3499	1.57	1730		4850		181		112
942S	1.69	1780	1780	3620	2960	103	67	112
AGR	1.59	550		1560		184		112
H3LM	1.68	1420	1420	2800	2750	97	94	112
H4LM		1500	1000	2700	2200	80	120	107
CK		1500		2600		73		107

6-6.3 FLEXURE

(a) *Elastic Modulus*. The stress-strain diagrams in flexure are similar to those obtained in pure tension and give similar values for the elastic modulus. The apparent elastic modulus, measured from the deflection of a beam loaded at the center, is dependent on the geometry of the specimen.⁶² The shear stresses are satisfactorily accounted for by the equation derived by Filon:¹¹³

$$\text{True modulus} = \text{apparent modulus} \left(1 + \frac{4h^2}{l^2} \times 2.73 \right) \quad (6.16)$$

where h is the height of the specimen and l is the span.

The elastic moduli obtained by this method agree with those obtained by direct tension and compression to an accuracy of about 10 per cent for values of h/l ranging from 0.38 to 0.1.

An alternative method of determining the modulus in flexure is to load the beam at four points, such that the maximum fiber stress between the center pins is constant, and to measure the radius of curvature of the beam by mirrors that are either fixed to or resting on the center span of the specimen. This method has been employed to determine some of the elastic constants of nuclear graphites.¹¹⁴

A number of workers^{111, 115, 116} have investigated the dynamic Young's modulus in flexure in the temperature range 0 to 2000°C (Fig. 6.11). In every case the Young's modulus rises with the test temperature, and for nuclear graphites the maximum increase is about 40 per cent. Larger increases for specimens cut perpendicular to the extrusion direction have been reported,¹¹⁶ the increase for ECA graphite being 87 per cent.

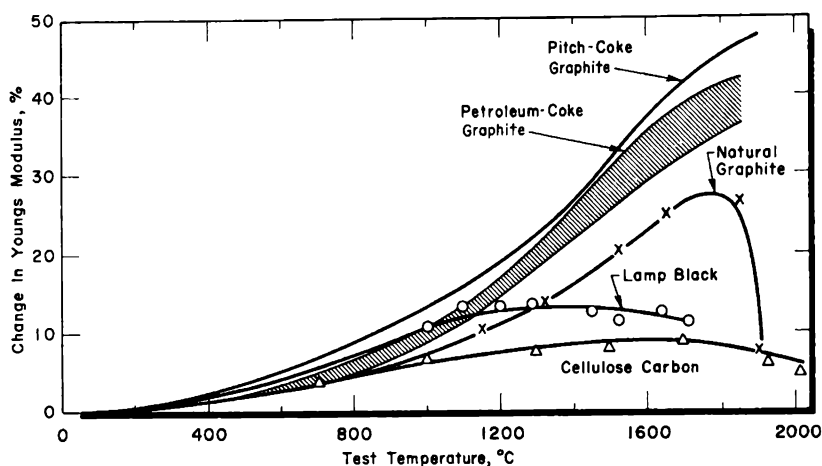


FIG. 6.11 Variation of Young's modulus with temperature for graphite cantilevers manufactured from a range of raw materials. The band for petroleum-coke graphite includes the results on specimens manufactured from calcined coke, 30 per cent binder (3 specimens); calcined coke, 33 per cent binder (2 specimens); and uncalcined coke, 48 per cent binder (1 specimen). (From Davidson et al., *Industrial Carbon and Graphite*, Ref. 115.)

(b) *Flexural Strength*. The measurement of the load necessary to break a beam in flexure is relatively simple and is often used for brittle solids to avoid the complication of a direct tension test. The beam can be loaded centrally (three-point method) or at two points along the beam (four-point method). In the latter case the maximum fiber stress is uniform for the central span, whereas in the former the maximum is at the point of application. The four-point method is said¹⁰⁸ to give values that are 20 to 35 per cent lower than the three-point method. Considerable data for the flexural strength occur in the literature and are summarized in Table 6.15.

The flexural strength of graphite increases with the test temperature. For example,¹⁹ the room-temperature flexural strength of ATJ graphite increases by 53 per cent at 2000°C and by 110 per cent at 2500°C.

6-6.4 SHEAR

(a) *Modulus of Rigidity*. The modulus of rigidity of graphite has been measured on graphite springs under both static loads and dynamic vibrations;^{115, 117} the behavior of a uniform bar in pure torsion has also been

Table 6.15 — FLEXURAL STRENGTHS OF A NUMBER OF GRAPHITES

Type of graphite	Manufacturer	Density, g/cm ³	Flexural strength, psi		Ref.
			(II)	(I)	
PGA	British Acheson Electrodes, Ltd.	1.74	2100	1530	105
R-0013	National Carbon Company	1.85	3250	3000	106
R-0018	National Carbon Company	1.85	3400	3200	106
ATJ	National Carbon Company	1.75	3300	3300	106
R-0025	National Carbon Company	1.90	4000	3900	106
R-0020	National Carbon Company	1.90	4100	3900	106
ATL-82	National Carbon Company	1.88	4600	4600	106
MH4LM-90	Great Lakes Carbon Corp.	1.90	2750	2900	106
CCN	National Carbon Company	1.92	2400	2050	106
AJL-82	National Carbon Company	1.88	2800	2400	106
Graph-i-tite G	Graphite Specialties Corp.	1.88	4400	3900	106
Graph-i-tite A	Graphite Specialties Corp.	1.93	4800	4000	106
R-4	National Carbon Company	1.98	3850	3550	106
AGOT	National Carbon Company	1.70	2400	2000	106
CS	National Carbon Company	1.68	2400	1970	19
CEQ	National Carbon Company		2530	2877	19

reported.^{114, 116, 118} The stress-strain diagram under static-load conditions is similar to that in tension and flexure.

Theoretically, the Poisson ratio is related to the Young's modulus and the modulus of rigidity. Poisson's ratio for an isotropic lampblack graphite is 0.27. However, because most nuclear graphites are anisotropic in their elastic moduli, no single value can be assigned.

The dynamic method of a bar in torsion has been used to examine the

effect of temperature on the modulus of rigidity of ECA and CEQ graphites.¹¹⁶ The maximum increases in moduli were 36 and 28 per cent, respectively. In both cases the maximum occurred below 2000°C, and an explanation in terms of grain-boundary relaxation was offered. An increase of 28 per cent has been measured from vibration of springs machined from petroleum-coke graphite.¹¹⁵

(b) *Shear Strength*. If a rod of graphite is twisted to failure, the crack occurs along a helix. This is typical of tensile failure rather than shear. One investigator¹¹⁸ has concluded that graphite always fails in tension and that the ultimate shear strengths are not obtained. Losty¹⁰⁴ has employed a double shear test and has measured values that were of the same order as the corresponding flexural strength.

6-6.5 IMPACT STRENGTH

The impact resistance of a completely elastic body is proportional to the elastic energy required to induce failure. This energy is given by $\frac{1}{2}Ed^2$, where E is the Young's modulus and d is the breaking strain. Direct measurement of the impact resistance by the conventional pendulum test is unsatisfactory for brittle solids because it is difficult to correct for spurious losses in the apparatus. The dynamic conditions at failure are similar to those under static loads, and it has been recommended¹⁹ that the impact strength be determined by

$$\text{Impact strength (ft-lb)} = 0.00463F^2/E \quad (6.17)$$

where F is flexural strength (psi) and E is Young's modulus (psi). The impact strength for petroleum-coke graphite calculated from Eq. 6.17 is in the range 0.01 to 0.03 ft-lb. The values depend on the size and orientation of the sample.¹⁹ Unpublished work¹⁰⁴ indicates that the deflections under dynamic loading are greater by 10 to 20 per cent than those predicted from static data; hence any estimate based on static data will be conservative.

Notch sensitivity is another measure of the static and impact behavior of graphite. If notch sensitivity is defined as the ratio of the strength of a 0.400-in.-thick test bar to that of a 0.500-in.-thick bar with a 0.100-in.-deep notch, typical values are 1.3 for AGSR and 1.7 for CEQ grades.¹⁹

6-6.6 EFFECT OF IMPREGNATION AND DENSITY

Polycrystalline nuclear graphites are manufactured from coke powder and pitch, and variations in the manufacturing processes can give rise to densities ranging from 1.5 to 1.7 g/cm³ (see also Sec. 6-7). The density can be further increased by impregnating the finished product with a variety of carbon-containing materials. The most common practice is to impregnate with a pitch similar to that used for the binder. The effect of such impregnation on the Young's modulus (E) is given by¹¹⁹

$$E = E_0(1 - k\epsilon) \quad (6.18)$$

where k and E_0 are constants and the void fraction (ϵ) is given in terms of the crystal density (ρ_c) and bulk density (ρ_B) by

$$\epsilon = \frac{\rho_c - \rho_B}{\rho_c} \quad (6.19)$$

To facilitate comparison with other experimental data, Eq. 6.18 can be rewritten

$$E = K(\rho_B - n) \quad (6.20)$$

where n and K are constants. Equations derived by other investigators can also be reduced to this form.

The values of the constants in Eq. 6.20 are given in Table 6.16 for pitch and sugar impregnants. Densification with sugar increases the modulus more rapidly than densification with pitch. The increase in modulus is greater on samples cut parallel to the extrusion axis.

Table 6.16 — EFFECT OF IMPREGNATION ON THE
CONSTANTS OF EQUATION 6.20

Impreg- nant	Final heat-treat- ment temperature after impregnation, °C	Orien- tation	K , dyne-cm/g	n , g/cm ³	Ref.
Pitch	2700	I	1.0×10^{11}	1.45	119
Pitch	2870	II	2.1×10^{11}	1.22	120
Sugar	1050	II	8.4×10^{11}	1.58	104
Sugar	2750	II	6.0×10^{11}	1.50	104
Sugar	1050	I	4.4×10^{11}	1.58	104
Sugar	2750	I	3.7×10^{11}	1.50	104

Impregnation also increases the strength of graphite. A linear relation between strength and density is most common,¹²⁰⁻¹²² although a power law has been suggested by one investigator.¹¹⁹ As a first approximation it is sufficient to assume that impregnation increases the Young's modulus and strength of graphite in the same proportion, causing no change in the breaking strain.

6-6.7 EFFECT OF HEAT-TREATMENT

Graphite is formed when petroleum cokes are heated to temperatures exceeding 2500°C (Sec. 5-9). During this heat-treatment the material changes from a hard abrasive solid to the soft machinable form of graphite. This change is reflected in a decrease in the elastic moduli by a factor of almost 2 between 1000 and 2000°C, with a further small decrease^{115, 117, 123} between 2000 and 2800°C (Fig. 6.12). The strength usually decreases with

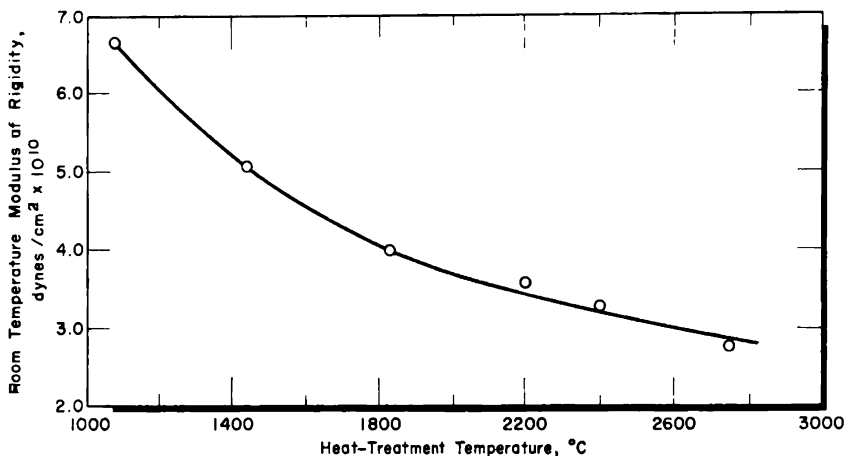


FIG. 6.12 Variation of the modulus of rigidity of graphite springs with heat-treatment temperature. The graphite was prepared from petroleum coke and graphitized at 2900°C. (From Davidson et al., *Industrial Carbon and Graphite*, Ref. 115.)

heat-treatment by a similar factor, although exceptions to this have been noted.¹²⁴

6-6.8 CREEP

The thermal creep of graphite has been studied in flexure,¹²⁴ torsion,¹²⁴ tension,^{107, 111, 112} and compression.¹⁰⁷ The measurements have been over the temperature range 1200 to 3000°C. The measurements in the temperature range 1200 to 2000°C, which were made in flexure and torsion, have been successfully unified into a single equation.¹²⁵

$$E_t = \sigma \left[\frac{1}{M_T} + \frac{C \log t}{M_0} \exp \left(-\frac{\Delta E}{RT} \right) + B_0 t \exp \left(-\frac{\Delta E'}{RT} \right) \right] \quad (6.21)$$

where E_t = strain at time t (min)

σ = applied stress (dynes/cm²)

M_0, M_T = the appropriate elastic moduli (dynes/cm²) at room temperature and test temperature ($T^\circ\text{K}$), respectively

C = constant for all graphites (approximately 13)

$\Delta E, \Delta E'$ = energies of activation for the transient and steady creep, respectively; $\Delta E = 20$ kcal/mole and $\Delta E' = 40$ kcal/mole for the nuclear graphite PGA

B_0 = a constant (3.31×10^{-11} cm²/dyne/min)

R = the gas constant

When the load is removed, the transient component of the creep is recovered according to

$$E_t = k \log t \quad (6.22)$$

Short-term tensile creep in the range 2400 to 3000°C has been measured on a number of different commercial electrographites.^{111, 126} The results can be fitted to an equation of the form

$$E_t = A + B (\log t) \exp\left(-\frac{\Delta E_B}{RT}\right) + Ct \exp\left(-\frac{\Delta E_C}{RT}\right) \quad (6.23)$$

where B and C are functions of the applied stress. The activation energies are higher ($E_B = 70$ to 112 kcal/mole and $E_C = 106$ to 204 kcal/mole) than those measured at lower temperatures,¹²⁵ and the creep appears to be proportional to the square of the stress. Recovery occurs when the load is removed, but it is generally less than half the transient creep deformation. Preliminary heat-treatment to 2800°C modifies the constants in Eq. 6.23 for tests at a lower temperature. This behavior may partially explain the differences between Eq. 6.21 and 6.23 since it has been found¹²¹ that creep in the range 1200 to 2000°C is markedly affected when the experiment is carried out within 200°C of the previous maximum heat-treatment temperature. If the previous maximum is exceeded, very large creep deformations are observed. The higher activation energies of Eq. 6.23 suggest that a spectrum of energies is present such that the higher the test temperature, the higher the observed activation energy.

The creep of several electrographites in tension and in compression has been measured¹⁰⁷ in the temperature range 2000 to 3000°C. No attempt was made to analyze the creep equation. The steady-state creep rate was obtained from the tangent to the curve. These data were expressed by the equation:

$$\frac{dE}{dt} = K \left(\frac{\sigma}{\sigma_B}\right)^{3.8} e^{-\Delta E/RT} \quad (6.24)$$

where dE/dt = the strain rate

K = a constant (= 40 for compression and 4 for tension)

σ = applied stress

σ_B = stress required to produce failure

ΔE = activation energy (50 kcal/mole for compression and 67 kcal/mole for tension)

From these data it is possible to calculate the creep of graphite over a wide range of temperatures. However, for temperatures in the range 2300 to 3000°C, the creep rate probably depends more on the maximum heat-treatment temperature than on the parameters given in Eq. 6.24.

6-6.9 COEFFICIENT OF FRICTION

The coefficient of friction (μ) is defined as

$$\mu = \frac{f}{F} \quad (6.25)$$

where f is the force necessary to either start (static) or maintain (dynamic) the motion and F is the force with which the two surfaces are pressed together normal to the direction of motion. The coefficient of friction depends upon the composition of the two surfaces in contact and the temperature, atmosphere, and load on the surfaces.¹⁹

The fact that graphite powder possesses lubricating properties has been known and used for many years. The precise nature of this phenomenon is not understood, and recent investigations have led to as many theories as the number of investigations. Some of these are in direct conflict.

The coefficients of friction for several grades of graphite are given in Table 6.17. The current state of knowledge is summarized in the following statements:¹⁰⁷

1. The static friction is always higher than the dynamic friction. When

Table 6.17 — COEFFICIENTS OF FRICTION FOR A NUMBER OF GRAPHITES

Material	Test temperature, °C	Atmosphere	Coefficient of friction		Ref.
			Static	Dynamic	
Graph-i-tite G on Graph-i-tite G	25	Air	0.35	0.25	107
Graph-i-tite G on Graph-i-tite G	2450	Helium	0.65	0.40	107
ATJ on ATJ	25	Air	0.33	0.24	107
ATJ on ATJ	2450	Helium	0.70	0.28	107
H4LM on H4LM	25	Air	0.34	0.26	107
H4LM on H4LM	2450	Helium	0.48	0.27	107
ATJ on H4LM	25	Air	0.33	0.26	107
ATJ on polished steel	25	Air		0.35	107
Graphitized lampblack:					
On silver	25	Air	0.31		19
On gold	25	Air	0.26		19
On zinc	25	Air	0.37		19
On nickel	25	Air	0.32		19
On copper	25	Air	0.30		19
On cadmium	25	Air	0.24		19
On graphitized lamp-black	25	Air	0.31		19
AGOT on AGOT	25	Air	0.24		19
AGOT on AGOT	900	Nitrogen	0.12		19
AGOT on 18-8 stainless steel	204	Air	0.35		19
AGOT on cold-rolled steel	204	Carbon dioxide	0.24		19

dynamic friction is being measured, the phenomenon of stick-slip occurs, giving rise to oscillating frictional forces.

2. The most pronounced effect on friction is that of surface finish. The coefficient of friction decreases as the number of unidirectional tests increases, the initial and final values being in the ratio of 1.5 for the static value and 1.1 for the dynamic value.

3. If the direction of motion is reversed, the friction increases.

4. The coefficients of friction are approximately independent of the force, stress, and orientation of the graphite.

5. The static coefficient of friction rises as the test temperature rises, whereas the dynamic coefficient is only slightly affected.

The last statement is perhaps the most difficult to substantiate since it involves the use of controlled atmospheres to prevent oxidation, the effect of which is not understood.

6-6.10 MACHINABILITY

The machinability of a graphite depends upon the raw materials used in its manufacture and upon the processing variables. All the conventional machining operations can be carried out on most of the common nuclear graphites (Chap. 3). However, departures from the conventional manufacturing techniques, for example, a low graphitizing temperature or the use of a poorly graphitizing coke, may result in a more abrasive material and cause excessive wear of the machining tools.

The machinability of graphite is defined as the depth a standard drill will penetrate at a fixed speed and torque under a given load in a fixed time. This index has been used to investigate a range of experimental and commercial nuclear graphites.^{127, 128} The machinability varies inversely with density and directly with particle size. The type of binder affects the machinability, and an increase in the temperature of graphitization causes an improvement in machining properties.

6-7 Density

The density of a graphite moderator is a factor in determining the degree of moderation. It must, therefore, be specified in the reactor design. Densities in the range 1.5 to 1.7 g/cm³ can be achieved by minor variations in the conventional processing of petroleum-coke electrographites, and a wider range is possible by special processing. Thus, at least from a neutron physics standpoint, the reactor designer has considerable latitude in the choice of graphite density. From an engineering standpoint, however, a high graphite density is usually desirable, primarily because the size of the reactor can be reduced with a potential savings in capital cost. For example, if it were practical to increase the density from 1.65 to 2.0 g/cm³, the volume of graphite could be reduced by 20 per cent while the same neutron-moderating effect was maintained. An increase in density is sometimes

Table 6.18 — COMPARISON OF GRAPHITE DENSITIES

Material	Density, g/cm ³						Ref.
	n-Hexane	Methanol	Benzene	Dibutyl phthalate	Helium	X-ray	
PGA rods	2.091	2.161	2.163	2.157	2.154	2.266	129
Polycrystalline graphite rods					2.093	2.261	130
Oxidized graphite dust		2.224			2.220		130
Ceylon natural flake		2.253			2.251	2.266	130

accompanied by certain other improvements in properties such as increased strength (Sec. 6-6.6) and low permeability to gases. The effects of density on the dimensional stability and chemical reactivity of the graphite are not predictable at present and should be determined for any cases where deviations are contemplated from the range 1.5 to 1.7 g/cm³.

6-7.1 DEFINITIONS AND MEASUREMENTS

A number of different kinds of densities are discussed in the graphite literature, their differences deriving from their method of measurement. The most common one is the bulk density (ρ_B). This is sometimes referred to as "apparent density" and is determined by the dimensions and weight of the body. Of the several densities this will have the lowest value.

The crystal, or real, density (ρ_c) is determined directly from the crystal parameters a and c . With a and c in angstroms, the density equation is:

$$\rho_c = \frac{91.93}{a^2c} \text{ g/cm}^3 \quad (6.26)$$

Thus well-crystallized graphite with $a = 2.46 \text{ \AA}$ and $c = 6.71 \text{ \AA}$ has a crystal density of 2.26 g/cm³. Because this is the density that the body would have if it were a single crystal with no voids, it is the highest density.

Other densities are measured by the displacement of various fluids (fluid densities) and will therefore depend upon the accessibility of the pores to the fluid. In practice the densities of polycrystalline graphite measured by the displacement of helium, methanol, and n -hexane do not differ significantly (Table 6.18). Although no molecular sieve effect is indicated by the densities measured with several displacing fluids, it has been reported¹²⁹ that the time required to reach equilibrium increases with molecular size from about 1 hr for helium to 100 hr for dibutyl phthalate.

The densities of a wide range of finely ground carbons heat-treated to 3000°C have been measured by the displacement of kerosene.¹⁰⁸ The lowest densities were found with the nongraphitic carbons such as activated carbon (1.46 g/cm³) and sugar carbon (1.50 to 1.58 g/cm³); the highest densities were found for petroleum cokes (2.20 to 2.26 g/cm³) and natural graphite (2.26 g/cm³). There is a strong correlation between fluid densities and graphitic character. The more closely the fluid densities approach the crystal densities, the more graphitic is the material. Bulk densities achievable in the final graphite are also in rough proportion to the fluid density of the graphitized filler.

6-7.2 METHODS OF ACHIEVING HIGH DENSITY

High densities in electrographites are achieved by maximizing the effects of particle packing, quantity and type of binder, puffing inhibitors, baking and graphitizing rates, and pitch impregnation. These factors are strongly interrelated; the gains in density realized by changing one factor

depend upon the other factors. Usually a gain in density achieved at some stage in the process will tend to decrease the gains possible at a later stage. Thus the entire fabrication process must be considered in evaluating the effects of a particular variable.

Very high densities (2.00 to 2.15 g/cm³) have been obtained by compacting natural flake graphite into blocks,^{131, 132} but they inherently have a very low shear strength because of the weak bonding between particles. Such materials may find some use if subjected only to compressive stresses.

Significant gains in density in more conventional graphites can be obtained by controlling the particle-size distribution of the coke filler. This has been accomplished to a limited extent with special blends of coke particles¹³¹ and to a greater extent by the addition of very fine carbon blacks.^{108, 131-133} Since petroleum-coke flour contains few particles less than 2 μ in diameter, the addition of a carbon black such as Thermax (average diameter 0.3 μ) fills some of the voids between coke particles and increases the density (Table 6.19).

Table 6.19 — EFFECT OF PARTICLE SIZE ON DENSITY OF GRAPHITE BLOCKS¹³³

Test No.	Blended filler, [†] %				Density, g/cm ³		
	Petroleum coke			Carbon black	Green block	Baked block	Graphitized block
	Grain	Powder	Flour				
1	25	75	0	0	1.73	1.61	1.62
2	25	45	30	0	1.73	1.63	1.72
3	25	65	0	10	1.73	1.68	1.72
4	25	55	0	20	1.77	1.76	1.80
5	25	50	0	25	1.80	1.76	1.81
6	40	35	0	25	1.76	1.71	1.77

[†] Filler particle size: grain, 20 to 40 mesh; powder, 20 to 150 mesh; flour, 90 per cent smaller than 10 μ ; carbon black, 0.2 to 0.3 μ .

High-density graphites formed by the addition of carbon blacks are less permeable than conventional materials. Unless precautions are observed during processing (extrusion-baking-graphitization), the entrapped gases produced distort and crack the bars (Sec. 2-3.1). Low rates of temperature rise during baking and graphitizing help to reduce this problem. Small stock (less than 1 in. in diameter) is more easily processed than larger stock because the gases formed during baking and graphitization are able to diffuse to the surface and are less likely to cause distortion and cracking. Gas purification is also less effective since the permeability of high-density stock is low.

Coking values[†] may vary considerably with the type of pitch employed,

[†] The coking value of a pitch is the percentage of pitch remaining after heating to 1000°C.

65 per cent being a common value in commercial practice. For a given process high coking values and high pitch density are reflected directly in a graphite of higher density. The coking value of binder in petroleum coke-Thermax-binder mixes has been increased¹³² by employing a preliminary penumatic-pressure bake at 80 to 500 psi and 540°C. However, volume shrinkage was lower and impregnation less effective on pressure-baked stock, making the net gains in density over conventionally baked stock negligible. A preliminary bake at 550°C under 5000-psi mechanical pressure also failed to increase the net density.¹³² It is possible that, in the future, density gains will be achieved by baking under mechanical pressure at the higher and more uniform temperatures attainable with electrical-resistance heating.

Some increase in density can be achieved with special resin binders that lead to high shrinkage rates during baking and graphitization. A high-density graphite has been produced¹³¹ on a laboratory scale with a phenol formaldehyde resin binder and petroleum-coke flour. Nonimpregnated resin-bonded specimens were formed with an average bulk density of 1.82 g/cm³ after graphitization at 2570°C, whereas the maximum density obtained on similar specimens bonded with coal-tar pitch averaged 1.62 g/cm³.

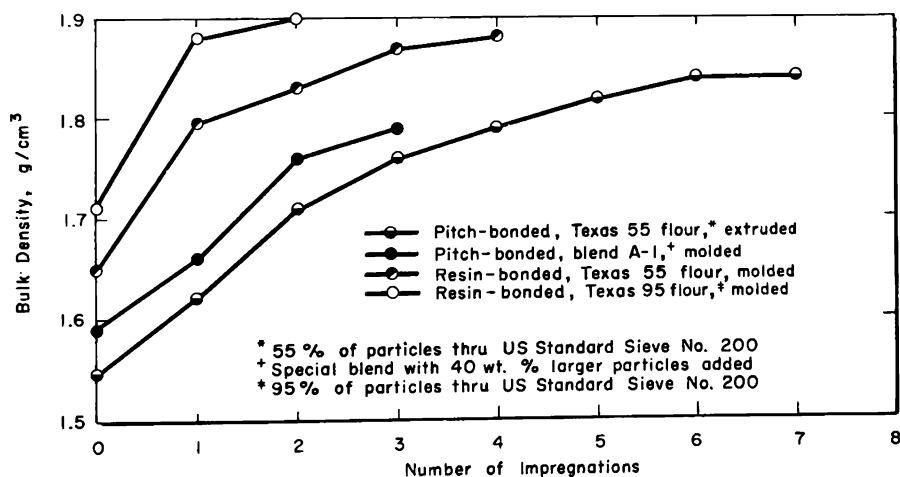


FIG. 6.13 Effect of pitch impregnation on density.¹³¹

The most widely used method of increasing the density of electrographites is that of impregnation of the baked stock with coal-tar pitch prior to graphitization (Sec. 2-4). In conventional electrographites the density is increased from 1.55 to 1.65 g/cm³ by a single impregnation. Additional impregnation-baking cycles result in decreasingly smaller gains in density (Fig. 6.13).

In the case of baked blocks in which a relatively high density has already been achieved either by the addition of carbon black or by the use

of a coke with small particle size, impregnation usually does not improve the density as much as it does in baked bars of lower density. Since multiple impregnations require additional baking-impregnation cycles, they add considerably to the cost of the material.

If one or more of the techniques discussed above are employed, it is possible to produce small graphitized bodies on an experimental basis with a density of 2.0 g/cm^3 or slightly higher. As mentioned earlier, difficulties are often encountered in producing material free from laminations, cracks and other defects when scaling up to the production of dense graphites in larger sizes. Perhaps the best measure of success is found in the densities of commercially available grades. Fully graphitized materials with densities in the range 1.85 to 1.95 g/cm^3 have been produced on a developmental or limited-production basis.¹⁰⁶ Although these materials are generally greatly improved in strength and impermeability, relatively little is known as yet about the effects of long-term reactor irradiation.

6-8 Surface Properties

6-8.1 SURFACE ACTIVITY

In view of the wide range of structural development found in carbons, it is no surprise that they vary widely in their ability to adsorb and hold gases on their surface. The active carbons that are employed as catalytic agents have BET surface areas of $1000 \text{ m}^2/\text{g}$ or more (Sec. 6-8.2), whereas those of well-crystallized electrographites are usually less than $1 \text{ m}^2/\text{g}$. Both the volume of gases held and the ease with which they may be desorbed depend upon the activity of the graphite surface. A large fraction of the gases adsorbed on graphite at room temperature is held by the adsorption of molecules on the surface and by capillary condensation. The gases are held through the physical adsorption of the molecules by van der Waals forces of attraction between the adsorbate molecules and surface atoms. The energy of these interactions is relatively weak, being similar in magnitude to the heat of sublimation of rare gases.

The difficulty with which the last traces of some gases are desorbed from graphite indicates that some molecules are held much more tightly by chemisorption. Because the binding energies in the case of chemisorption are comparable in magnitude to those in ordinary chemical bonds ($>10 \text{ kcal/mole}$), it is proper to consider these adsorbate surface groups as surface compounds. For intermediate cases of strong physical adsorption or weak chemisorption, the distinction is arbitrary, and it is difficult to assign the adsorption definitely to one type or the other.

The edge atoms of a crystallite, for which the valence forces may not be completely satisfied without adsorbed atoms or molecules, provide the most active sites. It is here that chemisorption most likely occurs. Atoms

in the basal plane of the surface are much less active, except in the vicinity of impurities or structural defects.

Very little is known about the forces restricting diffusion of adsorbates on a graphite surface. It has been calculated¹³⁴ that, in the limiting case of unrestricted mobility of a physically adsorbed gas, the adsorbed molecules repel each other. If this repulsion is assumed to be due to the repulsion of the induced dipoles, the magnitude of the induced dipole moment is physically reasonable, and the interaction energy of the induced dipoles leads to an appreciable contribution to the heat of adsorption.

6-8.2 SURFACE AREA

The volume of a gas adsorbed on the surface of a solid is a function of the temperature of the adsorbent and the gas pressure. As the temperature decreases or the pressure increases, more gas is adsorbed. The surface area of a porous solid is normally measured at constant temperature by determining the volume of gas adsorbed as a function of the relative saturation pressure (p/p_0), p being the pressure at which adsorption takes place and p_0 being the vapor pressure of the gas at the temperature of the adsorbent. Nitrogen, close to its normal boiling point, is most commonly employed. Figure 6.14 shows a typical nitrogen adsorption-desorption isotherm for

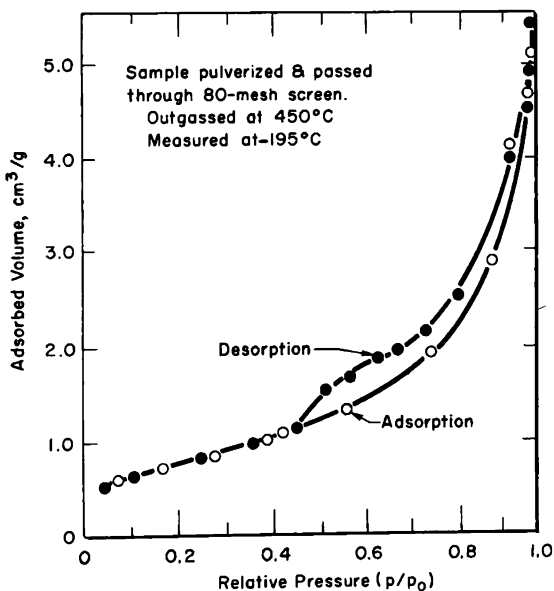


FIG. 6.14 Nitrogen adsorption-desorption isotherm for CSF graphite at -195°C . (From Spalaris, *Journal of Physical Chemistry*, Ref. 135.)

CSF graphite. The adsorption-desorption isotherms form a hysteresis loop at a value of p/p_0 greater than 0.45. Hysteresis loops were found for all

nuclear graphites studied by Spalaris.¹³⁶ Although several explanations have been offered for the existence of hysteresis loops, it is generally agreed that they are associated with the micropore structure.^{137, 138} However, a mechanism has been proposed¹³⁹ whereby hysteresis loops can occur on flat nonporous surfaces.

The surface area of graphite is normally calculated by the BET method¹⁴⁰ from the adsorption isotherm. This method is an extension of the Langmuir isotherm theory for molecular adsorption to account for multilayer adsorption on free surfaces and in pores of solids. If the number of layers is not restricted by the pore size, the volume of gas adsorbed is given by the equation

$$v = \frac{v_m c p}{(p_0 - p)[1 + (c - 1)(p/p_0)]} \quad (6.27)$$

where c is a constant and v_m is the volume of gas adsorbed when a monolayer has just formed. For particular values of c , this equation gives the S-shaped isotherm usually observed experimentally with porous solids. The BET areas are obtained by putting this equation in the form

$$\frac{p}{v(p_0 - p)} = \frac{1}{v_m c} + \frac{(c - 1)(p/p_0)}{v_m c} \quad (6.28)$$

and plotting $p/[v(p_0 - p)]$ vs. p/p_0 . For most isotherms a straight line is obtained for only the portion of the curve up to p/p_0 values of about 0.3. The values of v_m and c are obtained from the intercept and the slope of the low-pressure straight-line portion. Since v_m is the volume of gas necessary to cover the surface with one layer of gas molecules, it is a simple matter to calculate the surface area if the area covered by each molecule is known. Molecular areas calculated from the density of solid nitrogen (15.4 \AA^2) and liquid nitrogen (16.2 \AA^2) have both been used. The latter value has been more commonly used in recent years.

The magnitude of the surface area of unirradiated nuclear graphite varies between 0.25 and $1.0 \text{ m}^2/\text{g}$, depending upon the type of graphite and the treatment given the sample prior to measurement. The results for a number of nuclear graphites and some nongraphitic carbons are given in Table 6.20.

Grinding a graphite body opens new pores to the nitrogen; for CSF this increases the surface area by a factor of about 10. An extreme example is found in graphite wear dust, reported to be very small platelets about 20 \AA thick and 3500 \AA in diameter.

If graphite is not outgassed prior to surface-area measurement, those gases which are held on the surface cover potentially active sites capable of adsorbing nitrogen molecules after the gases are removed. Heating removes these gases and increases the surface activity as shown in Fig. 6.15. It is interesting to note that nitrogen surface areas are not greatly increased

Table 6.20 — BET NITROGEN SURFACE AREAS[†]

Carbon or graphite	Outgassing temperature, °C	Surface area, m ² /g	Ref.
CSF	200	0.32	136
CSGBF	550	0.36	136
KC	500	0.53	136
TS	200	0.66	136
WSF	500	0.87	136
CSF (pulverized to <170 μ)	500	6.70	141
Furnace black	250	27.0	142
Graphon (graphitized Spheron-6)		80.0	143
Spheron-6		120.0	143
Graphite wear dust	500	435.0	144

[†] All nuclear graphites in the form of cylinders 1 cm in diameter by 10 cm. Molecular area for nitrogen assumed to be 16.2 Å².

by degassing in the range 500 to 1000°C, even though a significant volume of gas is evolved at these temperatures (Sec. 6-8.5).

The BET surface area varies slightly within a bar of graphite. Values for randomly selected samples from the same bar (4 by 4 by 48 in.) of WSF or KC graphite agree to within about 5 per cent.¹³⁶ Variation between bars from the same grade is somewhat greater than 5 per cent.

Carbon dioxide at -78°C and argon at about -192°C have also been employed to measure the surface area of graphite.¹⁴⁵ With carbon dioxide the BET area of a graphitized carbon rod was found to be 0.6 m²/g; with nitrogen at about -192°C the BET area was 1.0 m²/g. On samples that had been oxidized to about 10 per cent weight loss at 1300°C, the surface areas measured with carbon dioxide, nitrogen, and argon were, respectively, 3.6, 4.1, and 4.2 m²/g.

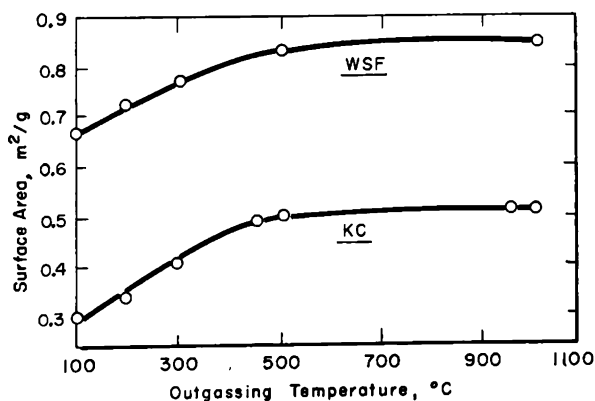


FIG. 6.15 The effect of outgassing temperature on the BET surface area. (From Spalaris, *Journal of Physical Chemistry*, Ref. 135.)

6-8.3 ADSORPTION OF WATER

The adsorption of atmospheric moisture by moderator graphite was measured by Horton and Roberts¹⁴⁶ to estimate the effects on pile reactivity. The results are also of importance to the high-temperature gas-cooled reactors now under construction since the quantity of oxidizing gases must be limited to prevent undesirable chemical reactions (Sec. 14-1.1). The adsorption of water as a function of its relative saturation pressure (p/p_0) is shown in Fig. 6.16 for AGXP graphite. The samples were exposed for

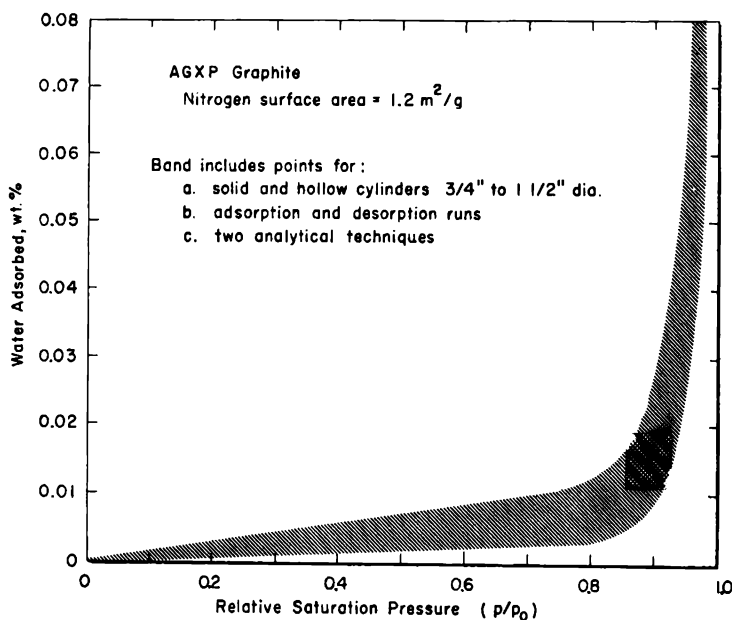


FIG. 6.16 The equilibrium amount of water adsorbed on nuclear graphite at 25°C. (From Horton and Roberts, British Report AERE-C-R-2219, Ref. 146.)

several days to different static pressures of water vapor in the absence of air. Even though the amount of water adsorbed under normal conditions is quite small, it constitutes the largest single source of the gases that are desorbed when graphite is heated (Sec. 6-8.5). The data of Fig. 6.16 are probably also valid for the adsorption of water vapor in air since the amount of physically adsorbed nitrogen, oxygen, and carbon dioxide is negligible near room temperature. A slight hysteresis in the adsorption-desorption isotherms was observed within the band in Fig. 6.16, the desorption isotherm being slightly above the adsorption isotherm. Most of the physically adsorbed water can be removed by evacuating the sample at room temperature. Assuming a nitrogen surface area of 1.2 m²/g, a unimolecular layer of water on AGXP graphite requires 0.034 wt.% of

adsorbed water. Thus at 25°C a monolayer is statistically complete at $p/p_0 = 0.94$.

The rate of water adsorption is affected by the presence of other atmospheric gases and also by the size of the specimen because interdiffusion of water and other gases in a porous body plays an important role. The percentage (by weight) of water adsorbed (W) on specimens of several geometries and sizes in a stream of air of controlled humidity has been fitted to the equation¹⁴⁶

$$W = W_{\infty}(1 - e^{-Bt}) \quad (6.29)$$

Equation 6.29 is an approximate solution of the classical diffusion equation for cylinders of radius R and length L . The saturation value (W_{∞}) depends upon p/p_0 , as shown in Fig. 6.16; B is a function determined by R and L ; and t is the time the graphite is exposed to water at a given partial pressure. When the curves are normalized to account for the sample-to-sample variation in W_{∞} , the data fit such an equation satisfactorily for $p/p_0 < 0.85$. For cylinders of $\frac{1}{2}$ -in. diameter by 2-in. length, saturation values were reached within a few hours. Extrapolation of the results to a cylindrical moderator block of 8.2-in. diameter by 29-in. length indicates that the half-saturation value would be reached in 4.5 days at $p/p_0 = 0.9$ and in 27 hr at $p/p_0 = 0.82$.

6-8.4 HEAT OF ADSORPTION

Just as heat is evolved during the condensation of a gas to a liquid, heat is also evolved when gases are adsorbed on solid surfaces. The heat of adsorption (ΔH_a) is a measure of the energy of interaction between adsorbed molecules and surface atoms. Values of ΔH_a for the first few layers of adsorbed molecules are generally higher than the heat of liquefaction (ΔH_L), indicating that the energy of interaction between surface and adsorbed molecules is greater than that between gas- and liquid-phase molecules of the adsorbing gas. For CSF graphite,¹³⁶ for example, the isosteric ΔH_a for the adsorption of nitrogen decreases from 1.95 kcal/mole, where 88 per cent of the surface is covered by statistical monolayer, to 1.65 kcal/mole, where 100 per cent is covered. These values can be compared to the ΔH_L for nitrogen of 1.36 kcal/mole.

As the number of adsorbed layers of gas increases, the average interaction between the carbon surface and the adsorbed gas molecules becomes weaker, and ΔH_a approaches ΔH_L . In the case of the adsorption of ethyl chloride on graphite,¹⁴⁷ ΔH_a exceeds ΔH_L by 25, 5, 2, and 1 per cent for 1, 2, 4, and 10 statistical layers, respectively.

6-8.5 DESORPTION OF GASES

Gases adsorbed on the surface and contained within the voids of the graphite moderator and reflector are a source of impurities, which, when

desorbed into the gas atmosphere by heating or displacement by other gases, may result in undesirable reactions with graphite and other core materials. From the preceding section it is clear that, of the atmospheric gases, only water has a high enough relative saturation pressure to be physically adsorbed in significant amounts near room temperature. However, gases other than water or the products of the reaction between graphite and water are also evolved when graphite is heated. These gases are probably held by chemisorption or are trapped in pores when the graphite contracts as it cools from graphitization temperature. Chemisorbed and trapped gases are released only at relatively high temperatures.

The volume and composition of gases evolved when graphite is heated have been measured by a number of workers.¹⁴⁸⁻¹⁵⁰ Although certain general features are common in all these studies, the volumes desorbed as a function of temperature vary considerably, reflecting differences in the experimental techniques and pretreatments employed and differences in the desorption properties of the materials themselves.

Desorption studies are usually conducted by pumping the gases away and collecting them in another part of the system while the sample is heated. After a period of time, the total gas volume is measured, and the composition is determined by mass spectrometry or gas chromatography.

The cumulative volume of gas desorbed from several materials is shown in Fig. 6.17. Differences in experimental methods account in part

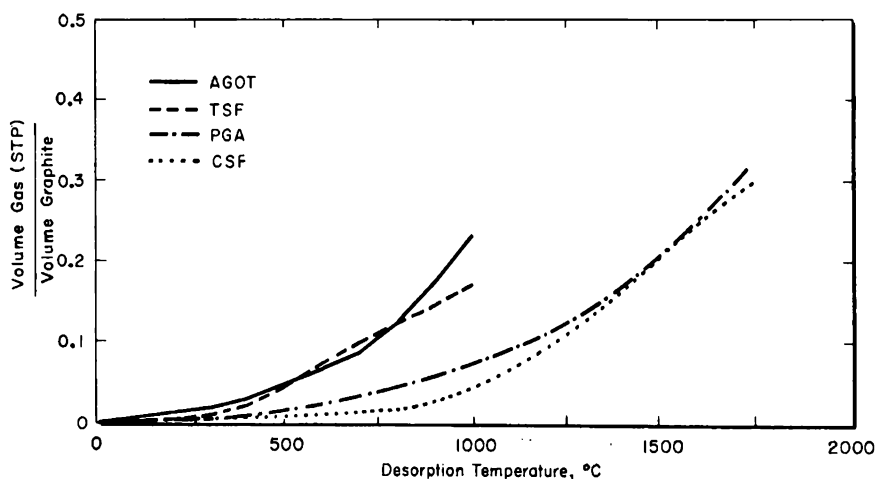


FIG. 6.17 The cumulative gas volume released during evacuation of nuclear graphites.

for the apparently different behavior of the four materials. The PGA sample¹⁴⁹ was heated in argon to 2600°C and stored for three months in clean air. This pretreatment probably resulted in a smaller volume of desorbed gas at each temperature. The TSF,¹⁴⁸ AGOT,¹⁴⁹ and CSF¹⁵⁰ sam-

ples were simply evacuated at room temperature prior to degassing. Gases were removed continuously during heating of the AGOT, TSF, and PGA samples, whereas the gas pressure was allowed to accumulate around the CSF sample for 8 min prior to removal. The quantity and composition of gases desorbed from a Speer Carbon Co. nuclear graphite¹⁵¹ were similar to that for the AGOT sample in Fig. 6.17, but the curve has been omitted to avoid crowding the figure.

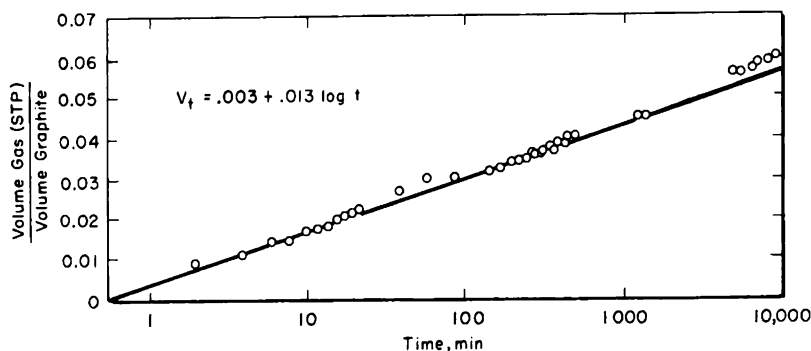
Gas-purified materials (Sec. 2-6), such as TSF, CSF, and TSGBF, desorb less gas than comparable thermally purified materials, probably because some impurity sites capable of holding gas at high temperature are removed. This fact is not readily apparent from Fig. 6.17 because experimental methods differ. In the case of the AGOT and TSF samples, where pretreatment was comparable, TSF evolved less gas at 1000°C. Overholser and Blakely,¹⁴⁸ in degassing a number of samples to 1000°C, report that the total volume of gas evolved varied from 0.06 to 0.26 cm³ of gas per cubic centimeter of graphite for TSF and from 0.22 to 0.33 cm³ of gas per cubic centimeter of graphite for AGOT. Walker and Redmond¹⁵² obtained 0.20 cm³ of gas per cubic centimeter of graphite when TSP (chlorine purified) was heated to 1500°C, as compared to 1.20 cm³ of gas per cubic centimeter of graphite from electrode-grade material heated to 1900°C. This difference could not be accounted for by the rather small difference in BET surface areas. Ryan¹⁵³ measured small gas volumes of 0.07 to 0.09 cm³ of gas per cubic centimeter of graphite for TSGBF at 975°C.

The rate at which gases are desorbed at a given temperature is determined by the strength with which the gases are held to active sites and the rate at which they can diffuse through the micropores and cracks to the surface of the body. If gases are pumped away as they are evolved, the desorption kinetics can often be approximated over an appreciable range of time by an equation of the form

$$V_t = A + B \log t \quad (6.30)$$

where V_t is the volume of gas desorbed per volume of graphite after time t and A and B are constants. This equation has been applied¹⁴⁹ to the gases evolved from PGA (Fig. 6.18). A plot of V_t vs. $\log t$ gives a straight line over a time factor of 10^4 . Other rate data¹⁵⁴ at 1000°C can also be fitted to an equation of this form, although some exceptions are found at 600°C.

The major components of the desorbate are nitrogen, water, carbon dioxide, carbon monoxide, hydrogen, and hydrocarbons (Figs. 6.19 and 6.20). Both AGOT and the purer TSF grade desorb a small amount of water in the range 200 to 500°C. In contrast to TSF, AGOT evolves a large volume of carbon dioxide at 500 to 700°C, the source of which is probably chemisorbed oxygen and surface oxides. The small quantity of carbon dioxide evolved from PGA may be the result of the pretreatment described previously. Above 600°C the carbon dioxide begins to react with the

FIG. 6.18 Gas desorption from PGA at 900°C.¹⁴⁹

graphite forming carbon monoxide. For both AGOT and TSF materials, the evolution of carbon monoxide begins to increase as the carbon dioxide decreases.

Above 400°C hydrogen begins to desorb; the evolution of hydrogen continues to a temperature of 1000°C and above. The most probable source is



It is possible also that some hydrogen is formed at higher temperatures by the decomposition of hydrocarbons into hydrogen and carbon.

According to Fig. 6.20 most of the gas desorbed from TSF above 800°C

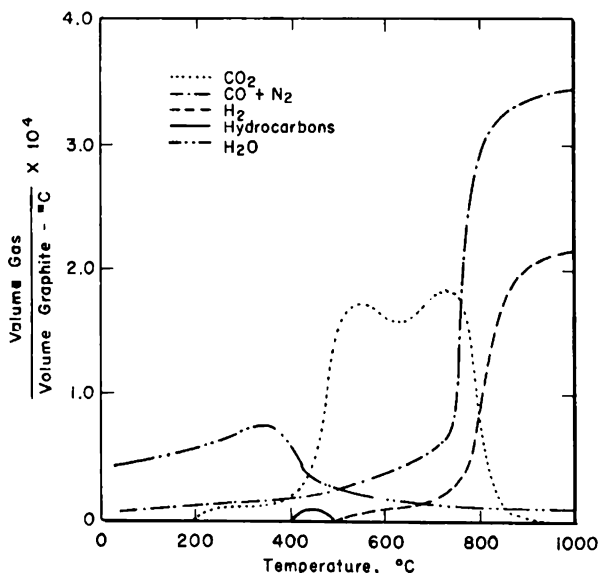


FIG. 6.19 Composition of gas desorbed from AGOT. Gases were collected at 100°C intervals during evacuation of the graphite. Cumulative volumes are given by the area under the curves.¹⁴⁸

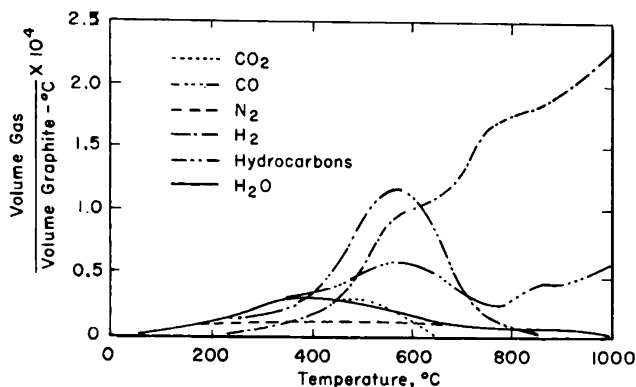


Fig. 6.20 Composition of gas desorbed from TSF. Gases were collected at 100°C intervals during evacuation of the graphite. Cumulative volumes are given by the area under the curves.¹⁴⁸

is hydrogen. This effect has also been observed¹⁵³ on another gas-purified material, TSGBF. After the gases had been pumped away for 1 hr at room temperature, the gas evolved in 18 hr at 975°C was collected and analyzed. Of the total gas volume (0.08 cm³ of gas per cubic centimeter of graphite), 90 per cent was hydrogen and the remainder was carbon monoxide, carbon dioxide, and nitrogen.

Although the composition of the hydrocarbon mixture shown in Figs. 6.19 and 6.20 was not determined, it may be predicted on the basis of other work¹⁴⁹ that the major component is methane. The source of the rather large volume evolved from TSF at 400 to 700°C is not clear. Any hydrocarbons not carbonized during graphitization at 2800°C would not be expected to desorb at 400 to 700°C. The most likely source of the hydrogen in the hydrocarbons is water. The amount of water adsorbed under normal conditions (Fig. 6.16) is of the right order of magnitude to account for the water, hydrogen, and hydrocarbons found in the desorbate. Methane, and other hydrocarbons, may be formed by the reaction with hydrogen



or water may react at the surface to form methane directly



Predications based on equilibrium considerations are not very helpful since under the degassing conditions, where gases are removed as they are formed, equilibrium is not attained.

Following degassing, graphite readsorbs much less gas on short exposure to air than was desorbed. If AGOT and TSF, which had been outgassed at 1800°C and cooled under vacuum, are exposed to air for about 10 days, the amount of gas released to 1800°C is only about 10 per cent of that released in the original degassing.¹⁴⁸

6-9 Permeability†

Low-permeability graphites have been used industrially for a decade or more as cascade coolers, heat exchangers, and reboilers.¹⁵⁵ With the increased interest in high-temperature gas-cooled reactors, more emphasis has been placed on the development of a material capable of serving at very high temperatures while remaining impermeable to the coolant gas.

Low-permeability graphites have several potential reactor applications. Those under current consideration include use as a high-temperature fuel-cladding material (Sec. 17-3.4) and as a fuel sleeve¹⁵⁶ to thermally insulate the graphite moderator from the coolant gas (Sec. 12-7.3). Another potential application is in the fabrication of an impermeable graphite-matrix fuel element (Sec. 16-2) in which the fission gases produced by the fuel would be contained in the matrix. The search for graphites suitable for these applications has led to the development of nearly impermeable graphite-based materials and to the methods for measuring their permeabilities quantitatively.

6-9.1 THEORIES OF GAS PERMEABILITY

The general law for the flow of a fluid through a body is^{157, 158}

$$\frac{dn}{dt} = \frac{KA}{L} \Delta \left(\frac{n}{V} \right) \quad (6.34)$$

where dn/dt = the number of molecules (n) flowing through a body per unit time (t)

A = the cross-sectional area of the body

L = the length of the body in the direction of flow

V = the gas volume

K = a permeability coefficient

For an ideal gas flowing at constant temperature, Eq. 6.34 can be written

$$\frac{d(PV)}{dt} = \frac{KA}{L} \Delta P \quad (6.35)$$

where the ΔP is the pressure drop across the body. For the viscous flow of a compressible gas

$$K = \frac{B}{\eta} \bar{P} \quad (6.36)$$

where B is a constant, η is the viscosity of the gas, and \bar{P} is the mean pressure in the porous body.

† This section was written by J. L. Jackson, Hanford Laboratories, General Electric Company.

Equation 6.35 can then be written in a form of Darcy's law

$$Q = \frac{B}{\eta} \bar{P} \frac{A}{L} \Delta P \quad (6.37)$$

where Q has been substituted for the rate of gas flow, $d(PV)/dt$.

Deviations from Darcy's law have been found at high flow rates for liquids and also for gases when the diameters of pores in the body are equal to, or less than, the mean free paths of the gas molecules.¹⁵⁸

Modern permeability theory recognizes three distinct types of flow in consolidated porous media: viscous flow, slip flow, and Knudsen (free molecular) flow. Normal flow in large-diameter capillaries is viscous with zero flow at the walls and a parabolic velocity profile. If the pressure of the gas is reduced until the mean free path of the molecules approaches the capillary diameter, slippage starts to take place at the capillary walls, and slip flow occurs. If the pressure or the capillary diameter is reduced until the mean free path is considerably greater than the capillary diameter, Knudsen (free molecular) flow takes place. Knudsen flow occurs by a diffusion process; it is independent of the gas viscosity and is dependent only on the partial pressure.

There is no simple relation between porosity (ratio of total void space to bulk volume) and the permeability of graphite. A fraction of the pores are sealed off and contribute nothing to the flow of gases. Only the connected pore system contributes to the permeability. The shapes of the pores influence the type of flow and length of the path the gas takes through the porous body. Since pores in different graphites vary greatly in size and shape, no general correlation between porosity and permeability can be expected.

6-9.2 PERMEABILITY EQUATIONS AND NOMENCLATURE

Several different permeability coefficients have been introduced in the graphite literature. Hutcheon¹⁵⁹ derived an expression for a permeability coefficient (K) defined by

$$K = \frac{B_0}{\eta} \bar{P} + \frac{4}{3} K_0 \sqrt{\frac{8RT}{\pi M}} = \frac{q_m \bar{P} L}{A \Delta P} \quad (6.38)$$

where M = the molecular weight of the gas

q_m = the volume flow rate

\bar{P} = the mean gas pressure in the body

B_0 = the permeability coefficient for viscous flow

K_0 = the permeability coefficient for the combined slip and Knudsen flow

Equation 6.38 is valid for the flow of several gases¹⁵⁹ through fine-pore graphites at temperatures up to 1000°C.

Eatherly¹⁰⁶ defines an admittance factor, F , as

$$F = \frac{Q_{pv}L}{A \Delta P} \quad (6.39)$$

where Q_{pv} is the pressure-volume flow and the other terms have the same significance as before. F is composed of two terms

$$F = F_0 + F_1 \bar{P} \quad (6.40)$$

where F_0 is the admittance factor for the combined slip and Knudsen flow and F_1 is the admittance factor for viscous flow.

If this expression is used, it is found¹⁰⁶ that the reimpregnation of graphite can either change the effective flow pore radius from the macro- to the microstructure or can decrease the pore radius in an already tight material.

When Eqs. 6.38 and 6.39 are compared, it is seen that K and F are equal. It should be noted, however, that B_0 and K_0 are not equivalent to F_1 and F_0 . The relations are

$$F_0 = \frac{4}{3} K_0 \sqrt{\frac{8RT}{\pi M}} \quad (6.41)$$

and

$$F_1 = \frac{B_0}{\eta} \quad (6.42)$$

B_0 and K_0 , in contrast to F_1 and F_0 , are independent of the gas used to measure the permeability.

6-9.3 UNITS OF GAS PERMEABILITY

It has been pointed out¹⁶⁰ that the units for expressing the permeability of a material to fluids are varied and confusing. The basic unit for many years has been the darcy, and, according to Carman,¹⁵⁷ "this corresponds to a flow of 1 ml/sec through a cm-cube with a pressure difference of 1 atm/cm² between the opposite faces and using a liquid with 1 centipoise viscosity." In metric units

$$1 \text{ darcy} = 9.87 \times 10^{-9} \text{ cm}^2 \quad (6.43)$$

Because Darcy's law is only applicable to the viscous flow of fluids, the darcy unit of permeability does not distinguish between the various flow processes and therefore does not reveal the effect of changes in the pore structure which occur with the newer impregnation methods. Permeability data are more useful when both viscous and slip flow are determined. The effects of impregnation or other treatments on the flow processes are then revealed.

The units for the different permeability coefficients are summarized in Table 6.21.

Table 6.21 — UNITS OF GAS PERMEABILITY COEFFICIENTS

Symbol	Unit	Type of flow
K ($\approx F$)	cm^3/sec	Viscous, slip, and Knudsen
B_0	cm^2	Viscous
F_1	$\text{cm}^2/\text{sec}/\text{atm}$	Viscous
K_0	cm	Slip and Knudsen
F_0	cm^2/sec	Slip and Knudsen

6-9.4 MEASUREMENT OF PERMEABILITY

Many methods have been devised for the determination of the various permeability coefficients of graphite. Those currently used are of two types: the steady-state and the dynamic (or pressure-change) methods.

In the steady-state method,¹⁶¹ a fixed forepressure is established on the sample, and the gas flow is measured after the pressure drop across the sample has become constant. The forepressure can be raised to the limits of the system; the back pressure can be controlled by a vent valve, or it may simply be atmospheric pressure or a vacuum. The differential pressure across the sample is read with a suitable instrument or is taken as the difference between the forepressure and the back pressure. For low-permeability graphites it may be necessary to measure the flow with a mass spectrometer.

For samples with very low permeability, a dynamic method is necessary.¹⁶²⁻¹⁶⁴ A fixed forepressure is established on the sample, the system is isolated, and the pressure decay is measured as a function of time. The pressure change is measured with either a closed-tube pressure gauge or a manometer.

6-9.5 PREPARATION OF LOW-PERMEABILITY GRAPHITE

The most common method of rendering graphite less permeable to gases is by impregnation with a carbonaceous liquid. The graphite body is heated to about 1000°C , or occasionally to higher temperatures, to carbonize the impregnant. Although the methods are generally similar to those used to increase the density (Sec. 2-4.2), the impregnating liquid is usually different. It is reported¹⁰⁶ that the conventional pitch impregnants increase the density without markedly reducing the permeability. Impregnants with low viscosities and greater wetting ability are more effective in reducing permeability.

The effect of several impregnants on the permeability of graphite is shown in Table 6.22. The permeabilities listed are in the units given in the references; they are not directly comparable because the experimental methods and analysis of the data were not the same. However, the improve-

Table 6.22 — EFFECT OF IMPREGNATION TECHNIQUES ON PERMEABILITIES

Base graphite	Permeability of base graphite	Measuring gas	Treatment	Permeability after treatment	Improvement factor	Ref.
1-in. -OD, 1/2-in. -ID tubes	2.7×10^{-3} cm ² /sec	N ₂	Two impregnations of furfuryl alcohol; carbonized at 1000 °C	1×10^{-7} cm ² /sec	2.7×10^4	165
2 1/4-in. -OD, 1 1/2-in. -ID tubes	2.8×10^{-2} cm ² /sec	N ₂	Two impregnations of furfuryl alcohol; carbonized at 1000 °C	2.1×10^{-6} cm ² /sec	10 ⁴	165
British Pile Grade A (PGA)	0.2 to 3 millidarcys	N ₂	One impregnation with sugar solution; heated to 1000 °C	0.004 to 0.06 millidarcys	50	156
British Pile Grade A (PGA)	0.2 to 3 millidarcys	N ₂	Five impregnations with sugar solution; heated to 1000 °C after each impregnation	0.2×10^{-6} to 3.0×10^{-6} millidarcys	10 ⁸	156
British Pile Grade A (PGA)	0.2 to 3 millidarcys	N ₂	Thermal decomposition of methane for 2 hr	0.004 to 0.10 millidarcys	30 to 50	156
National Carbon Grade AUF	4.0 millidarcys	Dry air	One furfuryl alcohol impregnation	0.35 millidarcys	10	166
National Carbon Grade AUF	4.0 millidarcys	Dry air	Multiple furfuryl alcohol impregnation	0.0039 millidarcys	1000	166
Fine-grained commercial stock		Air	Treated with benzene in nitrogen at 700 to 800 °C; pyrolytic carbon formed	1.5×10^{-9} cm ² /sec	10 ⁵ to 10 ⁷	165
Pyrolytic graphite	2.7×10^{-10} cm ² /sec	He	None			167

ment factor gives an indication of the relative effectiveness of the different treatments.

One of the more effective impregnants for graphite tubes is a furfuryl alcohol-catalyst mixture.¹⁶⁵ The mixture is deposited in the graphite pores by vacuum impregnation, and the resin that is formed is cured and then carbonized at 1000°C. Impregnation and carbonization are completed on one side before impregnation and carbonization of the other side to avoid bursting of the tube. This treatment reduces the permeability to gases by about a factor of 10^4 (Table 6.22).

The permeability of PGA graphite¹⁵⁶ is reduced by a factor of approximately 50 by one impregnation of a sugar solution, followed by slow heating of the body in an inert atmosphere to 1000°C. Four to five impregnations reduce the permeability by a factor of 10^6 .

A method that has been under extensive investigation is the reduction of permeability by the thermal decomposition of gases in the pores.¹⁵⁶ With suitable control of the pressure and the rate of decomposition of the hydrocarbon gases, the pores of the graphite can be partially filled. This method is similar to that used in forming pyrolytic carbon coatings (Sec. 14-7). The effect of this treatment on fine-grain commercial stock is shown in Table 6.22.

Graphite that has been impregnated to reduce the permeability is usually heated only to about 1000°C. Further heating to graphitization temperatures results in some opening of the closed pores. It is therefore very difficult to achieve permeabilities of less than 10^{-6} cm²/sec on fully graphitized material.

6-9.6 PERMEABILITY TO LIQUIDS

The fragmentary data that have been published indicate that Darcy's law (Eq. 6.37) does not hold for the flow of water through graphite.¹⁰⁶ The pressure applied to a liquid, in addition to maintaining the flow, must also

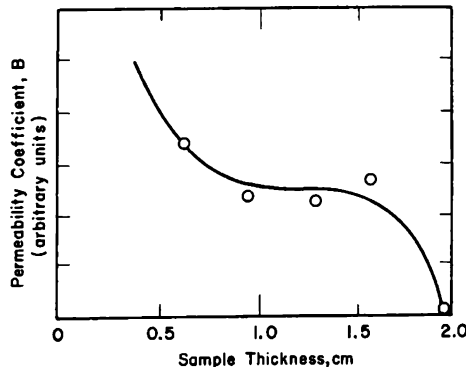


FIG. 6.21 Water permeability of R-0025 graphite.¹⁰⁶ The pressure differential across the sample is 150 psi.

Table 6.23 — MATERIAL DESIGNATIONS OF ELECTROGRAPHITES

Material designation	Manufacturer [†]	Description	Reference
AGOT	NCC		19
Nuclear-2	SCC	Current nuclear grades; $\delta \approx 3.9$ to 4.3 mb; $\rho = 1.6$ to 1.7 g/cm ³	169
R-1	GLCC		170
AGX	NCC	Early graphite used in first pile (see Sec. 1-1.2); selected from the commercial AGX grade for high purity; graphitized at 2600°C; absorption cross section (σ) ≈ 6.7 mb; $\rho = 1.58$ g/cm ³	111, 168
AGXP	BAEL	Graphite used in early British piles	
ATJ	NCC	Current grade of fine-grain high-density ($\rho = 1.73$ g/cm ³) graphite; molded	19, 106
ATJ-82	NCC	Same as ATJ except impregnated specifically for low permeability; $\rho = 1.88$ g/cm ³	106
ATL-82	NCC	A high-density ($\rho = 1.88$ g/cm ³) graphite manufactured in large sizes and impregnated for low permeability	106
AUF	NCC	Graphitized at 3000°C; $\rho \approx 1.67$ g/cm ³ ; formerly designated as ECA	111
AWG (also designated EBP)	NCC	An obsolete grade of a fine-grained molded graphite similar to AJT; $\rho = 1.75$ g/cm ³	177
C-18	NCC	Molded and graphitized at 2600°C; $\rho \approx 1.60$ g/cm ³ ; more isotropic than AUF	111
CK	Los Alamos Scientific Laboratory	$\rho = 1.71$ g/cm ³	107
CCN	NCC	High density ($\rho = 1.92$ g/cm ³); multiple pitch impregnations	106
CNG	NCC	Special sample prepared from Canadian natural-flake graphite to control electronic and structural factors.	12
CNG-B	NCC	Same as CNG but doped with boron	12
CS	NCC	Current grade used for hot-pressing molds; manufactured from coke of medium grain size; $\rho = 1.68$ g/cm ³ (This grade designation was also used for an early nuclear graphite similar to the current AGOT)	19

ECA (see AUF) EY9	Morgan Crucible Company, Ltd.	High-density ($\rho \approx 1.88 \text{ g/cm}^3$) graphite having a small, uniform pore size	106
French Nuclear Graphite	Compagnie Pechiney	Graphite used in the G-2 ($\sigma = 4.03 \text{ mb}$), G-3 ($\sigma = 3.95$), and the EDF reactors; purified with sodium fluoride; manufactured from Texas-Lockport coke; $\rho = 1.65 \text{ g/cm}^3$	174
GL-10	GLCC	A fine-grain experimental nuclear graphite manufactured from a needle coke and Standard pitch; not impregnated; $\rho = 1.60 \text{ g/cm}^3$	175
Graph-i-tite A	Graphite Specialties Corp.	High density ($\rho = 1.93 \text{ g/cm}^3$); heat-treated only to 700°C	106
Graph-i-tite G	Graphite Specialties Corp.	High density ($\rho = 1.88$); heat-treated to 3000°C	106
Graphon	Cabot Corporation	Spheron-6 heated to 3000°C	143, 178
H3LM	GLCC	Maximum particle size 0.033 in. ; $\rho = 1.68 \text{ g/cm}^3$	112
H4LM	GLCC	Maximum particle size 0.033 in. ; $\rho = 1.72 \text{ g/cm}^3$	107
KC (or AGOT-KC)	NCC	Early grade used in Hanford reactors made from Kendall coke and Chicago pitch; thermally purified, very well graphitized, anisotropic; $\rho \approx 1.7$; $\sigma = 4.40 \text{ mb}$	171
KCF	NCC	Same as KC except F purified; $\rho = 1.73 \text{ g/cm}^3$ and $\sigma = 3.78 \text{ mb}$	171
KS	NCC	Same as KC except made from Standard pitch; also designated as AGOT-KS	171
Korite graphite	Battelle Memorial Institute	An experimental graphite molded from No. 4 Korite petroleum asphalt coke; not well graphitized although heated to 2570°C or above; $\rho = 1.41$ to 1.59 g/cm^3	131

Table 6.23 (Continued)

Material designation	Manufacturer	Description	Reference
MH4LM-90	GLCC	Molded high density ($\rho = 1.90 \text{ g/cm}^3$); relatively high electrical and thermal conductivity; nearly isotropic	106
PBNG-G	NCC	Manufactured from natural flake graphite; bonded with pitch; very large crystallites	179
PGA	BAEL	The standard British moderator graphite; $\rho = 1.65$ to 1.75 g/cm^3 ; $\sigma \approx 4 \text{ mb}$	173
R-4	Graphite Specialties Corp.	High-density ($\rho = 1.98 \text{ g/cm}^3$) graphite made in large diameters; nearly isotropic	106
R-0013	NCC	A high-density (1.85 g/cm^3) base graphite; filler particles selected to optimize packing; carbon black added; pressure baked; no impregnations	106
R-0018	NCC	A high-density ($\rho = 1.85 \text{ g/cm}^3$) fine-grain graphite; pressure baked; no impregnations	106
R-0020	NCC	Same as R-0018 except impregnated; $\rho = 1.90 \text{ g/cm}^3$	106
R-0025	NCC	Same as R-0013 except impregnated, $\rho = 1.90 \text{ g/cm}^3$; now designated as RVA by manufacturer	106
SA-25	NCC	Manufactured from an oil-flame lampblack, pitch-bonded, molded, and graphitized at 3000°C ; isotropic with small crystallites; $\rho = 1.55 \text{ g/cm}^3$; now designated CEP by manufacturer	176, 177
SP7B	SCC	Experimental graphite made from Texas-Lockport coke and Standard pitch; gas purified; $\sigma = 3.65 \text{ mb}$, $\rho = 1.61 \text{ g/cm}^3$	172
SP24B	SCC	Experimental graphite made from a needle coke and Standard pitch; thermally purified; $\sigma = 4.27 \text{ mb}$, $\rho = 1.72 \text{ g/cm}^3$	172
Speer-3499	SCC	Molded and graphitized above 2260°C ; maximum particle size 0.005 in. ; $\rho = 1.57 \text{ g/cm}^3$	112
Speer gas purified	SCC	Similar to TSGBF except $\rho = 1.63 \text{ g/cm}^3$ and $\sigma = 3.68 \text{ mb}$	171
Spheron-6	Cabot Corporation	A medium processing channel black	143
Thermax	Thermax Atomic Carbon Co.	A furnace carbon; particle size $\approx 2750 \text{ \AA}$	181

Table 6.23 (Continued)

Material designation	Manufacturer [†]	Description	Reference
TSF	NCC SCC GLCC	Current nuclear grades structurally similar to AGOT but gas purified; $\sigma = 3.5$ to 3.85 mb	19
Nuclear-1			169
R-3			170
TSX	NCC	Manufactured from a fine-grain needle coke and graphitized at 3000°C; very anisotropic and well graphitized; $\sigma = 3.75$ to 3.85 mb; $\rho = 1.71$ g/cm ³ ; used in Hanford N Reactor	180
TSGBF	NCC	Made from Texas-Lockport coke and Standard pitch; graphitized and F purified in one step at 2450°C; more isotropic than CSF; $\rho = 1.65$ g/cm ³ ; $\sigma = 3.75$ mb; similar grade now designated GBF by manufacturer	171
WSF	NCC	Similar to CSF except made from Whiting coke	171

[†] NCC, National Carbon Company; SCC, Speer Carbon Co.; GLCC, Great Lakes Carbon Corp.; BAEL, British Acheson Electrodes, Ltd.

[‡] Consult manufacturer for exact value.

§ In addition to British Acheson Electrodes, Anglo-Great Lakes has recently begun production of this grade.

overcome the surface tension at the liquid-gas interface at the pores. This additional pressure (Δp) is given in terms of the pore radius (r) by

$$\Delta p = \frac{2\gamma \cos \theta}{r} \quad (6.44)$$

where γ is the surface tension of the liquid and θ is the contact angle.

As a result the permeability of a liquid through graphite might be expected to vary with the sample thickness in a way that depends on the pore-size distribution. Figure 6.21 shows this variation for a dense impregnated graphite, R-0025. A cutoff thickness, at which no measurable flow occurs, is approached very rapidly for a sample thickness greater than about 1.5 cm. The pore radius calculated from Eq. 6.43 for this case ($\theta = 0$, $\gamma = 72.8$ dynes/cm, $\Delta p = 150$ psi) is 1500 Å.

6-10 Material Designations of Electrographites

A wide variety of carbon materials have been irradiated or tested in other ways in the study of graphite for reactor applications. Many of these are not considered candidate reactor materials but have merely been used in basic studies to determine the effect of irradiation or other treatment on a particular property. They are usually referred to in the literature simply by a letter designation; occasionally this is accompanied by a general description of the properties.

The material designations referred to in this book are listed in Table 6.23. A brief description of the carbon material is given, and in some cases more information will be found in the references. The values of the properties given are those listed for the samples discussed in this book or given in the references; they are not necessarily typical of the material with that letter designation. Except where noted, all graphites were extruded from a mixture of petroleum coke and coal-tar pitch and were graphitized at 2750 to 3000°C.

References

1. J. Basset, Fusion of Graphite Under Argon Pressure of 1 to 11,500 kg/cm², Determination of the Triple Point, and the Establishment of a Provisional Diagram for the Solid, Liquid and Gaseous States of Carbon. I., *J. phys. radium*, **10**: 217-228 (1939).
2. M. T. Jones and W. Weltner, Jr., *The Phase Diagram of Carbon*, paper presented at the Fourth Conference on Carbon Held at the University of Buffalo, and private communication, 1959.
3. H. P. Bovenkerk et al., Preparation of Diamond, *Nature*, **184**: 1094-1098 (1959).
4. K. S. Pitzer and E. Clementi, *Large Molecules in Carbon Vapor*, USAEC Report UCRL-8675, University of California Radiation Laboratory, March 1959.
5. J. Drowart et al., Mass Spectrophotometric Study of Carbon Vapor, *J. Chem. Phys.*, **31**: 1131-1132 (1959).
6. J. E. Hove, Some Physical Properties of Graphite as Affected by High Temperature and Irradiation, in *Industrial Carbon and Graphite: Papers Read at the Conference*

- Held in London, September 24-26, 1957*, pp. 501-510, Society of Chemical Industry, London, 1958.
7. W. Desorbo and G. E. Nichols, A Calorimeter for the Temperature Region 1 to 20°K. The Specific Heat of Some Graphite Specimens, *Phys. and Chem. Solids*, **6**: 352-366 (1958).
 8. P. H. Keesom and N. Pearlman, Atomic Heat of Graphite Between 1 and 20°K, *Phys. Rev.*, **99**: 1119-1124 (1955).
 9. U. Bergenlid et al., The Specific Heat of Graphite Below 90°K, *Phil. Mag.*, **45**: 851-854 (1954).
 10. F. J. Webb and J. Wilks, The Measurement of Lattice Specific Heats at Low Temperatures Using a Heat Switch, *Proc. Roy. Soc. (London)*, **A230**: 549-559 (1955).
 11. J. C. Bowman et al., X-Ray and Low-Temperature Thermal Conductivity Study of Defects in Graphite, in *Industrial Carbon and Graphite: Papers Read at the Conference Held in London, September 24-26, 1957*, pp. 52-59, Society of Chemical Industry, London, 1958.
 12. J. C. Bowman and J. A. Krumhansl, The Low Temperature Specific Heat of Graphite, *Phys. and Chem. Solids*, **6**: 367-379 (1958).
 13. P. Flubacher et al., The Limiting Low-temperature Behavior of the Heat Capacity of Graphite, *Phys. and Chem. Solids*, **13**: 160-163 (1960).
 14. J. Krumhansl and H. Brooks, The Lattice-Vibration Specific Heat of Graphite, *J. Chem. Phys.*, **21**: 1663-1669 (1953).
 15. W. Desorbo and W. W. Tyler, The Specific Heat of Graphite from 13 to 300°K, *J. Chem. Phys.*, **21**: 1660-1663 (1953).
 16. F. D. Rossini et al., *Selected Values of Physical and Thermodynamic Properties of Hydrocarbons and Related Compounds Comprising the Tables of the American Petroleum Institute Research Project 44*, Carnegie Press, Pittsburgh, 1953.
 17. N. S. Rasor and J. D. McClelland, *Thermal Properties of Materials. Part I, Properties of Graphite, Molybdenum, and Tantalum to their Destruction Temperatures*, USAEC Report WADC-TR-56-400, North American Aviation, Inc., Oct. 26, 1956.
 18. J. E. Hove and A. W. Smith, Interpretation of the Low-Temperature Thermal Conductivity of Graphite, *Phys. Rev.*, **104**: 892-900 (1956).
 19. *Industrial Graphite Engineering Handbook*, Union Carbide Corporation, 1959.
 20. R. Berman, The Thermal Conductivity of Some Polycrystalline Solids at Low Temperatures, *Proc. Phys. Soc. (London)*, **A65**: 1029-1040 (1952).
 21. A. W. Smith and N. S. Rasor, Observed Dependence of the Low-Temperature Thermal and Electrical Conductivity of Graphite on Temperature, Type, Neutron Irradiation, and Bromination, *Phys. Rev.*, **104**: 885-891 (1956).
 22. R. W. Powell and F. H. Schofield, The Thermal and Electrical Conductivities of Carbon and Graphite to High Temperatures, *Proc. Phys. Soc. (London)*, **51**: 153-179 (1939).
 23. F. M. Collins, *The Thermal Expansion of Artificial Polycrystalline Carbons and Graphite*, Thesis, University of Buffalo, 1958.
 24. F. M. Collins, Thermal Expansion of Polycrystalline Carbons and Graphite, in *Proceedings of the Third Conference on Carbon Held at the University of Buffalo*, pp. 659-674, Pergamon Press, New York, 1959.
 25. L. Green, Jr., The Behavior of Graphite Under Alternating Stress, *J. Appl. Mechanics*, **18**: 345-348 (1951).
 26. G. J. Dienes, Mechanism for Self-Diffusion in Graphite, *J. Appl. Phys.*, **23**: 1194-1200 (1952).
 27. M. A. Kanter, The Mechanism for Atom Motion in Graphite Crystals, in *Conference on the Kinetics of High-Temperature Processes*, pp. 61-66, Technology Press, Massachusetts Institute of Technology, 1958.

28. M. A. Kanter, Diffusion of Carbon Atoms in Natural Graphite Crystals, *Phys. Rev.*, **107**: 655-663 (1957).
29. M. H. Feldman et al., Studies of Self-Diffusion in Graphite Using C^{14} Tracer, *J. Appl. Phys.*, **23**: 1200-1206 (1952).
30. R. R. Haering and S. Mrozowski, The Band Structure and Electronic Properties of Graphite Crystals, in *Progress in Semiconductors*, Vol. 5, pp. 273-316, Heywood & Company, Ltd., London, 1960.
31. R. R. Haering, Band Structure of Rhombohedral Graphite, *Can. J. Phys.*, **36**: 352-362 (1958).
32. P. R. Wallace, Band Theory of Graphite, *Phys. Rev.* **71**: 622-634 (1947).
33. J. C. Slonczewski and P. R. Weiss, Band Structure of Graphite, *Phys. Rev.*, **109**: 272-279 (1958).
34. D. E. Soule and J. W. McClure, Band Structure and Transport Properties of Single-Crystal Graphite, *Phys. and Chem. Solids*, **8**: 29-35 (1959).
35. J. W. McClure, Band Structure of Graphite and de Haas-van Alphen Effect, *Phys. Rev.*, **108**: 612-618 (1957).
36. P. Nozieres, Cyclotron Resonance in Graphite, *Phys. Rev.* **109**: 1510-1521 (1958).
37. W. S. Boyle and P. Nozieres, Band Structure and Infrared Absorption of Graphite, *Phys. Rev.*, **111**: 782-785 (1958).
38. J. W. McClure, Theory of Diamagnetism of Graphite, *Phys. Rev.*, **119**: 606-613 (1960).
39. R. R. Haering and P. R. Wallace, The Electric and Magnetic Properties of Graphite, *Phys. and Chem. Solids*, **3**: 253-374 (1957).
40. E. E. Loebner, Thermoelectric Power, Electrical Resistance, and Crystalline Structure of Carbons, *Phys. Rev.*, **102**: 46-57 (1956).
41. N. Ganguli and K. S. Krishnan, The Magnetic and Other Properties of the Free Electrons in Graphite, *Proc. Roy. Soc. (London)*, **A177**: 168-182 (1941).
42. K. S. Krishnan, Magnetic Anisotropy of Graphite, *Nature*, **133**: 174-175 (1934).
43. P. Kiive and S. Mrozowski, Changes in the Magnetic Susceptibility with the Degree of Carbonization, in *Proceedings of the Third Conference on Carbon Held at the University of Buffalo*, pp. 165-172, Pergamon Press, New York, 1959.
44. H. T. Pinnick and P. Kiive, Magnetic Susceptibility of Carbons and Polycrystalline Graphites. II., *Phys. Rev.*, **102**: 58-64 (1956).
45. D. Shoenberg, The de Haas-van Alphen Effect, *Phil. Trans. Roy. Soc. London*, **245**: 1-57 (1952).
46. T. G. Berlincourt and M. C. Steel, Oscillatory Hall Effect, Magnetoresistance, and Magnetic Susceptibility of a Graphite Single Crystal, *Phys. Rev.*, **98**: 956-961 (1955).
47. D. E. Soule, Magnetic Field Dependence of the Hall Effect and Magnetoresistance in Graphite Single Crystals, *Phys. Rev.*, **112**: 698-707 (1958).
48. J. W. McClure, Analysis of Multi-Carrier Galvanomagnetic Data for Graphite, *Phys. Rev.*, **112**: 715-721 (1958).
49. G. H. Kinchin, The Electrical Properties of Graphite, *Proc. Roy. Soc. (London)*, **A217**: 9-26 (1953).
50. D. R. Winder, National Carbon Company, unpublished data, 1960.
51. D. E. Soule, Fermi Surfaces in Graphite Determined from the de Haas-van Alphen Effect, in *Proceedings of the Fourth Conference on Carbon Held at the University of Buffalo*, pp. 183-188, Pergamon Press, New York, 1960.
52. J. K. Galt et al., Cyclotron Resonance in Graphite (Experimental), in *Proceedings of the Third Conference on Carbon Held at the University of Buffalo*, pp. 193-196, Pergamon Press, New York, 1959.
53. P. Nozieres, Cyclotron Resonance in Graphite, in *Proceedings of the Third Con-*

- ference on Carbon Held at the University of Buffalo, pp. 197-202, Pergamon Press, New York, 1959.
54. R. J. Elliott, Theory of the Effect of Spin-Orbit Coupling on Magnetic Resonance in Some Semi-Conductors, *Phys. Rev.*, **96**: 266-279 (1954).
 55. F. J. Dyson, Electron Spin Resonance Absorption in Metals. II. Theory of Electron Diffusion and the Skin Effect, *Phys. Rev.*, **98**: 349-359 (1955).
 56. G. Wagoner, Spin Resonance of Charge Carriers in Graphite, *Phys. Rev.*, **118**: 647-653 (1960).
 57. J. G. Castle, Paramagnetic Resonance Absorption in Graphite, *Phys. Rev.*, **92**: 1063 (1953).
 58. G. R. Hennig and B. Smaller, *Paramagnetism of Irradiated Graphite*, USAEC Report ANL-5385, Argonne National Laboratory, Jan. 20, 1955.
 59. W. Primak and L. H. Fuchs, Electrical Conductivities of Natural Graphite Crystals, *Phys. Rev.*, **95**: 22-30 (1954).
 60. W. Primak, *c*-Axis Electrical Conductivity of Graphite, *Phys. Rev.*, **103**: 544-546 (1956).
 61. W. Primak and L. H. Fuchs, Radiation Damage to the Electric Conductivities of Natural Graphite Crystals, *Phys. Rev.*, **103**: 541-544 (1956).
 62. J. Okada and T. Ikegawa, Electrical Resistivity of Artificial Graphite, *J. Appl. Phys.*, **23**: 1282-1283 (1952).
 63. I. B. Mason, The Electrical Resistance of Polycrystalline Carbons and Graphites, in *Industrial Carbon and Graphite: Papers Read at the Conference Held in London, September 24-26, 1957*, pp. 60-73, Society of Chemical Industry, London, 1958.
 64. L. C. F. Blackman et al., The Anisotropic Thermoelectric Power of Graphite, *Proc. Roy. Soc. (London)*, **A255**: 293-306 (1960).
 65. E. Taft and L. Apker, Photoelectric Emission from Polycrystalline Graphite, *Phys. Rev.*, **99**: 1831-1832 (1955).
 66. Y. H. Ichikawa, Characteristic Energy Loss of Electrons in Graphite, *Phys. Rev.*, **109**: 653-657 (1958).
 67. E. de B. Barnett and C. L. Wilson, *Inorganic Chemistry*, Longmans, Green & Co., Ltd., London, 1953.
 68. V. M. Sheplaine and R. J. Runck, Carbides, in *High Temperature Technology*, pp. 114-130, John Wiley & Sons, Inc., New York, 1956.
 69. J. F. Hogerton and R. C. Grass (Eds.), *Reactor Handbook. Vol. 3, Materials, Section 1, General Properties*, USAEC Report, AECD-3647, United States Atomic Energy Commission, March, 1955.
 70. G. R. Hennig, Interstitial Compounds of Graphite, in *Progress in Inorganic Chemistry*, Vol. 1, pp. 125-205, Interscience Publishers, Inc., New York 1959.
 71. A. F. Gerds and M. W. Mallett, Compatibility of a Number of Metals and Alloys with Graphite, *Trans. Am. Soc. Metals*, **53**: 1027-1045 (1960); see also this same title issued as USAEC Report BMI-1261, Battelle Memorial Institute, 1958.
 72. A. Herold, Recherches sur les composés d'insertion du graphite, *Bull. soc. chim. France*, Nos. 7-8, 999-1012 (1955).
 73. R. N. Lyon (Ed.), *Liquid-Metals Handbook*, U. S. Office of Naval Research Report NAVEXOS-P-733 Rev., 2nd ed., U. S. Government Printing Office, Washington, D. C., 1952.
 74. J. C. Bokros, *Graphite-Metal Compatibility at High Temperatures*, USAEC Report GA-782, General Atomic Division, General Dynamics Corp., June 1959.
 75. R. C. Asher and S. A. Wilson, Lamellar Compound of Sodium with Graphite, *Nature*, **181**: 409-410 (1958).
 76. *Metals Handbook*, p. 1183, American Society for Metals, Cleveland, 1948.
 77. J. J. Gangler, Resistance of Refractories to Molten Lead-Bismuth Alloy, *J. Am. Ceram. Soc.*, **37**: 312-316 (1954).

78. T. D. Chikalla, Hanford Laboratories, General Electric Company, unpublished data, June 1960.
79. E. L. Swarts, The Action of Molten Uranium on Graphite, *Trans. Met. Soc. of AIME*, **215**: 553-554 (1959).
80. P. D. Johnson, Behavior of Refractory Oxides and Metals, Alone and in Combination, in Vacuo at High Temperatures, *J. Am. Ceram. Soc.*, **33**: 168-171 (1950).
81. W. J. Kroll and A. W. Schlechton, Reactions of Carbon and Metal Oxides in a Vacuum, *J. Electrochem. Soc.*, **93**: 247-258 (1948).
82. Ya. A. Pavlov, paper presented at 2nd World Metallurgical Congress, Chicago, Nov. 6, 1957 (cf. Armed Services Technical Information Agency Document AD-220, 420, Ref. No. 2).
83. K. L. Komarek and A. Coucoulas, *Study of Reaction Rates Between Refractory Oxides and Graphite. Progress Report No. 5*, Report AD-234737, New York University, Sept. 16, 1959 to Mar. 15, 1960.
84. K. L. Komarek and N. Klinger, *Study of Reaction Rates Between Refractory Oxides and Graphite. Progress Report No. 7*, Report AD-254730, New York University, Sept. 16, 1960 to Mar. 15, 1961.
85. *Gas Cooled Reactor Project Quarterly Progress Report for Period Ending March 31, 1960*, USAEC Report ORNL-2929, pp. 98-100, Oak Ridge National Laboratory, June 21, 1960.
86. B. Craven and E. R. McCartney, Studies of Reactions between Uranium Dioxide and Graphite, *J. Am. Ceram. Soc.*, **44**: 12-15 (1961).
87. C. H. Prescott, Jr., and W. B. Hincke, The High-Temperature Equilibrium Between Thorium Oxide and Carbon, *J. Am. Chem. Soc.*, **49**: 2744-2753 (1927).
88. W. Rudorff, Graphite Intercalation Compounds, in *Advances in Inorganic Chemistry and Radiochemistry*, Vol. 1, pp. 223-266, Academic Press, Inc., New York, 1959.
89. R. C. Croft, Lamellar Compounds of Graphite, *Quart. Revs. London*, **14**: 1-45 (1960).
90. S. Mrozowski, Electric Resistivity of Interstitial Compounds of Graphite, *J. Chem. Phys.*, **21**: 492-495 (1953).
91. E. A. Kmetko, Electronic Properties of Carbons and of Their Interstitial Bisulfate Compounds, *J. Chem. Phys.*, **21**: 2152-2158 (1953).
92. J. Maire and J. Mering, Fixation of Bromine on Carbons of Various Degrees of Graphitization, in *Proceedings of the Third Conference on Carbon Held at the University of Buffalo*, pp. 337-346, Pergamon Press, New York, 1959.
93. G. R. Hennig, A Chemical Model of Radiation Damage in Graphite, *Nuclear Sci. and Eng.*, **3**: 514-528 (1958).
94. R. N. Smith, The Chemistry of Carbon-Oxygen Surface Compounds, *Quart. Revs. London*, **13**: 287-305 (1959).
95. A. Amorosi, Selection of Reactors, in *Nuclear Engineering Handbook*, pp. 12-2 to 12-77, McGraw-Hill Book Company, Inc., New York, 1958.
96. C. L. Mantell, *Industrial Carbon*, 2nd. ed., p. 418, D. Van Nostrand Co., Inc., New York, 1946.
97. E. M. Simons et al., *Corrosion and Components Studies on Systems Containing Fused NaOH*, USAEC Report BMI-1118, Battelle Memorial Institute, July 30, 1956.
98. D. P. Riley, The Thermal Expansion of Graphite: Part II. Theoretical, *Proc. Phys. Soc. (London)*, **57**: 486-495 (1945).
99. J. Basset, Researches on the Density of Graphite and Determination of the Mean Coefficient of Compressibility between 1 and 20,000 kg/cm², *Compt. rend.*, **213**: 829-831 (1941).
100. J. H. W. Simmons, The Effects of Irradiation on the Mechanical Properties of

- Graphite, in *Proceedings of the Third Conference on Carbon Held at the University of Buffalo*, pp. 559-568, Pergamon Press, New York, 1959.
101. F. Laves and Y. Baskin, Formation of the Rhombohedral Graphite Modification, *Z. Krist.*, **107**: 337-356 (1956).
 102. P. Arragon and R. M. Berthier, Mechanical Characterization of Artificial Graphite, in *Industrial Carbon and Graphite: Papers Read at the Conference Held in London, Sept. 24-26, 1957*, pp. 565-578, Society of Chemical Industry, London, 1958.
 103. R. Arnold, Elastische Eigenschaften von Kunstgraphit, *Z. angew. Phys.*, **11**: 179-183 (1959).
 104. H. H. W. Losty, General Electric Co., Ltd., unpublished data, 1960.
 105. A. B. McIntosh et al., Physical and Mechanical Properties of Graphite Moderators, in *Industrial Carbon and Graphite: Papers Read at the Conference Held in London, Sept. 24-26, 1957*, pp. 560-564, Society of Chemical Industry, London, 1958.
 106. W. P. Eatherly et al., Physical Properties of Graphite Materials for Special Nuclear Application, in *Proceedings of the Second United Nations International Conference on the Peaceful Uses of Atomic Energy, Geneva, 1958*, Vol. 7, pp. 389-401, United Nations, New York, 1959.
 107. P. Wagner et al., Some Mechanical Properties of Graphite in the Temperature Range 20 to 3000°C, in *Proceedings of the Second United Nations International Conference on the Peaceful Uses of Atomic Energy, Geneva, 1958*, Vol. 7, pp. 379-388, United Nations, New York, 1959.
 108. L. M. Currie et al., The Production and Properties of Graphite for Reactors, in *Proceedings of the First United Nations International Conference on the Peaceful Uses of Atomic Energy, Geneva, 1955*, Vol. 8, pp. 451-473, United Nations, New York, 1956.
 109. R. Berenbaum and I. Brodie, Measurement of the Tensile Strength of Brittle Materials, *Brit. J. Appl. Phys.*, **10**: 281-287 (1959).
 110. S. A. Bortz and H. H. Lund, Evaluation of a Tension Test for Brittle Materials, in *Proceedings of the Fourth Conference on Carbon Held at the University of Buffalo*, pp. 531-536, Pergamon Press, New York, 1960.
 111. C. Malmstrom et al., Some Mechanical Properties of Graphite at Elevated Temperatures, *J. Appl. Phys.*, **22**: 593-600 (1951).
 112. H. E. Martens et al., Tensile and Creep Behavior of Graphites Above 3000°F, in *Proceedings of the Fourth Conference on Carbon Held at the University of Buffalo*, pp. 511-530, Pergamon Press, New York, 1960.
 113. L. N. G. Filon, Approximate Solution for the Bending of a Beam of Rectangular Cross-Section under Any System of Load, *Phil. Trans. Roy. Soc. London*, **A201**: 63-155 (1903).
 114. G. H. Kinchin, The Effects of Irradiation on Graphite, Canadian Report CRNE-539, Apr. 7, 1953.
 115. H. W. Davidson et al., The Mechanical Properties of Graphite at Elevated Temperatures, in *Industrial Carbon and Graphite: Papers Read at the Conference Held in London, Sept. 24-26, 1957*, pp. 551-559, Society of Chemical Industry, London, 1958.
 116. F. E. Faris et al., The Thermal Dependence of the Elastic Moduli of Polycrystalline Graphite, *J. Appl. Phys.*, **23**: 89-95 (1952).
 117. H. W. Davidson and H. H. W. Losty, The Effect of Neutron Irradiation on the Mechanical Properties of Graphite, in *Proceedings of the Second United Nations International Conference on the Peaceful Uses of Atomic Energy, Geneva, 1958*, Vol. 7, pp. 307-314, United Nations, New York, 1959.
 118. J. O. Jeffrey et al., *Shear Tests of Graphite*, USAEC Report BNL-68, Brookhaven National Laboratory, July 15, 1950.

119. J. M. Hutcheon and M. S. T. Price, The Dependence of the Properties of Graphite on Porosity, in *Proceedings of the Fourth Conference on Carbon Held at the University of Buffalo*, pp. 645-656, Pergamon Press, New York, 1960.
120. S. Mrozowski, Physical Properties of Carbons and the Formulation of the Green Mix, in *Proceedings of the First and Second Conferences on Carbon Held at the University of Buffalo*, pp. 195-215, Waverly Press, Inc., Baltimore, 1956.
121. H. H. W. Losty, Effect of Impregnation and Heat Treatment on the Physical Properties of Graphite, in *Proceedings of the Fourth Conference on Carbon Held at the University of Buffalo*, pp. 671-674, Pergamon Press, New York, 1960.
122. A. F. Gorton and C. Malmstrom, *Tensile Strength of Type EBP Graphite at Elevated Temperatures and Its Relation to Apparent Density at Room Temperature*, USAEC Report NAA-SR-67, North American Aviation, Inc., Mar. 13, 1950.
123. S. Mrozowski, The Nature of Artificial Carbons, in *Industrial Carbon and Graphite: Papers Read at the Conference Held in London, Sept. 24-26, 1957*, pp. 7-18, Society of Chemical Industry, London, 1958.
124. H. W. Davidson and H. H. W. Losty, Elastic and Plastic Properties of Carbon and Graphite, in *Mechanical Properties of Non-Metallic Brittle Materials, London Conference of the National Coal Board, 1968*, pp. 219-238, Interscience Publishers, Inc., New York, 1958.
125. H. W. Davidson and H. H. W. Losty, An Interpretation of the Mechanical Behavior of Carbons, in *Proceedings of the Fourth Conference on Carbon Held at the University of Buffalo*, pp. 585-591, Pergamon Press, New York, 1960.
126. D. B. Fischbach, High-Temperature Creep of Graphite, *Nature*, **186**: 795-797 (1960).
127. J. C. Ballinger, *Graphite Machinability*, USAEC Report HW-30727, Hanford Works, Dec. 31, 1953.
128. E. M. Woodruff, *Machinability of Graphites for Future Piles*, USAEC Report HW-31578, Hanford Works, July 21, 1954.
129. R. L. Bond et al., The Structure and Reactivity of Pile Graphite, in *Proceedings of the US/UK Meeting on the Compatibility Problems of Gas-Cooled Reactors Held at Oak Ridge National Laboratory, Feb. 24-26, 1960*, pp. 374-385, USAEC Report TID-7597 (Bk. 1), 1961.
130. E. M. Dressl and L. E. J. Roberts, Closed Pores in Synthetic Graphite, *Nature*, **171**: 170 (1953).
131. W. A. Hedden et al., *Experimental Carbons and Graphites for Irradiation Studies*, USAEC Report BMI-962, Battelle Memorial Institute, Oct. 26, 1954.
132. M. W. Nathans, *High Density Graphite*, USAEC Report COO-202, Great Lakes Carbon Corp., Sept. 2, 1954.
133. T. Sawai et al., Some Problems of Manufacturing Reactor Graphite, *Proceedings of the Second United Nations International Conference on the Peaceful Uses of Atomic Energy, Geneva, 1958*, Vol. 4, pp. 257-268, United Nations, New York, 1959.
134. J. H. deBoer and S. Kruyer, The Two-Dimensional van der Waals Constants of Molecules Adsorbed on Charcoal and Graphite, *Trans. Faraday Soc.*, **54**: 540-547 (1958).
135. C. N. Spalaris, The Micropore Structure of Artificial Graphite, *J. Phys. Chem.*, **60**: 1480-1483 (1956).
136. C. N. Spalaris, *Adsorptive Properties of Virgin and Irradiated Graphite*, USAEC Report HW-33487 (AECD-3679), Hanford Atomic Products Operation, Nov. 24, 1954.
137. S. Brunauer, *Physical Adsorption of Gases and Vapors*, Princeton University Press, Princeton, 1943.
138. J. H. deBoer, The Shapes of Capillaries, in *The Structure and Properties of Porous Materials*, pp. 68-94, Academic Press Inc., New York, 1958.

139. C. Pierce and R. N. Smith, Adsorption-Desorption Hysteresis in Relation to Capillarity of Adsorbents, *J. Phys. & Colloid Chem.*, **54**: 784-794 (1950).
140. S. Brunauer et al., Adsorption of Gases in Multimolecular Layers, *J. Am. Chem. Soc.*, **60**: 309-319 (1938).
141. C. N. Spalaris, The Micropore Structure of Neutron Irradiated Graphite, in *Proceedings of the Third Conference on Carbon Held at the University of Buffalo*, pp. 575-578, Pergamon Press, New York, 1959.
142. F. E. Bartell and C. G. Dodd, Surface Areas of Crystalline Carbon and Carbide Powders as Measured by the Adsorption of Nitrogen, *J. Phys. & Colloid Chem.*, **54**: 114-128 (1950).
143. L. G. Joyner and P. H. Emmett, Differential Heats of Adsorption of Nitrogen on Carbon Blacks, *J. Am. Chem. Soc.*, **70**: 2353-2359 (1948).
144. R. H. Savage and C. Brown, Chemical and Physical Adsorption of Gases on Carbon Dust, *J. Am. Chem. Soc.*, **70**: 2362-2366 (1948).
145. P. L. Walker, Jr., et al., Surface Area Studies of Carbon-Carbon Dioxide Reaction, *Ind. Eng. Chem.*, **45**: 1703-1710 (1953).
146. C. C. Horton and L. E. J. Roberts, *The Adsorption of Water on Pile Graphite*, British Report AERE-C-R-2219, 1958.
147. C. Pierce and R. N. Smith, Heats of Adsorption. I., *J. Phys. & Colloid Chem.*, **52**: 1111-1115 (1948).
148. L. G. Overholser and J. P. Blakely, Studies of Gas Evolution by Graphite, in *Proceedings of the US/UK Meeting on the Compatibility Problems of Gas-Cooled Reactors Held at Oak Ridge National Laboratory, Feb. 24-26, 1960*, pp. 560-585, USAEC Report TID-7597 (Bk. 2), 1961.
149. R. C. Asher, The Degassing of Graphite, in *Proceedings of the US/UK Meeting on the Compatibility Problems of Gas-Cooled Reactors Held at Oak Ridge National Laboratory, Feb. 24-26, 1960*, pp. 504-522, USAEC Report TID-7597 (Bk. 2), 1961.
150. R. R. Eggleston et al., *Graphite Outgassing*, USAEC Report NAA-SR-Memo-1240, North American Aviation, Inc., Jan. 21, 1955.
151. S. Siegel et al., Basic Technology of the Sodium Graphite Reactor, in *Proceedings of the First United Nations International Conference on the Peaceful Uses of Atomic Energy, Geneva, 1955*, Vol. 9, pp. 321-330, United Nations, New York, 1956.
152. J. P. Redmond and P. L. Walker, Jr., The Gas Content of Graphites, *Nature*, **186**: 72-74 (1960).
153. B. A. Ryan, Hanford Laboratories, General Electric Company, unpublished data, May 1959.
154. L. G. Overholser, Oak Ridge National Laboratory, personal communication, August 1960.
155. W. M. Gaylord, Carbon and Graphite, *Ind. Eng. Chem.*, **51**: 1161-1164 (1959).
156. D. A. Boyland, The Reduction of the Permeability of Graphite, *G.E.C. Atomic Energy Rev.*, **2**: 44-50 (1959).
157. P. C. Carman, *Flow of Gases Through Porous Media*, Academic Press Inc., New York, 1956.
158. A. E. Scheidegger, *The Physics of Flow Through Porous Media*, The Macmillan Co., New York, 1957.
159. J. M. Hutcheon et al., The Flow of Gases Through A Fine-Pore Graphite, in *Industrial Carbon and Graphite: Papers Read at the Conference Held in London, September 24-26, 1957*, pp. 259-271, Society of Chemical Industry, London, 1958.
160. M. H. Dodson, *Permeability of Porous Solids: Units and Definitions*, British Report IGR-TM/CA-0143, Capenhurst Works, February, 1958.
161. R. N. Lyon, *Permeability of Graphite for Air*, Report Mont-291, Montsanto Chemical Company, Apr. 30, 1947.

162. S. D. Fulkerson and F. J. Lambert, *Apparatus and Method for Determining Gas Permeability of Carbon and Graphite*, USAEC Report Y-387, Carbide and Carbon Chemicals Corp., February 1959.
163. W. P. Eatherly, National Carbon Company, personal communication, 1959.
164. R. A. Penneman, *Diffusion of Helium Through Graphite*, USAEC Report N-1570, University of Chicago, Sept. 15, 1944.
165. W. Watt et al., Production of Impermeable Graphite, *Nuclear Power*, 4(34): 86-88 (1959).
166. R. D. Keen, *High Temperature Materials Studies. Semi-Annual Progress Report, January-July 1953*, USAEC Report, NAA-SR-279, North American Aviation, Inc., Mar. 1, 1954.
167. A. B. Riedinger and L. R. Zumwalt, The Noble Gas Permeability Characteristics of Graphite Materials for Use in Gas-Cooled Reactors, in *Proceedings of the US/UK Meeting on the Compatibility Problems of Gas-Cooled Reactors Held at Oak Ridge National Laboratory, Feb. 24-26, 1960*, pp. 391-409, USAEC Report TID-7597 (Bk. 1), 1961.
168. S. K. Allison, *The First Intermediate Pile at the University of Chicago*, USAEC Report CP-69, University of Chicago, no date.
169. Technical data sheet of the Speer Carbon Co., St. Marys, Penn.
170. Technical data sheet of the Great Lakes Carbon Corp., Electrode Division, P. O. Box 637, Niagara Falls, N. Y.
171. D. M. Knott, *Pile Moderator Graphite Considerations*, USAEC Report HW-27084, Hanford Works, Mar. 6, 1953.
172. W. T. Elston, Speer Carbon Co., unpublished data, 1959.
173. W. G. O'Driscoll and J. C. Bell, Graphite: Its Properties and Behavior, *Nuclear Eng.*, 3: 479-485 (1958).
174. A. Legendre et al., General Study on Nuclear Graphites Produced in France, in *Proceedings of the Second United Nations International Conference on the Peaceful Uses of Atomic Energy, Geneva, 1958*, Vol. 4, pp. 243-256, Geneva, 1959.
175. L. H. Juel, Great Lakes Carbon Corp., personal communication, 1959.
176. A. W. Smith and J. D. McClelland, *Electronic Properties of a Graphitized Lamp-black and Their Dependence on Neutron Irradiation*, USAEC Report NAA-SR-248, North American Aviation, Inc., June 2, 1953.
177. N. S. Rasor and A. W. Smith, *Low Temperature Thermal and Electrical Conductivities of Normal and Neutron Irradiated Graphite*, USAEC Report NAA-SR-862, North American Aviation, Inc., June 1, 1954.
178. R. N. Smith et al., Carbon-Oxygen and Carbon-Hydrogen Surface Complexes, *J. Phys. Chem.*, 60: 495-497 (1956).
179. S. B. Austerman, *Stored Energy Release in Graphite Irradiated at Low Temperatures*, USAEC Report NAA-SR-1564, North American Aviation, Inc., Oct. 1, 1956.
180. E. M. Woodruff, Hanford Laboratories, General Electric Company, personal communication, August 1961.
181. C. L. Mantell, *Industrial Carbon*, 2nd ed., p. 64. D. Van Nostrand Co., Inc., New York, 1946.

Theory of Radiation Effects in Graphite

D. R. DE HALAS†

7-1 Interaction of Radiation with a Solid

7-1.1 BASIC EFFECTS OF RADIATION ON A SOLID

Radiation induces permanent effects in solids either by displacing atoms or by exciting electrons into higher metastable energy levels. In some types of solids, particularly fissile materials, impurity atoms may be introduced by nuclear transmutations.

In metals conduction electrons are mobile and cannot be permanently displaced; all stable damage is the result of displaced atoms. Because graphite contains a significant number of free conduction electrons, the radiation effects produced in graphite are in many respects similar to those produced in metal. Thus this chapter is concerned mainly with the displacement of atoms. Displaced atoms can, of course, modify the electronic energy levels and thereby affect the electrical properties of a metal or graphite.

Although some nuclear transmutations will occur in graphite, the number of capture events is small compared to the total number of permanently displaced atoms; consequently neutron capture is of little significance in the radiation damage of graphite.

7-1.2 TRANSFER OF ENERGY TO A SOLID

During the radiation bombardment of a solid, the incident particle transfers its energy either by exciting the electrons in the solid or by colliding with its atoms. Because electron excitation can occur only when the incident particle is charged, the primary interaction in the case of neutron bombardment is always a collision. In a sufficiently energetic collision, the struck atom will be displaced and can in turn act as an energetic bombarding particle. This moving displaced atom is called the "primary knock-on atom." If it displaces other atoms, these atoms are called "secondary knock-on atoms," etc. The primary knock-on atom will generally be ionized and may therefore lose a significant portion of its energy by electron excitation. The phenomena associated with the passage of the primary knock-on atom through graphite are discussed in detail in Sec. 7-2.

In nonmetallic solids electron excitation can result in the breaking of

† Hanford Laboratories, General Electric Company, Richland, Wash.

chemical bonds and cause permanent rearrangement of atoms. Thus in organic materials all energy-transfer processes are likely to cause displaced atoms, and the amount of permanent damage is closely proportional to the total amount of energy absorbed in the solid. On the other hand, the amount of radiation damage in graphite is not proportional to the total energy absorption. Because of the weak interaction between unbonded electrons and the lattice atoms in graphite, the portion of energy expended by charged knock-on atoms in exciting electrons is rapidly dissipated through a relatively large volume of material and does not result in displacement of atoms. The fraction of energy lost by these ionization processes increases as the energy of the bombarding particle increases.

7-1.3 DISPLACEMENT ENERGY

The energy required to move an atom from its lattice position is called the "displacement energy" (E_d).[†] For most metallic solids E_d is about 25 ev. In Fig. 7.1 it can be seen that there is no change in the electrical

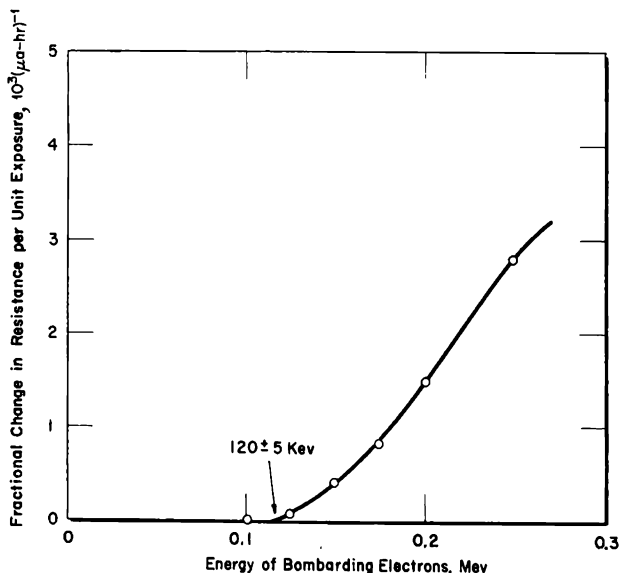


FIG. 7.1 Rate of fractional change in resistance of 0.0045-in.-thick graphite bombarded with electrons of various energies from a Van de Graaff generator.¹ No change in electrical resistivity is observed when the energy of the bombarding electrons is less than 120 kev.

resistivity of graphite bombarded with electrons until a rather sharp threshold is reached at about 120 kev electron energy.¹ Below this energy the electrons do not possess sufficient energy to displace carbon atoms. From

[†] A glossary of symbols used in Chap. 7 will be found at the end of the chapter (Sec. 7-7).

these data it can be calculated (see Eq. 7.2) that a minimum of 24.7 ± 0.09 ev is required to displace a carbon atom from the graphite lattice. The approximation of using 25 ev for E_d in solids is thus a good one for graphite.

In any crystalline material E_d probably varies with the direction of recoil. However, the exact value of E_d has only a minor influence on the radiation effects discussed in the following paragraphs, and the isotropic value of 25 ev will be used for subsequent discussions.

7-1.4 THRESHOLD ENERGY

For elastic collisions of particles, the expression giving the maximum energy (T_m) transferred (i.e., for the case of a head-on collision) from a moving particle of mass M_1 and energy E to a stationary atom of mass M_2 is

$$T_m = \frac{4M_1M_2}{(M_1 + M_2)^2} E \quad (7.1)$$

In the case of a knock-on atom of energy E' traveling through graphite, $M_1 = M_2$; consequently $T_m = E'$.

For bombardment with electrons of mass m_e , relativistic effects are usually important, and T_m is given by

$$T_m = \frac{2E(E + 2m_e c^2)}{M_2 c^2} \quad (7.2)$$

For gamma rays, which cannot cause atomic displacements directly, the important energy is that of the Compton or photoelectrons which result from the gamma ray-electron interactions, and therefore the threshold is the same as for electrons.

Using a value of 25 ev for the displacement energy, the minimum energy that the incident radiation must have to cause displaced atoms can be calculated. Table 7.1 gives the threshold radiation energies for producing displacements in graphite.

Table 7.1 — THRESHOLD ENERGIES FOR DISPLACEMENTS IN GRAPHITE

($E_d = 25$ ev)

Incident particle	Threshold energy, ev
Electrons, gamma rays	120,000
Neutrons, protons	88
Fission fragments of atomic mass 100	65
Alpha particles	33

7-1.5 THE PRIMARY DISPLACEMENT PROCESS IN GRAPHITE DURING IRRADIATION BY NEUTRONS

Two factors strongly influence the amount of damage produced in graphite during neutron irradiation: the energy of the primary knock-on

atoms and the number of primary knock-on atoms. The energy of the primary knock-on atom depends on the energy (E_n) of the colliding neutron. A neutron undergoing an elastic collision imparts to the primary knock-on atom energy ranging from 0 to a maximum of T_m , as given by Eq. 7.1. If the neutrons are scattered isotropically, the mean energy transferred (\bar{E}') to a primary knock-on atom is $T_m/2$. Thus, for isotropic neutron scattering by an atom of atomic mass A , $\bar{E}' = 4AE_n/(A+1)^2 = 0.142E_n$ in graphite. However, the scattering is isotropic only at low energies, and, in general, the mean energy transfer is related to E_n by a function (α) as indicated below:

$$\bar{E}' = \frac{\alpha}{2} E_n \quad (7.3)$$

Figure 7.2 gives $\alpha/2$ as a function of incident neutron energy as calculated from the angular scattering cross sections^{2,3} for neutrons. Dienes and

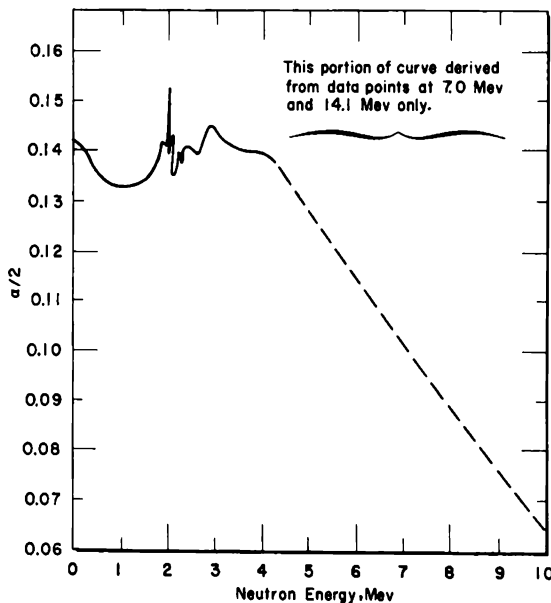


FIG. 7.2 Average fractional energy loss per collision ($\alpha/2$) for a neutron scattered in graphite. Values are calculated from the angular scattering cross section.^{2,3}

Vineyard⁴ have calculated from other data an average value of $\alpha/2 = 0.120$ for the complete fission spectrum, which is slightly lower than the average value of 0.130 calculated from the curve in Fig. 7.2.

The number of primary knock-on atoms is directly related to the number of collisions (N) that a neutron makes in slowing down from its initial energy (E_n^A) to some lower energy (E_n^B). N is given by

$$N = \frac{1}{\xi} \ln \frac{E_n^A}{E_n^B} \quad (7.4)$$

Table 7.2 — TOTAL NUMBER OF PRIMARY DISPLACEMENTS
CREATED IN GRAPHITE DURING THE SLOWING DOWN
OF A NEUTRON FROM ENERGY E_n^A

E_n^A , ev	ν_p , atoms
1×10^7	73
2×10^6	58
1×10^6	55
1×10^5	40
1×10^4	26
1×10^3	11

Corrected for anisotropic scattering.

In graphite $\xi = 0.158$ for isotropic scattering processes. However, ξ , like α , decreases at high neutron energies.† On the average, only neutrons with energies in excess of 175 ev will transfer enough energy to the graphite to cause a displacement. Setting E_n^B equal to 175 ev, the number of primary displacements (ν_p) created by a neutron of energy E_n^A is given by Eq. 7.4 by taking $\nu_p = N$. These results are given in Table 7.2.

In addition to the energy and number of primary knock-on atoms, fac-

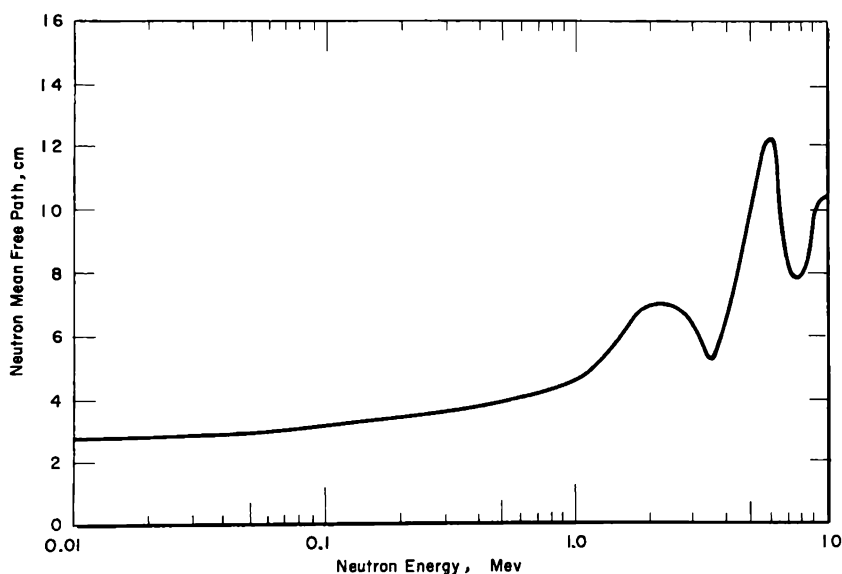


Fig. 7.3 The mean free path of neutrons in graphite of bulk density 1.7 g/cm^3 . On the average a neutron with the specified energy will create one primary knock-on atom for each mean free path length that it traverses through the graphite. Each collision degrades the neutron energy so that the mean free path changes constantly.

† ξ is related to α by the relationship $\xi = 1 + [(1 - \alpha)/\alpha] \ln (1 - \alpha)$.

tors that determine the amount of damage, the distribution of damage in the graphite is of interest. On the average, there is a neutron-carbon atom interaction every time the neutron travels one mean free path. Figure 7.3 gives the mean free path for neutrons in graphite as a function of the neutron energy. The distance between neutron scattering events is of the order of several centimeters. However, all the displaced atoms resulting from collisions of the primary and subsequent knock-on atoms occur within a total range of only a few microns from the position of the neutron-carbon atom interaction (see Sec. 7-2.5). Thus the passage of a neutron through graphite creates relatively widely spaced, discrete clusters of displaced atoms. Each cluster contains several hundred displaced atoms.

7-1.6 FISSION-FRAGMENT DAMAGE TO GRAPHITE

When graphite is mixed intimately with a fissionable material, the damage to the graphite is caused primarily by the dissipation of the kinetic energy of the fission fragments. Of the 200 Mev released during a fission event, about 160 Mev appears as kinetic energy of the fission fragments. Because of their extraordinarily high energy, fission fragments initially have about 20 units of net positive charge, which becomes neutralized as the fragment slows down.⁴ A large part of the energy of the fragment will therefore be dissipated by electronic excitation.

The fate of the primary and subsequent knock-on atoms produced by the fission fragment is the same as if these atoms had resulted from neutron bombardment. Thus, with the main exception of the number and the energy of the primary knock-on atoms, the considerations developed in subsequent sections concerning neutron damage to graphite can also be applied to fission-fragment damage.

7-2 Displacement of Atoms in Graphite by Knock-on Atoms

During the bombardment of graphite by energetic radiation, the primary displaced atom, that is, the atom displaced directly by interaction with the bombarding particle, will generally carry sufficient energy that it, in turn, will displace many more carbon atoms before coming to rest. A single primary knock-on atom created by the collision of a 2-Mev fission neutron can cause about 1500 further displacements before stopping. The study of radiation damage to graphite, especially that resulting from reactor neutron bombardment, is thus largely concerned with the phenomena associated with the slowing down of the primary knock-on atom.

7-2.1 COLLISIONS BETWEEN KNOCK-ON AND STATIONARY LATTICE ATOMS

Knock-on atoms undergo both elastic and inelastic collisions. In an elastic collision the moving atom interacts with a lattice atom transferring a fraction of its energy, up to 100 per cent, to the target atom. In an inelastic collision some energy is lost through electron excitation. In these

latter interactions the lattice electrons are excited by the Coulomb force between nuclear and electronic charges and are left in an excited state after the passage of the knock-on atom. Electron excitation is most important when the knock-on atom has several tens of thousand electron volts of energy (see Sec. 7-2.4).

In elastic collisions it is sufficient to consider that the electrons are not excited but only serve to partially screen the nuclear charges during a collision. There are two types of elastic collisions that can be considered in detail. When the moving atom has a high energy, it can more closely approach the lattice atom; thus the effect of electron screening is diminished. In this case the interaction between the Coulomb fields of the nuclei of the moving and of the stationary atom is dominant, and the collision is then termed a "Rutherford scattering event." The second type of elastic collision becomes important as the moving atom loses energy. Electron screening then becomes significant, and below a certain energy the scattering will correspond to that between rigid spheres since the electron fields are repulsive.

It is convenient and reasonably accurate for many purposes⁵ to assume that the screened Coulomb interaction potential has the form

$$\frac{q_1 q_2}{r} e^{-r/a} \quad (7.5)$$

where q_1 and q_2 are the charges on the incident and on the stationary nuclei, respectively, r is the separation of the two charges, and a is a screening constant for the pair. For calculations in subsequent sections, the screening constant (a) for a knock-on atom in a monatomic substance will be taken as related to the Bohr radius of the hydrogen atom (a_H) by the relation⁵

$$a = \frac{a_H}{\sqrt{2Z^{1/3}}} \quad (7.6)$$

For carbon, $a = 2.06 \times 10^{-9}$ cm.

If the classical distance of closest approach of the nuclei (b) is much less than a but much larger than the de Broglie wave length (λ) of the incident particle, then classical Rutherford scattering is valid down to angles θ as small as

$$\theta'_a \simeq \frac{b}{a} \quad (7.7)$$

The classical Rutherford scattering equations are therefore valid when

$$a \gg b \quad (7.8)$$

and when

$$b \gg \frac{\lambda}{2\pi} \quad (7.9)$$

For knock-on atoms of energy E' and mass M ,

$$\frac{2\pi b}{\lambda} = \frac{Z^2}{137} \left(\frac{2Mc^2}{E'} \right)^{1/2} \quad (7.10)$$

In graphite the condition expressed in Eq. 7.9 is satisfied even for knock-on atoms created by the most energetic fission neutrons.

The condition expressed by Eq. 7.8 is satisfied only at high knock-on atom energies. For knock-on atoms, b/a is given by the relation⁵

$$\frac{b}{a} = 4Z^2 \left(\frac{R_H}{E'} \right) \left(\frac{a_H}{a} \right) \quad (7.11)$$

Using the value of 13.6 ev for the Rydberg constant (R_H), this reduces to $b/a = 5050/E'(\text{ev})$ in graphite. It will be assumed that the condition in Eq. 7.8 is satisfied whenever b/a is less than 0.2 (equivalent to setting the exponential term in Eq. 7.5 to greater than 0.8). Elastic collisions can then be considered as Rutherford scattering events (i.e., collisions involving mutual repulsion between Coulomb barriers of the nuclei) when the energy of the moving carbon atom is greater than about 25,000 ev.

In the opposite case of strong screening, i.e., hard-sphere collisions, for which

$$b \gg a \quad (7.12)$$

classical mechanics is valid for a large range of scattering angles only if

$$a \gg \frac{\lambda}{2\pi} \quad (7.13)$$

In graphite this latter condition is satisfied for all energies of interest as far as radiation damage is concerned. The condition expressed in Eq. 7.12 will be assumed to be satisfied when b/a is greater than 4.6 (equivalent to assuming that the exponential term in Eq. 7.5 is less than 0.01). In this case hard-sphere scattering calculations are valid below a knock-on atom energy of about 1000 ev. Thus a broad and important energy region is left for which $1000 \text{ ev} < E' < 25,000 \text{ ev}$, where the mathematical treatments for both the hard-sphere and the Rutherford scattering are inexact. However, for simplicity in subsequent calculations, the point for which $b = a$, i.e., at $E' \simeq 5000 \text{ ev}$, will be considered as a sharp transition point between Rutherford and hard-sphere scattering.

7-2.2 HARD-SPHERE COLLISIONS

The energy transferred (E'') from a primary knock-on atom of energy E' in an elastic collision with a lattice atom, where the atoms are deflected through an angle θ in the center-of-gravity coordinate system, is given by

$$E'' = T'_m \sin^2 \frac{\theta}{2} \quad (7.14)$$

For a collision between like atoms, $T'_m = E'$ (see Eq. 7.1). An essential feature of hard-sphere collisions is that the scattering is spherically symmetric; thus all values of E'' between 0 and E' are equally probable. The average energy transferred in a hard-sphere collision between like atoms is therefore one-half that of the bombarding atom.

In a substance containing n_0 atoms per cubic centimeter,† the mean free path (L_s) for a knock-on atom of radius R undergoing hard-sphere collisions is given by

$$L_s = \frac{1}{\pi R^2 n_0} \quad (b \gg a) \quad (7.15)$$

However, in a highly anisotropic material such as graphite, a moving atom encounters significantly different densities of atoms depending on the crystallographic direction in which it is traveling. Thus, although the average mean free path is given by Eq. 7.15, the actual probability of a collision, and hence the distribution of displaced atoms, depends on the direction of travel of the moving atom. To investigate the relative importance of the anisotropy, an effective n_0 can be defined as

$$n_0 = \langle n \rangle^{3/2} \quad (7.16)$$

where $\langle n \rangle$ is the average number of atoms per square centimeter in the crystal plane under consideration. For an atom traveling perpendicularly to the c axis and in the (0 0 2) plane (see Fig. 5.2), $\langle n \rangle = 3.8 \times 10^{15}$ atoms/cm². In the (1 0 0) plane $\langle n \rangle = 1.2 \times 10^{15}$ atoms/cm². A fast-moving particle undergoing hard-sphere collisions behaves as if its radius (R) were less than the normal atomic radius. If the value of E'' is large compared with E_d and the interaction potential is of the form given by Eqs. 7.5 and 7.6, the radius associated with hard-sphere collisions is given approximately by⁵

$$R = \frac{a_H}{\sqrt{2}Z^{1/3}} \ln \left(\frac{Z^2 e^2}{R E''} \right) \quad (7.17)$$

When E'' decreases, R increases slowly toward the value of the atomic radius (0.7 Å for carbon). The value of R calculated by Eq. 7.17 and extrapolated down to E_d is given in Fig. 7.4 for a knock-on atom traveling through graphite. Because of the approximations employed in estimating the interaction potential, this value of R should be regarded as a crude estimate, especially as E'' approaches E_d . Based on the calculated collision radius, the mean free path is given in Table 7.3 for atoms traveling in the particular directions considered above.

The decrease in the mean free path near the end of the range of the knock-on atoms results in a tendency for the damage centers to cluster

† Unless otherwise noted, the value of n_0 used in calculations in this chapter is that corresponding to the crystal density rather than the bulk density of graphite.

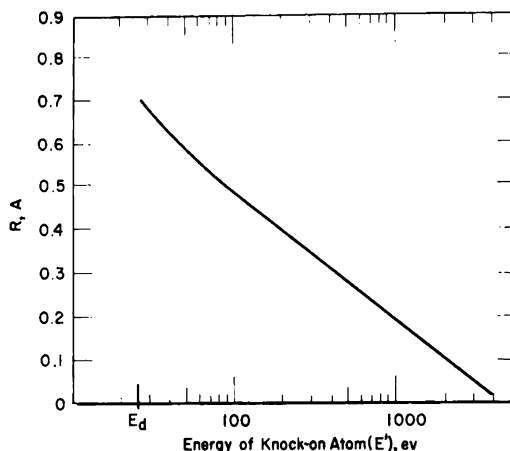


FIG. 7.4 The effective radius (R) associated with hard-sphere collisions for a knock-on atom moving through graphite.

near the tail end of the path of the moving particle. However, because of the relatively loose packing of atoms in the graphite lattice, there is

Table 7.3 — APPROXIMATE MEAN FREE PATH FOR KNOCK-ON ATOMS IN GRAPHITE AT LOW ENERGIES (HARD-SPHERE SCATTERING)

Energy of moving atom, ev	Mean free path, A		
	Travel in a random direction	Travel in the (002) plane	Travel in the (100) plane
4000	390	192	1060
1000	84	43	234
500	39	19	104
100	12	6	32
50	8	4	21

apparently no long region of the path of a knock-on atom where essentially every adjacent lattice atom is hit as the moving particle comes to rest, as is the case in many close-packed materials.

7-2.3 RUTHERFORD COLLISIONS

For close approach of the nuclei ($a \gg b$), the collision between the knock-on and the lattice atom obeys the classical Rutherford scattering laws for cases where the deflection angle is greater than θ'_a (see Eq. 7.7). When the collisions occur at angles smaller than θ'_a , the screening by the electron cloud becomes important. A comparison of Eqs. 7.14, 7.11, and 7.7 shows that the minimum amount of energy that can be transferred in a weakly screened Rutherford collision is given approximately by

$$T_a \simeq \frac{8Z^{1/3}R_H^2}{E'} \quad (7.18a)$$

For knock-on atoms in graphite, Eq. 7.18a reduces to

$$T_a \text{ (ev)} = \frac{6.4 \times 10^6}{E' \text{ (ev)}} \quad (7.18b)$$

Collisions involving transfer of less energy cannot be treated by classical Rutherford scattering formulas.

The differential scattering cross section for a collision in the Rutherford range is inversely proportional to the square of the amount of energy transferred. There is therefore a higher probability for low-energy scattering events. The average energy (\bar{T}_a) transferred in a Rutherford collision is

$$\bar{T}_a = T_a \ln \frac{T_m}{T_a} \quad (T_m \gg T_a) \quad (7.19)$$

and the total cross section (σ_a) for all collisions that lie in the Rutherford range is⁵

$$\sigma_a = \frac{\pi b^2}{4} \frac{T_m}{T_a} = \pi a^2 \quad (7.20a)$$

For carbon-atom collisions in graphite

$$\sigma_a = 1.33 \times 10^{-17} \text{ cm}^2 \quad (7.20b)$$

In cases where E_d lies between T_a and T_m , the displacement cross section (σ_d) for the limited class of collisions which transfer sufficient energy to create a displacement is given by⁵

$$\sigma_d = \frac{\pi b^2}{4} \frac{T_m}{E_d} = \frac{4\pi a_H^2 Z^4 R_H^2}{E' E_d} \quad (E_d > T_a) \quad (7.21a)$$

In graphite this reduces to

$$\sigma_d \text{ (cm}^2\text{)} = \frac{3.38 \times 10^{-12}}{E' \text{ (ev)}} \quad (E_d > T_a) \quad (7.21b)$$

The mean energy transferred in a displacement collision is

$$\bar{T}_d = E_d \ln \frac{T_m}{E_d} \quad \begin{matrix} (T_m \gg E_d) \\ (E_d > T_a) \end{matrix} \quad (7.22)$$

Equation 7.18 expressing the minimum energy (T_a) was derived by assuming that the Rutherford interaction between the incident atom and the lattice atom terminates abruptly at distances larger than the screening distance (a). Actually, the interaction decreases smoothly in accordance with Eq. 7.5. Equation 7.18b shows that in graphite $T_a > E_d$ in those cases where $E' \lesssim 255,000$ ev. Thus, if T_a is considered as a sharp cutoff energy, certain collisions occurring at angles less than θ'_a which may cause displacements will be neglected. However, collisions transferring less energy than T_a can be accounted for by considering them strongly screened (hard-sphere) events. In this case the differential scattering cross section for

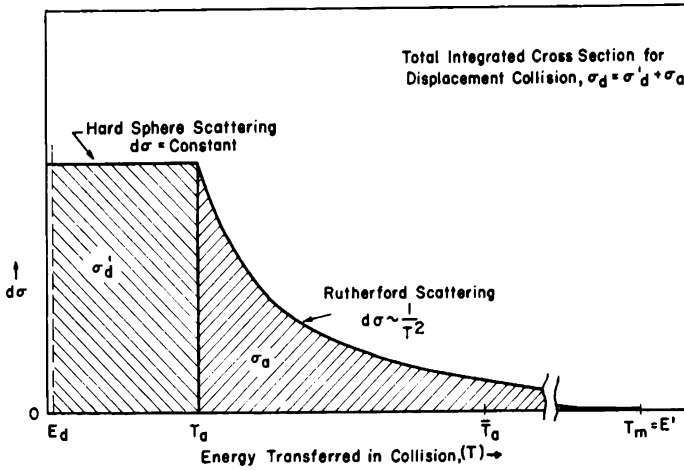


FIG. 7.5 Differential cross section for Rutherford scattering and low-angle hard-sphere scattering for $T_a > E_d$. It is assumed that T_a is a sharply defined energy and that interactions transferring more than this energy are Rutherford events, and those transferring less energy are hard-sphere events.

collisions transferring energy between E and $E + dE$ will behave approximately as indicated in Fig. 7.5. On the basis of this figure, the total cross section for displacement is given by

$$\sigma_d = \sigma_a + \sigma'_d = \sigma_a \left(\frac{2T_a - E_d}{T_a} \right) \quad (T_a > E_d) \quad (7.23)$$

The average energy transferred under the same set of conditions is

$$T_d = \frac{(\bar{T}_m/2)(T_a^2 - E_d^2) + \bar{T}_a T_a (T_m - T_a)}{2T_a T_m - T_a^2 - E_d T_m} \quad (T_a > E_d) \quad (7.24)$$

Although the low-angle scattering events, i.e., those collisions involving transfer of less energy than T_a , may significantly increase the number of secondary knock-on atoms created by a primary knock-on atom, these additional secondary atoms carry relatively little energy, with the result that the total number of displaced atoms (secondaries plus tertiaries, etc.) created by the primary knock-on atom is not appreciably increased (Sec. 7-2.10). If low-angle scattering is neglected, Eqs. 7.19 and 7.20 suffice to describe the collision when $T_a > E_d$.

For a high-energy (i.e., when $a \gg b$) knock-on atom traveling through graphite in a random direction, the mean free path between collisions that can cause displacements (L_d) is

$$L_d = \frac{1}{n_0 \sigma_d} \quad (7.25a)$$

From the cross sections in Eqs. 7.21 and 7.23,

$$L_d \text{ (cm)} = 2.6 \times 10^{-12} E' \text{ (ev)} \quad \begin{matrix} (a \gg b) \\ (E' > 255,000 \text{ ev}) \end{matrix} \quad (7.25b)$$

$$L_d \text{ (cm)} = \frac{4.2}{1.3 \times 10^7 - 25E' \text{ (ev)}} \quad \begin{matrix} (a \gg b) \\ (E' < 255,000 \text{ ev}) \end{matrix} \quad (7.25c)$$

If low-angle scattering is neglected, i.e., using the cross section in Eq. 7.20 for σ_d ,

$$L_d = 6.6 \times 10^{-7} \text{ cm} \quad \begin{matrix} (a \gg b) \\ (E' < 255,000 \text{ ev}) \end{matrix} \quad (7.25d)$$

7-2.4 ELECTRON EXCITATION

In general, inelastic collisions are much more frequent when the moving atom possesses high energy. The transition from inelastic to elastic behavior is not abrupt but can be fairly well fixed by the following argument.⁴ If a charged, moving atom (ion) has a velocity much less than that of the electron in the target, that electron will usually be left without excitation. If the moving ion has a velocity equal to, or greater than, that of the electron, electronic excitation becomes probable. A limiting energy (E_i) for excitation can be defined such that when the moving atom has an energy (E') less than E_i it will not lose energy to any appreciable extent by excitation, and also such that when E' is much greater than E_i the excitation losses will exceed those due to elastic collisions by a large factor.

Kinchin and Pease⁶ suggest that in materials where excitation of conduction electrons is important, E_i is related to the Fermi energy of the free electrons in the lattice (ϵ_F) by

$$E_i = \frac{1}{16} \left(\frac{M_1}{m_e} \right) \epsilon_F \quad (7.26)$$

where M_1 is the mass of the moving atom and m_e is the mass of an electron. The data of Watanabe⁷ indicate that there are two values of ϵ_F in graphite that should be considered: 1.6 ev, corresponding to the resonance energy between neighbors within the layer planes, and 0.33 ev, corresponding to the resonance energy between neighbors in adjacent layer planes. These numbers, when used in Eq. 7.26, give values for E_i of 2200 ev and 450 ev, respectively. However, the significance of these values is uncertain since there is a total of only about 10^{-4} charge carriers per carbon atom (Sec. 6-4.6). Thus the amount of energy that can be directly transferred to mobile carriers is not large (see below).

Inelastic-collision processes are still important because of excitation of bound lattice electrons. Since E_i is a complex function of the electronic energy levels for both conduction and bonding electrons, it is simpler to

consider the energy at which the moving knock-on atom regains its charge and becomes a neutral particle incapable of causing electron excitation. Based on the suggestion of Seitz⁸ that in insulators

$$E_i = \frac{1}{8} \left(\frac{M_1}{m_e} \right) I \quad (7.27)$$

where I is the lowest electronic excitation energy level, it has been assumed that the moving carbon atom regains its lost electron at the energy given by Eq. 7.27. The first ionization potential of carbon is about 11 ev, which gives a corresponding value of 30,000 ev for E_i . However, the moving carbon atom is probably not in its ground state, and the correct value of I for use in Eq. 7.27 should then be less than 11 ev. The highest bound excited state in carbon is about 2 ev below ionization. For the case of an excited atom, E_i equals about 5500 ev. The above considerations were used as guide lines in approximating the manner in which the average charge on the moving ion changes with its energy (Fig. 7.6). This figure serves to

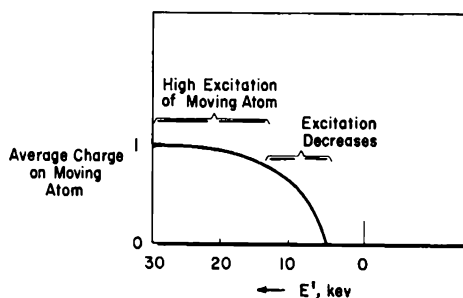


Fig. 7.6 An approximation to the average charge on a knock-on atom of energy E' .

emphasize that E_i is not actually a sharp cutoff energy but that the inelastic collision process tapers off over a range of energies. In general agreement with Fig. 7.6, an E_i value of from 10,000 to 30,000 ev has been used by several authors.^{4, 9-11} A value of 15,000 ev will be used in subsequent discussions.

The basic equation describing the loss of energy of a moving charge as a result of excitation of the electrons in the medium traversed is⁵

$$-\left(\frac{dE}{dx}\right)_e = 4\pi n_0 \frac{(Z_1)^2 e^4}{m_e V^2} Z'_2 \ln \frac{m_e V^2}{\bar{E}} \quad (7.28a)$$

where V is the velocity of the knock-on atom, Z_1 is the atomic charge on the moving particle, and Z'_2 is the number of electrons on the bound atom which are potentially capable of being excited by the incident particle. \bar{E} is an average of the excitation energies which can be stimulated by the incident particle; \bar{E} is difficult to estimate accurately. Equation 7.28a can be

modified to give the energy dissipated by conduction electrons.⁵ For this case

$$-\left(\frac{dE}{dx}\right)_e = 2\pi n_0 \frac{(Z_1)^2 e^4}{m_e V^2} z \ln \left[\frac{2m_e m E}{M h^2} \left(\frac{8\pi}{3n_0 z} \right)^{2/3} \right] \quad (7.28b)$$

Here z is the number of conduction electrons per atom, m is the effective mass of a conduction electron, and h is Planck's constant. Because of the small value of z , the conduction electrons can only dissipate about 10^{-4} ev/A of energy along the path of the knock-on atom. This rate of energy dissipation is too low to be of any importance.

To circumvent the problem of estimating \bar{E} in Eq. 7.28a, Brown¹² used experimental data for the penetration of carbon atoms in air and the stopping powers given by Livingstone and Bethe¹³ to calculate $(dE/dx)_e$ in graphite. The results of Brown's calculation are in approximate agreement with energy losses calculated by assuming that a knock-on atom of velocity V removes and accelerates to V both a π and a σ bonding electron from each adjacent carbon atom that it passes. The rate of energy loss due to electronic excitation is given in Fig. 7.7

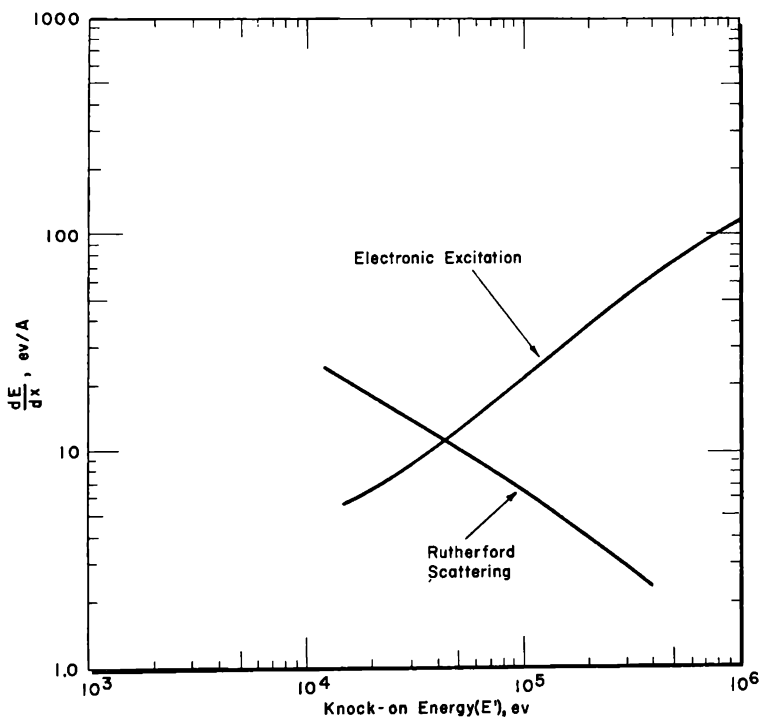


FIG. 7.7 Rate of energy loss of a knock-on atom in graphite due to electron excitation and to Rutherford scattering. The electron excitation losses are those calculated by Brown.¹² The Rutherford scattering losses are calculated from Eqs. 7.24 and 7.25c.

Rutherford scattering losses calculated from Eqs. 7.24 and 7.25c are also plotted in Fig. 7.7. This figure demonstrates the difficulty in choosing a value for E_i . The first condition for E_i , that excitation losses are significantly less than collision losses, is roughly satisfied at 15,000 ev. However, when the primary atom has higher energy, the elastic collisions cannot be neglected until the electron excitation exceeds the energy losses due to collisions by several orders of magnitude. Although the second condition for E_i , that collisional losses are unimportant when $E' \gg E_i$, is rather loosely defined, it is probably not satisfied at $E_i = 15,000$ ev. For comparative purposes an additional value of E_i , 75,000 ev, which more closely fits the second criterion, will also be used in subsequent calculations.

7-2.5 RANGE OF DISPLACED ATOMS

The model presented in the previous sections for the slowing down of a knock-on atom can be used to calculate the range that a moving atom will travel through the lattice. The rate of energy loss from scattering events can be derived from the mean free paths and average energy losses per collision. From the electron excitation losses from Fig. 7.7 and the scattering formulas given by Eqs. 7.22 and 7.23, the residual range (distance that the atom travels before stopping) has been calculated. This residual range is presented as a function of the energy of the atom in Fig. 7.8.

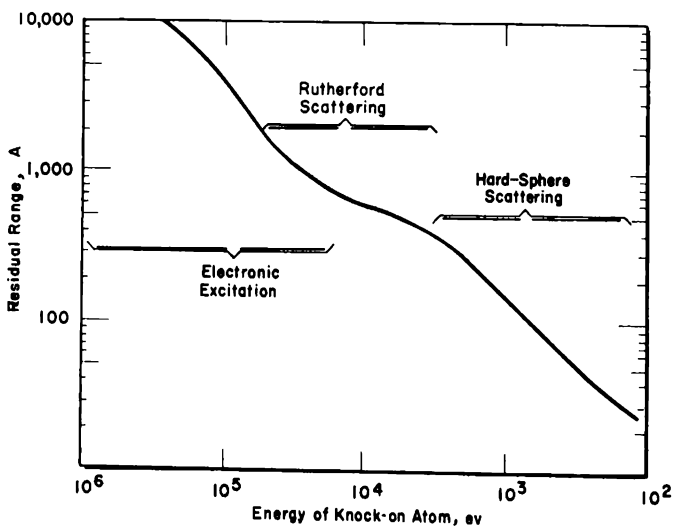


FIG. 7.8 The residual range of a knock-on atom in graphite as a function of the energy of the atom. The principal causes of energy loss in each energy range are indicated.

Even the most energetic knock-on atoms (a primary knock-on created by a 10-Mev neutron will have an average energy of 650 kev) have ranges

very short compared to the distances between primary displacement events (see Fig. 7.3).

7-2.6 ELECTRON SPIKES

The lattice electrons that are excited by the passage of a rapidly moving ionized knock-on atom are heated to very high equivalent kinetic temperatures. The energy of the electrons, in turn, is transferred back to the lattice atoms, and this results in localized heating of the lattice along the path of the moving atom. This localized heating of the electrons is referred to as an "electron spike." An electron spike differs from a thermal spike (to be discussed in Sec. 7-2.7) by the fact that the latter is considered to involve only the direct transfer of energy by collisions from the moving to the stationary atoms.

If the electrons are excited in a cylindrical volume about the path of the knock-on atom and are accelerated to the same velocity as the knock-on atom of energy E' and mass M_1 , then the initial electron temperature (T_e^*) is given by

$$T_e^* = \frac{m_e E'}{M_1 C_e} \quad (7.29)$$

where C_e is the electronic heat capacity per electron. Since the electrons are probably excited to the extent that they behave more like free electrons than conduction electrons, C_e is on the order of $3/2 k$ or 1.3×10^{-4} ev/°K. Thus an energetic knock-on atom of 300,000 ev will produce in its wake electron temperatures of about 100,000°K.

The lattice temperature (T_L) at time t after the formation of the spike of initial radius r_s is given approximately⁵ by the expression

$$T_L = \mu T_e^* \frac{r_s^2}{4D_e \tau} e^{-t/\tau} \ln \frac{4D_e t}{r_s^2} \quad (7.30)$$

where μ is the ratio of the electronic to lattice specific heats, D_e is the diffusion coefficient for electrons in the lattice, and τ is the relaxation time of electrons in the lattice. Using the assumptions of Seitz and Koehler,⁵ D_e in graphite is estimated to be 5.5×10^{-3} (°K)^{1/2} cm²/sec. Again following the assumptions of the same authors, τ is given approximately by 1.7×10^{-5} (°K)^{-3/2} sec. Taking the same value for the electronic heat capacity as used previously and a lattice heat capacity of 0.4 cal/g/°C (the mean value between 0.15 cal/g/°C at room temperature¹⁴ and 0.5 cal/g/°C, $3R$ per mole, at very high temperature), μ has the value of 0.6. Since it is unlikely that electrons more than one lattice unit away from the path of the moving atom will be initially excited, r_s is taken as one-half the average distance between atoms in the lattice, or roughly 1.5 Å. From Eq. 7.30 it is found that the lattice is only heated about 25°K by the electrons in a 100,000°K

spike. The electron spikes thus do not play any role in radiation damage or radiation annealing (Sec. 13-4) of graphite.

7-2.7 THERMAL SPIKES

The collision energy that is transferred to the lattice atoms and is not used in creating displacements initiates lattice vibrations and creates small high-temperatures zones near the point of collision. Each such point source of excitation gives rise to a thermal spike. Near the end of the path of a moving atom the mean free path for collision may become small enough that the spikes overlap and essentially the entire energy of the moving atom is dissipated in a very small region. Brinkman¹⁵ designates this terminal region as a displacement spike.

If Q is the amount of energy contained in a spherical spike when the temperature is T_L , the radius (r_i) can be calculated from

$$\frac{4\pi r_i^3}{3} n_0 = \frac{Q}{C_L T_L} \quad (7.31)$$

where C_L is the lattice specific heat per atom.

A 10-ev thermal spike will heat a spherical region with a radius of about 6 Å to 1000°K for a time that is long compared to the lattice vibrational period. Since it is likely that many interstitial-vacancy pairs are formed with initial separations less than this and since 10 ev is not a particularly high-energy spike, some of these pairs may be thermally reintegrated (annealed) immediately after formation. Thus, even for irradiations conducted at absolute zero, some of the displacements may be annealed so that the permanent damage would be less than that expected on the basis of the number of displacements which have occurred. On the other hand, this phenomenon would be practically independent of the actual lattice temperature and could not be solely responsible for the experimentally observed temperature-dependent radiation annealing process (see Sec. 13-4).

7-2.8 QUALITATIVE DESCRIPTION OF DISPLACEMENT PROCESSES

The preceding sections, although giving a mathematical description of the motion of a moving atom in a graphite lattice, are fraught with assumptions of various degrees of uncertainty. It is instructive to make these types of calculations, however, as they undoubtedly provide some insight into the displacement process. Furthermore, it is desirable to acquire an understanding of the type of assumptions that must be made in the calculations involving displacement processes.

Figure 7.9 summarizes in graphical form the conclusions of the preceding paragraphs. With this perspective, the preceding calculations will now be used to calculate the number of atoms displaced by neutron bombardment.

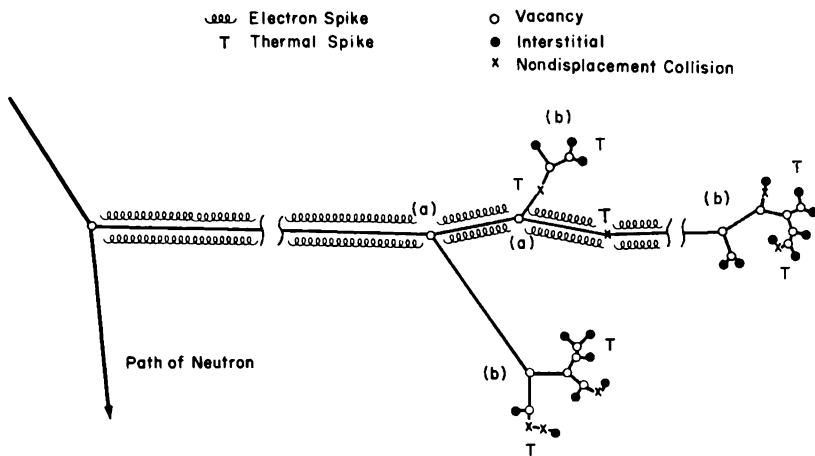


FIG. 7.9 Displacement processes in graphite. Over the initial path of the primary knock-on atom, electron excitation is responsible for the major dissipation of energy. In this region there are infrequent Rutherford collisions (a). The secondary atoms from these collisions undergo mostly hard-sphere collisions (b). Near the end of the path of the primary atom, hard-sphere collisions become increasingly frequent. The regions where atoms are struck without causing displacement and the final resting places of the displaced atoms are associated with thermal spikes.

7-2.9 AVERAGE NUMBER OF DISPLACEMENTS PRODUCED BY COLLISIONS

Consider the case where a knock-on atom transfers energy to the lattice only by elastic collisions. In the first collision the energy is shared by two atoms; in the second-collision generation the energy is shared by four atoms, etc. However, the struck atoms cannot be displaced unless they receive the minimum amount of energy E_d . From this general picture two models giving similar results are frequently used to calculate the mean number of displaced atoms. The first model, due to Kinchin and Pease,^{4,6} assumes:

1. An atom is invariably displaced from its lattice site if it receives kinetic energy greater than E_d and will never be displaced if it receives less than E_d .
2. The striking atom remains behind at the collision site if it is left with energy less than E_d . Thus there will be a net increase in the number of displaced atoms only if both atoms have kinetic energies greater than E_d after the collision.

The second model, developed by Seitz⁵ and others, differs in that it assumes the struck atom loses energy equal to E_d before moving off through the lattice to make other displacements. Also, this model does not allow for the possibility that the incoming atom will be captured on the lattice site from which the knock-on was displaced. Thus the models differ in two respects which tend to compensate each other:⁴ i.e., introducing a binding

energy reduces the net number of displacements; ignoring the capture process increases the number.

If only elastic collisions are considered, the result of the Kinchin and Pease calculation⁶ is that the total number of atoms displaced [$\nu(E')$] by a knock-on atom of energy E' , and including the knock-on atom itself, is given by

$$\nu(E') = \frac{E'}{2E_d} \quad (E' > 2E_d) \quad (7.32)$$

Seitz's model gives a result approximated by the formula

$$\nu(E') = 0.561 \left(1 + \frac{E'}{E_d} \right) \quad (E' > 4E_d) \quad (7.33)$$

Above an energy of a few E_d , Eqs. 7.32 and 7.33 predict approximately the same number for $\nu(E')$. For simplicity Eq. 7.32 will be used in subsequent calculations.

In the case of a Rutherford collision that transfers mean energy \bar{T}_d , it can usually be assumed that the secondary atom has only sufficient energy to undergo hard-sphere collisions. Thus the average number of atoms displaced in a Rutherford collision [$\nu_R(E')$] by a primary atom of energy E' , but *not* including the primary, is given by

$$\nu_R(E') = \frac{\bar{T}_d(E')}{2E_d} \quad (7.34)$$

The mean energy of a secondary atom [$\bar{T}_d(E')$] should be taken from the appropriate equation: Eqs. 7.19 (if low-angle scattering is neglected), 7.22, or 7.24.

7-2.10 TOTAL NUMBER OF DISPLACEMENTS PRODUCED BY A PRIMARY KNOCK-ON ATOM

The complete models of Kinchin and Pease⁶ and Seitz⁸ for calculating the number of displacements due to the primary knock-on atom of energy E' have included the following assumptions:

1. The knock-on atom loses energy entirely by ionization above the limiting energy E_i (see Sec. 7-2.4).
2. All knock-on atoms with kinetic energy less than E_i lose energy entirely by elastic collisions, and in these collisions they behave as hard spheres.

Kinchin and Pease thus give the number of displaced atoms as being equal to $E_i/2E_d$ if $E' > E_i$ and, in accordance with Eq. 7.32, equal to $E'/2E_d$ if $E' < E_i$. Seitz's calculation is similar except that the mean number of displacements produced when $E' < E_i$ is given by Eq. 7.33. Some early calculations of radiation damage to graphite have employed variations of Eq. 7.33; thus, several results have been obtained¹⁰ for the number of

displacements in graphite as calculated by Seitz's method. Recent values calculated by this method are essentially the same as those given by Kinchin and Pease.

Brown¹² has calculated the number of displacements in graphite by considering, in addition to the hard-sphere collisions occurring below E_i , those elastic collisions which occur while the primary knock-on atom has high energy and the principal cause of energy loss is electron excitation. Following Brown's general approach the calculations in the preceding paragraphs can be used to derive the number of displacements caused by a primary knock-on atom in the following manner:

1. At high energies it is assumed that electron excitation is primarily responsible for the slowing down of the primary knock-on atom. In this case Fig. 7.7 can be used to determine the distance that the atom travels in losing an increment of energy $\Delta E'$. With the appropriate mean free path for Rutherford displacement collisions given by Eq. 7.25, the number of displacements that occur while the primary atom loses energy $\Delta E'$ can be calculated. Each Rutherford collision that causes a displacement will transfer an amount of energy given either by Eq. 7.22 or by 7.24. (If low-angle scattering is neglected, Eqs. 7.18b and 7.25d can be used rather than Eqs. 7.24 and 7.25c.)
2. In this high-energy region, Eq. 7.34 is used to calculate the total number of displacements caused by the secondary atom.
3. When $(dE/dx)_e$ for electron excitation becomes of the same order as that due to elastic collisions, all energy transfer is assumed to be due to elastic collisions.
4. In this lower energy region, Eq. 7.32 is used to calculate the number of displacements.

The result of the calculation just outlined is compared in Fig. 7.10 to that based on the method of Kinchin and Pease. Consideration of the high-energy Rutherford collisions greatly increases the number of displacements calculated above that given by the Kinchin and Pease treatment with $E_i = 15,000$ ev. In the case of radiation damage to graphite, it therefore seems that Rutherford scattering cannot be neglected. As indicated in Fig. 7.10, the Kinchin and Pease treatment agrees more closely with the detailed Rutherford scattering treatment if a value of 75,000 ev is used for E_i . Justification for this higher value was mentioned in connection with Fig. 7.7.

Comparison of curves C and D in Fig. 7.10 shows that low-angle collisions at high energy do not contribute much to the damage. For simplicity these collisions will be ignored in the subsequent calculations.

7-3 Creation of Displacements in Graphite by Neutrons

If a neutron of energy E_n collides with a lattice atom, a primary knock-on atom is created with an energy between zero and a maximum of T_m , as given by Eq. 7.1. Since the energy of the primary knock-on atom

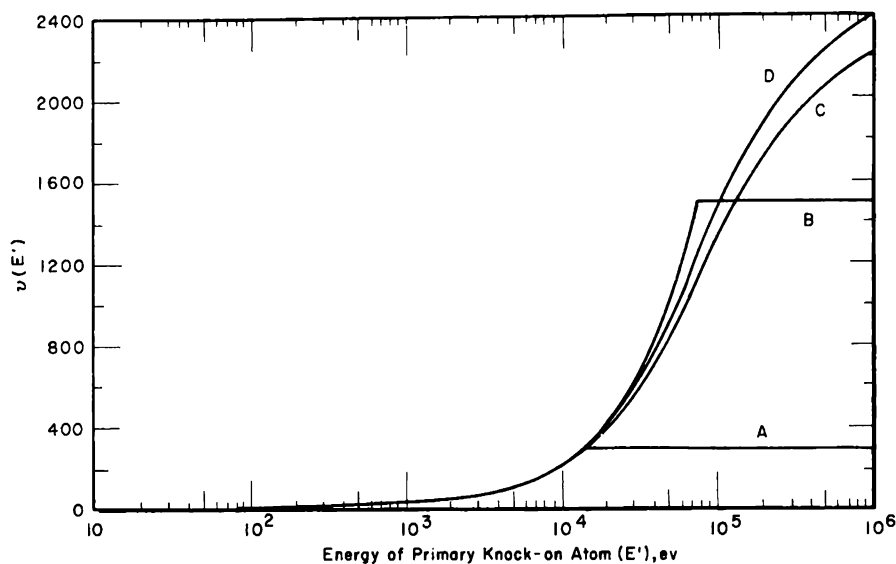


FIG. 7.10 Number of atoms displaced [$\nu(E')$] by a knock-on atom of initial energy E' before it comes to rest. Curve A, model of Kinchin and Pease with $E_i = 15,000$ ev. Curve B, model of Kinchin and Pease with $E_i = 75,000$ ev. Curve C, model including Rutherford collisions. Low-angle hard-sphere scattering at high energies is not considered. Curve D, same model but with the inclusion of low-angle scattering at high energies.

is not uniquely defined by the energy of the neutron, the treatments in Sec. 7-2.10 must be modified so that the average number of displacements caused by a neutron of a given energy can be calculated.

When neutrons are scattered elastically, all energies between zero and T_m are equally probable for the primary atom. If E_i is considered as a sharply defined energy and if $T_m < E_i$, then Eq. 7.32 can be used to calculate the number of displacements by substituting the average energy of the knock-on atom, i.e., $T_m/2$ for E' . When T_m exceeds E_i , then the primaries with the greatest energy will behave, as far as displacement production is concerned, as if they had only energy E_i . The effective average energy will thus be less than $T_m/2$. A consideration of the mathematics involved leads to the following more familiar forms of the Kinchin and Pease expression for calculating the number of displacements [$N(E_n)$] caused by a single collision of a neutron of energy E_n :

$$N(E_n) = \frac{\alpha E_n}{4E_d} \quad (\alpha E_n < E_i) \quad (7.35a)$$

$$N(E_n) = \left(2 - \frac{E_i}{\alpha E_n}\right) \frac{E_i}{4E_d} \quad (\alpha E_n > E_i) \quad (7.35b)$$

Curves C or D in Fig. 7.10 can be treated in an equivalent manner by graphically integrating these more complicated functions between zero and

αE_n . The results of this calculation are compared with those from Eq. 7.35 in Fig. 7.11.

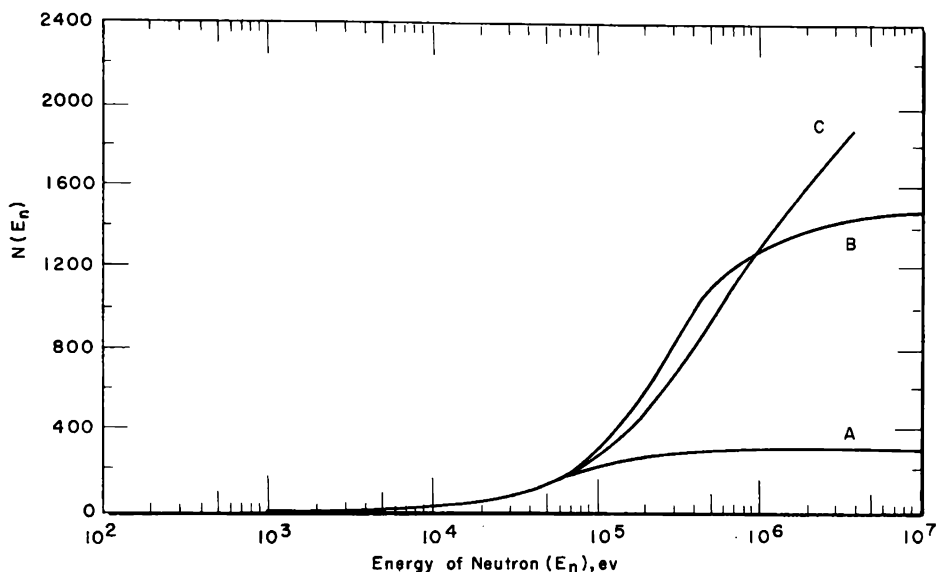


FIG. 7.11 Number of atoms displaced $[N(E_n)]$ by a single collision of a neutron of energy E_n . Curve A, model of Kinchin and Pease with $E_i = 15,000$ ev. Curve B, model of Kinchin and Pease with $E_i = 75,000$ ev. Curve C, model including Rutherford collisions. Low-angle hard-sphere scattering at high energies is not considered.

The calculations leading to Table 7.2 can be combined with the results of Fig. 7.11 to give an estimate of the total number of atomic displacements caused by a neutron with initial energy E_n^A during its lifetime in a graphite moderator. Curve A is disregarded since it is not believed to present as accurate a description of the displacement process as curves B or C. The results of this calculation are presented in Table 7.4.

Table 7.4 — TOTAL NUMBER OF DISPLACEMENTS PRODUCED BY A NEUTRON OF INITIAL ENERGY E_n^A DURING THERMALIZATION IN GRAPHITE

E_n^A , Mev	Total number of displacements based on Fig. 7.11	
	Curve B model	Curve C model
10	45,000	55,000
2	23,000	21,000
1	19,000	17,000
0.1	2,500	2,500

Based on either of the models considered, a fission neutron with an average energy of 2 Mev will cause approximately 22,000 displacements in the graphite during the time it is being thermalized.

7-4 Atomic Displacement Rates in Graphite in a Nuclear Reactor

The problem of calculating the rate of accumulation of damage in a given volume of graphite in a nuclear reactor involves an additional consideration; the energy distribution of the neutrons in that volume of graphite. Unfortunately, even at the present time and particularly during the time when many of the past experiments with graphite were conducted, knowledge of the neutron spectrum has generally been limited.

It is intuitively apparent and has been brought out in the previous sections that collisions by high-energy neutrons produce more displaced atoms than collisions by neutrons of lower energy. However, in a nuclear reactor the flux of neutrons of the highest energies is relatively low. Therefore most of the displaced atoms in graphite are caused by neutrons of some intermediate energy where the flux is higher. The exact limits of this range of energies are dependent upon the neutron spectrum at the irradiation position.

7-4.1 NEUTRON SPECTRA

All natural-uranium-fueled graphite-moderated reactors are restricted by reactor physics considerations to rather similar geometries. However, even within these reactors the neutron spectrum varies from point to point depending on such factors as distance to the fuel, control-rod positions, fuel-element configuration, and type and amount of coolant. If the fuel is enriched, the over-all design of a graphite-moderated reactor can be modified considerably. Such modifications can cause a significant change in neutron spectrum. The neutron spectrum in small high-flux test reactors may differ greatly from those in larger graphite-moderated reactors.

A general discussion of the components of the spectrum of the neutron flux will be helpful to an understanding of the methods that have been used to calculate atomic displacement rates in graphite. An unperturbed neutron-energy spectrum in a thermal reactor is illustrated in Fig. 7.12. Neutrons are created in fission with energies ranging from about 10 Mev down to about 100 kev. These neutrons constitute the so-called "fission spectrum." The fast neutrons are slowed down by collisions with the moderator in a manner such that the neutron flux per logarithmic energy interval is constant. These neutrons compose the epithermal region† of the spectrum, which is generally considered to extend from 1 Mev to about 0.2 ev. The presence of a strong resonance absorber will cause deviations from the ideal $1/E$ relation. Likewise, the neutron spectra in irradiation facilities located near the reflector, especially in small test reactors, do not follow closely a $1/E$ relation. Below approximately 0.2 ev the neutrons are in

† The differential flux, i.e., the flux per *unit energy* interval is inversely proportional to the energy (E) in the epithermal region. Thus this spectral region is often referred to as the " $1/E$ region."

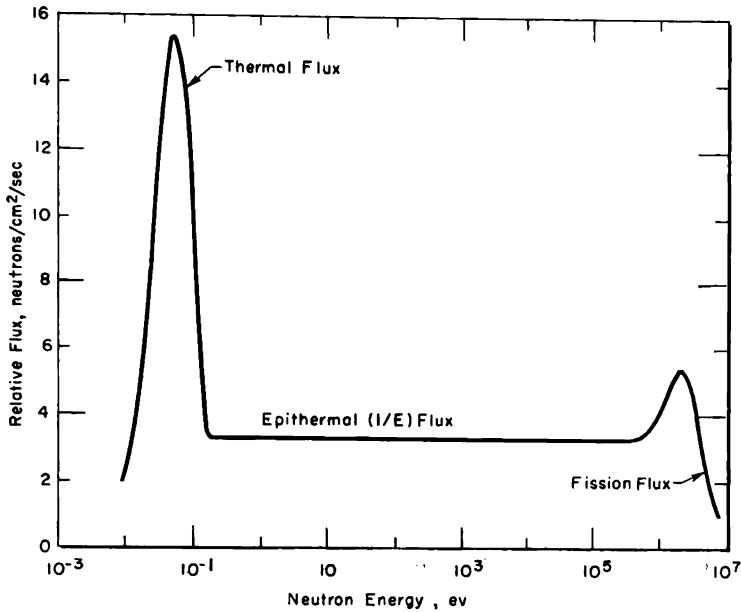


FIG. 7.12 Unperturbed neutron-energy spectrum in a thermal nuclear reactor. The flux per logarithmic energy interval is plotted against the neutron energy.

thermal equilibrium with the moderator, and a Maxwellian energy distribution of the neutrons results. The intensity and shape of the spectrum in these regions, the thermal-neutron, the epithermal-neutron, and the fission-neutron regions, are highly dependent upon the reactor geometry.

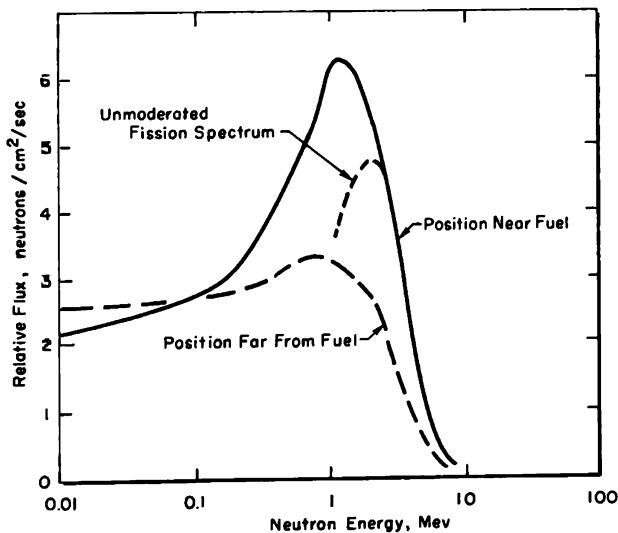


FIG. 7.13 The high-energy neutron spectrum at positions near and far from the fuel in a nuclear reactor. The two spectra, both of which have undergone some moderation, are compared with an unmoderated fission spectrum.

Figure 7.13 illustrates the high-energy regions of two different neutron spectra. In the absence of a moderator, the spectrum would have the shape indicated. Near the fuel the fast neutrons will not have undergone much moderation; consequently the shape of the spectrum above about 3 Mev is the same as for an unmoderated source. If the location of the irradiation position is several inches from the fuel, a fraction of the neutrons with energies of several million electron volts will have undergone some moderation. The spectral shape will then be similar to that indicated in the curve labeled "position far from fuel." A knowledge of the shape of the neutron spectrum above a few hundredths of a Mev is necessary for an accurate calculation of the displacement rates.

7-4.2 PRODUCTION OF DISPLACEMENTS IN REACTOR NEUTRON SPECTRA

If the flux per unit energy interval $[\phi(E)]$ is known, then D , the number of displacements per cubic centimeter per second occurring in the volume of graphite under consideration, can be calculated. Using the macroscopic scattering cross section $[\Sigma_s(E)]$ as a function of energy and the total number of displacements $[N(E)]$ produced per collision by a neutron of energy E , (see Fig. 7.11),

$$D = \int_0^{\infty} \phi(E) \Sigma_s(E) N(E) dE \quad \text{displacements/cm}^3/\text{sec} \quad (7.36)$$

It is instructive to evaluate this integral for several specific irradiation positions for which neutron spectra have been calculated by multigroup diffusion methods. These positions are:

1. The Experimental Gas Cooled Reactor at Oak Ridge.¹⁶ The neutrons at the positions investigated, the cell boundary, are moderated by about 3 in. of graphite.
2. A Hanford uncooled test-hole position. The neutrons at this point have also been moderated by about 3 in. of graphite.
3. A graphite-moderated reactor similar to a Hanford reactor but under-moderated and containing enriched fuel. Again, the neutrons are moderated by about 3 in. of graphite.
4. A central test position of the General Electric Test Reactor (GETR) at San Jose, Calif. A steel tube surrounds the irradiation position. This is a light-water-moderated reactor.
5. The same position in the GETR but with the graphite irradiation experiment enclosed in a fuel element and with no steel tube present.

The results in Table 7.5 have all been normalized to an integrated fast flux of 1 neutron/cm² ($E > 1$ Mev).

Although the number of displacements is approximately proportional to the fast flux above 1 Mev for the various graphite-moderated reactors, the proportionality does not remain constant when the graphite- and water-moderated reactors are compared.

Some general reactor types have been investigated by Hyder and Ken-

Table 7.5 — NUMBER OF DISPLACEMENTS PER CUBIC CENTIMETER IN GRAPHITE ($\rho = 1.7 \text{ g/cm}^3$) IRRADIATED IN VARIOUS POSITIONS TO A TOTAL DOSE OF 1 NEUTRON/CM² ($E > 1 \text{ Mev}$)

Irradiation position	Displacements/cm ³ (based on Fig. 7.11)	
	Curve B model	Curve C model
EGCR	880	870
Hanford uncooled test hole	890	870
Undermoderated graphite reactor	790	770
GETR	350	350
GETR, fueled position	540	540

ward,¹¹ who have performed similar calculations using the Kinchin and Pease damage model with five different values of E_i . They have used homogenized reactor models but have investigated the change in the number of displacements with different values of the geometric buckling.

The fraction of displacements $[F(E_n)]$ caused by neutrons with energy in excess of E_n is

$$F(E_n) = \frac{1}{D} \int_{E_n}^{\infty} \phi(E) \Sigma_s(E) N(E) dE \quad (7.37)$$

To investigate situations as widely different as possible, this fraction has been calculated for the curve A model and curve C model in Fig. 7.11 and

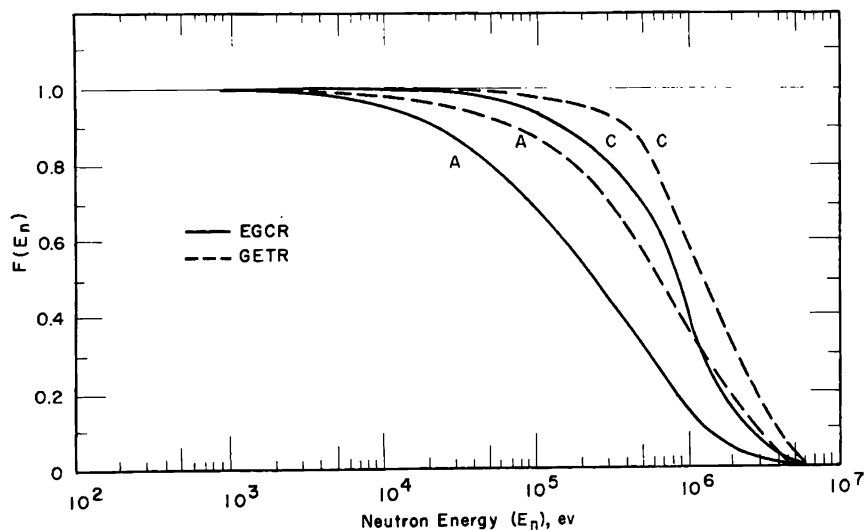


FIG. 7.14 Fraction of displacements $[F(E_n)]$ caused by neutrons with energy in excess of E_n . The curves designated A are based on the number of displacements given in curve A of Fig. 7.11 (Kinchin and Pease treatment with $E_i = 15,000 \text{ eV}$). The curves designated C are based on curve C of Fig. 7.11. The two neutron spectra are for the GETR (fueled position) and the EGCR. The C curves are believed to represent the actual situation more closely than do the A curves.

for the flux spectrum in the EGCR and the fueled position of the GETR. The first spectrum is an example of a highly moderated condition, whereas the second spectrum is that of essentially unmoderated neutrons. The results of these calculations are presented in Fig. 7.14. It is noted that for both of the considerably different models of displacement production and for both dissimilar spectra, most of the displacements in graphite are caused by neutrons with energies in the two decades between 30 keV and 3 MeV. This region of the spectrum would thus seem most important as far as the radiation effects to graphite are concerned. A similar observation has been made by Primak.¹⁷

7-4.3 COMPARISON OF CALCULATED AND EXPERIMENTAL DISPLACEMENT RATES

Table 7.8 shows that the integrated neutron flux above 1 MeV in a Hanford cooled test hole is 3.5×10^{16} neutrons/cm² per megawatt day per adjacent ton (Mwd/At). Although the positions are not identical in geometry, the neutrons in the Hanford cooled test holes and uncooled test holes have undergone approximately the same amount of moderation. Thus the number of displacements calculated for a Hanford uncooled test hole in Table 7.5 will be considered as applicable also to the Hanford cooled test holes. On the basis of the above theoretical treatments of displacement rates, it is calculated that there are 3.1×10^{19} displacements/cm³ produced in graphite per megawatt day per adjacent ton exposure. If all the displacements produce single interstitial carbon atoms, then the fraction produced per megawatt day per adjacent ton is 2.8×10^{-4} interstitials per carbon atom.

Hennig¹⁸ has reviewed a considerable amount of experimental data on radiation effects in graphite and has calculated, based on various assumptions, the fraction of interstitials that have been produced per megawatt day per adjacent ton Hanford cooled test-hole exposure. Hennig also estimates that about 30 per cent of the displacements that exist at absolute zero reintegrate at room temperature. Thus, to compare Hennig's calculations with the number derived above, which does not include any reintegration of interstitial and vacancy pairs. Hennig's numbers have been multiplied by 1.43, i.e., $100/(100 - 30)$. The results of the modified Hennig calculations are presented in Table 7.6.

The numbers in Table 7.6 lead to the conclusion that between 0.5×10^{-4} and 1.0×10^{-4} of the atoms are permanently displaced per megawatt day per adjacent ton. Values in this range are lower than those calculated from the strictly theoretical approach. The theoretical approach, however, makes no allowance for those close interstitial vacancy pairs that have been reintegrated by thermal spikes. It was pointed out in Sec. 7-2.7 that this reintegration may occur even at irradiation temperatures of absolute zero. About 65 to 80 per cent of the displacements would have to be reintegrated by this means to bring the experimental and theoretical calculations into

close agreement. This may be a high proportion of displacements to be thus affected. Similarly, if more than 30 per cent of the displacements existing at absolute zero are thermally annealed at room temperature, then the experimental numbers will come into closer agreement with the theo-

Table 7.6 — RATE OF PRODUCTION OF INTERSTITIALS AS CALCULATED FROM VARIOUS EXPERIMENTAL DATA BY HENNIG¹⁸

Property	Fraction of interstitials per Mwd/At
Stored energy	1.0×10^{-4}
X-ray spacings	0.9×10^{-4}
Neutron scattering	0.7×10^{-4}
Hall coefficient [†]	0.6×10^{-4}
Hall coefficient [†]	0.01×10^{-4}
Hall coefficient and susceptibility	0.4×10^{-4}

[†] Value obtained depends on assumptions.

retical ones; it is quite possible that the annealing has been underestimated. The assumption that all displacements lead to single interstitials is undoubtedly also a source of discrepancy between the theoretical and experimental calculations.

With all facts considered, the agreement between the two calculations is acceptable, and the theory for calculating the rate of displacement production in graphite appears to be correct in its basic principles.

7-5 Reactor Radiation Dosage Units

Radiation damage rates must be expressed as some function of the radiation dose received by the graphite. It has been pointed out that within a nuclear reactor most of the radiation effects on graphite are caused by neutrons within a fairly narrow range of energy. However, the magnitude of the neutron flux in this energy range has very seldom been known during experimental graphite irradiations, and consequently dosage has been expressed in a variety of less relevant units. For example, radiation damage to graphite has often been expressed in terms of the energy generated in the adjacent fuel elements (megawatt day per adjacent ton, or equivalent). However, unless reactor geometry, fuel enrichment, distance of the graphite from the fuel elements, and several other important factors remain identical, the amount of damage to graphite per unit of energy produced in the adjacent fuel will vary from one test facility to another. If comparisons are to be made of data obtained from different test facilities, the rate of radiation-induced property change must be expressed in terms of a basic unit that is independent of reactor geometry and other factors.

7-5.1 BASIS FOR MEANINGFUL DOSAGE UNITS

Many common types of radiation effects in graphite (e.g., stored energy growth, change in electrical resistance) are related to the number and type of lattice defects that are present. The existence of these defects after irradiation depends upon the number of radiation-induced atomic displacements that have occurred and also upon processes that may lead to annealing of a fraction of the defects. In principle, the number of atomic displacements that have occurred can be calculated by the methods used in Sec. 7-4.2.

This calculated number of atomic displacements is essentially a dosage unit that automatically includes any effects due to changes in neutron spectra. The problem of determining meaningful dosage units thus becomes primarily one of measuring the neutron flux and spectrum in the energy range of principal interest, approximately 0.03 to 3 Mev.

It should be recognized that to have a useful dosage unit the relation between dose and radiation-induced property changes does not need to be linear. Most property changes are proportional to the dose only up to a certain point, then the property change begins to saturate. Radiation effects on electrical conductivity, for example, saturate at very low dose.

7-5.2 MEASUREMENT OF NEUTRON EXPOSURES

Although it is necessary to know the neutron spectrum before a meaningful dosage can be established, there are unfortunately very few test facilities where the neutron spectra have been adequately determined. Measurements of the neutron flux at various energies must be made to determine experimentally a neutron spectrum. The most common method of accomplishing these measurements is to irradiate elemental "foils" that are strongly activated only by neutrons above a certain energy. At best, it is a very time-consuming process to expose the number of monitors required to completely define a neutron spectrum. Part of the difficulty in measuring the fast neutrons results from the fact that the only isotopes that can be activated to determine certain energy ranges yield products with very short half lives. Specialized equipment is necessary to count the activity before it decays to low value. There are several types of foils with convenient half lives which are commonly employed in the low-energy region and several long-life foils that can be utilized at the very high energy portion of the spectrum. However, these latter foils are activated at energies above the region of principal interest, i.e., above a few Mev, and the results must be extrapolated to lower energies. Because of the importance of the extrapolations from high energy, the experimental determination of fast flux will be discussed briefly.

Nickel undergoes a $\text{Ni}^{58}(n,p)\text{Co}^{58}$ reaction; sulfur undergoes a $\text{S}^{32}(n,p)\text{P}^{32}$ reaction; and neptunium undergoes a $\text{Np}^{237}(n,f)\text{Ce}^{137}$ reaction. All these

materials are commonly used as high-energy neutron monitors.† Nickel is convenient because it is easy to handle and will not melt in high-temperature experiments, whereas sulfur has a low melting point. However, the thermal cross section for the burn-out of Co^{58} from the $\text{Ni}^{58}(n,p)\text{Co}^{58}$ reaction is high; thus for high-exposure data to be obtained from activation of nickel, an accurate knowledge of the thermal flux is needed to allow corrections to the fast-flux calculations. Neptunium must be subjected to a chemical separation before it is counted, and hence it is not as convenient as the other two materials.

Aside from these difficulties, it is often impractical, because of experimental limitations, to include more than one type of foil in an irradiation facility simultaneously with the graphite. This means that no direct information can be obtained about the energy spectrum, and a spectrum must be assumed in calculating a flux from the foil activity. For example, nickel included in a graphite irradiation capsule is activated by neutrons with energy in excess of about 4 Mev. When the activity of the nickel foil is used to calculate the number of fast neutrons in the absence of any other data, it may be assumed, as is common practice, that the spectrum is unmoderated above 1 Mev, as illustrated in Fig. 7.13. This same figure demonstrates that this assumption may be in error. If the measurement were made in a moderated position, the flux greater than 1 Mev might be twice that calculated on the basis of an unmoderated spectrum. The determination of neutron flux from activation of a single foil can be improved by employing a computer calculation to estimate the spectral shape at high energy and the foil activation to determine the magnitude of the flux.¹⁹

7-5.3 DIRECT USE OF NEUTRON EXPOSURE AS A DOSAGE UNIT

Because of the common practice of reporting radiation effects on graphite either in terms of exposure to thermal neutrons or exposure to fast neutrons of greater than some given energy, usually 1 Mev, it is worth while to examine the limitations of this practice in some detail.

It has already been emphasized that the damage to the graphite results from neutrons having energies far above thermal. Furthermore, although radiation effects in graphite-moderated reactors are approximately proportional to the flux with energy greater than 1 Mev, Fig. 7.15 demonstrates that this proportionality does not hold for the thermal flux. Near the fuel the fast-neutron flux and the resulting damage are relatively high. Because the neutrons have not undergone much moderation and also because uranium absorbs thermal neutrons, the thermal flux is low at the same position. Away from the fuel the fast flux is depressed by the moderation

† There are many other materials used as high-energy flux monitors, e.g., Al^{27} , P^{31} , Fe^{54} , and Fe^{56} , but these either have inconveniently short half lives or their cross sections are not well established; hence their use is not as common at the present time as nickel, sulfur, and neptunium.

and the thermal flux is high. It is apparent that for the same thermal-flux exposure, the radiation effects in graphite, which are approximately proportional to the fast flux, will vary greatly depending upon the location of the graphite samples in the reactor (position A or B in Fig. 7.15).

Table 7.5 indicates that in similar positions in graphite-moderated reactors the damaging radiation dose to graphite is closely proportional to the flux above 1 Mev. However, this table also shows that this is not true when irradiations are conducted in vastly different types of reactors. If the neutron spectrum is known, the number of displacements per unit neutron

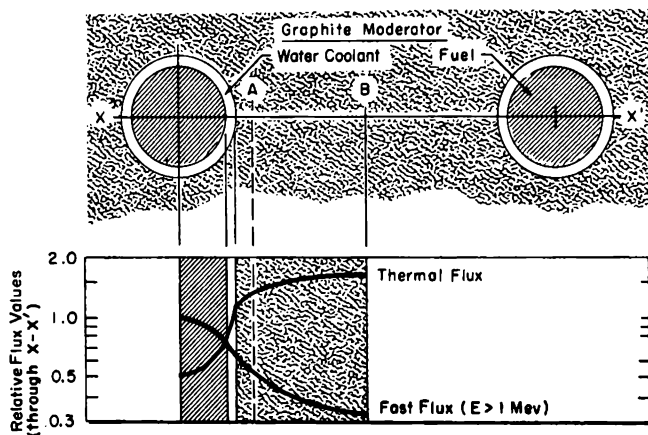


FIG. 7.15 Relative fast- and thermal-neutron fluxes as a function of distance into the moderator. Positions A and B indicate two different test positions for the irradiation of graphite.

dose can be calculated for each irradiation position, and the radiation effects can be compared at the dose calculated to produce the same number of displacements in each irradiation facility. As an example, either model in Table 7.5 shows that 1 neutron/cm² ($E > 1$ Mev) in the GETR (non-fueled position) produces about 0.40 as many displacements as the same neutron dose in a Hanford uncooled test hole. Thus graphite exposed to 10^{20} neutrons/cm² ($E > 1$ Mev) in the central position of the GETR should undergo the same changes as graphite irradiated to 0.40×10^{20} neutrons/cm² ($E > 1$ Mev) at Hanford.

In the absence of detailed information on the neutron spectra, the numbers in Table 7.7 can be used to make the same type correction discussed above. These numbers are based on the specific cases in Table 7.5. If an unmoderated fission spectrum has been assumed, the dose will be underestimated in each case. The appropriate column in Table 7.7, depending upon the type of foil measurement, should be used to correct for the error in dose.

Thus it can be estimated that, if graphite is irradiated to a true dose of

Table 7.7 — RELATIVE NUMBER OF DISPLACEMENTS PER UNIT VOLUME OF GRAPHITE CAUSED BY 1 NEUTRON/CM² ($E > 1$ Mev) EXPOSURE IN VARIOUS TYPES OF IRRADIATION FACILITIES

Irradiation facility	Relative number of displacements per neutron/cm ² ($E > 1$ Mev)		
	Neutron/cm ² is calculated from actual spectrum	Neutron/cm ² is calculated from unmoderated spectrum with foils indicated	
		Nickel activation	Sulfur activation
Graphite-moderated reactor, midway between fuel channels	1.0	2.3	1.9
Undermoderated graphite reactor, midway between fuel channels	0.90	1.5	1.6
Light-water-moderated test reactor, in-core position	0.40	0.75	0.070
Light-water-moderated test reactor, in-fuel "converter" position	0.60	0.75	0.070

10^{20} neutrons/cm² ($E > 1$ Mev) in a test reactor converter facility, the radiation effects will be the same as in graphite irradiated to 0.26×10^{20} neutrons/cm² ($E > 1$ Mev) as indicated by nickel activation in a graphite reactor when an unmoderated spectrum is assumed.

7-5.4 DOSAGE UNITS IN COMMON USE

Many of the data on the effects of irradiation on graphite reported in the literature are expressed in terms of dosage units such as total reactor energy, energy generated in adjacent fuel elements, or integrated thermal-neutron dose. As has been discussed above, none of these units can be directly related to the total number of atomic displacements that have occurred within the graphite. As long as the use of data expressed in terms of these dosage units is confined to comparisons of graphite behavior in the same irradiation facility, any of the above units is useful. The success with which data based on various dosage units can be utilized to make comparisons in the behavior of graphite irradiated in different reactor facilities depends on the convertibility of these dosage units to more generally useful units, such as integrated fast flux. The integrated fast flux can then be used in conjunction with calculations of the type given in Tables 7.5 and 7.7 to estimate the relative damaging dose in each facility.

Dosages in terms of total reactor power generation are perhaps the most nebulous of those in common use. Because of lack of a more exact knowledge of reactor conditions, many of the earlier data on the irradiation

Table 7.8 — INTEGRATED FLUX ABOVE 1 MEV FOR VARIOUS EXPOSURE UNITS[†] (Neutrons/cm²)

Facility	Reactor Mwd	Mwd/At	Thermal flux	Ref.
Hanford production reactor:				
Cooled test hole [†]		(3.5×10^{15})		20
K, cooled test hole		6.2×10^{15}		20
Uncooled test hole		5.5×10^{15}		20
K, uncooled test hole		9.6×10^{15}		20
Annulus Tube §		2.2×10^{15}		20
X-10 Graphite Reactor at Oak Ridge, hole 19		(7×10^{15})	0.2	21
Brookhaven Graphite Research Reactor (BGRR), hole E-25			0.2	22
Canadian National reactor Experiment (NRX), empty lattice position			0.03	23
British Experimental Pile (BEPO):				
Standard position, T-10			0.04	24
Hollow-slug converter			0.55	24, 25
Empty fuel channel			0.02	24
French reactor at Saclay:				
Aluminum thimble	2.2×10^{15}			26
Converter	9×10^{15}			26
British Windscale reactor, center of lattice			0.05	27

[†] Values are all based on flux measurements. The values in parentheses are based on flux measurements that cannot be compared directly and involve some additional calculations of reactor operating conditions. All data except the Hanford data are calculated on the basis of an unmoderated fission spectrum. The Hanford and BEPO data are based on nickel activation; the NRX, Saclay, and Windscale data, on sulfur activation; and the ORNL and BNL data, on a variety of methods.

Note that flux is not necessarily proportional to the damage. To compare damage rates in two facilities, use this table in conjunction with Table 7.7.

[‡] Unless otherwise stated, all Mwd/At (megawatt day per adjacent ton) exposures reported in this book for 30°C irradiation correspond to the cooled test-hole position. Those above 30°C correspond to the uncooled test-hole position.

§ Controlled-temperature irradiation device (see Fig. 8.4).

of graphite are expressed in this type unit. In column 2 of Table 7.8 are listed values of the integrated fast flux above 1 Mev after a total reactor energy production of 1 Mwd at several irradiation facilities. These data were calculated for particular positions and cannot be safely transposed to other positions within the reactor.

A slightly more satisfactory dose unit is the amount of energy generated in the adjacent fuel elements. The improvement lies in the fact that this unit is based upon the power generation in the vicinity of an irradiation facility rather than on the average power generation over the entire reactor. The majority of graphite irradiation data that have been obtained at Hanford are expressed in terms of two units of this type, megawatt-days per adjacent ton of uranium (Mwd/At) and megawatt-days per central ton of uranium (Mwd/Ct). These two units can be considered equivalent. However, the Mwd/Ct unit is determined from the average power generated in the central region of the reactor rather than on direct measurements of the power in the fuel immediately surrounding the irradiation experiment. For this reason there is approximately a 20 per cent greater uncertainty when converting Mwd/Ct units to integrated fast flux. Conversion factors based on a considerable amount of experimental data at the various Hanford irradiation facilities are listed in column 3 in Table 7.8.† It is obvious from the variation between the conversion factors, even within the same reactors, that it is not accurate to compare damage rates between various reactors on the basis of Mwd/At exposures.

Many studies on irradiation effects in graphite have been expressed in terms of thermal-neutron exposure. The danger inherent in this procedure has been discussed in Sec. 7-5.3. Conversion factors from thermal-neutron flux to fast-neutron flux have been derived from experimental measurements at several reactors and are listed in column 4 of Table 7.8.

Table 7.8 must be used with caution. The conversion factors are average values obtained under standard operating conditions. Changes in the operating conditions or in the experimental assembly may alter these conversion factors considerably. The only really satisfactory method of obtaining fast-neutron exposures is to irradiate foils with each experiment and to include a sufficient number of foils to obtain a measure of the flux gradient throughout the experimental apparatus.

7-5.5 DIRECT USE OF PROPERTY CHANGES AS A RELATIVE DOSAGE UNIT

Because of the lack of information on fast-neutron dose, several irradiation dosage units have been devised which are based upon property changes that occur in graphite during irradiation. The basis of this procedure is to assume that two pieces of graphite that have undergone the same property

† It should be noted that the previously published conversion factors for Hanford Mwd/At have been in terms of total rather than fast flux. The fast-flux conversion factors are based on more recent data than the previous conversion factors.

change have been exposed to the same integrated fluxes of damaging neutrons. Such units have been used to establish the relative dose rates in various irradiation facilities.

One of the earliest of these units to come into use was the L unit,[†] which was defined as the exposure necessary to cause a 25 per cent increase in the elastic modulus at 35°C in KC graphite.²⁸ This unit was utilized to compare the original radiation-damage studies in graphite, which were done in cyclotrons, to damage studies in the first nuclear reactors. The L units were assigned the following values in the available irradiation spaces. One L unit equals 2.2×10^5 μ a-hr in the Washington University cyclotron for exposure to neutrons produced in a beryllium target by deuterons. In the Berkeley cyclotron for neutron exposure, the conversion factor was 3.4×10^4 μ a-hr. As a comparison, one L unit equaled 1.16 Mwd in the CP-3 Reactor and 13 Mwd in the X-10 Reactor. An L unit is a very small dose, being approximately 1×10^{17} neutrons/cm² ($E > 1$ Mev) in a Hanford cooled test hole as estimated from the exposure required to produce a 25 per cent increase in elastic modulus.

The change in the electrical conductivity of graphite has likewise been proposed as a dosage unit.²⁹ Radiation-induced property changes in graphite have also been evaluated as a possible means of monitoring the fast flux in reactors for studies of radiation damage to other materials.³⁰

Table 7.9 — CONVERSION OF BEPO EQUIVALENT FLUX TO FAST FLUX IN SEVERAL BEPO IRRADIATION POSITIONS²⁴

Position	Fast flux, [†] neutrons/cm ² /sec ($E > 1$ Mev)	BEPO equivalent flux, neutrons/cm ² /sec
BEPO standard position [‡]	6.2×10^{10}	1.8×10^{12}
BEPO empty fuel channel	3.2×10^{10}	1.15×10^{12}
BEPO hollow slug	23×10^{10}	4.10×10^{12}

[†] Nickel activation, unmoderated fission spectrum is assumed.

[‡] In this position (T-10) the BEPO equivalent flux is defined as equal to the thermal flux.

Many British exposures have been reported in terms of BEPO equivalent flux. Various irradiation facilities have been calibrated in terms of the equivalent flux by comparing changes in electrical resistivity and Young's modulus with similar changes in BEPO. Within BEPO the conversion factors in Table 7.9 have been established. BEPO equivalent fluxes in other facilities have been reported.^{31, 32}

[†] L is the first letter of the name of the Norse god, Loki, the contriver of mischief and discord!

Recent British results have been reported in terms of equivalent Calder dose. Preliminary correlations give the result³³

$$\begin{aligned} \text{Equivalent Calder dose (Mwd/At}_e\text{)} \\ = 1.1 \times 10^{-18} \text{ equivalent BEPO dose (neutrons/cm}^2\text{)} \end{aligned} \quad (7.38)$$

The combination of this conversion factor with the value of BEPO equivalent flux for Hanford ($1 \text{ Mwd/At} = 5.5 \times 10^{17} \text{ BEPO equivalent flux}$) yields a conversion factor of

$$1 \text{ Mwd/At (Hanford)} = 0.6 \text{ Mwd/At}_e \text{ (Calder)}$$

This factor gives fair agreement between Hanford and Calder data.

7-5.6 EFFECT OF FLUX ON PROPERTY CHANGES

There is a potential error in the use of property changes or integrated fluxes as a basis for radiation-dosage units. The amount of change may depend not only upon exposure but also on flux. Theoretically flux dependence is possible whenever the rate of defect removal by annealing is significant with respect to the rate of defect production by radiation. Temperature-sensitive damage processes are in this category. A simplified treatment of the kinetics involved in the formation and recombination of single interstitials and vacancies shows that the concentration of defects at a given integrated fast-neutron exposure should be proportional to the square root of the fast-neutron flux.³⁴ Thus property changes that are proportional to the defect concentration may not be directly proportional to the exposure, but rather, may be approximately proportional to the exposure times the square root of the flux. However, a square-root relation with flux will not necessarily hold true because the simplified theory takes no account of such phenomena as the agglomeration of the interstitial carbon atoms into C_2 or higher complexes. Furthermore, this same simplified theory shows that a process that is controlled primarily by diffusion of defects to crystallite boundaries would depend on the product of the exposure and the first power of the flux.³⁴

British workers³⁵ have observed an apparent effect of flux in comparing damage between reactors with widely differing flux levels. To correct for this apparent effect, an equivalent temperature of irradiation has been defined as that temperature at which the observed rate of property change would occur in the standard BEPO position. Thus the higher the flux, the lower the equivalent temperature. If X is the ratio of flux in the irradiation position to that in the standard position, Eq. 7.39 gives the equivalent temperature.

$$\frac{1}{T_{\text{equiv}}} - \frac{1}{T_{\text{irrad}}} = 1.66 \times 10^{-4} \log X \quad (7.39)$$

This equation was derived from radiation-damage data obtained in the irradiation temperature range below about 350°C and is in a form that

accounts for only one activation energy for annealing at 1.2 ev. It is probable that the effective activation energy for annealing is greater at higher temperatures; in this case the constant term would be smaller. Equivalent and irradiation temperatures are given for stored-energy data in Sec. 12-2.3.

7-6 Nature of Radiation-induced Defects in Graphite

The formation of vacancies and displaced atoms has been discussed in the previous sections of this chapter, but very little attention has been given to the ultimate disposition of these defects. Single interstitials and vacancies are the initial products of displacement collisions, but, depending upon the temperature of irradiation and dose, these may agglomerate into complex damage centers. Near room temperature highly irradiated graphite contains so many displaced atoms that the observed property changes are primarily the result of these complex centers.

The nature and mobility of the lattice defects will be discussed in subsequent chapters in connection with the radiation effects that they produce in graphite. Two topics, not covered in detail elsewhere, warrant special mention here.

7-6.1 LATTICE STRAINS AND DISLOCATIONS

It has been proposed⁹ that in addition to interstitial complexes and vacancies, lattice strains are produced around vacancy centers during irradiation. A plausible source of a two-dimensional strain field that could occur in irradiated graphite is shown as type a in Fig. 7.16. These defects are most likely to be formed when displaced atoms try to reintegrate into the lattice and are presumably present only after some annealing has occurred. Also

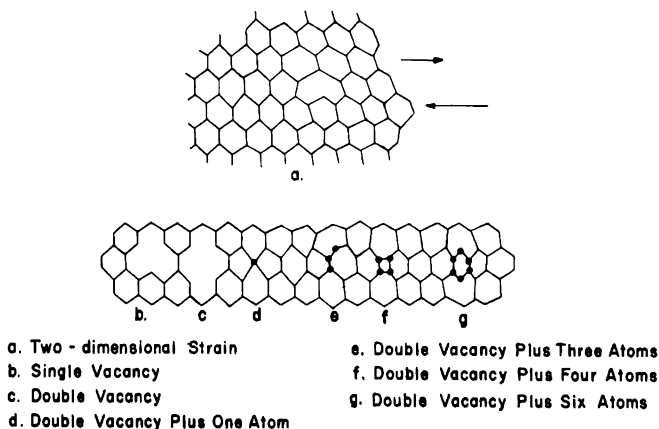


FIG. 7.16 Probable configurations of complex vacancy centers in a graphite lattice. These configurations are assumed to occur after some annealing has taken place. Two-dimensional strains may extend some distance into the lattice from the center.⁹

shown in Fig. 7.16 are several other possible configurations (types b through g) which might result from reintegrations. Type g, for example, represents the same configuration that would be produced by two close vacancy centers of type a.

The influence of vacancies may also extend to adjacent lattice planes. Dislocation loops have been observed³⁶ in graphite that has been thermally quenched from high temperature. It has been suggested that these loops are formed by the collapse of adjacent lattice planes into a vacancy cluster.

7-6.2 DESCRIPTION AND ANNEALING OF DEFECTS

A damage and annealing mechanism based on a large amount of annealing data of various types has been postulated⁹ which is consistent with the experimental results that are considered. However, this mechanism, which is discussed below, is not expected to apply to heavily irradiated samples in which more-complex damage centers are present.

During neutron bombardment at -200°C , nearly all the atoms that are displaced (with the exception of those annealed in thermal spikes) remain displaced. Approximately one third of the displaced atoms are present as close interstitial-vacancy pairs and are not able to trap electrons. The remainder of the interstitials are sufficiently far from the vacancies that they trap one electron and cause paramagnetic resonance absorption. Vacancies are predominantly single vacancies which trap a pair of electrons and are thus diamagnetic.

When annealed below room temperature, the close interstitial-vacancy pairs reintegrate. At the same time clustered interstitials drift apart because of the Coulomb repulsion of their negative charge. This proposed behavior is supported by evidence on thermal and electrical resistivities, X-ray spacing, paramagnetic resonance, and stored-energy measurements below room temperature.

As the temperature is raised to room temperature, a few close interstitial vacancy pairs remain to be annealed. Their annealing apparently coincides with the next process, recombination of single interstitials into C_2 molecules. This latter process requires an activation energy sufficiently high to overcome Coulomb repulsion of the charged interstitials. The considerable annealing of stored energy, electrical resistance, susceptibility, etc., in the range 100 to 200°C is presumably due to this reaction of single interstitials to form C_2 molecules.

The combination reaction is probably not complete before a third process begins to occur: annealing of complexes, predominantly C_2 , to vacancies and grain boundaries. The C_2 annealing decreases the c spacing because this process removes interstitial atoms. In lightly damaged graphite this process is practically complete near 600°C . However, in heavily damaged samples c -spacing annealing continues up to 2000°C . On the basis of experiments with radiocarbon tracers, it is concluded that this high-

temperature annealing results from the migration of C_2 complexes rather than vacancies.

At temperatures above 600°C a few interstitials are trapped at surfaces and imperfections, and an equal number of vacancies remain. Local strains are also probably formed, as discussed in Sec. 7-6.1. The vacancies should become mobile⁴ at about 1200°C .

Certain difficulties with this model are noted in Sec. 13-3.5. Dienes and Vineyard⁴ have also presented some objections to the above model; however, it is the best that can be suggested at the present time.

If graphite is irradiated at room temperature or above, some of the damage centers, e.g., close interstitial-vacancy pairs, will not be stable. Furthermore, single interstitials are relatively mobile above room temperature and may react with previously formed damage centers to form complexes. It is possible to explain some of the property changes observed after room-temperature irradiation as being due to a progressive conversion of single interstitial carbon atoms to complexes of two or more carbon atoms.

7-7 Glossary of Symbols

Symbol	Meaning	Defining equations
A	Atomic mass	
a	Screening constant	7.6
a_H	Bohr radius of hydrogen atom	
b	Classical distance of closest approach	7.10
C_e	Electronic heat capacity per electron	
C_L	Lattice specific heat per atom	
c	Velocity of light	
D	Number of displacements per cubic centimeter per second	7.36
D_e	Diffusion coefficient for electrons in lattice	
E	Neutron energy, also written as E_n	
\bar{E}	Average of excitation energies in lattice	
E'	Energy of primary knock-on atom	
\bar{E}'	Mean energy of primary knock-on atoms	7.3
E''	Energy of secondary knock-on atom	
E_d	Displacement energy required to remove an atom from a lattice position	
E_i	Limiting energy for excitation (see Sec. 7-2.4)	
E_n	Neutron energy, also written as E	
E_n^A	Initial neutron energy	
E_n^B	Final neutron energy	
e	Charge on an electron	
$F(E_n)$	Fraction of displacements caused by neutrons with energy greater than E_n	7.37

Symbol	Meaning	Defining equations
h	Planck's constant	
I	Lowest electronic excitation energy level	
k	Boltzman constant	
L_d	Mean free path between collisions that cause displacements	7.25a
L_s	Mean free path for hard-sphere collisions	7.15
M_1	Mass of moving particle	
M_2	Mass of stationary atom	
m	Effective mass of a conduction electron	
m_e	Electron mass	
N	Number of collisions	7.4
$N(E_n), N(E)$	Number of displacements caused by a single collision of a neutron of energy E_n or energy E	7.35a, 7.35b
$\langle n \rangle$	Average number of atoms per square centimeter in a crystal plane	7.16
n_0	Number of atoms per cubic centimeter	
Q	Amount of energy in thermal spike	
q_1, q_2	Charge on nuclei	
R	Effective atomic radius for hard-sphere collisions	7.17
R	Universal gas constant	
R_H	Rydberg constant	
r	Separation of two charges	
r_s	Radius of cylindrical electron spike	
r_t	Radius of spherical thermal spike	7.31
T	Energy transferred in a collision	
T_a	Minimum amount of energy that can be transferred in a Rutherford collision	7.18a
\overline{T}_a	Average energy transferred in a Rutherford collision	7.19
\overline{T}_d	Mean energy transferred in a displacement collision	7.22, 7.24
$\overline{T}_d(E')$	Mean energy of the secondary atom produced by a primary with energy E'	
T_e^*	Initial electron temperature in an electron spike	7.29
T_L	Lattice temperature	7.30
T_m	Maximum energy transferred in a collision	7.1, 7.2
T'_m	Maximum energy of a primary knock-on atom	
t	Time after formation of electron spike	
V	Velocity of knock-on atom	
Z	Atomic number of nucleus	
Z_1	Atomic charge on moving particle	

Symbol	Meaning	Defining equations
Z'_2	Number of excitable electrons on bound particle	
z	Number of conduction electrons per atom	
$(dE/dx)_e$	Rate of energy loss of moving charge	7.28a, 7.28b
α	Twice the average neutron energy loss per collision	
ϵ_F	Fermi energy of free lattice electrons	
θ	Angle of scattering	
θ'_a	Minimum scattering angle for which Rutherford scattering is valid	7.7
λ	de Broglie wave length of particle	
μ	Ratio of electronic to lattice specific heats	
$\nu(E')$	Total number of atoms displaced by a knock-on atom of energy E' (including the knock-on atom)	7.32
ν_p	Number of primary atomic displacements	
$\nu_R(E')$	Average number of atoms displaced in a Rutherford collision by a knock-on atom of energy E' (not including the knock-on atom)	7.34
ξ	Logarithmic energy decrement for neutron scattering	
$\Sigma_s(E)$	Macroscopic neutron scattering cross section at neutron energy E	
σ_a	Total cross section for all Rutherford collisions	7.20a
σ_d	Total cross section for producing displacements	7.21a, 7.23
σ'_d	Cross section for producing displacements by hard-sphere collisions	7.23
τ	Relaxation time of electrons in lattice	
$\phi(E)$	Neutron flux per unit energy interval	

References

1. D. T. Eggen, *Energy Required for Atomic Displacements in Graphite Determined by Electron Bombardment*, USAEC Report NAA-SR-69, North American Aviation, Inc., April 1950.
2. D. J. Hughes and R. S. Carter, *Neutron Cross-Sections: Angular Distributions*, USAEC Report BNL-400, Brookhaven National Laboratory, June 1956.
3. R. O. Lane et al., The Angular Distributions of Neutrons Scattered from Various Nuclei, *Ann. Phys.*, **12**: 135-171 (1961).
4. G. J. Dienes and G. H. Vineyard, *Radiation Effects in Solids*, Interscience Publishers, Inc., New York, 1957.
5. F. Seitz and J. S. Koehler, Displacement of Atoms During Irradiation, *Solid State Phys.*, **2**: 305-448 (1956).
6. G. H. Kinchin and R. S. Pease, The Displacement of Atoms in Solids by Radiation, *Repts. Prog. in Phys.*, **18**: 1-51 (1955).

7. H. Watanabe, Energy Loss of Electrons Passing Through a Graphite Single Crystal at Different Angles, *J. Phys. Soc. Japan*, **14**: 1453 (1959).
8. F. Seitz, On the Disordering of Solids by Action of Fast Massive Particles, *Discussions Faraday Soc.*, **5**: 271-282 (1949).
9. G. R. Hennig and J. E. Hove, Interpretation of Radiation Damage to Graphite, in *Proceedings of the First United Nations International Conference on the Peaceful Uses of Atomic Energy, Geneva, 1955*, Vol. 7, pp. 666-675, United Nations, New York, 1956.
10. W. Primak, Fast Neutron Damaging in Nuclear Reactors. II. The Radiation Damage Function of Graphite, *Nuclear Sci. and Eng.*, **2**: 117-125 (1957).
11. H. R. McK. Hyder and C. J. Kenward, *Fast Neutron Spectra in Thermal Reactors and Their Relation to Radiation Damage*, British Report AERE-R-2886, 1959.
12. F. W. Brown, *Studies on Nuclear Reactors. 4. Theory of Ionization and Atomic Displacement Produced by Fast Particles in Graphite*, USAEC Report NAA-SR-4, North American Aviation, Inc., Feb. 1, 1948.
13. M. S. Livingston and H. A. Bethe, Nuclear Physics. C. Nuclear Dynamics, Experimental, *Revs. Modern Phys.*, **9**: 245-390 (1937).
14. A. Yoshimori and Y. Kitano, Theory of the Lattice Vibration of Graphite, *J. Phys. Soc. Japan*, **11**: 352-361 (1956).
15. J. A. Brinkman, On the Nature of Radiation Damage in Metals, *J. Appl. Phys.*, **25**: 961-970 (1954).
16. C. A. Preskitt, Graphite Damage Resulting from the Moderation of Fast Neutrons, in *Gas Cooled Reactor Project Quarterly Progress Report for Period Ending December 31, 1959*, pp. 15-18, USAEC Report ORNL-2888, Oak Ridge National Laboratory, 1960.
17. W. Primak, Fast Neutron Damaging in Nuclear Reactors. III. The Radiation Damage Dosage, *Nuclear Sci. and Eng.*, **2**: 320-333 (1957).
18. G. R. Hennig, Review of Radiation Damage to Graphite, in *Metallurgy and Fuels, Progress in Nuclear Energy, Series V*, Vol. 1, pp. 587-651, Pergamon Press, New York, 1956.
19. J. M. Davidson and J. W. Helm, *The H-3 Irradiation Experiment: Irradiation of EGCR Graphite. Interim Report No. 1*, USAEC Report HW-71500A, Hanford Atomic Products Operation, Oct. 16, 1961.
20. H. H. Yoshikawa, *Fast Neutron Fluxes in Hanford Reactors*, USAEC Report HW-64393 Rev., Hanford Atomic Products Operation, 1960. (Classified)
21. R. E. Durand and F. E. Faris, *A Compendium of Radiation Effects on Solids, Supplement*, USAEC Report NAA-SR-1304, North American Aviation, Inc., Sept. 1, 1955. (Classified)
22. J. B. Trice, *Fast Neutron Flux Measurements in E-25 of the Brookhaven Graphite Reactor*, USAEC Report CF-55-7-130, Oak Ridge National Laboratory, July 27, 1955.
23. J. C. Roy and D. Wuschke, *Fast Neutron Reactions and Fast Neutron Flux in the NRX Reactor*, Canadian Report CRC-852, Atomic Energy of Canada Limited, July 1959.
24. J. H. W. Simmons, Atomic Energy Research Establishment (Harwell), personal communication, April 1960.
25. D. G. Martin and P. R. Stanwix, *The Measurement of Fast Neutron Flux for Irradiation Damage Studies*, British Report AERE-M/M-138, Nov. 20, 1956.
26. G. Mayer and J. Gigon, Effets des Neutrons Rapides sur quelques Constantes Physiques du Quartz Cristallin et de la Silice Vitreuse, *J. phys. radium*, **18**: 109-114 (1957).
27. J. S. Nairn, Windscale Laboratories, personal communication, June 7, 1960.
28. T. J. Neubert and M. Burton, *Wigner Effect in Graphite. Proposed Unit of Ex-*

- posure*, USAEC Report CC-2320, University of Chicago, Nov. 14, 1944. (Classified)
29. W. Primak and L. H. Fuchs, Fast Neutron Damaging in Nuclear Reactors. I. Radiation Damage Monitoring with the Electrical Conductivity of Graphite, *Nuclear Sci. and Eng.*, **2**: 49-56 (1957).
 30. E. Fast, *Graphite Damage as an Index to the Integrated Damaging Neutron Flux*, USAEC Report IDO-16182, Phillips Petroleum Co., Sept. 28, 1954.
 31. J. H. W. Simmons, *The Effects of Irradiation on Graphite*, British Report AERE-R/R-1954, June 5, 1956. (Classified)
 32. J. H. W. Simmons, The Effect of High Flux Neutron Irradiation on the Physical Properties of Graphite, *Proceedings of the Fifth Conference on Carbon, Held at Pennsylvania State University*, Pergamon Press (to be published).
 33. J. H. W. Simmons, *The Temperature Variation of High Flux Irradiation Damage in Graphite*, British Report AERE-M-661, March 1960. (Classified)
 34. G. J. Dienes and A. C. Damask, Radiation Enhanced Diffusion in Solids, in *Proceedings of the Second United Nations International Conference on the Peaceful Uses of Atomic Energy, Geneva, 1958*, Vol. 29, pp. 340-347, United Nations, New York, 1959.
 35. J. C. Bell et al., Stored Energy in Graphite of Power-Producing Reactors, *Phil. Trans. Roy. Soc. London Ser. A*, **254**: 361-395 (1962).
 36. S. Amelinckx and P. Delavignette, Dislocation Loops Due to Quenched-in Point Defects in Graphite, *Phys. Rev. Letters*, **5**: 50-51 (1960).

Irradiation Techniques

D. E. BAKER and J. M. DAVIDSON†

A number of unique problems are encountered in irradiation experiments. In addition to the usual considerations that determine the choice of materials in experimental equipment, the possible effects of high heat generation, radiation damage, and neutron absorption must be considered. Experiments must often be confined to a small space, which requires originality in experimental design. Because of the costs inherent in irradiation experiments, unusual demands are made upon the reliability and safety of the equipment.

Particle accelerators have been employed to a limited extent, particularly in early experiments, for the study of radiation effects in graphite (Sec. 1-1.3). Some irradiations of gas-graphite systems have been performed with gamma sources.^{1,2} However, by far the largest amount of testing has been conducted in reactors. Beginning with the Materials Testing Reactor (MTR) in 1953, several high-flux test reactors³⁻⁶ have been constructed in the United States and other countries for the purpose of serving experimental irradiation programs. The intense neutron flux available in these reactors makes high-exposure short-term irradiations possible, although difficulties may be encountered with high gamma heating rates and with the extrapolation of data to effects in other reactors.

It is not possible in a short chapter to discuss all the techniques applicable to graphite irradiations. The radiation-damage experiments that have been chosen for illustration come largely from experience at Hanford; however, in some cases experiments at other laboratories might have served equally as well. Although certain problems are peculiar to the testing of graphite, the techniques employed are largely applicable, with minor modification, to the testing of other nonfissionable materials.

8-1 Low-temperature Irradiations

8-1.1 CYCLOTRON IRRADIATIONS

Cyclotron irradiations^{7,8} have been performed under controlled conditions in the temperature range from -195 to 2000°C . Advantages in the use of cyclotrons are the high degree of reproducibility of irradiation conditions and exact knowledge of the energy of the monoenergetic charged

† Hanford Laboratories, General Electric Company, Richland, Wash.

particles. Experiments are generally performed more easily than they are in reactors; but the rate of damage accumulation is low, and the sample must necessarily be small.

Changes in electrical resistivity, thermoelectric power, and magneto-resistance of graphite have been determined⁷ following proton irradiation at 78°K in the 60-in. cyclotron (see Sec. 10-1.1). The targets, 1- by 0.1-in. graphite strips 0.003 or 0.010 in. thick, were oscillated in the beam to provide an area of uniform irradiation. The sample was cooled by forced convection with helium gas flowing at 0.6 lb/min. The cooling system consisted of a circulating compressor, heat exchangers, and a liquid-nitrogen boiler. Helium was led from the boiler to the target box at 78°K. Pulse annealing was carried out by heating the helium gas that cooled the targets during irradiation with a 4-kw stainless-steel bellows gas heater located in the inlet gas stream to the sample. Iron-constantan thermocouples, inserted into the target through Kovar seals, were attached to the sample for continuous temperature monitoring.

Graphite samples have also been irradiated with electrons at the temperature of liquid helium.^{9,10} An objective of this very low temperature experiment was to determine whether the amount of damage retained from irradiations at liquid-nitrogen temperatures represented essentially all the damage produced (see Sec. 12-4.2). Graphite samples 1.62 by 0.125 in. and 0.020 to 0.040 in. thick were immersed in liquid helium and irradiated with 1.25-Mev electrons. Four potential probes were placed along the sample to measure electrical resistivity during irradiation and annealing. Annealing was by resistance heating, each annealing pulse being followed by a resistivity measurement at 4°K.

8-1.2 REACTOR IRRADIATIONS

Studies of the nature of the damage caused by fast-neutron bombardment of graphite and other materials have necessitated irradiations in nuclear reactors at low temperatures for extended periods of time. Cryogenic devices have been operated successfully in the Brookhaven Graphite Research Reactor (BGRR), the Oak Ridge Graphite Reactor (X-10), the Low Intensity Test Reactor (LITR), and the British Experimental Pile (BEPO). Cooling by direct contact of liquid nitrogen with the sample was employed in the BGRR, LITR, and BEPO facilities. However, the methods of introducing the liquid coolant and the sample temperatures differed considerably.

In the BGRR facility¹¹ a small flask containing the test specimens was surrounded by a reservoir of liquid nitrogen. The reservoir was periodically replenished with liquid nitrogen forced by air pressure along an 18-ft length of horizontal tubing into the reactor. Automatic temperature control of the cryostat was accomplished by use of a chromel-alumel thermocouple located in the reactor and an external unit for injecting liquid nitrogen.

Whenever the temperature increased to -150°C , about 100 cm^3 of liquid nitrogen was automatically injected. The time for one cycle ranged from 4 to 10 min. Charge-discharge of samples during reactor operation was possible through four 0.4-in.-diameter tubes. Liquid-nitrogen consumption was 1 to 2 liters/hr, depending on the reactor power level and on the mass of the samples.

The BEPO cryostat¹² was installed in a vertical experimental hole of the reactor. Liquid nitrogen was drawn from a reservoir outside the reactor by a partial vacuum from a suction pump. Control was maintained by means of an iron-constantan thermocouple, which actuated the pump. The temperature ranged from -185 to -190°C . The cryostat was insulated by a vacuum jacket evacuated to 10^{-2} mm Hg. Liquid-nitrogen consumption was approximately 1 liter/hr. Oxides of nitrogen formed a sludge in the bottom of the cryostat, making removal of the sample difficult. Analysis of the cryostat off-gas after one month of operation showed 0.6 per cent nitrous oxide and 12 per cent oxygen.

In the LITR¹³ high-purity liquid nitrogen was circulated in a closed system at a pressure of 15 psig. An external heat exchanger cooled by liquid nitrogen boiling at atmospheric pressure maintained the circulating liquid nitrogen below its boiling point. Liquid-nitrogen consumption was about 16 liters/hr. Oxygen and water vapor were excluded from the closed circulating system, thereby reducing the explosion hazard. Two explosions have occurred in cryogenic devices inside the X-10 Reactor. It was believed that the explosive reaction may have involved ozone that was formed by the action of ionizing radiation on condensed oxygen in the cryostat.

A cryostat¹⁴ was operated in the X-10 Reactor for irradiations at temperatures near 15°K . The cryostat, located in a vertical hole of the reactor, was constructed almost entirely of aluminum and was supplied with cold helium gas from a helium refrigerator. The measured rate of heat removal by the helium refrigerator was 300 watts at 21.5°K . A vacuum jacket was the only insulation on the 22-ft in-pile assembly. Owing to the relatively low gamma heating rate of 4.7 mw per gram of aluminum at full reactor power, the refrigerator was able to maintain the wall of the sample chamber at 10 to 11°K . Copper-constantan thermocouples attached to the sample were checked against a gas thermometer in the cryostat. Stored-energy measurements and pulse annealing of the samples were carried out *in situ* utilizing reactor gamma heating.

8-2 Room-temperature Irradiations

Radiation-induced property changes in graphite near room temperature are a sensitive function of the irradiation temperature (Sec. 9-1.5). Fortunately in this temperature-sensitive region techniques are simpler and methods of temperature control are more successful than at higher temperature; thermal conductivities are better known, and the behavior of materials

of construction is more predictable. Even with these favorable factors, it is necessary to exercise special care to ensure successful irradiations. For example, gamma heating that is improperly accounted for or ignored may cause systematic errors in estimates of the temperature of nonmonitored samples.

Facilities for room-temperature irradiations are often relatively spacious, permitting large samples or many small samples to be irradiated and discharged conveniently. Some facilities are designed to afford the experimenter temperature control independent of the surroundings, a luxury not often available at other temperatures or in specialized experiments. For these reasons room-temperature irradiations have been widely used for the study of radiation-damage phenomena. The following sections discuss several room-temperature facilities and the irradiation techniques employed.

8-2.1 COOLED TEST HOLES (HANFORD)

Water-cooled test holes in the Hanford reactors have been used extensively for room-temperature irradiations. Figure 8.1 illustrates a typical room-temperature facility. The test hole penetrates the reactor shielding and the moderator transversely to the fuel channels. Water near room temperature is circulated between the inner and outer tubes, and, if desired,

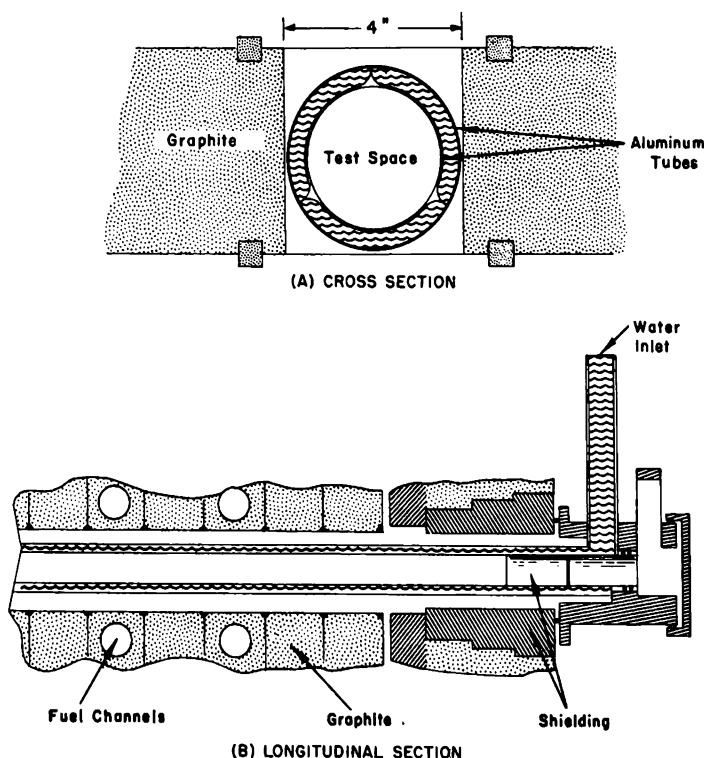


FIG. 8.1 Diagrams of a Hanford cooled test hole.¹⁵

the water can be steam-heated up to 80°C, thereby providing a range of irradiation temperatures. Large solid samples can be accommodated directly, whereas small samples require aluminum holders to keep them in the proper position during irradiation. Experiments up to 3 in. in diameter can be irradiated at a relatively constant temperature. Provision has been made for access of thermocouple wires to the experiment. Shielding plugs are inserted several feet into the facility to prevent neutron streaming.

The irradiation zone is nominally 40 ft long and varies in flux intensity as a modified cosine function. Superimposed on this variation is a periodic variation in fast flux caused by the transversely oriented fuel channels. Exposures are usually expressed in terms of megawatt-days per adjacent ton of uranium (Mwd/At), which is computed from the power delivered to the coolant from the neighboring fuel (Sec. 7-5). Although this method is generally satisfactory for the calculation of exposures for Hanford applications, foil dosimetry is more generally useful as a method of measuring the exposure. Recently interest in the damaging aspects of fast neutrons has evolved theoretical techniques for the calculation of neutron distributions above 0.18 Mev with high resolution.¹⁶ Such calculations have been used to estimate the fast-neutron spectra in several test facilities.¹⁶⁻¹⁸

8-2.2 ETR AND MTR X-BASKET IRRADIATIONS

Extensive use is made of X-basket capsule facilities in the Materials Testing Reactor (MTR) and the Engineering Test Reactor (ETR). These facilities, which represent the bulk of the irradiation space available in these reactors, are located in drilled filler blocks called "A" or "B" pieces. An X-basket is a ribbed thin-walled aluminum tube that centers capsules for proper coolant flow. In contrast to experiments that require lead wires, X-basket capsules can be employed to irradiate graphite and other materials in core positions that exclude the use of lead wires. If it is desired to position a capsule about the vertical mid-plane of the reactor for intensity measurements or for spectral considerations, this can be done through the use of other capsules or spacers. The reactor coolant flows through the X-baskets, setting a base temperature of 40°C in the MTR and 50°C in the ETR. Because of the high gamma heating rate of the MTR and the ETR, careful consideration must be given to heat transfer to avoid a systematic error in temperature estimates.

A typical aluminum capsule used for the irradiation of three graphite samples is shown in Fig. 8.2. The milled sides of the aluminum capsule (A) increase heat transfer and lessen gamma heating. Flux monitors (B) are imbedded in the small graphite carrier (C) to facilitate handling in the hot cell. The graphite samples (D) are canned in the aluminum tubes (E) before being assembled. The total capsule length is 6 in. In this irradiation it was desired to operate as close to the water-coolant temperature as possible. A dry atmosphere was ensured by encapsulating the samples in

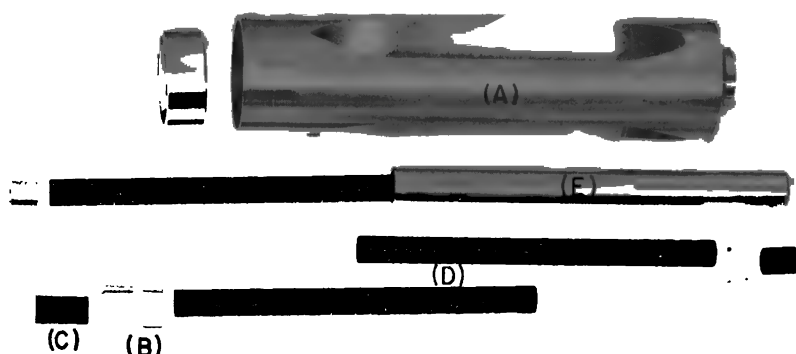


FIG. 8.2 Aluminum capsule for irradiations in MTR X-basket positions at 40°C. (A) Aluminum capsule. (B) Flux monitors. (C) Graphite carrier. (D) Graphite samples. (E) Aluminum sample canning tubes.

aluminum tubes, which were, in turn, sealed into the capsule with a cap weldment.

8-3 High-temperature Irradiations

For the study of radiation effects at high temperatures, a more elaborate class of experiments is necessary. With the exception of the experiments described in Sec. 8-3.1, high-temperature experiments differ from room-temperature experiments in the degree of complexity, and they generally include some method of heating and control to produce the desired test conditions.

8-3.1 UNCOOLED TEST-HOLE FACILITIES (HANFORD)

A large number of irradiations have been performed at elevated temperatures in uncooled test holes in the Hanford reactors. The uncooled test holes, like the cooled test holes, are large-volume irradiation facilities. They were constructed by omitting a line of moderator blocks, thus forming a square hole approximately 4 by 4 in. extending through the reactor. Shield plugs replace the normal reactor shielding and allow access to these holes.

Samples are normally contained in graphite carriers that enable the positioning of many small samples in an ordered configuration. A typical carrier is shown in Fig. 8.3. The properties of graphite make it an excellent material for construction, and the carrier itself can be measured for dimensional changes resulting from irradiation.

8-3.2 CONTROLLED-TEMPERATURE IRRADIATIONS

Without independent control sample temperatures are subject to variation during irradiation. Below 300°C it is especially important to maintain close control of the temperature because of the sensitivity of radiation

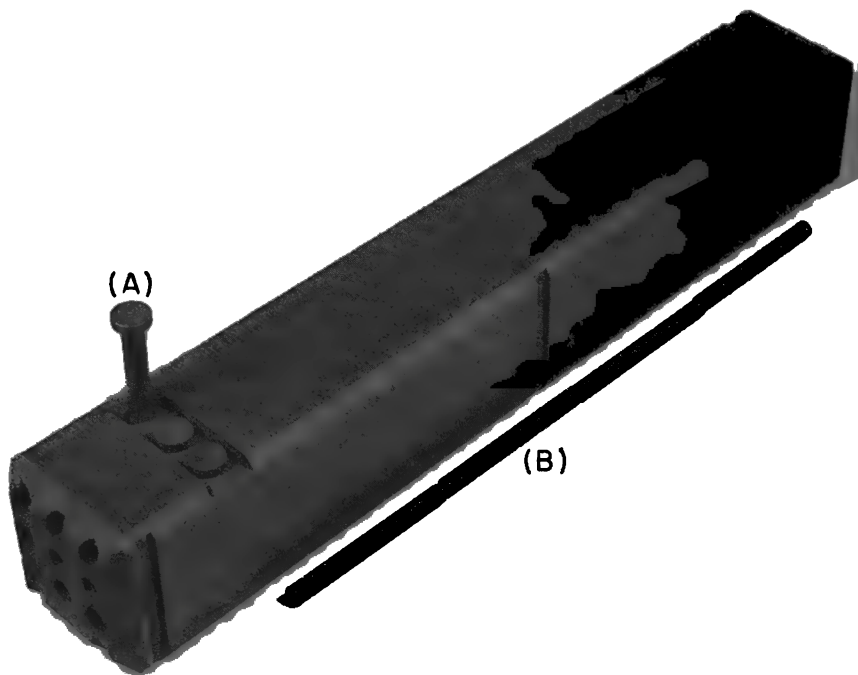


FIG. 8.3 A graphite carrier for positioning small samples for irradiation in an uncooled test hole. Graphite pins (A) retain the samples (B) during handling and irradiation. The graphite carrier is 2 ft long.

effects in graphite to the temperature of irradiation. Above 300°C radiation effects are less sensitive to temperature (see, for example, Fig. 9.20). The degree of control required is, therefore, dependent upon the irradiation temperature. Variations in gamma heating rates caused by shifts in control rods, by over-all changes in reactor power level, and by changes in coolant temperature result in a variable sample heating rate. Thus careful control of sample temperature is essential. In general, the control system should be capable of maintaining temperatures within a few degrees centigrade from room temperature to 300°C and within 50°C from 300 to 1000°C .

Shown in Fig. 8.4 is a device that has been used in Hanford reactors for

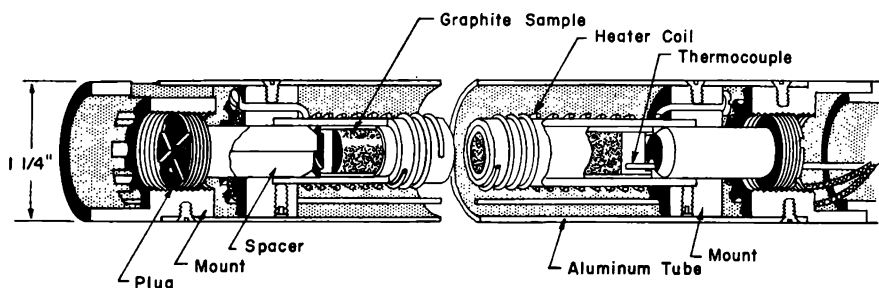


FIG. 8.4 Intermediate-temperature irradiation device.²⁰

irradiations^{19, 20} in the range from 150 to 400°C. The test assembly is made by joining four of the sub-assemblies end to end.

The experiment is contained in an annular tube facility, which is a coaxial-tube arrangement with water flowing between the inner and outer walls. From the relatively constant base temperature set by the coolant in the annulus, the temperature of the sample is raised to the desired operating point by the heaters. Lead wires for the heaters and for the thermocouples are brought out through an access flange. Test samples are cylinders 0.42 in. in diameter by 4 in. long. Two graphite samples contained in an aluminum capsule can be accommodated by each heater unit. All units are connected to a common ground, thus reducing the number of lead wires.

The heater unit was made by first spraying the aluminum tube with alumina, then winding Nichrome-V resistance wire over this, and finally spraying again with alumina. When multiple units are used in one facility, the heaters are operated independently to provide the desired control for each pair of samples. Aluminum, because of its good thermal conductivity and low absorption cross section, is used to maintain uniform temperatures within the sample and to minimize depression of the neutron flux. If operation at higher temperatures were desired, the aluminum parts could be replaced by stainless steel with some reduction in the neutron flux.

8-3.3 EXPERIMENTS AT VERY HIGH TEMPERATURES

A number of graphite irradiations at temperatures in excess of 800°C and a few irradiations to 1200°C have been performed.²¹ At high temperatures materials are seriously affected by the combination of high temperature and neutron flux, and ceramics are usually required for the test devices. In addition, the measurement of temperatures with thermocouples is a difficult problem at irradiation temperatures above 1000°C.

To date, irradiations at very high temperatures have been accomplished in high-flux test reactors, taking advantage of the inherent high gamma heating rate. Two basic concepts based on gamma heating have been employed. In the first, electrical heating is used to control the temperature of irradiation above a base temperature set by gamma heating. In the other, gamma heating alone, in conjunction with a carefully designed irradiation capsule, is used to achieve the desired temperature. In both types of experiments, insulated samples allow operation at high temperatures. The container operates at relatively low temperatures, and the thermal load (about 48,000 Btu/hr/sq ft) is not particularly high.

A temperature-controlled electrically heated irradiation device²¹ used successfully in the MTR core is shown in Fig. 8.5. Three graphite wafer samples (A) are contained in a graphite holder (B). Platinum heaters (C) are encased in alumina and connected mechanically to copper leads (D). Alumina caps (E) cover the sample and contribute to the heating. Small holes in aluminum base plates (F) contain flux monitors. Four holders

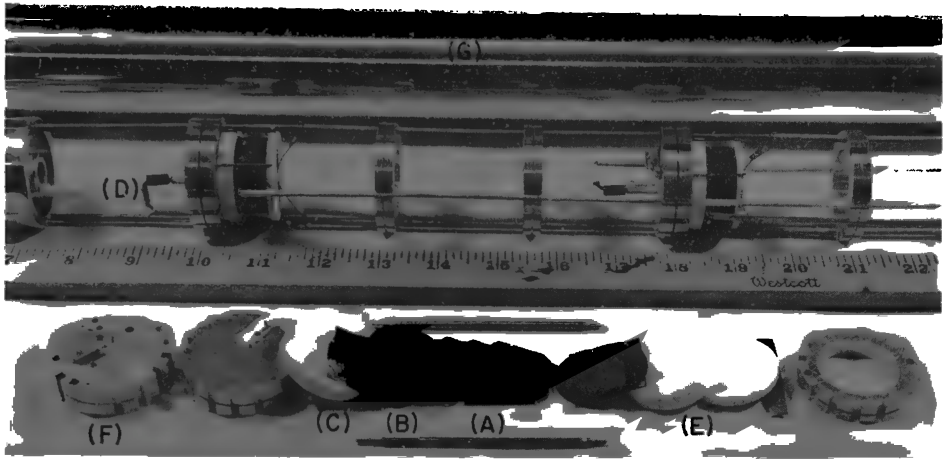


FIG. 8.5 A temperature-controlled capsule for high-temperature irradiations. (A) Graphite (wafer) samples. (B) Graphite holder. (C) Platinum heater. (D) Copper leads. (E) Alumina caps. (F) Aluminum base plate. (G) Aluminum capsule.

with associated heater units are inserted into a 2-in.-diameter aluminum capsule (G), which penetrates the reactor core. In typical operation the samples are heated primarily by gamma radiation, and the heater acts as a thermal barrier to control the heat loss to the aluminum base plate, thereby controlling the temperature of the sample. The heater, sample, and caps are held in tight contact by a molybdenum leaf spring between two supporting molybdenum posts. Aluminum cooling rings are spaced between the sample units to prevent the thermocouple and heater wires from melting. Helium gas is used to provide an inert atmosphere. Similar capsules have been operated in the ETR and in an MTR safety rod. Long-term temperature stability of $\pm 10^\circ\text{C}$ at 1000°C has been maintained for experiments of four months duration at fluxes of 3×10^{14} neutrons/cm²/sec ($E > 0.18$ Mev).

Noncontrolled experiments heated entirely by gamma radiation have provided a substantial amount of very high temperature graphite irradiation data. Figure 8.6 shows a capsule¹⁷ that has been used in a high-flux position of the General Electric Test Reactor (GETR). Four quarter-round samples (A) form a cylinder and fit into graphite retaining caps (B). A molybdenum disk (C) is used to position the samples within the aluminum cooling rings (D). The holder is designed to accommodate thermal expansion of the samples. The temperature is attained by gamma heating in the sample and related parts, all being designed to afford the proper heat leakage to attain the desired irradiation temperature of 800°C . Thermocouples are placed in the samples to monitor the temperatures during irradiation. Such a capsule is subject to variations in the gamma heating rate as reactor conditions change but is relatively stable ($\pm 20^\circ\text{C}$) at temperatures near 1000°C owing to high heat losses by thermal radiation.

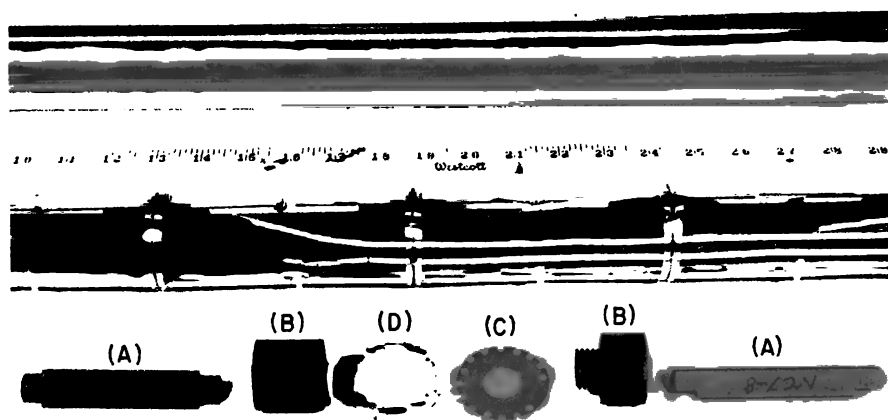


FIG. 8.6 A noncontrolled high-temperature capsule. (A) Quarter-round samples. (B) Graphite retaining caps. (C) Molybdenum positioning disk. (D) Aluminum cooling rings.

Irradiation temperatures up to 1200°C have been maintained with similar capsules.

Only a limited number of samples can be irradiated in instrumented tests, which are themselves limited by both cost and available irradiation space. Therefore noninstrumented gamma-heated experiments have been used to provide preliminary information. In this type experiment the temperature of the sample is calculated on the basis of the gamma heating rate and is assumed to be the irradiation temperature attained. A typical device for such an experiment consists of four quarter-round samples, similar to those shown in Fig. 8.6, banded together at their ends and insulated from the capsule with aluminum oxide rods. The rods fit axially drilled holes in the sample group and serve to skewer the samples in the capsule. If higher temperatures are desired, the capsule can be evacuated to reduce heat loss by gas convection and conduction.

8-4 Controlled-atmosphere Irradiations

Gas reactions with graphite are accelerated by formation in the reactor of active gaseous species. Irradiation experiments are conducted to study the effect of radiation on the kinetics of these reactions and on the nature of the products formed. Special problems are encountered in conducting controlled-atmosphere irradiations. The materials of construction must not react with gaseous or solid test materials. Other considerations in the selection of materials are strength, susceptibility to radiation damage, flux depression, and activation. Provisions for emergency cooling and reactor safety may be required in the design of the experiment.

The methods used in the study of gas-graphite reactions are described in this section. The results are discussed in Chap. 14.

8-4.1 LOW-PRESSURE GAS LOOPS

(a) *BEPO Glass Apparatus*. A low-pressure gas loop^{22,23} constructed entirely of borosilicate glass and fused silica was operated in BEPO to study the radiation-induced carbon dioxide-graphite reaction and the decomposition of carbon dioxide. The characteristics of the loop are given in Table 8.1. Since gas analysis was selected as the method to be used in following the course of the reaction, it was essential that all contaminants be excluded from the system. Glass and fused silica were selected as the materials of construction to eliminate contaminants that could form carbon monoxide from carbon dioxide during the irradiation. The loop contained no greased surfaces.

Table 8.1 — CHARACTERISTICS OF THE BEPO GLASS LOOP²²

Graphite sample dimensions:	
Length, in.	8
Outside diameter, in.	0.75
Inside diameter, in.	0.375
Temperature range, °C	27 to 450
Gas pressure range, atm	0.3 to 3
Gas flow rate, grams CO ₂ /min	0.9 to 3.7
Thermal-neutron flux at reactor power of 6 Mw, neutrons/cm ² /sec	9.7 x 10 ¹¹

The loop, shown in Fig. 8.7, consisted of a gas-handling and -purification system, a circulating system, an in-pile assembly, and a gas-transfer and -analysis system. The gas was purified by conventional methods utilizing oxidizing and reducing agents and was finally fractionated before being introduced into the circulating system. Circulation of the gas was accomplished with an all-glass electromagnetically operated pump.²⁴ Each stroke of the glass piston, which contained a soft-iron core, forced gas past check valves and into the in-pile assembly.

The in-pile assembly was 21¼ ft long and contained a shielding plug from which aluminum support tubes were suspended to hold the sample heater. A cylindrical graphite sample was centered within a Nichrome wire-wound heater. Temperatures were measured by means of glass-insulated chromel-alumel thermocouples. Gas samples were withdrawn from the loop periodically and analyzed by a Blacet-Leighton gas micro-analysis apparatus.²⁵

In addition to providing data on the radiation-induced carbon dioxide-graphite reaction (see Sec. 14-2.6), the loop demonstrated the suitability of quartz for in-pile experimentation.

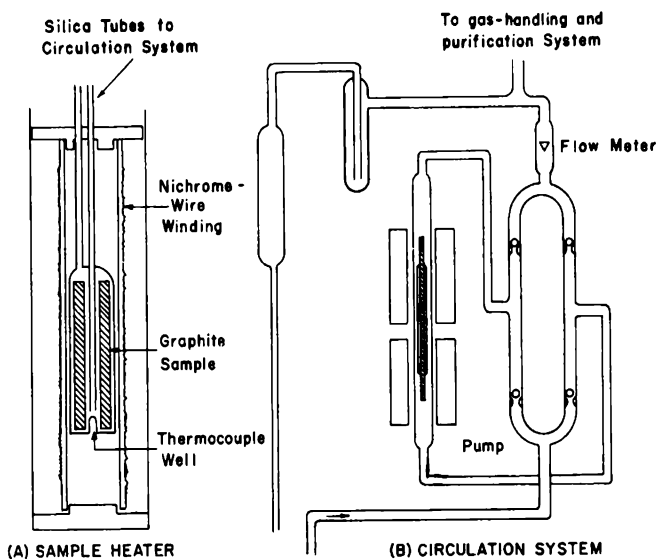


FIG. 8.7 Sample-heater assembly (A) and gas-circulation system (B) of the BEPO loop. (From Davidge and Marsh, British Report AERE-C/R-1374, Ref. 22.)

(b) *Hanford Gamma Facility.* A Co^{60} gamma irradiation facility has been constructed at Hanford to investigate the effect of gamma radiation on the rates of reaction of various gases with graphite (Table 8.2). The source

Table 8.2 — HANFORD Co^{60} GAMMA FACILITY

Dimensions of cylindrical test spaces:	
Diameter, in.	2
Length, in.	7
Dose rate in test spaces, rad/hr	1.2×10^6
Strength of source, curies	1.5×10^4
Usable temperature range, °C	25 to 700
Maximum gas pressure, atm	1
Maximum flow rate, grams CO_2 /min	4

is located at the bottom of a water-filled stainless-steel tank 7 ft in diameter by 14 ft deep. The source holder, constructed of stainless steel, positions the radioactive cobalt rods on a 6-in.-diameter circle. The cobalt pieces, with aluminum spacers to provide a more uniform field, are enclosed in stainless-steel tubing with welded end caps. The source holder is designed to accept four 2-in.-diameter stainless-steel tubes. The irradiation tubes extend from the bottom of the tank to 3 ft above the water level. The dose rate in the 2-in.-diameter tubes, as measured by ceric sulfate dosimeters,

was 1.2×10^6 rad/hr when the facility was completed in July 1959. The maximum variation in gamma flux is 6 per cent over a length of 7 in.

Glass loops of the reentrant type are employed to circulate gas over the graphite samples, which are maintained at a constant temperature in the radiation flux. The annulus between the metal and glass tubes impedes heat transfer to the shielding water. The 2000-watt sample heater consists of a Nichrome winding completely enclosed in quartz so that circulating gas does not contact the hot heater wires. Gas is supplied from a purification train and is either exhausted after a single pass through the loop or recirculated with an all glass pump similar to the type described previously for the BEPO loop. Positioned over the glass-loop tubes are recording semi-microanalytical balances enclosed in glass bell jars. Cylindrical graphite samples 0.5 in. in diameter by 2 in. long are suspended within the radiation flux by a platinum wire attached to one arm of the balance. Radiation-induced chemical reactions have been studied in this facility at controlled temperatures as high as 700°C.

8-4.2 HIGH-PRESSURE GAS LOOPS

(a) *Model Channel in BEPO.* The carbon dioxide-cooled PIPPA model channel²⁶ in BEPO and the Plutonium Recycle Test Reactor (PRTR) gas-cooled loop²⁷ are examples of high-pressure recirculating facilities that have been constructed to investigate gas-graphite reactions at conditions expected to prevail in gas-cooled reactors. The purpose of the model-channel loop (Table 8.3) was to study the graphite-carbon dioxide reaction under

Table 8.3 — PIPPA MODEL CHANNEL IN BEPO

Diameter of test section, in.	6
Inlet gas temperature, °C	140
Outlet gas temperature, °C	336
Gas pressure, atm	7.5
Maximum gas flow rate, grams CO ₂ /sec	148
Thermal-neutron flux, neutrons/cm ² /sec	10^{12}

irradiation conditions representative of a channel in the Calder Hall reactors. Inlet and outlet loop gas temperatures, gas pressure, and the fraction of the total gas under irradiation were equivalent to the operating conditions in the Calder Hall reactors.

The main loop of the model channel consisted of a longitudinal test section, a filter, a gas cooler, gas circulators, a delay vessel, and a gas heater. A block diagram of the gas flow circuit is shown in Fig. 8.8. The reactor test section was constructed from a stainless-steel tube 6 in. in inside diameter by 48 ft long with an 0.08-in.-thick wall. The graphite sample train consisted of blocks 1 ft in length. The top half of the train could be unloaded without disturbing either the lower half or the fuel

elements supported by the lower graphite pieces. Blocks forming the top half of the train also contained removable graphite samples. The gas filtration agent was coarse-fibered boron-free glass wool. Two gas-bearing compressors, one of which was maintained as a stand-by unit, circulated the

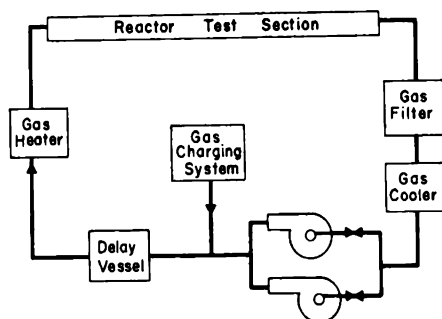


FIG. 8.8 Block diagram of the gas flow circuit in the carbon dioxide-cooled PIPPA model channel in BEPO. Carbon dioxide is circulated by gas-bearing compressors over a removable graphite stringer.²⁶

loop gas. The gas flow rate was controlled by a variable-frequency generator supplying power to the gas circulators. The delay vessel was internally baffled and sized to satisfy the in-pile to out-of-pile ratio requirement. The gas-charging system consisted of a Cardice converter, a reducing valve, a silica gel drier, and a metering vessel to measure the make-up volume.

Welded joints were used wherever possible to minimize gas leakage. Flanges with annealed copper gaskets also proved satisfactory. A silicone rubber O-ring seal was selected for the gas inlet end of the in-pile test section (outside the radiation field) since the temperature at this point was about 150°C.

(b) *The PRTR Gas-cooled Loop.* The PRTR gas-cooled loop²⁷ will be installed in the PRTR at Hanford during 1962. The design characteristics are listed in Table 8.4. Although the loop is intended primarily for the study of reactions of reactor coolant gases with graphite, it was designed

Table 8.4 — PRTR GAS LOOP²⁷.

Dimensions of cylindrical test space:	
Diameter, in.	2.9
Length, ft.	9
Maximum gas outlet temperature, °C	815
Heat-removal capacity, kw	500
Maximum gas pressure, atm	35
Maximum gas flow rate, grams CO ₂ /sec	1900
Thermal-neutron flux, neutron/cm ² /sec	4 x 10 ¹³

as a versatile general-purpose irradiation testing facility and will be capable of removing up to 500 kw of fission heat.

The PRTR is of vertical-pressure-tube design, employing heavy water both as coolant and moderator, and has a rated thermal power level of 70 Mw. The in-pile section of the gas loop will replace one of the 85 reactor process tubes. Carbon dioxide will flow through the loop test section from top to bottom. The test section, consisting of an outer pressure tube and an inner removable liner, is to be fabricated from Hastelloy-X alloy. The liner will be suspended within the pressure tube from a support and will be free to expand independently of the outer tube. A stagnant layer of carbon dioxide at loop pressure will fill the annulus between the tubes and will provide thermal insulation.

A flow diagram²⁷ of the loop is shown in Fig. 8.9. Under typical operating conditions gas at the inlet to the blowers is controlled at 450 psig and 425°C. As the gas passes through the blowers, which have self-acting gas-lubricated bearings, the gas pressure will be increased to 500 psig. The gas

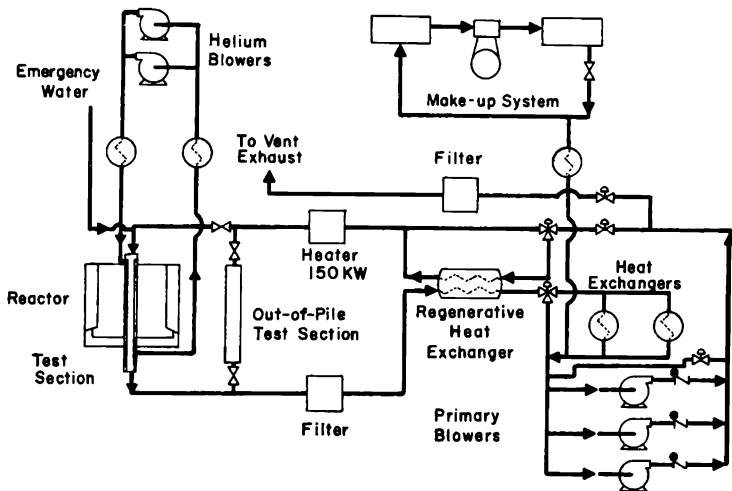


FIG. 8.9 Flow diagram of the PRTR gas loop. (From Baker et al., Monograph No. 7 of the Franklin Institute, Ref. 27.)

will then pass through a regenerative heat exchanger and an electrical preheater, which supplements fission heat whenever necessary to maintain the desired temperature. The heater will utilize a bath of sodium-potassium alloy (NaK) as the heat-transfer agent. A bundle of Hastelloy-X tubes carrying the carbon dioxide will traverse this bath, and tubes near the periphery of the heater will carry electrical heating elements. This heater design minimizes the portions of the vessel which must withstand loop pressures and utilizes easily replaceable heating elements that will not contact the carbon dioxide.

From the preheater the gas will pass through one of two test sections before entering the high-temperature filter, where 99.5 per cent of the particles larger than $1\text{ }\mu$ will be removed. The filtration agent will be a spun alumina-silica fiber that will withstand the 815°C gas temperature. The gas will then be returned to the regenerative heat exchanger and will pass through two water-cooled heat exchangers operating in parallel, where the gas temperature will be lowered to the allowable blower inlet temperature of 425°C . Helium will be circulated in the annulus between the loop tube and the surrounding reactor shroud tube.

The purpose of the out-of-pile test section is to separate the radiation effects from thermal effects. It will be capable of closely duplicating conditions in the in-pile test section except for radiation.

Instruments will control the process variables automatically and provide a graphic display of conditions existing in the loop. Alarms will warn of abnormal conditions within the loop, and interlocks will shut down both the loop and the reactor under certain conditions. The analysis of gases in the loop and make-up system will be obtained from a continuous-process mass spectrometer and a gas chromatograph.

Graphite samples will be removed from the loop by means of retrieving tools and a special sample cask. Samples containing fissionable materials will be discharged with the reactor fueling machine.

8-4.3 ELECTRICAL-DISCHARGE EXPERIMENTS

A microwave glow discharge is a convenient method of producing free radicals or atoms in gases to simulate some of the effects of reactor radiation. The reaction between carbon dioxide and graphite in a microwave glow discharge has been studied by Clark²⁸ with a microwave generator

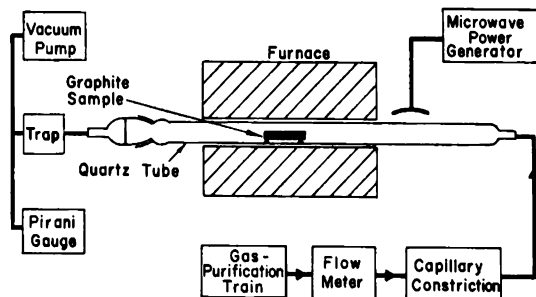


FIG. 8.10 Block diagram of microwave glow-discharge assembly.²⁸

providing 125 watts at 2450 Mc. A block diagram of the equipment is shown in Fig. 8.10. The glow is started with a Tesla coil and can be maintained at carbon dioxide pressures from 50 to $500\text{ }\mu$ with a clean reaction tube.

Although microwave glow-discharge experiments are relatively simple to perform, there is not yet enough experience with this type radiation to

correlate the data readily with results from graphite oxidation experiments in nuclear reactors.

The reaction between graphite and electrically activated carbon dioxide has been studied in England²⁹ by means of an electrodeless discharge from high-frequency generators operating at 19 and 1.5 Mc/sec. A sample was suspended from a calibrated silica spring, and weight changes were observed with a cathetometer. The pressure of carbon dioxide was maintained at 3 mm or less, and provisions were included for adding a second gas or volatile liquid to study inhibition reactions. The emission spectrum of the activated gas was examined with a spectrograph, and several active species, including atomic oxygen, were identified. Studies were also conducted at atmospheric pressure in a bank of ozonizers.

The possibility of a radiation-induced reaction between helium and graphite was investigated³⁰ in a helium plasma generated by 2400-Mc/sec microwave radiation. Thin carbon films deposited on silica rods were suspended in the plasma. No evidence was found for a reaction between excited helium atoms or ions and carbon.

8-5 Reactor-graphite Monitoring Methods

The experimental study of radiation effects in graphite is complemented by measurements of dimensional changes in a graphite moderator itself and by extraction of small samples for property measurements. The study of gross moderator behavior is extremely useful from an engineering standpoint and cannot be fully duplicated with small samples. Conversely, the extreme complexity of evaluating the actual behavior of the moderator and the samples therefrom annuls the self-sufficiency of this technique. This section discusses the methods used for monitoring Hanford moderators. They are, with suitable modification, general enough to be used with other graphite-moderated reactors.

8-5.1 DIMENSIONAL CHANGES

Vertical-height and horizontal-bowing measurements are made to observe gross dimensional changes of the graphite moderator. The simplest and also the most accurate measurement of distortion is accomplished by pulling a target through a selected channel in a moderator and observing it with a transit that has been referenced to some fixed point.³¹ For measurement of the relative vertical height through horizontal channels, a mercury-manometer arrangement is used in which the level of mercury in a tube is measured while a connecting mercury reservoir is being pulled through the channel.

8-5.2 MODERATOR SAMPLING

Samples can be removed from the moderator in the form of solid pieces or powder. Small cylindrical samples are obtained by coring through the wall of the tube blocks.³² This is accomplished by inserting a device such

as that shown in Fig. 8.11 into a fuel channel from which the process tube has been removed. The saw is a tungsten carbide-tipped threaded cylinder with a very thin wall. The saw is pinned in slots of the containing housing to prevent rotation but to allow translation. When the housing is rotated, the saw moves through the threaded upper bearing plate into the graphite.

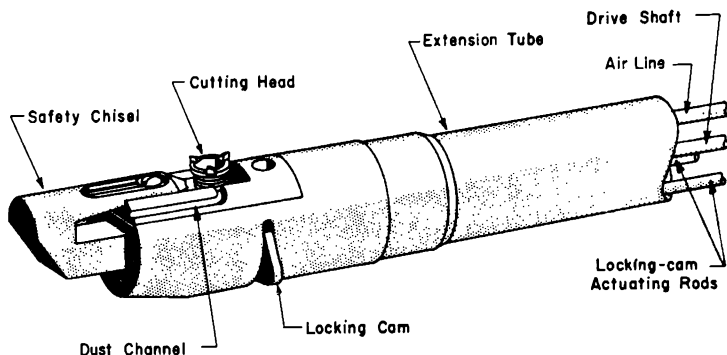


FIG. 8.11 Graphite core borer.²² Rotation of the driveshaft causes the threaded saw to be rotated out from the housing. Each rotation of the saw extends the cutters 0.04 in.

The drive shaft is turned until the saw, passing through the block, reaches its limit of travel. During the cutting operation compressed air is forced through the saw to blow away graphite chips and dust. The operation is reversed after a core has been cut. A chisel capable of shearing the saw is mounted on the core borer to enable removal of the core borer from the channel in the case of malfunction.

If a complete core is not required, channel scrapings can be removed to a depth of $\frac{1}{4}$ in. by a device with protruding teeth which is rotated in the channel. The sample is gathered by vacuuming the scrapings into a collection bottle. Although powder samples can be obtained more easily than cores, it should be recognized that only the surface of the channel is sampled, and this may or may not be typical of the entire graphite block. The core sample, on the other hand, can be studied for average properties or can be sectioned for a study of damage gradients.

8-5.3 OXIDATION MONITORING

The reaction of oxidizing gases with the graphite moderator results in the removal of graphite from the reactor core. The extent of oxidation of a permanent graphite-moderator structure can be measured from the weight loss of replaceable samples that are removed at intervals from the core.²⁶ Sample positions should be selected to cover a range of temperature and radiation-flux conditions. This is most easily accomplished if suitable sample positions and the mechanical details for sample removal are in-

cluded in the core design. Postirradiation measurements of the monitoring samples may also reveal changes in moderator strength due to the combined effects of oxidation and irradiation.

References

1. G. R. Hennig et al., Radiation Effects on the Oxidation Rate and on Other Chemical Properties of Graphite, in *Proceedings of the Second United Nations International Conference on the Peaceful Uses of Atomic Energy, Geneva, 1958*, Vol. 7, pp. 301-306, United Nations, New York, 1959.
2. R. E. Woodley, *Promotion of Chemical Reaction in Gas-Graphite Systems by Gamma Radiation*, USAEC Report HW-31929, Hanford Atomic Products Operation, May 24, 1954.
3. J. H. Buck and C. F. Leyse, *Materials Testing Reactor Project Handbook*, USAEC Report TID-7001, May 7, 1951.
4. P. D. Bush et al., *Engineering Test Reactor Engineering Design and Safeguards Report*, USAEC Report IDO-24020, Idaho Operations Office, July 1956.
5. S. S. Jones, W. R. Langdon, and T. T. Naydon, General Electric Company, New Radiation Test Facilities in the General Electric Company, in *Third Semiannual Radiation Effects Symposium, October 28, 29, 30, 1958*, Vol. 1, Paper 4 Lockheed Aircraft Corporation.
6. *Westinghouse Testing Reactor Facility Description*, Westinghouse Electric Corporation, Pittsburgh 30, Pa.
7. H. P. Yockey et al., Cyclotron Techniques for Radiation Damage Studies, *Rev. Sci. Instr.*, **25**: 1011-1019 (1954).
8. H. P. Yockey et al., *The Use of Cyclotron Irradiation in the Study of Radiation Effects on Materials*, USAEC Report NAA-SR-186, North American Aviation, Inc., Dec. 16, 1952.
9. S. B. Austerman and J. E. Hove, Irradiation of Graphite at Liquid Helium Temperatures, *Phys. Rev.*, **100**: 1214-1215 (1955).
10. S. B. Austerman, *Low-Temperature Irradiation and Annealing Experiments in Graphite*, USAEC Report NAA-SR-2457, North American Aviation, Inc., July 15, 1958.
11. A. W. McReynolds et al., Neutron Irradiation Effects in Cu and Al at 80°K, *Phys. Rev.*, **98**: 418-425 (1955).
12. M. W. Thompson and D. W. Jefferson-Loveday, A Cryostat for Reactor Irradiations in Liquid Nitrogen, *J. Sci. Instr.*, **35**: 397-399 (1958).
13. C. C. Sartain and H. P. Yockey, Cryostat for Reactor Irradiation, *Rev. Sci. Instr.*, **29**: 118-121 (1958).
14. R. R. Coltman et al., Techniques and Equipment Utilized in Low Temperature Reactor Irradiations, *Rev. Sci. Instr.*, **28**: 375-380 (1957).
15. J. C. Fox, *Special Irradiations Manual*, USAEC Report HW-29548, Hanford Atomic Products Operation, May 16, 1954. (Classified)
16. C. A. Preskitt, Oak Ridge National Laboratory, personal communication, August 1960.
17. J. M. Davidson and J. W. Helm, *The H-3 Irradiation Experiment: Irradiation of EGCR Graphite. Interim Report No. 1*, USAEC Report HW-71500-A, Hanford Atomic Products Operation, Oct. 16, 1961.
18. H. H. Yoshikawa, *Fast Neutron Fluxes in Hanford Reactors*, USAEC Report HW-64393, Hanford Atomic Products Operation, May 3, 1960. (Classified)
19. J. F. Fletcher, *Controlled Temperature Irradiations of Graphite, Interim Report No. 3, PT106-403-P*, USAEC Report HW-36221, Hanford Atomic Products Operation, Sept. 5, 1956. (Classified)

20. K. Koyama, *Controlled Temperature Irradiation of Graphite, Interim Report No. 4 PT-IP-22A*, USAEC Report HW-62453, Hanford Atomic Products Operation, Oct. 21, 1959.
21. J. M. Davidson, Hanford Laboratories, General Electric Company, unpublished data, 1956.
22. P. C. Davidge and W. R. Marsh, *The Effect of Pile Radiation on the Carbon Dioxide-Graphite Reaction*, British Report AERE-C/R-1374(Del.), January 1956.
23. H. B. F. Gow and W. R. Marsh, Temperature Effects on the Radiation Induced Reaction of Carbon Dioxide with Graphite, in *Proceedings of the US/UK Meeting on the Compatibility Problems in Gas-cooled Reactors, Held at Oak Ridge National Laboratory, February 24-26, 1960*, pp. 16-38, USAEC Report TID-7597(Bk. 1), 1961.
24. N. S. Corney et al., *A Glass Enclosed Gas Circulating Pump*; British Report AERE-C/M-364, 1959.
25. F. E. Blacet and P. A. Leighton, A Dry Method of Microanalysis of Gases, *Ind. Eng. Chem., Anal. Ed.*, **3**: 266-269 (1931).
26. A. R. Anderson et al., Chemical Studies of Carbon Dioxide and Graphite Under Reactor Conditions, in *Proceedings of the Second United Nations International Conference on the Peaceful Uses of Atomic Energy, Geneva, 1958*, Vol. 7, pp. 335-373, United Nations, New York, 1959.
27. D. E. Baker et al., The PRTR Gas-cooled Loop, in *Gas-cooled Reactors: Proceedings of the Symposium Sponsored Jointly by the Franklin Institute and the American Nuclear Society, Delaware Valley Section, February 10 and 11, 1960*, Franklin Institute Monograph No. 7, pp. 313-325, May 1960.
28. T. J. Clark, *Gas-Graphite Reactions. I. Thermal and Microwave Oxidation of Various Reactor-grade Graphites*, USAEC Report HW-63855, Hanford Atomic Products Operation, Feb. 10, 1960.
29. H. C. Cowen and R. Lind, The Reaction Between Graphite and Carbon Dioxide in Electric Discharges, in *Proceedings of the US/UK Meeting on the Compatibility Problems of Gas-cooled Reactors Held at Oak Ridge National Laboratory, Feb. 24-26, 1960*, pp. 173-187, USAEC Report TID-7597(Bk. 1), 1961.
30. I. N. Onslow MacAulay and M. Tomlinson, On the Possibility of Radiation Induced Transport of Carbon in Helium, in *Proceedings of the US/UK Meeting on the Compatibility Problems of Gas-Cooled Reactors Held at Oak Ridge National Laboratory, Feb. 24-26, 1960*, pp. 191-205, USAEC Report TID-7597(Bk. 1), 1961.
31. R. W. Powell et al., Control of Radiation Effects in a Graphite Reactor Structure, in *Proceedings of the Second United Nations International Conference on the Peaceful Uses of Atomic Energy, Geneva, 1958*, Vol. 7, pp. 282-294, United Nations, New York, 1959.
32. J. M. Davidson, *Pile Graphite Core Borer*, USAEC Report HW-41884, Hanford Atomic Products Operation, Mar. 12, 1956.

Radiation-induced Structural and Dimensional Changes

R. E. NIGHTINGALE, H. H. YOSHIKAWA, and E. M. WOODRUFF†

9-1 Radiation Effects on Crystal Structure

Radiation-induced changes to the crystal structure of graphite were first observed by Zachariasen^{1,2} in 1945. He noted that, as a result of short exposures in a Hanford reactor, the c spacing increased. A small decrease in the a spacing was also observed. Because crystal-structure changes seemed to provide an explanation for macroscopic length changes and because they were also basic to an understanding of the changes in other properties, a great deal of effort has been expended on subsequent structure studies. An excellent review³ summarizes the results of room-temperature irradiations conducted in England and the United States to about 1955. Subsequent work has not significantly changed the interpretation of crystal-structure changes near room temperature. The effects of irradiation at higher exposures and higher temperatures have been reported^{4,5} since 1955.

9-1.1 X-RAY LINE SHAPES

In many ways the X-ray diffraction patterns of irradiated graphite resemble the patterns of poorly graphitized carbon. Neutron irradiation causes the lines to become diffuse and to shift in the direction expected for an expanded c spacing. There are some significant differences, however, which become apparent, particularly when the effects of annealing are studied. Figure 9.1 illustrates the continuous deterioration of the X-ray powder diffraction pattern for a series of irradiations.

The first observable change is a shift of the (006) and (004) lines to lower angles caused by an increase in the c spacing. This occurs initially with very little broadening of the lines. As the dose increases, the (006) and (004) lines become more diffuse and finally disappear entirely.

The changes of the (002) line, which have been extensively used to calculate changes in c spacing and apparent crystallite size, L_c , have been studied in considerable detail. The changes in line profiles for exposures up to 1500 Mwd/At are given in Fig. 9.2. The relative intensities are not to scale since different amounts of powder were used in obtaining the profiles. The (002) peak for unirradiated graphite appears to shift with little

† Hanford Laboratories, General Electric Company, Richland, Wash.

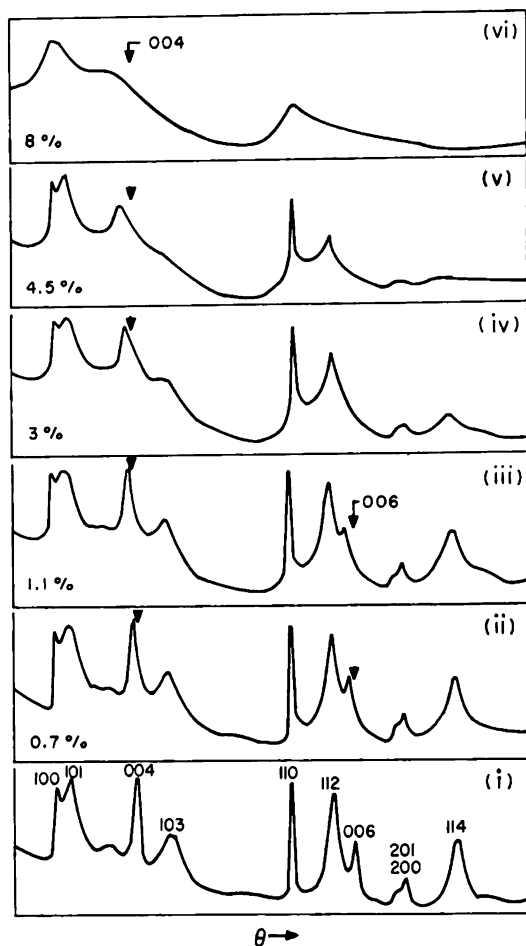


FIG. 9.1 Photometer traces of X-ray diffraction photographs of irradiated graphite showing the continuous deterioration of structural perfection. The arrows on curves ii-vi indicate the position of the (004) and (006) peaks before irradiation (curve i). The numbers to the left of the curves give the increase in c dimension, thus serving as an index of the degree of irradiation. The (002) line is outside the range (to the left) of these photometer traces. (From Bacon and Warren, *Acta Crystallographica*, Ref. 3.)

change in shape for exposures up to 680 Mwd/At, after which the lines rapidly become broadened. A very pronounced shoulder on the high-angle side of the peak appears on the 860 Mwd/At sample, giving an appreciable intensity even at angles corresponding to a c spacing of 6.70 Å. With increasing exposures the tail increases in relative intensity and the sharp component decreases; the result is, finally, a very broad symmetrical line.

This increase in scattering at higher angles has been reported by others³ for both the (002) and (004) peaks of irradiated graphite. The line profiles have the appearance of sharp crystalline reflections superimposed on a broad background of temperature-diffuse scattering. Since tempera-

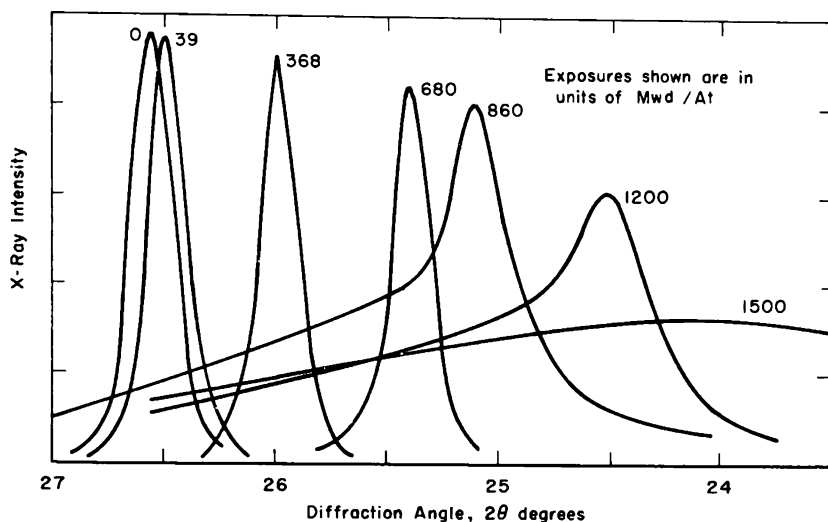


FIG. 9.2 Effect of irradiation at 30°C on the (002) line. Note the initial peak shift with little broadening. After 1500 Mwd/At the line is very broad and diffuse.⁶

ture-diffuse scattering is greater at higher orders of reflection, this analogy suggests that the sharp component should form a smaller part of the (004) peak than it does of the (002) peak. The fact that the sharp component disappears³ at a lower exposure on the (004) peak than on the (002) peak indicates that this is the case.

9-1.2 LINE BROADENING

Changes in the breadth of the (002) line with exposure at 30°C are plotted in Fig. 9.3. The accelerated broadening between 800 and 2000 Mwd/At is a distinguishing feature of this curve. There are no rapid changes in the physical properties corresponding to this exposure, although in the more crystalline nuclear graphites (KC and to a lesser extent CSF) the growth rate increases slightly in this exposure range (see Fig. 9.12). One might speculate that at an exposure of about 800 Mwd/At expansion of the *c* spacing becomes increasingly restricted as the voids into which the crystallites expand become smaller. The resulting compressive stresses on the crystallites would then be reflected in broadened diffraction lines. In this case a reduced rate of broadening would be possible only when the stresses are relieved by crystal twinning and fracture. No investigations have been reported on the line broadening of extremely fine particles such as graphite wear dust or on single crystals where crystallite motion would be less restricted.

Although the cause of line broadening over other parts of the exposure range in Fig. 9.3 has been discussed by several workers (Refs. 3, 6, and 8 to 11), the explanations are not entirely clear and satisfying. Some of the difficulties were noted in Sec. 5-6.3. The work of Bacon and Warren³ indi-

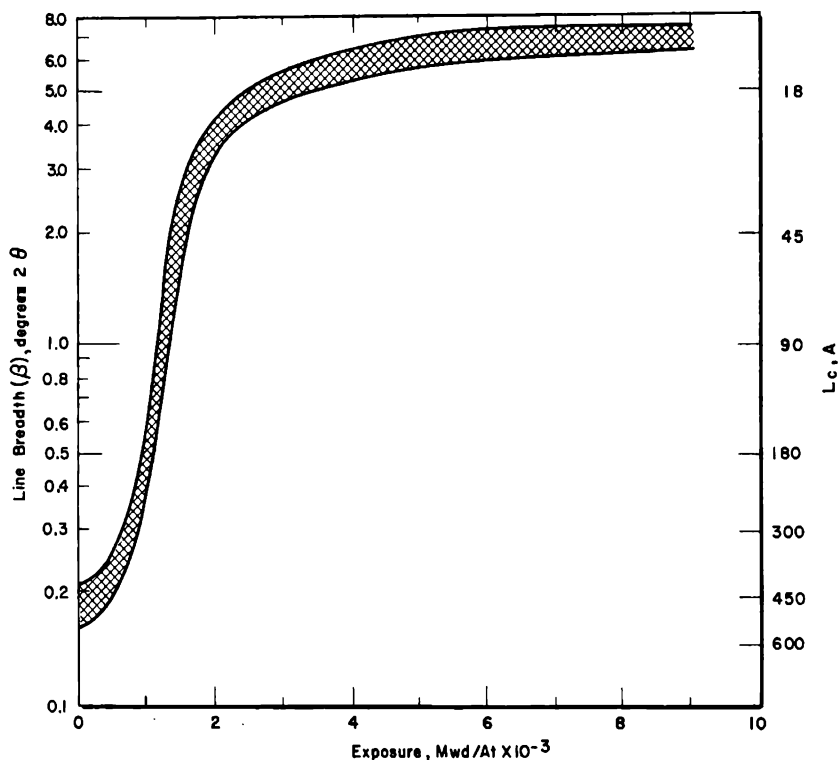


FIG. 9.3 Broadening of the (002) line in CSF at 30°C. The band shows the scatter of data for different samples. Line breadth has been corrected for instrumental broadening by the Jones method⁷ using $d = 0.08^\circ$ and $b = 0.106^\circ$. L_c values, calculated by assuming that the broadening is due entirely to crystallite size, are shown on the right.

cates that at least to $\Delta c/c_0 = 6$ per cent (~ 1200 Mwd/At at 30°C) the crystals do not break up and that line broadening is therefore associated with short-range lattice distortions. This conclusion is based upon the observation that after irradiation the diffraction patterns of two graphites with initially different crystallinities were restored by annealing to 1500°C. It was concluded that, although the layers may buckle and bend, their dimensions and the probability of layer displacement within the stacks of layers are largely unchanged, and atomic displacements in graphite irradiated to moderate exposures take place without permanently disrupting the layers.

Townsend and Lund⁶ compared the (002) peak shapes of irradiated graphite with the diffraction patterns of carbon blacks and lampblacks, which are known to consist of minute crystallites. Based on the similarity of physical properties and diffraction patterns, they ascribed the broadening in highly irradiated graphites (> 2000 Mwd/At at 30°C) to a decrease in crystallite size. The results of annealing studies also favor this theory since temperatures sufficient to cause crystallite growth in carbons are required

to reduce the line breadths to unirradiated values. For example, the (0 0 2) line breadth of highly irradiated (5700 Mwd/At at 30°C) graphite anneals very little below 1250°C. Most annealing occurs in the 1400 to 1800°C range (Sec. 13-3.1).

Broadening of the other peaks in highly damaged graphite results in a diffraction pattern characteristic of the two-dimensional turbostratic stacking described by Warren.¹² The (1 0 1) and (1 1 2) peaks disappear, and the (1 0 0) and (1 1 0) peaks show a characteristic asymmetry with the low-angle side of the peak dropping off more rapidly than the high-angle side. The apparent crystallite size calculated¹³ from the (1 0 0) peak of CSF after an exposure of 3000 Mwd/At at 30°C is 12 Å; for the (1 1 0) peak it is 14 Å. After this same exposure L_c , measured from the (0 0 2) peak, is 12 Å.

9-1.3 CHANGES IN c AND a SPACING

The increase in c spacing measured from the shift in the (0 0 2) reflection is shown as a function of dose in Fig. 9.4. The scatter in experimental points encompassed by the band reflects slight differences in structure of

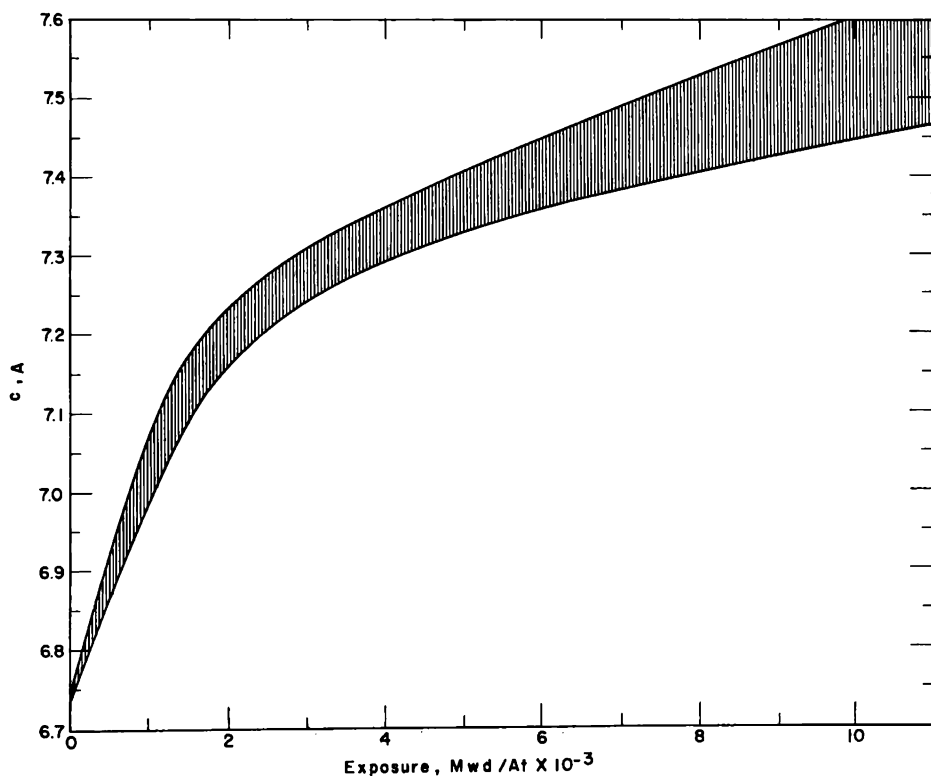


FIG. 9.4 Expansion of c spacing at 30°C in CSF graphite. The band shows the range of values obtained for different samples.

the unirradiated samples and differences in the temperature and neutron flux to which the samples were exposed. Other nuclear graphites show the same general behavior. The c values in Fig. 9.4 lie below most earlier published values for two reasons. Line profiles must be corrected for geometrical, polarization, and form factors, especially at the higher exposures. These corrections, which have the effect of reducing c , were made in Fig. 9.4, whereas they were not, in some cases, applied to earlier data. At 2000 Mwd/At these corrections reduce the c spacing by about 0.08 Å. At 4000 Mwd/At the reduction is about 0.20 Å. The values of c also depend upon the method used to determine the Bragg angle, θ . Two methods, which yield considerably different values for c in the case of the broad asymmetrical peaks obtained at exposures greater than about 700 Mwd/At, have generally been employed. In the first method θ is taken as the center of the peak at half-peak intensity. In the second θ is taken from the maximum intensity of the profile. The former method, which results in smaller values of c , was used in Fig. 9.4. At 2000 Mwd/At the difference in c calculated by the two methods is about 0.10 Å. At 4000 Mwd/At the difference is 0.20 Å. As the peaks become broader, both methods become more difficult to apply accurately, and the physical significance of the calculated c is less clear.

A limited amount of data has been reported on the effect of the initial crystallinity on radiation-induced c -spacing changes. In contrast to the definite effect of crystallinity on bulk dimensional changes (Sec. 9-3), the c expansion is rather insensitive to the crystallinity of the unirradiated graphite. The Δc of an experimental Korite graphite ($c_0 = 6.87$ Å) remains approximately equal¹⁴ to that of CSF ($c_0 = 6.73$ Å) to 4000 Mwd/At. Similar c expansion rates for low doses (<1000 Mwd/At) have also been observed¹⁵ for a variety of materials, with only one exception, a poorly crystallized phenol formaldehyde resin graphite ($c_0 = 6.94$ Å). It might be expected that at very high exposures the c spacing of all graphites would approach the same value irrespective of the initial value, but, on the basis of the data now available, this state of damage is not reached for exposures less than 4000 Mwd/At at 30°C.

The a spacing decreases during room-temperature irradiation. However, the change is small and is difficult to detect after short exposures. The ratio of c expansion to a contraction is about 10. The decrease in a is approximately linear, at least at low exposures where the (00 l) lines are still symmetrical and well defined.³

9-1.4 INTERPRETATION OF LINE BROADENING AND LATTICE-PARAMETER CHANGES

A simple physical model has been proposed by Bacon and Warren³ to explain the changes to the X-ray diffraction lines. They consider that, as the result of the displacement of atoms into interlayer positions, there is the

probability, α , that any given layer spacing will be increased by a small amount, ϵ , from the normal spacing of $\frac{1}{2}c_0$. The measured Δc will then be $2\alpha\epsilon$. For a random distribution of localized displacements, the diffraction peak should be broadened symmetrically. Because very pronounced asymmetric broadening is observed, it can be concluded that the increased spacings do not occur randomly but are spaced with approximate regularity once every $1/\alpha$ layer. Exact regularity would produce superstructure reflections, which are not observed.

Table 9.1 gives the values of α and ϵ for well-crystallized natural flake graphite after two exposures. On the basis of this model, an exposure of 460 Mwd/At caused about 10 per cent of the layers to expand to 4.29 Å, and 12 per cent were expanded to 4.99 Å after 1480 Mwd/At. The values of Δc measured from the displacement of the $(00l)$ reflections and the values of $2\alpha\epsilon$ are in fair agreement considering the simplicity of the model.

Table 9.1 — VALUES OF ϵ and α FOR A NATURAL FLAKE GRAPHITE³

Exposure, Mwd/At	ϵ , Å	α	$2\alpha\epsilon$ [†]	ΔC , Å [‡]
460	0.94	0.097	0.182	0.208
1480	1.64	0.124	0.406	0.610

[†] Average of values calculated from the Fourier coefficients and the phase angles of the (002) and (004) reflections.

[‡] Measured from the $(00l)$ peak positions; c_0 is assumed to be 6.70 Å.

That this model produces an asymmetrical diffraction line can be seen from the following. The distance, L , between any given pair of planes can be written as

$$L = \frac{1}{2}nc \quad (9.1)$$

where n is an integer.

The average spacing between layers is $\frac{1}{2}c_0 + \alpha\epsilon$. For large values of n (the case where many layer planes contribute), the variation of L is symmetrical above and below $L = n(\frac{1}{2}c_0 + \alpha\epsilon)$. However, for small values of n (the case where only a few layer planes contribute), there is a small probability of a large fractional increase in L , corresponding to the inclusion of an expanded spacing, and a large probability of a small decrease in L below the average value, $n(\frac{1}{2}c_0 + \alpha\epsilon)$. Thus the diffraction peak will be asymmetrical and will tail off slowly to high diffraction angles.

A schematic representation of this model of irradiated graphite is illustrated in Fig. 9.5. Suppose that during the irradiation one interstitial group lodges at position P and another arrives at Q' . The latter position is highly compressed by the interstitial already at P , and, since lateral movement of single interstitials between the layers should be very easy, the

interstitial at Q' moves away from P to some new position Q . This minimizes the distortion energy and positions the interstitials in a fairly regular way, as assumed in the model.

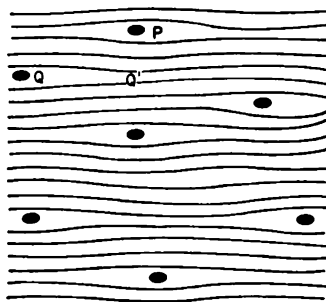


FIG. 9.5 Schematic representation of radiation-damaged graphite showing the approximate regularity in the positioning of the interstitial groups and the local increase in layer spacing at each interstitial. (From Bacon and Warren, *Acta Crystallographica*, Ref. 3.)

The exact nature of the interstitial groups and other damage centers is uncertain. Even an approximate description of the many damage centers that probably are formed is an extremely complex problem on which progress has been understandably slow. One general feature, which is now quite well established, is that, as the damage accumulates with increasing exposure, the damage centers become more complex. As the concentration of single displaced carbon atoms (or ions) increases, the probability becomes greater that they will diffuse along the layer planes and combine with other displaced atoms or ions. These larger, less mobile groups are more difficult to anneal.

Hennig and Hove¹⁶ suggested that the linearity of the c expansion to moderate exposures indicates that each displaced atom has about the same effect on the c spacing when combined in an interstitial cluster as it does when separate. It is generally believed³ that a vacancy does not have as much effect on the c spacing as an interstitial.

The apparent a contraction is usually attributed to the distortion of the layer planes. It probably is not due to an actual decrease in the C—C bond distance since it is not likely that the vacancies and interstitials would cause an average increase in the interatomic binding forces within the layers. Zachariasen,² who first observed the a contraction, suggested that it is caused by “blistering” of the layers and likened it to “frozen heat motion.” The effects on the X-ray diffraction patterns caused by heating graphite can be predicted from theory.¹⁷ They are: (1) a shift in the peaks corresponding to the thermal expansion of the lattice; (2) a decrease in peak intensity which arises from the less periodic arrangement of the atoms caused by thermal displacements; and (3) no change in peak shape or peak

width. All these properties are observed⁶ in the (002) peak of graphite with exposures up to 680 Mwd/At at 30°C. For example, the peak shown in Fig. 9.2 for 680 Mwd/At has the same displacement as would be expected for an unirradiated sample at a temperature of 1500°C. The peak intensity is also reduced with no change in peak shape.

9-1.5 STRUCTURAL CHANGES AT DIFFERENT TEMPERATURES

Partial annealing of the radiation-induced property changes occurs at a significant rate even during irradiations below room temperature. The net result is that all those radiation effects associated with disordering of the crystal structure occur at lower rates as the irradiation temperature increases. This is, perhaps, one of the most important features of radiation damage in graphite, the marked sensitivity of property changes to the temperature of irradiation. At -196°C, for example, the *c* expansion rate of natural flake graphite¹⁸ is more than twice the rate observed at 50°C. About half this expansion anneals at room temperature. Similar effects are observed at -138°C on pitch-bonded natural graphite.¹⁹

The temperature dependence of *c* expansion at room temperature and above is shown in Fig. 9.6. At low exposure these curves are approximately

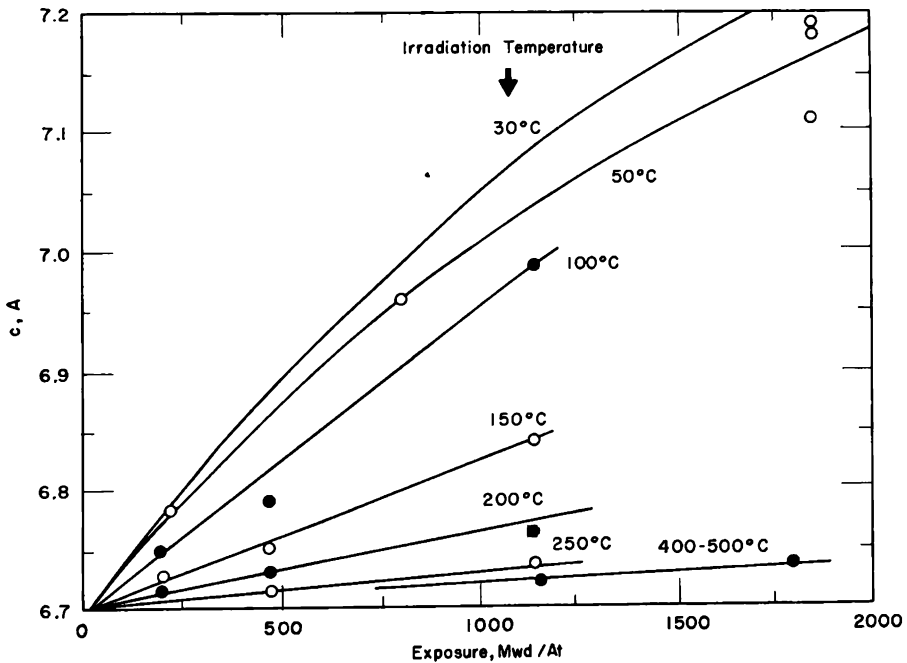


FIG. 9.6 Expansion of *c* spacing at different irradiation temperatures.^{5, 20, 21}

linear. When the initial slopes are plotted against irradiation temperature, it is seen that the *c* expansion becomes increasingly less sensitive to tem-

perature changes as the temperature increases. The a spacing and X-ray line broadening at these intermediate temperatures also show that the rate of disordering of the structure is much less than at room temperature.

In the 400 to 500°C range, some damage to the crystallites still occurs (Fig. 9.7). The c spacing continues to expand slowly, and the apparent crystallite size decreases.

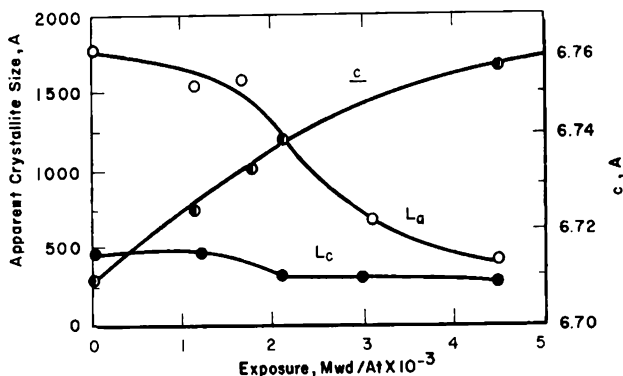


Fig. 9.7 Crystallite changes⁵ in CSF graphite at 400 to 500°C.

The c values in Fig. 9.7 are not quantitatively comparable to those in Figs. 9.4 and 9.6 because the former were computed from 2θ peak positions. The c spacings are therefore slightly larger than they would have been if the center at half-peak intensity had been used.

For irradiations at 1050°C some c -spacing expansion is barely detectable, being on the order of 0.08 per cent per 10^{20} neutrons/cm² ($E > 1$ Mev) for TSGBF graphite.⁵ Line broadening is quite significant, however. After 2×10^{20} neutrons/cm² ($E > 1$ Mev), the apparent L_c and L_a were reduced from 525 to 140 Å and from 900 to 430 Å, respectively.† It is significant that, even though some crystal expansion occurs at these very high temperatures, the bulk density increases (Sec. 9.4).

Hennig and Hove¹⁶ have discussed some of the basic processes underlying the strong dependence of radiation-induced property changes on the irradiation temperature. The results of irradiations at higher temperatures⁴ agree with the general features of their theory. At a very low irradiation temperature ($< -150^\circ\text{C}$), the interstitial groups (probably single carbon atoms or ions) are relatively immobile. One would expect that under these conditions the concentration of interstitials and vacancies would increase in proportion to the total dose.

As the irradiation temperature increases, some of the defects will anneal. The most probable fate of interstitials (i) and vacancies (v) can be represented by the following:

† An error in the calculation of L_a in Ref. 5 resulted in values which are too small by a factor of 10.

Diffusion of interstitials to surface of crystals



Reintegration



Clustering



or, in general,



Vacancy diffusion can be represented by a similar set of processes:
Diffusion to surface of crystals



Clustering



or, in general,



The effect of temperature on the relative rates of each of these reactions is difficult to predict. However, it is possible to arrive at some qualitative conclusions with the following assumptions:

1. The reaction rates can be expressed by an Arrhenius equation. For the decrease in i by Eq. 9.2 this is

$$-\frac{di}{dt} = iA_2e^{-E_2/RT} \quad (9.7)$$

and the ratio of the loss of i by Eq. 9.2 to the loss of i by Eq. 9.3 at a given irradiation temperature is

$$\frac{(di/dt)_2}{(di/dt)_3} \equiv \frac{R_2}{R_3} \quad (9.8)$$

2. Since single interstitials are generally considered to be more mobile than vacancies, it will be assumed that Eq. 9.3 occurs by the diffusion of interstitials. Therefore,

$$E_2 = E_3 = E_4 \quad (9.9)$$

3. Equations 9.5 and 9.6 are controlled by diffusion of single vacancies. It will be assumed that the activation energy for the diffusion of vacancies is greater than for the diffusion of interstitials, i.e.,

$$E_5 = E_6 > E_2 \quad (9.10)$$

4. It will be assumed that after any given neutron dose the concentration of single interstitials and single vacancies decreases with the irradiation

temperature, i.e., v and i decrease with temperature. The annealing processes in graphite are not yet well enough understood to carry out the complex analysis of all possible kinetic processes required to test this assumption rigorously. On an intuitive basis, however, this assumption appears physically reasonable.

With these assumptions, consider the effect of raising the irradiation temperature on each pair of reactions individually. The ratio of the two rates for Eqs. 9.2 and 9.4 is

$$\frac{R_2}{R_4} = \frac{iA_2e^{-E_2/RT}}{i^2A_4e^{-E_4/RT}} = \frac{A_2}{iA_4} \exp \left[-\frac{(E_2 - E_4)}{RT} \right] \quad (9.11)$$

Since it is assumed that $E_4 = E_2$ and that i decreases with temperature, the ratio R_2/R_4 increases with temperature. This means that as the irradiation temperature increases, the interstitial-to-surface reaction is favored over the clustering reaction.

Table 9.2 lists the results of comparisons of several pairs of reactions. The effect of temperature on all other combinations cannot be predicted, either because the effect on concentration ratios is unknown or because the direction indicated by the difference in activation energies of a pair of reactions is opposite to the direction indicated by the concentration effect. Some knowledge of the magnitudes of the opposing effects is necessary to carry the argument further.

Table 9.2 — PREDICTED EFFECT OF IRRADIATION TEMPERATURE ON THE RELATIVE RATES OF INTERSTITIAL AND VACANCY REACTIONS

Ratio of rates	Effect of temperature increase on ratio
R_2/R_3	Increase
R_2/R_4	Increase
R_5/R_3	Increase
R_5/R_6	Increase

Table 9.2 indicates that the effect of increasing the irradiation temperature is to increase the rate of interstitial-to-surface reaction by Eq. 9.2 to a greater extent than by other interstitial reactions, Eqs. 9.3 and 9.4; similarly, the vacancy-to-surface reaction rate by Eq. 9.5 increases faster than the rate of vacancy clustering by Eq. 9.6 and the rate of interstitial-vacancy reintegration by Eq. 9.3.

This oversimplified description is most likely to apply at low total damage. Several complicating factors arise as the damage increases. Large immobile clusters will block diffusion between the layer planes. Extreme buckling of the layers will result in some cross linking between planes at

vacancy sites, and this will also restrict diffusion. The net result is that very high temperatures will be required to anneal the damage.

One would expect that the accumulation of damage could be more effectively prevented by continuous irradiation at some temperature T_2 than by irradiation at a lower temperature T_1 with periodic anneals at T_2 ; this has been observed by measurements of thermal conductivity and dimensional changes (Sec. 13-4.3). The phenomenon of radiation annealing is predicted as a logical extension of these ideas.

9-1.6 NEUTRON TRANSMISSION AT LONG WAVE LENGTHS

Neutrons have a characteristic wave length (λ) that depends upon their energy (E). If E is expressed in electron volts, the relation is

$$\lambda(\text{\AA}) = 0.286E^{-1/2} \quad (9.12)$$

Neutrons, like X rays and electrons, are diffracted by crystals when the Bragg condition is satisfied, and neutron-diffraction patterns resemble the patterns obtained with X rays.²² There are differences, however, arising from the fact that neutrons are scattered primarily by nuclei, rather than by electrons. The intensities of neutron-diffraction patterns of graphite agree within 5 per cent with those calculated from the Bernal structure (Sec. 5-2). However, the intensities of X-ray patterns do not agree with those calculated from the Bernal structure if one assumes that the electron cloud around the carbon atoms is symmetrical. Bacon²³ has shown that the X-ray intensities agree much more closely with calculated values when it is assumed that the electron cloud around the carbon nuclei departs slightly from spherical symmetry.

If a polycrystalline material of sufficient length is placed in a beam of neutrons, Bragg scattering removes all neutrons from the incident beam except those having wave lengths greater than twice the largest interplanar spacing. For graphite $\lambda = 2d_{002} = 6.7$ \AA. The intensity of the transmitted beam is reduced by neutron absorption, inelastic scattering, disorder scattering (isotopic, spin, etc.), and defect scattering. If only the defect scattering is changed by the irradiation of a material, then neutrons of long wave length can be used to measure the number of defects produced.

The intensity of neutrons transmitted by an unirradiated nuclear graphite has been compared²⁴ with the intensity transmitted by a sample irradiated near room temperature (Fig. 9.8). From the area under the curves, the ratio of the transmitted intensity for the unirradiated sample to that for the irradiated sample is 0.608. According to the theory, this would require that the fraction of defects (interstitials plus vacancies) in the irradiated sample be 0.0526. The fraction of displaced atoms is just one-half this number, or 0.0263.

The fraction of displaced atoms for 1.1×10^{20} neutrons/cm² estimated from Seitz's theory²⁵ is 0.021. Considering the fact that there are many

sources of error in both the experimental and theoretical values, the good agreement is probably fortuitous. The clustering of defects during irradiation also causes some error in the fraction of displaced atoms measured by this method because scattering by clusters is not equivalent to scattering from isolated defects. Furthermore, since some annealing occurs during irradiation, the fraction of displaced atoms measured is not exactly equal to the displacement rate calculated by the Seitz theory.

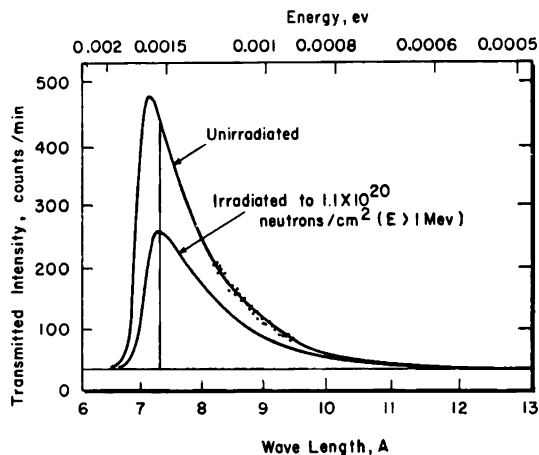


FIG. 9.8 Slow-neutron intensity transmitted by an irradiated and by an unirradiated graphite specimen. For clarity only a typical group of experimental points has been reproduced along one curve to indicate the number and spread. Only those intensities to the right of the vertical line at 7.30 Å were considered in computing intensities. (From Antal et al., *Physical Review*, Ref. 24.)

It should be possible, in principle, to distinguish between defects of different size by examining the wave-length dependence of the neutron attenuation at long wave lengths. However, the rapid decrease in intensity of the neutron source with wave length makes this difficult, and it has not yet been possible to detect any wave-length dependence.

9-1.7 ELECTRON MICROSCOPY

Recent observations with the electron microscope have helped to characterize defects produced in graphite. Electron transmission pictures of irradiated graphite (10^{20} neutrons/cm² at 30°C) taken in dark-field illumination are found to contain black and white dots 10 to 100 Å in diameter and loops about 100 Å in diameter.²⁶ The dots, which are not found in unirradiated graphite, are presumed to be interstitial and vacancy clusters. Heating to 400°C makes the loops larger and the dots smaller. Upon further heating to 2200°C, the pictures appear the same as before irradiation. In this connection it will be seen in Sec. 13-3 that the properties of graphite irradiated at room temperature to low neutron doses are almost completely annealed by heating to 2000°C.

Transmission electron micrographs of single crystals of graphite irradiated at 200°C to a dose of 4.8×10^{20} neutrons/cm² are found²⁷ to contain very fine speckles, barely resolvable at a magnification of 120,000. The damage centers of similar specimens irradiated at 650°C are larger, rounder, and more sparse.

The damage centers formed during 200°C irradiations²⁷ cluster upon annealing at temperatures up to 1500°C. Above 1500°C the clusters begin to break up and disappear, and further heating to 1700°C anneals almost all the damage. Although the evidence is not conclusive, it is tentatively suggested that the clusters are composed of interstitial atoms.

When the symmetry properties of probable structures for interstitial groups and vacancy groups were used, evidence was obtained to indicate that the large dislocation loops formed by quenching-annealing treatment of thin graphite flakes are composed of vacancies.²⁸ Similar deductions²⁹ suggest that large interstitial loops are formed in graphite crystals by an irradiation of 3×10^{20} neutrons/cm² at 300°C.

Damage centers 100 to 2000 Å in diameter produced by fission fragments have been reported.³⁰ From fringes in the damaged region, it is inferred that the damage centers are lenticular voids with a height of a few atomic distances in the *c* direction.

Thus far electron microscopy studies have been confined to observations with the electron beam perpendicular to the basal planes because of the difficulty of preparing thin samples with basal planes perpendicular to the surface of the flake. A further difficulty is that sample preparation often introduces large amounts of cold work into the specimen. In spite of these difficulties, electron microscopy promises to be a useful tool for the study of radiation effects in graphite crystals.

9-2 Radiation Effects on Macrostructure

9-2.1 CHANGES IN SURFACE AREA AND PORE SIZE NEAR ROOM TEMPERATURE

The BET surface area decreases when graphite is irradiated near room temperature. After a rapid initial change, the fractional decrease in area ($-\Delta S/S_0$) is approximately linear with exposure (Fig. 9.9). When the graphite is heated above the irradiation temperature, the surface area gradually increases to almost the preirradiation value.

The change in the size distribution of pores accessible to gases indicates that irradiation near room temperature causes the pores to shrink (Fig. 9.10). This behavior has been observed on both powdered and solid samples of several nuclear graphites. Samples irradiated at room temperature in carbon dioxide, carbon monoxide, oxygen, and vacuum are reported³¹ to show about the same behavior.

As might be expected from the surface and pore-size changes, the helium density of graphite is reduced by irradiations near room temperature.³¹ At

temperatures high enough to oxidize the sample, this decrease in density may be more than offset by oxidation of the porous part of the graphite body.

The decrease in surface area and helium density and the general shrinkage of the micropores are probably direct results of radiation-induced

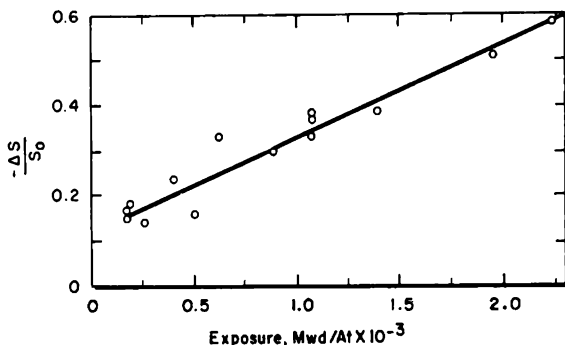


FIG. 9.9 Decrease in the BET surface area of nuclear graphite by irradiation near room temperature. (From Spalaris et al., *Journal of Physical Chemistry*, Ref. 31.)

expansion of the crystallites, which reduces the intercrystalline void spaces. It is likely that many pores become inaccessible to the measuring gas as the crystal expansion seals off some of the small bottle-neck openings to

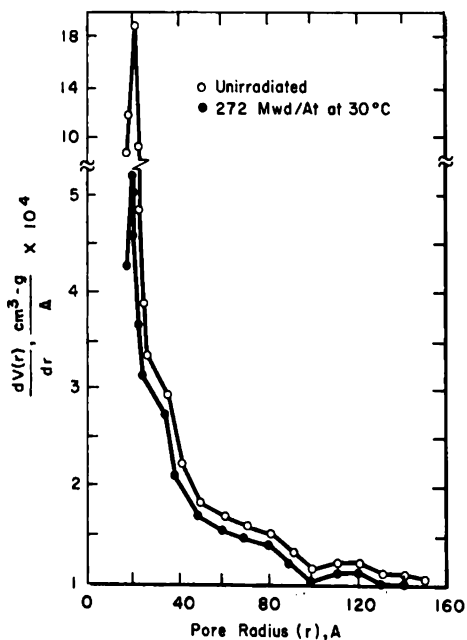


FIG. 9.10 Pore-size distribution for a powdered TSGBF graphite before and after irradiation. (From Spalaris et al., *Journal of Physical Chemistry*, Ref. 31.)

the pores. Crystal expansion into pores is also suggested from the relative magnitudes of bulk and crystal expansion (Sec. 9-3.3).

9-2.2 CHANGES IN SURFACE AREA AND PORE SIZE AT HIGH TEMPERATURE

Changes to the microstructure are considerably reduced when graphite is irradiated above room temperature. Woodley³² found that the surface area of CSF graphite samples irradiated at 400 to 500°C actually increased. Although the samples were slightly oxidized during irradiation, the increase in surface area was greater than could be accounted for by oxidation alone.

The pore-size distribution is also significantly changed (Fig. 9.11). The

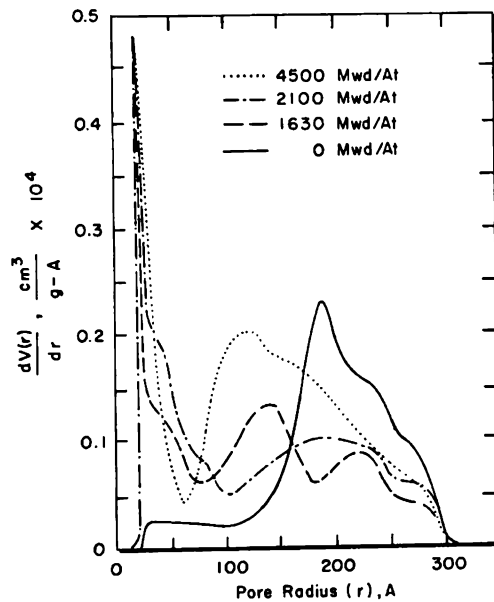


FIG. 9.11 Pore-size distribution⁸ in CSF graphite irradiated at 400 to 500°C.

appearance of the narrow peak at 20 to 30 Å is probably the result of a small amount (less than 0.5 per cent) of oxidation during irradiation, which made the very small pores accessible to the nitrogen.

Woodley³² has suggested that irradiation at 400 to 500°C may result in a slow change in the crystallite-size distribution over a long period of time. This would allow the crystallites to pack more efficiently, reducing the average size of the larger pores. This redistribution of crystallites may be thought of as a radiation-induced densification process. In view of the limited understanding of the processes occurring in graphite during high-temperature irradiations (Sec. 9-4.3), an explanation of the apparent shift of pores to smaller sizes must be conjectural at this time.

9-3 Dimensional Changes Near Room Temperature

The structural changes discussed in previous sections are manifest in bulk dimensional changes, although, as might be expected for an anisotropic, imperfectly oriented, and porous substance, the result is indirect and difficult to predict. Speculation on the dimensional behavior of graphite before the first reactors began operation included predictions of growth, contraction, and even disintegration. Subsequent experience has shown that both expansion and contraction occur under certain conditions. Table 9.3 reviews the historical development of the problems and the research associated with dimensional changes in graphite in the United States.

Table 9.3 — EVENTS ASSOCIATED WITH THE STUDY OF RADIATION-INDUCED DIMENSIONAL CHANGES IN GRAPHITE IN THE UNITED STATES

Date	Event
1942-1945	Predictions and first observations of radiation-induced dimensional change ³³⁻³⁶
1946-1947	Graphite expansion becomes a problem in reactor operation ³⁹⁻⁴¹ Contraction parallel to extrusion axis first noted ⁴²
1948-1951	Increases in reactor operating temperature reduce expansion ^{43, 44} Reactor designs improved to reduce expansion ⁴⁵⁻⁴⁸
1952-1956	Special methods of manufacturing graphite developed to reduce expansion ^{15, 49} First observation ⁵⁰ of contraction perpendicular to extrusion direction in irradiations above 300°C
1957-1961	Contraction recognized as a problem in the design and operation of reactors ^{5, 51-53}

It is evident that while the solutions to early expansion problems were being successfully applied, new problems with contraction were developing as a result of increases in reactor operating temperatures. Current research efforts are concentrated on developing methods of reducing high-temperature contraction by structural modifications to conventional nuclear graphites.

The demand for graphites having special properties for reactor applications is increasing. Low permeability, oxidation resistance, high strength, or properties that are suited to the application of oxidation-resistant coatings are attained in graphite through structural changes. However, these changes may result in high contraction rates. Further studies are required to develop methods of reducing contraction in these special graphites or

to provide sufficient irradiation data on them to permit the design of components that can accommodate contraction.

9-3.1 NUCLEAR GRAPHITES

The extrusion process, by which almost all nuclear graphites have been formed, aligns the coke particles and produces an anisotropic body (Sec. 5-8.2). The radiation-induced dimensional changes depend on the direction of measurement with respect to the extrusion direction. In this section the discussion is divided into those changes measured transverse to the extrusion direction and those changes measured parallel to the extrusion direction.

(a) *Transverse to the Extrusion Direction.* During irradiation at 30°C all nuclear graphites expand transverse to the extrusion direction. Considerable variation in the rate of growth of nuclear graphites has been noted and is illustrated in Fig. 9.12. The transverse growth rates are approximately

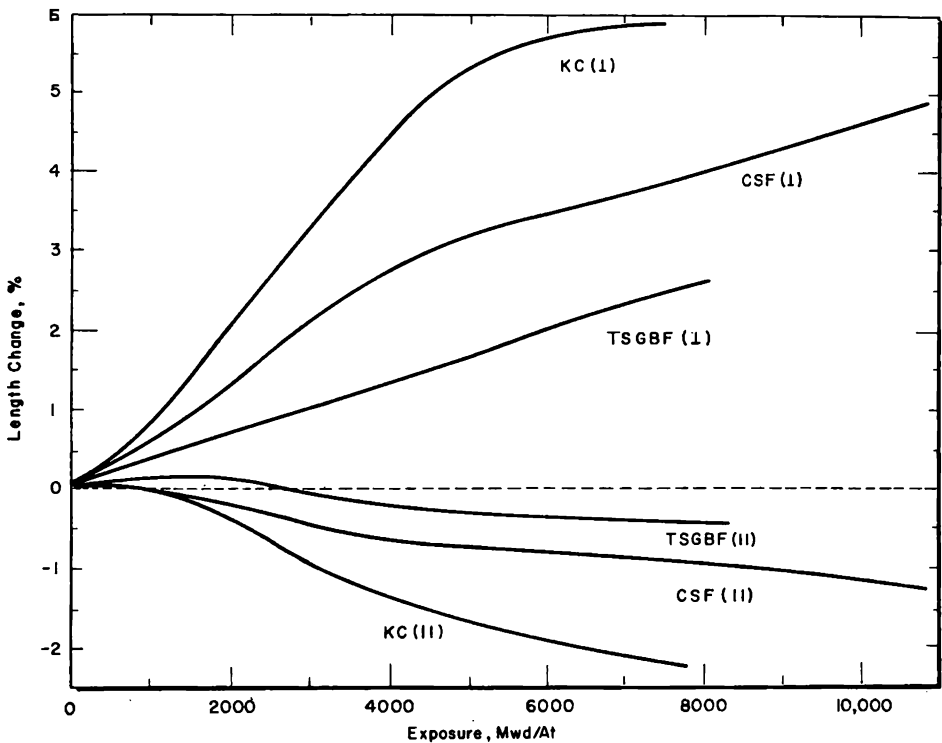


Fig. 9.12 Dimensional changes of nuclear graphites caused by irradiation at 30°C. (From Davidson et al., *Fourth Conference on Carbon*, Pergamon Press, Ref. 54.)

constant to 1000 Mwd/At. Thereafter the growth rate increases for KC and CSF and decreases for TSGBF. Early investigators⁵⁵ found a correlation between the growth rates above and below 1000 Mwd/At for several nuclear graphites. After 5000 Mwd/At the rates for KC and CSF decrease and a

slight increase is noted for TSGBF. The growth of KC graphite apparently saturates near 6 per cent.

The different growth rates shown for KC, CSF, and TSGBF can be attributed to structural differences. Although the size of the extruded bars was the same for each graphite (4 by 4 by 48 in.), the cokes and particle sizes used in manufacturing each of these grades were different. This resulted in different degrees of preferred orientation evidenced by ratios of transverse to parallel thermal expansion coefficients: 3.9, 2.3, and 1.6 for KC, CSF, and TSGBF, respectively.⁵⁶ The crystal structure is also most highly developed in KC graphite and the least developed in TSGBF (see Table 5.1).

A variation in the rate of growth due to an orientation gradient across a bar has also been observed.⁴⁰ After an exposure of 188 Mwd/At, transverse samples cut from the center of a bar expand 0.18 per cent, whereas those cut from the edge of the same bar expand 0.14 per cent. Uniform sampling methods thus become important when different types of graphite are to be compared. Transverse samples, from which data for Fig. 9.12 were obtained, were cut from layers adjacent to surfaces exposed by cutting bars in half longitudinally.⁵⁷ Parallel samples were cut from layers adjacent to those used for transverse samples; however, no samples were taken from the highly oriented graphite near the surface of a bar.

The expansion rates for samples from different bars of the same grade can also differ appreciably. Initial expansion rates of 0.65 and 0.50 per cent per 1000 Mwd/At were noted for two bars of CSF graphite.⁵⁷ After 11,000 Mwd/At the transverse expansions for these two bars were 5.5 and 4.3 per cent respectively.²¹ Thus several bars from different graphitizing heats should be tested to obtain the average length changes on graphites to be used in reactor construction.

Linear growth is generally observed transverse to the extrusion axis in British and French nuclear graphites. One exception is reported⁵⁸ for AGXP graphite irradiated in the Canadian NRX reactor. It was found that the growth rate initially increased with exposure. At 20°C linearity was established after an exposure of 2×10^4 Mw-hr.† The exposure required to produce linear growth decreased as the irradiation temperature was increased. The initial nonlinearity of growth is attributed⁵⁹ to internal stresses that must be overcome before dimensional changes are evident.

Graphites processed at several graphitizing temperatures were included⁶⁰ in NRX irradiations at 20°C. A graphite processed below 2600°C grew less than those processed at 2600 and 2800°C. This comparison is similar to that which can be made between TSGBF processed at 2450°C and CSF or KC processed at 2800°C. The qualitative agreement between results of irradiation

† One megawatt-hour at the position of maximum flux in the fast-neutron plugs in NRX is equivalent to $(1.9 \pm 0.2) \times 10^{18}$ thermal neutrons/cm² in an experimental hole in BEPO.⁶¹

tions conducted in different facilities is generally satisfactory when the effects of graphite properties or manufacturing processes on growth are compared. Attempts to compare growth rates of different graphites in different facilities on a quantitative basis have been inconclusive owing to uncertainties in corrections for the different irradiation temperatures, doses, and sampling procedures.⁶¹

(b) *Parallel to the Extrusion Direction.* In the direction parallel to extrusion, a slight growth is usually observed at low exposures (Fig. 9.12). However, with increasing exposure graphite begins to contract, and the rate increases up to an exposure of 2500 Mwd/At. The rate then decreases and becomes linear at 4000 Mwd/At.

It is evident from Fig. 9.12 that the anisotropy and crystalline perfection which result in the high transverse growth rates for KC graphite also produce the highest parallel contraction rate. No saturation of parallel contraction has been observed which would correspond with the saturation of growth in transverse KC graphite.

It is interesting to note that in the NRX irradiations of AGXP graphite⁵⁸ a very small initial contraction is observed parallel to the extrusion axis at low exposures where transverse growth is nonlinear. The contraction soon ceases, and linear growth is established at the same exposure that growth becomes linear in transverse samples. These irradiations were not carried to high enough exposures to observe linear parallel contraction.

9-3.2 EXPERIMENTAL GRAPHITES

The wide range of expansion behavior noted in early nuclear graphites led to investigations of the properties of many experimental graphites and their effects on radiation-induced dimensional changes. A comprehensive study of the effects of irradiation at 30°C has been conducted on 54 groups of specimens. The raw materials, preparation and properties of test specimens prior to irradiation,⁴⁹ and the effects of irradiation have been reported.^{15,62} Variations in the properties of the experimental graphites were achieved by variations in filler and binder materials and variations in the heat-treatment, forming, impregnation, and graphitization steps. Irradiation results show that for the range of variables investigated, the raw materials produce the largest change in radiation-induced growth. The filler fraction in particular has greater influence on dimensional changes than the binder. Figure 9.13 illustrates the dimensional changes of graphites with different fillers. It is significant that, when resin binder was coked and used for a filler, contraction occurred during irradiation; however, when it was used as binder with skeletal graphite filler (obtained from the high-temperature zone of a silicon carbide production furnace), the resin did not prevent the highest expansion of all the experimental graphites.

The expansion rate of the pitch-coke graphite is even higher than that

of KC graphite. The Thermax carbon-black graphite expanded at a rate slightly higher than CSF graphite. However, a graphite (not shown in Fig. 9.13) made from Sterling-S, a carbon black whose particles are smaller and more difficult to graphitize, expanded at a rate comparable to the petroleum-asphalt coke graphite.

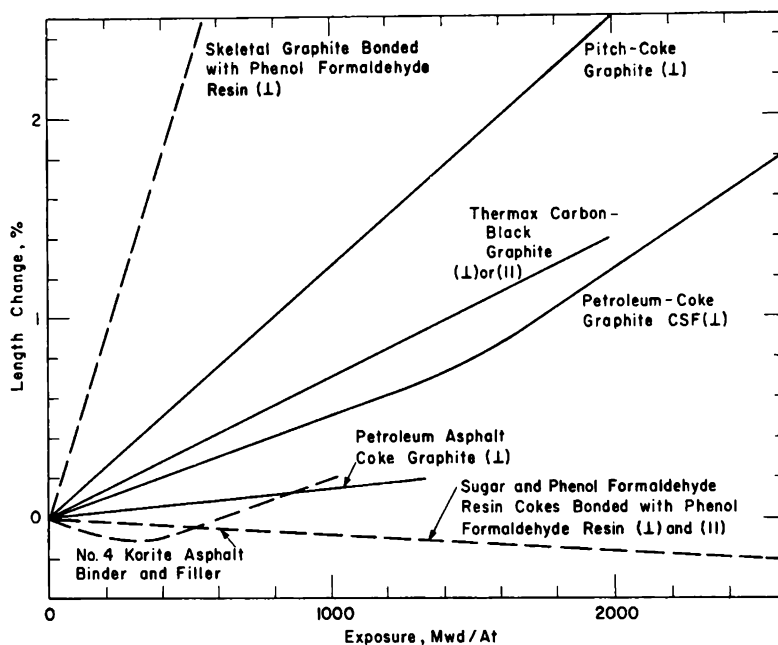


FIG. 9.13 Length changes observed after irradiation at 30°C. The solid curves represent graphites prepared with different fillers but with the same medium-hard coal-tar pitch binder.^{16, 21}

The petroleum-asphalt coke was prepared in the laboratory using No. 4 Korite, a commercially available asphalt. When the asphalt was used as both binder and filler, the material first contracted to 0.1 per cent and then began to expand at a constant rate of 0.2 per cent per 1000 Mwd/At. The resin and sugar coke graphites continued to contract at a low rate.

The effects of density changes are shown in Fig. 9.14. All samples were prepared from Texas coke and Standard (medium-hard coal tar) pitch and were graphitized at 2570°C. The different densities were achieved by variations in the molding pressure for all samples except the two highest densities. The sample with a density of 1.67 g/cm³ was given a single impregnation; the 1.83 g/cm³ sample was triply impregnated. Samples with higher densities expanded at a higher rate, particularly those in the range requiring impregnation.

Increasing the graphitization temperature usually increases the expansion rate, as indicated in Fig. 9.15. The 2700°C sample does not follow this

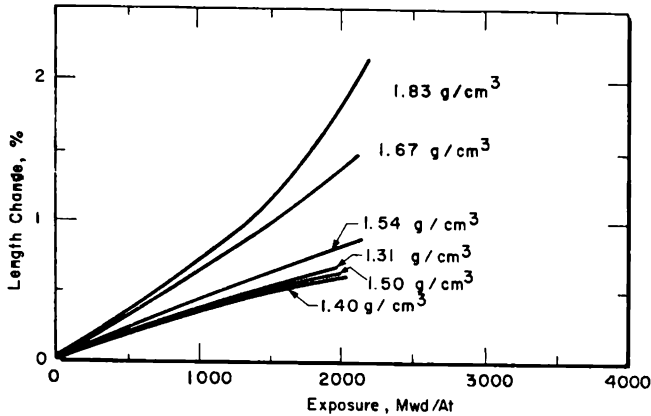


FIG. 9.14 Effect of density on expansion of graphites irradiated at 30°C. All samples were molded, and length changes were measured in the direction of the molding force. (From Fletcher and Snyder, *American Ceramic Society Bulletin*, Ref. 14.)

trend. Anomalous behavior of this sample also occurs in irradiations at 500°C and has been traced to the preferred orientation, which is lower than either the 2300 or 2570°C graphites.

Graphites that appeared to be most promising for low-temperature reactor applications were never developed on a production scale because

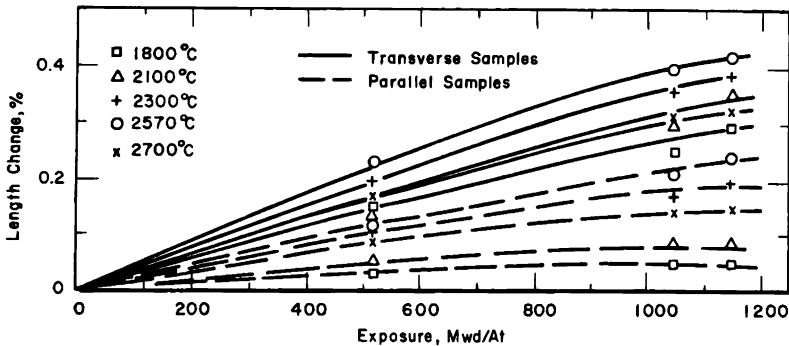


FIG. 9.15 Effect of graphitization temperature on expansion of molded Texas coke graphites⁴³ irradiated at 30°C.

the general trend toward higher graphite temperatures has reduced the expansion problems. Many specimens prepared for potential low-temperature application were, however, irradiated at 400 to 500°C and have provided valuable information pertinent to the radiation-induced contraction of graphite.

9-3.3 INTERPRETATION OF DIMENSIONAL CHANGES NEAR ROOM TEMPERATURE

Correlations of dimensional changes with other properties offer some insight into the mechanisms operative during room-temperature irradiation.

Of particular interest are the relations between the changes in bulk dimensions, c spacing, and the preirradiation values of the coefficients of thermal expansion.

As shown in Fig. 9.16, at low exposures the rate of c -spacing expansion is about eight times the rate of bulk dimensional change transverse to the extrusion axis. This ratio decreases to about 3 for exposures greater than 4000 Mwd/At. Assume that the relative orientation of the crystallites with respect to the extrusion direction is approximately proportional to the coefficients of thermal expansion. For CSF the ratio CTE (\perp)/CTE (\parallel) is 2.3. Then, in an orthogonal coordinate system in which z is in the extrusion

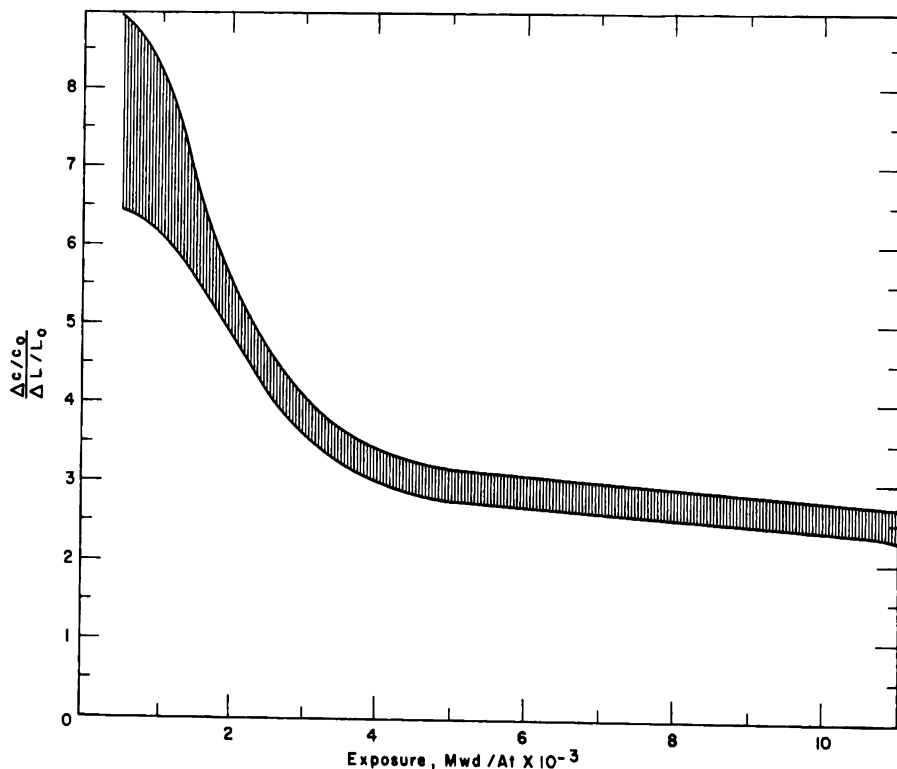


FIG. 9.16 Ratio of the rate of c -spacing change to transverse-length change $\left(\frac{\Delta c/c_0}{\Delta L/L_0}\right)$ for irradiation of CSF graphite at 30°C. (Data from Figs. 9.4 and 9.12.)

direction, the average number of crystallites aligned with their c axes along the x , y , and z directions will be in the ratio of 2.3:2.3:1. The fraction of crystallites oriented with c axes along one of the transverse directions is $2.3/(2.3 + 2.3 + 1) = 2.3/5.6$. Neglecting the small effect due to contraction of the a spacing, this leads to $(\Delta c/c_0)/(\Delta L/L_0) = 5.6/2.3 = 2.5$, which is in good agreement with Fig. 9.16 for high exposures. The higher value

for this ratio at lower exposures may be partially due to an absorption of a fraction of the c expansion in the pores. This fraction would become smaller as the exposure increases because, as the readily available pores are filled, more of the lattice expansion would be transmitted into bulk expansion.

A correlation⁶⁴ between radiation-induced dimensional changes and the coefficients of thermal expansion has been reasonably successful for several nuclear graphites manufactured from petroleum coke by conventional processes (Fig. 9.17). However, the correlation is not as satisfactory for graphites¹⁵ made by nonconventional processes.

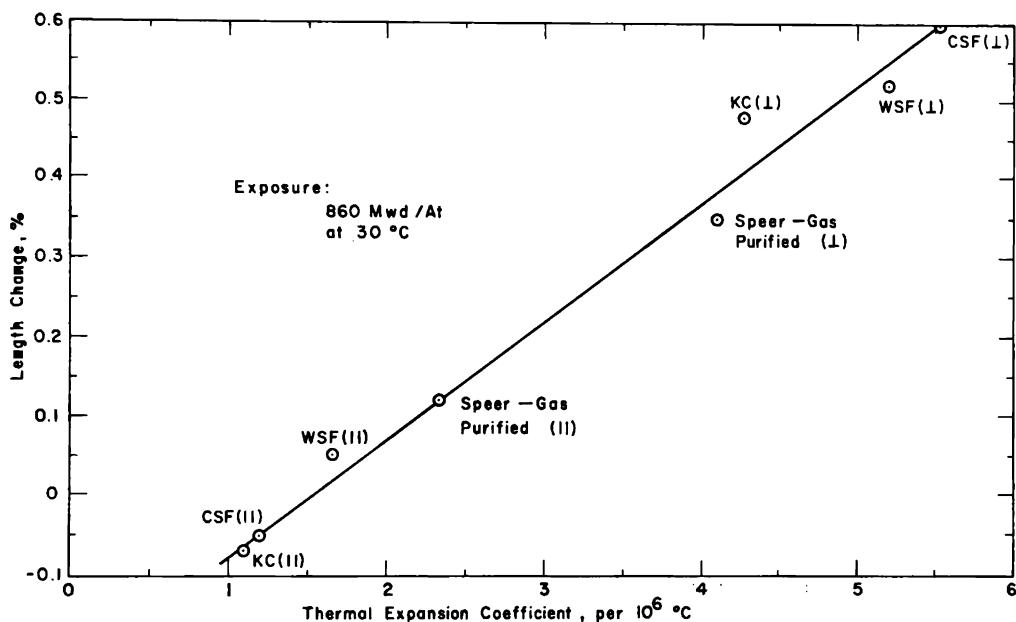


FIG. 9.17 Length changes after an exposure of 860 Mwd/At at 30°C for nuclear graphites as a function of the thermal expansion coefficients. The thermal expansion coefficients are averages between 25 and 425°C measured prior to irradiation.⁶⁴

9-4 Dimensional Changes at Elevated Temperatures

As the irradiation temperature increases above room temperature, the expansion of graphite perpendicular to the extrusion direction decreases; above 300°C contraction is observed. In the direction parallel to the extrusion axis, contraction is observed in most nuclear graphites at all irradiation temperatures, and, as the temperature increases, the amount of contraction decreases.

The magnitude of the dimensional changes at elevated temperatures varies widely with different graphites. Although the reasons for these variations are not fully understood, most of the properties of graphite which have

an important effect on the dimensional changes have been identified, and some progress has been made in relating dimensional changes to the structural properties of the graphites.

9-4.1 GENERAL TEMPERATURE EFFECTS

The effect of irradiation temperature on length changes transverse to the extrusion axis is illustrated in Fig. 9.18. Length changes, like other radiation-induced effects, are very sensitive to the irradiation temperature in

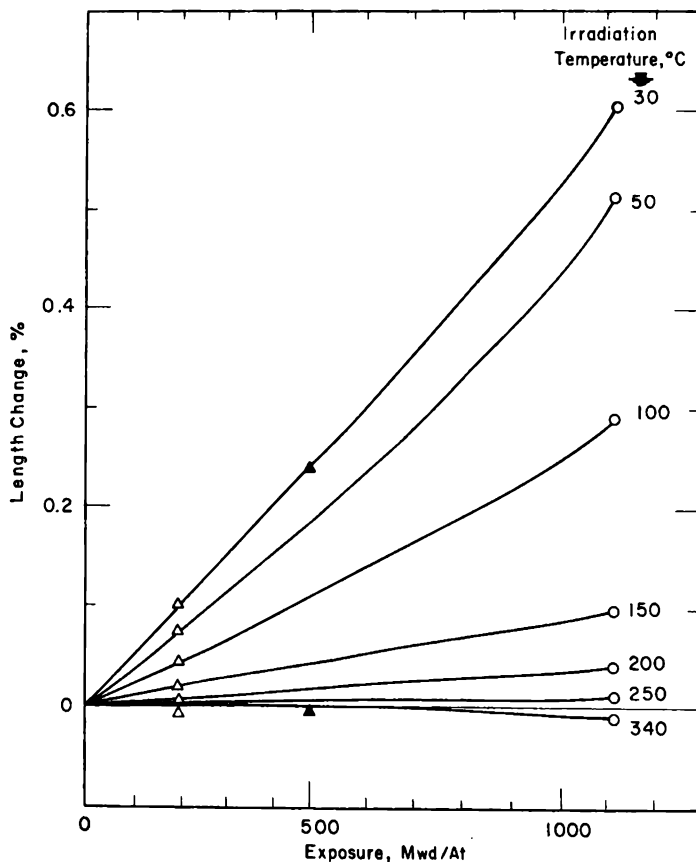


FIG. 9.18 Length changes of CSF (\perp) graphite at several irradiation temperatures.²⁰

this temperature range. No comparable studies on length changes parallel to the extrusion axis have been reported, although it can be assumed from measurements at higher irradiation temperatures that a continual decrease in the contraction rate would be observed between 30 and 300°C.

Above 300°C the relation between length change and exposure is complex (Fig. 9.19). In the transverse direction an initial expansion is generally observed to an exposure of at least 1500 Mwd/At, and at higher exposures

a contraction is observed. The contraction is linear with exposure to 12,000 Mwd/At (the maximum exposure for which data are available), and published contraction rates usually refer to the slope of this linear region.

A small initial expansion is also observed parallel to the extrusion axis, but the expansion is generally less than in the transverse direction. After approximately 1000 Mwd/At, the contraction becomes linear with exposure.

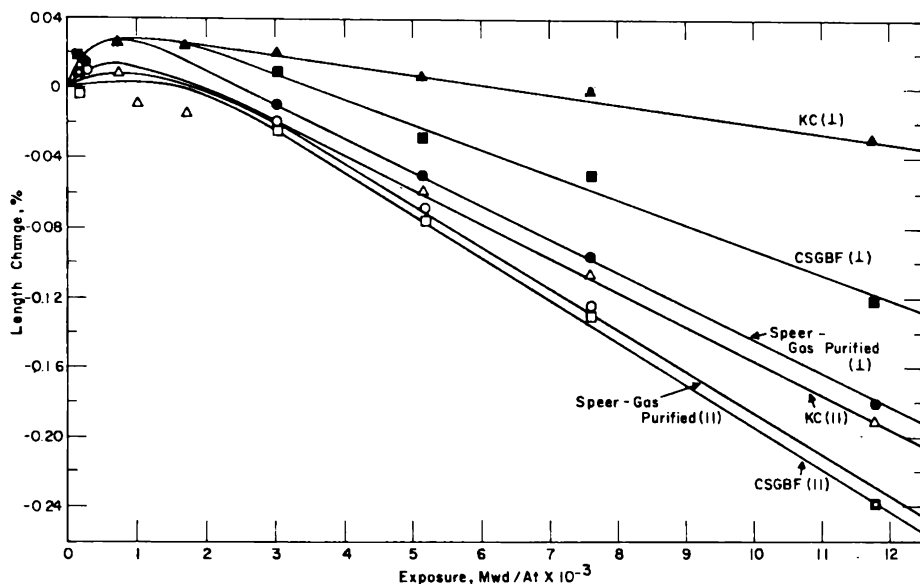


Fig. 9.19 Dimensional changes in nuclear graphites^{21,54} irradiated at 400 to 500°C.

It has been established that a portion of the initial expansion reported in earlier work⁵ was caused by the annealing of strains introduced into the samples by machining. After this effect was recognized,⁵⁴ irradiations at 500 to 600°C of samples annealed to 1000°C after machining disclosed that a small initial expansion still occurred.⁶⁵ However, the magnitude of the expansion in the transverse direction was reduced by the preannealing treatment from about 0.04 to 0.02 per cent.

The rate of length change of CSF graphite up to 1200°C is shown in Fig. 9.20. Above room temperature the rate of transverse expansion decreases rapidly owing to concurrent annealing effects. The "200°C peak" observed in annealing samples exposed at 30°C is a manifestation of the strong effect of temperature between 30 and 200°C.

In the vicinity of 300°C, CSF and similar graphites are relatively stable, but above this temperature contraction occurs in the transverse direction. A broad maximum between 600 and 900°C is indicated in Fig. 9.20. This

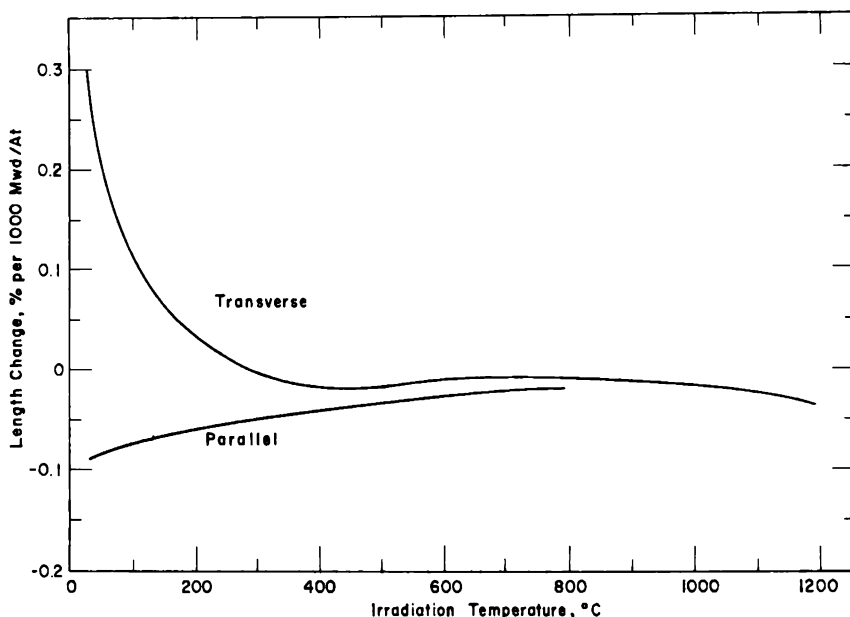


FIG. 9.20 Effect of irradiation temperature on the rate of dimensional change in CSF graphite.⁶⁶ The rates were derived from the linear region (>5000 Mwd/At) of the exposure curves. Above 500°C the rates were measured in high-flux test reactors, and the exposures were converted to megawatt-days per adjacent ton by the relation: $1 \text{ Mwd/At} = 1.3 \times 10^{17} \text{ neutrons/cm}^2$ ($E > 0.18 \text{ Mev}$).

part of the curve is based upon relatively few irradiations,⁶⁶ and additional data are necessary before this behavior can be conclusively demonstrated. From the fragmentary data at 1000°C and above, the contraction rate of transverse samples at 1200°C appears to be about three times the rate at 1000°C .

9-4.2 DEPENDENCE ON GRAPHITE

The contraction rate in the transverse direction depends upon the graphitization temperature, the graphitizability of the coke, the extent of grain orientation, and probably upon other factors that have not been investigated. Some of these factors are responsible for the different contraction rates in Fig. 9.19. The KC graphite, which has the lowest transverse contraction rate, was manufactured from a well-graphitizing coke and has a high degree of preferred orientation (see Table 6.23). The Speer gas-purified and CSGBF materials were not fully graphitized and are not as highly oriented as KC.

The effects of maximum heat-treatment temperature are shown in Fig. 9.21. Samples that were heated to the higher graphitization temperatures are more stable. Although the 2570°C and 2700°C samples appear to be reversed, dimensional changes in both samples are very small; the apparent

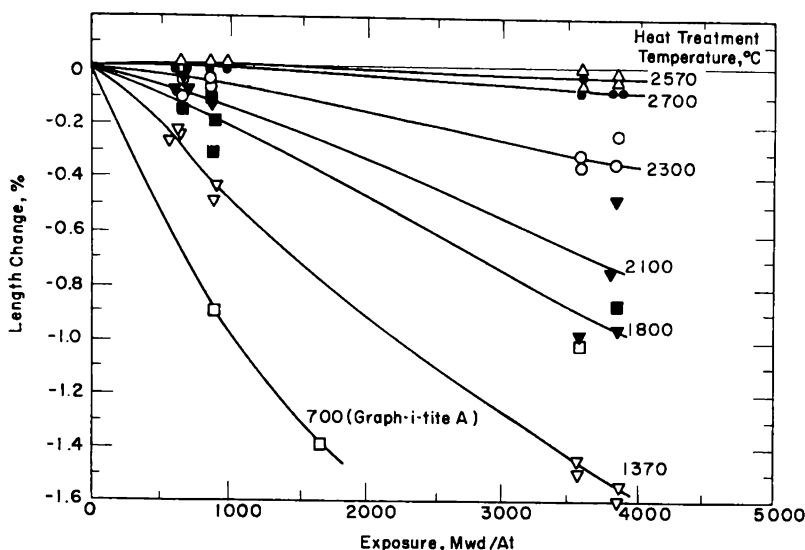


FIG. 9.21 Effect of maximum heat-treatment temperature on radiation-induced dimensional changes measured parallel to the molding force (transverse sample).^{5, 67} All graphites except Graph-i-tite A were made from Texas-Lockport coke and the same pitch binder. The irradiation temperature was in the range 400 to 500°C.

reversal may be related to a difference in degree of orientation, as suggested in Sec. 9-3.2.

As more data are obtained, the conclusion that materials which are not fully graphitized contract at a higher rate when irradiated at high temperatures is becoming more certain. This conclusion is supported by the following additional observations:

1. For two graphites that were identical except that one was graphitized at 2900°C and the other at 3140°C, the transverse contraction after exposures of 1.6 to 3.3×10^{21} ($E > 0.18$ Mev) at 850 to 1200°C was lower in the material graphitized at the higher temperature.⁶⁸

2. An additional pitch impregnation⁶⁷ caused a slight increase in the transverse contraction rate at 500 to 600°C.

3. A lampblack-base graphite⁶⁹ that had been heat-treated at 3000°C contracted rapidly at 500 to 600°C. Both the c spacing and length decreased, the latter showing the larger percentage change.

9-4.3 MECHANISM OF DIMENSIONAL CHANGES AT ELEVATED TEMPERATURES

The mechanism of dimensional changes in graphite should account for the following observations:

1. Graphite shrinks when irradiated above 300°C, while at the same time the c spacing expands.

2. Factors that increase the ultimate crystallinity of graphite reduce the rate of contraction.

3. The shrinkage transverse to the extrusion axis does not anneal, whereas shrinkage parallel to the extrusion axis does anneal when the sample is heated to high temperatures (see Sec. 13-3.3).

A mechanism that accounts for these observations has been proposed.⁷⁰ Two processes appear to operate concurrently during irradiation. The first may be broadly classed as a damaging effect. It is the predominant process below 300°C. The effects of this process, e.g., *c* expansion, transverse length expansion, parallel length contraction, and stored energy, are annealed by heating to high temperatures.

The second process may be broadly classed as radiation-induced densification, and the effects produced are not annealed by heating to high temperatures. Densification of nongraphitic carbons and lampblack-based materials occurs at a relatively rapid rate during irradiation at 500°C. It is presumed that in electrographites there also exist nongraphitic regions that densify during irradiation. On the atomic level there is no direct evidence concerning the mechanism by which this may occur. However, evidence has been obtained for the ordering of disordered alloys by radiation-enhanced diffusion, and radiation-induced phase transformations have also been observed in metals.⁷¹ It is probable that similar effects occur in graphite leading to atomic rearrangement in poorly ordered regions with a consequent increase in density.

9-5 Dimensional Changes in Moderator Structures

The dimensional changes observed in samples cut from bars of nuclear graphites or from small specimens of experimental graphites have been discussed in the preceding sections. The extent to which these changes cause distortion of moderator structures is influenced by additional factors⁷² such as the geometric arrangement of the block; the amount of restraint provided by keys or external devices; thermally induced distortion (or thermal "ratcheting," as it is called when the displacement is irreversible); and variations of flux and temperature which are held as constant as possible in small-sample irradiations.

Graphite moderator structures can be constructed by stacking the blocks with the extrusion axes in either a vertical or a horizontal direction. Since fuel channels are usually parallel to the long dimension or extrusion axis of blocks, the two types of structures correspond with vertically and horizontally fueled reactors. The general features of dimensional changes in horizontal and vertical structures are discussed in the following sections. The design of specific reactors and the methods used to control distortion in each are discussed in more detail in Chap. 17.

9-5.1 HORIZONTAL STRUCTURES

A relatively simple stack in which bars are arranged horizontally will illustrate the complexity of reactor distortion. Reflector graphite at the top,

bottom, and sides of the stack normally will not cause significant dimensional changes because the fast-neutron flux is low. In regions of the core where graphite temperatures are below 300°C, growth will occur, whereas in the central region temperatures may be high enough to cause radiation-induced contraction. The net change in height measured at the top of the stack will therefore depend on a combination of temperature and flux parameters. Contraction may be observed at the top center position. In fringe regions the balance between growth and contraction may shift to produce a zone in which growth is observed. In the Brookhaven reactor⁷³ a single maximum is observed at a gap in the central region where graphite temperatures are lowered by coolant gas that enters through the gap. However, the graphite temperatures are not sufficiently high to cause the graphite to contract.

Horizontal dimensional changes of the stack are influenced by behavior transverse and parallel to the axis of extrusion. If the bars in all layers are parallel to each other, side-to-side dimensional changes of the stack will be controlled by changes transverse to the extrusion axis of the bar (growth or contraction depending on temperature). Dimensional changes parallel to the fuel channels will be controlled by parallel behavior (contraction at all temperatures after a short period of growth at low exposures). Figure 9.20 illustrates the transverse and parallel behavior in CSF graphite. Growth in the horizontal direction will be transmitted to the sides of the stack when gaps between blocks are not provided. Horizontal contraction, however, will not be cumulative from block to block unless a keyed or interlocking arrangement is used. Since fuel channels are usually bored along the extrusion axis of blocks, contraction parallel to the bore can cause gaps to develop along the channel between blocks.

If layers of blocks are crisscrossed, horizontal dimensional behavior in one direction may vary considerably from layer to layer. Alternately recessed and protruding layers may develop at the sides parallel to fuel channels unless interlayer compensation is provided.

The inherent advantage of the horizontal structure is that considerable distortion can be accommodated before external support is necessary. The principal disadvantage is that fuel channels are transverse to the vertical distortion, which is unavoidably cumulative and may result in distortion of fuel or control rod channels, especially in the upper regions of the reactor.

9-5.2 VERTICAL STRUCTURES

Vertical arrangement of blocks and fuel channels reduces the problems associated with vertical distortion. The cumulation of vertical distortion prevents the formation of gaps along channels that may develop in horizontal reactors as a result of contraction parallel to the extrusion axis of blocks. The natural tendency of vertical columns to move with respect to the central axis of the reactor is, however, aggravated by horizontal

distortion and necessitates the use of keys and external restraints. In reactors where graphite temperatures are below 300°C, transverse growth in blocks results in the bowing of peripheral columns away from the central axis of the reactor. This type of distortion has been controlled by providing gaps at the sides of blocks for growth as in the Calder Hall reactors.⁷⁴ Transverse contraction in reactors operating at temperatures above 300°C results in the formation of gaps at the sides of blocks. If these gaps are closed by external forces, the vertical channels are bowed toward the central axis. Keyed blocks and layers of interlocked tiles were developed in the designs of the Tokai-Mura,⁷⁵ EDF 2,⁷⁶ and Trawsfynydd⁷⁷ reactors to accommodate contraction as well as growth. The unusual feature of these designs is that as the blocks or tiles change dimension their central axes remain fixed in space with respect to the restraint structure. Both designs have been satisfactorily tested in small-scale models; however, information on the dimensional behavior of these reactors during operation is not yet available.

References

1. W. H. Zachariasen, *X-Ray Evidence for Structural Change in Irradiated Graphite*, USAEC Report MUC-FWHZ-126, University of Chicago, Apr. 4, 1945.
2. W. H. Zachariasen, *X-Ray Diffraction Studies of Irradiated Graphite*, USAEC Report CP-3010, University of Chicago, May 24, 1945.
3. G. E. Bacon and B. E. Warren, X-Ray Diffraction Studies of Neutron-Irradiated Graphite, *Acta Cryst.* **9**: 1029-1035 (1956).
4. R. E. Nightingale and J. F. Fletcher, Radiation Damage to Graphite from 30 to 185°C, in *Proceedings of the French-American Conference on Graphite Reactors Held at Brookhaven National Laboratory, November 12 to 15, 1957*, pp. 32-41, USAEC Report BNL-489, Brookhaven National Laboratory, September 1958.
5. R. E. Nightingale et al., Damage to Graphite Irradiated up to 1000°C, in *Proceedings of the Second United Nations International Conference on the Peaceful Uses of Atomic Energy, Geneva, 1958*, Vol. 7, pp. 295-300, United Nations, New York, 1959.
6. J. R. Townsend and C. A. Lund, *X-Ray Diffraction Peak Shapes from Irradiated Graphites*, USAEC Report HW-25019, Hanford Works, May 12, 1952. (Classified)
7. F. W. Jones, The Measurement of Particle Size by the X-Ray Method, *Proc. Roy. Soc., (London)*, **A166**: 16-43 (1938).
8. E. P. Warekois, *X-Ray Diffraction Studies of Irradiated Graphites, (Interim Report No. 12)*, USAEC Report HW-20435, Hanford Works, Mar. 1, 1951. (Classified)
9. J. R. Townsend, *The Microcrystalline Structure of Neutron-Irradiated Graphite*, USAEC Report HW-24982, Hanford Works, May 10, 1952. (Classified)
10. V. I. Klimenkov and Yu. N. Aleksenko, Change in the Properties of Graphite When Irradiated by Neutrons, in *Conference of the Academy of Sciences of the USSR on the Peaceful Uses of Atomic Energy, July 1-5, 1955*, Session of the Division of Physical and Mathematical Sciences, USAEC Report AEC-TR-2435 (Pt. 1), pp. 227-237, (English translation).
11. A. E. Austin and R. J. Harrison, Annealing of Crystal Distortion in Irradiated Graphite, in *Proceedings of the Third Conference on Carbon Held at the University of Buffalo*, pp. 585-605, Pergamon Press, New York, 1959.
12. B. E. Warren, X-Ray Diffraction in Random Layer Lattices, *Phys. Rev.*, **59**: 693-698 (1941).

13. J. R. Townsend, Disorder in Neutron-Irradiated Graphite, *Reactor Sci. Technol.*, **3**(4): 67-77 (December 1953), USAEC Report TID-2011. (Classified)
14. J. F. Fletcher and W. A. Snyder, Use of Graphite in the Atomic Energy Program, *Am. Ceram. Soc. Bull.*, **36**: 101-104 (1957).
15. L. D. Loch et al., *Effect of Constitution of Graphites on Their Stability Under Low-Temperature Irradiation*, USAEC Report BMI-1042(Del.), Battelle Memorial Institute, Sept. 30, 1955.
16. G. R. Hennig and J. E. Hove, Interpretation of Radiation Damage to Graphite, in *Proceedings of the First United Nations International Conference on the Peaceful Uses of Atomic Energy, Geneva, 1955*, Vol. 7, pp. 666-675, United Nations, New York, 1956.
17. R. W. James, *The Crystalline State, Vol. II. The Optical Principles of the Diffraction of X-Rays*, George Bell & Sons, Ltd., London, 1948.
18. D. T. Keating, X-Ray Measurements on Low-Temperature Neutron-Irradiated Graphite, *Phys. Rev.*, **98**: 1859-1860 (1955).
19. S. B. Austerman, *Low-Temperature Irradiation and Annealing Experiments in Graphite*, USAEC Report NAA-SR-2457, Atomics International, July 15, 1958.
20. J. F. Fletcher, *Controlled Temperature Irradiation of Graphite (Interim Report No. 3)*, USAEC Report HW-36221, Hanford Atomic Products Operation, Sept. 5, 1956. (Classified)
21. E. M. Woodruff, Hanford Laboratories, General Electric Co., unpublished data, January 1960.
22. J. Cockcroft, The Scientific Work of the Atomic Energy Research Establishment, *Proc. Roy. Soc., (London)*, **A211**: 155-168 (1952).
23. G. E. Bacon, The Powder Diffraction Intensities of Graphite for X-Rays and Neutrons, *Acta Cryst.*, **5**: 492-499 (1952).
24. J. J. Antal et al., Long-Wavelength Neutron Transmission as an Absolute Method for Determining the Concentration of Lattice Defects in Crystals, *Phys. Rev.*, **99**: 1081-1085 (1955).
25. F. Seitz, On the Disordering of Solids by Action of Fast Massive Particles, *Discussions Faraday Soc.*, No. 5, pp. 271-282 (1949).
26. W. Bollmann, Electron Microscopic Observations of Radiation Damage in Graphite, *Phil. Mag.*, **5**: 621-624 (1960).
27. W. N. Reynolds et al., Aggregation and Dispersal of Radiation Damage in Graphite, *Nature*, **189**: 824-826 (1961).
28. S. Amelinckx and P. Delavignette, Dislocation Loops Due to Quenched-in Point Defects in Graphite, *Phys. Rev. Letters*, **5**: 50-51 (1960).
29. G. K. Williamson and C. Baker, A Comparison of Vacancy and Interstitial Loops in Graphite, *Phil. Mag.*, **6**: 313-314 (1961).
30. K. Izui and F. E. Fujita, Observation of Lattice Defects in Fission-Fragment Irradiated Graphite, *J. Phys. Soc. Japan*, **16**: 1032-1033 (1961).
31. C. N. Spalaris et al., Surface Properties of Irradiated Graphite, *J. Phys. Chem.*, **61**: 350-354 (1950).
32. R. E. Woodley, *A Preliminary Study of the Effect of Neutron Irradiation and Oxidation at Moderate Temperatures on the Structural Characteristics of CSF Graphite*, USAEC Report HW-52375, Hanford Atomic Products Operation, Sept. 4, 1957.
33. E. Fermi, *Report for Month Ending December 15, 1942*, Physics Division, USAEC Report CP-387, University of Chicago, December 1942.
34. S. K. Allison et al., *Technical Council Meeting of Dec. 31, 1942*, USAEC Report CS-404, University of Chicago, Dec. 31, 1942.
35. J. Franck and M. Burton, *Chemical Research—Radiation Chemistry Report for Month Ending May 15, 1943*, USAEC Report CC-649, University of Chicago, May 15, 1943.

36. *Laboratory Council—Information Meeting (Chemistry)*, USAEC Report CS-679, University of Chicago, May 24, 1943.
37. J. Franck and M. Burton, *Chemical Research, Radiation Chemistry, Report for Month Ending June 19, 1943*, USAEC Report CC-734, University of Chicago, June 19, 1943.
38. W. K. Woods, *Tube Alignment, Final Report on Production Test 106-44-P*, USAEC Report HW-7-3336, Hanford Works, Jan. 30, 1946. (Classified)
39. R. M. Evans, *Evidence of Graphite in the Piles Increasing in Volume at Alarming Rate*, USAEC Report DUH-7814, Feb. 20, 1946. (Classified)
40. W. K. Woods, *Graphite Expansion Committee Meeting of October 4, 1946*, USAEC Report HW-7-5172, Hanford Works, Oct. 7, 1946. (Classified)
41. W. K. Woods, *Graphite Expansion Committee Meeting of December 6, 1946*, USAEC Report HW-7-5493, Hanford Works, Dec. 12, 1946. (Classified)
42. W. K. Woods, *Graphite Expansion Committee Meeting of January 10, 1947*, USAEC Report HW-7-5691, Hanford Works, Jan. 23, 1947. (Classified)
43. W. R. Lewis, *Expansion of Graphite Blocks, Production Test 106-147-P*, USAEC Report HW-8392, Hanford Works, Dec. 30, 1947. (Classified)
44. W. K. Woods, *Graphite Expansion in the Piles*, USAEC Report HW-14522, Hanford Works, Oct. 4, 1949. (Classified)
45. J. T. Carleton, *Construction of Pile Moderator to Minimize Effects of Dimensional Changes*, USAEC Report HW-8890, Hanford Works, Jan. 29, 1948. (Classified)
46. A. A. Johnson and J. T. Carleton, *Reduction of Graphite Expansion Rate in a New Pile*, USAEC Report HW-15138, Hanford Works, Nov. 18, 1949. (Classified)
47. A. A. Johnson, W. R. Lewis, and P. H. Reinker, *Graphite Radiation Damage, Its Effects and Control in the Hanford Piles*, USAEC Report HW-16075, Hanford Works, Feb. 20, 1950. (Classified)
48. W. R. Lewis, *Invention Report HWIR-173*, USAEC Report HW-20573, Hanford Works, Mar. 19, 1951. (Classified)
49. W. A. Hedden et al., *Experimental Carbons and Graphites for Irradiation Studies*, USAEC Report BMI-962, Battelle Memorial Institute, Oct. 26, 1954.
50. J. F. Music and H. F. Zuhr, *Technical Activities Report June 1952—Graphite Development—Pile Graphite*, USAEC Report HW-24836, Hanford Works, July 10, 1952. (Classified)
51. W. A. Snyder, *Radiation Damage to Graphite at 500°C*, USAEC Report HW-52030RD, Hanford Atomic Products Operation, Sept. 23, 1957.
52. D. H. Curtiss and R. E. Trumble, *Technical Data Pertinent to Graphite Contraction*, USAEC Report HW-58026, Hanford Atomic Products Operation, Dec. 8, 1958. (Classified)
53. R. F. Corlett, *Discussion of NPR Contraction*, USAEC Report HW-57654, Hanford Atomic Products Operation, Oct. 2, 1958. (Classified)
54. J. M. Davidson et al., High Temperature Radiation-induced Contraction in Graphite, in *Proceedings of the Fourth Conference on Carbon Held at the University of Buffalo*, pp. 599–605, Pergamon Press, New York, 1960.
55. W. K. Woods, et al., Irradiation Damage to Artificial Graphite, in *Proceedings of the First United Nations International Conference on the Peaceful Uses of Atomic Energy, Geneva, 1955*, Vol. 7, pp. 455–471, United Nations, New York, 1956.
56. F. W. Albaugh, *Reactor and Fuels Research and Development Operation Monthly Report—May 1959*, USAEC Report HW-60505A, Hanford Atomic Products Operation, June 15, 1959. (Classified)
57. W. A. Snyder and W. C. Riley, *Low Temperature Radiation Damage to Pile Grade Graphites*, USAEC Report HW-35869, Hanford Atomic Products Operation, July 1, 1955. (Classified)

58. H. Sheard and N. J. Pattenden, *The Effect of Pile Irradiation on the Linear Dimensions of AGXP Graphite*, Canadian Report CRNE-496, June 1952.
59. G. H. Kinchin, The Effects of Irradiation on Graphite, in *Proceedings of the First United Nations International Conference on Peaceful Uses of Atomic Energy, Geneva, 1955*, Vol. 7, pp. 472-478, United Nations, New York, 1956.
60. G. H. Kinchin, *The Effects of Irradiation on Graphite*, Canadian Report CRNE-539, Apr. 7, 1953.
61. H. Hering et al., Intercomparison of Graphite Irradiations, in *Proceedings of the French-American Conference on Graphite Reactors Held at Brookhaven National Laboratory, November 12 to 15, 1957*, pp. 2-8, USAEC Report BNL-489, Brookhaven National Laboratory, September 1958.
62. W. C. Riley, *Pile Material Evaluation of Experimental Graphites*, USAEC Report HW-33705, Hanford Atomic Products Operation, Nov. 8, 1954. (Classified)
63. E. M. Woodruff, Dimensional Changes in Irradiated Graphite, in *US/UK Graphite Conference Held at St. Giles Court, London, December 16-18, 1957*, USAEC Report TID-7565 (Pt. 1), pp. 1-10, 1959.
64. W. C. Riley and E. M. Woodruff, *Thermal Expansion of Pile Graphites*, USAEC Report HW-43395, Hanford Atomic Products Operation, May 25, 1956.
65. H. H. Yoshikawa, *Irradiation Effects on NPR Core Graphite, Initial Short Term Irradiation Results*, USAEC Report HW-58762, Hanford Atomic Products Operation, Mar. 24, 1961.
66. J. M. Davidson and J. W. Helm, Effect of Temperature on Radiation-induced Contraction of Reactor Graphite, in *Proceedings of the Fifth Conference on Carbon Held at Pennsylvania State University, June 19-23, 1961*, Pergamon Press, 1962.
67. J. M. Davidson et al., *Technical Basis for NPR Graphite Recommendations*, USAEC Report HW-64287, Hanford Atomic Products Operation, Mar. 30, 1960. (Classified)
68. J. M. Davidson and J. W. Helm, *The H-1 High Temperature Graphite Irradiation Experiment*, USAEC Report HW-64286, Hanford Atomic Products Operation, Apr. 9, 1961.
69. F. W. Woodfield, *Unclassified R&D Programs Executed for the Division of Reactor Development and the Division of Research for January 1961*, USAEC Report HW-68542, Hanford Atomic Products Operation, Feb. 10, 1961.
70. D. R. de Halas and H. H. Yoshikawa, Mechanism of Radiation Damage to Graphite at High Temperatures, in *Proceedings of the Fifth Conference on Carbon Held at Pennsylvania State University, June 19-23, 1961*, Pergamon Press, 1962.
71. G. J. Dienes and G. H. Vineyard, *Radiation Effects in Solids*, Interscience Publishers, Inc., New York, 1957.
72. D. H. Curtiss, Graphite Radiation Damage as a Reactor Operational Problem, in *US/UK Graphite Conference Held at St. Giles Court, London, December 16-18, 1957*, USAEC Report TID-7565 (Pt. 2), February 1959. (Classified)
73. R. W. Powell, Control of Radiation Damage in a Graphite Reactor Structure by Annealing, in *US/UK Graphite Conference Held at St. Giles Court, London, December 16-18, 1957*, USAEC Report TID-7565 (Pt. 1), pp. 46-63, February 1959.
74. E. Long, The Calder Hall Graphite Structure, *Nuclear Power*, 3(22): 58-63 (February 1958).
75. R. W. Bailey and J. L. Head, Earthquake-Resistant Core for Tokai-Mura, *Nuclear Eng.*, 6: 25-27 (1961).
76. M. Roux and M. Bienvenu, The Chinon Nuclear Power Plant EDF 1 and EDF 2, in *Proceedings of the Second United Nations International Conference on the Peaceful Uses of Atomic Energy, Geneva, 1958*, Vol. 8, pp. 356-379, United Nations, New York, 1959.
77. P. C. Warner, Design of the Trawsfynydd Graphite Cores, *Nuclear Eng.*, 6: 21-23 (1961).

Radiation Effects on Electrical and Thermal Properties

R. E. NIGHTINGALE†

10-1 Electrical Resistance

The mean free path of the conduction electrons in unirradiated electrographites is relatively large, being limited only by scattering at the crystallite boundaries. The introduction of crystal defects by neutron and heavy-particle radiation changes the concentration of the charge carriers (electrons and holes) and also the number of scattering centers. The study of these changes has aided the understanding of the nature of the radiation-induced defects.

The impact of changes in electrical resistivity per se on the engineering aspects of reactor technology has been relatively minor. Such changes have introduced no problems in the operation of graphite-moderated reactors.

Primak¹ has suggested the use of resistivity of graphite as a means of monitoring the damaging portion of the neutron flux in radiation-damage studies (Sec. 7-5.5).

10-1.1 PARTICLE-ACCELERATOR IRRADIATIONS

A number of studies have been conducted on the effects of charged-particle irradiation on the electrical resistivity of graphite. The irradiation temperatures range from that of liquid helium to 250°C; the bombarding particles include protons,² deuterons,^{3,4} alpha particles,^{3,4} and electrons.⁵⁻⁷ In terms of the energy dissipated during the irradiations, the efficiency of the particles of the same energy for increasing the resistivity increases in the order: electron, proton, deuteron, and alpha particle.⁴

The effects of proton bombardments have been compared with neutron irradiations at several temperatures. As shown in Fig. 10.1, the changes resulting from proton and neutron irradiations are similar. The initial slopes of the curves and the saturation values decrease with irradiation temperature, whereas the exposures where saturation begins increase with irradiation temperature. By assuming that the two-dimensional electron-band model is applicable and by making certain other simplifying assumptions, Hove⁸ has concluded that the number of electrons trapped per effective scatterer decreases with increasing irradiation temperature. The rapid decrease with irradiation temperature of the initial slopes of the curves in Fig. 10.1 is believed to reflect the fact that fewer free electrons are trapped

† Hanford Laboratories, General Electric Company, Richland, Wash.

at the higher temperatures; the change in saturation values is attributed to the decrease in the relative number of trapped electrons per scattering center.

These conclusions are compatible with the damage model proposed by Hennig and Hove⁹ wherein it is suggested that at low temperatures (-200°C) close interstitial-vacancy pairs are produced which trap only

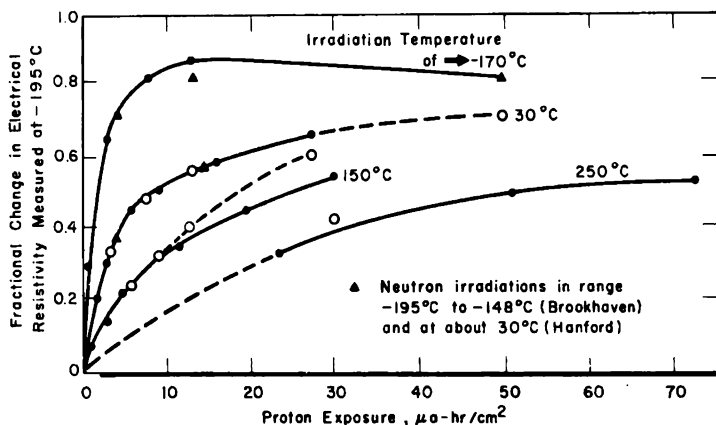


FIG. 10.1 Change in electrical resistivity of graphite irradiated with neutrons and 8.6-Mev protons. The open symbols refer to samples irradiated at a lower temperature and annealed at the temperature indicated. An equivalence of $1 \mu\text{a-hr/cm}^2$ to 1.5 Mwd/At is assumed. (From Hove, *Progress in Nuclear Energy, Series V, Metallurgy and Fuels*, Pergamon Press, Ref. 8.)

one electron. Those defects that anneal only at higher irradiation temperatures are believed to include isolated interstitials that trap one electron, isolated vacancies that trap two electrons, and clustered defects that trap several electrons. Presumably all these act as single scatterers, and therefore, when the close pairs are annealed, the ratio of trapped electrons to scatterers decreases.

It will be noted from Fig. 10.1 that proton irradiations at 30°C and above, followed by annealing at a higher temperature, result in a slightly larger change in electrical resistivity than irradiations carried out at higher temperatures. The phenomenon of irradiation annealing is suggested; however, of all the physical properties studied, electrical resistivity has been found to be the least affected by annealing during neutron irradiation (Sec. 13-4).

10-1.2 REACTOR IRRADIATIONS

The effects of reactor radiation on the electrical resistivity of graphite have been measured on a wide variety of materials ranging from graphitized lampblack to carefully selected single crystals. Nuclear graphites, which lie between these two extremes, have been most thoroughly studied. The data on two grades are shown in Fig. 10.2. In contrast to most other proper-

ties, the changes in electrical resistivity rapidly approach a saturation value, and the changes thereafter occur over a long period of time. This rapid approach to saturation has been explained^{9,12} in terms of the relative change in the number of charge carriers and scattering centers. At low doses the increase in the concentration of positive holes is almost balanced by the

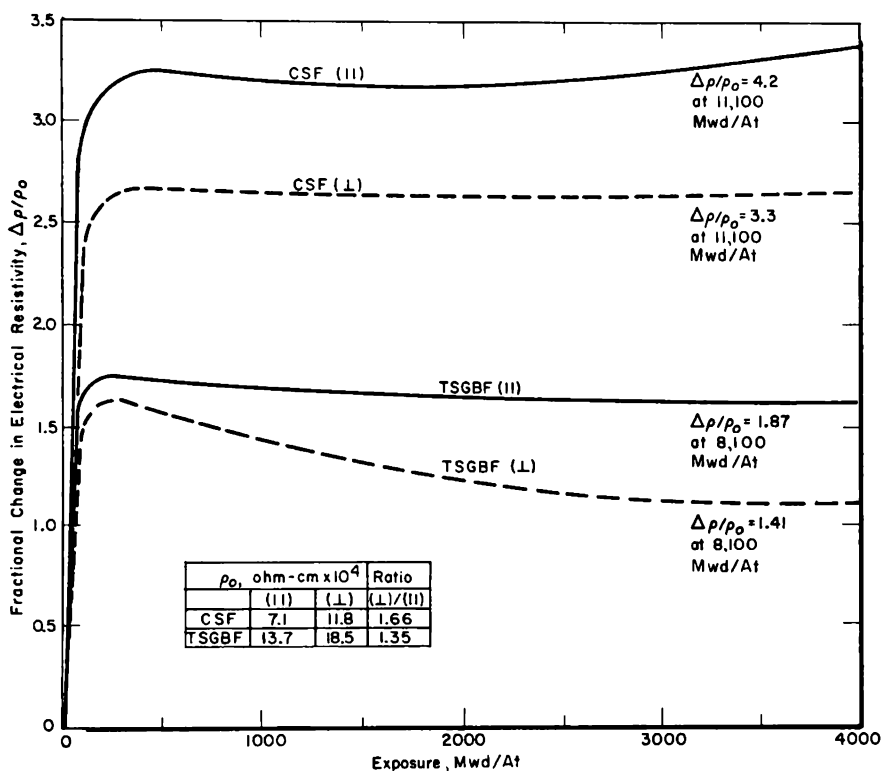


Fig. 10.2 The fractional change in the room-temperature electrical resistivity ($\Delta\rho/\rho_0$) resulting from irradiations near room temperature.^{10, 11}

decrease in the concentration of free electrons, and therefore the increase in resistivity is almost proportional to the number of scattering centers. After a relatively low dose (~ 200 Mwd/At at 30°C), the free-electron concentration is greatly reduced and does not contribute significantly to the conductivity. At this point the increasing concentration of holes counteracts the decreasing mean free path between scattering centers, and the resistivity remains relatively constant.

Although there is little change in ρ after 200 Mwd/At, the changes that continue to occur in the graphite cause the activation energy for annealing electrical resistivity to increase (see Fig. 13.12). Apparently the scattering centers become more complex and more difficult to anneal as the structure becomes heavily damaged.

Because the initial resistivity of graphite is strongly dependent on the degree of crystallinity, the fractional increase in resistivity caused by irradiation is also sensitive to the crystallinity. Relatively large differences in the saturation value of fractional resistivities are found, even between different grades of nuclear graphite (see Fig. 10.2). The differences in the graphitization temperatures of CSF and TSGBF (2800 and 2450°C, respectively) and the graphitizability of the starting cokes largely account for the different degree of crystallinity (Table 5.2) and different values of ρ_0 . More extreme examples may be found in the literature. For example, graphitized carbon black ($\rho_0 = 60 \times 10^{-4}$ ohm-cm) saturates¹³ at $\Delta\rho/\rho_0 \simeq 0.15$ when irradiated at 30°C; whereas natural flake crystals with a very high anisotropy ratio [$\rho_0(\perp)/\rho_0(\parallel) \simeq 140$] saturate¹⁴ at $\Delta\rho/\rho_0(\parallel) \simeq 19$ and $\Delta\rho/\rho_0(\perp) \simeq 2$. Saturation values of $\Delta\rho/\rho_0$ for nuclear graphites reported by other investigators^{12,15} are similar to those shown in Fig. 10.2.

The changes in electrical resistivity of graphite irradiated above room temperature are shown in Fig. 10.3. If the changes are compared with those

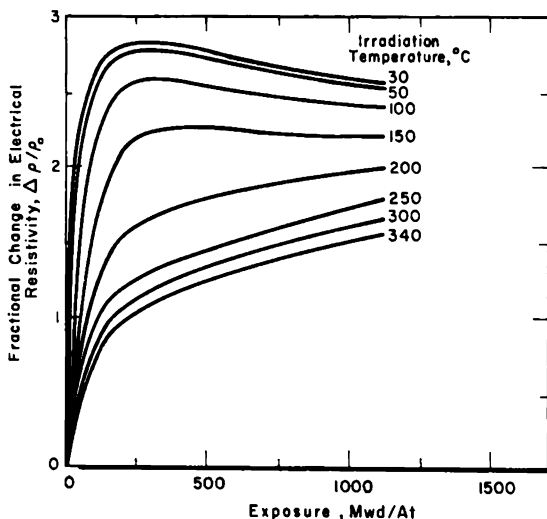


FIG. 10.3 The fractional change in the room-temperature electrical resistivity ($\Delta\rho/\rho_0$) of CSF (L) graphite at several irradiation temperatures.¹⁶

of stored energy, length, c spacing, and thermal conductivity, it will be seen that electrical resistivity is the least sensitive to the irradiation temperature. At 1000 Mwd/At the ratios of the fractional changes in various properties at 30°C to those at 300°C vary from about 12 to 25 for most cases; this ratio is only 1.7 for electrical resistivity. The fact that irradiation does not greatly enhance annealing of electrical resistivity (Sec. 13-4) is undoubtedly related to this temperature dependence.

10-2 Magnetoresistance

The magnetoresistance decreases very rapidly as the electron mobility decreases (Sec. 6-4.4). For example, the magnetoresistance coefficient (A) defined† by

$$\frac{\Delta\rho}{\rho} = AH^2 \quad (10.1)$$

where H is the magnetic-field strength, is reduced in KC (||) graphite from 5.1×10^{-10} to $<0.01 \times 10^{-10}$ emu even before the Hall coefficient reaches a maximum.¹⁷ At an exposure of approximately 50 Mwd/At at 30°C, the magnetoresistance coefficient becomes negative and then slowly approaches zero at higher exposures. The detailed changes following the rapid initial decrease are not well understood, particularly the anomalous negative values.

10-3 Hall Coefficient

The Hall coefficient is of considerable interest because it provides direct information on the nature and number of electron carriers (Sec. 6-4.3). The effect of irradiation on the Hall coefficient has been reported by several investigators with generally similar results. The studies include short-term (<200 Mwd/At) irradiations,^{18,19} and longer term irradiations followed by annealing.²⁰ The effects of exposure on two materials with widely different crystallite sizes are illustrated in Fig. 10.4.

In Sec. 10-1.2 the changes in electrical resistivity were explained in terms of the scattering due to damage centers and the change in the number of charge carriers. The Hall effect can be qualitatively explained in a similar fashion.²¹ Since the Hall coefficient is negative in unirradiated graphite, the charge carriers are predominantly electrons [i.e., $n_e\mu_e^2 > n_h\mu_h^2$ (see Eq. 6.8)]. As traps are produced by irradiation, the ratio of the charge carried by free electrons to the charge carried by positive holes decreases. The Hall coefficient passes through zero and attains a maximum positive value. At higher exposures when $n_e\mu_e^2 \ll n_h\mu_h^2$ the Hall coefficient becomes inversely proportional to the number of holes and decreases with continued irradiation as illustrated in Fig. 10.4.

The changes in the Hall coefficient can be described quantitatively on the basis of equations derived for a two-band conductor,¹⁹ and the number of trapped electrons and the change in mean free path due to scattering from lattice defects can be estimated. These calculations have been extended to an estimate of the density of electron-trapping defects.²²

The curve of Hall coefficient vs. exposure in Fig. 10.4 lies above that

† $\Delta\rho/\rho$ varies approximately as H^2 only at low field strengths (several kilogauss). Kinchin¹⁹ has found an $H^{1.63}$ dependence at 77°K and an $H^{1.88}$ dependence at 290°K.

for KC (||). It reaches a maximum value (not shown in the figure) of 2.1 emu at 24 Mwd/At. The difference in these two curves has been attributed¹³ to additional trapping of free electrons at the crystallite boundaries of the graphitized lampblack.

Changes in the Hall coefficient of irradiated graphite have been correlated with the changes produced chemically by a known concentration of bisulfate ions.²³ The bisulfate ions were introduced quantitatively by the electrolysis of concentrated sulfuric acid between graphite electrodes.

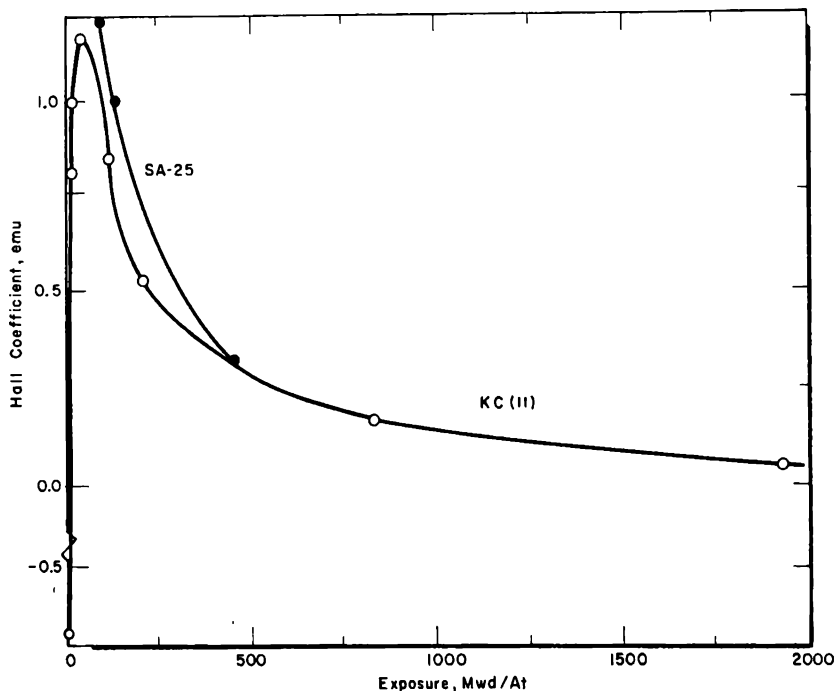


FIG. 10.4 The effects of room-temperature irradiation on the Hall coefficient for a nuclear graphite, KC (||), and a graphitized lampblack, SA-25. The crystallite size of SA-25 is approximately one-tenth that of KC.^{13, 17}

Both the chemical impurities and the radiation-induced defects act as electron traps. It was found that 9×10^{-5} chemical traps per carbon atom produce the same change in the Hall coefficient as a reactor exposure of 1 Mwd/At. The Hall coefficient of the irradiated graphite and of the graphite containing bisulfate ions was described satisfactorily by the two-band conductor model,²⁴ although the electrical resistance and magnetoresistance of the latter material were not.

10-4 Thermoelectric Power

As does the Hall coefficient, the thermoelectric power provides information on the effects of irradiation on the electronic band structure. The

thermoelectric power is an extremely sensitive function of the dose (Fig. 10.5). If it is assumed that the number of electrons trapped from the conduction band is proportional to the exposure, the two-dimensional band theory correctly predicts the shape of the curves in Fig. 10.5 for KC (||) graphite.^{25, 26} For graphites with relatively large crystallites, the mean free path of the conduction electrons appears to be independent of their energy.

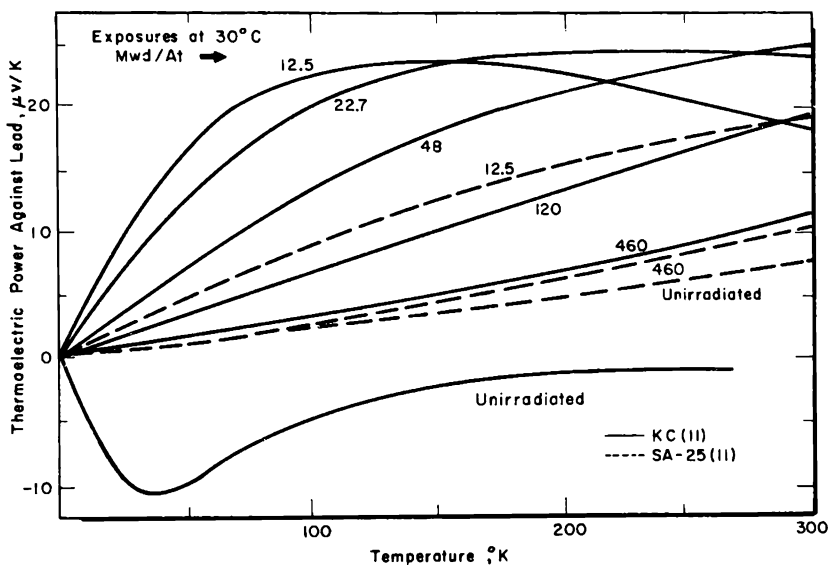


Fig. 10.5 The thermoelectric power of irradiated KC (||) and SA-25 graphitized lampblack.²⁵

The thermoelectric power of SA-25 is not as sensitive to irradiation effects as that of KC, and it is not until high exposures are reached that their thermoelectric behaviors become similar. This has been explained in terms of the type of scattering center.²⁶ In graphites with large crystallites, defect scattering is also relatively important even in unirradiated samples, and irradiation only increases the number of defects. In graphites with small crystallites, boundary scattering is expected to predominate until the crystallites have suffered appreciable damage. This explanation cannot account for the different behavior of the unirradiated sample. Although it has been noted¹³ that the difference could be due to the fact that scattering at boundaries and scattering at internal defects probably depend differently upon the energy of the electrons, no calculations have been published.

Although the Hall coefficient and magnetic susceptibility give a common value of about 9×10^{-5} traps per carbon atom per megawatt-day per adjacent ton,^{23, 26} no such correlation exists for the thermoelectric power.² Moreover, the correlation between neutron and proton irradiations which has been derived from other properties does not apply to thermoelectric

power. One must conclude that thermoelectric effects in graphite are not well understood at the present time.

10-5 Magnetic Properties

The theory of electronic phenomena in graphite indicates that the magnetic susceptibility should depend only on the free-electron concentration. In contrast to other electronic properties, it should be independent of scattering effects. The magnetic susceptibility is unique in another respect. Although the susceptibility is highly anisotropic, the total susceptibility (the sum of the susceptibilities measured in any three orthogonal directions) is almost independent of direction of measurement and crystallite size for materials that have been heated to graphitization temperatures.

Graphite is highly diamagnetic. Values of the total susceptibility measured in electromagnetic (cgs) units range from -21.5×10^{-6} for graphitized lampblack (SA-25) to -23.2×10^{-6} for compressed flakes of natural Ceylon graphite.²⁷ A slightly lower diamagnetism of -20.8×10^{-6} emu has been measured for nuclear KC graphite.

The diamagnetism is attributed to the presence of electrons near the edge of the Brillouin zone (Sec. 6-4.1). These electrons are trapped by damage centers, and therefore the susceptibility is rapidly reduced by

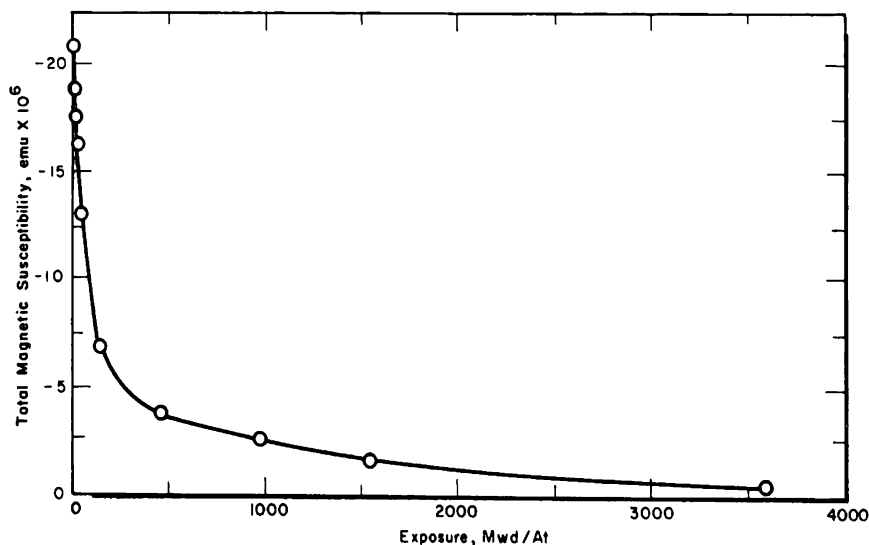


Fig. 10.6 The change in total magnetic susceptibility of KC graphite due to irradiation at 30°C. The total susceptibility is the sum of the susceptibilities measured in any three orthogonal directions.³⁰

irradiation as illustrated in Fig. 10.6. A correlation²⁸ with the susceptibility resulting from chemical traps indicates that over the exposure range 0 to 20 Mwd/At approximately 9×10^{-5} electron traps per atom are formed per megawatt-day per adjacent ton.

As neutron bombardment proceeds, trapping centers having an associated spin will make a paramagnetic contribution to the susceptibility. If it is assumed that the paramagnetic centers are isotropic and the Peierls type diamagnetism is anisotropic, then the ratio of susceptibilities measured parallel and perpendicular to the axis of extrusion can be used to separate the paramagnetic and diamagnetic contributions. The data²⁷ indicate that the paramagnetic contribution is small for exposures less than 1000 Mwd/At, although the evidence on this point would be more conclusive on graphites having a higher anisotropy. From an analysis²⁸ of the available data, it was concluded that the paramagnetic contribution to the susceptibility is proportional to the square root of the neutron exposure and attains a value of only 0.5×10^{-6} emu at 1000 Mwd/At.

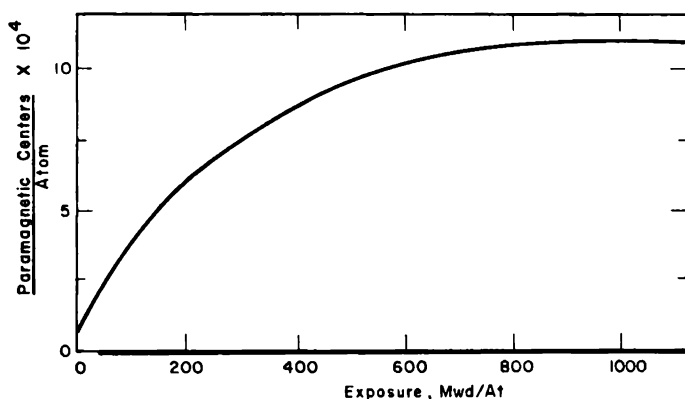


FIG. 10.7 Paramagnetic resonance⁹ of graphite irradiated at 30°C.

The measurement of paramagnetic spin centers by magnetic susceptibility is difficult because of the large diamagnetism. A paramagnetic resonance method has been employed²⁹ for this purpose, and the results are shown in Fig. 10.7. The number of paramagnetic spin centers formed per carbon atom (N_c) during room-temperature irradiations is given approximately by

$$N_c = 4 \times 10^{-5} E^{1/2} \quad (10.2)$$

where E is the room-temperature exposure in megawatt-days per adjacent ton. Thus the rate of production of electron traps is several times the rate of production of paramagnetic centers in the exposure range (0 to 20 Mwd/At) over which the former has been measured.

The concentration of paramagnetic centers appears to saturate at about 1000 Mwd/At, which suggests that the centers are simple defects, perhaps single interstitials or single vacancies. Since paramagnetic centers produced at -196°C are mobile at -100°C , it is more probable that the centers are predominantly interstitials.

10-6 Thermal Conductivity

10-6.1 REACTOR IRRADIATIONS

Conduction of heat in polycrystalline graphite takes place mainly by lattice waves rather than by electronic transport. The evidence for this comes largely from the Wiedemann-Franz ratio for graphite, which is about 100 times larger than the theoretical value for purely electronic conduction (Sec. 6-2.1). The mean free path of the lattice waves, to which the thermal conductivity is roughly proportional, is of the same order of magnitude as the size of the individual crystallites, indicating that the lattice waves are scattered at crystal boundaries.

The thermal conductivity (k) is markedly reduced by radiation-induced scattering centers created within the crystallites. This reduction in thermal conductivity in the moderator structure is not necessarily undesirable. However, it is necessary to be able to anticipate changes in thermal conductivity so that the reactor lattice can be designed to accommodate the accompanying changes in heat transfer which will occur during the life of the reactor.

The radiation-induced changes in the thermal resistivity measured at room temperature are shown in Figs. 10.8 and 10.9. As with electrical resis-

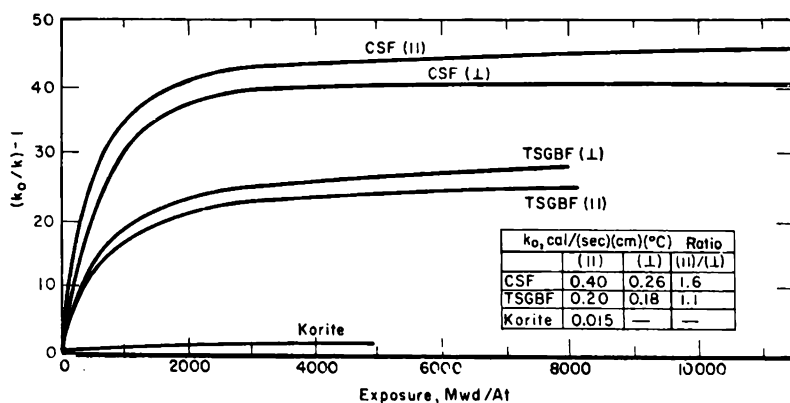


FIG. 10.8 Fractional change in the room-temperature thermal resistivity due to reactor irradiation near 30°C. The crystallinity of the unirradiated materials decreases in the following order: CSF, TSGBF, and Korite. The curves for exposures >3000 Mwd/At are based upon only a few points that are scattered about the curves. The uncertainty in the values above 3000 Mwd/At is ± 10 per cent.^{10, 11, 30}

tivity, the fractional change in thermal resistivity, $(k_0/k) - 1$, is greater in the more crystalline materials. Prolonged neutron irradiation at 30°C reduces the thermal conductivity of each graphite to a common value, which approaches 0.005 to 0.007 cal/(sec)(cm)(°C).

Data on the thermal conductivity of graphite irradiated in the temperature range 50 to 400°C are limited to low exposures (<1200 Mwd/At).

More information is available at higher temperatures; after 4500 Mwd/At the fractional change³¹ in the thermal resistivity of CSF (\perp) is 3.4 at 400°C and 2.3 at 500°C.

Of more direct interest in reactor applications is the effect of high-temperature irradiation on the thermal conductivity measured at high

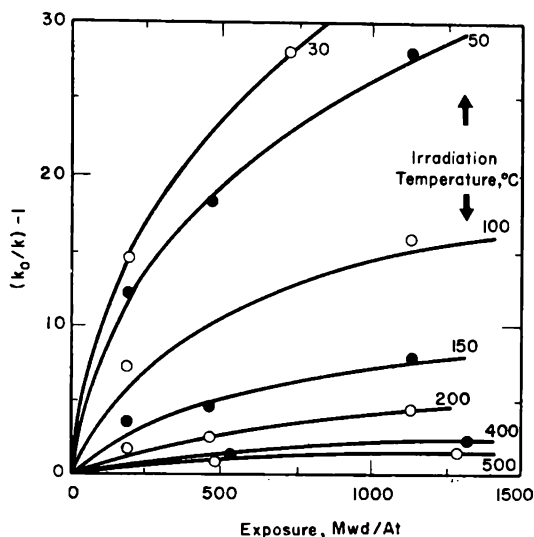


Fig. 10.9 The fractional change in the room-temperature thermal resistivity of CSF (\perp) graphite irradiated at several temperatures.^{16, 31}

temperatures. Only fragmentary results have been reported, and one must be guided by measurements made on unirradiated material and by theoretical predictions.

The lattice thermal conductivity of solids is given approximately by the Debye relation

$$k = \frac{1}{3} C_p \lambda v \quad (10.3)$$

where C_p is the lattice specific heat, λ is the mean free path of the scattered lattice waves, and v is the effective velocity of the waves (see also Sec. 6-2.1). Carter³² has derived a family of curves of k vs. T , each curve representing a graphite characterized by a ratio λ_i/λ_θ , where λ_i is the temperature-independent wave length determined by the boundary scattering and λ_θ is the temperature-dependent wave length assumed to be inversely proportional to the absolute temperature.† The value of λ is given by the equation

$$\frac{1}{\lambda} = \frac{1}{\lambda_i} + \frac{1}{\lambda_\theta} \quad (10.4)$$

† Recent work⁴¹ indicates that better agreement with experiment is obtained if λ_θ is assumed to be inversely proportional to the square of the absolute temperature.

The product $C_p\lambda$ contains the temperature-dependent part of the thermal conductivity. A set of curves normalized by choosing $\nu\lambda_i$ to give the peak thermal conductivity of CSF (\perp) graphite at 300°K is shown in Fig. 10.10. As λ_i/λ_0 decreases, the curves tend to flatten out, and the maximum in the curves shifts to higher temperatures.

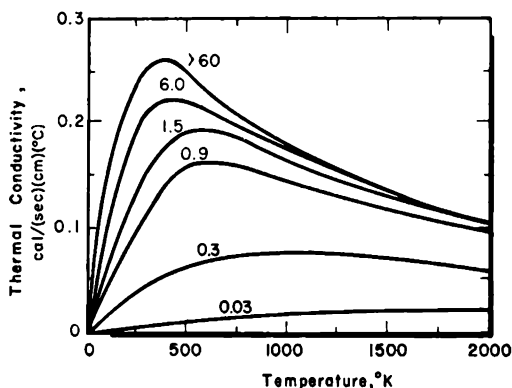


FIG. 10.10 Theoretical curves for the thermal conductivity of graphite for various values of λ_i/λ_0 at 300°K. The value of λ_i/λ_0 is less than 60 for graphites that are incompletely graphitized or that have suffered radiation damage.³²

The trends suggested by experimental measurements are in general accord with these predictions in those few cases where it is possible to make valid comparisons. The experimental work is summarized in Fig. 10.11.

The KC graphite is a well-graphitized material having a preferred orientation somewhat greater than CSF. Figure 10.11 and additional measurements at low temperature³² show that the maximum thermal conductivity occurs near 0°C, slightly lower than that for CSF. Other generally similar curves have been reported on unirradiated polycrystalline graphites.³²⁻³⁵

The graphites MH4LM-90, R-0025, and ATL-82 are high-density ($\rho \simeq 1.90$ g/cm³) low-permeability materials (see Table 6.23). The high thermal conductivity of MH4LM-90 suggests that it is highly crystalline; the anisotropy is low, and little difference is expected in the thermal conductivity measured in the transverse and parallel directions. After a short irradiation† at 360 to 420°C, the thermal conductivity is reduced to 50 per cent of its original value at 30°C and is almost independent of the measuring temperature.

The thermal conductivities of ATL-82 and R-0025 are lower than that of MH4LM-90. In the case of the R-0025, this may be due to the non-graphitizing carbon black that was added to the base formulation. Again

† The changes in thermal conductivity suggest that the dose of 3.6×10^{19} neutrons (thermal)/cm² in the Materials Testing Reactor is roughly equivalent to 100 Mwd/At.

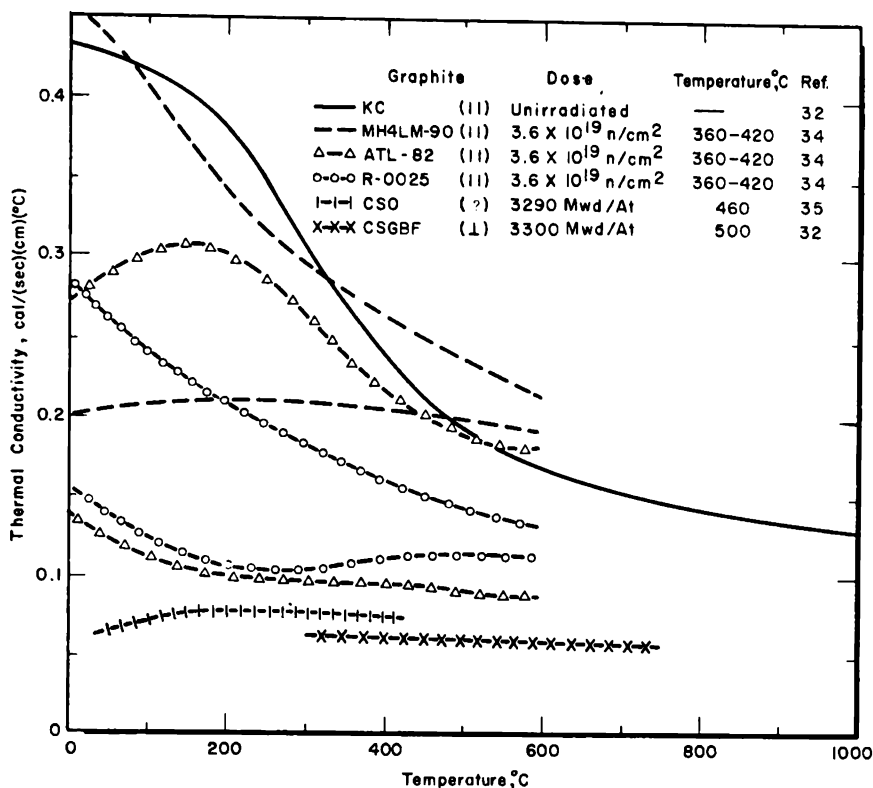


FIG. 10.11 The change in the thermal conductivity of graphite with temperature. Where two curves are shown for a given material, the lower one pertains to the irradiated sample.

the effect of irradiation on both materials is to reduce the conductivity and displace the maximum of the curves to higher temperatures.

The CSO and CSGBF (I) curves show that irradiation to much higher doses reduces the thermal conductivity further and almost completely eliminates the maximum in the curves.

10-6.2 INTERPRETATION

The radiation-induced changes in the low-temperature ($<100^\circ\text{K}$) thermal conductivity have been interpreted on the basis of a two-phase structure composed of graphitic particles, each consisting of many single crystallites, and bonded by a thin isotropic layer of carbon.³⁶ It is suggested that the isotropic layer is formed from some of the pitch that does not graphitize completely. Since the extent of graphitization of the pitch binder is at present a controversial point and is not essential to the argument, it is perhaps best to simply assume that well-crystallized grains are separated by isotropic carbon regions whose dimensions are large compared with the wave length of the thermal wave. The equation that gives the

temperature dependence of thermal conductivity for this model has the form³⁷

$$\frac{T^3}{k} = AT + BT^2 + C \quad (10.5)$$

where A is inversely proportional to the crystalline size, B is directly proportional to the number of internal defects of the crystallite, and C is a function of the thickness of the isotropic regions. Experimental values of T^3/k are shown as a function of T^2 in Fig. 10.12. The slopes of the curves

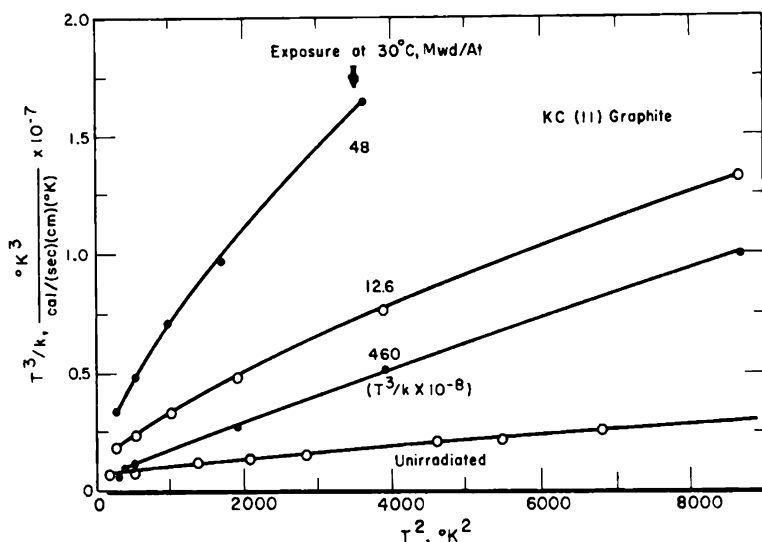


FIG. 10.12 The function T^3/k vs. T^2 for KC (11) graphite at several exposures at 30°C. Note the change in scale for the 460 Mwd/At curve. (From Hove and Smith, *Physical Review*, Ref. 36.)

decrease with temperature, as predicted from Eq. 10.5, and become almost constant at the higher temperatures. Similar behavior is found with AWG graphite and the graphitized lampblack SA-25. The slope of the linear portion of each curve should be proportional to the number of defects in the crystalline phase. As expected, these slopes increase rapidly with increasing exposure. By subtracting the slope of the unirradiated sample and correcting for the type of graphite, Hove and Smith³⁶ derived a function proportional to the number of radiation-induced defects as a function of exposure for KC, AWG, and SA-25. This function indicates that, although the crystallite size of SA-25 is of the order of one-tenth that of KC and AWG, about twice as many defects appear to be retained by SA-25 as by the other two materials. This result is contrary to expectations (Sec. 12-4.2) and has not been explained.

The validity of Eq. 10.5 is supported by the dependence on temperature

of the thermal conductivity of dilute bromine-graphite residue compounds. Since the residual bromine in these compounds is thought to be at the boundary sites, the linear portion of T^3/k vs. T^2 curves should have the same slope until bromine begins to enter the lattice (>1 per cent bromine); then the slope should increase. This behavior has been observed experimentally.³⁶

A detailed interpretation of the radiation-induced changes to the thermal conductivity above about 100°K in terms of the structure of graphite has not been developed. It is apparent that Eq. 10.5 is not valid in the temperature range of 30°C and above because it incorrectly predicts that the thermal conductivity increases monotonically with temperature.

10-7 Specific Heat†

Irradiation causes a small increase in the specific heat (C_p) of graphite. De Sorbo and Tyler³⁸ have measured the effect over the temperature range 13 to 300°K on a nuclear graphite irradiated to about 2200 Mwd/At at 30°C . Goodman et al.³⁹ have measured the increase in specific heat between 20 and 80°K for three different neutron exposures.

The increase in C_p can be understood if it is assumed that the atoms which are displaced to interstitial positions have an effective Debye temperature much less than that of the average lattice atom. If the displaced atoms are assumed to be isolated interstitials, they will contribute to the specific heat at low temperatures like simple Einstein oscillators. The fraction (f) of displaced interstitial atoms has been estimated³⁸ by fitting the excess specific heat, ΔC_p , to an Einstein function with a characteristic temperature of 180°K . The ΔC_p is normalized to a saturation value at 300°K of $3Rf$, where R is the gas constant. This gives a value of $f = 0.014$, which is about an order of magnitude less than the average value calculated from other properties for this exposure (Sec. 7-4). The lower value may be due to the considerable amount of clustering which would be expected in a severely damaged sample. In any case, the agreement is satisfactory in view of the uncertainties in such estimates.

Goodman et al.³⁹ calculated the characteristic frequency of an atom displaced to an interplanar position directly below the center of a carbon hexagon. The characteristic frequency normal to the (001) planes was calculated with two different forms of the potential function and was found to be several times greater than that calculated for the two vibrational modes parallel to the planes. It was therefore concluded that ΔC_p is determined by the two parallel modes.

The ΔC_p vs. T curves of Goodman are represented quite well by Einstein functions with a characteristic temperature of $105 \pm 5^\circ\text{K}$. The calcu-

† Specific heat as used in this section refers to the specific heat measured at temperatures low enough that no annealing of irradiation damage takes place during measurement.

lated frequencies of the parallel vibrational modes were equated to the frequency derived from the characteristic Einstein temperature, and an average value was calculated for the local expansion of the planes of 1.4 ± 0.4 Å. This compares favorably with the value of ϵ calculated by Bacon and Warren⁴⁰ (see Sec. 9-1.4).

To calculate f , Goodman assumed that ΔC_p approaches the value $2Rf$ since the calculations indicated that only two vibrational modes contributed to ΔC_p . At low neutron exposures (E), the ratio f/E approached a value of $(3.4 \pm 0.5) \times 10^{-22}$ per thermal neutron/cm². Comparison with other calculations of f is difficult because E is given in terms of thermal neutrons per square centimeter in an unreported facility. However, if a reasonable equivalence of $1 \text{ Mwd/At} = 10^{17}$ to 10^{18} neutrons/cm² is assumed, these results are in good agreement with other estimates of the displacement rate.

The pre- and postirradiation measurements of De Sorbo and Tyler were not performed on the same sample. Goodman has reported that a scatter in C_p of up to 10 per cent may be expected on different samples. Hence the uncertainties in De Sorbo and Tyler's values of the characteristic temperature and of f , which are derived from the ΔC_p curves, are probably large enough that they are not in serious disagreement with Goodman's values.

References

1. W. Primak and L. H. Fuchs, Fast Neutron Damaging in Nuclear Reactors. I. Radiation Damage Monitoring with the Electrical Conductivity of Graphite, *Nuclear Sci. and Eng.*, **2**: 49-56 (1957).
2. G. E. Deegan, *Thermal and Electrical Properties of Graphite Irradiated at Temperatures from 100 to 425°K*, USAEC Report NAA-SR-1716, Atomic International, Dec. 15, 1956.
3. C. R. Malmstrom, *Studies on Nuclear Reactors. 10. Experimental Method for the Determination of Resistivity Change in Graphite Bombarded with Deuterons and Alpha Particles*, USAEC Report NAA-SR-10, North American Aviation, Inc., Mar. 1, 1948.
4. F. Faris, *Results of Resistivity-Range Measurements on Graphite Bombarded with Charged Particles*, USAEC Report NAA-SR-14 (Del.), North American Aviation, Inc., Oct. 12, 1950.
5. D. T. Eggen and W. E. Parkins, *Preliminary Experiments on Radiation Damage Due to Electron Bombardment*, USAEC Report NAA-SR-37, North American Aviation, Inc., Sept. 12, 1949.
6. D. T. Eggen, *Energy Required for Atomic Displacements in Graphite Determined by Electron Bombardment*, USAEC Report NAA-SR-69, North American Aviation, Inc., Apr. 10, 1950.
7. S. B. Austerman and J. E. Hove, Irradiation of Graphite at Liquid Helium Temperatures, *Phys. Rev.*, **100**: 1214-1215 (1955).
8. J. E. Hove, Low Temperature Irradiation and Annealing Effects in Graphite, in *Progress in Nuclear Energy, Series V, Metallurgy and Fuels*, H. M. Finniston and J. E. Hove (Eds.), Vol. 2, pp. 551-569, Pergamon Press, New York, 1959.
9. G. R. Hennig and J. E. Hove, Interpretation of Radiation Damage to Graphite, in

- Proceedings of the First International Conference on the Peaceful Uses of Atomic Energy, Geneva, 1955*, Vol. 7, pp. 666-675, United Nations, New York, 1956.
10. W. K. Woods et al., Irradiation Damage to Artificial Graphite, in *Proceedings of the First International Conference on the Peaceful Uses of Atomic Energy, Geneva, 1955*, Vol. 7, pp. 455-471, United Nations, New York, 1956.
 11. E. M. Woodruff, Hanford Laboratories, General Electric Company, unpublished data, November 1960.
 12. G. H. Kinchin, The Effects of Irradiation on Graphite, in *Proceedings of the First International Conference on the Peaceful Uses of Atomic Energy, Geneva, 1955*, Vol. 7, pp. 472-478, United Nations, New York, 1956.
 13. A. W. Smith and J. D. McClelland, *Electronic Properties of a Graphitized Lamp-black and Their Dependence on Neutron Irradiation*, USAEC Report NAA-SR-248, North American Aviation, Inc., June 1, 1953.
 14. W. Primak and L. H. Fuchs, Radiation Damage to the Electrical Conductivities of Natural Graphite Crystals, *Phys. Rev.*, **103**: 541-544 (1956).
 15. V. I. Klimenkov and Yu. N. Aleksenko, Change in the Properties of Graphite When Irradiated by Neutrons, in *Conference of the Academy of Sciences of the USSR on the Peaceful Uses of Atomic Energy, July 1-5, 1955*, Session of the Division of Physical and Mathematical Sciences (in English translation as USAEC Report AEC-TR-2435, Pt. 1, pp. 227-237).
 16. J. F. Fletcher, *Controlled Temperature Irradiation of Graphite, Interim Report No. 3, PT-105-403-P*, USAEC Report HW-36221, Hanford Atomic Products Operation, Sept. 5, 1956. (Classified)
 17. W. P. Eatherly and J. J. Donoghue, *A New Circuit for Precision Measurement of the Hall and Magneto-Resistive Effects with Results of Observations on Reactor Irradiated Graphite*, USAEC Report NAA-SR-68, North American Aviation, Inc., Apr. 5, 1950.
 18. R. J. Maurer and R. C. Ruder, *The Hall Effect in Neutron Irradiated and Annealed Graphite*, USAEC Report CP-2890, Carnegie Institute of Technology, Apr. 25, 1945.
 19. G. H. Kinchin, Changes in the Electrical Properties of Graphite Due to Neutron Irradiation, *J. Nuclear Energy*, **1**: 124-129 (1954).
 20. C. J. Delbecq and G. R. Hennig, *The Hall Coefficient of Pile Irradiated Graphite*, USAEC Report ANL-4416, Argonne National Laboratory, Mar. 9, 1950.
 21. H. Brooks, Nuclear Radiation Effects in Solids, *Ann. Rev. Nuclear Sci.*, **6**: 215-276 (1956).
 22. D. F. Johnston, A Calculation of the Density of Electron-Trapping Defects in Neutron-Irradiated Graphite from Measurements of the Temperature Variation of the Hall Coefficient, *J. Nuclear Energy*, **1**: 311-318 (1955).
 23. G. R. Hennig, A Chemical Model of Radiation Damage in Graphite, *Nuclear Sci. and Eng.*, **3**: 514-528 (1956).
 24. G. L. Montet, Interstitial Compounds of Irradiated Graphite, *Nuclear Sci. and Eng.*, **4**: 112-133 (1958).
 25. W. P. Eatherly and N. S. Rasor, *The Thermoelectric Power of Graphite Dependence on Temperature, Type and Neutron Irradiation*, USAEC Report NAA-SR-196, North American Aviation, Inc., Nov. 21, 1952.
 26. J. E. Hove, Radiation Damage Effects on Graphite, in *Proceedings of the First and Second Conferences on Carbon Held at the University of Buffalo*, pp. 125-136, Waverly Press Inc., Baltimore, Md., 1956.
 27. J. J. Donoghue and J. D. McClelland, *The Magnetic Susceptibility of Graphite and the Effect of Irradiation on Artificial Graphite*, USAEC Report NAA-SR-153, North American Aviation, Inc., Dec. 18, 1951.

28. J. E. Hove and J. D. McClelland, Magnetic Susceptibility of Neutron-Damaged Graphite, *J. Chem. Phys.*, **26**: 1028-1030 (1957).
29. G. R. Hennig and B. Smaller, *Paramagnetism of Irradiated Graphite*, USAEC Report ANL-5385, Argonne National Laboratory, Jan. 20, 1955.
30. J. F. Fletcher and W. A. Snyder, Use of Graphite in the Atomic Energy Program, *Am. Ceram. Soc. Bull.*, **36**: 101-104 (1957).
31. R. E. Nightingale et al., Damage to Graphite Irradiated up to 1000°C, in *Proceedings of the Second United Nations International Conference on the Peaceful Uses of Atomic Energy, Geneva, 1958*, Vol. 7, pp. 295-300, United Nations, New York, 1959.
32. R. L. Carter et al., Recent Developments in the Technology of Sodium-Graphite Reactor Materials, in *Proceedings of the Second United Nations International Conference on the Peaceful Uses of Atomic Energy, Geneva, 1958*, Vol. 7, pp. 72-81, United Nations, New York, 1959.
33. R. W. Powell and F. H. Schofield, The Thermal and Electrical Conductivities of Carbon and Graphite to High Temperatures, *Proc. Phys. Soc. (London)*, **51**: 153-172 (1939).
34. W. P. Eatherly et al., Physical Properties of Graphite Materials for Special Nuclear Applications, in *Proceedings of the Second United Nations International Conference on the Peaceful Uses of Atomic Energy, Geneva, 1958*, Vol. 7, pp. 389-401, United Nations, New York, 1959.
35. D. E. Baker, Hanford Laboratories, General Electric Company, unpublished data, 1958.
36. J. E. Hove and A. W. Smith, Interpretation of the Low-Temperature Thermal Conductivity of Graphite, *Phys. Rev.*, **104**: 892-900 (1956).
37. J. E. Hove, Thermal Properties of Graphite, in *Proceedings of the Third Conference on Carbon Held at the University of Buffalo*, pp. 515-527, Pergamon Press, New York, 1959.
38. W. De Sorbo and W. W. Tyler, Effect of Irradiation on the Low-Temperature Specific Heat of Graphite, *J. Chem. Phys.*, **26**: 244-247 (1957).
39. B. B. Goodman et al., L'effet de l'irradiation neutronique sur la chaleur spécifique du graphite, *Compt. rend.*, **248**: 956-959 (1959).
40. G. E. Bacon and B. E. Warren, X-ray Diffraction Studies of Neutron-Irradiated Graphite, *Acta Cryst.*, **9**: 1029-1035 (1956).
41. R. L. Carter, Atomics International, unpublished data, 1961.

Radiation Effects on Mechanical Properties

H. H. W. LOSTY†

Nuclear graphite, in addition to serving as a neutron moderator, is also employed as a structural component to locate and support the fuel assemblies and to provide channels for the coolant. Except in a few special cases, it is not possible to replace the graphite core, and it is therefore necessary to ensure that the mechanical integrity of the core is preserved throughout the life of the reactor. The effects of the reactor environment on the mechanical properties are discussed in this chapter.

11-1 Single Crystals

The published work on the mechanical properties of irradiated single crystals of graphite is extremely limited. Some observations on the load-deflection characteristics of a cantilever made from a flake of Travancore natural graphite have been reported.¹ The unirradiated specimen showed a small elastic recovery with a large permanent set when the load was removed. After neutron irradiation the deflection was completely elastic and very much smaller.

11-2 Elastic Moduli of Nuclear Graphites

11-2.1 YOUNG'S MODULUS

The effect of neutron irradiation on the Young's modulus of graphite has been studied by a number of workers.¹⁻⁶ For irradiations carried out at room temperature, the modulus rises to two or three times the unirradiated value for a dose between 100 and 200 Mwd/At. The modulus then begins to decrease, and, after a dose of 600 Mwd/At, it reaches a value at least twice the unirradiated value. A typical curve is shown in Fig. 11.1. As the irradiation temperature rises, the change in modulus decreases² and at 350°C is only 1.4 times the unirradiated value at a dose of 4×10^{20} neutrons/cm².‡ No data have yet been published for irradiations at higher temperature.

11-2.2 MODULUS OF RIGIDITY

The fractional increase in the modulus of rigidity due to neutron irradiation is the same as that for Young's modulus.¹ The changes depend

† Research Laboratories of the General Electric Co., Ltd., Wembley, England.

‡ Exposures expressed in this chapter are the integrated thermal flux at a standard position in the center of the lattice cell in BEPO. For this position 1 Mwd/At $\simeq 5.5 \times 10^{17}$ neutrons/cm².

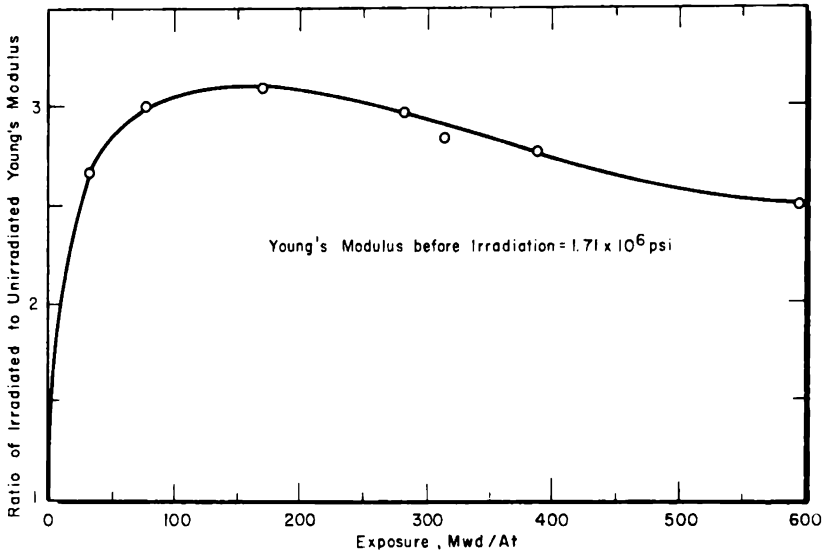


FIG. 11.1 The effect of room-temperature irradiation on the Young's modulus of KC (II) graphite.⁴

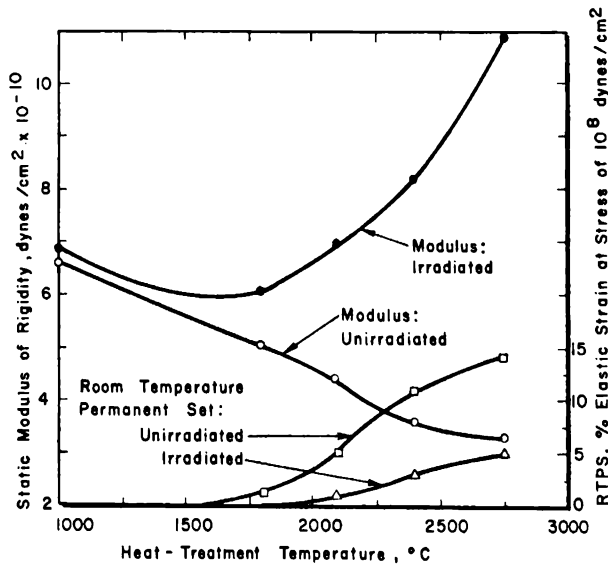


FIG. 11.2 Modulus of rigidity and room-temperature permanent set (RTPS) before and after irradiation as a function of the maximum temperature reached in manufacture. Irradiated samples were exposed to 7.3×10^{19} neutrons (thermal)/cm² at 60°C.

upon the maximum temperature reached during manufacture,⁵ as illustrated in Fig. 11.2. The modulus of ungraphitized material is not greatly increased by irradiation, and it is not until the heat-treatment temperature has reached about 2200°C that the modulus begins to increase rapidly. The modulus of fully graphitized material reaches a maximum value after irradiation of nearly twice that of the ungraphitized material.

Figure 11.2 also shows the effect of neutron irradiation on the stress-strain behavior of previously unstressed graphite. The nonlinearity of the stress-strain diagram is illustrated by the permanent set that can be produced by a stress of 10^8 dynes/cm². For unirradiated and ungraphitized material, the permanent set is small and increases with the heat-treatment temperature. Irradiation reduces the amount of permanent set that can be induced for all heat-treatment temperatures.

11-2.3 INTERPRETATION OF MODULUS CHANGES

An attempt⁷ has been made to rationalize the out-of-pile behavior of the elastic moduli of graphites in terms of crystal shear. It is suggested that all elastic deformation of graphite occurs by the movement of the layer planes of crystallite elements relative to each other. This movement can be resisted by the presence of imperfections that distort the layer structure. This hypothesis has been successfully employed to explain the relation between the elastic moduli of graphitized and ungraphitized carbon and of graphites manufactured from a wide range of raw materials.

Neutron irradiation introduces a specific type of imperfection which, for low doses at room temperature, can be regarded as single interstitial atoms. These atoms resist the shear motion and so increase the elastic modulus. The presence of gross imperfections in the lattice such as are found in nongraphitic carbons lessens the effect of the displaced atoms and results in a smaller increase in the modulus. In quantitative terms this hypothesis requires elaboration since the absolute value of the elastic modulus is greater for irradiated graphite than for ungraphitized material (Fig. 11.2). The presence of gross imperfections causes the layer spacing to increase, and it is this increased spacing rather than the imperfections themselves which lessens the effect of the interstitial atoms. Figure 11.2 shows that the modulus is not sensitive to neutron-induced damage until the treatment temperature reaches about 2200°C. Since the layer spacing for petroleum coke heat-treated to this temperature is approximately 3.39 Å and decreases to a value of about 3.36 Å as graphitization proceeds,⁸ it would appear that the effect of single interstitials is markedly reduced for values of the layer spacing greater than 3.39 Å.

So far only the effect of neutron irradiation in small doses at room temperature, i.e., up to 75 Mwd/At at 30°C, has been considered. As the irradiation proceeds, the single displaced atoms join together and considerably more complex damage results. This, in turn, causes the layer

planes to move apart, and, when the dose has reached 100 Mwd/At at 30°C, the layer spacing reaches the value of 3.39 Å. At this dose the effect of single displaced atoms is being reduced at a greater rate than it is being created, and the modulus begins to decrease. At very high doses the accumulation of complex damage makes the contribution of the single interstitials negligible. It is then found that the modulus saturates at a value of the same order of magnitude as that found for ungraphitized carbon.

As the temperature of irradiation increases, the single displaced atoms are thermally annealed to vacant sites in the lattice, to sites in the relatively disordered regions at the crystallite boundaries, or to favorable interstitial sites, where they join together to form complex damage arrays. Under these conditions the large initial increase in the modulus does not occur, and only the latter stage of a progressive increase to a value characteristic of ungraphitized carbon is observed.

11-3 Strength

11-3.1 COMPRESSIVE STRENGTH

The increase in compressive strength induced by irradiation at 30°C is shown in Fig. 11.3. The changes are similar to those observed for Young's

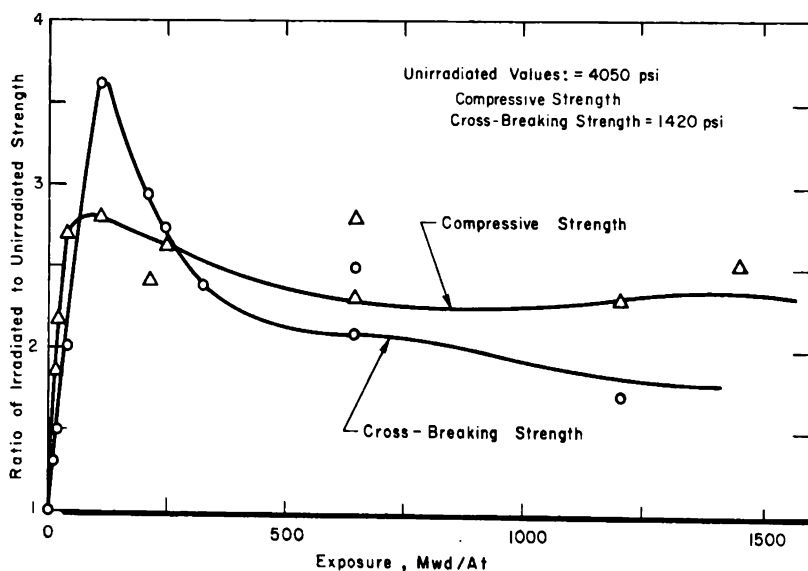


FIG. 11.3 The effect of room-temperature irradiation on the strength of KC (II) graphite.⁴

modulus and imply that the elastic breaking strain is little altered by neutron irradiation. Meyer and Bourdeau⁹ reported similar findings, although their results indicate a large decrease in the breaking strain. It is

apparent that the large permanent sets that can be induced in unirradiated graphite are almost completely absent after irradiation. Since the apparent breaking strain is composed of the elastic strain plus the permanent set, the large changes in the apparent breaking strain are partially accounted for.

11-3.2 FLEXURAL STRENGTH

The effect of irradiation at 30°C on the flexural strength is also shown in Fig. 11.3. A sharp peak in the curve occurs at a dose of 100 Mwd/At, at which point the ratio of maximum to initial strength attains a value of 3.6. The strength decreases for larger doses and tends to saturate at a value of about 2. A comparison with the change in modulus⁴ again shows that the breaking strain does not appreciably change as a result of neutron irradiation.

Davidson and Losty⁵ have found a linear correlation between Young's modulus and flexural strength for graphite irradiated to a range of doses. The breaking strain decreased initially by about 40 per cent. Similar behavior was found for ungraphitized material, where the change in both the elastic modulus and the strength was only about 20 per cent.

11-3.3 TENSILE STRENGTH

No data have been published on direct tensile measurements of irradiated graphite; the difficulties of performing such tests were discussed in Chap. 6. Davidson and Losty⁵ have carried out such tests on ungraphitized material and have shown that the fractional increase in tensile strength is equal to that for the flexural strength.

11-3.4 IMPACT STRENGTH

No direct measurements of the impact strength of graphite after irradiation have been reported in the literature. It has been found⁵ that, when such measurements are carried out on ungraphitized material, the impact strength increases in a similar proportion to the other measured strengths. If the criterion given in Chap. 6 is adopted, i.e., that the impact strength (I) is proportional to the square of the flexural strength (F) divided by the Young's modulus (E), then, provided F and E increase by the same fraction, the impact strength will also increase by this fraction. This can be expressed by

$$\frac{dI}{I} = -\frac{dE}{E} + 2\frac{dF}{F} \quad (11.1)$$

If, however, the fractional increase in modulus is greater than the fractional increase in flexural strength, as has been suggested by some of the data considered in the earlier paragraphs, then the impact strength may not increase appreciably. The most pessimistic estimates predict no decrease in the impact strength.

11-3.5 INTERPRETATION OF STRENGTH CHANGES

It has been shown that the elastic modulus and the strength increase in similar proportion as a result of neutron irradiation, and indeed they show the same characteristics of an initial increase to a dose of about 100 Mwd/At followed by a decrease to a level characteristic of ungraphitized carbon. It would appear therefore that graphite fails at a breaking strain characteristic of each grade and that this strain is not markedly changed as a result of neutron irradiation.

Out-of-pile experiments^{7, 10, 11} have shown that the elastic deformations of graphite occur within the grains and are almost independent of the nature of the binder. The constancy of the breaking strain implies that the graphite fails when these grains achieve a characteristic deformation. If the elastic moduli of the grains are increased, the stresses necessary to achieve this deformation are also increased in the same proportion. It would appear from this that graphite first fails within the grains, i.e., within the region of ordered crystallites, and not at the bridges between the grains as other theories¹² have suggested. Failure within the grains concentrates the stresses at bridges and results in failure of the body.

11-4 Irradiation Under Stress

11-4.1 MODULUS CHANGES

In practical application graphite is irradiated under stress. This stress arises either from some external source, such as the structure in which it is contained, or from internal sources such as the differential dimensional changes that arise from anisotropy or from a nonuniform distribution of radiation damage. It has been demonstrated that the elastic moduli increase during irradiation, and their influence on the stress (or strain) leads to an interesting dilemma. As an illustration of the problem, consider a graphite spring carrying a fixed load during irradiation. The increase in the elastic modulus could lift the weight, or the weight could remain at a fixed deflection with only partial recovery of the original elastic strain when the load is removed after irradiation. This problem can be stated in terms of the model described in Sec. 11-2.3 for the increase in the elastic modulus. The problem is to decide whether the interstitial atoms will increase the potential energy of the structure by doing work on the stress-strain diagram or whether they will merely impede the capacity for the shear to recover when the stress is removed. A similar distinction arises when the graphite spring is irradiated at a fixed deflection (i.e., constant strain) in that the increase in modulus can either cause the stress to increase or result in a permanent set when the deflection is released. If the latter is true, then the constant-stress and constant-strain behavior are clearly identical. Experiments¹³ to distinguish between these two cases have been inconclusive since

it is not possible to produce changes in the modulus at ordinary temperature without incurring plastic behavior. The evidence tends to support the view that the weight will not be lifted and a permanent set will be observed on removing the load after irradiation.

11-4.2 IRRADIATION CREEP

In the experiments carried out on graphite springs under irradiation, an induced plasticity is observed; for springs carrying a weight, a steady creep is observed. This creep can be represented by the simple equation

$$E_t = E_0 + k F(\phi) St \quad (11.2)$$

where E_t = strain at time t

E_0 = initial strain

k = specific creep constant, $(\text{cm}^2/\text{dyne})/(\text{neutrons}/\text{cm}^2)$

$F(\phi)$ = a function of the neutron flux, $\text{neutrons}/\text{cm}^2/\text{sec}$

S = stress, dynes/cm^2

t = time, sec

For springs maintained at a fixed deflection, the load necessary to produce the deflection after irradiation is always less than that before irradiation.

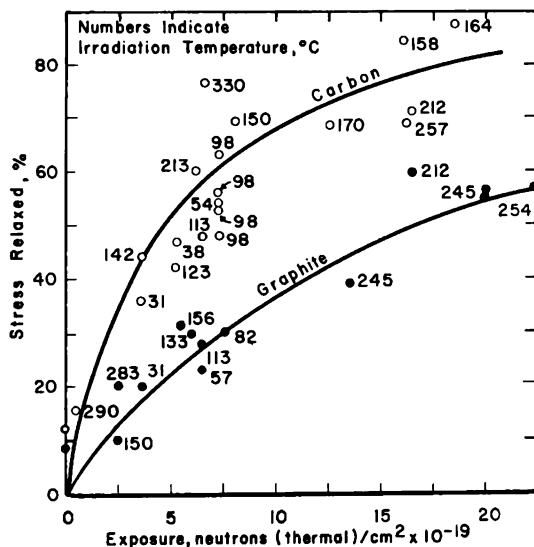


FIG. 11.4 The radiation-induced stress relaxation in constant-strain springs. (From Losty, *Proceedings of the Fourth Conference on Carbon*, Pergamon Press, Ref. 13.)

The difference in load corresponds to a relaxation of stress. The results, which are shown in Fig. 11.4, can be fitted to the equation

$$S_t = \frac{S_0}{Mk F(\phi) t + 1} \quad (11.3)$$

where S_t = stress at time t , dynes/cm²
 S_0 = initial stress, dynes/cm²
 M = average elastic modulus, dynes/cm²

Assuming a flux of 5×10^{12} neutrons/cm²/sec, the values of $k F(\phi)$ are 1.6×10^{-18} and 0.8×10^{-18} cm²/dyne-sec for ungraphitized and graphitized carbon, respectively.

The effect of the maximum temperature reached during manufacture on the relaxation of stress has been measured.⁵ The creep constants calculated from Eq. 11.3 decrease almost linearly with heat-treatment temperatures between 1000 and 2750°C.

Figure 11.4 shows that between 30 and 300°C the irradiation temperature has no detectable effect on the relaxation of stress.

11-4.3 EFFECT OF CREEP ON DIFFERENTIAL GROWTH STRESSES

If it is assumed that the distribution of radiation damage is not uniform over a single piece of graphite in a reactor, then the rate of growth or shrinkage will vary from place to place, and stresses will be generated by this lack of uniformity. These stresses will, in turn, promote irradiation creep and will then be relaxed. There are not yet sufficient data to calculate these effects precisely. Since, however, radiation-induced dimensional changes diminish with increasing temperature in the range of 30 to 300°C and since the relaxation of stress is independent of temperature, the equilibrium stress for a given flux distribution will diminish as the temperature rises.

11-4.4 INTERPRETATION OF IRRADIATION CREEP

It has been demonstrated that plastic deformation is induced in carbons and graphite by irradiation. The effect is largely independent of the temperature and therefore of the accumulation of damage. The most probable explanation would appear to depend on the annealing effects that occur during irradiation. When graphite is irradiated, even at room temperature, some of the displaced atoms are simultaneously annealed and return to sites of lower energy in the structure. Little is known of the precise nature of this annealing, but it is thought that at least some of the atoms take up positions in the less-ordered regions at the crystallite boundaries. The diffusion of the atoms through these regions of relatively high stress could cause the observed plastic deformation. If the crystallite diameter is reduced, the mean free path for diffusion is also reduced, and an enhanced effect would be expected. This is consistent with the fact that the creep rate falls as the graphitization temperature rises. The temperature dependence of the creep process is small since the primary displacements outnumber the permanently displaced carbon atoms in the temperature range studied.

11-5 Hardness and Machinability

The Young's modulus and Brinell hardness of graphite are affected in a similar manner by neutron irradiation⁶ as a function of both dose and temperature. This result is to be expected since it has been shown that strength and modulus change in the same way and hardness is a function of these parameters.

The effect of irradiation on machinability is shown in Fig. 11.5. For

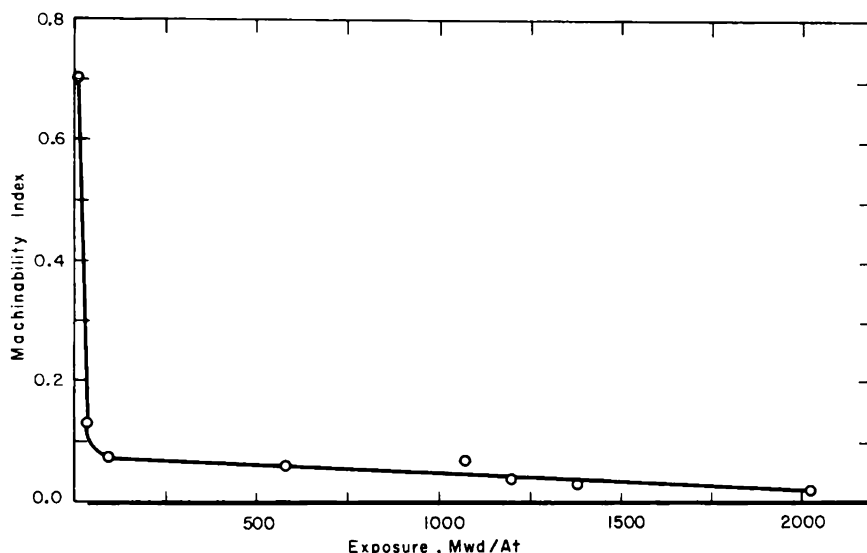


Fig. 11.5 Machinability of CSF graphite as a function of exposure. The machinability index is a measure of the depth of penetration of a carbide-tipped drill in a standardized drilling test.⁴

irradiations at 30°C the machinability index decreases by a factor of 10 for a dose of about 150 Mwd/At. The machinability index after this exposure is the same as that for unirradiated material¹⁴ heat-treated to less than 1400°C. Clearly, graphite irradiated to a dose of 150 Mwd/At is not as amorphous as unirradiated graphite heat-treated to only 1400°C. This is further evidence that irradiation is not simply the reversal of the process of graphitization and that an additional hypothesis, such as has been suggested to explain the increase in the elastic modulus, must be employed for machinability.

11-6 Coefficient of Friction

Measurements of the static coefficient of friction¹⁵ on unirradiated and irradiated TSGBF graphite bars $3\frac{3}{4}$ in. in cross section indicate that no large change in this property results from irradiations up to 2000 Mwd/At

at 400 to 500°C. The initial friction coefficients and those after up to fifty tests are slightly higher for unirradiated bars than for irradiated bars (Table 11.1). It is possible that a small amount of oxidation, which is difficult to prevent during long irradiations, may have altered the surface characteristics sufficiently to lower the coefficients of the irradiated samples.

**Table 11.1 — COEFFICIENTS OF FRICTION OF TSGBF GRAPHITE
MEASURED AT ROOM TEMPERATURE¹⁶**

	Unirradiated	Irradiated [†] (1500 to 2000 Mwd/At at 400 to 500°C)
Maximum initial static coefficient	0.41	0.35
Average initial static coefficient	0.40	0.32
Average final static coefficient after 25 tests	0.31	0.27

[†]Weight loss due to oxidation was ≈ 0.07 per cent.

Table 11.1 shows that a surface-conditioning effect occurs similar to that reported by other investigators.¹⁶ This results in a decrease in the friction coefficients for successive tests using the same surfaces. The travel of one bar with respect to the other was about $\frac{1}{8}$ in. during each test shown in Table 11.1.

The rate of decrease in the coefficient of friction with successive tests increases when the load is increased and when the movable bar is allowed to slide in only one direction with respect to the stationary bar. When the bar is moved in the reverse direction to position it for successive tests, some of the surface conditioning is altered. This does not occur when the upper bar is lifted during repositioning. The influence of preferential alignment of graphite particles on the contact surfaces is suggested by this behavior.

Values of the static coefficient of friction in Table 11.1 apply to tests in which the extrusion axes of the two test bars are rotated 90° in planes parallel to each other. If tests are conducted in which the bars are oriented with their extrusion axes parallel, no significant difference is observed.

11-7 Mechanical-property Changes in Graphite-moderator Stacks

The radiation-induced changes that are known to occur in the mechanical properties of graphite are, in themselves, unlikely to have any major effect on the operation, safety, or life of a graphite-moderated reactor. Irradiation creep, however, can have a beneficial effect in relieving stresses that arise from any nonuniform changes in dimension. It appears from the limited data currently available that, in a simple graphite stack where the only stresses are those due to the dead load of the stack itself, irradiation

creep will only produce dimensional changes comparable with those anticipated in the absence of such stress. A more serious problem may arise in the stability of a vertical stack if the vertical columns are inadequately located in the horizontal plane. In this case, bowing of the columns could occur, and plastic deformation in the high-stress regions on the inside radius of the bow could cause the columns to become unstable (see also Chap. 17).

References

1. J. H. W. Simmons, The Effects of Irradiation on the Mechanical Properties of Graphite, in *Proceedings of the Third Conference on Carbon Held at the University of Buffalo*, pp. 559-568, Pergamon Press, New York, 1959.
2. J. H. W. Simmons, The Effects of Neutron Irradiation on the Physical Properties of Graphite, in *Industrial Carbon and Graphite: Papers Read at the Conference Held in London, Sept. 24-26, 1957*, pp. 511-518, Society of Chemical Industry, London, 1958.
3. G. H. Kinchin, The Effects of Irradiation on Graphite, in *Proceedings of the First United Nations International Conference on the Peaceful Uses of Atomic Energy, Geneva, 1955*, Vol. 7, pp. 472-478, United Nations, New York, 1956.
4. W. K. Woods et al., Irradiation Damage to Artificial Graphite, in *Proceedings of the First United Nations International Conference on the Peaceful Uses of Atomic Energy, Geneva, 1955*, Vol. 7, pp. 455-471, United Nations, New York, 1956.
5. H. W. Davidson and H. H. W. Losty, The Effect of Neutron Irradiation on the Mechanical Properties of Graphite, in *Proceedings of the Second United Nations International Conference on the Peaceful Uses of Atomic Energy, Geneva, 1958*, Vol. 7, pp. 307-314, United Nations, New York, 1959.
6. V. I. Klimenkov and Yu. N. Alekshenko, Change in the Properties of Graphite When Irradiated by Neutrons, in *Conference of the Academy of Sciences of the USSR on the Peaceful Uses of Atomic Energy, July 1-5, 1955*, Session of the Division of Physical and Mathematical Sciences (in English translation as USAEC Report AEC-TR-2435, Pt. 1, pp. 227-237).
7. H. W. Davidson and H. H. W. Losty, Elastic and Plastic Properties of Carbon and Graphite, in *Mechanical Properties of Non-Metallic Brittle Materials, London Conference of the National Coal Board, 1958*, pp. 219-238, Interscience Publishers, Inc., New York, 1958.
8. J. C. Bowman, Imperfections in the Graphite Structure, in *Proceedings of the First and Second Conferences on Carbon Held at the University of Buffalo*, pp. 59-64, Waverly Press, Inc., Baltimore, Md., 1956.
9. R. A. Meyer and R. G. Bourdeau, Effect of Pile Radiation on Mechanical and Other Properties of Graphite, in *Proceedings of the Third Conference on Carbon Held at the University of Buffalo*, pp. 569-574, Pergamon Press, New York, 1959.
10. J. F. Andrew et al., Elastic Constants and Permanent Set in Carbons and Graphite at Room Temperature, in *Proceedings of the Fourth Conference on Carbon Held at the University of Buffalo*, pp. 559-575, Pergamon Press, New York, 1960.
11. H. H. W. Losty, The Effect of Impregnation and Heat Treatment on the Physical Properties of Graphite, in *Proceedings of the Fourth Conference on Carbon Held at the University of Buffalo*, pp. 671-674, Pergamon Press, New York, 1960.
12. S. Mrozowski, Physical Properties of Carbons and the Formulation of the Green Mix, in *Proceedings of the First and Second Conferences on Carbon Held at the University of Buffalo*, pp. 195-215, Waverly Press, Inc., Baltimore, Md., 1956.
13. H. H. W. Losty, The Problems Raised by the Influence of Neutron Irradiation on

- the Stress-Strain Relationships of Graphite, in *Proceedings of the Fourth Conference on Carbon Held at the University of Buffalo*, pp. 593-597, Pergamon Press, New York, 1960.
14. E. M. Woodruff, *Machinability of Graphites for Future Piles*, USAEC Report HW-31578, Hanford Works, July 21, 1954.
 15. E. M. Woodruff, Hanford Laboratories, General Electric Company, unpublished data, 1959.
 16. P. Wagner et al., Some Mechanical Properties of Graphite in the Temperature Range 20 to 3000°C, in *Proceedings of the Second United Nations International Conference on the Peaceful Uses of Atomic Energy, Geneva, 1958*, Vol. 7, pp. 379-388, United Nations, New York, 1959.

Stored Energy

R. E. NIGHTINGALE†

12-1 Definition and Origin

A fast-fission neutron with energy near 2 Mev displaces about 60 carbon atoms before reaching the threshold energy where it is no longer traveling fast enough to cause further displacements (Chap. 7). The average primary knock-on carbon atom displaces about 350 more atoms from their lattice positions. Thus, for every fast neutron moderated in graphite, approximately 20,000 atoms are knocked from their lattice sites. Many of the displaced atoms do not anneal during the irradiation period, and the net result is an increase in the heat content of the graphite. This increase in heat content is called the "total stored energy," S . In the European literature it is usually referred to as "total Wigner energy."

When irradiated graphite is heated above the irradiation temperature, some of the stored energy is released as heat. The specific heat of the sample thus appears to be lower than that of an unirradiated sample. An informative and useful way of characterizing the stored energy in irradiated graphite is to plot the stored energy annealed per degree Centigrade temperature rise (dS/dT) as a function of the annealing temperature (T). These plots have been termed "stored-energy release spectra" in the United States and "Wigner energy-release curves" in France and England.‡ A stored-energy release curve is illustrated in Fig. 12.1. External heating to T_1 triggers a spontaneous release of energy, and under adiabatic conditions the temperature will quickly rise to a higher temperature, T_2 , such that the two shaded areas are equal. Continued heating results in no further spontaneous increase in temperature unless there is another peak in the release curve at some higher annealing temperature which exceeds the specific heat. However, the graphite will have a lower apparent specific heat equal to the difference between the specific heat and stored-energy release curve.

The possibility of a large spontaneous temperature rise in the graphite moderator is the main source of concern associated with the accumulation of stored energy in an operating reactor. The necessity of assessing this possibility in every reactor in which graphite is employed as the moderator has resulted in investigations leading to a fair understanding of the accumulation and release of stored energy. This chapter is concerned with

† Hanford Laboratories, General Electric Company, Richland, Wash.

‡ The term "stored-energy spectrum" is also frequently used in the graphite literature.

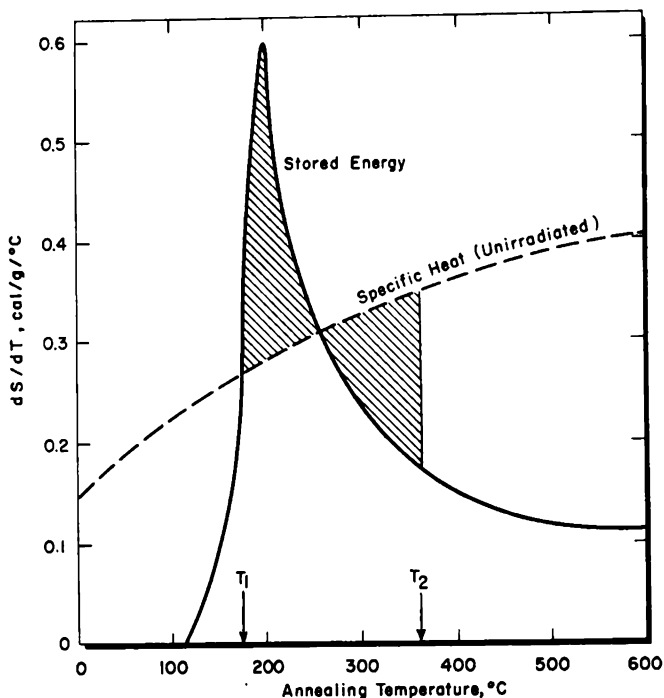


FIG. 12.1 The stored-energy release curve of graphite irradiated to 400 Mwd/At at 30°C. Heating to T_1 causes the temperature of the graphite to rise spontaneously to T_2 , where the shaded areas are equal. The total stored energy for this sample was 150 cal/g.

the effects of neutron exposure and irradiation temperature on both the total stored energy and the stored-energy release curve.

12-2 Total Stored Energy

12-2.1 MEASUREMENT OF TOTAL STORED ENERGY

The release of the last traces of stored energy requires very high temperatures. Strong carbon-carbon bonds must be broken before all the radiation-induced defects can anneal. The customary method of making certain that no stored energy remains unannealed is to determine S by measuring the increase in the room-temperature heat of combustion. If ΔH_i and ΔH_u are, respectively, the heats of combustion of an irradiated and a similar but unirradiated sample, then

$$S = \Delta H_i - \Delta H_u$$

Although conventional methods of bomb calorimetry are employed in the measurement of the heat of combustion of graphite, the relatively small contribution of S to the heat of combustion makes very precise measurements necessary. An accuracy of ± 1 or 2 cal/g is required in some studies

of lightly damaged samples. Since the heat of combustion is approximately 7800 cal/g, measurement of the heat of combustion to about 0.01 per cent is required to attain an accuracy of ± 1 cal/g.

Most measurements of S have been made at the United Kingdom Atomic Energy Authority's Windscale Laboratory or at the U. S. National Bureau of Standards. Both laboratories employ an isothermal-jacket bomb calorimeter. The heat of combustion is measured from the reaction of a small amount of graphite with oxygen. In the NBS method¹⁻³ the graphite sample is crushed in a pellet press and desiccated under vacuum at room temperature to degas and dry the sample. About 1 g of graphite is necessary for each determination. A 0.3-g pellet of standard benzoic acid is placed on top of the graphite to facilitate combustion. The oxygen is purified and admitted to the bomb at 30 atm, and an iron- or platinum-wire fuse is used to ignite the sample.

The carbon dioxide formed by combustion is accurately weighed, and the amount produced from the combustion of benzoic acid is subtracted to yield the mass of carbon dioxide produced from the graphite. This mass of carbon dioxide is used to determine the amount of graphite burned. With this procedure neither inert impurities nor incomplete combustion of the graphite affects the heat of combustion. However, because the unreacted graphite may be partially annealed during the combustion, it is desirable to burn as much of the graphite as possible. In the NBS method it is found that only negligible amounts of graphite and none of the benzoic acid remain unburned. No products of incomplete combustion have been found in the gaseous products.

The heat produced is measured by the rise in temperature of water surrounding the bomb, and the heat capacity of the calorimeter is determined from the temperature rise produced by a known amount of electrical energy. When the heat of combustion is calculated, corrections are made for the heat produced in ignition (if any), the combustion of the benzoic acid, and the production of a small amount of nitric acid.

The Windscale method⁴ is similar in most respects to that described above, except that the weight of graphite burned is determined from the original weight minus the residue weight rather than from the weight of carbon dioxide formed. Residues amounting to approximately 0.4 per cent of the sample weight are obtained; part of these residues are impurities. The Windscale bomb is calibrated by the combustion of benzoic acid, rather than by the generation of a known amount of electrical energy. The errors have been carefully examined, and it is estimated that the heat of combustion of graphite can be determined with a standard deviation of ± 1.75 cal/g. At 98 per cent confidence limits (i.e., $\pm 2\sigma$), this corresponds to a precision in S for a single measurement of about ± 4 cal/g. About the same precision (± 3.4 cal/g) has been reported for measurements of stored energy by the National Bureau of Standards.⁵

Two other methods for measuring total stored energy have been tried but have met with little success. One involved an attempt to measure the free energy of graphite from electrode potentials established by graphite in various solutions.⁶ The second consisted in measuring the heat of reaction with potassium.⁷ Although this latter method was attractive because of the relatively low heat of reaction of graphite with potassium compared with the heat of combustion (81 ± 2 cal/g at 66 to 95°C vs. 7800 cal/g at 25°C), the excess heat of reaction of irradiated graphite did not agree with the excess heat of combustion; nor was there a constant relation between them for different samples. Furthermore, the excess heat of reaction did not decrease when an irradiated sample was annealed. It was concluded that the final state of the products of the potassium-graphite reaction was different for irradiated and unirradiated graphite both with respect to the composition of the graphite-potassium compounds formed and with respect to the structure of the residual graphite lattice.

In summary, we may conclude that it is possible to measure S quite accurately by differences in heats of combustion if a great deal of care is taken. Often only one irradiated sample is available for a determination. In this case the precision in S is limited in present techniques to ± 3 to 4 cal/g. This is sufficiently precise for most requirements, particularly for heavily damaged samples (>100 cal/g). Some improvement in precision is desirable for samples with small amounts of stored energy.

12-2.2 BUILD-UP OF TOTAL STORED ENERGY WITH EXPOSURE

The accumulation of stored energy as a function of reactor irradiation is shown in Fig. 12.2. The exposures for the measurements from the Wind-scale Laboratories were reported in units of Mwd/At_e (Sec. 7-5.5). The recommended⁹ conversion 1 Mwd/At = 0.6 Mwd/At_e was used. Kinchin's data¹¹ at 30°C, which are reported in thermal neutrons/cm², fall on the 30°C curve of Fig. 12.2 if

$$\frac{\text{Thermal nvt (BEPO equivalent)}}{\text{Mwd/At}} = 6.4 \times 10^{17}$$

This is slightly higher than the value of 5.5×10^{17} derived from other property changes (Sec. 7-5). The general character of the 30°C curve is similar to that of most other radiation-induced property changes. The initial rate of accumulation is about 500 cal/g per 1000 Mwd/At. This decreases to 25 cal/g per 1000 Mwd/At in the 4000 to 5000 Mwd/At exposure range.

A relatively large amount of energy, 630 cal/g, is stored when graphite is exposed to 5000 Mwd/At at 30°C. This is equal to 7.5 kcal/gram atom, several times the estimated interlayer binding energy in unirradiated graphite (Sec. 5-3). This amount of energy also corresponds to the integrated heat capacity of unirradiated graphite between 100 and 1550°C.

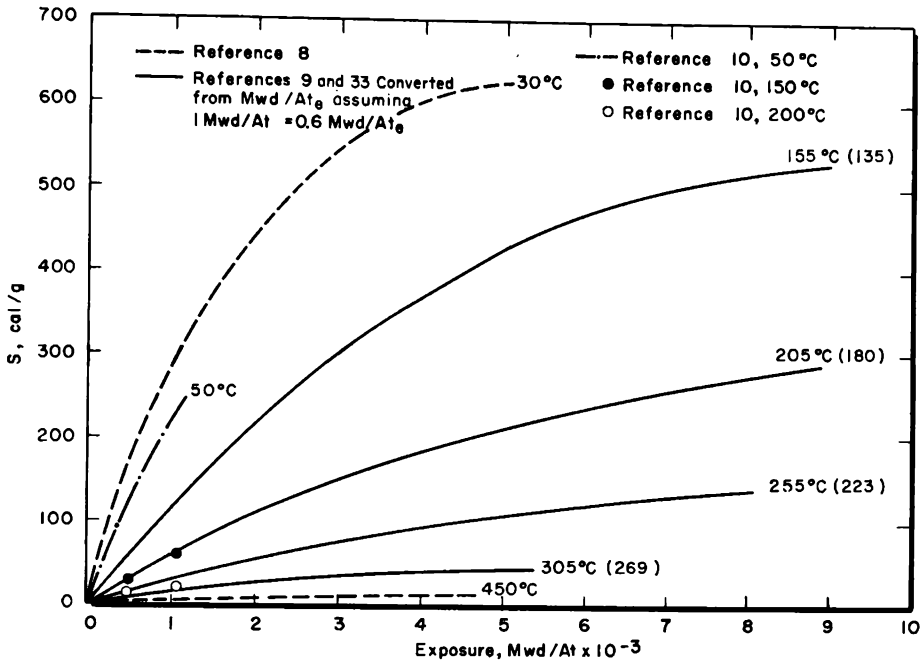


FIG. 12.2 The accumulation of total stored energy (S) at several irradiation temperatures. Equivalent Calder irradiation temperatures are shown in parentheses for each curve (see Sec. 12-2.3).

12-2.3 EFFECT OF IRRADIATION TEMPERATURE

The rate of accumulation of stored energy and the saturation value that S approaches after very long exposures (S_{∞}) decrease with the irradiation temperature. From Fig. 12.2 the value of S_{∞} at 30°C appears to be in the range 650 to 700 cal/g. Newgard¹² has pointed out that the exposure data (the 30°C curve to 3000 Mwd/At) can be fitted to semiempirical equations of the form,

$$S = S_{\infty}(1 - e^{-kE}) \quad (12.1)$$

or

$$S = S_{\infty} \tanh k'E \quad (12.2)$$

where k and k' are constants and E is the neutron exposure. Equations 12.1 and 12.2 predicted slightly different values for S_{∞} of 647 cal/g and 594 cal/g, respectively. Applying these equations to the 30°C curves in Fig. 12.2 results in an excellent fit in the case of Eq. 12.1 with $S_{\infty} = 685$ cal/g and $k = 0.526$ (1000 Mwd/At)⁻¹. Equation 12.2 does not fit the data as well over the complete exposure range.

Equation 12.1 can also be fitted quite accurately to the data above 30°C using the parameters given in Table 12.1. The values of k suggest that

longer times are required to reach saturation at the higher temperatures. The ratio k_{30}/k_T shown in the last column is equal to the dose required to attain a given per cent of S_∞ at T divided by the dose required to attain the same per cent of S_∞ at 30°C. Thus at 200°C three times the 30°C dose is necessary to get to any given fraction of S_∞ . The 300°C curve seems to be an exception; however, at this temperature the amount of stored energy is small, and the values of S_∞ and k are sensitive to changes in S of 5 to 10 cal/g.

Table 12.1 — PARAMETERS FOR THE EQUATION $S = S_\infty (1 - e^{-kE})$

Irradiation temperature, °C	S_∞ , cal/g	k , per 1000 Mwd/At	k_{30}/k_T
30	685	0.526	1
150	600	0.242	2.2
200	375	0.169	3.1
250	200	0.151	3.5
300	50	0.393	1.3

In the original derivation of Eq. 12.1 by Newgard, k is the rate constant for annealing displaced atoms. The numerical value of k should increase with irradiation temperature. However, except for the 300°C curve, the k derived from Fig. 12.2 decreases with temperature. There are several possible explanations for this apparent anomaly, all of which relate to the likelihood that the simple model assumed in the derivation of the equation is not adequate, particularly when the graphite becomes highly damaged. Therefore k depends not only on T but also on E . The k in Table 12.1 should be regarded only as an empirical parameter and should not be interpreted as having the physical significance that Newgard originally attached to it.

The 150 and 200°C points on Fig. 12.2 from the curves of Davidson¹⁰ were obtained from samples irradiated in the Hanford controlled-temperature facility (Sec. 8-3.2). These points fall below the curves at the corresponding temperatures. The curves were obtained from irradiations carried out inside hollow fuel elements in high-flux reactors (DIDO, PLUTO, and DMTR) for which the intensity of the damaging flux was considerably greater than normal for a graphite-moderated reactor. It is possible that under such conditions the radiation effects produced at a given total dose are significantly greater (Sec. 7-5.6). In fact, an "equivalent Calder temperature" (indicated in parentheses in Fig. 12.2) has been assigned^{9,33} to the irradiations to convert to the irradiation temperature in a Calder reactor at which the observed stored energy would be predicted. Although this brings the points and curves of Fig. 12.2 into better agreement, further studies will be necessary to establish with certainty the effects of flux intensity on stored energy and other radiation-induced changes in properties.

A useful equation¹³

$$S(T) = \alpha e^{-T/\beta} \quad (12.3)$$

relates the total energy stored $[S(T)]$ at a given exposure to the irradiation temperature (T). The stored energy accumulated at 0°C (α) is a constant for any given exposure. All the data of Fig. 12.2 are satisfactorily reproduced with $\beta = 71.2^\circ\text{C}$. A different α must be used to fit the Windscale and Hanford data, and in this sense the data from these two sources do not produce a consistent set of curves. The explanation for this is not clear.

Very little stored-energy data have been reported for irradiations above 450°C . A single CSGBF sample irradiated¹⁴ to 15,000 Mwd/At at about 500°C accumulated 40 cal/g. Another measurement⁸ on one sample after an exposure of 1.8×10^{20} neutrons/cm² ($E > 1$ Mev) at 750°C gave 9 cal/g. These results and the extrapolation of results obtained at lower temperatures indicate that stored-energy build-up will be of no practical concern at temperatures in the 500 to 1000°C range contemplated for future high-temperature graphite reactors.

12-3 Measurement of Stored-energy Release Curves

As soon as stored energy in graphite was observed, it was recognized that measurement of the total stored energy alone would be inadequate for the prediction of possible temperature excursions in the graphite moderator. It is necessary to know the amount of stored energy released as a function of the annealing temperature. Numerous experimental methods for determining stored-energy release curves have been developed, and, in fact, each laboratory concerned with radiation effects in graphite has developed one or more methods. For a discussion of the basic principles of these methods, it is convenient to classify them as isothermal, linear rise, and adiabatic.

12-3.1 ISOTHERMAL METHODS

In theory, stored-energy release curves can be derived from heat-of-combustion measurements in the following type of experiment. An irradiated sample is sectioned into several smaller samples. One section is isothermally annealed at T_1 , another section at a higher temperature, T_2 , etc. The ΔH is measured on each section, and the stored energy released in each temperature interval (ΔT) is calculated. A plot of $\Delta S/\Delta T$ as a function of the annealing temperature is a stored-energy release curve, the resolution of which is determined by the magnitude of ΔT (see Fig. 12.7).

This method has the disadvantage of requiring a large number of ΔH measurements to block out the spectrum with satisfactory resolution. Also a stored-energy gradient may exist throughout a sample large enough that, if the sample were sectioned into a number of smaller samples, each would have a different amount of stored energy. As assurance that each sample will have the same amount of stored energy, the original sample can be

ground prior to annealing. In this case, however, one must be satisfied with the average stored energy, and nothing can be learned of any gradients.

An advantage of this method is that the region in which high-temperature annealing takes place can be more easily studied. In fact, the only information on the stored-energy release curve at annealing temperatures above 800°C has been obtained by this method.

Somewhat similar information can be obtained from a calorimetric measurement of the apparent decrease in specific heat. This type of isothermal method consists in suddenly inserting the sample in a gas or liquid at an elevated temperature for a predetermined period of time. From an analysis of the heating-rate curve, the stored energy released up to the temperature of the heating fluid can be calculated. Variations of the isothermal method have been employed at Argonne,⁶ Hanford,¹⁵ and in England.¹⁶ The results of these experiments, while providing a measure of stored energy released under the conditions of the experiments, are difficult to apply in a general way, and this method has been replaced by more refined and more generally useful methods.

Wechsler et al.¹⁷ have described another type of isothermal method based upon radiative exchange of heat between the sample and the calorimeter. In common with other isothermal methods, this method does not give the stored energy as a continuous function of the annealing temperature; it gives only the total stored energy released up to the temperature of the calorimeter.

12-3.2 LINEAR RISE

Those methods that can be broadly classified as linear rise include a modification of the Sykes method¹⁸ employed at Argonne,¹⁹ Hanford,²⁰ and Chalk River;²¹ the twin-crucible method;²² the differential thermal-analysis method;²³ and the linear-rise method most recently improved and reported in England.^{16, 24} They all employ a calorimeter whose temperature rise is only approximately linear, but, since the stored energy is determined from the difference in two annealing curves, a small deviation from linearity is not serious if the temperature-time program is the same for the two curves.

In early versions¹⁹ of the linear-rise method, the difference between the temperature of the sample and the calorimeter was recorded during the run. The procedure normally employed was to record the temperature differential as a function of time or temperature up to 400 to 500°C. The release of stored energy was indicated by a temperature rise in the sample. The run was repeated on the partially annealed sample. Assuming that no stored energy was released during the second run, dS/dT could be calculated as a function of annealing temperature.

A modification of the above procedure, and the one now commonly employed,^{16, 22, 25} is to measure the additional heat necessary to keep the sample and calorimeter at the same temperature during the temperature

rise. The linear-rise calorimeter described by Cottrell et al.¹⁶ will serve as a good example. Two samples, one irradiated and one unirradiated, are placed in a copper enclosure, which, in turn, is mounted in a space that can be evacuated (Fig. 12.3). The samples and enclosures are provided with

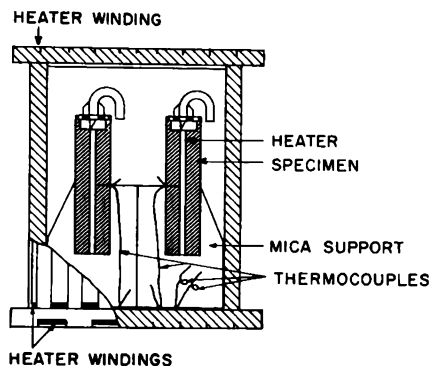


FIG. 12.3 A linear-rise calorimeter. Two graphite samples, one irradiated and one unirradiated, are heated, and the power required to maintain the samples at the same temperature is measured.¹⁶

electrical heaters and thermocouples, the heater currents being controlled so that the electromotive forces (emf) from the thermocouples follow the output from a potential source. The latter consists of a motor-driven potentiometer, which provides an emf increasing linearly with time.

During an experiment the difference in the power supplied to the two samples is recorded. Assuming the specimens were identical prior to irradiation, this difference in power is just the rate of stored-energy release, dS/dT . To allow for any lack of symmetry, two runs are made, and the stored energy is determined from the difference in the two power curves. A third run can be made to verify that no stored energy was released during the second run. One can then plot dS/dT as a function of the annealing temperature.

For a sample in which dS/dT exceeds the specific heat, such as is illustrated in Fig. 12.1, it is necessary to remove heat to maintain a constant rise in temperature. In this case the temperature of the enclosure can be controlled at a fixed interval below the temperature of the samples by inserting a suitable potential (lag voltage) in series with the sample thermocouples.

Most linear-rise calorimeters are limited to temperatures less than 500°C. This is, of course, the region of most practical interest since dS/dT often exceeds the specific heat between 125 and 400°C. This is also the temperature range within which most graphite moderators operate. Koyama²⁵ has recently described a linear-rise calorimeter to measure dS/dT to 1200°C. A single graphite sample is employed, and instrumentation is used to maintain a constant temperature rise of 10°C/min. Tests with un-

irradiated graphite show that the power curve is reproducible to ± 5 per cent. No data on irradiated samples have yet been reported.

The detailed shapes of the release curves obtained in different laboratories by linear rise depend upon the operating characteristics of the particular instrument, the operating procedures, and treatment of the data because heat-transfer conditions are inevitably slightly different, heating rates and lag voltages (if any) have not been standardized, and various corrections and approximations are often applied to the data. For example, significant differences¹⁶ in the shape and maximum position of the "200°C peak" are obtained with heating rates of 2.5°C/min and 13°C/min. These variables can be held sufficiently constant that reproducible results can be obtained on a given instrument. However, some cross-checking and standardization between the laboratories measuring stored energy by linear rise methods are needed. In spite of the experimental difficulties encountered and the careful work required, linear rise is probably the most generally useful of the methods of measuring stored energy.

12-3.3 ADIABATIC RISE

The adiabatic-rise method is really not a method of measuring the release curve; rather it is a means of determining the total energy released to a given temperature, usually in the range 200 to 400°C. It is only applicable to those regions of the release curve for which

$$\int \frac{dS}{dT} dT > \int C_p dT$$

i.e., from 175 to 360°C in Fig. 12.1.

The adiabatic-rise method has been found especially valuable in predicting the spontaneous temperature rise of irradiated graphite under approximately adiabatic conditions. It has been refined to a high degree by Simmons and coworkers at Harwell²⁶ and was used extensively in predicting the annealing behavior of the graphite during the release of stored energy in BEPO.²⁴ In this method the temperature of the sample is raised rapidly to promote a fairly rapid release of stored energy. The sample is then maintained in adiabatic surroundings, and the temperature rise is followed as a function of time.

A typical experimental arrangement is shown in Fig. 12.4. The sample (normally $\frac{3}{8}$ in. in diameter by $\frac{1}{2}$ in. long) rests on three mica supports. The bottom and top parts of the calorimeter are heated separately on the outer surface by the nichrome heaters. One of the two thermocouples attached to the sample measures the sample temperature, and the second is connected in opposition to a thermocouple in the lower half of the calorimeter. The signal, which is proportional to the temperature difference, controls the heat supplied to the lower part of the calorimeter. A differential thermocouple, which uses the copper calorimeter as one part of the constantan-

copper-constantan circuit, indicates the temperature difference between the top and bottom halves of the calorimeter and controls the heat supplied to the top half. Thus the bottom half of the calorimeter follows the sample, and the top half of the calorimeter follows the bottom half.

A small radiant heater, consisting of a coil of platinum wire, is used to initiate the stored-energy release. By this means the temperature of the sample is raised as quickly as possible to the temperature where energy

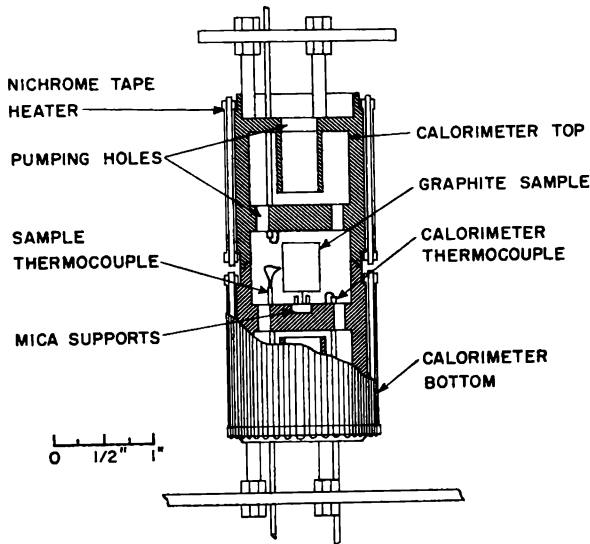


FIG. 12.4 A vacuum calorimeter used in the adiabatic-rise method. This assembly is placed inside a water-cooled enclosure and evacuated during a run. (From Henson and Simmons, Ref. 26.)

release begins. The heat supply is then cut off, but the temperature of the sample continues to rise owing to the release of stored energy. The temperature of the calorimeter is maintained close to the temperature of the sample to minimize heat losses, and the amount of stored energy released is determined from the increase in the sample temperature and the known specific heat of the graphite. A correction is applied for the heat gained or lost from the calorimeter under nonadiabatic conditions.

Typical adiabatic-rise curves are shown in Fig. 12.5. The differences in the curves for a high-energy sample and a low-energy sample are shown. The starting temperature may be raised in steps until a suitable starting rate is obtained. The curves show that at times the calorimeter must follow a slow drift, during which time precise temperature control is needed to keep the heat transfer small. At other times the rate of temperature rise is rapid, and the calorimeter must be able to follow this without lagging or overshooting.

The stored energy released in an adiabatic-rise experiment is well

defined only if the starting and finishing conditions are specified. In most Harwell measurements a starting temperature is chosen to produce an initial rate of rise of $1^{\circ}\text{C}/\text{min}$, and the measurement is terminated when the rate has fallen to $0.2^{\circ}\text{C}/\text{min}$.

The adiabatic-rise calorimeter is a versatile instrument. It can be used to make pseudo linear-rise measurements, or the heat losses can be adjusted to approximate specific reactor conditions to obtain an estimate of the temperature rise during a reactor anneal.

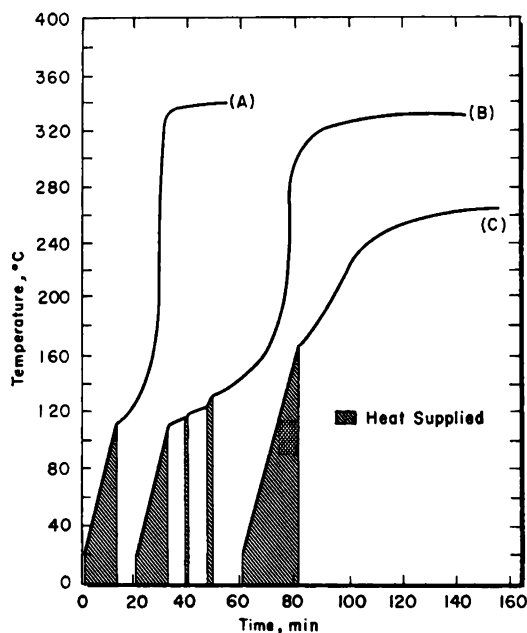


FIG. 12.5. Adiabatic-rise curves. Curves for a typical high-energy sample (A) and a typical low-energy sample (C) are shown. Curve B illustrates the way in which the starting rate can be changed until a suitable rate is obtained.²⁴

The largest uncertainty in the adiabatic-rise measurements with this type calorimeter is the uncertainty in the starting conditions, partly because it is not possible to reach the starting temperature instantaneously and partly because some heat is added to the sample after the heater current has been switched off. Even so, it is reported²⁴ that a reproducibility of ± 1.5 cal/g in the energy released up to 400°C can be expected in the adiabatic-rise method.

12-4 Release Curves in Irradiated Graphite

12-4.1 IRRADIATIONS NEAR 30°C

The changes in stored-energy release curves caused by irradiation at $30 \pm$ $^{\circ}\text{C}$ in Hanford cooled test holes are illustrated in Fig. 12.6. The

release curves were determined by the linear-rise method described in the previous section with a lag voltage of $400\ \mu\text{V}$ up to about 300°C . The most important feature of the curves is the behavior of the familiar 200°C peak. The maximum of the peak increases in intensity to greater than twice the specific heat in the range 400 to 600 Mwd/At and then decreases with increasing exposure to a fairly constant value of $0.45\ \text{cal/g}/^\circ\text{C}$ after 1200

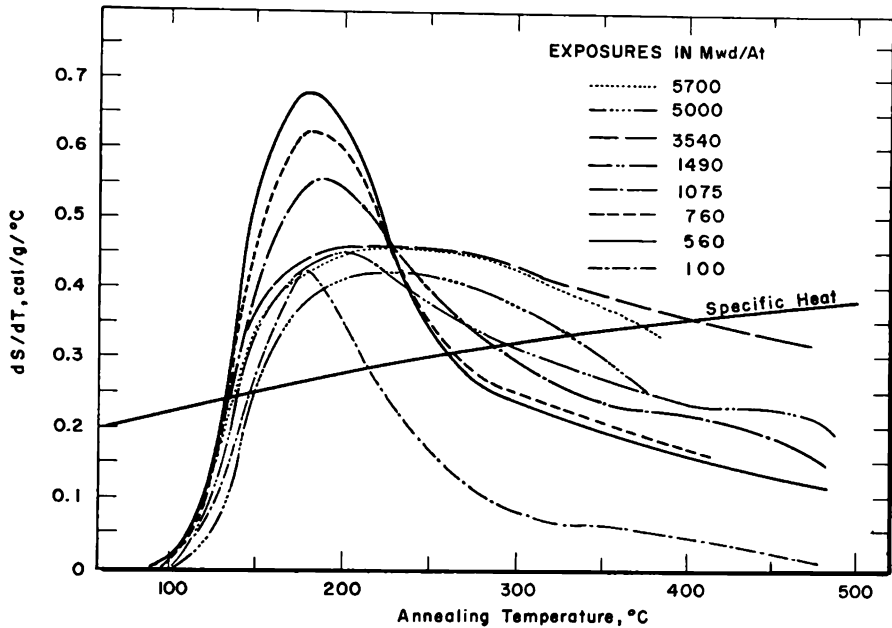


Fig. 12.6 Stored-energy release curves²⁷ of CSF graphite irradiated near 30°C .

to 1500 Mwd/At. The stored energy releasable above 200°C continues to increase, however, and results in the continuous increase in total stored energy shown in Fig. 12.2. The decrease of the peak intensity at high exposures and the general shift to higher annealing temperatures are important from a reactor-safety standpoint since the kinetics of the heat release are obviously closely related to the shape and intensity of the release curves. Earlier stored-energy release curves[†] reported by Woods et al.²⁸ and the activation energy spectra by Neubert and Lees¹⁹ show the same general behavior.

It is important to know if the release curve contains any peaks at higher temperatures which greatly exceed the specific heat. Unfortunately the determination of reliable release curves to high temperature is experimentally difficult, and practically no data have been reported above

[†] The stored-energy investigations reported by Woods et al. at the 1955 Geneva Conference are a part of the early work carried out at the Hanford Engineer Works and published in classified reports during the period 1945-1953 by L. McClaine, L. P. Bupp, P. H. Reinker, J. C. Ballinger, and others.

500°C. Ballinger²² has measured the release curve to 800°C for a sample exposed at approximately 30°C for 650 Mwd/At. In this case the curve contains a broad minimum between 400 to 600°C, followed by an increase at higher temperatures. However, the curve does not exceed the specific heat in the high-temperature region.

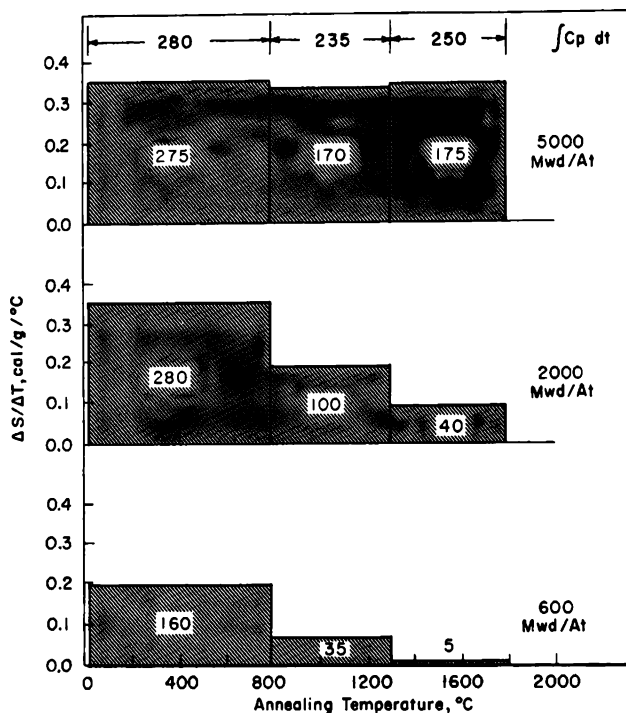


FIG. 12.7 Stored energy released from TSGBF graphite irradiated at 30°C. The numbers inside the areas give the stored energy released in the corresponding temperature range. The specific heat integrated over each temperature range is given at the top of the figure. All stored energy was removed by the 1800°C anneal.¹⁰

Some indication of the shape of release curves at high temperatures is given by the measurement of total stored energy after annealing at different temperatures (Fig. 12.7). The apparent heat content $H(T_1, T_2)$ between T_1 and T_2 defined by

$$H(T_1, T_2) = \int_{T_1}^{T_2} C_p dT - \int_{T_1}^{T_2} \frac{dS}{dT} dT \quad (12.4)$$

will be negative if there is sufficient stored energy for the graphite to be self-heating between T_1 and T_2 ; if there is insufficient stored energy for the graphite to be self-heating, the amount of energy required to raise the temperature from T_1 to T_2 is given by $H(T_1, T_2)$. For the samples exposed at 2000 and 5000 Mwd/At, $H(25, 800) \simeq 0$. Above 800°C, $H(800, T_2)$ is

greater than zero for these samples, but it is appreciably less than the value for unirradiated graphite.

It is interesting to note that the average stored energy apparently builds up to a maximum of about 280 cal/g in the 25 to 800°C range. There is some indication of this type of behavior in the 3540-, 5000-, and 5700-Mwd/At curves of Fig. 12.6, where the stored energy releasable at 400°C remains about the same, or decreases slightly. Woods et al.²⁸ report similar results for anneals at 1000°C.

12.4.2 EFFECTS OF IRRADIATION TEMPERATURE

The stored-energy release curves of graphite irradiated near the temperature of liquid nitrogen have revealed several interesting aspects of radiation effects in graphite. A number of small pieces of AWG graphite†

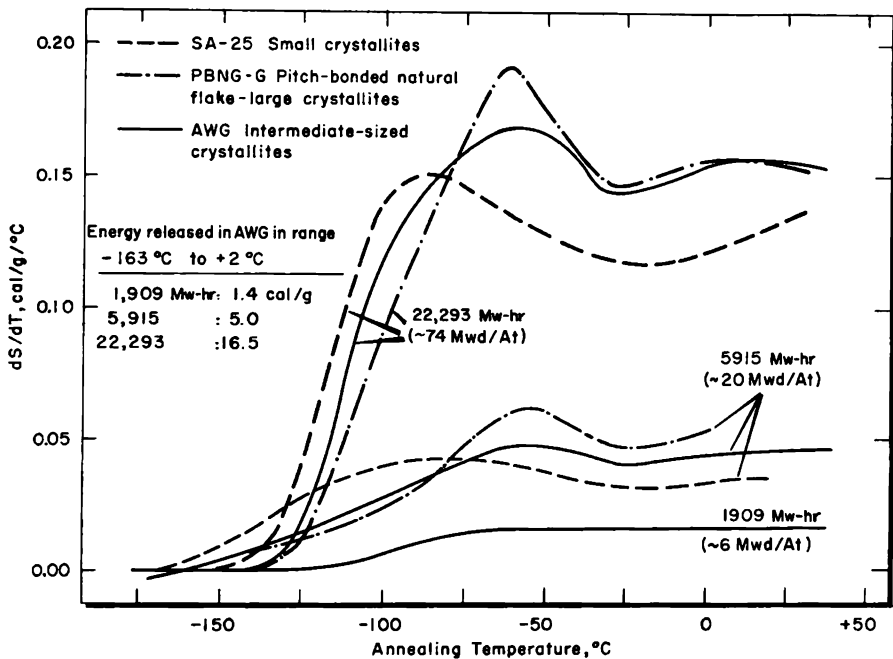


FIG. 12.8 Stored energy released following irradiation^{29, 30} at -150°C .

were irradiated²⁹ in the low-temperature facility of the Brookhaven Graphite Research Reactor (BGRR) under conditions such that the temperature was held below -150°C .

The release curves for AWG, which represent the average for several samples, are shown in Fig. 12.8.

† AWG is an obsolete grade of a fine-grained molded electrographite similar to the current ATJ grade manufactured by the National Carbon Co. (see Table 6.23). AWG was fully graphitized, and the stored-energy accumulation and release characteristics should be similar to those for current nuclear grades.

It is clear that a considerable amount of damage was retained at low temperature which would have annealed during room-temperature irradiations. For example, after 22,293 Mw-hr (~ 75 Mwd/At), 16.5 cal/g annealed in the range -163°C to $\pm 2^\circ\text{C}$; this is approximately one-third of the total energy released above 30°C .

The more intense maximum in the 22,293 Mw-hr AWG curve at about -60°C suggests that a discrete defect is forming that anneals over a narrow temperature range. Crystallinity has a slight effect on the shape of the curves. The release curves of SA-25, having small crystallites, have broad maxima at about -110°C . In the case of the pitch-bonded natural flake graphite, the maxima are at -60°C , and they are more distinct.

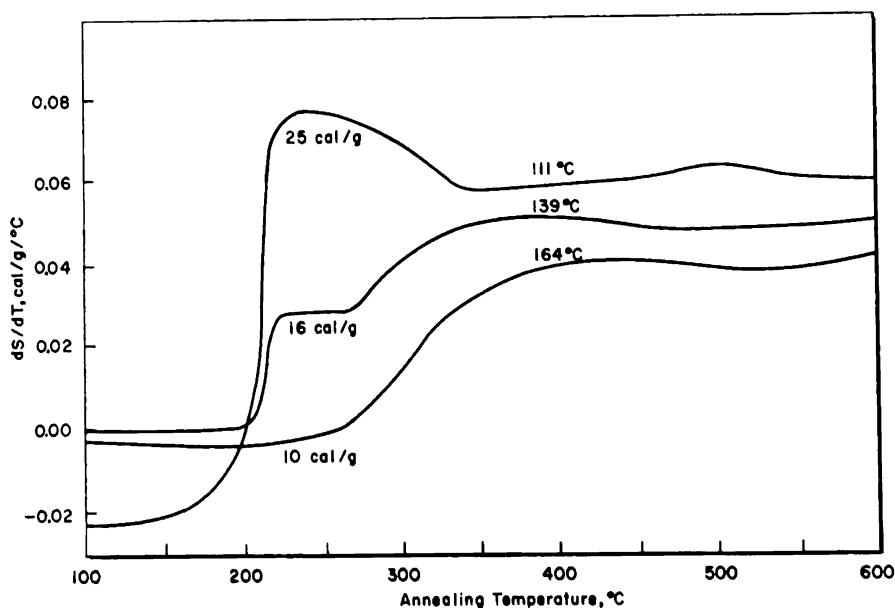


FIG. 12.9 Stored-energy release curves of CSF graphite²⁹ exposed to 193 Mwd/At. The higher irradiation temperatures greatly reduced the 200°C peak. Numbers under the curves give the stored energy released to 600°C .

Austerman²⁹ states that this can be explained if it is assumed that interstitial defects, initially distributed uniformly, diffuse during annealing to sinks at crystallite boundaries. The crystallites in SA-25 are about one-tenth the size of those in the natural flake material. Thus diffusion to boundaries might be expected to occur more rapidly in SA-25 and would be detected at a lower temperature.

Austerman and Hove³¹ found that, after irradiations at -263°C with 1.25-Mev electrons, practically no change occurs in the electrical conductivity until the samples are heated to -190°C . It is probable therefore that irradiation at the temperature of liquid nitrogen would result in almost

as much stored energy as irradiation at the temperature of liquid helium.

Changes in stored energy²² and other properties²² have been reported on CSF graphite irradiated above room temperature. A comparison of Figs. 12.6 and 12.9 shows that irradiation temperatures of substantially less than 200°C very effectively reduce the 200°C peak. Other investigators^{14,23} have also made this observation.

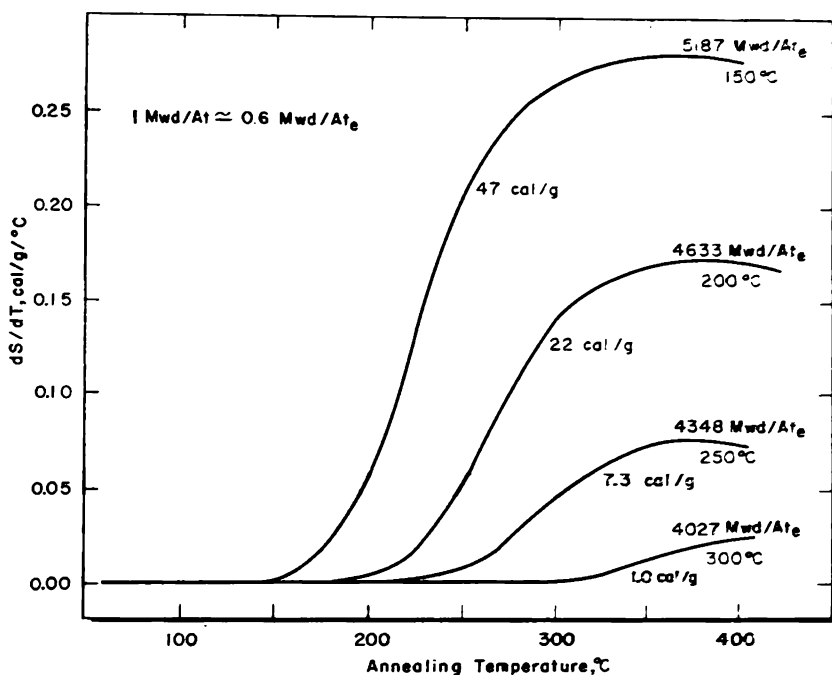


FIG. 12.10 The effect of irradiation temperature on stored-energy release curves for high exposures.^{9, 33} Numbers under the curves give the stored energy released to 400°C.

The effects of irradiation temperature at much higher exposures are shown in Fig. 12.10. Although the stored energy releasable to 400°C continues to increase, the amount tends toward saturation.

12.4.3 EFFECTS OF GRAPHITE STRUCTURE

In several ways highly damaged graphite appears to approach a microcrystalline state. Radiation-induced expansion is substantially reduced in noncrystalline carbons during room-temperature irradiations, and one might therefore hope that microcrystalline graphites would be less susceptible to the build-up of stored energy. The only data published on this subject indicate that in extreme cases of noncrystallinity such is the case.³⁴ The effects of irradiation at room temperature on the release curves of microcrystalline carbon powders are shown in Fig. 12.11. The 200°C peak vanishes, and the stored energy released up to 600°C becomes less as

the crystallite size is reduced. These effects lend support to the suggestion by Austerman²⁹ that during irradiation interstitials are trapped at the crystal boundaries and at other defects in the noncrystalline carbons. It should be noted that carbon black and polymer carbon are extreme examples of noncrystalline carbons. Differences in the rate of stored-energy

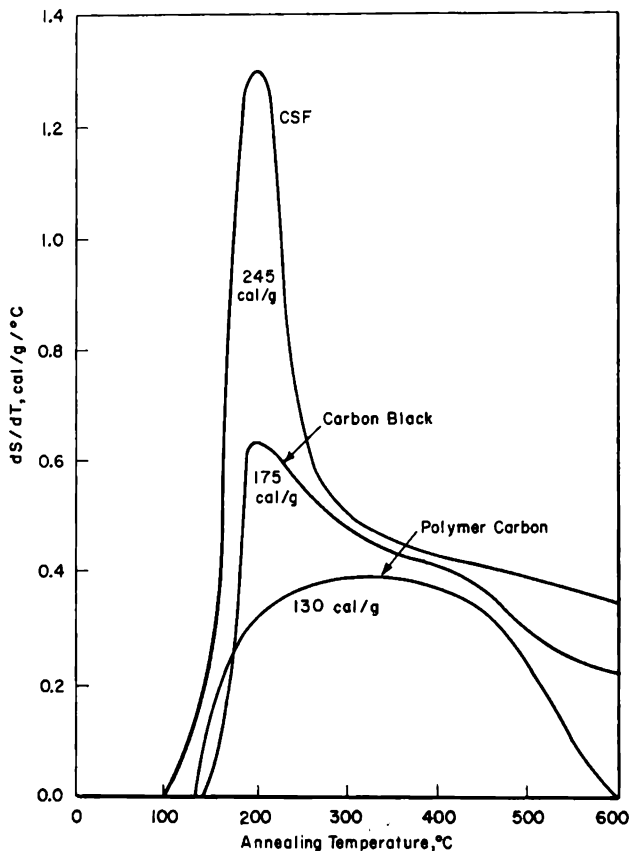


FIG. 12.11 Stored energy in special carbons (exposure, 530 Mwd/At). CSF, carbon black, and polymer carbon have decreasingly smaller crystallites. The stored energy released to 600°C is given by the numbers under the curves.³⁴

build-up between CSF and a less graphitic material such as a Korite graphite, which might be of practical interest for low-temperature moderator applications, have not been studied; the differences would probably be slight, however.

The stored energy released from the CSF sample of Fig. 12.11 is somewhat more than would be predicted for this exposure by Fig. 12.6. This difference is believed to be due to the fact that the release curves in Fig. 12.11 were measured prior to improvements in the twin-crucible method; however, intracomparison of the curves in Fig. 12.11 should be valid.

12-5 Theory of Energy Storage

12-5.1 HEAT CONTENT OF AN INTERSTITIAL-VACANCY PAIR

The heat content of an interstitial-vacancy pair has not been measured directly, but it is possible to estimate a value from a consideration of the energy relations of the following processes:

1. Formation of an interstitial-vacancy pair.
2. Formation of a gaseous carbon atom from an interstitial atom.
3. Formation of a gaseous carbon atom and a vacancy from a lattice atom inside the crystal.
4. Evaporation of a surface carbon atom (sublimation).
5. Formation of a vacancy by diffusion of an atom to the surface.

These processes are illustrated schematically in part a of Fig. 12.12, and the energy relations for the formation and annealing of vacancies are shown in part b.

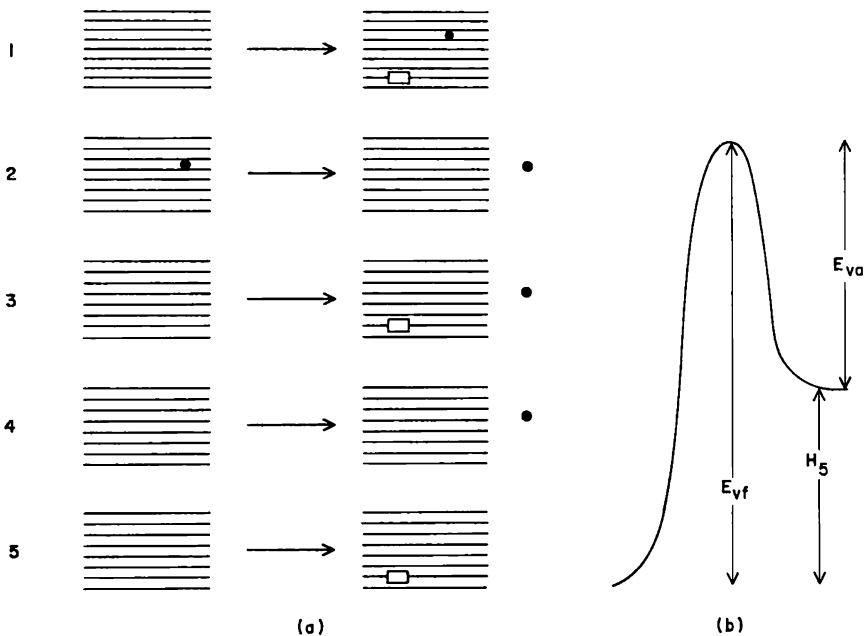


FIG. 12.12 (a) Schematic illustration of several idealized processes in the formation of vacancies and interstitials. Vacancies are represented by the symbol \square , and interstitials and gaseous carbon atoms, by the symbol \bullet . (b) Energy relations in vacancy formation and annealing (process 5). Activation energies are shown for vacancy formation (E_{vf}) and vacancy annealing (E_{va}). H_s is the heat of formation of a vacancy.

The rate of accumulation of stored energy (S) with exposure (E) is given in terms of the displacement rate (R) by

$$\frac{dS}{dE} = H_1 R \quad (12.5)$$

where H_1 is the energy of formation of an interstitial-vacancy pair.

In any estimate of H_1 , it has always been assumed that the energy of formation of a gaseous carbon atom (H_2) from an interstitial atom is approximately zero. This implies that the energy evolved by the relaxation of the undistorted lattice about an interstitial carbon atom is small. The fact that interstitial atoms diffuse at low temperatures suggests that the relaxation energy about the interstitial is low, and therefore the approximation has some justification.

The energy of formation of a gaseous carbon atom and a vacancy (H_3) is the sum of the heat of sublimation (H_4) and the energy of formation of a vacancy (H_5). Therefore, since $H_3 = H_1 + H_2$ and $H_2 \simeq 0$,

$$H_1 \simeq H_4 + H_5 \quad (12.6)$$

The heat of sublimation of graphite has been measured experimentally, and, although some uncertainty has existed in the past as to the proper value, most investigators now favor a value of 170 kcal/gram atom.

The energy of formation of a vacancy has not been measured and must be inferred from indirect evidence. The formation of a vacancy involves the transfer of an interior lattice atom to the surface. The atom combines with the edge atoms and becomes a part of the surface. The annealing of a vacancy by diffusion along a layer plane to an edge surface site, where it is annihilated, is the reverse of this process.

The energy relations for vacancy formation are shown in part b of Fig. 12.12. The activation energy for self-diffusion³⁵ in graphite is 163 kcal/gram atom. However, it is not possible to choose between a vacancy diffusion and a direct interchange mechanism (see also Sec. 6-2.6). If the vacancy mechanism is the correct one, the activation energy for vacancy formation (E_{vf}) is 163 kcal/gram atom; if not, E_{vf} probably does not differ greatly from this value.

The activation energy for vacancy annealing calculated by Dienes' method³⁶ is 93 kcal/gram atom if the heat of sublimation is taken as 170 kcal/gram atom. This value corresponds to vacancy annealing beginning above 1000°C, which seems reasonable. Therefore, since, from part b of Fig. 12.12, $H_5 = E_{vf} - E_{va}$, the energy of formation of vacancies is approximately 70 kcal/gram atom.

Other values for H_5 have been suggested: Kanter and Hennig³⁷ state that H_5 is greater than 69 kcal/gram atom; Neubert and Lees¹⁹ assume a value of 80 kcal/gram atom; a later estimate by Kanter³⁸ places the value of H_5 in the range 10 to 80 kcal/gram atom. A value of 70 kcal/gram atom will be assumed in the subsequent discussion.

From Eq. 12.6 $H_1 \simeq 170 + 70 = 240$ kcal/gram atom. Most other esti-

mates of the energy stored by interstitial-vacancy pairs give values of this magnitude. The following values in kilocalories per gram atom have been assumed or calculated for H_1 by various investigators: 250 (Ref. 19), 230 (Ref. 11), and 207 (Ref. 39).

Clustering will, of course, decrease the average energy stored per displaced atom. If it is assumed that interstitial C_2 groups have a binding energy equal to that of C_2 vapor (140 kcal/mole),⁴⁰ then the net increase in energy content for the formation of C_2 interstitials and vacancies is $240 - (140/2) = 170$ kcal/gram atom.

12-5.2 DISPLACEMENT RATE FROM STORED-ENERGY MEASUREMENTS

For the calculation of displacement rates, the rate of stored-energy build-up with exposure (dS/dE) must be measured near zero exposure at temperatures low enough to ensure that no clustering or annealing to surfaces has occurred. The alternative is to estimate the energy stored for each atom originally displaced at the temperature for which dS/dE is measured.

The lowest temperature for which dS/dE has been measured is about 30°C. On the basis of property changes produced by irradiation at liquid-helium and liquid-nitrogen temperatures (Sec. 12-4.2), it is estimated that 30 per cent or more of the displaced atoms reintegrate during irradiations at 30°C. The displacement rate is therefore

$$R \simeq \frac{4}{3} \frac{dS/dE}{H_1} \quad (12.7)$$

At 30°C dS/dE from Fig. 12.2 is 0.5 cal/Mwd/At. More-accurate values derived from measurements at very low exposures range from 0.6 to 1.0 cal/Mwd/At.† Assuming a value of 1 cal/Mwd/At,

$$R \simeq \frac{4}{3} \frac{6 \times 10^{23}}{240 \times 1000} = 3.3 \times 10^{18} \frac{\text{displacements}}{\text{g} - \text{Mwd/At}}$$

which, for nuclear graphite with a density of 1.7 g/cm³, is

$$R = 5.7 \times 10^{18} \frac{\text{displacements}}{\text{cm}^3 - \text{Mwd/At}}$$

Values of R calculated from displacement theory and from other property changes agree within an order of magnitude with this number (Sec. 7.4).

12-6 Relation of Stored Energy to Other Radiation-induced Property Changes

Careful and time-consuming measurements are required for the determination of stored energy. In addition, the radiation effects are at least partially removed when stored-energy release curves are determined, and

† See Ref. 41 for a discussion of dS/dE measurements.

the sample is destroyed when total stored energy is measured. Thus samples cannot be reinserted into the reactor to study the effects of exposure on stored energy. It is natural therefore that there has been considerable interest in estimating stored energy from the measurements of other property changes that are both quicker and nondestructive. The most successful attempts in this direction have employed correlations of stored energy with changes in c spacing and thermal conductivity.

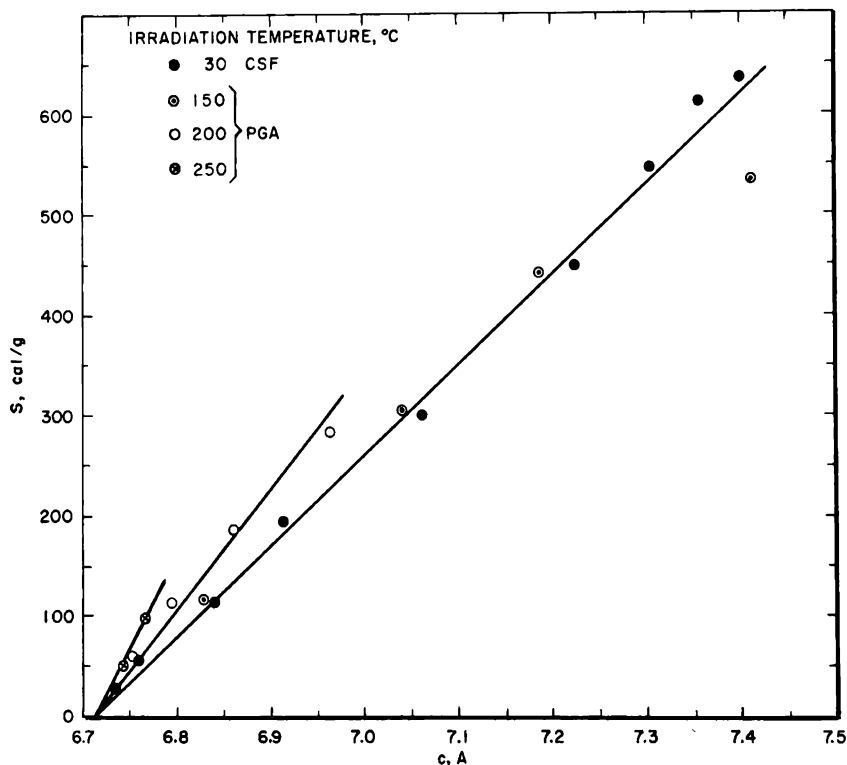


FIG. 12.13 The relation of radiation-induced c -spacing changes and total stored energy (S). Polarization and geometrical corrections have been applied to the c -spacing measurements.

The correlation of stored energy and c -spacing changes is shown in Fig. 12.13. It should be noted that the c spacings in Fig. 12.13 have been taken from Fig. 9.6 to which polarization and geometrical corrections have been applied. The slopes of the lines in Fig. 12.13 are therefore steeper than would be obtained from c measurements to which these corrections have not been applied. The stored-energy vs. c -spacing curves are linear, and the slopes appear to increase with irradiation temperature above approximately 150°C. The close correlation between stored energy and c spacing indicates that the radiation effects responsible for stored energy and lattice expansion are similar. Since c spacing can be measured from small powdered samples,

this correlation is useful in estimating stored-energy gradients throughout a moderator structure.

Figure 12.14 shows the relation of stored energy and thermal conductivity. Changes in the thermal conductivity of CSF graphite measured

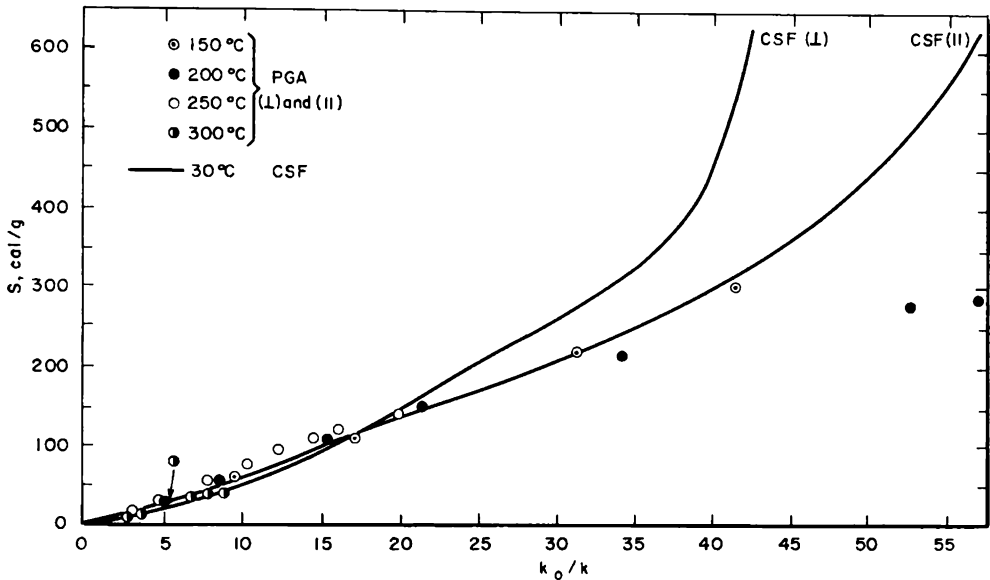


FIG. 12.14 The relation of stored energy (S) and the room-temperature thermal conductivity ratio (k_0/k).

transverse (\perp) to the extrusion axis saturate more quickly than the changes measured parallel (\parallel) to the extrusion axis. This causes the curve for stored energy vs. thermal conductivity for CSF (\perp) to rise steeply beyond $k_0/k = 35$. Points for PGA graphite exposed at intermediate temperatures lie close to the 30°C curve for CSF (\perp) except at higher exposures, where k_0/k apparently saturates very slowly. If data for other graphites, such as TSGBF (Fig. 10.8), were added to Fig. 12.14, it would become apparent that changes in thermal conductivity are more sensitive to the structure of the graphite than are changes in stored energy. From this standpoint, the correlations with c spacing are more generally useful for estimating stored energy.

12-7 Reactor Safety and Operational Aspects of Stored Energy

12-7.1 HANFORD REACTORS

The accumulation of stored energy in the Hanford reactors first became of concern when Szilard pointed out the possibility that a sudden release of stored energy might cause an undesirably large temperature rise.[†] The first actual measurements of stored energy in graphite were made almost

[†] The historical aspects of stored energy are described elsewhere^{10, 12} in more detail.

simultaneously in the fall of 1944 by Babcock, Gast, and Wende⁴³ at Hanford and by R. J. Maurer⁴⁴ at the University of Chicago. These and subsequent measurements revealed that stored energy accumulated at a considerably slower rate in the Hanford reactors than the 20 to 50 cal/g per day that had been predicted earlier. Subsequent periodic assessments of the stored energy have involved the determination of stored-energy release curves and total stored energy on samples removed by mining and coring from the moderator stack itself and on samples inserted into cooled and uncooled test channels. These data have been analyzed in terms of four moderator zones.⁴⁵ These zones consisted of a central graphite region (characterized by a fairly high, uniform temperature) and a fringe graphite region (having a less uniform and lower temperature); each of these regions was further divided into the tube-block graphite and the filler-block graphite. Figure 12.15 shows the stored-energy release curves

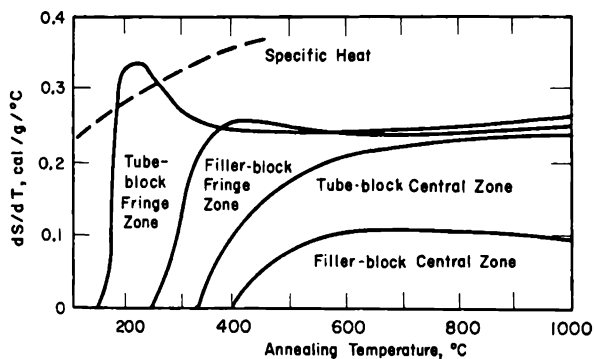


FIG. 12.15 Stored-energy release from four zones of the Hanford graphite moderator.⁴⁵

for graphite taken in 1952 from each of these zones. It is seen that the curves exceed the specific heat only in the fringe zone (10 per cent of the graphite moderator). From this type of information and total stored-energy measurements, it was concluded that, although a considerable amount of stored energy had accumulated in the cooler parts of the graphite stack, it did not constitute a major safety problem. Limitations were placed on reactor operation to control rates of temperature change from established temperature levels and the periods of time necessary to establish these levels. Under these conditions the rate of self-annealing has been sufficient to keep the stored energy at a safe level, and it has never been considered necessary to anneal the reactors.

12-7.2 BEPO, WINDSCALE, X-10, AND OTHER REACTORS

The graphite moderator in the British Experimental Pile Zero (BEPO), Windscale, Oak Ridge X-10, and French G-1 reactors is cooled by air brought in at atmospheric temperature and discharged at 220°C or lower

(Table 1.2). The graphite, therefore, operates at a temperature low enough to accumulate stored energy at a significant rate. Each of these reactors has been annealed one or more times for the purpose of removing stored energy. In addition, the BGRR, which is also air cooled, has received several anneals, although the purpose for these has been to anneal radiation-induced dimensional changes in the graphite rather than stored energy. The results of these anneals and their relation to the design and operating characteristics of the graphite moderator are discussed in Sec. 17-3.2.

12-7.3 CALDER TYPE REACTORS

The Calder Hall reactors are carbon dioxide cooled, having an inlet temperature of 135°C and an outlet temperature of 333°C. The graphite temperatures are, therefore, low enough in the cooler parts of the core to allow the accumulation of a significant amount of stored energy. Following the Windscale incident, the effect of stored energy on the safety and operation of the Calder reactors was reevaluated. It was concluded that after two years of operation the stored energy was insufficient to produce a self-sustaining release and that it was likely to remain so for at least another two years.⁴⁶⁻⁴⁸ Furthermore, it was recognized that the consequences of a sudden release of energy would be less serious than in an air-cooled reactor since uranium reacts with carbon dioxide only at appreciably higher temperatures than with air. In addition, the carbon dioxide-graphite reaction is endothermic, thereby allowing the coolant to be used safely for removal of stored energy released from the graphite. There was, however, little information from which the effects of long-term irradiation at intermediate temperatures might be predicted, and so the extent of the problem, if any, after four years of operation could not be completely evaluated.

It now appears that the problem will be dealt with in the Calder reactors and the Chapel Cross No. 1 Reactor by the insertion of Magnox sleeves in the coolant channels between the fuel elements and the graphite.⁴⁹ This will create an insulating barrier of stagnant gas through which heat generated in the graphite (6 to 8 per cent of the fission heat) will have to pass. The expected increase in the graphite temperatures has not been reported, but presumably it will be sufficient to reduce the rate of accumulation of stored energy to an acceptable level. Sleeves will be used only in the lower parts of the channels since the temperature in the upper parts of the graphite structure is expected to be sufficiently high.

The Berkeley, Bradwell, Hunterston, and later reactors of the Calder type will employ graphite sleeves. Although some energy storage will occur on their cooled inner surfaces, the sleeves will have only a limited life since they will be discharged with the fuel. It has been estimated⁴⁹ that the Hunterston reactors can be operated about 50 years before energy storage in any region of the moderator will necessitate a release of energy.

12-7.4 STORED ENERGY IN ADVANCED HIGH-TEMPERATURE REACTORS

Several high-temperature prototype reactors under construction are intended to pilot the development of gas-cooled graphite-moderated reactors. Graphite in the Advanced Gas-cooled Reactor in England and the Experimental Gas-cooled Reactor at Oak Ridge will operate in the range 300 to 600°C. The High Temperature Gas-cooled Reactor in the United States and the Dragon Reactor in England will employ graphite sleeves so that the bulk of moderator will be considerably above 300°C. Reference to Fig. 12.2 shows that under these conditions it is unlikely that stored energy will be a problem in any of these reactors. It should be noted, however, that above 400°C the highest exposure for which data have been obtained is less than 10 per cent of the expected lifetime of a power reactor. Since there is as yet no evidence of saturation of the stored-energy level at high temperatures, irradiation experiments in high-flux reactors must be continued to provide the high-exposure data required.

Other graphite-moderated reactors listed in Table 1.2 (the Urals Power Station reactors, the Sodium Graphite Reactor, and the Hanford N Reactor) are cooled by pressurized liquids, which do not come in direct contact with the graphite. It would appear that even in the lowest temperature regions of these reactors the stored energy will remain at an acceptably low level.

12-7.5 STORED ENERGY IN GRAPHITE REFLECTORS

Many reactors employ graphite as a neutron reflector. The build-up of stored energy in reflector graphite is usually not considered a problem since the component of damaging neutrons is relatively low. However, consideration should be given to this problem during the design of the reactor. Experience with the Canadian NRX reflector graphite has been reported in detail and serves to illustrate this point.

The NRX, built in 1947, is a natural-uranium heavy-water-moderated reactor.⁵⁰ The core is surrounded by a graphite reflector consisting of two cylindrical sections separated by a 2.5-in. annular gap. The neutron flux at the inner reflector was sufficiently high and the temperature sufficiently low for a significant amount of stored energy to accumulate over the six-year period 1947–1953. Measurements made in 1953 indicated that a maximum of 81 cal/g releasable between 100 and 500°C had accumulated in the vertical center of the inner reflector and that 52 cal/g of this was released²¹ in a peak between 100 and 240°C. It was estimated that a maximum temperature rise of 50°C could be expected under adiabatic conditions and that a more serious temperature rise might occur with increasing exposure.

In 1958 additional stored-energy measurements were made which showed that much of the stored energy had been annealed.⁵¹ The amount releasable up to 400°C was in the range of 4 to 8 cal/g. Examination of

temperature records of the inner reflector showed that an increase in the reactor power level from 30 to 40 Mw in 1953 caused an increase in the temperature from 95 to about 175°C at the center of the inner reflector. It was concluded that the stored energy was annealed by the higher temperatures.

The experience with the NRX reflector emphasizes the need for a thorough knowledge of temperatures in representative parts of graphite reflectors and also the desirability of installing easily removable samples of graphite in the reflector during construction.

References

1. E. J. Prosen and F. D. Rossini, Some Experimental Data on the Heats of Combustion of Benzoic Acid and Carbon (Graphite), *J. Research Nat. Bur. Standards*, **33**: 439-446 (1944).
2. E. J. R. Prosen and F. D. Rossini, Heats of Isomerization of the Five Hexanes, *J. Research Nat. Bur. Standards*, **27**: 289-310 (1941).
3. H. C. Dickinson, Combustion Calorimetry and the Heats of Combustion of Cane Sugar, Benzoic Acid, and Naphthalene, *Bulletin of the Bureau of Standards*, **11**: 189-257 (1915).
4. G. F. Jackson and D. Cordall, *The Windscale Bomb Calorimeter*, British Report IG-189 (RD/W), 1959.
5. E. J. Prosen and D. R. Valent, *The Energy Content of Irradiated Graphite Samples*, Report NBS-D-104, U. S. National Bureau of Standards, 1951. (See also other similar reports such as NBS-D-101 to NBS-D-111).
6. J. R. Gilbreath and O. C. Simpson, *Chemistry Division, Section C-11, Summary Report April through September, 1949*, USAEC Report ANL-4380, p. 33, Argonne National Laboratory, 1950. (Classified)
7. L. A. Quarterman and W. L. Primak, *The Heat of Reaction of Irradiated Graphite with Potassium*, USAEC Report ANL-4749, Argonne National Laboratory, 1952.
8. R. E. Nightingale et al., Damage to Graphite Irradiated up to 1000°C, in *Proceedings of the Second United Nations International Conference on the Peaceful Uses of Atomic Energy, Geneva, 1958*, Vol. 7, pp. 295-300, United Nations, New York, 1959.
9. G. B. Greenough, Windscale Laboratories, unpublished data, April 1960.
10. J. M. Davidson, Stored Energy in Irradiated Graphite, in *US/UK Graphite Conference held at St. Giles Court, London, Dec. 16-18, 1957*, USAEC Report TID-7565 (Pt. 1), pp. 11-20, 1959.
11. G. H. Kinchin, The Effects of Irradiation on Graphite, in *Proceedings of the First United Nations International Conference on Peaceful Uses of Atomic Energy, Geneva, 1955*, Vol. 7, pp. 472-478, United Nations, New York, 1956.
12. J. J. Newgard, Simple Semiempirical Model for Neutron Induced Stored Energy in Graphite, *J. Appl. Phys.*, **30**: 1449-1451 (1959).
13. C. Dalmaso and G. F. Nardelli, The Wigner Release in Graphite-moderated Reactors, *Energia Nucleare (Milan)*, **6**: 307-321 (1959). (English translation in USAEC Report AEC-tr-4545, May 1961).
14. J. M. Davidson, Hanford Laboratories, General Electric Company, unpublished data, August 1960.
15. J. A. Wheeler and J. J. O'Conner, *Effect of Pile Operation on Storage of Energy in Graphite*, USAEC Report HW-7-3020, Hanford Works, 1945. (Classified)
16. A. H. Cottrell et al., Theory of Annealing Kinetics Applied to the Release of

- Stored Energy from Irradiated Graphite in Air-Cooled Reactors, in *Proceedings of the Second United Nations International Conference on the Peaceful Uses of Atomic Energy, Geneva, 1958*, Vol. 7, pp. 315-327, United Nations, New York, 1959.
17. M. S. Wechsler et al., Use of a Radiation-Calorimeter in Measurement of Stored Energy in Irradiated Graphite, *J. Appl. Phys.*, **30**: 42-45 (1959).
 18. C. Sykes, Methods for Investigating Thermal Changes Occurring During Transformations in a Solid Solution, *Proc. Roy. Soc. (London)*, **A148**: 422-446 (1935).
 19. T. J. Neubert and R. B. Lees, Stored Energy in Neutron-Bombarded Graphite, *Nuclear Sci. and Eng.*, **2**: 748-767 (1957).
 20. G. P. Kerr, *Summary of Sykes Stored Energy Determinations*, USAEC Report HW-17446, Hanford Atomic Products Operation, 1950. (Classified)
 21. R. W. Attree et al., *The Release of Stored Energy from N. R. X. Reactor Reflector Graphite*, Canadian Report CRC-541, 1953.
 22. J. C. Ballinger, *Twin Crucible Calorimeter for Graphite Stored Energy Study*, USAEC Report HW-24692, Hanford Atomic Products Operation, 1952. (Classified)
 23. G. Mayer et al., Some Physical Methods for Studies of Irradiation Effects in Graphite, in *Proceedings of the French-American Conference on Graphite Reactors, Brookhaven National Laboratory, Nov. 12-15, 1957*, USAEC Report BNL-489, Brookhaven National Laboratory, pp. 42-45, 1958.
 24. J. L. Dickson et al., BEPO Wigner Energy Release, in *Proceedings of the Second United Nations International Conference on the Peaceful Uses of Atomic Energy, Geneva, 1958*, Vol. 7, pp. 250-281, United Nations, New York, 1959.
 25. K. Koyama, *A Linear Rise Calorimeter for Measuring Stored Energy in Graphite*, USAEC Report HW-63552, Hanford Atomic Products Operation, 1960.
 26. R. W. Henson and J. H. W. Simmons, *An Adiabatic Rise Calorimeter for Measuring Stored Energy in Irradiated Graphite*, British Report AERE-M/R-2564, 1959.
 27. J. C. Bell and G. B. Greenough, Windscale Laboratories, unpublished data, April 1960.
 28. W. K. Woods et al., Irradiation Damage to Artificial Graphite, in *Proceedings of the First United Nations International Conference on the Peaceful Uses of Atomic Energy, Geneva, 1955*, Vol. 7, pp. 455-471, United Nations, New York, 1956.
 29. S. B. Austerman, *Stored Energy Release in Graphite Irradiated at Low Temperatures*, USAEC Report NAA-SR-1564, North American Aviation, Inc., 1956.
 30. J. E. Hove, Low Temperature Irradiation and Annealing Effects in Graphite in *Metallurgy and Fuels, Progress in Nuclear Energy, Series V*, Vol. 2, pp. 551-569, Pergamon Press, New York, 1959.
 31. S. B. Austerman and J. E. Hove, Irradiation of Graphite at Liquid Helium Temperatures, *Phys. Rev.*, **100**: 1214-1215 (1955).
 32. J. F. Fletcher, *Controlled Temperature Irradiation of Graphite. Interim Report No. 3*, USAEC Report HW-36221, Hanford Atomic Products Operation, September 1956. (Classified)
 33. J. C. Bell et al., Stored Energy in the Graphite of Power-Producing Reactors, *Phil. Trans. Roy. Soc. London*, **A254**: 361-395 (1962).
 34. J. C. Ballinger, Graphite Stored Energy, *Reactor Sci. Technol.*, **3**(4): 55-66 (December 1953), issued as USAEC Report TID-2011. (Classified)
 35. M. A. Kanter, Diffusion of Carbon Atoms in Natural Graphite Crystals, *Phys. Rev.*, **107**: 655-663 (1957).
 36. G. J. Dienes, Mechanism for Self-Diffusion in Graphite, *J. Appl. Phys.*, **23**: 1194-1200 (1952).
 37. M. A. Kanter and G. R. Hennig, Quenched-In Lattice Defects in Graphite, *Bull. Am. Phys. Soc.*, **1**(2): 119 (1956).
 38. M. A. Kanter, The Mechanism for Atom Motion in Graphite Crystals, in *Kinetics*

- of *High-Temperature Processes*, pp. 61-66, Conference on the Kinetics of High-Temperature Processes, Massachusetts Institute of Technology, 1958, W. D. Kingery (Ed.), Technology Press of Massachusetts Institute of Technology, Cambridge, 1959.
39. G. R. Hennig, Review of Radiation Damage to Graphite, in *Metallurgy and Fuels, Progress in Nuclear Energy, Series V*, Vol. 1, pp. 581-651, Pergamon Press, New York, 1956.
 40. G. Glockler, The Heat of Sublimation of Graphite and the Composition of Carbon Vapor, *J. Chem. Phys.*, **22**: 159-161 (1954).
 41. W. Primak, Some Aspects of Stored Energy in Irradiated Graphite. Part II. Storage of Energy in Graphite on Irradiation, *Nuclear Sci. Technol.*, **2**(1): 7-26 (February 1956), issued as USAEC Report TID-2021. (Classified)
 42. M. Burton and T. J. Neubert, Effect of Fast Neutron Bombardment on Physical Properties of Graphite: A Review of Early Work at the Metallurgical Laboratory (Argonne National Laboratory), *J. Appl. Phys.*, **27**: 557-572 (1956).
 43. Hanford Works Technical Division. *Weekly Report for Period Ending Sept. 26, 1944*, USAEC Report HW-3-758, Hanford Works, Sept. 27, 1944. (Classified)
 44. S. K. Allison, *Dislocation Energy in Graphite*, USAEC Report MUC-SKA-803, University of Chicago, Sept. 29, 1944.
 45. J. C. Ballinger, *Status of Stored Energy in the B, D, and F Hanford Piles*, USAEC Report HW-29064, Hanford Works, Aug. 17, 1953. (Classified)
 46. *Accident at Windscale No. 1 Pile on 10th October, 1957*, Her Majesty's Stationery Office (White Paper), Command 302, 1957.
 47. *Final Report—Committee to Evaluate Design and Operation of Windscale Piles and Review Controlled Release of Wigner Energy*, Her Majesty's Stationery Office (White Paper), Command 471, 1958.
 48. G. Brown et al., Safety Aspects of the Calder Hall Reactor in Theory and Experiment, in *Proceedings of the Second United Nations International Conference on the Peaceful Uses of Atomic Energy, Geneva, 1958*, Vol. 11, pp. 202-216, United Nations, New York, 1959.
 49. P. J. Grant, Wigner Energy Storage—Its Relation to Reactor Design, *Nuclear Eng.*, **4**: 69-72 (1959).
 50. *Nuclear Reactor Plant Data*, Vol. 2, Research and Test Reactors, American Society of Mechanical Engineers, McGraw-Hill Book Company, Inc., New York, 1959.
 51. H. B. Hilton and E. A. G. Larson, *Measurement of Stored Energy in the N. R. X. Reactor Reflector Graphite*, Canadian Report CRIO-865, July 1959.

Annealing Radiation Effects

R. E. NIGHTINGALE†

13-1 Introduction

At ordinary temperatures some annealing of radiation-induced defects in graphite occurs during irradiation. The net result of these concurrent damaging and annealing processes has been discussed in previous chapters. This chapter is concerned primarily with the property changes that result from heating graphite above the temperature at which it was irradiated.

The importance of the annealing of radiation effects in relation to the useful life and safe operation of graphite-moderated reactors is self-evident. Annealing studies have played an equally important role in the characterization and understanding of radiation effects in graphite.

13-2 Analysis of Annealing Experiments‡

Annealing experiments provide information on property changes as a function of temperature and time. They may be conducted in many ways. In what is probably the most common type, the sample is held at a constant temperature for a given time, and the property change is measured at room temperature (occasionally at some other temperature). Then the procedure is repeated on the same sample at a higher annealing temperature. In a second type of experiment, the property is measured during an isothermal anneal. In still another type, such as a linear-temperature-rise anneal, neither the annealing time nor the annealing temperature is held constant.

Through various methods of analysis, one seeks (1) to condense the results of annealing experiments into a single relation between property change, temperature, and time which will allow interpolation to a wide range of annealing conditions or (2) to obtain information that will lead to a better understanding of the damage state.

For the first purpose a knowledge of time, temperature, and property change during any particular anneal does not completely characterize the annealing process. The extent of property change also depends upon the previous history of the sample, i.e., type of graphite, irradiation exposure and temperature, and the extent to which the graphite has already been annealed in previous heat-treatments. Because it is not practical to study the annealing effects for all the conditions for which annealing characteristics are required, one is usually faced with the problem of deriving some empirical relation between time, temperature, and the sample history from

† Hanford Laboratories, General Electric Company, Richland, Wash.

‡ A glossary of symbols used in Chap. 13 is given at the end of the chapter.

a few experiments such that the results will be useful in predicting annealing effects over the widest possible range of conditions. To further relate parameters in such an empirical relation with fundamental physical parameters adds another degree of complexity to the problem.

Many approaches to the analysis of annealing experiments have been suggested and tried. Some of the general methods of analysis which have been most widely used to date will be discussed here.

13-2.1 CONSTANT-FREQUENCY FACTOR

Rate processes are generally considered to follow an equation of the form

$$-\frac{dq}{dt} = k'q^n \quad (13.1)$$

where q is the concentration of the species participating in the kinetic process at any time t , k' is the specific rate constant, and n is the kinetic order of the process. The specific rate constant is related to the activation energy (E) by the equation

$$k' = Ce^{-E/RT} \quad (13.2)$$

where C is the frequency factor, R is the gas constant, and T is the absolute temperature.

These equations are usually applied to discrete chemical reactions in a gas or a solution. If they are to be applied to the annealing of disordered solids, a number of simplifying assumptions must be made. In the case of irradiated graphite, one must deal, not with a single well-defined process, but rather with a whole distribution of processes, each of which may have its own characteristic value of q , n , C , and E .

Changes in q cannot be measured directly; only a property or property change (p) which is proportional to q can be measured. Thus, for the case where the property change is linearly dependent on the concentration of participating species,

$$p = fq \quad (13.3)$$

where f is the change in property accompanying the occurrence of one kinetic process. Equation 13.1 then becomes

$$-\frac{dp}{dt} = Cf\left(\frac{p}{f}\right)^n e^{-E/RT} \quad (13.4)$$

Some simplifying assumptions must be made before Eq. 13.4 can be integrated. First, consider the case where the annealing processes can be characterized by a constant frequency factor and a distribution of activation energies. Primak^{1,2} has discussed this case in considerable detail. In Sec. 13-2.2 the effect of assuming a constant E and variable C will be considered.

The integrated form of Eq. 13.4 with a constant C and f is

$$p = p_0[1 - (1 - n)Bte^{-E/RT}]^{1/(1-n)} \quad (13.5)$$

where B is defined by

$$B = C \left(\frac{f}{p_0} \right)^{1-n} \quad (13.6)$$

The expression $p \, dE$ is the contribution to the property change of those defects which anneal to more-stable positions with an activation energy between E and $E + dE$. The measured property change (P) is then

$$P = \int_0^\infty p(E) \, dE = \int_0^\infty p_0(E) \theta_n(E, t) \, dE \quad (13.7)$$

where

$$\theta_n(E, t) = [1 - (1 - n)Bte^{-E/RT}]^{1/(1-n)} \quad (13.8)$$

The form of θ , which Primak¹ calls the "characteristic isothermal annealing function," is shown in Fig. 13.1. The inflection point occurs at $E = E_0$,

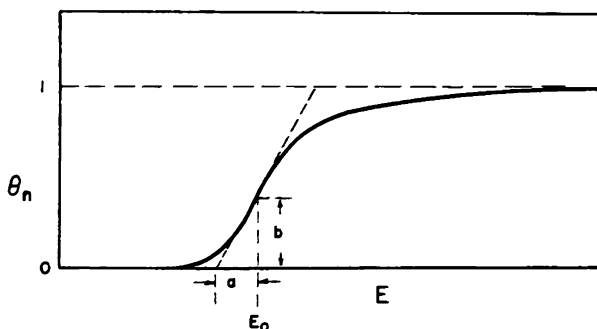


FIG. 13.1 The characteristic annealing function for isothermal annealing. The constants shown are related to parameters in the equation for θ in the following way: $a = nRT$, $b = n^{1/(1-n)}$, and $E_0 = RT \ln(Bt)$. (From Primak, *Physical Review*, Ref. 1.)

for which

$$E_0 = RT \ln(Bt) \quad (13.9)$$

As isothermal annealing progresses, the characteristic annealing function is displaced along E but does not change shape. With a broad spectrum of activation energies, the annealing behavior is dominated by the exponential dependence on E appearing in θ and by the initial activation-energy spectrum, $p_0(E_0)$.

Isothermal annealing in the case of a broad activation-energy spectrum (which includes practically all cases of graphite annealing) can be visualized with the help of Fig. 13.2. As the annealing time or temperature

increases, the initial activation-energy spectrum is swept out with the advance of the characteristic annealing function. A good approximation to

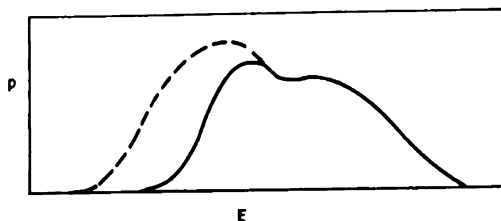


FIG. 13.2 An idealized activation-energy spectrum in isothermal annealing. The portion of the initial activation-energy spectrum which has been annealed is shown as a dashed curve. (From Primak, *Physical Review*, Ref. 1.)

θ when the activation-energy spectrum covers a range of several times nRT is the step function suggested by Vand:³

$$\begin{aligned} \theta &= 0 & \text{for } E < E_0 \\ \theta &= 1 & \text{for } E > E_0 \end{aligned} \quad (13.10)$$

in which case

$$P(t) = \int_{E_0}^{\infty} p_0(E) dE \quad (13.11)$$

and

$$\frac{dP(t)}{dt} = -p_0(E_0) \frac{dE_0}{dt} = -\frac{RT}{t} p_0(E_0) \quad (13.12)$$

Equations 13.9 and 13.12, which are the working equations of the Vand method of analysis, are a special case of Primak's general theory. It is not necessary to assume a first-order rate law as was done by Vand, although if $n \neq 1$, B is not the frequency factor usually employed in rate processes but is a function of f , p_0 , and n . The Vand method of analysis requires the measurement of the rate of property change as a function of time during an isothermal anneal. The quantity $p_0(E_0)$ is then plotted as a function of E_0 . This plot is termed the initial activation-energy spectrum or, simply, the activation-energy spectrum.

Figure 13.3 is an example of an activation-energy spectrum determined from the isothermal annealing of c spacing. The dotted lines are drawn through the experimental points for isothermal anneals at a single temperature. According to the Vand-Primak theory, the envelope of these dotted lines gives the distribution of the radiation-induced increase in c spacing among the activation energies before annealing begins. Kinetic processes involving the entire range of activation energies from 26 to 80 kcal/gram atom contribute to the annealing.

Although there is a sharp peak at 33 kcal/gram atom, the height is not

well defined. This peak corresponds to the "200°C peak" found in stored-energy release curves (Chap. 12).

The effect of making the Vand approximation to θ is to decrease the resolution of the activation-energy spectrum so that any sharp peaks will be broadened out to a width of the order of nRT . This is still quite satisfactory for distributions that extend over a range many times nRT .

The assumption of a constant B is less well justified when there is a desire to preserve some physical significance to the parameters in Eqs. 13.9 and 13.12. It is certainly not unrealistic to consider that B changes over the wide range of kinetic processes represented in Fig. 13.3. However, E_0 is not particularly sensitive to changes in B since it appears as a logarithm in Eq. 13.9.

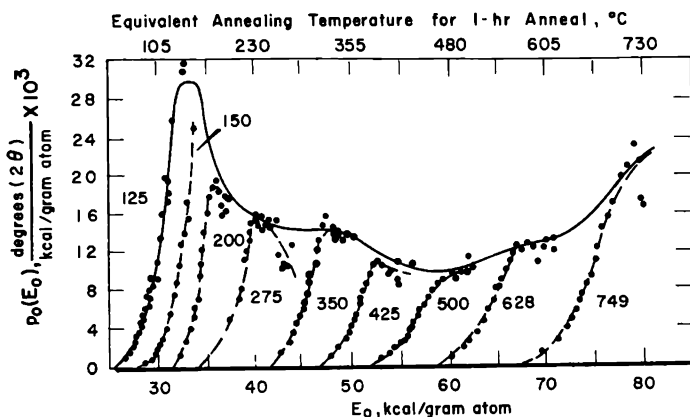


FIG. 13.3 The activation-energy spectrum for c-spacing annealing in CSF graphite. Exposure was 556 Mwd/At at 30°C. The value of B was assumed to be $7.5 \times 10^{13} \text{ sec}^{-1}$. Annealing temperatures (°C) are shown for each dotted curve.⁴

Primak^{1,2} has pointed out that, if B is not chosen correctly, the parts of the spectrum revealed at different temperatures will not fit together. Thus one could presumably determine the B that makes the experimental curves (the dotted curves in Fig. 13.3) fit best to a smooth envelope. This approach has a practical limitation, however, because annealing data over several decades of time are required to obtain data beyond the initial S-shaped portion. Since dP/dt has by this time decreased to a very low value, the uncertainty in $p_0(E_0)$ is very large. This is illustrated by the scatter of the points at the end of the dotted curves in Fig. 13.3.

Perhaps an even more serious limitation than variations in B , if this theory is to be interpreted literally, is the effect of successive kinetic processes. It is most probable that the observed annealing effect consists of processes which produce property changes and which thereby generate other processes that occur at a higher activation energy. An example is the agglomeration of two interstitial carbon atoms to form a C_2 group at a

relatively low activation energy, followed by the diffusion of the C_2 group to a crystal boundary at a higher activation energy. For this case $p_0(E_0)$ cannot be considered the initial activation-energy spectrum. The extent to which successive reactions occur and their effect on the interpretation of $p_0(E_0)$ is unknown. For this reason and because of other uncertainties mentioned previously, the identification of any of the parameters in the theory with fundamental physical parameters is questionable, at least for any experiments reported to date.

The Vand approximation of the constant frequency factor model is, nevertheless, useful as an empirical method of presenting annealing data. Once $p_0(E_0)$ has been determined or estimated, the amount of property change can be calculated for any t and T . The theory has also been applied to linear-rise and other experiments in which the annealing temperature is increased continuously with time.^{1,5} In fact, if the purpose of an annealing experiment is simply to obtain $p_0(E_0)$, from which the annealing behavior can be predicted, the linear-rise method is preferred to the isothermal method because it is more rapid. One or more activation-energy spectra may be obtained in an 8-hr period by the linear-rise method, whereas a week or more may be required if annealing is done isothermally.

The fact that it is possible to reduce annealing data obtained under a wide variety of conditions to a single type of presentation, i.e., property change vs. E_0 , is an important feature of the variable-activation-energy method as an empirical method of analysis. Further examples of this application are presented in later sections of this chapter.

13-2.2 CONSTANT ACTIVATION ENERGY

A method of analysis (the constant activation-energy method) has been developed^{6,7} specifically to predict the characteristics of stored-energy release in the region of the 200°C peak. The identification of parameters in the theory with fundamental physical constants is abandoned from the very beginning. It is an empirical method that has been used with considerable success to systematize and correlate laboratory annealing studies of a few hours so that the results can be used to guide the controlled release in a reactor over a period of several days. Although it is applicable to other property changes as well, the method will be discussed here in terms of the annealing of stored energy.

The rate of release of stored energy is assumed to be governed by an equation of the form

$$\frac{dS}{dt} = -F(S)e^{-E/RT} \quad (13.13)$$

where S is the stored energy remaining in the sample after an anneal at T (°K) for a time t and $F(S)$ is some function that characterizes the state of the sample and will therefore depend on such variables as the irradiation

temperature, exposure, and the amount of stored energy in the sample at any instant. In terms of Eq. 13.4

$$F(S) = Cf\left(\frac{p}{f}\right)^n \quad (13.14)$$

Integration of Eq. 13.13 gives

$$\int_{S_0}^S \frac{dS}{F(S)} = \int_0^t e^{-E/RT} dt \equiv \tau \quad (13.15)$$

where τ is a "reduced time," i.e., the time weighted by the activation-energy factor to compensate for differences in temperature experienced by the specimen during an anneal.

Here τ serves the same function that E_0 does in the constant-frequency factor method. Both contain the entire functional dependence of t and T on which the property changes depend. If τ is to be used, a value for E must be assumed or estimated. In early applications $E = 39$ kcal/gram atom was used. More recently $E = 32$ kcal/gram atom has been suggested as being slightly better.⁸

The reduced time, τ , is used in the following way. During a laboratory anneal the quantities dS/dt , T , and t are measured. This information is condensed into a relation between S and τ such as is illustrated in Fig. 13.4.

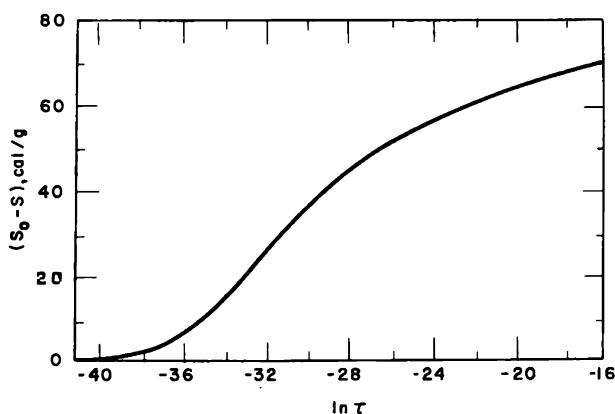


FIG. 13.4 A typical relation⁶ between the stored energy annealed ($S_0 - S$) and the reduced time (τ).

This figure contains all the information on the release of stored energy for this particular sample, and it can be used in several ways.

In the case of isothermal annealing, $\tau = te^{-E/RT}$. Therefore changes in ($S_0 - S$) during an isothermal anneal can be calculated from Fig. 13.4. For a linear-rise experiment in which the temperature is constrained to rise at a uniform rate α to a temperature T ,

$$\tau = \int_0^t \exp \left[- \frac{E}{R(T_0 + \alpha t)} \right] dt \quad (13.16)$$

which for large values of E/RT reduces to

$$\tau = \frac{RT^2 e^{-E/RT}}{\alpha E} \quad (13.17)$$

Finally, for an adiabatic anneal all the stored energy released is used in heating the sample, and

$$-dS = C_p(T) dT \quad (13.18)$$

where $C_p(T)$ is the specific heat. Since, from Eq. 13.15, $d\tau = e^{-E/RT} dt$, a T vs. t curve can be synthesized from a curve such as that given in Fig. 13.4. The case where the sample exchanges heat with the surrounding air has also been treated. Calculated curves for isothermal, linear-rise, and adiabatic annealing are given by Cottrell et al.⁶ to illustrate the information that can be derived from $(S_0 - S)$ vs. $\ln \tau$ curves.

An activation-energy model in which $E(S)$ is a function of the amount of stored energy released has also been considered. The function $E(S)$, which was determined from dissimilar linear-rise anneals of similar specimens, was found to increase from 26.4 kcal/gram atom for no stored energy annealed to 36.8 kcal/gram atom for 60 cal/g annealed.⁸ It is probable that $E(S)$ would depend also on the irradiation temperature and exposure, but there is no information on this. It is interesting to note that, if it is assumed that the range of annealing temperatures in these experiments was from about 100 to 300°C,[†] the corresponding range in activation energies of 26 to 37 kcal/gram atom would agree satisfactorily with those in Fig. 13.3.

The determination of $E(S)$ is experimentally difficult and requires an electronic computer for the practical analysis of the data. Since tests have shown that the theory based on Eq. 13.13 with a constant E is capable of predicting the general features of stored-energy release, the use of the more cumbersome theory with a variable E has been very limited.

13.2.3 ACTIVATION ENERGY OF DISCRETE ANNEALING PROCESSES

If an annealing process occurs with a single activation energy or a narrow band of activation energies, it is possible to determine⁹ the activation energy with a minimum of restrictive assumptions concerning the value and the constancy of n and f . When E is constant, Eq. 13.1 can be integrated directly, giving

$$\frac{q_0^{1-n} - q^{1-n}}{C(1-n)} = t e^{-E/RT} \quad (13.19)$$

[†] This appears to be a reasonable assumption since it is stated⁸ that 85 cal/g was removed up to 400°C.

for $n \neq 1$. The method is applicable if $n = 1$ with the appropriate solution for Eq. 13.1.

The physical property (P) is related in some manner to q . Letting h represent some unspecified function of P ,

$$\frac{h(P_0) - h(P)}{C(1 - n)} = te^{-E/RT} \quad (13.20)$$

The value of E is determined by annealing several samples, each having the same value of P_0 , at different temperatures to the same final value of P . Under these conditions

$$te^{-E/RT} = \text{constant} \quad (13.21)$$

The value of E is measured from the slope of the straight line of the $\log t$ vs. $1/T$ plot. If the activation energy changes over the range of annealing temperatures, the slope of the line will not be constant.

Application of this method to the isothermal annealing of c spacing of irradiated graphite (556 Mwd/At at 30°C) results in a line with considerable curvature between 175 and 225°C. The average activation energy is of the order of 40 kcal/gram atom (compare with Fig. 13.3). The curvature suggests that the activation energy increases with temperature.

13-3 Thermal Annealing

13-3.1 RADIOCARBON TRACER STUDIES

The characterization of defects produced by fast neutrons has been an elusive and difficult problem. Some aspects of concurrent damaging and annealing processes are discussed in Chap. 9. The annealing studies by Hennig and coworkers^{10,11} provide further information on the mobility of displaced atoms. These investigators employed C^{11} atoms as tracers for those atoms displaced to relatively large distances from their original lattice site. The C^{11} was produced by $(n,2n)$ or (γ,n) reactions on C^{12} . Both processes impart enough recoil energy to the transmuted carbon atoms to displace them from their lattice sites and eject many secondary carbon atoms before coming to rest. The annealing behavior of displaced atoms was studied by first determining the distribution of C^{11} throughout irradiated graphite particles. This was accomplished by oxidizing samples in air at temperatures sufficiently low (400°C) that only the outer surfaces of the particles burned. The oxidation products were continuously analyzed for radiocarbon.

It was found¹¹ that the surface enrichment (Σ_s) of C^{11} increased with the annealing temperature† (Fig. 13.5). This result is strong evidence for the annealing of the displaced atoms by diffusion to the surface. The crystal perfection and size of the graphite particles were also found to change the

† Σ_s is the fraction of all C^{11} atoms which annealed to surfaces accessible to the air.

surface enrichment. The fraction of displaced atoms migrating to the surface was higher for natural graphite than for nuclear (KCF) graphite, and the fraction decreased with increasing particle size.

Based upon the measured surface enrichment and the dimensions of the crystals, it was estimated that, on the average, displaced atoms traveled a linear distance of 2000 Å in being annealed. However, the C^{11} atoms are not completely representative of displaced atoms produced by neutron bombardment since, in this case, a considerable number of displaced atoms do not travel far from their original sites. Thus the C^{11} atoms are only typical of those atoms which are removed from the potential field of the remaining vacancy.

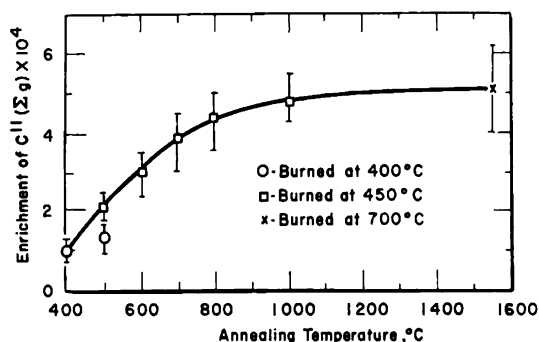


FIG. 13.5 Effect of annealing temperature on the enrichment of C^{11} in graphite crystals. (From Montet, *Nuclear Science and Engineering*, Ref. 11.)

For samples that had been given a light reactor irradiation (0 to 2.5 Mwd/At) prior to introduction of the C^{11} tracer, the fraction of displaced atoms which reached the surface of the graphite decreased rapidly with neutron exposure. Apparently the vacancies created by neutron bombardment trapped the displaced atoms quite effectively before they reached a surface.

It was estimated that less than 8 per cent of the atoms that were displaced far from their vacancies reintegrated with the lattice during room-temperature irradiations. Atoms that, unlike C^{11} , remain in the potential field of their vacancies may reintegrate to a greater extent during bombardment.

During annealing below 400°C it was estimated that about 80 per cent of the atoms reintegrate into vacancies and the remainder form interstitial groups, perhaps C_2 . Between 400 and 1000°C these interstitial groups drift to defects within the crystal and to external surfaces. If an appreciable concentration of damage is present, further extensive reintegration with vacancies would be likely to occur in this temperature region.

Based upon a rather complex model of annealing, an estimate of the displacement rate, and an estimate of the probability that a displaced

complex will reach the boundary of a perfect region, it was concluded that the concentration of vacancies remaining after annealing at 1000°C did not exceed 10^{-6} per atom. Figure 13.5 suggests that all displaced atoms have become trapped at 1000°C. However, the results of oxidation with chromic acid, rather than with air, suggest that reintegration of the displaced C^{11} atoms is not complete below 1700°C; annealing at lower temperatures leaves some of the displaced atoms in a more-active condition and renders them more susceptible to attack by the oxidant. Reintegration between 1000 and 1700°C accounts for the annealing of some properties above 1000°C.

Tracer studies with diamond indicate that the annealing process is different from that in graphite. Displaced atoms in the diamond structure do not migrate over large distances since no excess radioactivity is found on external surfaces after annealing. It has been suggested¹¹ that annealing in diamond may occur by a replacement process that removes the displaced C^{11} atoms so that they do not migrate to the surface.

13-3.2 LATTICE PARAMETERS AND CRYSTALLITE DIMENSIONS

The annealing of c -spacing changes in irradiated graphite has been studied by several investigators.¹²⁻¹⁵ The different time-temperature relations make direct comparison of the various experiments difficult. However,

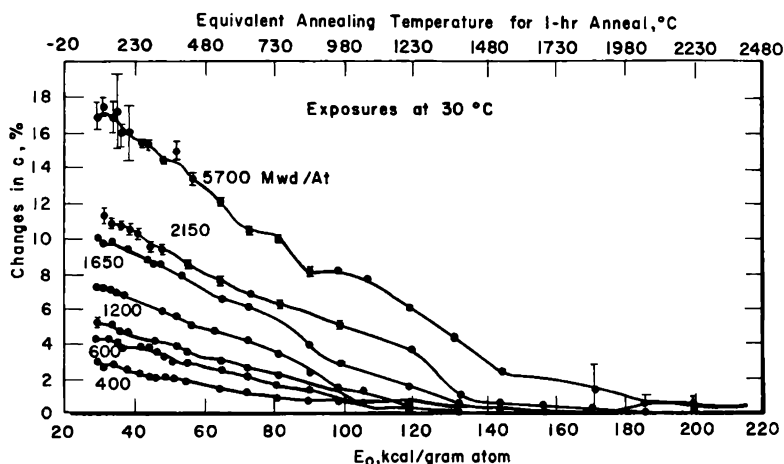


FIG. 13.6 Annealing of c spacing in CSF graphite based on $c_0 = 6.71$ Å. The apparent activation energy is given by $E_0 = RT \ln (Bt)$ for which $B = 7.5 \times 10^{13} \text{ sec}^{-1}$. (From Nightingale and Snyder, *Proceedings of the Third Conference on Carbon*, Pergamon Press, Ref. 14.)

when the data are replotted as a function of E_0 , defined by Eq. 13.9, the studies show the same general features and are in fair agreement. Figure 13.6 is a typical example¹⁴ for irradiations near room temperature.† Recov-

† The c -spacing changes were determined from the maximum intensity of the (002) line profile. No corrections were made for geometrical, polarization, and form factors (see Sec. 9-1.3).

ery of c expansion is approximately linear with E_0 below 100 kcal/gram atom. As the exposure increases, a larger fraction of the increase in c spacing anneals at high activation energies. For example, an $E_0 = 100$ kcal/gram atom is necessary to anneal one-half the c expansion after 5700 Mwd/At, whereas only 65 kcal/gram atom is required after 400 Mwd/At. This is the result of the larger probability for the formation of multiple interstitial and vacancy groups at higher exposures.

The decrease in intrinsic line breadth (β) with E_0 is shown for the (002) line in Fig. 13.7. It is interesting to note that after 5700 Mwd/At

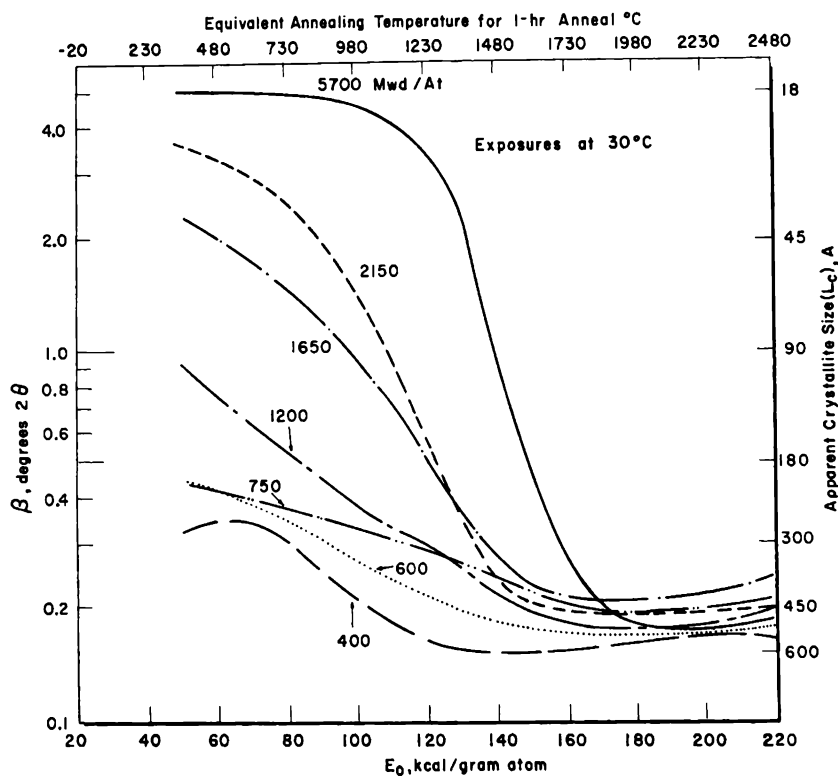


FIG. 13.7 The reduction of intrinsic line breadth (β) with E_0 for the (002) reflection of CSF graphite. The apparent crystallite size assuming no strain broadening is given on the right side of the figure.¹⁴

the structure was so severely disrupted that annealing was slight below $E_0 = 130$ kcal/gram atom. As with c spacing, a greater fraction of increase in line broadening is distributed in the higher activation energies in the more highly irradiated samples.

The changes in c , a , β_{002} , and β_{110} during annealing have been studied by Austin and Harrison¹⁵ on KC graphite irradiated to 400, 1000, and 1500 Mwd/At at 30°C. The c spacing and β_{002} annealing were qualitatively sim-

ilar to that described above. In addition, the nature of the intralayer distortions was studied by Fourier analysis of the (110) line profiles for the 400 and 1000 Mwd/At samples. The (110) line of the 1500 Mwd/At sample was apparently too diffuse in the unannealed state to make analysis possible. It was concluded that for irradiations of less than 1000 Mwd/At the intralayer distortion is due principally to an inhomogeneous strain with little crystal breakup. The stored energy associated with the strain was estimated to be of the order of 80 cal/g for the 1000 Mwd/At exposure. Most of this strain was relieved by a 1-hr anneal at 200°C. Figure 12.6 shows that 80 cal/g represents an appreciable fraction of the stored energy released by such treatment.

13.3.3 DIMENSIONS

Very high temperatures are required¹⁴ to anneal all the expansion effects produced by reactor irradiations (Fig. 13.8). In general, annealing begins immediately at the lowest activation energy. An exception is the 5700

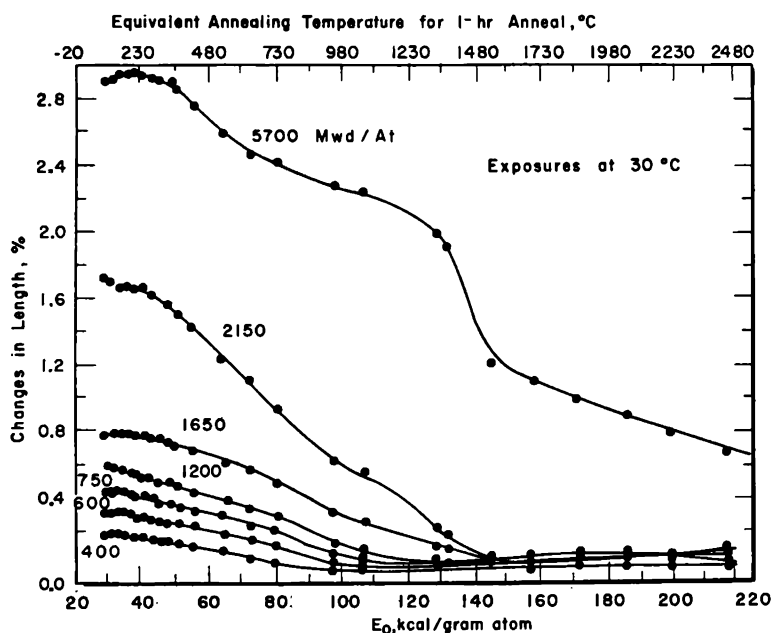


FIG. 13.8 Annealing of length changes in irradiated CSF (\perp) graphite. (From Nightingale and Snyder, *Proceedings of the Third Conference on Carbon*, Pergamon Press, Ref. 14.)

Mwd/At samples for which a small but significant amount of expansion occurs before contraction begins. Woods et al.¹² have observed an initial expansion in samples with lower exposures by very sensitive interferometric measurements.

Length annealing does not closely parallel the line-breadth annealing

shown in Fig. 13.7, particularly in the highly damaged samples. Length and c -spacing annealing are more similar, the percentage of change in c being about six times as great as the percentage of change in length. It appears that many of the crystallites contract when the c spacing is annealed, leaving voids or amorphous carbon volumes; therefore only a fraction of the c contraction results in length contraction.

The bulk contraction parallel to the extrusion axis produced by room-temperature irradiations is also annealable. For CSF graphite¹⁶ exposed to 4200 Mwd/At near room temperature, most of the contraction is annealed by heating to 1000°C.

If the radiation-induced contraction that occurs above 300 to 400°C in transverse samples results from a relief of stresses introduced during fabrication, annealing should not cause the sample to return to its original length. Annealing studies¹⁶ on CSF and other nuclear graphites have demonstrated that contraction transverse to the extrusion direction does not anneal; instead, a small additional contraction occurs, possibly as the result of annealing the c expansion. This suggests that the net transverse contraction observed during high-temperature irradiations results from two effects: (1) a small bulk expansion caused by the c expansion (this is annealable) and (2) a larger contraction caused, perhaps, by the relief of stresses. The latter is apparently not annealable.

Additional information on this point is provided by annealing experiments on incompletely graphitized transverse samples. Figure 9.21 shows that the radiation-induced contraction at high temperatures is much greater in materials that have not been fully graphitized. When the sample is heated, this contraction is not annealed; in fact, some additional contraction occurs above the original graphitization temperature, presumably as a result of further graphitization.

Contraction parallel to the extrusion axis during room-temperature irradiations is due, at least in part, to a different mechanism (Sec. 9-4.3). Parallel contraction, which decreases as the irradiation temperature increases, is due to a damaging process. It seems reasonable that the a contraction causes a small bulk contraction just as c expansion results in bulk expansion in transverse samples. Both the a contraction and parallel bulk contraction produced by room-temperature irradiations can be annealed. In contrast to the behavior of transverse samples, the contraction produced in parallel samples at high temperatures is to a large extent annealable.

13-3.4 MECHANICAL PROPERTIES

Figure 13.9 shows the change in the unannealed fraction of Young's modulus for a series of isothermal anneals.† These data, reported by

† These annealing experiments were conducted at the Metallurgical Laboratory of the University of Chicago during the period 1943 to 1946 by T. J. Neubert and A. Novick.¹¹ The data were analyzed by them in terms of an activation-energy spectrum having a broad maximum at $E_0 = 40$ kcal/gram atom.

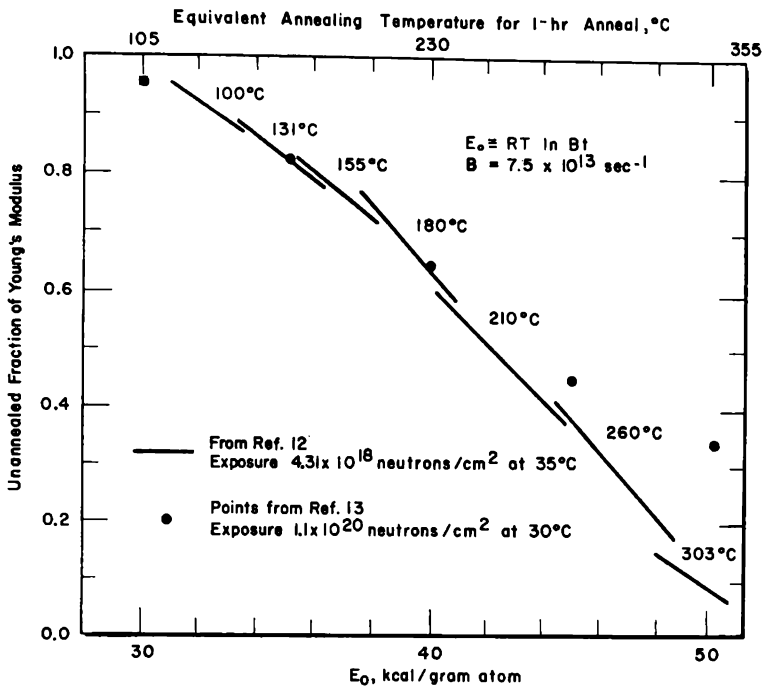


Fig. 13.9 Young's modulus changes in KS (II) graphite for a series of isothermal anneals. Data points for 1-hr anneals at several temperatures are also shown for a sample with higher exposure.^{12, 13}

Woods,¹² have been replotted as a function of E_0 . It is interesting to note that, although the data represent annealing periods from a few hours to one month and annealing temperatures from 100 to 303°C, they fall quite well on a single curve when time and temperature are incorporated in E_0 . Each set of isothermal anneals has been approximated by a straight line, and each line overlaps quite well with the next.

Also included in Fig. 13.9 are some points from a different type experiment, i.e., 1-hr anneals at increasingly higher temperatures.¹³ Agreement with the isothermal anneals is satisfactory below 42 kcal/gram atom. The disagreement at higher activation energies is not unexpected since the exposure was considerably greater for the samples annealed for 1 hr. A larger fraction of the change in Young's modulus anneals only at higher activation energies in this case.

Figure 13.10 is a graph of the same data using τ as the annealing parameter. Again, the data fall approximately on a smooth curve. A slightly better fit to the data is obtained with $E = 40$ to 45 kcal/gram atom. As an empirical method of correlating these annealing data, the use of E_0 and τ seems to be equally satisfactory. A wider range of values for E_0 and τ is necessary to make a more critical comparison.

The decrease in modulus of rigidity with annealing temperature resembles that of Young's modulus. Davidson and Losty¹⁸ have shown that most annealing occurs in the region 100 to 400°C for small graphite springs irradiated to 8 to 9×10^{19} thermal neutrons/cm² at 50 to 100°C. In connection with this work, it was noted that graphite acquires a significant permanent set when stressed at room temperature. The set is not completely

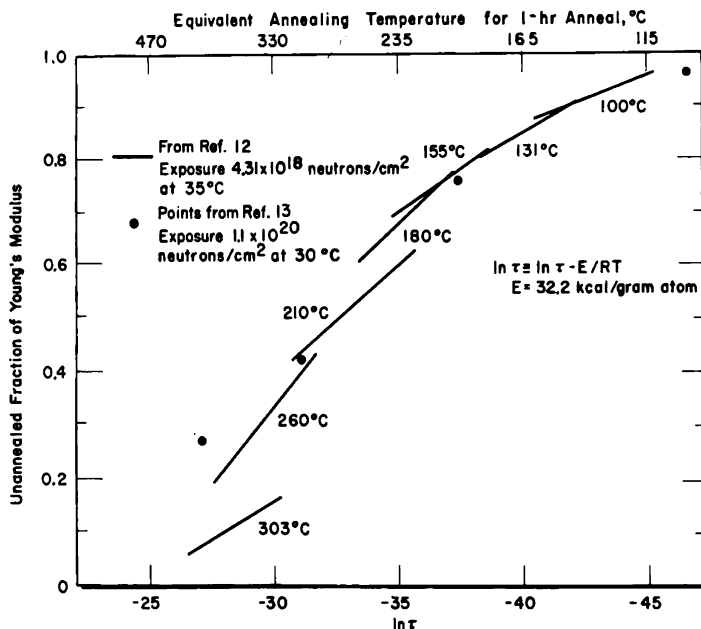


FIG. 13.10 The data of Fig. 13.9 plotted as a function of τ . Either Fig. 13.9 or Fig. 13.10 may be used to calculate annealing changes for a wide range of temperatures and times.

annealed until very high temperatures are reached. This effect has also been noted by others¹⁹ in connection with the preparation of samples for irradiation-induced dimensional studies. Length changes occurring during annealing to 2500°C on samples machined from large bars range up to 0.2 per cent or higher depending on the hardness, anisotropy, and other factors. It is concluded that machined graphite specimens should be thoroughly annealed to remove any permanent set prior to the study of small dimensional changes brought about by irradiation or other treatment.

13-3.5 ELECTRICAL AND THERMAL PROPERTIES

(a) *Low-temperature Annealing.* A number of annealing studies have been conducted at very low temperatures in an effort to learn more about the damage centers produced in irradiated graphite. These studies include neutron irradiations²⁰ near the boiling point of liquid nitrogen, electron irradiation²¹ near the boiling point of liquid helium, and proton irradiation

tions²² at four temperatures between -170 and 150°C . Some representative data are illustrated in Fig. 13.11.

An important feature of the electrical and thermal resistivity annealing is the initial *increase* in $\Delta\rho/\Delta\rho_0$ and coincident *decrease* in $\Delta k_0/\Delta k$. A mechanism to account for this and other observations during low-temperature annealing was proposed by Hennig and Hove¹⁰ (see Sec. 7-6.2). Hove²³ has subsequently noted one of the difficulties with this model arising from

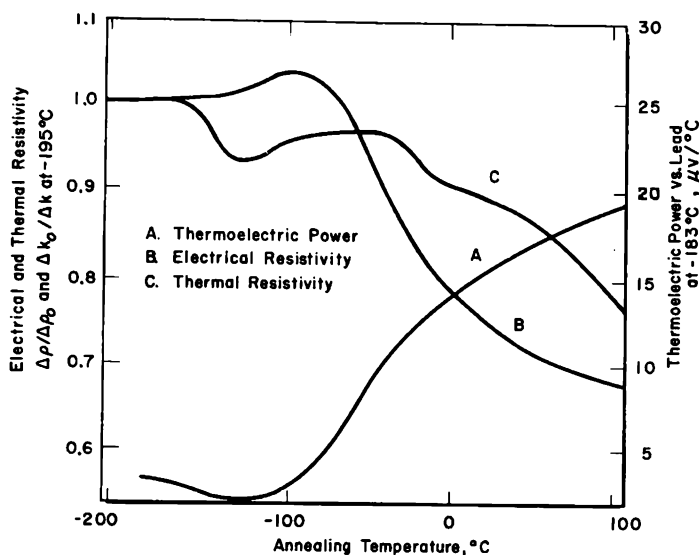


Fig. 13.11 Annealing of AWG graphite at low temperatures.¹⁰ The resistivity ordinate gives the fraction of property change remaining after annealing. Irradiations were performed in the liquid-nitrogen facility at the Brookhaven Graphite Research Reactor at about -150°C . The exposure, 5915 Mw-hr, is approximately equivalent to 20 Mw-d/At.

additional low-temperature annealing experiments. Graphite irradiated with 1.25-Mev electrons near 4°K has an even more prominent peak between -190 and -170°C ($\Delta\rho/\Delta\rho_0 = 1.3$ to 1.4) than the peak in Fig. 13.11. Assuming the paramagnetic resonance results to be correct, it is difficult to explain such a large and abrupt increase in ρ as due to a declustering effect at this low temperature. However, no explanation has been offered which is more satisfactory than that originally proposed.

Reynolds and Goggin²⁴ have also observed an anomalous increase of about 40 per cent in the electrical resistivity of irradiated graphite (4-Mev electrons at -194°C) during annealing in the range -190 to -150°C . In addition, they found that the initial changes in the magnetoresistance and the Hall coefficient also increase further by 40 to 50 per cent during annealing in this temperature range. A simplified band-theory calculation indicates that the concentrations of both electrons and holes increase during irradiation and also in the anomalous annealing range.

(b) *Electrical Resistivity.* The annealing of electrical resistivity at room temperature and above is shown in Fig. 13.12. For short irradiations most annealing is complete at 400°C. The activation energy from isothermal

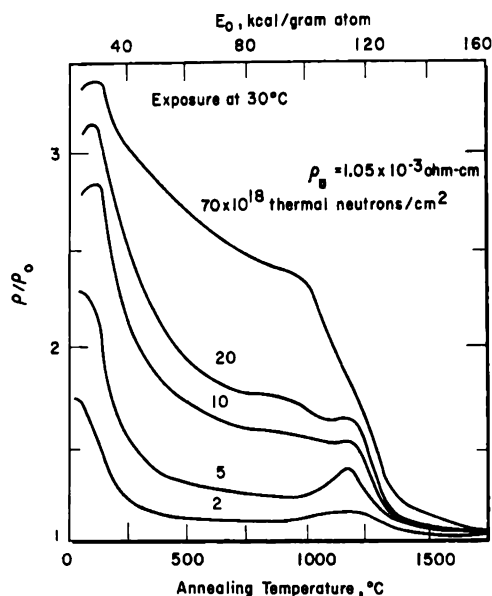


FIG. 13.12 Recovery of resistivity changes for 1-hr anneals.¹³ Samples were cut parallel to the extrusion axis. An exposure of 10^{18} thermal neutrons/cm² is equivalent to approximately 2 Mwd/At.

experiments¹³ is 28 kcal/gram atom up to 200°C, and thereafter it rises rapidly. Klimenkov and Aleksenko²⁵ measured an activation energy of 34.5 kcal/gram atom for samples irradiated to 20×10^{18} neutrons/cm² (total) and annealed at 150°C. These activation energies are in approximate agreement with the activation energies predicted from the E_0 scale in Fig. 13.12. For higher exposures recovery is continuous to 1000°C, and the annealing is not well characterized by a single activation energy.

The value of ρ/ρ_0 increases in the region 1000 to 1300°C except at the highest exposure. Kinchin¹³ suggested that the increase results from changes in the electron trapping level as the groups of vacancies spread out in the early stages of diffusion; the decreasing interaction between vacancies may raise the energy of the trapping levels and release electrons. Other investigators^{17, 26} have observed an increase in ρ at almost exactly the same temperature. Neubert et al.¹⁷ have noted that no unexpected changes in the annealing of Young's modulus occur for samples in which this increase in ρ/ρ_0 is observed.

The general character of the isothermal annealing curves¹⁷ for electrical resistivity and for Young's modulus is somewhat different, at least for graphite irradiated to low doses (10 Mwd/At). In contrast to the annealing

of electrical resistivity, Young's modulus continues to change for relatively long periods of time in the range 180 to 300°C. Activation-energy spectra calculated from the isothermal annealing curves show that electrical-resistivity annealing is centered about a rather sharp peak at $E_0 = 32$ kcal/gram atom, whereas Young's modulus anneals over a wider range of activation energies centered about a broad peak at 42 kcal/gram atom.

(c) *Thermal Conductivity.* Changes in the ratio of unirradiated to final thermal conductivity (k_0/k) are shown in Fig. 13.13. There is no indication

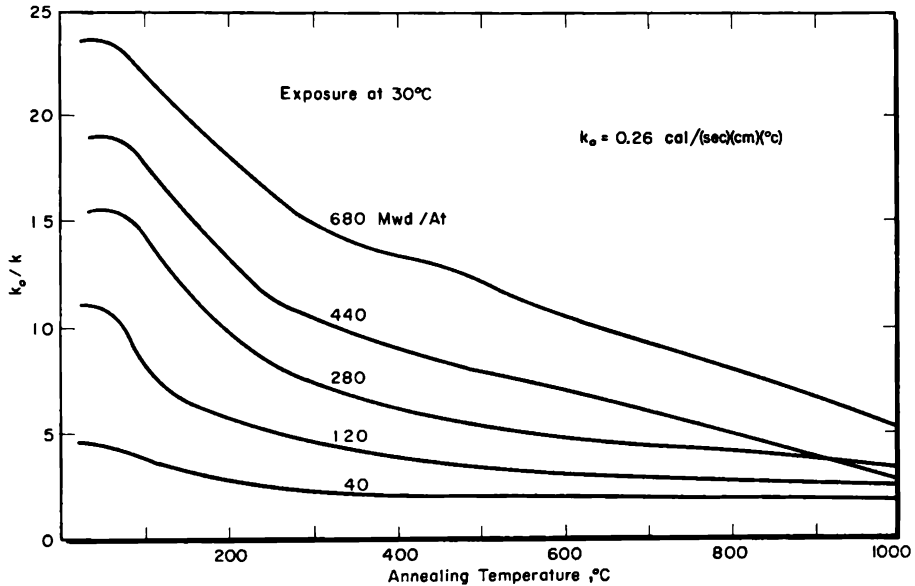


FIG. 13.13 Annealing room-temperature thermal conductivity¹² in CSF (\perp) graphite irradiated at 30°C.

of an increase in thermal resistivity near 1000°C similar to that found for electrical resistivity. Moreover, it is found¹² that the thermal resistivity decreases continuously to 2000°C during pulse annealing.† Since the conduction of heat by electrons is negligible in polycrystalline graphites, any purely electronic changes, such as proposed by Kinchin to explain the increase in electrical resistance at 1000 to 1300°C, would have a negligible effect on the thermal conductivity. The migration of vacancies at this temperature would therefore lead to a continuous decrease in k_0/k as observed.

Pulse-annealing curves of the Hall coefficient,²⁷ thermoelectric power,²⁸ magnetic susceptibility,²⁹ and magnetoresistance²⁷ are shown in Figs. 13.14 to 13.17, respectively. Irradiations were performed in the Hanford reactors

† Pulse annealing is a particularly convenient method of annealing in which property changes are measured at room temperature or below between short temperature pulses. In the method developed at Atomics International,⁹ the thermal response of the system was sufficiently rapid that practically all annealing was done at the pulse temperature.

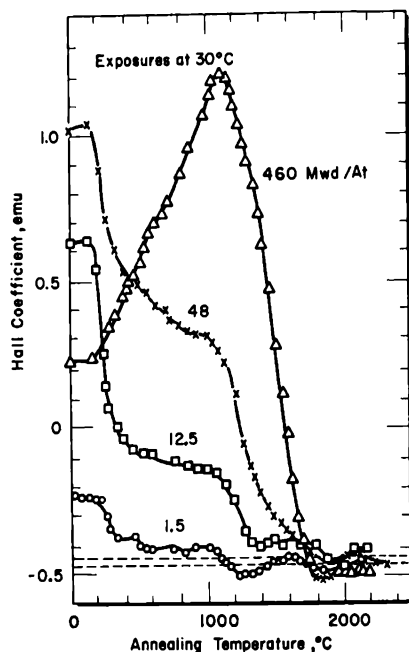


FIG. 13.14 Pulse-annealing spectrum of the Hall coefficient in AWG (||) graphite. Dotted lines show the range of values for unirradiated samples. (From Hove, *Proceedings of the First and Second Conferences on Carbon*, Waverly Press, Inc., Ref. 28.)

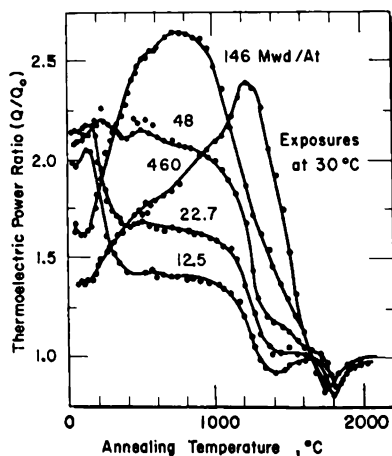


FIG. 13.15 Pulse-annealing spectrum of the thermoelectric power ratio, Q/Q_0 , in AWG (||) graphite. (From Hove, *Proceedings of the First and Second Conferences on Carbon*, Waverly Press, Inc., Ref. 28.)

near room temperature. The annealing time at each temperature was about 1 min. It is apparent from the curves that the annealing processes are complex. Hove²⁸ has noted that all attempts to analyze these curves on the

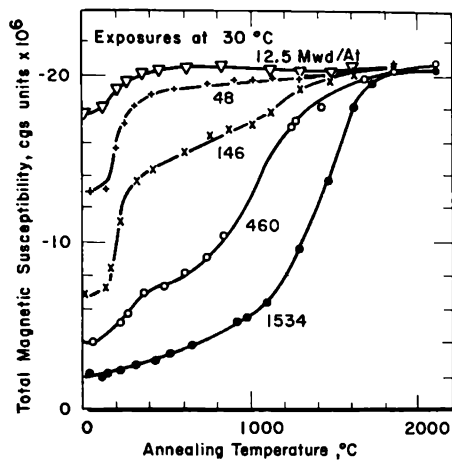


FIG. 13.16 Pulse-annealing spectrum of the magnetic susceptibility of KC graphite. The total susceptibility shown on the ordinate is defined as the sum of the susceptibilities in the three orthogonal directions. (From Hove, *Proceedings of the First and Second Conferences on Carbon*, Waverly Press, Inc., Ref. 28.)

basis of first- or second-order kinetics have been unsuccessful unless a spectrum of activation energies is employed. However, the general features of the annealing curves are consistent with theoretical predictions, as demon-

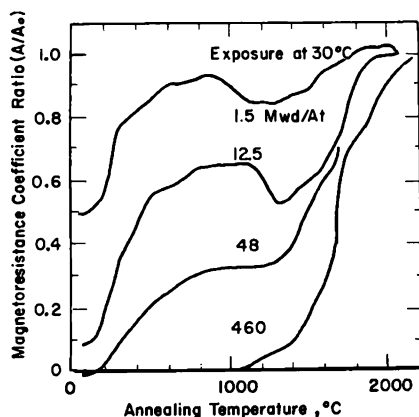


FIG. 13.17 Pulse-annealing spectrum of the magnetoresistance coefficient ratio, A/A_0 , of AWG (II) graphite. (From Hove, *Proceedings of the First and Second Conferences on Carbon*, Waverly Press, Inc., Ref. 28.)

strated quite remarkably when the magnetoresistance annealing curves, calculated from the annealing of electrical resistivity and susceptibility, are compared with experimental curves.²⁸

13-3.6 STORED ENERGY

The annealing of stored energy is discussed in Chap. 12 in connection with annealing spectra. Annealing of total stored energy has been reported,¹² and the results are in satisfactory agreement with those deduced from Fig. 12.7.

13-4 Radiation Annealing

A number of early investigators^{30,31} reported that the annealing of irradiated graphite is more extensive when conducted in the presence of reactor radiation than when done in the absence of radiation. A striking example of this effect was observed by H. Sheard in England and reported by Woods et al.¹² Two samples from the same graphite were irradiated at 30°C, and the increases in length were noted. One of the samples was annealed at 150°C, and the second was returned to the reactor and irradiated at 150°C. In the absence of radiation, the anneal resulted in a slight additional expansion of the sample, a common observation during the initial stages of annealing. About 40 per cent of the expansion was annealed in the second sample in the same period of time. Moreover, it was noted that annealing continued over a long period of time. The net expansion of a third sample, which was irradiated continuously at 150°C, was considerably less than either of the samples that were irradiated at 30°C and subsequently annealed in the absence of radiation or in the reactor.

This phenomenon has been termed by various investigators as nuclear, neutronic, reactor, pile, radiation, and irradiation annealing. In the subsequent discussion the term "radiation annealing" will include all those annealing effects occurring under the influence of radiation which cannot be accounted for by thermal annealing alone. All annealing effects (thermal and radiation) occurring in the reactor will be called "reactor annealing."

Although a radiation-annealing effect is expected on theoretical grounds, it is difficult to predict to what extent it may occur or even that it should be large enough to be detectable. Similar effects in other materials are suggested by certain experimental results,³² but none have been so conclusively demonstrated as in graphite.

13-4.1 PROPERTY ANNEALING

The effect of radiation annealing is illustrated in Figs. 13.18 and 13.19. Samples were first irradiated at 30°C, and then annealed at 375°C for several days. Samples that were returned to the reactor and irradiated at 335°C continued to anneal over a long period of time, whereas samples heated to 335°C in the laboratory underwent only a small additional amount of annealing. Comparison of the curves for the 1177 and 950 Mwd/At samples with the 1400 Mwd/At sample shows that the enhanced reactor annealing is quite striking. Stored energy and thermal conductivity behave

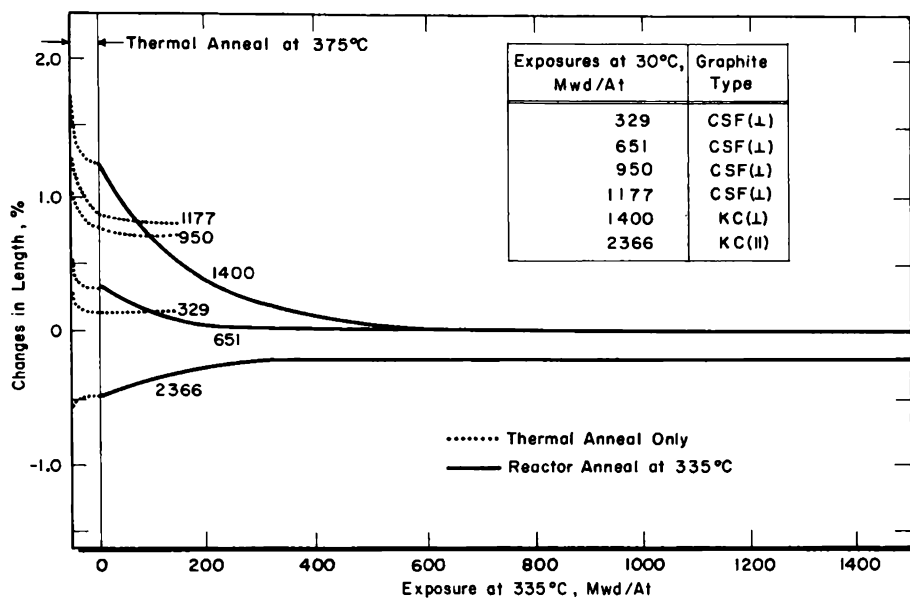


FIG. 13.18 Radiation annealing of length changes. Thermal anneals to the left of the zero exposure were performed at 375°C; those to the right, at 335°C. Exposures (in Mwd/At) at 30°C are indicated for each curve.³³

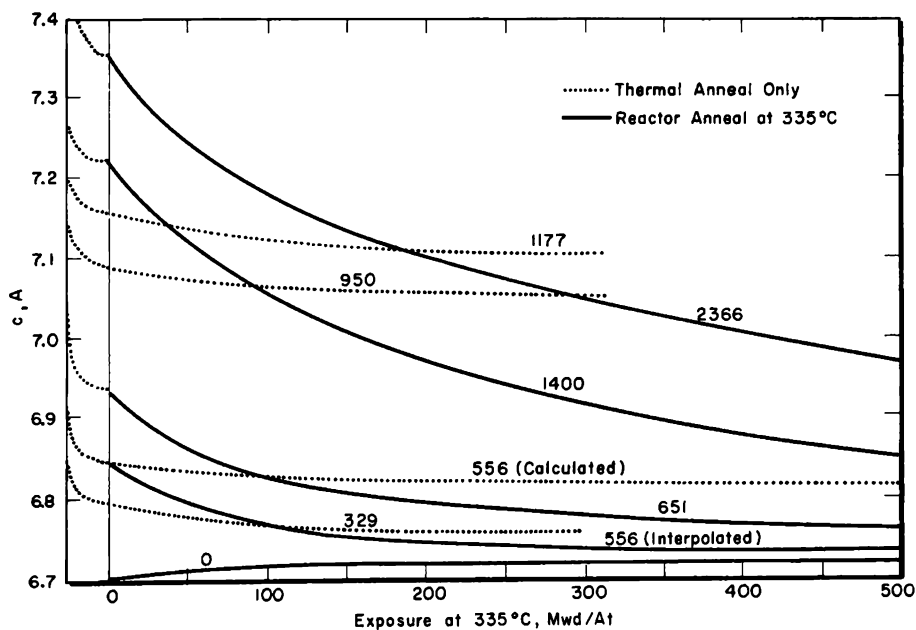


FIG. 13.19 Radiation annealing of c spacing. Thermal anneals to the left of zero exposure were performed at 375°C; those to the right, at 335°C. Exposures (in Mwd/At) at 30°C are indicated for each curve.³³

in a similar fashion, whereas radiation annealing is much less effective in annealing electrical-resistivity changes.³³

The experimental results of long-term radiation and thermal annealing are compared with those calculated for thermal annealing in Fig. 13.19. The 556 (calculated) curve was obtained from the activation-energy spectrum in Fig. 13.3. The fact that this curve parallels the long-term thermal-annealing curve for other exposures lends some confidence to the use of activation-energy spectra for predicting annealing behavior.

An assumed reactor-annealing curve, 556 (interpolated), is shown which could not be greatly in error. It has been calculated³⁴ that to accomplish by purely thermal means the amount of annealing observed at the

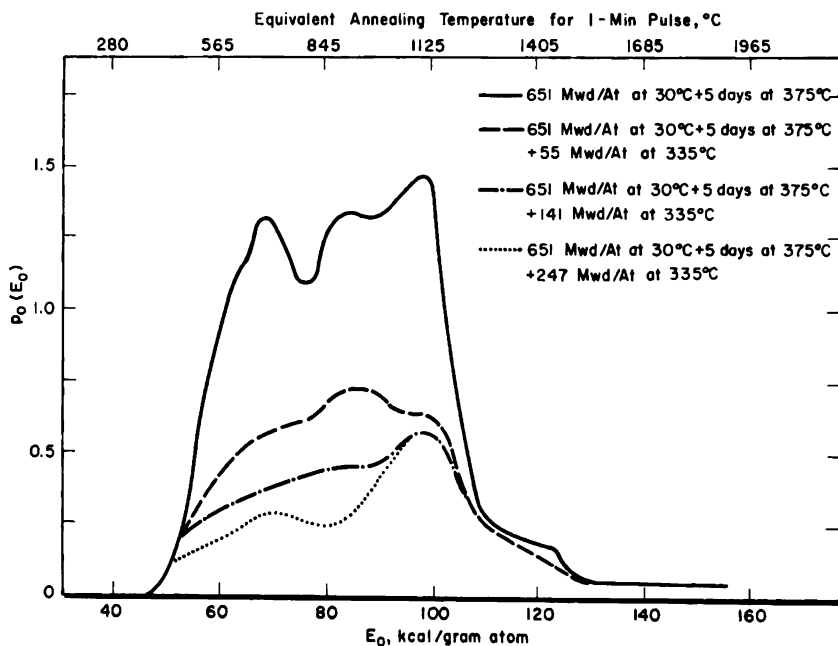


FIG. 13.20 The activation-energy spectra for annealing thermal resistivity in CSF (\perp) graphite subjected to radiation annealing. The quantity, $p_0(E_0)$, is the change in thermal resistivity (cgs units) per kilocalorie per gram atom.³³

end of the 556 Mwd/At exposure would have required a temperature greater than the irradiation temperature by more than 100°C. Examination of the 950 and 1177 Mwd/At curves shows that the contrast between thermal and radiation annealing is even greater for more highly damaged samples.

Whereas the total change in a property demonstrates that radiation enhances annealing, it is more revealing to study the manner in which the activation-energy spectrum is affected by radiation annealing. Activation-energy spectra, calculated by the method of Neubert and Lees,⁵ are shown

in Fig. 13.20 for samples irradiated near room temperature, annealed for five days at 375°C, and then reirradiated to various exposures at 335°C. Pulse annealing was employed for the final annealing. The analysis assumes that the 1-min pulses at 50°C intervals are equivalent to a tempering experiment in which t (min) = $0.02 T$ (°C). The activation-energy spectra are entirely different from those which could be obtained after an equivalent amount of property change brought about by thermal annealing. During a thermal anneal the characteristic annealing function (almost a vertical line) advances, sweeping out damage from left to right, as illustrated in Fig. 13.2. Damage is not removed in this way during radiation annealing. In addition to thermal annealing,† a considerable amount of damage is removed from top to bottom, reaching into damage states with very high activation energies. On the temperature scale some damage is removed during the 335°C irradiation that requires 1300°C to accomplish thermally.

13-4.2 MECHANISM

Although the detailed mechanism of radiation annealing is not known, it would appear that the knock-on atoms are in some way responsible for the enhanced annealing. The three principal processes by which energy is transferred to the lattice are: (1) primary collisions between fast neutrons and carbon atoms, (2) ionization and excitation of lattice atoms by ionized recoil atoms, and (3) further collisions between energetic recoil carbon atoms and lattice atoms.

Attempts to produce radiation annealing with purely ionizing radiation have failed.^{35, 36} Although the question should not be considered conclusively settled, in the calculations to follow it is assumed that only processes (1) and (3) above are capable of causing radiation annealing.

When energy is transferred by either (1) or (3), two possibilities exist for a lattice atom. The lattice atom may receive sufficient energy to be permanently displaced, or, upon being struck, the atom may remain bound and dissipate its energy to nearby atoms through the coupling forces in the lattice. Radiation annealing can occur in the latter case if lattice defects receive enough energy to become mobile. It is instructive to estimate the fraction of atoms excited per second to energies between some activation energy (E_0) and the threshold energy (E_d) for displacement of normal lattice atoms. In the case of neutron-carbon-atom collisions, this fraction is³⁷

$$F = \sigma \gamma \ln \frac{E_d}{E_0} \quad (13.22)$$

where σ is the scattering cross section and the damaging part of the neutron-flux spectrum is approximated by

† The five-day thermal anneal at 375°C should have advanced the inflection point of the characteristic annealing function to 58 kcal/gram atom; this is approximately what is observed in Fig. 13.20.

$$\begin{aligned}\phi &= \frac{\gamma}{E_n} & E_n < 6 \text{ Mev} \\ \phi &= 0 & E_n > 6 \text{ Mev}\end{aligned}\quad (13.23)$$

F is also the fraction of the *displaced* atoms which is excited per second between E_0 and E_d . With typical values of $\sigma = 4.5 \times 10^{-24}$ cm², $\gamma = 10^{12}$ neutrons/cm²/sec, $E_0 = 3$ ev, and $E_d = 25$ ev, the relaxation time (time to anneal 63 per cent of the displaced atoms) is about 2100 years.³⁷ For reactor-annealing experiments at 335°C, for which purely thermal annealing is negligible, the relaxation time varies with different properties between 1 and 10 months, the average being 4 months. Excitation by neutron-carbon-atom collisions therefore is insufficient to account for the enhanced annealing observed, and the conclusion is that secondary collisions must be included. Although a precise treatment requires some knowledge of the way in which excess energy is dissipated throughout the lattice, the problem can be approximated by considering that at some time after the struck atom receives an energy (E') there will be a volume occupied by E'/E_0 atoms wherein all atoms have an energy E_0 . The secondary energy transfer can then be accounted for by weighting those collisions for E' less than E_d by a factor E'/E_0 . This leads to

$$F = \sigma\gamma \left(\frac{E_d}{E_0} - 1 \right) \quad (13.24)$$

which, with the values of the constants used above, gives a relaxation time of 600 years. Since weighting the collisions of E'/E_0 is the most efficient way that recoil energy can be utilized in annealing collisions, the relaxation time calculated in this way should be less than the true value.

Primary recoil atoms with energy greater than about 50 kev† lose their energy principally through ionization and electronic excitation, with only an occasional collision. For example, a 2-Mev primary neutron upon striking a carbon atom will produce a recoil atom with an average energy of about 280 kev, but only a fraction of this energy is used in producing displaced atoms. It is reasonable to expect that part of the primary recoil energy will be transmitted to displaced lattice atoms, supplying the activation energy for annealing. If the fraction of primary recoil energy in excess of E_d going into annealing reactions is ξ , then, for each such primary atom, a number of atoms given by $\xi(E' - E_d)/E_0$ may undergo annealing. This gives³⁷

$$F = \xi\sigma\gamma \frac{E_m}{E_0} \quad (13.25)$$

where E_m , the maximum recoil energy, is of the order of 1 Mev. For a relaxation time of 1/3 year, $\xi = 0.04$. Thus approximately 4 per cent of the primary recoil energy is effective in producing annealing collisions.

† The difficulty of assigning an exact value is discussed in Sec. 7-2.4.

Approximately 20,000 displacements are produced by a 2-Mev neutron during its thermalization (see Table 7.4). Since each atom requires an average of 50 ev to be displaced, 50 per cent of the initial energy of the neutron is transferred by elastic collisions. Hence a value of 4 per cent for ξ , which should be the lowest value possible owing to the method of weighting, appears possible considering the uncertainties in such calculations.

Although the above estimates are very crude, they do indicate that, at least qualitatively, the annealing rates observed in radiation annealing of graphite can be attributed to the slowing down of displaced recoil atoms produced by high-energy neutrons. If one inquires further into the mechanism, there appears to be another observation, which is at present unexplained: Why, if activation is due to "hot atoms," is the radiation-annealing rate so sensitive to temperature between 30 and 300°C?

This question is closely related to the marked sensitivity of the damage rate to temperatures in the 30 to 300°C range. A possible explanation is that the "hot" reactions, which occur at all ambient temperatures, provide the activation energy to free displaced atoms from the immediate vicinity in which they are bound, but they cannot easily diffuse away to more-stable positions unless the ambient lattice temperature is sufficiently high. At an irradiation temperature of 300°C, the annealing rate is rapid for defects at the time that they are created, i.e., before large clusters are formed. Therefore, in graphite that has been irradiated at 30°C, the rate of radiation annealing at 300°C should be controlled by the rate at which cluster atoms are broken into smaller, more-mobile groups by the hot reactions. This would explain why radiation annealing, unlike thermal annealing, continues over long periods of time at a given temperature. This mechanism, in addition to accounting for the sensitivity to the irradiation temperature, also retains the features of hot-atom activation, which seem necessary to explain the observation that defects with very high activation energies are affected by radiation annealing.

13-4.3 REACTOR-EXPOSURE-THERMAL-ANNEAL CYCLING

It is always found, at least in the range 30 to 300°C, that irradiation at some temperature, T_1 , followed by annealing at a higher temperature, T_2 , results in more damage than irradiation for the same period at T_1 . The simple damage centers formed during short exposures are much more easily annealed than those formed when damage is allowed to accumulate at a low irradiation temperature. Moreover, of those complex damage centers that do form, some are removed by radiation annealing if the temperature is sufficiently high. It is, then, of interest to ask: How effectively can radiation damage be reduced by thermal anneals?

Figures 13.21 and 13.22 show the changes in length and thermal conductivity, respectively, during reactor-exposure-thermal-anneal cycling. Annealing methods in order of increasing effectiveness are: (1) 20 hr at 500°C

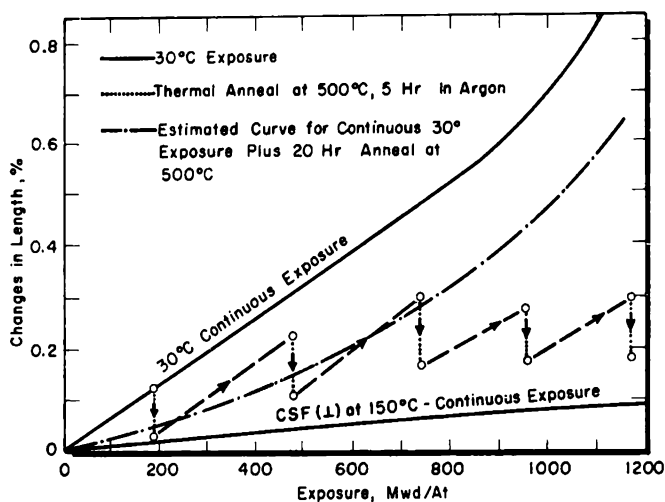


FIG. 13.21 Length changes in KC (\perp) graphite during reactor-exposure-thermal-anneal cycling.³⁸

after continuous exposure at 30°C, (2) periodic 5-hr anneals at 500°C after short periods of irradiation at 30°C, and (3) continuous irradiation at 150°C.

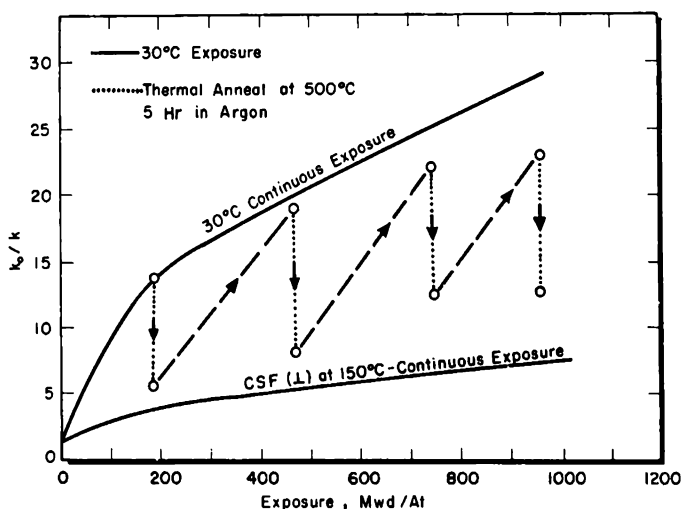


FIG. 13.22 Changes in the thermal-conductivity ratio (k_0/k) during reactor-exposure-thermal-anneal cycling.³⁸

The extent to which these conclusions can be extended to irradiations at very low or very high temperatures is not known. The results of proton irradiations at -170°C suggest that the particular manner of annealing may not be as important as it appears to be with 30°C irradiations.²² The effects of different types of anneals following irradiations at high tempera-

tures have not been studied. If differences do exist, they will be difficult to detect since the property changes are so small.

A novel application of annealing has been suggested by Carter.³⁹ He points out that there should be a self-limitation to the radiation damage sustained by a graphite-moderator structure since damage to the graphite at the surface of coolant channels decreases the thermal conductivity. The graphite temperature in the interior is thereby increased, which reduces the rate of damage. Thus, after some long period of time, the graphite should consist of a highly damaged region near the coolant channels and an inner region at high temperature which is largely undamaged. However, as Charrault⁴⁰ has pointed out, an error of a factor of 10 occurred in the ordinate of Fig. 11 of the paper;³⁹ therefore the calculated temperature gradients were overestimated. However, this self-limitation of radiation damage may become of practical interest in future reactors having much higher heat fluxes than those of current design.

13.5 Glossary of Symbols

Symbol	Meaning	Equation
A	Magnetoresistance	10.1
A_0	Magnetoresistance prior to an irradiation	
a		$a \equiv nRT$
B		13.6
b		$b \equiv n^{1/(1-n)}$
C	Frequency factor	13.2
$C_p(T)$	Heat capacity as a function of temperature	
c	Crystal lattice spacing	
E	Activation energy	13.2
E_0	An approximate activation energy	13.9
$E(S)$	Activation energy as a function of stored energy released	
E_n	Neutron energy	
E'	Energy of knock-on atom	
E_d	Threshold energy for atomic displacement	
E_m	Maximum energy of a knock-on atom	
F	Fraction of atoms excited per second to an energy between E_0 and E_d	13.22, 13.24, and 13.25
f	Change in property accompanying one kinetic process	13.3
$F(S)$	A function of the stored energy, S	13.13
$h(P)$	A function of a property (P) of graphite	13.20
$h(P_0)$	A function of a property of graphite prior to annealing	13.20
k	Thermal conductivity	
k_0	Thermal conductivity prior to an irradiation	

Symbol	Meaning	Equation
k'	Specific rate constant	13.2
n	Kinetic order of an annealing process	13.1
P	Property change in graphite	
$p dE$	Property change when defects anneal with activation energies between E and $E + dE$	
$p_0(E_0)$	Initial activation-energy spectrum	13.12
Q	Thermoelectric power	
Q_0	Thermoelectric power prior to an irradiation	
q	Concentration of defects that anneal with a rate constant k' and kinetic order n	13.1
q_0	Concentration of defects (q) when $t = 0$	
R	The ideal gas constant	$R = 0.001987$ kcal/mole/°C
S	Total stored energy	
S_0	Total stored energy prior to annealing	
T	Temperature	
t	Time	
α	Rate of temperature rise	
β	Intrinsic X-ray diffraction-line breadth	
γ	A constant related to the neutron spectrum	13.23
θ_n	Characteristic isothermal annealing function	13.8
ξ	Fraction of primary recoil energy in excess of E_d going into annealing reactions	13.25
ρ	Electrical resistivity	
ρ_0	Electrical resistivity prior to an irradiation	
Σ_g	Fraction of all C^{11} atoms annealed to surfaces exposed to air	
σ	Scattering cross section of carbon	
τ	A reduced time	13.15
ϕ	Neutron spectrum	13.23

References

1. W. Primak, Kinetics of Processes Distributed in Activation Energy, *Phys. Rev.*, **100**: 1677-1689 (1955).
2. W. Primak, Large Temperature Range Annealing, *J. Appl. Phys.*, **31**: 1524-1533 (1960).
3. V. Vand, A Theory of the Irreversible Electrical Resistance Changes of Metallic Films Evaporated in Vacuum, *Proc. Phys. Soc. (London)*, **55**: 222-246 (1943).
4. R. E. Nightingale, *Thermal Annealing Kinetics of Interlayer Spacing Damage in Irradiated Graphite*, USAEC Report HW-37406, Hanford Atomic Products Operation, June 21, 1955.
5. T. J. Neubert and R. B. Lees, Stored Energy in Neutron-bombarded Graphite, *Nuclear Sci. and Eng.*, **2**: 748-767 (1957).
6. A. H. Cottrell et al., Theory of Annealing Kinetics Applied to the Release of Stored

- Energy from Irradiated Graphite in Air-cooled Reactors, in *Proceedings of the Second United Nations International Conference on the Peaceful Uses of Atomic Energy, Geneva, 1958*, Vol. 7, pp. 315-327, United Nations, New York, 1959.
7. D. E. Rimmer and W. M. Lomer, *Calculations on the Release of Stored Energy in Graphite*, British Report AERE-M/R-2603, June 1958.
 8. D. E. Rimmer, *The Validity of the Constant Activation Energy Model for the Release of Stored Energy in Graphite*, British Report AERE-R-3061, August 1959.
 9. W. E. Parkins et al., Pulse Annealing for the Study of Relaxation Processes in Solids, *J. Appl. Phys.*, **22**: 1012-1019 (1951).
 10. G. R. Hennig and J. E. Hove, Interpretation of Radiation Damage to Graphite, in *Proceedings of the First United Nations International Conference on the Peaceful Uses of Atomic Energy, Geneva, 1955*, Vol. 7, pp. 666-675, United Nations, New York, 1956.
 11. G. Montet et al., Tracer Studies on Radiation Damaged Graphite, *Nuclear Sci. and Eng.*, **1**: 33-52 (1956).
 12. W. K. Woods et al., Irradiation Damage to Artificial Graphite, in *Proceedings of the First United Nations International Conference on the Peaceful Uses of Atomic Energy, Geneva, 1955*, Vol. 7, pp. 455-471, United Nations, New York, 1956.
 13. G. H. Kinchin, The Effects of Irradiation on Graphite, in *Proceedings of the First United Nations International Conference on the Peaceful Uses of Atomic Energy, Geneva, 1955*, Vol. 7, pp. 472-478, United Nations, New York, 1956.
 14. R. E. Nightingale and W. A. Snyder, Distribution of Radiation Damage in Graphite, in *Proceedings of the Third Conference on Carbon Held at the University of Buffalo*, pp. 579-584, Pergamon Press, New York, 1959.
 15. A. E. Austin and R. J. Harrison, Annealing of Crystal Distortion in Irradiated Graphite, in *Proceedings of the Third Conference on Carbon Held at the University of Buffalo*, pp. 585-605, Pergamon Press, New York, 1959.
 16. R. E. Dahl, Hanford Laboratories, General Electric Company, unpublished data, April 1960.
 17. T. J. Neubert et al., *Neutron-Induced Discomposition of Graphite*, USAEC Report ANL-5472, Argonne National Laboratory, January 1956.
 18. H. W. Davidson and H. H. W. Losty, The Effect of Neutron Irradiation on the Mechanical Properties of Graphite, in *Proceedings of the Second United Nations International Conference on the Peaceful Uses of Atomic Energy, Geneva, 1958*, Vol. 7, pp. 307-314, United Nations, New York, 1959.
 19. F. W. Albaugh, *Reactor and Fuels Research and Development Operation Monthly Report, March 1959*, p. A-18, USAEC Report HW-59717A, Hanford Atomic Products Operation, Apr. 15, 1959. (Classified)
 20. S. B. Austerman, *Stored Energy Release in Graphite Irradiated at Low Temperatures*, USAEC Report NAA-SR-1564, Atomics International, Oct. 1, 1956.
 21. S. B. Austerman and J. E. Hove, Irradiation of Graphite at Liquid Helium Temperatures, *Phys. Rev.*, **100**: 1214-1215 (1955).
 22. G. E. Deegan, *Thermal and Electrical Properties of Graphite Irradiated at Temperatures from 100 to 425°K*, USAEC Report NAA-SR-1716, Atomics International, Dec. 15, 1956.
 23. J. E. Hove, Low Temperature Irradiation and Annealing Effects in Graphite, in *Metallurgy and Fuels, Progress in Nuclear Energy, Series V*, Vol. 2, pp. 551-569, Pergamon Press, New York, 1959.
 24. W. N. Reynolds and P. R. Goggin, The Annealing of Electron Irradiation Damage in Graphite, *Phil. Mag.*, **5**: 1049-1058 (1960).
 25. V. I. Klimenkov and Yu. N. Aleksenko, Change in the Properties of Graphite When Irradiated by Neutrons, in *Conference of the Academy of Sciences of the USSR on*

- the Peaceful Uses of Atomic Energy, July 1-5, 1955*, Session of the Division of Physical and Mathematical Sciences, USAEC Report AEC-tr-2435 (Pt. 1), pp. 227-237, 1956.
26. W. E. Parkins et al., *Results of Pulse-Annealing Measurements on the Electric Resistivity of Irradiated Graphite*, USAEC Report NAA-SR-23, North American Aviation, Inc., Oct. 17, 1949.
 27. W. P. Eatherly, *Changes in the Hall and Magneto-Resistivity Coefficients During Pulse Annealing of Irradiated Graphite*, USAEC Report NAA-SR-76, North American Aviation, Inc., Sept. 25, 1951.
 28. J. E. Hove, *Radiation Damage Effects on Graphite*, in *Proceedings of the First and Second Conferences on Carbon Held at the University of Buffalo*, pp. 125-136, Waverly Press, Inc., Baltimore, 1956.
 29. J. D. McClelland, *Change in Magnetic Susceptibility of Irradiated Graphite During Pulse Annealing*, USAEC Report NAA-SR-211, North American Aviation, Inc., Dec. 18, 1952.
 30. T. J. Neubert, *Thermal Annealing of Neutron Induced Discomposition in Artificial Graphite. III Heating-During-Irradiation Experiments*, USAEC Report ANL-5025, Argonne National Laboratory, Apr. 13, 1953.
 31. J. A. Wheeler and J. J. O'Connor, *Effect of Pile Operation on Storage of Energy in the Graphite. The Theory of Energy Storage and Its Application to Operating Procedure*, USAEC Report N-2191a, Hanford Works, Nov. 9, 1945. (Classified)
 32. R. S. Barnes and M. J. Makin, *On the Mechanism of Irradiation Annealing*, *J. Nuclear Energy*, **2**: 291-298 (1956).
 33. R. E. Nightingale, *Irradiation Annealing in Graphite. I. An Experimental Study*, in *Proceedings of the US/UK Graphite Conference Held at St. Giles Court, London, Dec. 16-18, 1957*, pp. 21-32, USAEC Report TID-7565 (Pt. 1), Mar. 16, 1959.
 34. R. E. Nightingale, *An Experimental Study of Irradiation Annealing of Graphite*, USAEC Report HW-40795, Hanford Atomic Products Operation, Apr. 18, 1956. (Classified)
 35. J. R. Gilbreath and O. C. Simpson (Comps.) *Chemistry Division, Section C-II Summary Report, October, November, and December 1952*, USAEC Report ANL-5024 (Rev.), Argonne National Laboratory, Aug. 14, 1953.
 36. J. D. McClelland et al., *Role of Ionization in Radiation Annealing*, USAEC Report NAA-SR-1025, North American Aviation Inc., Oct. 1, 1954 (Classified).
 37. J. R. Townsend and R. E. Nightingale, *Irradiation Annealing of Graphite*, USAEC Report HW-40796, Hanford Atomic Products Operation, May 14, 1956. (Classified)
 38. E. M. Woodruff, *Dimensional Changes in Irradiated Graphite*, in *Proceedings of the US/UK Graphite Conference Held at St. Giles Court, London, Dec. 16-18, 1957*, pp. 1-10, USAEC Report TID-7565 (Pt. 1), Mar. 16, 1959.
 39. R. L. Carter et al., *Recent Developments in the Technology of Sodium Graphite Reactor Materials*, in *Proceedings of the Second United Nations International Conference on the Peaceful Uses of Atomic Energy, Geneva, 1958*, Vol. 7, pp. 72-81, United Nations, New York, 1959.
 40. J. C. Charrault, *Différences de température entre surfaces des canaux et profondeur du graphite*, French CEA Report DPC C Ph/59-523, CEN Saclay, July 22, 1959.

Gas-Graphite Systems

T. J. CLARK, R. E. WOODLEY, and D. R. DE HALAST†

14-1 Survey of Gas-Graphite Systems

14-1.1 NUCLEAR APPLICATIONS

Certain gases are of interest as nuclear-reactor coolants in power-recovery systems because they can be utilized at high temperatures with high thermodynamic efficiency and without the use of costly high-pressure equipment. The type of gas to be used as a coolant depends to a large extent upon the temperature at which the reactor is to operate. Unless an inert gas such as helium is used, corrosion of many structural materials may become serious above approximately 650°C. If the gas comes into direct contact with graphite, gasification of the carbon will generally limit the temperature at which an oxidizing gas can be used as a coolant. However, because of the inherent simplicity of passing gas directly through an unprotected graphite moderator, this concept has been widely utilized in reactor design.

For reactors operating below approximately 200°C, air can be used directly as the coolant with little adverse effect on the graphite. This mode of cooling has been successfully used for the large production reactors at Windscale as well as the Oak Ridge X-10 Reactor, the Brookhaven Graphite Research Reactor (BGRR), and several test reactors. At temperatures approaching 300°C oxidation of graphite by air becomes serious. Carbon dioxide is inexpensive and relatively abundant and can be used as a coolant at outlet temperatures where power recovery becomes economically feasible. The Calder Hall reactors have successfully operated at outlet temperatures of about 300°C, and the Advanced Gas Cooled Reactor (AGR) in England will operate at a maximum carbon dioxide temperature of about 575°C. However, even below 500°C oxidation by carbon dioxide in a radiation field is not entirely negligible. The oxidation can be retarded somewhat by the addition of inhibitors such as carbon monoxide to the carbon dioxide, but for practical purposes the use of carbon dioxide is probably limited to graphite temperatures of about 600°C. Hydrogen or nitrogen will most likely be successfully utilized as coolants above this temperature, but at present helium seems most attractive for use at very high temperatures. The High Temperature Gas Cooled Reactor (HTGR) to be built at Peach Bottom, Pa., and the Dragon Reactor in England, will be cooled with helium at an outlet temperature of 750°C.

† Hanford Laboratories, General Electric Company, Richland, Wash.

In addition to the direct cooling of nuclear reactors, gas can be used to regulate the temperature of the graphite moderator in water-cooled reactors. In the Hanford reactors a mixture of carbon dioxide and helium has been utilized to adjust the transfer of heat from the moderator to the water-coolant passages. The graphite temperatures are thereby adjusted to minimize radiation damage to the moderator.

Reactions that might occur under abnormal conditions form an important aspect of gas reactions with graphite as far as nuclear reactors are concerned. As an example, if small traces of water come in contact with the hot graphite moderator, not only will the graphite be oxidized, but the hydrogen resulting from the reaction may embrittle essential reactor components such as zirconium pressure tubes containing water coolant.

Probably the most widely studied hazard of gas-graphite reactions has been the self-sustained combustion of graphite in air. If a large quantity of air is introduced by accident into a graphite moderator operating at high temperature or if an air-cooled reactor undergoes a temperature excursion, the graphite may ignite. Once combustion starts, the exothermic reaction with oxygen can sustain the combustion even in the absence of nuclear heating. The partial destruction of one of the air-cooled Windscale reactors in 1957 resulted from rapid oxidation of the graphite following a temperature excursion during a graphite-annealing operation (Sec. 17-3.2).

14-1.2 PROPERTIES OF GAS COOLANTS

The choice of any particular gas as a reactor coolant depends principally upon its reactivity with graphite, heat-transfer properties, cost, and corrosive effects on other reactor components. The first limitation is often the most restrictive for a graphite-moderated reactor. The approximate relative rates of gas-carbon reactions at 800°C and 0.1 atm are given in Table 14.1;

Table 14.1 — APPROXIMATE RELATIVE RATES OF THE GAS - CARBON REACTIONS AT 800°C and 0.1 ATM PRESSURE[†]

Reaction	Relative rate
C - O ₂	1 x 10 ⁵
C - H ₂ O	3
C - CO ₂	1
C - H ₂	3 x 10 ⁻³

[†]From Walker et al., *Advances in Catalysis*, Ref. 3.

however, each reaction shows a different dependence upon pressure and temperature. The physical properties of gases of interest for reactor operations have been tabulated extensively in the literature.^{1,2}

The absorption of neutrons by the various gases may have significant effects on the reactivity of the reactor. In Table 14.2 the macroscopic cross

Table 14.2 — MACROSCOPIC CROSS SECTION FOR THERMAL-NEUTRON ABSORPTION

Gas at 500°C and 10 atm	$\Sigma_a \times 10^6, \text{ cm}^{-1}$
N ₂	36
Air	28
H ₂	6.3
He	0.07
CO ₂	0.04
O ₂	0.00
<u>Moderator</u>	
BeO	73
C (for $\rho = 1.7 \text{ g/cm}^3$ and $\sigma = 3.4 \text{ mb}$)	29

sections of several gases are compared with the cross sections of graphite and beryllium oxide. Under the conditions considered air will absorb about as many neutrons as an equal volume of moderator.

14-1.3 THERMODYNAMICS OF GAS-GRAPHITE SYSTEMS

The heats of reaction at 18°C and 1 atm pressure are given in Table 14.3 for a number of gas-graphite and related reactions.³ On the basis of $\Delta H =$

Table 14.3 — HEATS OF REACTION OF SEVERAL GAS-GRAPHITE SYSTEMS AT 18°C and 1 ATM PRESSURE[†]

	$\Delta H, \text{ kcal/mole}$
<u>C - O₂:</u>	
(1) $\text{C} + \text{O}_2(\text{g}) = \text{CO}_2(\text{g})$	-94.03
(2) $\text{C} + 1/2 \text{O}_2(\text{g}) = \text{CO}(\text{g})$	-26.62
(3) $\text{CO}(\text{g}) + 1/2 \text{O}_2(\text{g}) = \text{CO}_2(\text{g})$	-67.41
<u>C - CO₂:</u>	
(4) $\text{C} + \text{CO}_2(\text{g}) = 2\text{CO}(\text{g})$	+40.79
<u>C - H₂O:</u>	
(5) $\text{C} + \text{H}_2\text{O}(\text{g}) = \text{CO}(\text{g}) + \text{H}_2(\text{g})$	+31.14
(6) $\text{CO}(\text{g}) + \text{H}_2\text{O}(\text{g}) = \text{CO}_2(\text{g}) + \text{H}_2(\text{g})$	- 9.65
(4) $\text{C} + \text{CO}_2(\text{g}) = 2\text{CO}(\text{g})$	+40.79
(7) $\text{C} + 2\text{H}_2(\text{g}) = \text{CH}_4(\text{g})$	-17.87
<u>C - H₂:</u>	
(7) $\text{C} + 2\text{H}_2(\text{g}) = \text{CH}_4(\text{g})$	-17.87

[†] From Walker et al. , *Advances in Catalysis*, Ref. 3.

0 for graphite, various types of amorphous carbons are reported to have positive heats of formation ranging from 1.7 to 2.6 kcal/mole. The heat of formation of irradiated graphite is also positive by an amount equal to the stored energy; the highest value reported to date is 7.5 kcal/mole (Chap. 12).

The extent to which some reactions occur, such as the formation of carbon monoxide from carbon dioxide and graphite, is limited by kinetic considerations. On the other hand, reactions such as the production of methane from hydrogen and carbon are severely restricted by equilibrium considerations under normal reactor-temperature conditions.

Equilibrium constants for gas-graphite and associated reactions listed in Table 14.3 are presented in Table 14.4. At ordinary temperatures the

Table 14.4 — EQUILIBRIUM CONSTANTS FOR GAS-CARBON AND ASSOCIATED REACTIONS[†]
(Gas Pressures in Atmospheres)

Temp., °K	Log K						
	(1)	(2)	(3)	(4)	(5)	(6)	(7)
300	+68.67	+23.93	+44.74	-20.81	-15.86	+4.95	+8.82
400	+51.54	+19.13	+32.41	-13.28	-10.11	+3.17	+5.49
500	+41.26	+16.26	+25.00	- 8.74	- 6.63	+2.11	+3.43
600	+34.40	+14.34	+20.06	- 5.72	- 4.29	+1.43	+2.00
700	+29.50	+12.96	+16.54	- 3.58	- 2.62	+0.96	+0.95
800	+25.83	+11.93	+13.89	- 1.97	- 1.36	+0.61	+0.15
900	+22.97	+11.13	+11.84	- 0.71	- 0.37	+0.34	-0.49
1000	+20.68	+10.48	+10.20	+ 0.28	+ 0.42	+0.14	-1.01
1100	+18.80	+ 9.94	+ 8.86	+ 1.08	+ 1.06	-0.02	-1.43
1200	+17.24	+ 9.50	+ 7.74	+ 1.76	+ 1.60	-0.16	-1.79
1300	+15.92	+ 9.12	+ 6.80	+ 2.32	+ 2.06	-0.26	-2.10
1400	+14.78	+ 8.79	+ 5.99	+ 2.80	+ 2.44	-0.36	-2.36
4000	+ 5.14	+ 5.84	- 0.70				

[†] From Walker et al., *Advances in Catalysis*, Ref. 3.

equilibrium for the reaction of graphite with oxygen favors the formation of products. The same is true of the carbon-hydrogen reaction below about 400°C; however, above 900°C the latter reaction does not proceed to any appreciable extent. The reactions of carbon dioxide and water with graphite do not give large concentrations of products until temperatures are in excess of 700°C. Additional information on entropies and enthalpies for gas-graphite reactions has been tabulated by K. K. Kelley.⁴

14-1.4 THERMODYNAMICS UNDER IRRADIATION

Many highly active species, such as O, H, OH, O₃, and O₂⁺, can be formed in the gas phase in a radiation field. Their concentrations depend upon such factors as radiation intensity, type of radiation, and the geometry of the system. The reaction of these short-lived species with graphite is

exceedingly rapid, and the equilibrium lies far on the product side. The formation of these active species changes the relative importance of reaction routes leading from reactant to product. Thus the equilibrium position in a reaction can be shifted by factors not normally taken into account by the thermodynamics of systems in thermal equilibrium. For example, Anderson et al.⁵ have reported that under irradiation the steady-state concentration of CO in CO₂ in contact with graphite is well in excess of the thermodynamic equilibrium values.

In a strict sense the change in equilibrium values caused by the opening of alternate reaction paths is actually a kinetic phenomenon rather than the result of any basic change in thermodynamics. Additionally, however, the radiation undoubtedly excites some gaseous molecules without supplying sufficient energy for dissociation. The molecules thus affected will upset the Boltzmann energy distribution at a given temperature, and thus a normal chemical thermodynamic equilibrium cannot exist. The importance of such an effect is difficult to ascertain.

The above considerations are all concerned with the gas phase. It was noted in the preceding section that the heat of formation of graphite is increased by irradiation at low temperature. Likewise, the entropy of the graphite is increased by lattice disorders. These effects change the free energy, and hence the equilibrium constant, of the reaction. However, most of the lattice defects responsible for these changes are annealed out at temperatures below 300°C, and thus their influence on equilibria for reactions occurring above this temperature is small.

The effects of radiation on reaction rates are usually of more practical interest than any changes in the equilibrium constants of the reactions. Under irradiation most reactions proceed at a significant rate at temperatures considerably below the thermal threshold for detectable reaction.

14-1.5 ACTIVE SITES

Before starting the discussion on kinetics, it is worth while to consider briefly the role that active sites play in the reactions of graphite with gases. There is much evidence to show that one of the steps in a thermal gas-graphite reaction is the adsorption of the gas on the carbon surface.³ The subsequent desorption of the gaseous products often plays an important role in the kinetics. Sorption of gases occurs preferentially on certain sites on the graphite. Although these sites are generally believed to be associated with the atoms located at the edges of the crystallites, their exact nature is not well understood.

As might be expected, there are several different types of active sites specific to certain gases. Sites for the water reaction with charcoal occupy about 2 per cent of the total microscopic carbon surface,[†] whereas those

[†] Microscopic surface estimated from the adsorption isotherm for water vapor at room temperature.

for the carbon dioxide reaction only occupy about 0.5 per cent.^{6,7} Furthermore, sites that adsorb water do not adsorb carbon monoxide, whereas carbon monoxide is adsorbed⁶ on sites that adsorb carbon dioxide.

The surface activity of different grades of polycrystalline graphites and carbons varies over a wide range (Sec. 6-8), thus introducing some uncertainty and confusion into the interpretation of rate data. Generally, rate equations are expressed in such a manner that the total number of active sites, C^* , is incorporated into the value of the rate constant. The number of unoccupied active sites available for reaction, C_f , is given by the relation

$$C_f = C^*(1 - \theta) \quad (14.1)$$

where θ is the fraction of sites occupied by adsorbed species. The manner in which C^* is included in the experimental rate constant, k' , is shown by the following example. A reaction step in the oxidation of graphite by oxygen is



for which

$$\frac{dp_{CO_2}}{dt} = kC_f p_{O_2} = kp_{O_2}(1 - \theta)(C^*) = k'p_{O_2}(1 - \theta) \quad (14.3)$$

The experimental rate constant, k' , is determined by measuring the ratio of carbon dioxide to oxygen under conditions where $\theta \ll 1$ and includes the value of C^* as well as the specific rate constant, k . Thus any change in the number of active sites, such as may result from changing the degree of crystallinity of the carbon, will change the experimental rate constant. It is probable that the number of active sites also changes with temperature and with the impurity content of the graphite. It is necessary to keep these considerations in mind when interpreting rate data on gas-graphite reactions.

The total concentration of active sites does not significantly affect the equilibrium constant for reactions with carbon. Whereas the availability of active sites has an important bearing on reaction rates, the considerations during the (unlimited) time available to establish thermodynamic equilibrium are different than in the kinetic case. New active sites are continually being formed in the carbon as the reaction takes place; thus each carbon atom in the graphite is potentially available for reaction. Although it is not always explicitly stated, the kinetic treatments of graphite reactions also assume the generation of new active sites so as to maintain C^* constant.

The fact that C^* , the number of active sites, remains approximately constant during oxidation is evidenced by the observation that oxidation rates[†] remain constant over a wide range of graphite oxidation. For exam-

[†] Rates expressed as grams of weight loss per unit time. All other rates in this chapter, unless otherwise specified, refer to fractional weight loss per unit time.

ple, after an initial increase the oxidation rate of graphite in carbon dioxide does not change in some cases⁸ until as much as 55 per cent of the graphite has been oxidized (see Fig. 14.7). Eventually the rate starts to decrease.

This eventual decrease is to be expected because, as the gasification of carbon progresses, the *concentration* of active sites, i.e., $C^*/\text{total } C$, must increase. At some point a limiting concentration or crowding together of active sites will result, and thereafter C^* , and hence the reaction rate, will decrease as the total number of carbon atoms decreases. Obviously C^* must equal zero when there is no graphite remaining.

14-1.6 INTERPRETATION OF MULTISTEP REACTIONS

Most gases react with carbon through a series of steps involving the adsorption and desorption of several types of graphite surface compounds. As a consequence the rate equation is generally quite complicated. The rate equation for the reaction of graphite with carbon dioxide, which is derived in Sec. 14-2.3, is of the form

$$\text{Rate} = \frac{k_A p_{\text{CO}_2}}{1 + k_B p_{\text{CO}} + k_C p_{\text{CO}_2}} \quad (14.4)$$

where p_{CO_2} and p_{CO} are the partial pressures of carbon dioxide and carbon monoxide and the constants, k_A , k_B , and k_C are combinations of one or more specific rate constants for the reaction steps. Although the individual specific rate constants or combinations thereof will vary with temperature according to the Arrhenius equation, the over-all rate for such a complicated relation does not. Thus, for the example given above, attempts to determine the activation energy of the carbon-carbon dioxide reaction by plotting the logarithm of the rate at constant carbon dioxide pressure vs. the inverse absolute temperature will yield a constant value for the activation energy only under special conditions.

A change in the experimental conditions can change both the order of the reaction and the apparent rate constant. It can be seen from Eq. 14.4 that at low pressures the rate approaches first order with respect to the carbon dioxide pressure, and the activation energy will be determined by k_A . Physically the first-order dependence can be interpreted as showing that only a very small fraction of the active sites are covered and that the coverage increases linearly with pressure. Furthermore, it can be seen that at very high carbon dioxide pressures the initial rate is independent of the carbon dioxide pressure, and the measured activation energy will be determined by k_A/k_C . In this case all the active sites are covered. Furthermore, k_A , k_B , and k_C do not have the same activation energies, and the relative importance of the various terms in the rate equation will change with temperature even at constant pressure. Large temperature changes may therefore result in apparent changes in the order of the reaction and in the activation energy.

14-1.7 DIFFUSION CONTROL

In the above discussions it has been tacitly assumed that the reaction rates are controlled by the chemical reactivity of the gases and the graphite. However, heterogeneous reactions involving a porous solid and a gas can be controlled by one or more of three idealized steps.†

1. Mass transport of the reacting gas or reaction products across a relatively stagnant gas film between the exterior surface of the graphite and the main gas stream.
2. Mass transport of the reacting gas from the exterior surface to an active site beneath the exterior surface and mass transport of the products in the opposite direction.
3. Chemical reaction at the active sites.

The temperature is of prime importance in determining which of these steps controls the gas-graphite reactions. The sample geometry, permeability, and reactivity and the gas pressure and flow conditions are of secondary importance.

Ideally the variation of reaction rate with temperature can be divided into three main zones, as shown in Fig. 14.1. Consider a porous graphite body exposed to a reactive gas at a temperature T . At low temperatures, when the reaction rate is low, the gas diffuses into the solid much more rapidly than it reacts at active sites, i.e., step 3 is the slow step. In this low-temperature zone (zone I), the reaction rate is controlled solely by the chemical reactivity of the solid. The measured (apparent) activation energy, E_a , is, by definition, equal to the true activation energy, E_t . Furthermore, η , which is defined as the ratio of the experimental reaction rate to the reaction rate that would be found if the gas concentration were constant throughout the interior of the sample, is virtually equal to one.

In the intermediate-temperature zone (zone II), step 2 becomes important, and the concentration of the reactant species approaches zero at a distance from the exterior surface less than the radius, R . In this zone η is less than one-half. Furthermore, the apparent activation energy is $E_t/2$. At higher temperatures the concentration gradient of the reacting gas becomes steeper within the graphite, and the gas concentration approaches zero at a distance nearer the surface. Thus, even though the reaction rate between gaseous molecules and active sites increases with temperature, the total amount of carbon available to the gas decreases. The temperature dependence of the reaction rate is then determined by $E_t/2$ rather than by E_t .

In the high-temperature zone (zone III), the concentration of the

† The following discussion closely follows the work of Walker et al.³ This reference should be consulted for details of derivations and original references to experimental work.

reacting gas is low at the exterior of the solid, and the rate is controlled by step 1. Increasing the temperature affects the reaction rate by changing the amount of reactant that can reach the exterior surface per unit time. However, since bulk gas-transfer processes have low activation energies, the apparent activation energy for gas-carbon reactions in zone III is low. In zone III, η is very much less than one, and, because of the behavior of the surface film, the reaction rate is proportional to the square root of the gas-stream velocity.

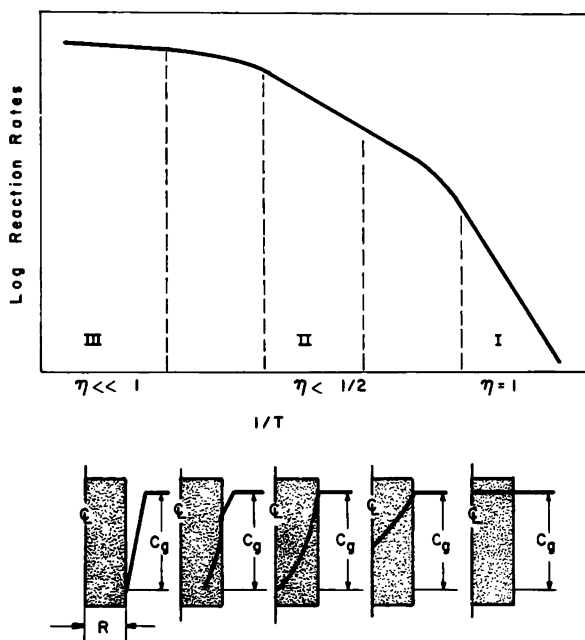


Fig. 14.1 Ideal reaction zones in graphite. Zone I is controlled by the reactivity of the carbon. Zone II is controlled by diffusion through the solid. Mass transport of the gas to the exterior surface of the graphite controls the reaction of zone III. η is the ratio of the rate in a given zone to the rate that would be observed if zone I conditions applied. C_g is the concentration of the reactant. (From Walker et al., *Advances in Catalysis*, Ref. 3.)

The most common experimental method of determining the reaction zone is to vary the surface-to-volume ratio of the graphite. If the reaction rate is dependent only on the total volume of graphite, then the reaction is in zone I. Similarly, if the rate is directly proportional to the exterior surface area, the reaction is in zone III. If the reaction rate is sensitive to the surface-to-volume ratio, the reaction is in zone II or an intermediate zone.

14-1.8 INITIAL KINETICS

The formation of a surface compound is one of the steps in all gas-graphite reactions. There is therefore a short initial period during which the

concentration of surface compounds changes; during this time the reaction does not proceed according to steady-state kinetics. Unless graphite is very carefully degassed at high vacuum and high temperature, surface compounds will always be present initially. Also, during experiments in small-volume systems, where the progress of the reaction is followed by measuring changes in the gas pressure, enough gas may be adsorbed or desorbed during the initial stages to cause difficulty in interpretation of results. This difficulty may be especially troublesome in experiments such as capsule irradiations where only pre- and postexperiment pressure measurements are performed.

Another factor that normally affects the initial rate of reaction more than a change in concentration of surface compounds is the opening of pores in the graphite by oxidation. The rate of oxidation of graphite has been shown to increase as the accessible pore volume increases.⁹ After a small amount of oxidation, the rate generally levels off to a steady-state value and no longer seems to be affected by the opening of pores (see Fig. 14.7). The length of the induction period during which the rate increases depends upon the over-all rate of reaction. In carbon dioxide below 750°C, where the reaction is relatively slow, the steady-state oxidation rate is generally obtained after a few tenths of 1 per cent oxidation. In the rapid reaction of oxygen with graphite above 500°C, the rate does not level off until about 5 per cent oxidation. Since the fastest reactions are those most subject to diffusion control, it is likely that the opening of pores not only increases the available surface area for reaction but also increases the rate at which gases can diffuse through the graphite.

14-1.9 EFFECT OF IMPURITIES

The reaction rates of different grades of electrographites are seldom the same. This may be attributed in part to differences in crystalline perfection and porosity. However, these differences are more generally related to the impurity level of inorganic compounds in the graphite. Iron, cobalt, nickel, copper, and manganese are all known to catalyze graphite oxidation. Boron, titanium, and tungsten have an inhibiting effect.³

Long and Sykes⁶ suggest that impurities affect carbon reactivity by interaction with the π -electrons of the carbon basal plane. This interaction is attributed to a change in the bond order of the surface atoms, which affects the ease with which they can leave the surface with a chemisorbed species. According to this theory removal of an electron by an impurity increases the rate of reaction, whereas addition of an electron decreases the rate of reaction. Since the π -electrons in carbon are known to have high mobility in the basal plane, it is not necessary that the impurity be adjacent to the reacting carbon atom. It has been suggested that an impurity at any position in the basal plane will affect the reaction.³

In some cases it has been found that the catalytic effect of the impurity

depends upon the particular salt present in the graphite.³ Lead acetate is an effective catalyst, whereas lead sulfate exhibits only a slight catalytic effect.

14-1.10 ACTIVE SPECIES IN THE GAS PHASE

The primary effect of radiation upon the reaction between gases and graphite is to produce highly reactive species in the gas phase. The activation energy for the reaction between these active species and graphite is approximately zero. Thus, if the reaction rate is measured as a function of temperature in a radiation field, a transition temperature will generally be found above which the reaction is thermally controlled and below which the rate is independent of temperature. This behavior is illustrated in Fig. 14.2.

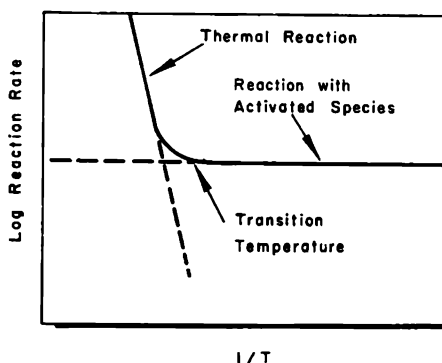


Fig. 14.2 Idealized temperature dependence of reaction rates in the presence of radiation. Below the transition temperature the reaction is controlled by the concentration of active species in the gas and displays a very low activation energy. Above the transition temperature the normal thermal reaction predominates.

In a radiation field graphite is subject to oxidation by species activated in two regions. Molecules are activated in the space surrounding the graphite; these may then diffuse to the graphite surface and react. Only those molecules activated within several mean free paths of the graphite surface have a high probability of reaching the graphite without deactivation in the gas phase. Active species are also formed from the gas present within the pores of the graphite. In this case the activated molecules have a higher probability of reaching the graphite surface before deactivation since many of the pores are small. Experiments on the radiation-induced reaction of carbon dioxide with graphite have shown that, at least under certain conditions, the reaction occurs largely by activation of the carbon dioxide in the pores.¹⁰

14-2 Carbon Dioxide-Graphite System

The reactions between carbon dioxide and graphite are of importance in nuclear reactors where carbon dioxide is used as a coolant or as a protec-

tive atmosphere around the moderator or where it may be present as an impurity at very high temperatures. The universal availability and low neutron cross section of carbon dioxide are factors in its favor for nuclear-reactor applications. At high temperatures, however, the thermal-reaction rates with graphite are appreciable for this system. This limitation can be reduced by the use of coatings, relatively impermeable graphite, and gas-phase inhibitors, as discussed in Sec. 14-7. The low activation energies of the radiation-induced reactions in this system make such reactions important only at lower temperatures.

14-2.1 THERMAL REACTION

Recent general reviews^{3,11} summarize most of the research on the thermal carbon dioxide-carbon system.

The over-all reaction



is endothermic, with $\Delta H = 41$ kcal/mole. This feature is of interest in nuclear-reactor design since it does not lead to the exothermic self-sustained oxidation possible with air or oxygen (Sec. 14-3.2).

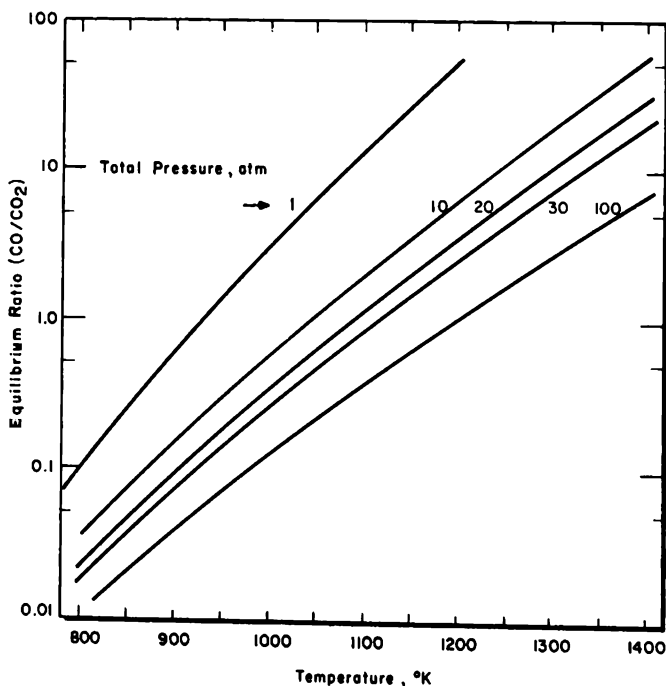


FIG. 14.3 Variation of the equilibrium ratio (CO/CO_2) with temperature. No carbon monoxide was present initially.

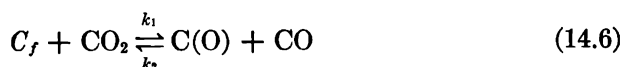
Equation 14.5 correctly indicates the stoichiometric relation and the production of a single gaseous product, carbon monoxide. The equilibrium

constant for this reaction is given in Table 14.4. Figure 14.3 shows the equilibrium ratio (CO/CO_2) as a function of temperature.

Ideally the over-all reaction might be followed manometrically in a closed system since 2 moles of carbon monoxide are formed per mole of carbon dioxide reacted. As might be expected, however, the actual reaction mechanism is more complex. At temperatures below 625°C , carbon dioxide sorption on clean graphitic carbon is observed to give rise to carbon monoxide production without gasification of the solid.⁵ The rate of carbon monoxide production in this case decreases with time, and only a small amount of carbon monoxide is observed in the gas phase.

14-2.2 MECHANISM OF THE THERMAL REACTION

To explain these and other experimental observations, Ergun¹² proposed the mechanism



where the free active-carbon sites, C_f , react to form gaseous carbon monoxide and a bound surface oxide C(O) .

The first of these reactions (Eq. 14.6) is the so-called "oxygen-exchange" reaction. It gives rise to carbon monoxide production while forming the bound surface oxide C(O) . The approach of this reaction to equilibrium for carbon that initially contains no adsorbed gases explains the decreasing rate of carbon monoxide production without gasification.

The second of these reactions (Eq. 14.7) is the gasification reaction that transfers carbon from the solid to the gas phase. Since C(O) is actually attached to the graphite lattice, Eq. 14.7 can be written as



to account for regeneration of active sites, C_f . In this case n is an integer having a value from zero to 2; the most probable average value¹² is 1.

Gadsby and coworkers¹³ have proposed a different mechanism



where a portion of the carbon monoxide is adsorbed to form a bound complex C(CO) . However, the bulk of experimental work¹⁴⁻¹⁶ supports the Ergun mechanism. In work with radioactive C^{14}O_2 , Bonner and

Turkevich¹⁷ found the forward reaction (Eq. 14.6) to be very rapid, resulting in a large build-up of surface oxide. They found no evidence for the reverse of Eq. 14.7, and their work lends strong support to Ergun's mechanism.

The equilibrium constant for Eq. 14.6 is

$$K = \frac{p_{\text{CO}}}{p_{\text{CO}_2}} \frac{[\text{C(O)}]}{[\text{C}_f]} \quad (14.10)$$

In Fig. 14.4, $\ln K$ is plotted as a function of $1/T$ for three types of carbon. The average heat of reaction in the 800 to 1400°C range is 23 kcal/mole.

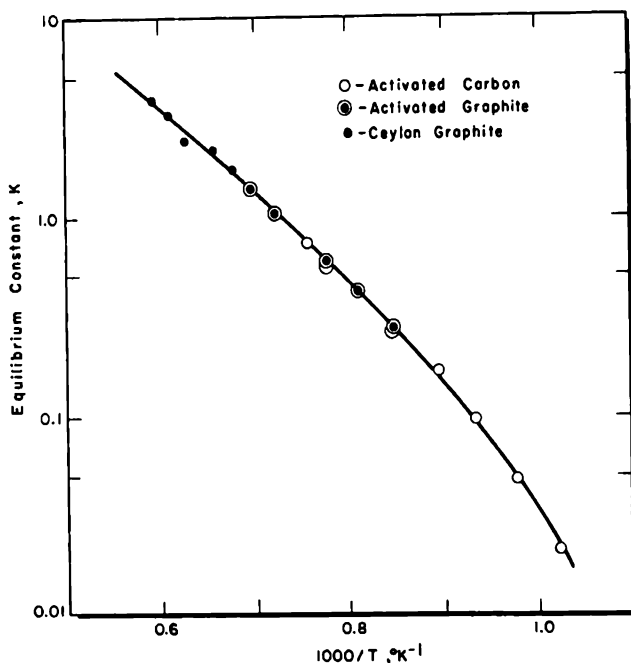


FIG. 14.4 Temperature dependence of the equilibrium constant (Eq. 14.10) for the reaction $\text{C}_f + \text{CO}_2 \rightleftharpoons \text{C(O)} + \text{CO}$. (From Ergun, *Journal of Physical Chemistry*, Ref. 12.)

14-2.3 KINETICS OF THE THERMAL REACTION

Thermal-reaction rates for the carbon dioxide-graphite reaction are measured by observing either the loss in weight of the graphite or the change in gas composition and volume as a function of time. Although the gas-composition method is capable of greater sensitivity,¹⁸ the weight-loss method is more convenient and more easily instrumented. Adsorption of product carbon monoxide on the graphite surface makes the correlation of results for the two methods difficult. Both methods are useful for a complete understanding of the reaction. A number of variables including temperature,

pressure, diffusion, concentration of available active sites, and extent of oxidation have been examined in kinetic studies of this system.

(a) *Temperature.* Graphite weight losses in pure carbon dioxide are difficult to detect at temperatures below 625°C. At higher temperatures gasification occurs at a measurable rate and can be expressed by a differential equation of the general form

$$\text{Rate} = -\frac{dC}{dt} = \frac{k_A p_{\text{CO}_2}}{1 + k_B p_{\text{CO}} + k_C p_{\text{CO}_2}} \quad (14.11)$$

where p_{CO} and p_{CO_2} are the partial pressures of carbon monoxide and carbon dioxide and the constants are combinations of one or more specific rate constants.

A relation of this form can be derived from consideration of active surface coverage.³ If θ_1 is the fraction of active surface covered by oxygen atoms, the relative number of free active-carbon sites, C_f , can be expressed as $1 - \theta_1$. Considering the reaction mechanism (Eqs. 14.6 and 14.7) and assuming steady-state conditions, where the rates of formation and removal of the surface complex are equal,

$$k_1 p_{\text{CO}_2} (1 - \theta_1) = k_2 \theta_1 p_{\text{CO}} + k_3 \theta_1 \quad (14.12)$$

from which

$$\theta_1 = \frac{k_1 p_{\text{CO}_2}}{k_3 + k_2 p_{\text{CO}} + k_1 p_{\text{CO}_2}} \quad (14.13)$$

Since the gasification rate is $k_3 \theta_1$,

$$\text{Gasification rate} = \frac{k_1 p_{\text{CO}_2}}{1 + (k_2/k_3) p_{\text{CO}} + (k_1/k_3) p_{\text{CO}_2}} \quad (14.11a)$$

which is of the same form as Eq. 14.11.

It is interesting to note that a similar rate equation results for the Gadsby mechanism. If θ_1 is defined as before and θ_2 is the fraction of active surface covered by bound carbon monoxide, then the relative number of free active sites can be expressed as $(1 - \theta_1 - \theta_2)$. Thus, for a steady-state concentration of C(O) ,

$$k_1 p_{\text{CO}_2} (1 - \theta_1 - \theta_2) = k_3 \theta_1 \quad (14.14)$$

After the equilibrium for Eq. 14.9 is established,

$$k_4 p_{\text{CO}} (1 - \theta_1 - \theta_2) = k_5 \theta_2 \quad (14.15)$$

which gives

$$\text{Gasification rate} = \frac{k_1 p_{\text{CO}_2}}{1 + (k_4/k_5) p_{\text{CO}} + (k_1/k_3) p_{\text{CO}_2}} \quad (14.11b)$$

Thus both mechanisms lead to rate equations of the same form.

(b) *Pressure.* The order of reaction, as well as the rate, can be varied by changing experimental conditions. At very low pressures, where p_{CO} and p_{CO_2} are small, Eq. 14.11 shows that a first-order dependence with respect to carbon dioxide pressure will be observed, whereas, at very high carbon dioxide pressures, the reaction should be independent of carbon dioxide pressure. It is not surprising therefore that values from zero to one have been reported³ for the order of reaction for different experimental conditions of temperature and carbon dioxide pressure.

(c) *Diffusion.* Diffusion was discussed in Sec. 14-1.8 in general terms. For the carbon dioxide-graphite system, zone I conditions prevail from about 625°C, where the thermal reaction becomes significant, to 900 or 950°C. The activation energy in zone I is believed³ to be approximately 93 kcal/mole. Visual inspection of broken graphite rods reacted with carbon dioxide at temperatures greater than 950°C indicates a definite reactant penetration depth that increases with time.⁸ The transition³ from zone I to zone II is gradual and extends to approximately 1250°C for spectroscopic carbon rods in carbon dioxide at 1 atm. Figure 14.5 shows

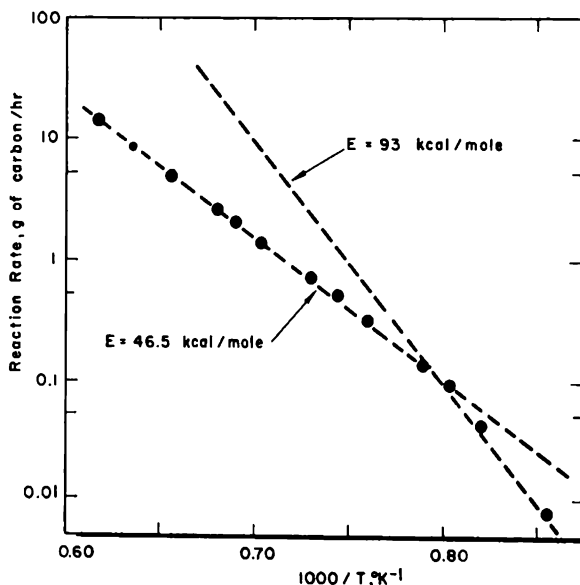


FIG. 14.5 Temperature dependence of the rate of reaction of spectroscopic carbon rods³ with carbon dioxide at 1 atm. The carbon rods were manufactured from lamp-black and heat-treated at 3000°C.

the Arrhenius plot. The apparent activation energy in zone II is about half that in zone I, or about 46.5 kcal/mole. The activation energy is still lower in zone III, where the rate is controlled by diffusion through a relatively stagnant gas layer at the carbon surface.

Bulk-density profiles provide a means for estimating the depth of reac-

tion. Figure 14.6 shows the difference in the profile when graphite samples are reacted at various temperatures to the same weight loss. The profiles are prepared by removing outer layers on a lathe and determining bulk densities for the remainder of the sample. High turning speeds and needle-point tools are used to minimize pore clogging by the machining.

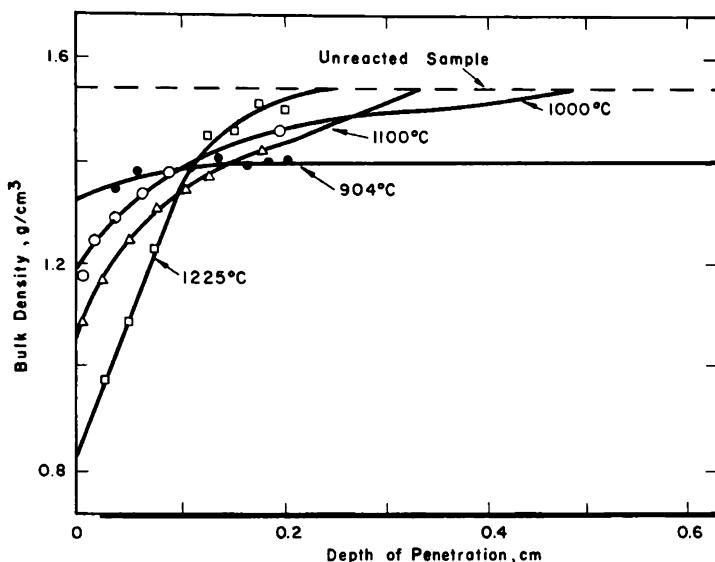


FIG. 14.6 Bulk-density profiles for graphite rods oxidized to about 10 per cent weight loss at various temperatures. (From Petersen and Wright, *Industrial and Engineering Chemistry*, Ref. 8.)

(d) *Available Active Sites*. In zone I, where reaction rates are controlled by chemical reactivity, the rates are a function of the concentration of free active sites, C_f . Although the presence of such sites has not been unequivocally established, it is probable that they occur at edge locations in the graphite lattice. Thus, if the number of edge locations is proportional to the available surface area, the surface area of a sample should be one measure of its reactivity. Correlations have been made¹⁹ between the initial increase in oxidation rates for graphite samples and the surface area measured by nitrogen adsorption.

Certain metallic impurities produce pits at locations other than at edges on single crystals of graphite. The pits probably form at catalyzed active sites.²⁰

From the detailed discussion of the manufacture and structure of electrographite (Chaps. 2 and 5), it can be concluded that a number of variables influence the concentration of available active sites. Among these are coke type and particle size; the type and quantity of binder and impregnant; graphitization temperature and time; and the density, purity, surface area, and pore-size distribution of the finished graphite.

Because of the interdependence of the many possible variables, it is difficult to establish any quantitative relation between the oxidation rate of an electrographite and any one property. In one extensive study²¹ no precise correlation could be found between carbon gasification rates in carbon dioxide and any of the following: quantitative and qualitative ash analyses, hydrogen content, interlayer spacing, average crystallite size, true and apparent density, porosity, surface area, and effective diffusion coefficients of hydrogen through the carbons.

(e) *Extent of Oxidation.* Experimentally, graphite weight-loss rates display three definite phases with respect to the extent of oxidation at a given temperature.^{8, 22, 23} During the first phase, which is usually complete at less than 1 per cent oxidation, reaction rates increase as oxidation proceeds. This increase may be due to a combination of factors:

1. An increase in available surface area with oxidation, which increases the concentration of C_f .
2. The presence of machining dust in exposed pores as a result of sample preparation.
3. Surface contamination due to sample handling.
4. Establishment of equilibrium with respect to surface oxide formation.

It is from the linear weight-loss rates observed in the second phase that activation energies are usually calculated. In Sec. 14-1.5 it was shown that the linear rates are a result of steady-state conditions with respect to the

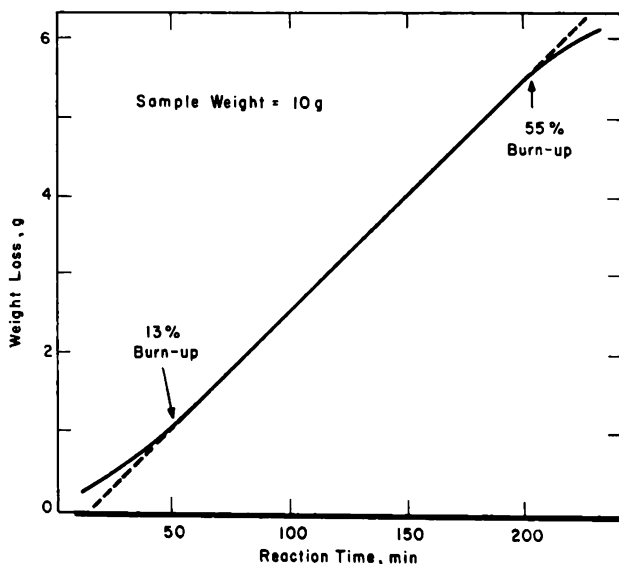


FIG. 14.7 The reaction of graphite rods with carbon dioxide at 1100°C, illustrating the three phases of the reaction. (From Petersen and Wright, *Industrial and Engineering Chemistry*, Ref. 8.)

formation and destruction of active sites. Under steady-state conditions one active site is created for each site destroyed.

A third phase, in which the oxidation rate decreases, is observed at higher total weight losses (Sec. 14-1.5). Such effects are not observed below approximately 55 per cent total weight loss.⁸ The three phases are shown in Fig. 14.7.

14-2.4 EFFECTS OF OXIDATION ON THE PHYSICAL PROPERTIES OF GRAPHITE

The rapid initial increase in the rate of the carbon dioxide-graphite reaction is accompanied by a corresponding increase in BET surface area.^{19, 23, 24} Apparently oxidation opens up pores not initially available to the adsorbing nitrogen molecules employed in the surface-area determinations.

Changes are also observed in the relative number of micropores (radius < 300 Å) as a result of oxidation. Figure 14.8 shows the micropore distri-

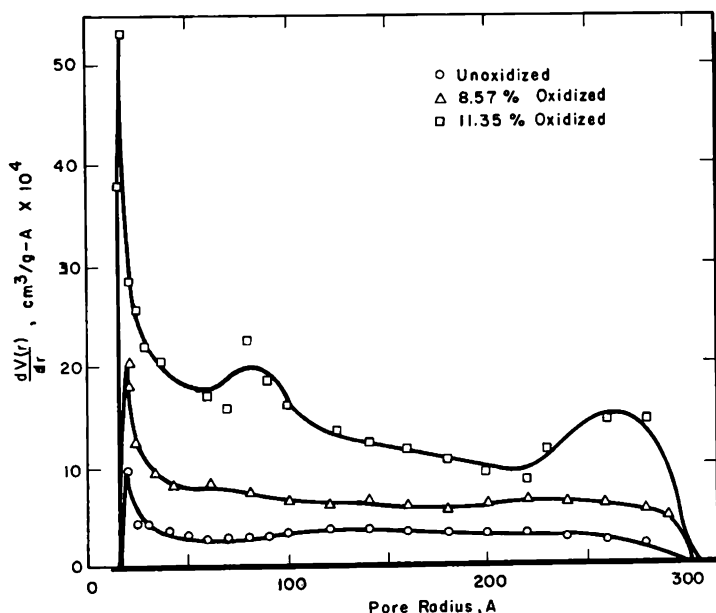


FIG. 14.8 Changes in pore-size distribution with oxidation in CSF graphite. Samples were outgassed at 350°C prior to measurement of the pore-size distribution.²⁵

butions observed for three samples taken from the same bar of CSF graphite. It can be seen that the peak intensity at 17 to 22 Å increases with increasing oxidation. This has been attributed to the removal of carbon that previously blocked access to some of these pores.

Figure 14.6 and the explanations given in Sec. 14-1.7 for the temperature zones lead to the conclusion that the micropore structure of graphite is probably of little importance at temperatures above those for zone I. This is analogous to the case of the fast reaction of a gas with a porous

catalyst;^{26, 27} small pores remote from the surface of the particle play a small part in the catalysis of the reaction. For the carbon dioxide-graphite system then, at temperatures above 900°C, the macropore system with radii greater than 300 Å is the one of interest.

Most of the macropore volume (radius > 300 Å) is concentrated in a relatively narrow size range for electrographites. This fact and the effects of oxidation at 900 and 1100°C are illustrated in Fig. 14.9. The voids

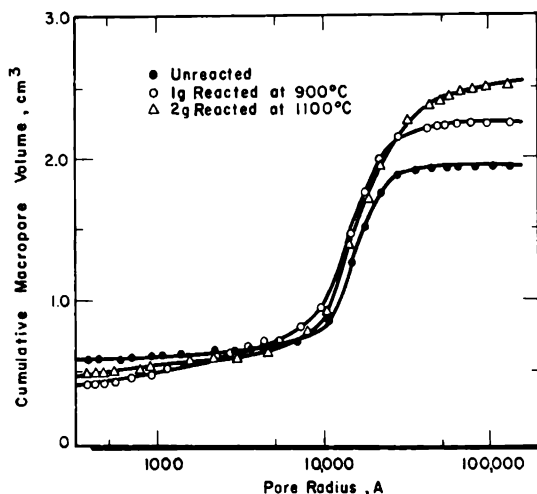


FIG. 14.9 Changes in macropore volume of graphite rods resulting from gasification. (From Walker et al., *Journal of Physical Chemistry*, Ref. 28.)

between grains result in a concentration of a large fraction of the macroporosity between 10,000 and 25,000 Å. This is also indicated by the fact that the void volume of lampblack, with a much smaller average grain size, is concentrated in the region of 1300 Å. In addition, the bimodal particle-size distribution gives a bimodal macropore-volume system. An attempt was made to correlate the macropore structure with gasification rates at 900 and 1100°C in carbon dioxide and with hydrogen diffusion coefficients for the graphites, but no positive correlations were found for the conditions studied.²¹

The bulk density and compressive strength of graphite are reduced by oxidation. The decrease is rapid initially. In the case of CSGBF graphite,²⁹ 10 per cent oxidation reduces the strength by about a factor of 2. The rate of decrease becomes less as the sample is oxidized further. Preirradiated materials show the same effect but have greater compressive strength than the unirradiated material for a given amount of oxidation.

14-2.5 RADIATION EFFECTS ON CARBON DIOXIDE AND CARBON MONOXIDE

Any account of the carbon dioxide-graphite reaction in a radiation field must consider the radiation effects on the solid, the carbon dioxide, and the

product carbon monoxide. In addition, it may be necessary to differentiate between the gas surrounding the graphite body and the gas in the pores of the graphite (Sec. 14-1.10).

Gaseous CO_2 is stable under irradiation.^{30,31} Harteck and Dondes³² irradiated CO_2 at 5 atm pressure under conditions such that each CO_2 molecule was dissociated an average of 150 times. Even for these extreme conditions, the yield of decomposition products, $\text{CO} + \text{O}_2$, was less than 2 per cent. The stability of CO_2 under reactor irradiation has been demonstrated by experiment; only 5 ppm of CO was found³³ after a radiation dose of 1.2×10^{22} ev/g.

The radiation stability of pure CO_2 is due to efficient reactions for the re-formation of CO_2 from the primary dissociation products. The presence^{30,34} of mercury, phosphorus, methane, hydrogen, and other substances that can react with decomposition products leads to the decomposition of irradiated CO_2 . When NO_2 is added the G value† for the decomposition of CO_2 is 8 ± 1 . No evidence of equilibrium has been found after 25 per cent of the CO_2 has decomposed.³² Calculations show that the equilibrium is not expected to occur at less than 90 per cent decomposition. In liquid or solid CO_2 or in the gas phase at high pressures, the decomposition of pure CO_2 becomes appreciable. Wall effects may be important even in pure CO_2 gas.^{32,35}

Direct oxidation of CO by O_3 was suggested³¹ as an explanation of the apparent radiation stability of CO_2 . More recent work, however, has demonstrated that the activation energy for the reaction between CO and O_3 is high (28 kcal/mole), and more elaborate mechanisms have been proposed.³⁶

Carbon monoxide is less stable than CO_2 in a radiation field. Decomposition of CO yields CO_2 , C, and carbon suboxide polymers.³⁷

14-2.6 RADIATION-INDUCED CARBON DIOXIDE-GRAPHITE REACTION

In a nuclear reactor most of the energy absorbed by carbon dioxide is from the gamma rays. For example, in BEPO approximately 81 per cent of the energy absorbed is from gamma radiation, whereas the remaining 19 per cent is from fast neutrons.³⁸ The energy-absorption rates of carbon atoms and oxygen atoms are nearly identical under similar conditions. Nuclear-capture reactions are not an important source of energy in a carbon-oxygen system because of the low cross sections.

Although more energy per unit volume is absorbed in the graphite than in the carbon dioxide, most of this energy is apparently quickly dissipated before reaction with the carbon dioxide can occur. Of much greater importance is the energy absorbed in the gas phase.³⁵ When carbon dioxide is first passed through a large gas volume within a radiation field before

† The G value is the number of molecules decomposed per 100 ev of energy absorbed.

contacting graphite, the oxidation rate increases. This enhanced reaction rate is observable over a wide temperature range, and the effect is orders of magnitude larger than the enhancement of the reaction rate brought about by energy absorption in the solid.

(a) *Mechanism.* When carbon dioxide is irradiated in the presence of carbon or graphite, the solid is oxidized, producing carbon monoxide, until steady-state conditions are reached. This is to be expected because carbon is a substance capable of competing for the active species produced in the primary process and thus may partially prevent re-formation of carbon dioxide molecules. This steady-state condition has been observed in static and flowing systems.^{31, 33, 39} With carbon monoxide production in the radiation field, deposits of carbon and carbon suboxides are expected and are, indeed, observed on surfaces within the radiation field. In flowing systems deposits are observed on surfaces well outside the field.⁵

No unequivocal mechanism has yet been proposed for the radiation-induced carbon dioxide-graphite reaction.³⁵ When such a mechanism is proposed, it must include the primary dissociations of CO_2 and CO , yielding CO , C and O . These primary dissociations then may lead to a number of secondary reactions, including (1) formation of carbon and carbon suboxide deposits and reaction of such deposits with O or O_3 to regenerate CO_2 ; (2) reactions of oxygen atoms at surfaces, leading to the formation of O_2 or O_3 ; (3) reactions of oxygen atoms with deposited carbon to form CO and with CO to form CO_2 ; and (4) heterogeneous oxidation of graphite by oxygen atoms. At temperatures above approximately 625°C in a radiation field, the effects of the concurrent thermal reaction must also be considered.

(b) *Kinetics.* The lack of any formal mechanism for the radiation-induced carbon dioxide-graphite reaction prevents the development of an applicable differential rate equation. As yet, the kinetic studies of this reaction are limited to the study of single reaction variables and their effects, and no empirical differential rate equation has been formulated from the experimental results. Thus a discussion of the kinetics of this reaction must be limited, for the present, to the discussion of the effects of variables such as temperature, pressure, flow, and radiation intensity.

(c) *Temperature.* As indicated in Sec. 14-1.10, the reaction of oxygen atoms with carbon takes place with a near-zero activation energy. Thus very little change in oxidation rates is observed^{40, 41} for the radiation-induced carbon dioxide-graphite reaction at temperatures up to approximately 625°C . Above this temperature the thermal reaction becomes important,⁵ and its relatively high activation energy determines the temperature coefficient of reaction, as shown in Fig. 14.2. The change in rates observed in a typical reactor experiment is illustrated in Fig. 14.10. For the temperature range from 30 to 300°C , the rate increases by only a factor of 2. The apparent activation energy is about 1 kcal/mole.

(d) *Pressure.* Variations in pressure affect not only the energy absorp-

tion in carbon dioxide but also the mean free path of the resultant active species. It is not surprising then that the relation between carbon dioxide pressure and the radiation-induced reaction rate is a complex one that depends on conditions of flow and geometry. In typical experiments with flowing carbon dioxide, the reaction rate increased less than threefold for a sevenfold increase in pressure;³³ in another case the rate increased by a factor of 5 for a fivefold increase in pressure.⁴² In capsule experiments a decrease in the radiation yield of product carbon monoxide with increasing pressure was observed.¹⁰

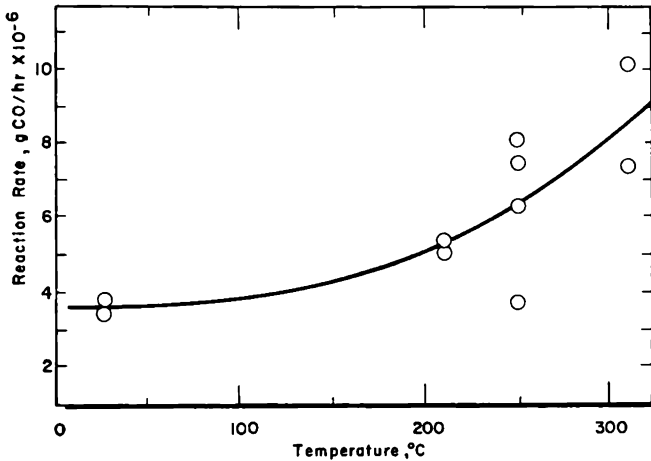


FIG. 14.10 The effect of temperature on the radiation-induced reaction rate for the carbon dioxide-graphite reaction at low temperature. AGXP graphite was irradiated for 10 to 20 hr in a thermal flux of 5.65×10^{11} neutrons/cm²/sec. (From Davidge and Marsh, Ref. 33.)

(e) *Flow.* The rate of reaction in flowing carbon dioxide can be considered as the product of the following terms:³³ (1) the rate of formation of active species in the system; (2) the fraction of the active species arriving at the graphite surface; and (3) the fraction of active species which, having reached the graphite, react with it. Both (2) and (3) are sensitive to the flow rate. At very low flow rates (2) is small because of recombinations in the gas phase and at the walls. At high flow rates (3) also decreases as a result of the reduced time of contact between the graphite and active species in the gas phase. In an experiment in BEPO³³ an increase in mass flow rate of carbon dioxide from 1 to 5 g/min reduced the radiation-induced reaction rate by a factor of about 3. For this system the flow conditions for maximum reaction had been exceeded at 1 g/min, and the observed reaction rates decreased for all higher values of flow rate.

Recirculating flow systems offer a method of studying the approach to steady-state conditions in the CO₂-C-CO system. For example, in the PIPPA model-channel loop (Sec. 8-4.2), a steady state was observed at a

CO concentration of 1.35 per cent in CO_2 flowing at 148 g/sec at 290 to 340°C in the radiation field in BEPO.⁵

Static capsule experiments offer another experimental approach to the study of this reaction. Such experiments have been performed with gamma-radiation sources and in reactors.^{10, 39, 43} The approach to equilibrium can be observed in capsules, but adsorption of product carbon monoxide may obscure the results because of the relatively intimate contact of the carbon monoxide with the graphite surface. Estimates of the contribution of in-pore

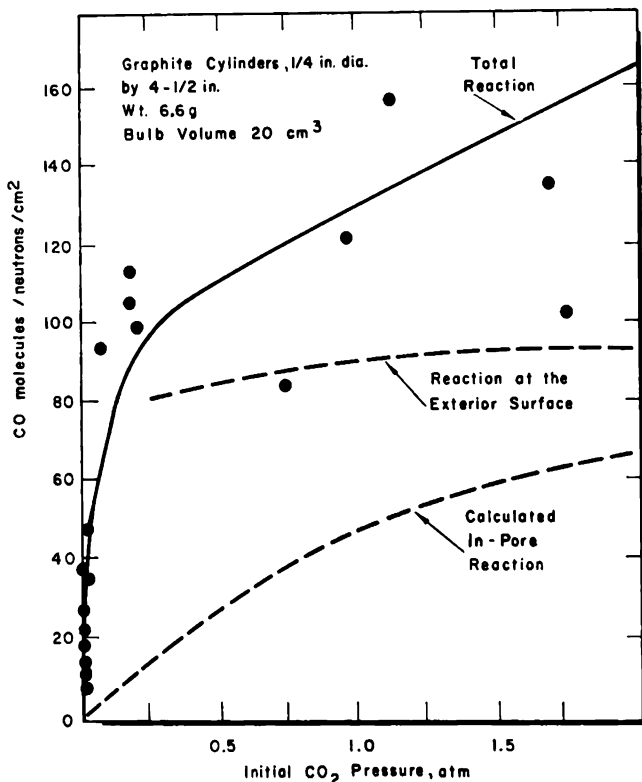


FIG. 14.11 Surface and in-pore contributions to the reaction of PGA graphite with carbon dioxide. The total reaction was determined in capsules containing a large free volume. The in-pore contribution was measured in tight-fitting capsules.¹⁰

reactions can be made by inserting carefully machined samples into tight-fitting capsules to minimize the free volume outside the graphite. Figure 14.11 shows the results when graphite was exposed to a number of carbon dioxide pressures. For initial carbon dioxide pressures greater than about 0.25 atm, the contribution of the surface reaction was nearly independent of the pressure, indicating a balance between the effects of the increased activation of the gas and the decreased mean free path of the oxygen atoms for this geometry. The in-pore contribution continued to increase with

carbon dioxide pressure, but the deviation from linearity shows that the fraction of active molecules which reached the graphite decreased with increasing pressure.

(f) *Radiation Intensity.* The rate of energy absorbed by carbon dioxide determines the rate of formation of oxygen atoms and thus determines the rate of oxidation for the radiation-induced reaction. If other factors are held constant, the radiation-induced reaction rate is directly proportional to flux intensity.³³

14-2.7 OXIDATION IN GRAPHITE MODERATORS

A number of carbon dioxide-cooled graphite-moderated reactors are now in operation or under construction (Table 1.2). Successful operation of these reactors must take into account the gas-graphite reaction rates and the effect of such reactions on the graphite moderator.

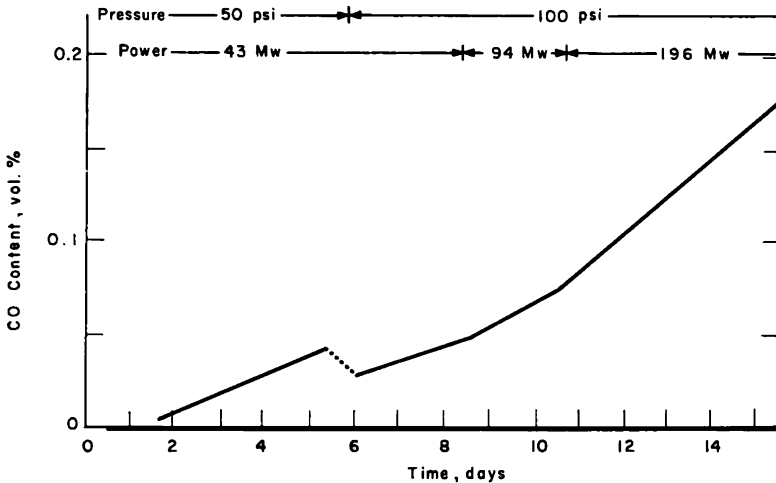


FIG. 14.12 Increase of the carbon monoxide in the carbon dioxide coolant during a start-up of the Calder-2 reactor.⁵

The initial increase in carbon monoxide concentration in Calder-2 has been observed experimentally.⁵ Figure 14.12 shows the build-up of carbon monoxide as the reactor is brought to power. Increasing the reactor power level, and thus the radiation intensity, increased the rate of carbon monoxide build-up by increasing the concentration of active species. The rate of carbon monoxide build-up was found to be directly proportional to the reactor power and to the carbon dioxide pressure.

In passing through a reactor moderator structure, the coolant gas is exposed to continuous variations in temperature and radiation intensity. The variation in the radiation-induced reaction rate is shown in Fig. 14.13 as a function of position in the Calder-2 reactor. It is clear that the weight loss is approximately proportional to the radiation dose.

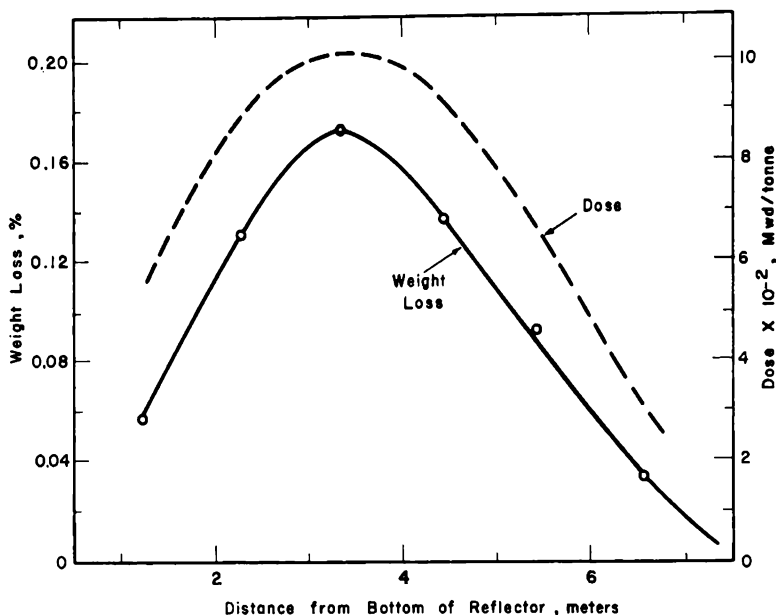


FIG. 14.13 Variation of graphite weight loss and dose with position in the Calder-2 reactor. Gas flow in the reactor is from bottom to top.⁵

14-3 Oxygen-Graphite System

Air is employed as a reactor coolant in several graphite-moderated reactors (Table 1.2) but, because coolant temperatures are severely restricted by the oxygen-graphite reaction, it is unlikely that any additional ones will be built with a specific power high enough to be useful as a power plant or as a materials-testing reactor. Moreover, since the oxygen-graphite reaction is exothermic, it is possible under certain conditions for more heat to be generated by this reaction than can be removed by the coolant. Operation of the Windscale reactors was discontinued in 1957 when one of the reactors was damaged by such an incident (Sec. 17-3.2).

The oxygen-graphite reaction will continue to be of interest in all graphite-moderated gas-cooled reactors regardless of coolant as long as the potential exists for air to enter accidentally into the coolant stream. Oxygen may also occur as an impurity in gas coolants or may diffuse into the gas atmosphere surrounding the graphite in liquid-cooled reactors.

14-3.1 THERMAL REACTION

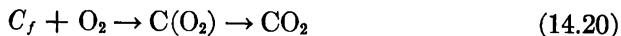
The reactions occurring in the oxygen-graphite system are



The heats of reaction and the equilibrium constants are given in Tables 14.3 and 14.4. The formation of both CO and CO₂ probably occurs through one or more surface complexes



and



Although Eq. 14.20 indicates that CO₂ is a primary reaction product, this has not always been the accepted view. Walker et al.³ have reviewed the controversy and have presented experimental evidence that favors the mechanism indicated by Eqs. 14.19 and 14.20. This evidence has been obtained from studies under the following conditions where oxidation of CO takes place at a negligible rate: low pressure;⁴⁴⁻⁴⁸ high gas velocities;⁴⁹⁻⁵² in the presence of substances inhibiting CO oxidation;^{49, 53-56} and at low temperatures.^{57, 58} It is generally accepted that the ratio CO/CO₂ is not constant but increases with increasing temperature.

(a) *Kinetics*. As in the case of the carbon dioxide-graphite reaction, the kinetic studies are carried out by observing either the changes in the weight of graphite or the rate of formation of carbon dioxide and carbon monoxide. To date, no empirical equation has been devised for describing the rate of the oxygen-graphite reaction analogous to Eq. 14.11 for the carbon dioxide-graphite system. When a satisfactory equation is developed, it can doubtless be synthesized from surface-coverage equations similar to Eq. 14.3. Most observers^{47, 49, 57, 58} find the thermal oxygen-graphite reaction to be first order, or nearly first order, with respect to oxygen, corresponding to low surface coverage by the carbon-oxygen complex.

(b) *Temperature*. As indicated in Table 14.1, the thermal oxygen-graphite reaction is much faster than the thermal carbon dioxide-graphite reaction at comparable temperatures and pressures. Figure 14.14 shows typical rates for the reaction of air with nuclear graphite. Since the reaction is first order under these conditions, the rate in pure oxygen can be calculated from these results.

The apparent activation energy derived from Fig. 14.14 is 38 kcal/mole, which agrees well with the value of 38.6 kcal/mole found by others for the reaction of oxygen with CSF graphite.⁶⁰⁻⁶² Observed activation energies for the reaction of oxygen or air with carbons are as varied as those observed for the carbon dioxide-graphite reaction. Reported values range from less⁵⁸ than 20 kcal/mole to about^{46, 63} 90 kcal/mole, depending on the temperatures and pressures used.

(c) *Pressure*. High activation energies are reported by experimenters working at low oxygen pressures.^{46, 63, 64} These same experimenters also report a zero-order dependence on the oxygen pressure, and one group⁶⁴ finds carbon monoxide to be the primary product. It is difficult to reconcile these results with the lower activation energies, first-order dependence, and pro-

duction of both carbon monoxide and carbon dioxide as primary products that most studies have shown. The interrelation of temperature and diffusion effects apparently complicates these studies,⁶⁴ but more work must be done to clarify the results.

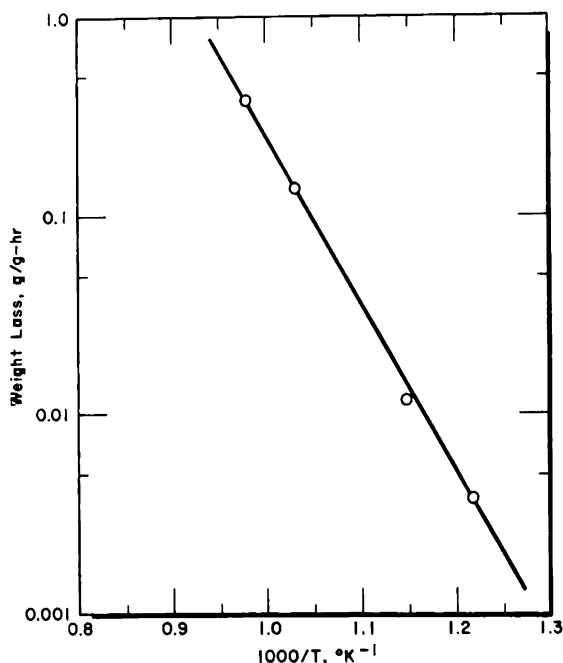


FIG. 14.14 The reaction of CSF graphite with air⁶⁵ at 1 atm and a flow of 2 cu ft/hr. The samples were hollow 2-in.-long cylinders with an outside diameter of 0.43 in. and an inside diameter of 0.25 in.

(d) *Flow*. The reaction of oxygen with ungraphitized carbon has been studied⁶⁵ at very high flow rates and temperatures from 1225 to 2025°C. At these temperatures the rate is determined by the mass transport of the reacting gas at the surface of the carbon (zone III). The rate was observed to increase as the square root of the velocity of the impinging gas stream at an injection velocity of 5000 to 60,000 ft/min. The reaction was first order and was not strongly affected by the type of carbon or the temperature. Others⁶⁶ have observed a similar flow dependence at somewhat lower temperatures and flows (900 to 1200°C and 1700 to 32,500 ft/min).

(e) *Geometry*. At temperatures where in-pore diffusion plays a role (zone II), the sample geometry is important. Cowen et al.,⁶⁷ upon oxidizing a 4-in. cube of nuclear graphite at 500°C in flowing air, found that the rate (expressed as fractional weight loss per hour) increased as the cube was machined to a smaller and smaller size. However, no simple function of the size could be found to express the results. Obviously care must be exer-

cised when extrapolating oxidation rates from laboratory-scale samples to larger samples at temperatures where the reaction is in zone II.

(f) *Preirradiation*. The effects of prior irradiation on the thermal oxidation rate have been determined in air and in oxygen.^{20, 68-70} When samples were irradiated in the BGRR to a thermal-neutron dose of 4×10^{20} neutrons/cm², a marked increase in the subsequent thermal reaction rates was observed, as shown in Fig. 14.15. The rate was increased by a factor of 6 at

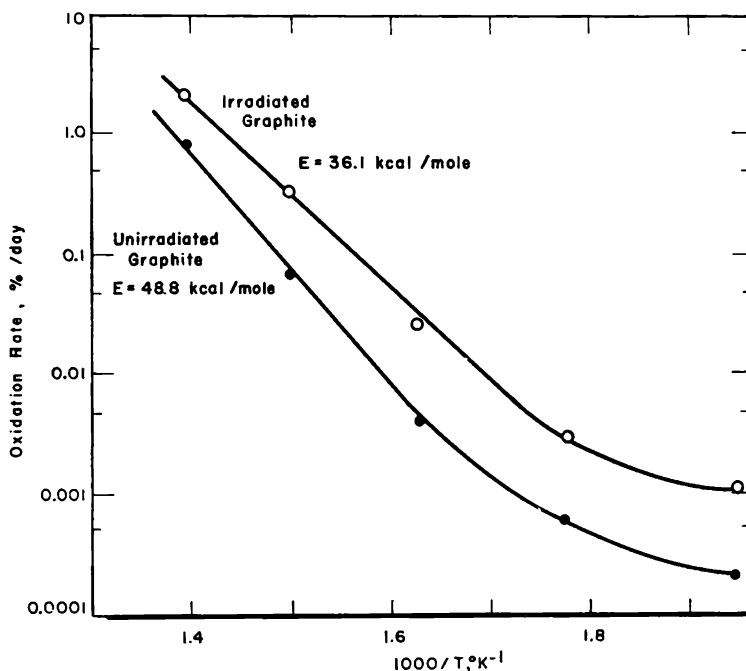


FIG. 14.15 The oxidation of irradiated and unirradiated graphite by oxygen in the absence of radiation.⁶⁸

250 to 350°C and a factor of 2.3 at 450°C. The increase in rate is the result of radiation-induced structural changes, as discussed in Sec. 14-1.4. After annealing at 2800°C, the reactivity was reduced to the unirradiated value.

Experiments with single crystals of graphite have shown that neutron irradiation not only increases the number of active sites at the edges of the crystals, but also causes active sites to appear on the crystal faces.²⁰ Unirradiated crystals were attacked by oxygen only at crystal edges and crystal steps, whereas irradiated crystals burned at all surfaces and, as a result, became covered with minute pits visible under the microscope. The pits presumably are initiated at lattice defects caused by the irradiation.

14-3.2 SELF-SUSTAINED BURNING

Self-sustained burning occurs when more heat is generated by the exothermic oxygen-graphite reaction than can be carried away by the

coolant. A number of studies⁷¹⁻⁷⁴ of this condition have been reported for different systems, but it is difficult to form generalizations as yet because of the varying geometries, flows, temperatures, and pressures. Diffusional effects are known to play an important role⁷⁵ and must be evaluated for each system.

Figure 14.16 shows the relation of graphite temperature to the rate of air flow when varying amounts of supplemental heat are added. This experiment was performed in a channel that simulates a fuel channel in the

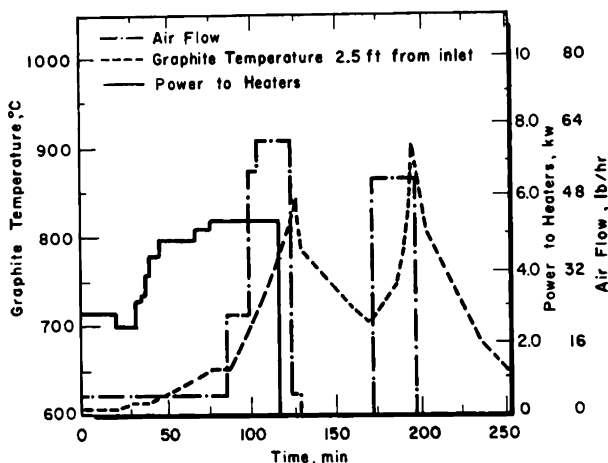


FIG. 14.16 An example of self-sustained burning of Speer-Nuclear 2 graphite in air.⁷³ Inlet temperature is 150°C.

Experimental Gas Cooled Reactor. If the temperature is sufficiently high, increasing the flow rate produces more heat by reaction than can be removed. This is a peculiar case where lower graphite temperatures are obtained when the flow of coolant air is reduced.

14-3.3 IRRADIATION EFFECTS IN OXYGEN

Excitation and ionization of O_2 by irradiation lead to the formation of oxygen atoms and ozone. In the gas phase the steady-state concentration of ozone ranges from 0.04 to 0.4 mole %. An average of 0.5 to 1 molecule of O_3 is formed per ion pair.⁷⁶ Studies in condensed phases indicate that most O_3 is formed as a result of excitation rather than ionization. Little is known about the radiation stability of O_3 itself, but, assuming that formation and decay both occur as first-order processes, the rate constant for decomposition is two or three orders of magnitude higher than the rate constant for formation. The temperature dependence of the decomposition has not been studied.

The dissociation of O_2 in a radiation field is sensitive to the presence of gaseous impurities. A trace of H_2O is an effective catalyst.^{77,78} When a microwave generator is used to dissociate O_2 , a strong catalytic effect is

observed for the production of oxygen atoms when traces of N_2 , NO, N_2O , or H_2 are present.⁷⁹ No effect is found when He, A, or CO_2 are added.

14-3.4 RADIATION-INDUCED OXYGEN-GRAPHITE REACTION

As in the case of the carbon dioxide-graphite system, a radiation-induced reaction also occurs between oxygen and graphite, although no mechanism has been generally accepted. Only fragmentary results have been reported on the effects of temperature, pressure, flow, and radiation intensity.

(a) *Temperature.* Since the radiation-induced reaction occurs by the formation and subsequent reaction of oxygen atoms or ozone (acting as an oxygen-atom carrier) with graphite, little temperature effect is expected or found.⁸⁰ One report,⁶⁸ not yet fully explained, presents data which indicate that a reproducible inhibition takes place at 350 to 400°C in a radiation field. The observed reaction rate is about six times slower than the thermal rate. Further work is necessary to clarify this anomalous result.

(b) *Pressure.* Oxidation rates are dependent on the total gas pressure and in most circumstances are directly proportional to it. When the partial pressure is reduced by addition of an inert gas such as helium, the reaction rate decreases, probably as a result of the reduction in the energy absorbed per unit volume by oxygen molecules.⁸⁰ The resultant rate, however, is greater than for pure oxygen at a pressure equal to its partial pressure in the mixture. Thus the inert gas transfers absorbed energy to the oxygen molecules, increasing the production of oxygen atoms.

(c) *Irradiations in Air.* In the thermal reactions with graphite discussed here, oxygen and air have been used interchangeably, and only the necessary corrections for the partial pressure of oxygen have been made. Under irradiation, however, it may not be proper to consider nitrogen as an inert diluent. In fact, in the absence of carbon, much of the oxygen is known³⁴ to be consumed in the formation of NO_2 and N_2O . In a sealed quartz vessel at 85°C and a total pressure of 3.29 atm, irradiation⁸¹ at 1.8×10^7 rad/hr for a few months produces 62.5 per cent N_2 , 20.3 per cent NO_2 , and 5.7 per cent N_2O with no detectable O_2 . Thus, in the air-graphite system, the gaseous species and the solid may compete for oxygen atoms. No experimental evidence on this point has been reported.

(d) *Flow.* The effects of flow and geometry are closely related. Here again, as in the carbon dioxide-graphite system, at a given flow rate the reaction rate varies with the volume of gas upstream within the radiation field. The effect of changing the flow rate is complex⁸⁰ and involves the rate of production of oxygen atoms and/or ozone in the gas, residence time in the prereaction volume, and the rate of recombination of oxygen atoms. It is difficult to compare results from one experimental system to another.

(e) *Radiation Intensity.* To a first approximation the reaction rate is directly proportional to the reactor power.⁸⁰ The approximation is best

under conditions in which the rate of oxidation by the gas activated within the pores is much greater than the reaction at the external surface.

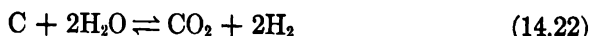
14-4 Steam-Graphite System

Steam reacts too rapidly to be used as a reactor coolant with unprotected graphite. The interest in this reaction from a technological standpoint arises from the fact that water may be present as an impurity in an inert coolant gas. One potential source is water from the secondary heat-transfer system, which may enter the primary coolant through small leaks in the heat exchanger. Water may also be added in small quantities for a specific purpose. The reduction of hydriding in metal tubing⁸² is an example of this type of application.

There is a striking similarity between the steam-graphite system and the carbon dioxide-graphite system. It is generally held that the mechanisms of both reactions involve surface complexes; the differential rate equations are of similar form; the reaction rates for given conditions of temperature, pressure, and flow are of about the same order of magnitude; and the observed orders and activation energies are similar.

14-4.1 THERMAL REACTION

Steam reacts with carbon to produce CO, CO₂, H₂ and CH₄. The distribution of products is a function of the temperature and pressure, as illustrated in Fig. 14.17. The primary reactions are probably



although it would be difficult to distinguish between the direct formation of CO₂ by Eq. 14.22 and a two-step production involving Eq. 14.21 and a secondary reaction between CO and H₂O to produce CO₂ and H₂.

Secondary reactions that definitely occur are



Although more elaborate mechanisms have been suggested^{7,14} for the steam-graphite reaction, the one proposed by Gadsby⁸³ and by Johnstone⁸⁴ is sufficient to describe most of the experimental results. The mechanism for the primary reactions may be written as



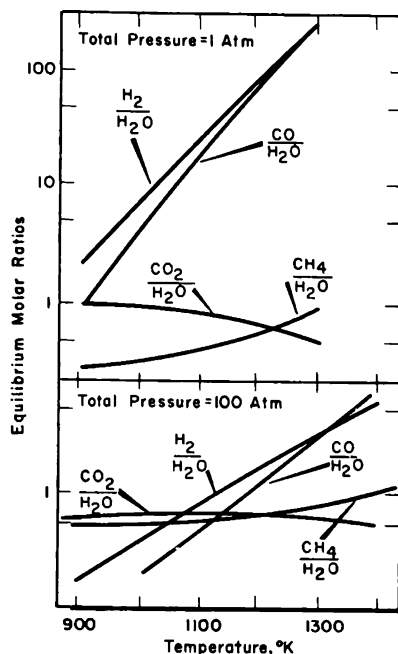


FIG. 14.17 Equilibrium product-steam ratios for the steam-graphite system in which only steam and graphite are present initially. (From Walker et al., *Advances in Catalysis*, Ref. 3.)

which is analogous to Eqs. 14.7, 14.8, and 14.9 for the carbon dioxide-graphite reaction.

14-4.2 KINETICS OF THE THERMAL REACTION

Using the Gadsby mechanism and considering surface coverage, Walker et al.³ have shown that the appropriate differential rate equation for the steam-graphite reaction is

$$\text{Gasification rate} = \frac{[k_1 k_3 / (k_2 + k_3)] p_{\text{H}_2\text{O}}}{1 + (k_4 / k_5) p_{\text{H}_2} + [k_1 / (k_2 + k_3)] p_{\text{H}_2\text{O}}} \quad (14.28)$$

This equation is similar in form to Eq. 14.11 for the carbon dioxide-graphite reaction. In general, the rate of the steam-graphite system is greater but only by a factor of about 3.

The analysis that gives the kinetic order of the reaction at various pressures in the steam-graphite system is analogous to that for the carbon dioxide-graphite system, and again reaction orders from zero to one are observed experimentally³ for different conditions of temperature and pressure. Activation energies of 60 to 80 kcal/gram atom have been reported^{57, 85} for the gasification of carbon by steam, except under conditions where mass-transport control is important. In this case somewhat lower activation energies are observed.⁸⁰⁻⁸⁹

Figure 14.18 shows the effects of small amounts of water in argon. In the range 0 to 600 ppm by volume, the gasification rate increases linearly with increasing water content. The difference in rates of PGA and EY9 at

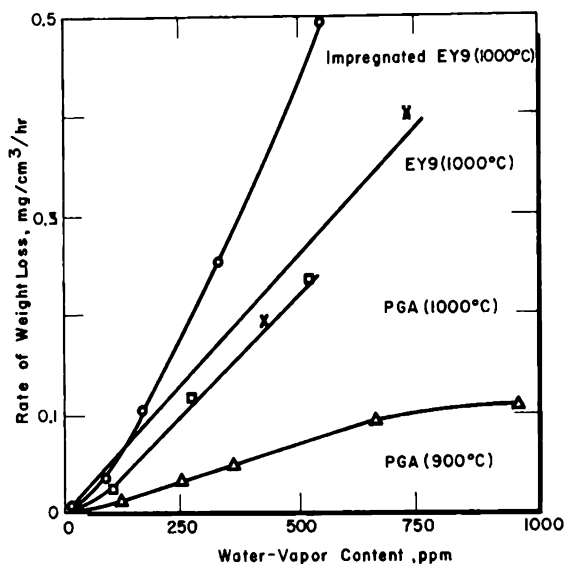


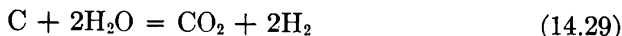
FIG. 14.18 Gasification rates of several graphites in argon containing water vapor. (From Antill and Peakall, *Journal of Nuclear Materials*, Ref. 90.)

1000°C is related to the purity of the graphite. The high oxidation rate of EY9 impregnated with furfuryl alcohol is attributed to the increased reactivity of the ungraphitized impregnant char.

14-4.3 RADIATION-INDUCED STEAM-GRAPHITE REACTION

Although no information has been reported on the effects of radiation on the steam-graphite reaction, the general results can be predicted from radiation effects observed in water vapor and pure liquid water and in water solutions.^{76, 91-95} Primary recombination of the ions and radicals that result from energy absorbed in a radiation field leads to the formation of H_2 and H_2O_2 . Secondary reactions produce O_2 and H_2O from the H_2O_2 , which is not stable under irradiation. The net result is the radiolytic decomposition of water into hydrogen and oxygen. Figure 14.19 shows the effect observed in bubbling (oxygenated) water in an X-ray field. A small steady-state concentration of H_2O_2 is formed, and H_2 and O_2 are released from the liquid. The effect of bubbling is to aid in the release of the gases as they are formed.

To date, no experimental information is available on the steam-graphite reaction in a radiation field. However, some results have been obtained⁴³ on the radiation-induced reaction of graphite with liquid water at a temperature of about 30°C. In this case the equation for the over-all reaction is



It might be anticipated that, when studies are conducted on the steam-graphite system, they will reveal the complex effects of carbon oxidation by the ordinary thermal reactions in addition to the attack of graphite by the active species produced by irradiation of the steam. These species may

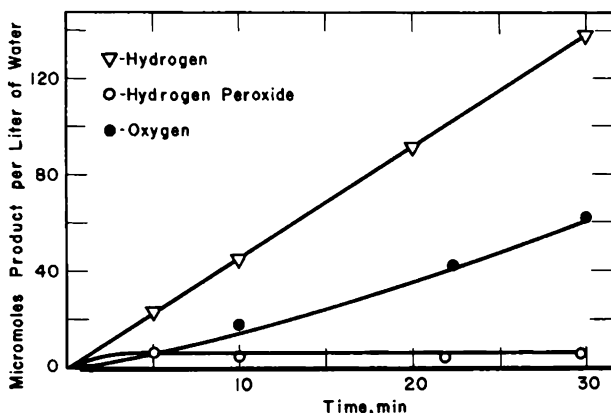


FIG. 14.19 Decomposition of oxygenated water⁹⁶ at 25°C. The X-ray dosage was 7.5×10^{20} ev/liter/min.

include H, H₂, O, O₂, CO₂, OH, and H₂O₂ in ionized or excited forms. The products and their relative distributions are expected to be complex functions of the system geometry, temperature, pressure, and flow. Above some temperature in the range of 500 to 600°C, the thermal reaction, by virtue of its higher activation energy, may be expected to predominate over the radiation-induced reaction (see Sec. 14-1.10).

14-5 Hydrogen-Graphite System

14-5.1 THERMODYNAMICS

The thermodynamic properties of the graphite-hydrogen reaction have interesting implications in the use of hydrogen as a high-temperature coolant in graphite-moderated reactors. The over-all reaction occurs according to the equation



Under most conditions methane is the sole product.⁹⁷ As shown in Fig. 14.20, hydrogen is virtually inert to graphite at high temperatures and pressures in the vicinity of 1 atm. At atmospheric pressure and temperatures in excess of 800°C, less than 5 per cent CH₄ exists at equilibrium, whereas at temperatures above 1000°C less than 1 per cent CH₄ is present. Thus, irrespective of the rate of attaining equilibrium, the loss of H₂ and conse-

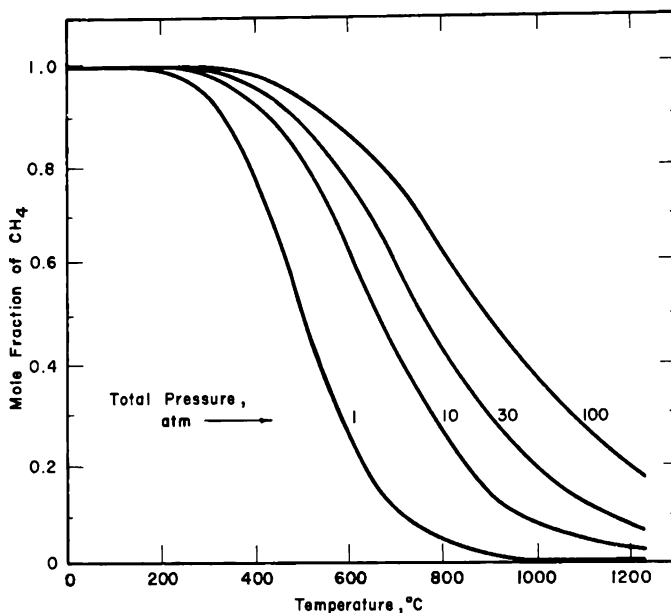


FIG. 14.20 The mole fraction of methane formed at equilibrium for the hydrogen-graphite reaction. Hydrogen and methane are assumed to behave as ideal gases, with no methane present initially.⁹⁸

quently of graphite is small. At higher total pressures the extent of CH_4 production increases markedly, but again the equilibrium mole fraction of CH_4 decreases rapidly with increasing temperature.

The equilibrium constants presented in Table 14.5 demonstrate that the production of the higher hydrocarbons, C_2H_6 , C_2H_4 , and C_2H_2 , is severely

Table 14.5 — EQUILIBRIUM CONSTANTS FOR THE FORMATION OF HYDROCARBONS FROM GRAPHITE AND HYDROGEN^{98, 100, 101}
(Gas pressures in atmospheres)

Hydro-carbon	Log K						
	300°K	500°K	700°K	900°K	1100°K	1300°K	1500°K
C_2H_6	5.665	- 0.514	- 3.409	- 5.106	- 6.220	- 7.001	- 7.577
C_2H_4	-11.887	- 8.417	- 7.082	- 6.400	- 5.990	- 5.717	- 5.520
C_2H_2	-36.406	-20.629	-13.892	-10.170	- 7.816	- 6.196	- 5.013

limited by the preferential formation of CH_4 . At extremely high temperatures, in the range from 2000 to 3000°K, significant amounts of C_2H_2 as well as CH_3 , CH_2 , CH , and atomic hydrogen are formed.⁹⁹

In general, experimental investigations of the thermal equilibrium between H_2 and various forms of carbon agree reasonably well with the results obtained by calculation. Travers,¹⁰² in an investigation of the reac-

tion between sugar charcoal and H_2 , found about 13 per cent CH_4 at $712^\circ C$ and atmospheric pressure. At $800^\circ C$ and a total pressure of 1.05 atm, 3.2 per cent CH_4 was present in the H_2 in equilibrium with nuclear graphite.⁹⁷ At higher temperatures in the equilibrium between H_2 and arc-lamp carbon, the CH_4 content decreased¹⁰³ to a minimum value of 0.26 per cent at $1450^\circ C$. At temperatures in excess of $2000^\circ C$, C_2H_2 and C_2H_4 appeared in the gas phase. The hydrogen-carbon equilibrium can also be approached from the CH_4 side.¹⁰⁴

An interesting feature of the hydrogen-carbon equilibrium is that carbon removed from the cooler fringe regions of a graphite moderator will be deposited in regions where the temperature is higher. This behavior may be contrasted to the carbon dioxide-graphite system, where mass transfer of carbon proceeds in the opposite direction.

14-5.2 MECHANISM AND KINETICS

The kinetics and mechanism of the hydrogen-graphite reaction have not been thoroughly studied. A number of investigations have been concerned primarily with the sorption of hydrogen on various forms of carbon. Perhaps the most complete investigation to date is a study¹⁰⁵ of the interaction of hydrogen with a low-temperature carbon char in the temperature range 816 to $927^\circ C$. Several mechanisms for the hydrogen-carbon reaction can be postulated which lead to rate expressions showing qualitatively similar behavior. In general, these mechanisms include the establishment of a steady-state concentration of a surface hydride, which, in turn, reacts with H_2 to form CH_4 . In the case of the carbon char, the rate law derived¹⁰⁵ is of the form

$$\frac{d(CH_4)}{dt} = \frac{Ap_{H_2}^2}{1 + Bp_{H_2}} \quad (14.31)$$

where A and B are constants.

From Eq. 14.31, it is evident that at high pressures where $Bp_{H_2} \gg 1$ the rate of CH_4 production should be first order with respect to H_2 , whereas at low pressures where $Bp_{H_2} \ll 1$ a second-order dependence is expected. At $927^\circ C$ and high burn-offs, the order of the hydrogen-char reaction decreased with increasing pressure as predicted.¹⁰⁵ The range of pressures (10 to 30 atm) was, however, believed to be too small to provide a rigorous test of Eq. 14.31.

It is further observed that the CH_4 formed does not retard the reaction other than through the approach to equilibrium.¹⁰⁵ The back reaction, the thermal decomposition of CH_4 , is first order with respect to the CH_4 concentration.⁹⁷

(a) *Temperature.* In the temperature range from 600 to $800^\circ C$, the reaction of nuclear graphite with H_2 proceeds with an activation energy of 65 kcal/mole (Fig. 14.21). At temperatures below $600^\circ C$, the activation

energy appears to decrease. It has been suggested^{97,102,104} that the production of CH_4 at these lower temperatures is of secondary importance to the chemisorption of H_2 . The activation energy of 65 kcal/mole for nuclear graphite is in fair agreement with the value found for a low-temperature char at high burn-off.¹⁰⁵ In the latter case Arrhenius plots give good straight lines at a given burn-off, the activation energies increasing with increasing burn-off. At 0 per cent burn-off, an activation energy of about 17 kcal/mole

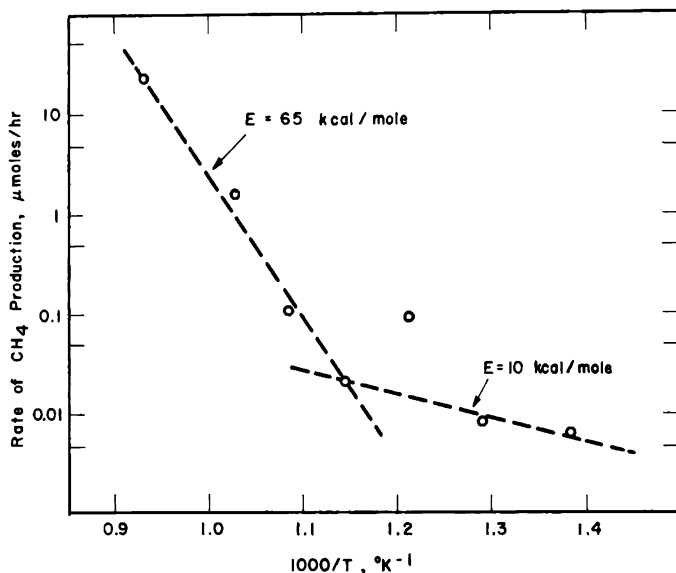


FIG. 14.21 Temperature dependence of the rate of reaction of PGA graphite with hydrogen at 1.05 atm. (From Corney and Thomas, Ref. 97.)

is observed, whereas at 60 per cent burn-off the value increases to approximately 50 kcal/mole and approaches a limiting value. Although this increase in activation energy might be attributed to the attainment of a more uniform structure, the interpretation is highly complicated by the variable composition of the char, which initially contained about 82 per cent carbon, 14 per cent ash, and 1 per cent hydrogen.¹⁰⁶ The remaining 3 per cent consisted of sulfur, nitrogen, and oxygen.

(b) *Catalysis.* The effect of catalysts on the rate of reaction of graphite with hydrogen has not been studied directly. Catalysts have been employed, however, to investigate the carbon-hydrogen equilibrium at low temperatures where the study would otherwise have been precluded by time limitations. Browning and Emmett¹⁰⁷ studied the equilibrium in the temperature range 380 to 838°C, using carbon prepared by decomposing iron carbide, the iron catalyzing the reaction. Troesch¹⁰⁸ obtained equilibrium values at temperatures as low as 143°C by employing carbon supported on

a nickel catalyst. It is readily apparent from these examples that impurities could have a pronounced effect on the rate of reaction of hydrogen and graphite.

(c) *Adsorption.* Active sites on the graphite surface play an important role in the reactions of gases with graphite. In the case of hydrogen, the effect of active sites is especially pronounced at temperatures below 600°C, where adsorption is presumably rate controlling. If the graphite sample is carefully outgassed, a small amount of fast nonactivated chemisorption of hydrogen occurs on nuclear graphite even at -196°C where physical adsorption is predominant.¹⁰⁹ A temperature of 400°C is required to adsorb additional hydrogen, but at this temperature the rate of adsorption is very slow. In the range 600 to 750°C, adsorption is rapid, whereas above 900°C methane appears in the gas phase. In general, the adsorption isotherms observed^{109,110} are equivalent to Temkin isotherms.¹¹¹ It is of interest to note that, although no adsorption of hydrogen molecules occurs at room temperature, large amounts of hydrogen atoms created at low pressure by an electric discharge are adsorbed.¹¹²

It is generally agreed that adsorption occurs on the edge atoms of the graphite lattice with little or no adsorption occurring on or between the basal planes. Dzurus et al.¹¹³ have shown by measuring the Hall coefficient and magnetoresistance that no true homogeneous lamellar compound of graphite and hydrogen is formed.

Hydrogen and oxygen compete for active sites, and at -196°C a pre-adsorbed film of oxygen completely inhibits¹⁰⁹ the fast nonactivated chemisorption of hydrogen. At 400°C hydrogen reacts¹¹⁴ with oxygen adsorbed on bone char to form water. At 1000°C hydrogen treatment is very effective in removing carbon-oxygen complexes from a partially graphitized carbon black (Graphon)¹¹⁵ and from graphite.¹⁰⁹ Two hydrogen atoms replace every oxygen atom removed from the surface, suggesting that the surface oxide is ketonic.¹⁰⁹

The activation energy for adsorption of hydrogen increases, and the heat of adsorption and activation energy for desorption decrease with increasing surface coverage. For a nuclear graphite¹¹⁰ outgassed at 2000°C, the activation energy for desorption, E' , as a function of the fractional surface coverage, θ , is given by

$$E' \text{ (kcal/mole)} = 137 - 42\theta \quad (41.32)$$

where $0.32 < \theta < 0.68$ and $1035^\circ\text{C} < T < 1375^\circ\text{C}$. From isotherms at 1335 and 1475°C, the heat of adsorption, Q , is approximated by the relation

$$Q \text{ (kcal/mole)} = 58 - 56\theta \quad (14.33)$$

for $0.50 < \theta < 0.80$. Since the activation energy for adsorption is given by

$$E = E' - Q \quad (14.34)$$

$$E \text{ (kcal/mole)} = 79 + 14\theta \quad (14.35)$$

for $0.50 < \theta < 0.68$.

14-5.3 RADIATION EFFECTS

The presence of radiation has a pronounced effect on the reaction of graphite with hydrogen, primarily as a result of the formation of highly reactive intermediates in the gas phase. As previously indicated, hydrogen atoms formed by an electrical discharge are readily adsorbed by graphite at room temperature. Hydrogen atoms also react with soot at 45°C to form methane and lesser amounts of higher hydrocarbons.¹¹⁶

When the hydrogen-graphite system is exposed to radiation within a nuclear reactor, CH₄ is formed at temperatures where the thermal reaction is extremely slow.⁹⁷ In an experiment of more than 500 hr duration, the combined amount of C₂H₆ and C₃H₈ did not exceed about 2 per cent of the CH₄ produced.

The active species formed during irradiation are believed to be hydrogen atoms or ionized hydrogen molecules with very short lifetimes. Only those molecules activated near the graphite surface react before becoming deactivated. The rate of methane production⁹⁷ is approximately proportional to the hydrogen pressure in the range 400 to 800 mm Hg. At the higher pressure more energy is absorbed by the hydrogen, and hence more active species are formed, leading to faster rates. Insufficient data are available to permit an Arrhenius plot; however, the results of Corney and Thomas⁹⁷ indicate that the activation energy for the radiation-induced reaction is probably less than 10 kcal/mole. The *G* value (the number of molecules of methane formed per 100 ev absorbed by the hydrogen) depends upon the volume of hydrogen used in the calculation. Consideration of only the hydrogen within the pores of the graphite results in an average *G* value of about 10.

The radiation-induced decomposition of methane is of interest with regard to the possible back reaction indicated by Eq. 14.30. The decomposition has been investigated using alpha particles^{117, 118} and 12-Mev deuterons.¹¹⁸ In both cases hydrocarbons up to pentane are formed. Alpha particles produce a small amount of unsaturated liquid with the empirical formula C_{*n*}H_{1.98*n*}. With increasing exposure the concentration of higher hydrocarbons decreases, and ultimately hydrogen is the predominant species in the gas phase. The ion-pair yield (the number of molecules of methane decomposed per ion pair formed in the methane) ranges from 2.0 to 2.5.

In several respects hydrogen holds considerable promise as a coolant for nuclear reactors, especially for high-temperature applications. Further investigation of both the thermal and radiation-induced reactions will be

necessary, however, to clarify the reaction mechanisms and to determine precisely the temperature and pressure dependence of the reaction rates.

14-6 Other Gases

Of the gases that are not considered in the preceding sections, only helium and nitrogen are of current interest as reactor coolants. The reactions of graphite with gases that might enter the reactor as impurities will, however, also be examined.

14-6.1 HELIUM

Helium has found extensive use as a reactor coolant, and, although it is generally considered to be completely inert, the possibility of mass transport of graphite by excited helium atoms and by helium ions has caused some concern. Experiments employing microwave activation of helium have demonstrated that no carbon transport occurs which cannot be accounted for by impurities in the helium.¹¹⁹ In addition, studies of the graphite-helium system under reactor irradiation have revealed no carbon transport.¹²⁰

The erosion of graphite by high-temperature helium jets has also been investigated.¹²¹ With the helium and the graphite surface heated to 2000°C, it is found that, after the loosely bound particles resulting from machining are blown free, no further erosion occurs if the helium is free from oxygen and entrained particles.

14-6.2 NITROGEN

Although pure nitrogen has not been employed extensively as a coolant, under most conditions it is relatively inert to graphite. The formation of significant amounts of cyanogen by the reaction



is not thermodynamically feasible in the temperature range 300 to 3000°K. The equilibrium constant derived from free-energy functions for graphite,¹²² nitrogen,¹²³ and cyanogen^{124,125} is 2.7×10^{-52} at 300°K; this increases to 8.7×10^{-4} at 3000°K. It is clear that only at very high nitrogen pressures will the pressure of cyanogen be significant even at 3000°K.

The only rate data on the nitrogen-graphite system must be considered preliminary;¹²⁶ no products were analyzed nor mechanisms proposed. The data did suggest, however, that the activation energy is about 78 kcal/mole in the temperature range 2500 to 2900°K.

In contrast to the reaction with molecular nitrogen, the reaction of graphite with atomic nitrogen to form cyanogen theoretically goes to completion in the temperature range 300 to 1500°K. At 300°K the calculated equilibrium constant is 1.2×10^{67} , whereas at 1500°K it has decreased to 1.0×10^{10} . On the other hand, experimental investigations have often

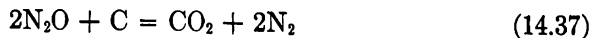
indicated that no reaction occurs. Strutt,¹²⁷ employing nitrogen activated by an electric discharge, found no interaction with carbon at room temperature. Zinman¹²⁸ subjected nitrogen to a 6-Mc radio-frequency field and then allowed it to flow over spectroscopic carbon rods at 800°C which were located 25 cm downstream from the discharge. Neither cyanogen nor paracyanogen were formed, although, when a small amount of hydrogen was added, significant amounts of hydrogen cyanide were obtained. Giberson,¹²⁹ using microwave-activated nitrogen, found that the active nitrogen reacts with graphite to form paracyanogen but only when the graphite sample is positioned directly in the discharge glow.

Two explanations for the observed behavior of the graphite-nitrogen atom system are plausible. Either the lifetime of the nitrogen atoms is so short that few reach the carbon surface, or the concentration of cyanogen is rapidly diminished by the reverse of Eq. 14.36. Prolonged heating of cyanogen at 1250°C results in the formation of cyanide radicals and ultimately of paracyanogen.¹³⁰ Negligible carbon deposition occurs in the absence of a catalyst. When subjected to an electric discharge, cyanogen reverts to paracyanogen rather than to carbon and nitrogen.¹³¹ It therefore appears that the former explanation is correct.

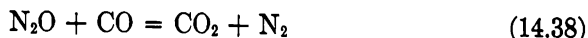
14-6.3 OXIDES OF NITROGEN AND AMMONIA

The radiolysis of air results in the formation of oxides of nitrogen.^{34, 81} These gases may be present therefore when air is employed as a coolant or when air leaks into a coolant stream.

The reaction of nitrous oxide with carbon filaments at temperatures between 900 and 1600°C shows a remarkable similarity to the reactions of CO₂ and H₂O with carbon.¹³² However, in contrast to CO₂ and H₂O, which do not react with charcoal at 400°C at a measurable rate, N₂O reacts rapidly with charcoal at this temperature to give CO₂. At higher temperatures CO rather than CO₂ is formed. Nitrous oxide also reacts with CO in the presence of charcoal to give CO₂. The over-all reactions are represented by



and



Between 278 and 380°C the activation energy for Eq. 14.37 is 32 kcal/mole; the activation energy¹³³ for Eq. 14.38 is 12 kcal/mole.

Nitric oxide reacts with sugar charcoal below 200°C to give N₂ and surface oxides, whereas, in the temperature range 450 to 600°C, N₂, CO₂, and CO are obtained as major products.¹³⁴ Some N₂O is also found,¹³⁵ but no C₂N₂. Depending upon the nature of the surface, the activation energy¹³⁴ varies from 15.0 to 18.3 kcal/mole.

Ammonia, which may occur in minor amounts in a coolant stream, forms HCN upon reaction¹³⁶ with amorphous carbon in the temperature range 700 to 900°C. Neither Ceylon graphite nor diamond heated in NH₃ for 3 hr at 700°C react, however.

14-6.4 HALOGENS

Chlorine and bromine have been investigated as inhibitors of graphite oxidation (Sec. 14-7.2) and as such may enter a reactor coolant system.

Chlorine reacts with graphite at temperatures below 0°C to form a series of lamellar compounds (Sec. 6-5.3) with chlorine concentrations up to C₈Cl, but no reaction occurs above this temperature which can be detected by changes in the magnetic susceptibility.¹³⁷ Even at temperatures up to 1650°C, dry Cl₂ does not measurably attack graphite.¹³⁸

At room temperature natural graphites react with bromine from an atmosphere saturated with Br₂ vapor to form^{139,140} the lamellar compound C₈Br. Under similar conditions pyrolytic graphite¹⁴⁰ attains the composition C_{9.2}Br, whereas electrographite¹³⁹ forms C₁₀Br. The rate of bromination is more rapid with natural graphite than with pyrolytic graphite. When the external pressure of Br₂ vapor is reduced, Br₂ is evolved from the compound, leaving a residue containing from 3 to 10 per cent bromine.¹³⁷ The graphite cannot be completely freed from bromine even at red heat.

Of the remaining halogens, iodine does not react with graphite, and below about 400°C graphite is stable to fluorine.¹³⁷ At 420°C the reaction with fluorine yields carbon monofluoride.¹⁴¹ From 500 to 700°C the reaction is often explosive. Above 700°C graphite burns in F₂, yielding a mixture of fluorocarbons including CF₄ and C₂F₆.

14-7 Inhibitors and Protective Coatings†

The trend to higher temperatures in graphite-moderated gas-cooled reactors accentuates two problems: (1) In considering possible catastrophic accidents, one must assess the consequences of a coolant-line rupture that would allow the displacement of the inert coolant by air. This could lead to serious damage to the reactor core and to the spread of radioactive contamination. (2) The reaction of trace impurities in the coolant with the graphite moderator could substantially reduce the reactor life. The necessity of reducing or eliminating gas-graphite reactions in these reactors has led to increased activity in the investigation and to the development of inhibitors and protective coatings. These agents have the potential of reducing the rate of gas-graphite reactions in the event of a catastrophe or during normal operation. If successfully developed, they would allow a wider choice of coolant gases with less stringent purity requirements and would make gas-cooled reactors more attractive to nations lacking a natural supply of helium.

† This section was written by J. L. Jackson and R. E. Dahl, Hanford Laboratories.

14-7.1 SOLID-PHASE INHIBITORS

Solid-phase inhibitors are chemical compounds which, when deposited on or within the graphite in trace quantities, reduce gas-graphite reaction rates by reduction of the concentration of active carbon sites. These inhibitors are adsorbed on active carbon sites, in contrast to the deposition of thicker refractory coatings.

Phosphate compounds, certain of which significantly improve the oxidation resistance of graphite, have been the most thoroughly studied of the solid-phase inhibitors.^{5,142} Figure 14.22 shows the reaction rate of carbon

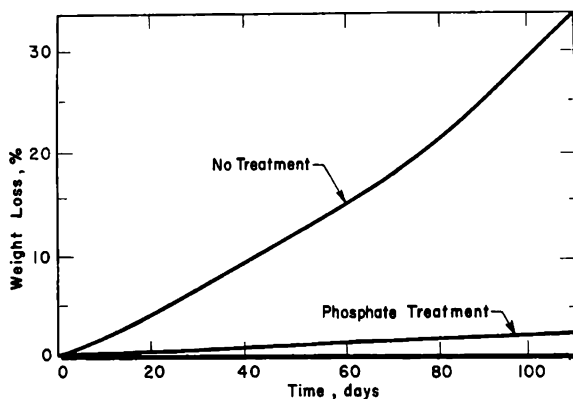


FIG. 14.22 Oxidation of phosphate-treated graphite in carbon dioxide at 700°C. The curves are the averages for three pairs of specimens.⁵

dioxide with phosphate-treated samples compared to the rate with untreated samples. The samples were pretreated by exposure to vapors of refluxing trimethyl phosphate, followed by rapid heating to 1000°C in an argon atmosphere. Comparable results have been obtained by pretreatment with phosphorus pentoxide, followed by a similar heating step. Many phosphate compounds, including syrupy phosphoric acid, have been found¹⁴³ to inhibit the oxidation of graphite.

The inhibition of oxidation appears to occur by formation of a chemisorbed layer of the inhibitor over the active carbon atoms. The effectiveness of trace quantities of phosphate added to the samples is consistent with this theory. In the case of phosphorus inhibitors, the actual chemisorbed species is not known. However, the quantity of phosphorus in the graphite is of the order of that required for the formation of a monolayer of a species such as P_4O_{10} or for the coverage of edge sites by phosphate groups.⁵

In-pile experiments indicate that phosphate pretreatment in its present state of development will not provide suitable oxidation resistance for nuclear-reactor applications.⁵ Phosphate-treated samples exhibit approximately the same oxidation rate as untreated samples during in-pile ir-

radiation in carbon dioxide in which the gamma flux is about 1.3×10^8 r/hr and the graphite temperature is 460 to 500°C. The rate-determining factor is evidently the production of active species in the gas phase. Because the irradiated gas is sufficiently active to react with any surface carbon atom, simply covering the active sites on the graphite does not reduce the rate.

Although phosphate treatment does not reduce the in-pile oxidation rate, it does reduce the postirradiation oxidation rate.⁵ This indicates that the chemisorbed layer is not dislodged by irradiation. The irradiations performed to date have been of short duration (nine days), but the results offer some hope that at high temperature, where the thermal oxidation rate is much greater than the radiation-induced rate, phosphate compounds will effectively inhibit oxidation.

14-7.2 GAS-PHASE INHIBITORS

Certain gases, when admixed in trace quantities in a gas-graphite system, retard the reaction rate of graphite. These gas-phase inhibitors have been studied for a number of years^{55, 144} as an aid to understanding carbon oxidation; however, with the development of the high-temperature gas-cooled reactors, interest has centered on this type inhibitor because it appears to have potential as a reactor safeguard.

Halogen compounds are the most effective gas-phase oxidation inhibitors that have been studied to date. Among those which have been investigated are chlorine, bromine, carbon tetrachloride, and phosphorus oxychloride.¹⁴⁵ Of these, chlorine has been most seriously considered for reactor applications because it is readily available and is inexpensive. Relatively low concentrations effectively reduce the oxygen-graphite reaction rate (Fig. 14.23). This reduction has also been observed in combustion experi-

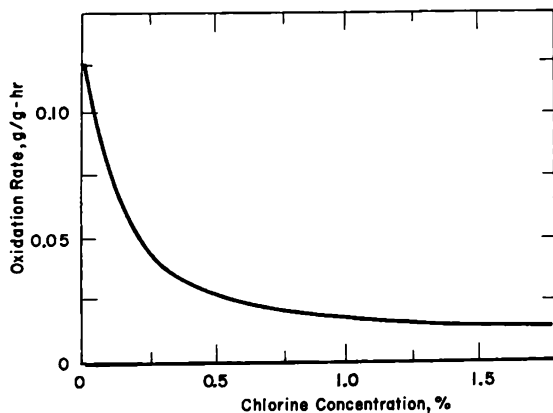


FIG. 14.23 Inhibition of the oxidation of graphite in a stream of air by chlorine.¹⁴⁶

ments in which 2 per cent chlorine in an oxygen stream extinguished petroleum coke⁴⁹ burning at 1730°C and nuclear graphite¹⁴⁶ at 1200°C.

Several mechanisms have been proposed to account for the manner in which chlorine and other halogens inhibit oxidation of carbon compounds. A plausible explanation is that chlorine chemisorbs at active sites on the surface, effectively denying access to them by the oxidant. The rate law derived on this assumption indicates that the oxidation rate is inversely proportional to the square root of the chlorine concentration.¹⁴⁶

A gas-phase inhibitor has several desirable features as a reactor safeguard. It can be stored out of the radiation zone prior to use, whereas a solid-phase inhibitor or protective coating must be subjected to an extended reactor environment, which is potentially damaging. A disadvantage in the case of halogens is their toxic and corrosive nature; however, if used in averting a serious accident, the corrosion effects would be of secondary importance. The testing of chlorine in a reactor environment has only recently begun, and a complete evaluation of gas-phase inhibitors cannot be made at this time.

14-7.3 PROTECTIVE CARBIDE COATINGS

To fulfill the requirements for use in a nuclear reactor, a coating should have the following properties: it must protect the graphite from oxidation, resist wear, have a low cross section for thermal neutrons, and maintain its structural integrity under severe thermal stress. Many investigators have produced coatings that meet these requirements in part. In the subsequent paragraphs some of the methods used for coating graphites and the type and quality of the coatings produced will be discussed.

One method¹⁴⁷ used to produce protective coatings for graphite involves the vapor decomposition of a suitable halide. Silicon coatings approximately 0.01 in. thick are formed by the hydrogen reduction of silicon tetrachloride on a graphite surface heated to 1075°C. Coatings of this type afford protection for several hundred hours at 1370°C in air. Failures result at temperatures in excess of 1370°C, at which temperature silicon is rapidly converted to silicon dioxide and silicon carbide. Cracks that develop in the coating seldom lead to failure because they are soon filled with silicon dioxide.

A slightly different approach employs a process in which halides of niobium, tantalum, and zirconium are thermally decomposed on graphite tubes to form carbides.¹⁴⁸ The coating temperature and pressure are chosen to prevent metal deposition but to allow the formation of the carbide. The rate of formation of the carbide is believed to be dependent on the diffusion of carbon to the reacting surface. The coatings that have been produced appear adherent, but no oxidation tests have been reported.

Other attempts¹⁴⁹ have been made to coat graphite using the thermal decomposition of silicon halides at 1900 to 2200°C. Below 1900°C the rate of formation of silicon carbide appears to be too slow to be practical, and above 2200°C the silicon carbide formed is very porous.

Graphite can be coated with solid suspensions by brushing or by dipping. For example, a molybdenum disilicide powder has been applied in a phenolic resin by brushing it on the graphite, air drying for 1 hr, heating to 176°C to polymerize the resin, and then heating further to 217°C in a neutral or reducing atmosphere for 15 min.¹⁵⁰ A glazed, dense coating of molybdenum silicon carbide results, which affords protection at temperatures below 1875°C in a high-velocity stream of oxidizing gases for several 2-min cycles. Failures that occur are at thin spots or pin holes.

A modification¹⁵¹ of the dipping technique involves the impregnation of graphite by quenching in special solutions to form SiC, ZrC, B₄C, and Cr₃C₂. All except the chromium compounds appear to offer some protection from oxidation, but the most effective oxidation barrier is silicon carbide. This method involves heating graphite to 400°C, quenching it in a solution of ethyl orthosilicate suspended in ethyl alcohol, drying, and then firing at 2000°C for 1 min to produce SiC. Additional quenching cycles increase the effectiveness of the coating and reduce the oxidation of the graphite substrate.

Of the different coatings tested to date, the one that most closely meets the requirements for in-pile use is silicon carbide. When properly applied, silicon carbide provides excellent protection for graphite exposed to air at temperatures to 1000°C and above. It is very resistant to wear, has good thermal-shock characteristics, and has a low thermal-neutron cross section. There are, however, several problems associated with its use. At present continuous adherent coatings for reactor use have been applied only to special graphites of small sizes. Most of these test specimens range in size from 2 to 4 in. in length and are from 1/4 to 1/2 in. in diameter. In addition, isotropic graphites with a thermal expansion close to that of silicon carbide are required for the substrate. No really good coatings have been reported for existing nuclear-grade graphites.

Very little information is available on the radiation stability of the silicon carbide coatings. Some current work¹⁵² indicates siliconized silicon carbide (a silicon carbide coating, the pores of which are filled with silicon dioxide) may be very useful in containing fission-product gases in a coated uranium dioxide-graphite fuel element. Development studies¹⁵³ are under way on a number of commercially applied coatings to determine the effect of reactor conditions on the coating integrity.

A silicon carbide coating applied to graphite is shown in Fig. 14.24. Of particular interest is the penetration of the coating material into the substrate pore structure. Coatings of this type have afforded protection to graphite for 160 hr in 1000°C air with no indication of failure, as measured by weight loss from the sample.¹⁵⁴

In addition to the application of a coating to the complete graphite moderator, there are several other potential uses. Process tubes with an impermeable coating of silicon carbide could prevent an oxidizing coolant,

such as carbon dioxide, from reaching the main moderator structure. Silicon carbide-coated graphite tubes in a helium-cooled reactor could serve as a safety backup in case the primary-coolant piping was ruptured and allowed air to enter. The use of a siliconized silicon carbide-coated



FIG. 14.24 Silicon carbide coating on graphite. The dark material at the top is the resin used to hold the sample. The next band of grey and white is the coating (the light grey regions of the coating are silicon carbide; the white regions are silicon dioxide). The bottom dark-grey band is the graphite substrate.

tube either to prevent diffusion of fission products from the fuel to the coolant gas or to keep the contaminated coolant gas from the main moderator structures has also been considered. In the next few years considerably more data will be available to better evaluate the use of carbide-coated graphite bodies for use in nuclear reactors.

14-7.4 PYROLYTIC CARBON COATINGS

Pyrolytic carbon has been produced experimentally for many years. However, it was only with the advent of the space and high-temperature reactor technologies that serious consideration was given to the use of pyrolytic carbon or graphite as a structural material. A considerable research effort is now being devoted to the preparation and properties of this material.

Pyrolytic carbon is prepared by the decomposition of a carbonaceous gas on a heated surface. The reaction has been carried out over a wide range of temperatures from 1400 to over 2000°C. The structure and density of the deposited carbon depend upon the deposition temperature and other factors,¹⁵⁵ and the crystallinity can be developed further by heating the deposit to still higher temperatures after it has been formed. The activation energies for the formation of the carbons are low, ranging from 21 kcal/mole for methane to 32 kcal/mole for benzene. The mechanism proposed by Brown and Watt¹⁵⁴ is quoted below:

1. "The parent hydrocarbon dissociates on the hot surface, with or without deposition of carbon, forming free radicals and possibly complex molecules which pass back into the gas phase.
2. "The products of this reaction undergo repeated decomposition on the hot surface and combination in the gas-phase, in the course of which carbon is deposited and aromatic compounds produced."

It has been reported¹⁵⁶ that the temperature of the deposition surface affects the hydrocarbon composition as well as the mobility of the deposited carbon atoms. It has been noted that the geometry of the deposition chamber has a decided effect on the quality of the deposited material.

Photomicrographs, such as the one shown in Fig. 14.25, illustrate the striking structural development found in pyrolytic carbons. The deposits are highly oriented, with the carbon-layer planes parallel to the surface of the substrate.

Pyrolytic graphite has several distinct properties that set it apart from electrographites. It is highly anisotropic, as can be seen from some of the typical properties listed in Table 14.6. Pyrolytic graphite is a good thermal insulator transverse to the layer planes and is almost as good a conductor as copper parallel to the layer planes.

In contrast to electrographites, pyrolytic graphite is impermeable to gases. It has been reported¹⁵⁷ that pyrolytic graphite is impermeable to helium, even in films 1 to 2 mils thick.

The oxidation rate of pyrolytic graphite is less than that of electrographites. Improvements by a factor of 3 to 10 have been reported.^{154, 156}

The properties of pyrolytic graphite suggest several possible reactor applications for this material. Being impermeable to gases, it is being seriously considered for use as a fuel tube, as a sleeve to isolate the moderator structure from the fuel coolant gases, as insulation for the moderator in the normally cool peripheral region to reduce low-temperature radiation damage, and as a coating on fuel particles.

Pyrolytic graphite as a nuclear material is still in the development stage. Additional research and development work is required to solve certain problems before it can be considered a reliable engineering material. Methods are needed to prevent delamination of thick deposits and to

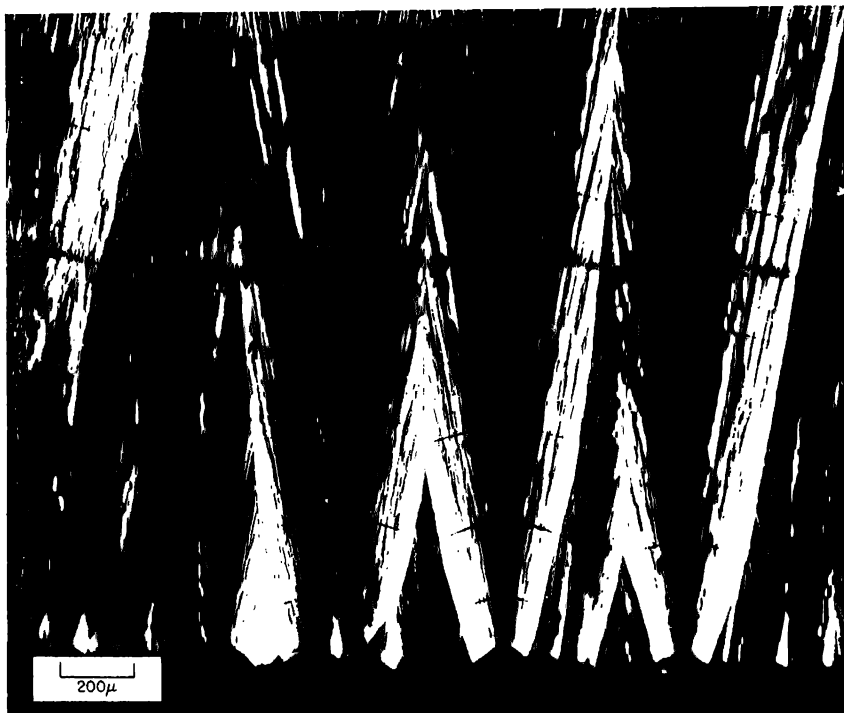


FIG. 14.25 Structure of pyrolytic graphite. The black area at the bottom is the resin holding the sample. The fine black lines in each cone are cracks. The heavy dark line approximately two-thirds of the distance from the bottom of the figure is a soot layer, probably caused by some small variation in gas composition.¹⁵³

Table 14.6 — PROPERTIES OF PYROLYTIC GRAPHITE AND ELECTROGRAPHITE¹⁵⁷

Property at room temperature	Pyrolytic graphite	Electrographite
Bulk density, g/cm ³	1.80 - 2.22	1.60 - 2.0
Tensile strength, psi	15,000 - 20,000	2000 - 4000
Thermal conductivity:		
(II), cal/(sec)(cm)(°C)	0.38 - 0.93	0.45
(I), cal/(sec)(cm)(°C)	0.0048 - 0.0083 [†]	
Electrical resistivity, ohm-cm		
(II)	200 - 250 x 10 ⁻⁶	800 x 10 ⁻⁶
Coefficient of thermal expansion per °C (III)	0.67 x 10 ⁻⁶	1 - 2 x 10 ⁻⁶
Strength/density, psi/g/cm ³	10,000	1340

[†] Absolute value depends on density.

permit production of larger pieces. Engineering properties need to be more carefully defined. The effects of radiation must be determined, and means of obtaining a material of reproducible quality will need to be devised. All these problems can be solved to some degree, and it is probable that in a few years this laboratory curiosity will become a useful material for high-temperature reactor applications.

References

1. J. Hilsenrath and Y. S. Touloukian, The Viscosity, Thermal Conductivity, and Prandtl Number for Air, O₂, N₂, NO, H₂, CO, CO₂, H₂O, He, and A, *Trans. Am. Soc. Mech. Engrs.*, **76**: 967-985 (1954).
2. P. C. Davidge et al., Gas Coolants, in *Reactor Handbook, Vol. 1, Materials*, pp. 979-993, 2nd ed., Interscience Publishers, Inc., New York, 1960.
3. P. L. Walker, Jr., et al., Gas Reactions of Carbon, *Advances in Catalysis*, **11**: 133-221 (1959).
4. K. K. Kelley, Contributions to the Data on Theoretical Metallurgy. X. High-Temperature Heat Content, Heat Capacity, and Entropy Data for Inorganic Compounds, and XI. Entropies of Inorganic Substances. Revision (1948) on Data and Methods of Calculation, *U. S. Bur. Mines Bull.*, No. 476, 1949, and No. 477, 1950.
5. A. R. Anderson et al., Chemical Studies of Carbon Dioxide and Graphite Under Reactor Conditions, in *Proceedings of the Second United Nations International Conference on the Peaceful Uses of Atomic Energy, Geneva, 1958*, Vol. 7, pp. 335-373, United Nations, New York, 1959.
6. F. J. Long and K. W. Sykes, The Catalysis of the Oxidation of Carbon, *J. chim. phys.*, **47**: 361-378 (1950).
7. F. J. Long and K. W. Sykes, The Mechanism of the Steam-Carbon Reaction, *Proc. Roy. Soc. London*, **A193**: 377-399 (1948).
8. E. E. Petersen and C. C. Wright, Reaction of Artificial Graphite with Carbon Dioxide, *Ind. Eng. Chem.*, **47**: 1624-1629 (1955).
9. C. N. Spalaris, *Role of Surface Area in the Kinetics of Oxidation of Graphite*, USAEC Report HW-31928, Hanford Atomic Products Operation, May 24, 1954.
10. T. B. Copestake and N. S. Corney, The Reactions Between Carbon and Carbon Dioxide under Irradiation, in *Proceedings of the US/UK Meeting on the Compatibility Problems of Gas-Cooled Reactors Held at Oak Ridge National Laboratory, February 24-26, 1960*, pp. 76-123, USAEC Report TID-7597 (Bk. 1), March 1961.
11. F. J. Vastola, *A Mass Spectrometric Study of the Carbon-Carbon Dioxide Reaction*, Ph.D. Thesis, Pennsylvania State University, 1958.
12. S. Ergun, Kinetics of the Reaction of Carbon Dioxide with Carbon, *J. Phys. Chem.*, **60**: 480-485 (1956).
13. J. Gadsby et al., The Mechanism of the Carbon Dioxide-Carbon Reaction, *Proc. Roy. Soc. London*, **A193**: 357-376 (1948).
14. A. E. Reif, The Mechanism of the Carbon Dioxide-Carbon Reaction, *J. Phys. Chem.*, **56**: 785-788 (1952).
15. A. Key, The Investigation of the Use of Oxygen and High Pressure in Gasification. V. The Reactions Between Coke and Steam at High Pressure, in *Fifty-third Report of the Joint Research Committee of the Gas Research Board and the University of Leeds*, Gas Research Board, copyright publication No. 40, 1948.
16. R. F. Strickland-Constable, Some Comments on the Work of Key on the Reactions

- Between Coke and Carbon Dioxide and Between Coke and Steam, *J. chim. phys.*, **47**: 356-360 (1950).
17. F. Bonner and J. Turkevich, Study of the Carbon Dioxide-Carbon Reaction Using C-14 as a Tracer, *J. Am. Chem. Soc.*, **73**: 561-564 (1951).
 18. N. S. Corney et al., Experimental Techniques in the Study of the Reaction Between Carbon Dioxide and Graphite Under Irradiation, in *Proceedings of the US/UK Meeting on the Compatibility Problems of Gas-Cooled Reactors Held at Oak Ridge National Laboratory, February 24-26, 1960*, pp. 2-15, USAEC Report TID-7597 (Bk. 1), March 1961.
 19. C. N. Spalaris, *Surface Studies of Irradiated Graphite*, USAEC Report HW-29082, Hanford Atomic Products Operation, July 14, 1953.
 20. G. R. Hennig et al., Radiation Effects on the Oxidation and on Other Chemical Properties of Graphite, in *Proceedings of the Second United Nations International Conference on the Peaceful Uses of Atomic Energy, Geneva, 1958*, Vol. 7, pp. 301-306, United Nations, New York, 1959.
 21. P. L. Walker, Jr., and F. Rusinko, Jr., Gasification of Carbon Rods with Carbon Dioxide, *J. Phys. Chem.*, **59**: 241-244 (1955).
 22. P. V. N. Ramachandra Rao and E. E. Petersen, Effect of Carbon Dioxide Concentration on Gasification of Artificial Graphite, *Ind. Eng. Chem.*, **50**: 331-336 (1958).
 23. P. L. Walker, Jr., et al., Surface Area Studies of Carbon-Carbon Dioxide Reaction, *Ind. Eng. Chem.*, **45**: 1703-1710 (1953).
 24. C. N. Spalaris, *Role of Surface Area in the Kinetics of Oxidation of Graphite*, USAEC Report HW-31928, Hanford Atomic Products Operation, May 24, 1954.
 25. R. E. Woodley, Hanford Laboratories, General Electric Company, unpublished data, January 1961.
 26. A. Wheeler, Reaction Rates and Selectivity in Catalyst Pores, in *Advances in Catalysis*, **3**: 249-327 (1951).
 27. P. B. Weisz and C. D. Prater, Interpretation of Measurements in Experimental Catalysis, *Advances in Catalysis*, **6**: 143-196 (1954).
 28. P. L. Walker et al., Changes of Macropore Distribution in Carbon Rods upon Gasification with Carbon Dioxide, *J. Phys. Chem.*, **59**: 245-249 (1955).
 29. B. Griggs, *The Effect of Oxidation on the Compression Strength of CSGBF Graphite*, USAEC Report HW-42498 (Del.), Hanford Atomic Products Operation, Apr. 11, 1956.
 30. S. C. Lind and D. C. Bardwell, The Chemical Action of Gaseous Ions Produced by Alpha Particles. VI. Reactions of the Oxides of Carbon. *J. Am. Chem. Soc.*, **47**: 2675-2697 (1925).
 31. J. O. Hirschfelder and H. S. Taylor, The Alpha-Particle Reactions in Carbon Monoxide, Oxygen and Carbon Dioxide Systems, *J. Chem. Phys.*, **6**: 783-790 (1938).
 32. P. Hartek and S. Dondes, Radiation Chemistry of Gases, in *Proceedings of the Second United Nations International Conference on the Peaceful Uses of Atomic Energy, Geneva, 1958*, Vol. 29, pp. 415-419, United Nations, New York, 1959.
 33. P. C. Davidge and W. R. Marsh, *The Effect of Pile Radiation on the Carbon Dioxide-Graphite Reaction*, British Report AERE-C/R-1374, 1955.
 34. A. T. Cameron and W. Ramsey (Sir), The Chemical Action of Radium Emanation. Part III. On Water and Certain Gases, *J. Chem. Soc., Trans.*, **93**: 966-992 (1908).
 35. J. Wright, The Radiation-Induced CO₂/Graphite Reaction—A Tentative View of the Mechanism, in *Proceedings of the US/UK Meeting on the Compatibility Problems of Gas-Cooled Reactors Held at Oak Ridge National Laboratory, February 24-26, 1960*, pp. 148-172, USAEC Report TID-7597 (Bk. 1), March, 1961.
 36. P. Hartek and S. Dondes, Decomposition of Carbon Dioxide by Ionizing Radiation. Part I., *J. Chem. Phys.*, **23**: 902-908 (1955).

37. S. C. Lind, *The Chemical Effects of Alpha Particles and Electrons*, 2nd ed., Chemical Catalog Company, Inc., New York, 1928.
38. A. R. Anderson and R. J. Waite, *The Calorimetric Measurement of Energy Absorbed from Reactor Radiation in BEPO*, British Report AERE-C/R-2253, 1960.
39. R. E. Woodley, *Promotion of Chemical Reaction in Gas-Graphite Systems by Gamma Radiation*, USAEC Report HW-31929, Hanford Atomic Products Operation, May 24, 1954.
40. H. B. F. Gow and W. R. Marsh, Temperature Effects on the Radiation Induced Reaction of Carbon Dioxide with Graphite, in *Proceedings of the US/UK Meeting on the Compatibility Problems of Gas-Cooled Reactors Held at Oak Ridge National Laboratory, February 24-26, 1960*, pp. 16-45, USAEC Report TID-7597 (Bk. 1), March 1961.
41. H. B. F. Gow and W. R. Marsh, *The Effect of Temperature on the Carbon Dioxide-Graphite Reaction Under Pile Radiation*, British Report AERE-C/M-361, 1958.
42. H. C. Cowen and R. Lind, High Flux Experiments in the System CO₂-CO-Graphite, in *Proceedings of the US/UK Meeting on the Compatibility Problems of Gas-Cooled Reactors Held at Oak Ridge National Laboratory, February 24-26, 1960*, pp. 46-75, USAEC Report TID-7597 (Bk. 1), March 1961.
43. R. E. Woodley, *The Promotion of Chemical Reaction by Pile Radiation*, USAEC Report HW-40142, Hanford Atomic Products Operation, Nov. 22, 1955.
44. I. Langmuir, Chemical Reactions at Low Pressures, *J. Am. Chem. Soc.*, **37**: 1139-1167 (1915).
45. V. Sihvonen, The Influence of Keto- and Ketene Groups, Adsorbed Molecules, and Ions on the Mechanism of Carbon Oxidation, *Trans. Faraday Soc.*, **34**: 1062-1074 (1938).
46. L. Meyer, The Surface Reaction of Graphite with Oxygen, Carbon Dioxide and Water Vapour at Low Pressures, *Trans. Faraday Soc.*, **34**: 1056-1061 (1938).
47. R. F. Strickland-Constable, The Interaction of Oxygen and Carbon Filaments at High Temperatures, *Trans. Faraday Soc.*, **40**: 333-343 (1944).
48. X. Duval, Réaction de l'Oxygène avec des Filaments de Carbone à Hautes Températures et sous Très Basses Pressions, *J. chim. phys.*, **47**: 339-347 (1950).
49. R. J. Day, *Kinetics of the Carbon-Oxygen Reaction at High Temperatures*, Ph.D. Thesis, Pennsylvania State University, 1949.
50. Z. Chukhanov and N. Karzharina, Burning of Carbon, *Fuel*, **19**: 17-20, 49-50, 64-67 (1940).
51. M. K. Grodzovskii and Z. F. Chukhanov, Primary Reactions of the Combustion of Carbon, *Fuel*, **15**: 321-328 (1936).
52. T. F. E. Rhead and R. V. Wheeler, The Mode of Combustion of Carbon, *J. Chem. Soc., Trans.*, **103**: 461-489 (1913).
53. J. R. Arthur, Combustion of Carbon, *Nature*, **157**: 732-733 (1946).
54. G. W. Bridger, Combustion of Carbon and Carbon Monoxide, *Nature*, **158**: 236 (1946).
55. J. R. Arthur, Reactions Between Carbon and Oxygen, *Trans. Faraday Soc.*, **47**: 164-178 (1951).
56. E. Wicke, Contributions to the Combustion Mechanism of Carbon, in *Fifth Symposium on Combustion*, pp. 245-252, Reinhold Publishing Corp., New York, 1955.
57. M. Rossberg, Experimentelle Ergebnisse über die Primärreaktionen bei der Kohlenstoffverbrennung, *Z. Elektrochemie*, **60**: 952-956 (1956).
58. W. K. Lewis et al., Low-Temperature Oxidation of Carbon, *Ind. Eng. Chem.*, **46**: 1327-1331 (1954).

59. R. E. Dahl, *Oxidation of Graphite Under High Temperature Reactor Conditions*, USAEC Report HW-68493, Hanford Atomic Products Operation, July 1961.
60. H. H. Burton, *Graphite Oxidation*, USAEC Report HW-14376, Hanford Works, Sept. 6, 1949. (Classified)
61. R. E. Woodley, *AEC Technical Cooperation Program, UK-USA Discussion on Graphite Oxidation, Hanford Contribution*, USAEC Report WASH-690, Hanford Atomic Products Operation, Apr. 16, 1956. (Classified)
62. P. H. Reinker, *Oxidation and Irradiation of Pile Graphite*, USAEC Report HW-18365, Hanford Atomic Products Operation, July 18, 1950. (Classified)
63. L. Meyer, *Der Mechanismus der Primärreaktion zwischen Sauerstoff und Graphit*, *Z. physik. Chem. Leipzig*, **B17**: 385-404 (1932).
64. G. Blyholder and H. Eyring, *Kinetics of Graphite Oxidation*, *J. Phys. Chem.*, **61**: 682-688 (1957).
65. R. J. Day et al., *The Carbon-Oxygen Reaction at High Temperatures and High Gas-Flow Rates*, in *Industrial Carbon and Graphite. Papers Read at the Conference Held in London, Sept. 24-26, 1957*, pp. 348-370, Society of Chemical Industry, London, 1958.
66. J. M. Kuchta et al., *Combustion of Carbon in High Temperature, High Velocity Air Streams*, *Ind. Eng. Chem.*, **44**: 1559-1563 (1952).
67. H. C. Cowen et al., *The Rate of Oxidation of Large Blocks of Graphite in Air*, in *Proceedings of the US/UK Meeting on the Compatibility Problems of Gas-Cooled Reactors Held at Oak Ridge National Laboratory, February 24-26, 1960*, pp. 359-373, USAEC Report TID-7597 (Bk. 1), March 1961.
68. W. L. Kosiba and G. J. Dienes, *The Effect of Radiation on the Rate of Oxidation of Graphite*, in *US/UK Graphite Conference Held at St. Giles Court, London, December 16-18, 1957*, pp. 121-132, USAEC Report TID-7565 (Pt. 1), 1959.
69. W. L. Kosiba and G. J. Dienes, *The Effect of Displaced Atoms and Ionizing Radiation on the Oxidation of Graphite*, in *Advances in Catalysis*, **9**: 398-405 (1957).
70. J. S. Nairn and P. J. Robinson, *The Reaction of Graphite with Gaseous Coolants in the Windscale and Calder Reactors*, in *US/UK Graphite Conference Held at St. Giles Court, London, December 16-18, 1957*, pp. 148-156, USAEC Report TID-7565 (Pt. 1), 1959.
71. P. J. Robinson and J. C. Taylor, *Thermal Instability Due to Oxidation of a Graphite Channel Carrying an Air Flow*, in *Proceedings of the US/UK Meeting on the Compatibility Problems of Gas-Cooled Reactors Held at Oak Ridge National Laboratory, February 24-26, 1960*, pp. 471-503, USAEC Report TID-7597 (Bk. 2), March 1961.
72. J. S. Nairn and V. J. Wilkinson, *The Prediction of Conditions for Self-Sustaining Graphite Combustion in Air*, in *Proceedings of the US/UK Meeting on the Compatibility Problems of Gas-Cooled Reactors Held at Oak Ridge National Laboratory, February 24-26, 1960*, pp. 453-470, USAEC Report TID-7597 (Bk. 2), March 1961.
73. R. E. Dahl, *Experimental Evaluation of the Combustion Hazard to the Experimental Gas-Cooled Reactor—Preliminary Burning Rig Experiments*, USAEC Report HW-67792, Hanford Atomic Products Operation, November 1961.
74. R. Aubeau et al., *Essai de Determination des Conditions d'Inflammation de Un Canal de G-1*, French Report CP/58-533/PM/MLL, Department de Physico Chimie, Centre de Etudes Nucléaires de Saclay, 1958.
75. P. J. Robinson, *The Effects of Diffusional Control of Oxidation of Graphite on the Highest Safe Temperatures in Air*, British Report IGR-143(RD/W), May 20, 1959.
76. S. Ya. Pshezhetskii and M. T. Dmitriev, *The Mechanism of Some Simple Chemical*

- Reactions Taking Place Under the Action of Ionizing Radiations, *Uspekhi Khimii*, **26**: 225-267 (1957); translated in British Report AERE-Lib Trans-800, 1958.
77. L. C. Copeland, The Heat of Formation of Molecular Oxygen, *Phys. Rev.*, **36**: 1221-1231 (1930).
78. J. C. Greaves and J. W. Linnett, Recombination of Atoms at Surfaces. Part 5. Oxygen Atoms at Oxide Surfaces, *Trans. Faraday Soc.*, **55**: 1346-1361 (1959).
79. F. Kaufman and J. R. Kelso, Catalytic Effects in the Dissociation of Oxygen in Microwave Discharges, *J. Chem. Phys.* **32**: 301-302 (1960).
80. P. C. Davidge et al., *The Oxidation of Graphite During Irradiation in Oxygen*, British Report AERE-C/R-1450-DEL, 1959.
81. P. Harteck and S. Dondes, The Kinetic Radiation Equilibrium of Air, *J. Phys. Chem.*, **63**: 956-961 (1959).
82. D. W. Shannon, *The Role of the Oxidation Rate on the Hydriding of Zircaloy-2 by Gaseous Hydrogen*, Interim Report 3, USAEC Report HW-67811, Hanford Atomic Products Operation, Dec. 15, 1960.
83. J. Gadsby et al., The Kinetics of the Reactions of the Steam-Carbon System, *Proc. Roy. Soc. London*, **A187**: 129-151 (1946).
84. H. F. Johnstone et al., Kinetics of the Steam-Carbon Reaction in Porous Graphite Tubes, *Ind. Eng. Chem.*, **44**: 1564-1569 (1952).
85. J. S. Binford, Jr., and H. Eyring, Kinetics of the Steam-Carbon Reaction, *J. Phys. Chem.*, **60**: 486-491 (1956).
86. J. M. Pilcher et al., Kinetic Study of the Steam-Carbon Reaction, *Ind. Eng. Chem.*, **47**: 1742-1749 (1955).
87. M. A. Mayers, Reduction of Carbon Dioxide by Graphite and Coke, *J. Am. Chem. Soc.*, **61**: 2053-2058 (1939).
88. B. E. Hunt et al., Reaction of Carbon with Steam at Elevated Temperatures, *Ind. Eng. Chem.* **45**: 677-680 (1953).
89. J. A. Dodson et al., Rate of the Steam-Carbon Reaction by a Falling-Particle Method, *Ind. Eng. Chem.*, **49**: 148-154 (1957).
90. J. E. Antill and K. A. Peakall, Attack of Graphite by an Oxidizing Gas at Low Partial Pressures and High Temperatures, *J. Nuclear Materials*, **2**: 31-38 (1960).
91. A. O. Allen, A Survey of Recent American Research in the Radiation Chemistry of Aqueous Solutions, in *Proceedings of the First United Nations International Conference on the Peaceful Uses of Atomic Energy, Geneva, 1955*, Vol. 7, pp. 513-520, United Nations, New York, 1956.
92. A. O. Allen, Mechanism of Decomposition of Water by Ionizing Radiations, *Discussions Faraday Soc.*, **12**: 79-87 (1952).
93. A. O. Allen and H. A. Schwarz, Decomposition of Water Under High Energy Radiation, in *Proceedings of the Second United Nations International Conference on the Peaceful Uses of Atomic Energy, Geneva, 1958*, Vol. 29, pp. 30-37, United Nations, New York, 1959.
94. E. J. Hart, Chemical Effects of Ionizing Radiations on Aqueous Inorganic Solutions, *J. Chem. Educ.*, **34**: 586-593 (1957).
95. R. F. Firestone, The Radiation Chemistry of Water Vapor. The Indirect Effect on Deuterium of the Exchange of D-Atoms with Water Molecules, *J. Am. Chem. Soc.*, **79**: 5593-5598 (1957).
96. S. Gordon and E. J. Hart, Radiation Decomposition of Water Under Static and Bubbling Conditions, in *Proceedings of the Second United Nations International Conference on the Peaceful Uses of Atomic Energy, Geneva, 1958*, Vol. 29, pp. 13-18, United Nations, New York, 1959.
97. N. S. Corney and R. B. Thomas, *The Effect of Pile Radiation on the Reaction Between Hydrogen and Graphite*, British Report AERE-C/R-2502, June 1958.

98. D. D. Wagman et al., Heats, Free Energies, and Equilibrium Constants of Some Reactions Involving O_2 , H_2 , H_2O , C , CO , CO_2 , and CH_4 , *J. Research Nat. Bur. Standards*, **34**: 143-161 (1945).
99. K. Wieland, Vorkommen und Nachweis freier Radikale in Gasgleichgewichten bei hohen Temperaturen, *Österr. Chem.-Ztg.*, **55**: 329-332 (1954).
100. D. D. Wagman et al., Heats, Equilibrium Constants, and Free Energies of Formation of the Acetylene Hydrocarbons through the Pentynes, to $1500^\circ K$, *J. Research Nat. Bur. Standards*, **35**: 467-496 (1945).
101. F. G. Brickwedde et al., Equilibrium Constants of Some Reactions Involved in the Production of 1,3-Butadiene, *J. Research Nat. Bur. Standards*, **37**: 263-279 (1946).
102. M. W. Travers, On the System Carbon, Hydrogen, Methane, between 442 and $712^\circ C$, *Trans. Faraday Soc.*, **34**: 580-584 (1938).
103. Z. Szabó, The Examination of a System Carbon and Hydrogen in the Temperature Range 1100 - $2600^\circ C$, *J. Am. Chem. Soc.*, **72**: 3497-3502 (1950).
104. R. M. Barrer, The Interaction of Hydrogen with Micro-Crystalline Charcoal, II—Activated Sorption of Hydrogen and Methane by Carbon, *Proc. Roy. Soc. London*, **A149**: 253-269 (1935).
105. C. W. Zielke and E. Gorin, Kinetics of Carbon Gasification, Interaction of Hydrogen with Low Temperature Char at 1500 to $1700^\circ F$, *Ind. Eng. Chem.*, **47**: 820-825 (1955).
106. G. E. Goring et al., Kinetics of Carbon Gasification by Steam. Effect of High Temperature Pretreatment on Reactivity of Low Temperature Char to Steam and Carbon Dioxide, *Ind. Eng. Chem.*, **44**: 1051-1057 (1952).
107. L. C. Browning and P. H. Emmett, Equilibrium Measurements in the System $C-CH_4-H_2$, *J. Am. Chem. Soc.*, **73**: 581-583 (1951).
108. A. Troesch, La Dissociation du Méthane en Présence d'un Catalyseur au Nickel, *J. chim. phys.*, **47**: 274-282 (1950).
109. W. J. Thomas, The Adsorption of Hydrogen at Graphite Surfaces, in *Proceedings of the US/UK Meeting on the Compatibility Problems of Gas-Cooled Reactors Held at Oak Ridge National Laboratory, February 24-26, 1960*, pp. 523-544, USAEC Report TID-7597 (Bk. 2), March 1961.
110. J. P. Redmond and P. L. Walker, Jr., Hydrogen Sorption on Graphite at Elevated Temperatures, *J. Phys. Chem.*, **64**: 1093-1099 (1960).
111. M. I. Temkin, Adsorption Equilibrium and the Kinetics of Processes on Non-homogeneous Surfaces and in the Interaction Between Adsorbed Molecules, *J. Phys. Chem. U.S.S.R.*, **15**: 296-332 (1941).
112. D. H. Bangham and J. Stafford, "Activated" Graphite as a Sorbent of Oxygen, *J. Chem. Soc.*, **127**: 1085-1094 (1925).
113. M. Dzurus et al., Chemical Reactions of Graphite, in *Proceedings of the French-American Conference on Graphite Reactors Held at Brookhaven National Laboratory, November 12-15, 1957*, USAEC Report BNL-489, Brookhaven National Laboratory, 1958.
114. W. V. Loebenstein and V. R. Deitz, Oxygen Chemisorption on Carbon Adsorbents, *J. Phys. Chem.*, **59**: 481-487 (1955).
115. R. N. Smith et al., Carbon-Oxygen and Carbon-Hydrogen Surface Complexes, *J. Phys. Chem.*, **60**: 495-497 (1956).
116. G. M. Harris and A. W. Tickner, Reaction of Hydrogen Atoms with Solid Carbon, *Nature*, **160**: 871 (1947).
117. S. C. Lind and D. C. Bardwell, The Chemical Action of Gaseous Ions Produced by Alpha Particles. IX. Saturated Hydrocarbons, *J. Am. Chem. Soc.*, **48**: 2335-2351 (1926).

118. R. E. Honig and C. W. Sheppard, An Experimental Comparison of the Chemical Effects of Deuterons and of Alpha Particles on Methane and *n*-Butane, *J. Phys. Chem.*, **50**: 119-143 (1946).
119. I. N. Onslow MacAulay and M. Tomlinson, On the Possibility of Radiation Induced Transport of Carbon in Helium, in *Proceedings of the US/UK Meeting on Compatibility Problems of Gas-Cooled Reactors Held at Oak Ridge National Laboratory, February 24-26, 1960*, pp. 191-206, USAEC Report TID-7597 (Bk. 1), March 1961.
120. W. L. Kosiba, Irradiation Effects on Carbon Mass Transport by Impurities in Helium, in *Proceedings of the US/UK Meeting on the Compatibility Problems of Gas-Cooled Reactors Held at Oak Ridge National Laboratory, February 24-26, 1960*, pp. 124-147, USAEC Report TID-7597 (Bk. 1), March 1961.
121. L. Green, *The Erosion of Graphite by High Temperature Helium Jets*, USAEC Report NAA-SR-77, North American Aviation, Inc., May 24, 1950.
122. J. O. Clayton and W. F. Giauque, The Heat Capacity and Entropy of Carbon Monoxide. Heat of Vaporization. Vapor Pressures of Solid and Liquid. Free Energy to 5000°K from Spectroscopic Data, *J. Am. Chem. Soc.*, **54**: 2610-2626 (1932).
123. W. F. Giauque and J. O. Clayton, The Heat Capacity and Entropy of Nitrogen. Heat of Vaporization. Vapor Pressures of Solid and Liquid. The Reaction $\frac{1}{2}\text{N}_2 + \frac{1}{2}\text{O}_2 = \text{NO}$ from Spectroscopic Data, *J. Am. Chem. Soc.*, **55**: 4875-4889 (1933).
124. E. Rutner et al., Thermodynamic Functions of Cyanogen and the Equilibrium Constant for the Reaction $\frac{1}{2}\text{C}_2\text{N}_2 \rightleftharpoons \text{CN}$ between 1000 and 4500°K, *J. Chem. Phys.*, **24**: 173 (1956).
125. M. W. Thompson, The Free Energy of Methyl Cyanide, and Equilibrium Constants of Some Related Reactions, *Trans. Faraday Soc.*, **37**: 344-352 (1941).
126. A. Maimoni, *Corrosion of Graphite by Nitrogen. A Summary of Blowpipe Data*, USAEC Report UCID-4135, University of California, Mar. 10, 1958.
127. R. J. Strutt, A Chemically Active Modification of Nitrogen Produced by the Electric Discharge, *Proc. Roy. Soc. London*, **A85**: 219-229 (1911).
128. W. G. Zinman, *A Study of the Interaction Between Carbon and Dissociated Gases*, Report R59SD457, Aerosciences Laboratory, General Electric Company, Nov. 5, 1959.
129. R. C. Giberson, *Reactions of Graphite with Microwave-Activated Nitrogen*, USAEC Report HW-68380, Hanford Atomic Products Operation, February 1961.
130. G. B. Kistiakowsky and H. Gershinowitz, The Thermal Dissociation of Cyanogen into Cyanide Radicals, *J. Chem. Phys.*, **1**: 432-439 (1933).
131. M. Kondo, The Decomposition Reaction of Cyanogen Compounds by Electric Discharge. VII. Decomposition of Dicyanogen by Silent Discharge, *J. Chem. Soc. Japan, Pure Chem. Sect.*, **77**: 486-490 (1956).
132. R. F. Strickland-Constable, The Kinetics of the Oxidation of Carbon, A Survey of Some Recent Results, *J. chim. phys.*, **47**: 322-327 (1950).
133. D. G. Madley and R. F. Strickland-Constable, The Kinetics of the Oxidation of Charcoal with Nitrous Oxide, *Trans. Faraday Soc.*, **49**: 1312-1324 (1953).
134. R. N. Smith et al., The Oxidation of Carbon by Nitric Oxide, *J. Phys. Chem.*, **63**: 544-547 (1959).
135. H. Watts, The Oxidation of Charcoal by Nitric Oxide and the Effect of Some Additives, *Trans. Faraday Soc.*, **54**: 93-105 (1958).
136. P. H. Van Der Ley and J. P. Wibaut, On the Properties of Nitrogen in Nitrogenous Carbons as Compared with the Properties of Nitrogen in Coke, *Rec. trav. chim.*, **51**: 1143-1156 (1932).

137. W. Rudorff, Graphite Intercalation Compounds, in *Advances in Inorganic Chemistry and Radiochemistry*, Vol. 1, H. J. Emeleus and A. G. Sharp (Eds.), pp. 223-265, Academic Press Inc., New York, 1959.
138. L. C. Werking, Carbon, Graphite, *Chem. Eng.*, **54**: 226, 228 (February 1947).
139. A. Hérold, Sur le système graphite-brome, *Compt. rend.* **239**: 591-592 (1954).
140. L. C. F. Blackman et al., Electrical Properties of Crystal Compounds of Graphite. I. Conductance of Graphite/Bromine, *Proc. Roy. Soc. London*, **A256**: 15-27 (1960).
141. O. Ruff, Reactions of Solid Carbon with Gases and Liquids, *Trans. Faraday Soc.*, **34**: 1022-1033 (1938).
142. F. K. Earp and M. W. Hill, Oxidation of Carbon and Graphite, in *Industrial Carbon and Graphite. Papers Read at the Conference Held in London, Sept. 24-26, 1957*, pp. 326-333, Society of Chemical Industry, London, 1958.
143. A. B. McIntosh et al., Compatibility Problems of Graphite Moderators, in *Industrial Carbon and Graphite. Papers Read at the Conference Held in London, Sept. 24-26, 1957*, pp. 519-526, Society of Chemical Industry, London, 1958.
144. J. R. Bowring and H. G. Crone, The Rate of Combustion of Carbon. Some Effects of Internal Structure and Inorganic Impurities, *J. chim. phys.*, **47**: 543-547 (1950).
145. K. Hedden and E. Wicke, About Some Influences on the Reactivity of Carbon, in *Proceedings of the Third Conference on Carbon Held at the University of Buffalo*, pp. 249-256, Pergamon Press, New York, 1959.
146. R. E. Dahl, *Evaluation of Chlorine Inhibition of Graphite Oxidation as a Reactor Safeguard*, USAEC Report HW-67255, Hanford Atomic Products Operation, April 1961.
147. R. Wehrmann, *Topical Progress Report to NEPA Project; September, 1958 to March, 1959*, USAEC Report NEPA-1402, Fansteel Metallurgical Corporation, April 1959.
148. J. M. Blocher et al., *Carbide Coatings on Graphite*, USAEC Report BMI-1200, Battelle Memorial Institute, June 1957.
149. J. M. Blocher et al., *Coating of Graphite with Silicon Carbide by Reaction with Vapor of Controlled Silicon Activity*, USAEC Report BMI-1349, Battelle Memorial Institute, June 1959.
150. J. F. Lynch et al., *Molybdenum Disilicide Coating for Graphite*, Report WADC-TR-53-457, Battelle Memorial Institute, September 1954.
151. P. T. Whelan, *Effects of Several Impregnants on the Oxidation Resistance of Graphite*, Report WAL-TR-371/49, Watertown Arsenal Laboratory, November 1957.
152. C. E. Raines and W. H. Goldthwaite, Fission Product Release During Irradiation of Uranium Oxide Carbide-Graphite Spheres, in *Progress Relating to Civilian Application During April 1959*, p. 72, R. W. Dayton and C. R. Tipton, Jr. (Eds.), USAEC Report BMI-1340, Battelle Memorial Institute, May 1959.
153. J. L. Jackson, *The Effect of Irradiation on Siliconized Silicon Carbide Coatings for Graphite*, USAEC Report HW-68494, Hanford Atomic Products Operation, February 1961.
154. A. R. G. Brown and W. Watt, The Preparation and Properties of High-Temperature Pyrolytic Carbon, in *Industrial Carbon and Graphite. Papers Read at the Conference Held in London, Sept. 24-26, 1957*, pp. 86-100, Society of Chemical Industry, London, 1958.
155. A. R. G. Brown et al., Some Interesting Properties of Pyrolytic Carbon. I. The Structure and Density of Pyrolytic Carbon, *J. Less-Common Metals*, **1**: 94-100 (1959).
156. E. Stover, General Electric Research Laboratories, unpublished data, November 1959.
157. Oriented Graphite Produced by Commercial Process, *Materials in Design Engineering*, **51**(2): 16, 170 (1960).

Graphite-Metal and Graphite-Molten-salt Systems

R. A. MEYER and J. C. BOKROS†

The development of reactor concepts has been directed for economic reasons toward higher temperatures. However, the performance of solid fuel elements at high temperatures is limited by the effects of fission-product gases and the loss of physical strength. For these and other reasons, the design of liquid-fueled reactors was undertaken. In such a system fissile material in solution is circulated between the reactor core and the heat-exchanger equipment. Graphite is used as the moderator because it has desirable neutron properties and also because it can serve as a container for the liquid fuel.

The high-temperature gas-cooled reactor is another approach to the attainment of high coolant temperatures. Some of these reactors require that structural metals operate in contact with graphite for long periods of time. In others there is opportunity for carburization or graphitization to occur in metallic parts of the coolant system through the reaction of gases evolved from the graphite or the reaction with products of gas-graphite reactions.

The reactions of graphite with metals, metallic oxides, and other materials have been summarized in Chap. 6. In this chapter certain of these reactions that may occur in high-temperature liquid- or gas-cooled reactor systems will be discussed in more detail.

15-1 Liquid Metals

The advantages of an impermeable or low-permeability graphite for use as a moderator were recognized early in the design of liquid-fueled reactors. In 1955 an intensive program was initiated in the United States to find a graphite with a small pore volume accessible to bismuth for the proposed Liquid Metal Fuel Reactor (LMFR). Other reactor systems, the Molten Salt Reactor (MSR), the High Temperature Gas Cooled Reactor (HTGR), and the Dragon Reactor, have also been designed using a graphite with a low permeability to salt or gas.

15-1.1 BISMUTH-GRAPHITE COMPATIBILITY

The LMFR concept requires that the liquid-bismuth heat-transfer fluid contain enriched uranium in solution. Therefore the graphite must be rela-

† John Jay Hopkins Laboratory for Pure and Applied Science, General Atomic Division, General Dynamics Corporation, San Diego, Calif.

tively impermeable to bismuth so that uranium and fission products cannot penetrate and accumulate in the moderator. A number of graphites have been evaluated by the measurement of their absorption of liquid bismuth.¹ These studies indicate that absorption varies from 3 to 4 g of bismuth per cubic centimeter of graphite for large-pore AGOT graphite or its equivalent to less than 0.1 g/cm³ for graphites with smaller pores.

From data obtained in other types of experiments, it has been found that the degree of uptake is a function of the surface tension of bismuth.¹ Sessile drop tests conducted in vacuum using bismuth droplets in contact with the graphite indicate that without additives to the bismuth the surface tension ranges from 147 to 259 dynes/cm (Table 15.1). That these values are some-

Table 15.1 — SURFACE TENSIONS AT 550°C[†]

Test liquid	Solid-surface preparation	Surface tension, dynes/cm
Bi	Ultrasonic cleaning	253
Bi	Blown free of loose particles	259
Bi	Loose particles left on surface	147
Bi + 350 ppm Mg	Loose particles left on surface	66
Bi + 350 ppm Zr	Loose particles left on surface	281
Bi + 250 ppm Zr	Loose particles left on surface	330
Bi + $\begin{cases} 250 \text{ ppm Zr} \\ 350 \text{ ppm Mg} \end{cases}$	Loose particles left on surface	64
Bi + $\begin{cases} 50 \text{ ppm Zr} \\ 1000 \text{ ppm Mg} \\ 1500 \text{ ppm U} \end{cases}$	Loose particles left on surface	100

[†] The bismuth and graphite were loaded into a quartz tube and evacuated at approximately 700°C for 12 to 15 hr. This procedure produced a shiny metallic surface on the bismuth.

what lower than usually reported is attributed to variations in the surface of the graphite. For example, the lowest value is obtained if loose particles are left on the surface. When the graphite is ultrasonically cleaned, or freed of these loose particles by some other means, the surface tension increases by approximately 100 dynes/cm. Under these conditions it has not been possible to cause the bismuth to wet the graphite even for testing times in excess of 50 hr.

In the bismuth reactor system, magnesium and zirconium additives are commonly used to inhibit oxidation of the fuel and corrosion of the metal components. Surface-tension tests similar to those mentioned above have been conducted with these additives; the data are shown in Table 15.1. It will be noted that the addition of zirconium increases the surface tension. No explanation has been suggested for this behavior. The presence of mag-

nesium decreases the surface tension. It is not known whether this is due to gas evolution from the graphite or whether the magnesium cleans the surface of the bismuth. When zirconium and magnesium in combination are added to bismuth, the magnesium is still effective in reducing the surface tension and is not influenced by the presence of 250 ppm of zirconium.

The effect of uranium has been tested by adding a combination of 50 ppm of zirconium, 1000 ppm of magnesium, and 1500 ppm of uranium. The resulting surface tension is 100 dynes/cm. Although the concentration of magnesium is higher, the surface tension is not reduced to the 66 dynes/cm value previously obtained for the magnesium and bismuth system.

The effects of pressure on the absorption of bismuth by graphite are shown in Fig. 15.1. In these tests the sample was placed in an evacuated

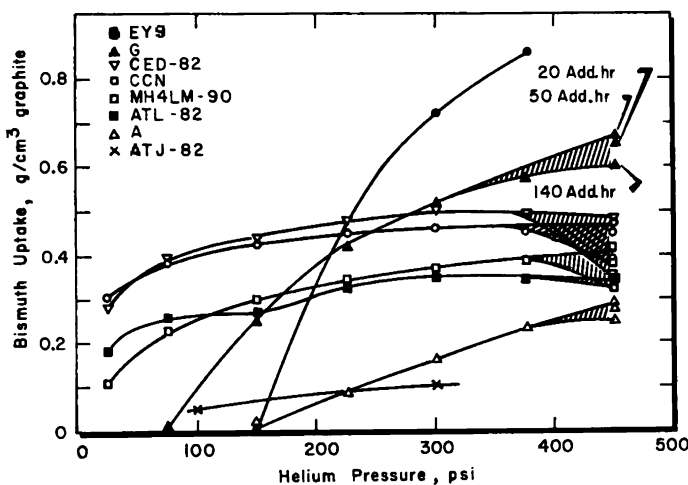


Fig. 15.1 Bismuth uptake vs. pressure for successive immersions of 20 hr at 550°C. All materials tested were high density ($\rho = 1.88$ to 1.93 g/cm³) graphites.¹ A detailed description of other properties is given in Table 6.23 and Ref. 1.

system and outgassed at 550°C for 14 to 18 hr. The system was kept closed, and the sample was submerged in a pool of bismuth. Helium pressure was then applied to the surface of the bismuth for 20 hr. After each run the graphite was removed, reweighed, and inserted for the next run. The results indicate that the bismuth uptake varies over a rather wide range for the different graphites tested. In five of the graphites, the uptake is rather insensitive to pressure in the range tested; i.e., most of the bismuth absorption occurs at pressures less than 100 psi. On the other hand, types A, G, and EY9† show no gain in weight until a threshold pressure is exceeded; then the pressure dependence is marked. Since the macropore spectra of A,

† See Ref. 1 for a description of A and G graphites. EY9 is a graphite from the Morgan Crucible Company, Ltd., with a smaller and more-uniform pore distribution (0.01 to 1.0μ) than types A or G.

G, and EY9 are similar, this suggests that the absorption is a function not only of the surface tension of the bismuth solution but also of the pore structure of the graphite. The lower threshold pressure of G graphite indicates that its pores are slightly larger than those of EY9. This has been confirmed by mercury porosimeter measurements.

Bismuth absorption is also a function of pressure and submersion time. For example, after several hundred hours at 125 psi, EY9, A, and G graphites absorb bismuth in amounts equal to those obtained after only 20 hr at 250 psi. Figure 15.2 gives the results of long-term tests on several grades of graphite. It will be noted that some variation in weight occurs, which

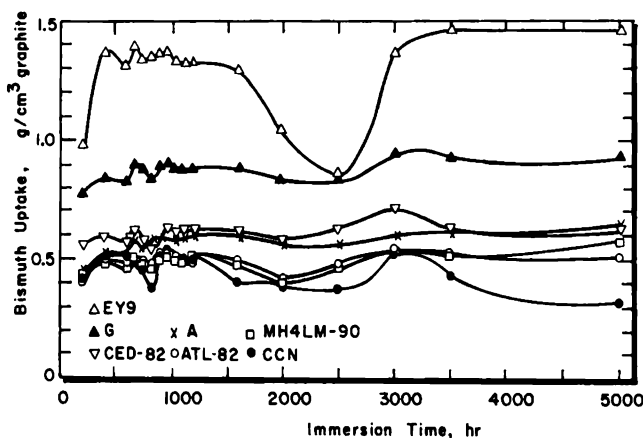


FIG. 15.2 Bismuth uptake vs. time¹ at 550°C and 250 psi. Samples were outgassed 20 hr at 550°C.

usually does not exceed more than 0.2 g/cm³. This effect is tentatively attributed to the expulsion and reabsorption of bismuth caused by the build-up and relief of gases within the pores. Temperature has no effect on the uptake of bismuth up to 600°C. In the case of a comparatively open pore structure, the absorption values shown on the graph can be approximated by submerging samples for 10 sec.

Whether or not graphite is weakened when bismuth contained in the pores expands by freezing has been determined as follows: Samples of AGOT graphite were submerged in bismuth and thermally cycled from below the melting point (272°C) to 700°C. After a successively greater number of thermal cycles, 0, 3, 9, 27, etc., the crushing strength of the graphite was measured with the bismuth in a molten condition. It was found that there is no reduction in strength up to at least 129 cycles. It would seem that the bismuth is able to expand into other available pores in the graphite or that the graphite deforms in local regions to accommodate the increased volume of the solid bismuth.

The surfaces of graphite which had been submerged in bismuth or in

uranium-bismuth-zirconium solutions were examined metallographically for effects attributable to static submersion and/or dynamic conditions in a loop. For tests as long as 10,000 hr and at bismuth velocities up to 10 ft/sec, there is no evidence of erosion, spalling, or fracturing of the surfaces.² Penetration of bismuth into graphite occurs to the same degree as that measured with the graphite in a static bismuth solution.

Graphite samples have been exposed to fission recoils from a uranium-bismuth-magnesium solution. Exposure in the Brookhaven Graphite Research Reactor (BGRR) was in excess of 5×10^{16} fissions/cm³ with a concentration of 1000 ppm of uranium, 350 ppm of magnesium, and 250 ppm of zirconium in the bismuth solution. Postirradiation examination did not reveal any detrimental effects due to fission recoils or lamellar compounds formed from the fission products.

When solutions of bismuth with uranium and fission products are contained in graphite, it is found that cesium precipitates reversibly if the temperature is near 450°C but remains in solution at 600°C. The formation of lamellar compounds (Sec. 6-5.3) is suggested.

It has been reported that UC, UC₂, and U₂C₃ are formed as stable carbides.³ However, such formation does not seem to occur unless the uranium in the bismuth exceeds 1 per cent and the temperature is above 1200°C.

15-1.2 LEAD-BISMUTH AND LEAD-BISMUTH-TIN LIQUID METALS

The eutectic of 55 per cent lead-45 per cent bismuth enters graphite more readily⁴ than pure bismuth at 300°C and pressures up to 20 psi. This indicates that the surface tension of the eutectic is lower than that of bismuth. However, when the pressure is increased to 90 psi, the two absorption curves merge.

The lead-bismuth eutectic has also been subjected to tests⁵ in which the alloy was circulated in contact with graphite for 466 hr at 260°C. There was no evidence, however, of erosion or corrosion of the graphite. As the test progressed, the flow decreased. This probably resulted from the formation of metal oxides, which restricted the flow, rather than from spallations from the graphite impeller or any other graphite parts in the loop.

15-1.3 LIQUID SODIUM

Sodium wets graphite readily in the temperature range from 250 to 735°C, filling 60 to 90 per cent of the available pores.⁶ The sodium can be removed almost quantitatively by vacuum distillation. In contrast to the very extensive reaction between potassium, rubidium, and cesium (Sec. 6-5.1), pure sodium reacts only very slowly with graphite.

The uptake of sodium is accompanied by an anisotropic swelling of the graphite, which increases with temperature; at 400°C the linear expansion is about 1 per cent. No increase in the lattice constants accompanies the

swelling, which indicates that the effect is an intercrystalline one. Carniglia⁶ has suggested that sodium may react with the nongraphitic intergranular carbon, thereby weakening the bonding between grains and causing the structure to expand. The observation⁷ that the rate of reaction with sodium increases in the order, single crystals,⁸ polycrystalline graphite, and lampblack, supports the idea that the nongraphitic carbon is preferentially attacked.

If certain impurities are present, sodium reacts much more rapidly with graphite. A small amount (<1 per cent) of potassium is sufficient to greatly increase the swelling. Also, if care is not taken to remove oxygen from the sodium, a vigorous interaction with graphite is observed.⁸ In fact, sodium oxide, sodium hydroxide, sodium peroxide, ammonia, and amines all cause an interaction of sodium with graphite so vigorous that in most cases polycrystalline graphites are completely disintegrated.

It has been proposed⁸ that the impurity atoms act as spacer groups and allow the sodium to penetrate the layer planes. Thermal decomposition of compounds formed by the reaction of impure sodium and single crystals of graphite results in large-scale disintegration of the crystals. Although no X-ray structural evidence has been reported to confirm the formation of lamellar compounds, the crystals have been observed to swell in the direction of the *c* axis to many times their former thicknesses by such treatment.

It has been reported recently^{9,10} that a dilute interlamellar compound, $C_{64}Na$, is formed by heating powdered graphite and sodium to 400°C. The formation of a compound is indicated by the disappearance of several X-ray diffraction lines characteristic of graphite. The compound is believed to have a lamellar structure in which the sodium is intercalated in every eighth layer plane, analogous to the potassium-graphite compound.

It will be concluded that sodium, if used as a coolant in a graphite-moderated reactor, should not be allowed to contact the graphite. In the Sodium Reactor Experiment (SRE)¹¹ the graphite is clad in zirconium to prevent the reaction of sodium and the undesirable reduction of reactivity of the reactor.

The effect of a sodium-graphite reaction is also detrimental to the metal components of the external coolant system. At elevated temperatures metal specimens encapsulated with graphite in sodium and exposed to 100 to 200 hr between 800 and 920°C show marked corrosion.¹² Above 500°C stainless steels are carburized in a sodium-graphite system.

15-1.4 OTHER LIQUID METALS

Although they do not fulfill all the requirements of a reactor coolant, several other liquid metals may be of interest in special nuclear applications.

(a) *Magnesium*. Liquid magnesium at temperatures as high as 1100°C can be contained by graphite without difficulty.¹³ As a nuclear material

magnesium has the advantage of a low thermal-neutron cross section and a reasonably low melting point of 651°C. Magnesium can also be successfully contained in ferrous pipes. At the melting point of magnesium, the resistance to corrosion is good, but at 800°C the solubility of iron in magnesium is sufficient to cause mass transfer of iron in a circulating system.^{14, 15}

(b) *Aluminum*. For many years graphite has been used as a container material for aluminum.¹⁶ The solubility of carbon in aluminum is very low for temperatures less than 1200°C. At temperatures of 1700 to 1800°C, the carbide Al_4C_3 is formed, but the rate is limited by diffusion through the carbide^{4, 16} (see also Sec. 6-5.1). Although aluminum has a low thermal-neutron cross section, its usefulness is limited in the molten state because it is strongly corrosive to almost all metallic container materials.¹⁷

(c) *Tin*. Tin is compatible with graphite and possesses a reasonably low neutron-absorption cross section, making it an attractive metal for reactor systems. The surface tension of tin is reported¹³ to be 526 dynes/cm at 300°C and 510 dynes/cm at 500°C. Since these values are greater than those of bismuth, it might be expected that graphite would be less permeable to tin than to bismuth. However, limited studies conducted at 2000°C indicate otherwise.¹⁸ Metallographic sections show a high degree of penetration and a wetting contact angle of less than 90° at the tin-graphite interface. Micrographs also indicate that a large percentage of the available pores is filled by the tin, even though no gas pressure is exerted on the liquid metal. This is further evidence that tin wets graphite. If 3 wt.% zirconium is added, a distinct zirconium carbide layer forms at all the interfaces, including the interior pores of the graphite. After 4 hr at 2000°C, these pore layers grow in thickness to approximately 1 mil.

Other studies have also been conducted on the compatibility of graphite and tin in an all-graphite loop.⁵ Liquid tin was circulated for 60 hr at temperatures ranging between 850 to 1000°C. The graphite was examined and found to be completely intact without any evidence of erosion or corrosion. In a series of static tests conducted to determine the relative corrosion resistance of refractory materials to tin, no corrosive or deleterious effects were observed¹⁹ between the graphite and tin up to 1800°C.

Two properties of tin make it attractive as a nuclear material. First, the neutron-absorption cross section is 0.55 barns, only twice that of aluminum. Second, uranium is soluble in tin, thereby making tin an excellent fuel carrier for liquid reactors. Unfortunately it is difficult to contain tin in other metals. One possible material¹⁶ is low-carbon cast iron, which shows limited corrosion resistance up to 510°C.

(d) *Uranium*. Uranium and graphite react to form uranium carbides at temperatures in excess of 1150°C. This reaction may place an upper temperature limit on uranium-bearing liquid systems in which uranium is in contact with graphite. Between 1150 and 1300°C, UC is formed, and at 1400°C traces of UC_2 may be observed metallographically.^{3, 20} These car-

bides form a layer that grows at the expense of the graphite and may spall in the presence of molten uranium.

The long-term diffusion of uranium through graphite at elevated temperatures may be another limiting factor in the usefulness of graphite as a container material. This transport, which has been measured between 1600 and 2400°C, apparently occurs either by volume diffusion or by migration along pores.²¹ The extent of penetration for volume diffusion is small (<40 mils for 100 hr at 2400°C), although the uranium concentration is high. In contrast, the extent of penetration by migration along pores is large, but the uranium concentration is much less. The duration of these tests was short compared to normal reactor operating conditions. No long-term studies have been conducted.

15-2 Compatibility of Solid Metals and Graphite

The use of graphite as the moderator or reflector in nuclear reactors often requires that structural or cladding materials operate in contact with graphite for long periods of time. Many of the alloying elements commonly used in engineering alloys are strong carbide formers and will react with graphite at elevated temperatures. Other metals, which do not form carbides at elevated temperatures, dissolve carbon, which can then be precipitated as graphite when the temperature is reduced. When a metal reacts with graphite to form a carbide or a solid solution, the attack is termed "carburization"; when a metal dissolves carbon or forms an unstable carbide at elevated temperatures and subsequently rejects graphite at lower temperatures, the process is called "graphitization."

Carburization can affect metals and alloys in a variety of ways, depending upon the amount of carbon absorbed and the size and distribution of the carbides that form. For example, an alloy may be weakened owing to the removal, as carbides, of elements in solid solution. Carbides may also weaken or embrittle the alloy if they agglomerate and collect at grain boundaries. On the other hand, the carbides that form can, by a dispersion hardening mechanism, increase the strength when they are fine and widely distributed. In any event it is obvious that, unless the carburization can be closely controlled, the properties of an alloy can vary in an unpredictable and erratic manner.

Graphitization of most metals does not usually impair the properties of the metal in the early stages. However, during thermal cycling in a carburizing environment, the graphite precipitate can build up continuously, link-up, and form cracks. Eventually the accumulated graphite results in a general deterioration of the metal.

15-2.1 PURE METALS

(a) *Copper*. At moderate temperatures copper is probably the metal most compatible with graphite. It does not form a carbide, and the solu-

bility of carbon in copper is immeasurably small at temperatures up to the melting point of copper; in fact, this solubility is so low that carbon will not diffuse through copper. This property is utilized in commercial carburization processes where copper plate is used as a masking material on steel parts during carburization. Gerds and Mallett²² have exposed copper to graphite in an argon atmosphere for 250 hr at 1010°C. Based on metallography and hardness, very slight, if any, reaction was found. Copper tensile specimens pack carburized† for 500 hr at 930°C exhibit stress-strain curves identical to control specimens having the same thermal history.^{23, 24}

(b) *Nickel*. Nickel, like copper, does not form a stable carbide, but it does dissolve 0.65 wt.% carbon at the eutectic temperature (1316°C). No significant reaction has been observed between graphite and nickel at temperatures up to 1010°C, although considerable evidence of graphitization

Table 15.2 — THICKNESSES OF Mo_2C LAYERS FORMED ON MOLYBDENUM HELD IN CONTACT WITH GRAPHITE† AT VARIOUS TEMPERATURES IN HELIUM²³

Temperature, °C	Carbide-layer thicknesses, mils	
	Zirconium-gettered helium	Ungettered helium
705	‡	0.2
815	‡	0.8 to 1.1
930	1.0 to 1.2	1.7 to 2.3
1010	0.5 to 1.0	3.5 to 5.0

† A 2000-psi bearing pressure maintained for 2000 hr.

‡ No test.

has been reported.²³ Nickel exposed to graphite at 1020°C for long periods of time or thermally cycled from 930°C to room temperature or from 980 to 540°C exhibits considerable graphitization. Combined carburization and carburization-aging treatments indicate that graphitization of nickel supersaturated with carbon occurs at 430°C and above.²³ The graphitization reduces the room-temperature strength and hardness, but it does not affect the ductility.

(c) *Molybdenum*. Molybdenum reacts with graphite in the temperature range 650 to 980°C to form a single-phase carbide layer, Mo_2C , which is continuous and protective.^{22, 23} The thicknesses of the carbide layers formed at various temperatures on molybdenum in contact with graphite in helium are shown in Table 15.2.

The tensile strength²⁴ of molybdenum sheet specimens (30 mils thick)

† Pack carburization was carried out in a mixture of graphite powder containing 5 per cent BaCO_3 .

increases 20 per cent and the elongation decreases more than 50 per cent due to pack carburization at 930°C for 1000 hr.

(d) *Tungsten*. The diffusion of carbon into tungsten has been measured by Pirani and Sandor.²⁵ Small tungsten beads pack carburized in pure degassed carbon black in flowing, dry hydrogen formed a uniform layer of WC, which penetrated uniformly into the metal. The depth of penetration observed in 1 hr at various temperatures is shown in Table 15.3. These data give an activation energy of 59 ± 5 kcal/gram atom.

Table 15.3 — THICKNESSES OF WC FORMED ON TUNGSTEN PACK²⁶ CARBURIZED IN CARBON BLACK AND DRY HYDROGEN FOR 1 HR

Temperature, °C	Carbide-layer thicknesses, mils
1535	1.5
1640	2.1
1705	3.0
1800	4.3

Lower rates than those in Table 15.3 have been observed at 1600°C in cases where the contact is poor. These results²⁶ (on 20-mil tungsten sheet wired to graphite) show 0.5-mil penetration in 30 min at 1600°C. At 2100°C a carbide layer 5 mils thick is formed in 1 hr; this grows to a thickness of 20 mils in 20 hr.

(e) *Tantalum*. Numerous data have been reported for the carburization of metallic tantalum^{27,28} by gases at temperatures as low as 1300°C and for the carburization from solid carbon²⁹⁻³¹ under hydrogen at temperatures as low as 1400°C. A summary of this work is given by Schwarzkopf and Kieffer.³² The carburization of tantalum wires in contact with graphite occurs in helium.³³ A carbide layer 0.5 mil thick forms in 24 hr at 1400°C, and a layer 1.5 mils thick forms at 1800°C in 24 hr.

Very little reaction occurs between carbon black and tantalum sheet in 2 hr at 2000°C, whereas complete carburization results³⁴ in 3 min at 2600°C.

(f) *Niobium*. Niobium reacts with graphite above 815°C to form a protective surface layer composed of the two niobium carbides, NbC and Nb₂C (Table 15.4). This layer diffuses into the metal very slowly, penetrating to a depth of 2 to 3 mils in 2000 hr at 1010°C.

In addition to reacting with graphite, niobium also getters impurities evolved from graphite (Sec. 6-8.5), which increases the hardness, decreases the ductility, and leads ultimately to embrittlement.

(g) *Vanadium*. Very little information on the carburization of vanadium by graphite has been reported in the literature. Tammann and Schönert³⁵ found that carbon does not diffuse into vanadium at 800 to 980°C.

(h) *Zirconium*. Zirconium has been evaluated as a cladding material for graphite moderators at temperatures as high as 600°C and shows no

evidence of carburization up to this temperature. At 750°C, however, carburization has been observed.³⁶ Zirconium is even more reactive than niobium and getters impurities evolved from graphite. Therefore, unless

Table 15.4 — METALLOGRAPHIC RESULTS OF GRAPHITE-NIOBIUM REACTIONS AT VARIOUS TEMPERATURES IN HELIUM†²³

Material	Time, hr	Temperature, °C	Maximum penetration, mils		Remarks
			Ungettered helium	Zirconium-gettered helium	
Niobium	2000	705	11.0	‡	Carbide-oxide layer
	2000	815	2.0	‡	
	1000	870	4.5	1.7	Carbide layer
	2000	930	3.0	‡	
	2000	1010	3.0	1.5	
Nb + 1% Zr	2000	705	<0.1	‡	Carbide layer
	2000	815	0.5	‡	
	1000	870	1.5	0.3	
	2000	925	1.0	‡	
	2000	1010	2.0	1.5	

†A 2000-psi bearing pressure.

‡Not measured.

extreme care is taken to outgas the graphite prior to exposure to zirconium, the zirconium will absorb these impurities and be embrittled by them.

15-2.2 ALLOYS

(a) *Iron-Chromium Alloys.* The rate of carburization of iron-chromium alloys is apparently related to the microstructure existing at the carburization temperature. Figure 15.3 shows the increases in hardness observed²³ in specimens of a series of iron-chromium alloys carburized for 2000 hr at 704 and 816°C in contact with graphite in helium. At 816°C only those alloys which contain austenite in their microstructure (alloys containing less than 17 per cent chromium) show evidence of carburization. The two alloys that resisted carburization at 816°C (17 and 25 wt.% chromium) carburized rapidly at 870°C and above.²³

(b) *Iron-Chromium-Aluminum Alloys.* The ferritic alloys in this group exhibit thermal expansion coefficients similar to those of the ferritic steels and differ from them only in that they have been modified by the addition of aluminum to improve their oxidation resistance. The DB-2 alloy (7 wt.% aluminum-5 wt.% chromium) resists carburization by graphite in impure helium at 705 and 815°C in 2000 hr, but at 930°C there is extensive internal oxidation of aluminum and complete carburization in 1000 hr. The 25 wt.%

chromium-5 wt.% aluminum alloy shows a behavior similar to that of the DB-2 alloy. At 815°C some carburization and surface oxidation occur; at 930°C the reactions are extensive.²³

(c) *Nickel-Copper Alloys*. As has been pointed out, nickel is susceptible to graphitization when exposed to graphite during thermal cycling. Monel, a nickel-base alloy containing 30 wt.% copper, shows little evidence of

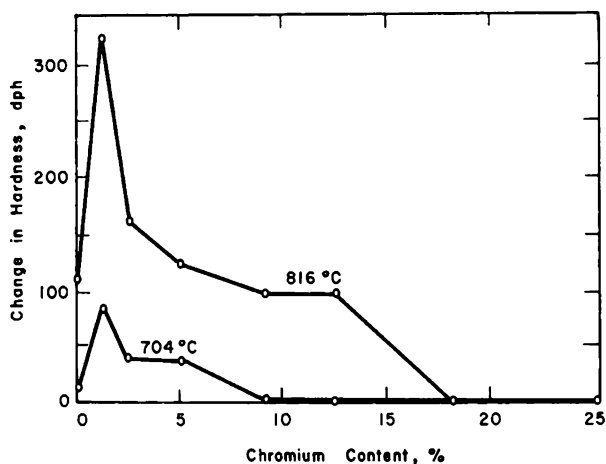


FIG. 15.3 The increase in hardness of iron-chromium alloys carburized in helium for 2000 hr in contact with graphite. (From Bokros, *Journal of Nuclear Materials*, Ref. 23.)

graphitization during thermal cycling in contact with graphite in helium. The effects of the carburizing and of the combined carburizing-aging treatments, which cause graphitization, on the tensile properties of "A" nickel and monel are illustrated²³ in Fig. 15.4. Tensile specimens of "A" nickel and monel saturated with carbon at 930°C were aged for 1000 hr at 315, 430, 540, and 650°C. Values for the tensile properties of control specimens that were subjected to the same thermal treatment used during the carburization are also included in Fig. 15.4 for comparison. The carburizing treatments do not decrease the room-temperature ductility of either material but do result in an increase in strength of both "A" nickel and monel. Subsequent aging of "A" nickel above 430°C causes a decrease in the room-temperature strength and hardness, whereas the strength and hardness of monel are increased slightly by the aging treatments. Metallographic examination reveals that extensive graphitization of carburized "A" nickel occurs during aging above 430°C, whereas graphitization of carburized monel does not occur even after 1000 hr at 650°C.

In a subsequent investigation it was found that both the solubility of carbon in nickel and the graphitization rate are reduced substantially for nickel-copper alloys containing 25 wt.% copper or more.³⁷

(d) *Nickel Alloys with Chromium, Molybdenum, and Iron.* The solubility of carbon in nickel in the range 705 to 930°C is appreciable. Nickel is particularly vulnerable to carburization when alloyed with carbide formers such as chromium, iron, or molybdenum. All tests²³ made on alloys of this type in contact with graphite in helium show carburization at 705°C. The alloy most resistant to carburization, Inconel X, forms a network of

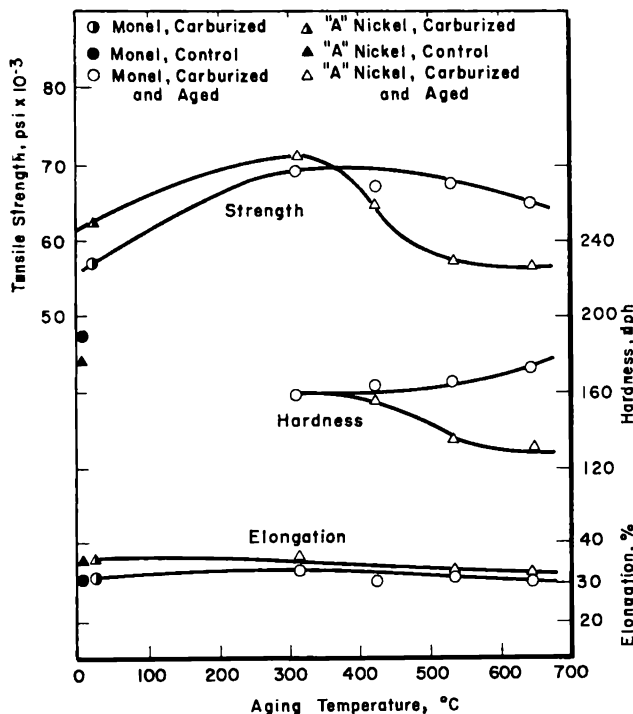


FIG. 15.4 The effects of carburization and subsequent graphitization on the properties of "A" nickel and monel. Aging time is 1000 hr. (From Bokros, *Journal of Nuclear Materials*, Ref. 23.)

carbide at the grain boundaries, which penetrates more than 10 mils in 2000 hr at 705°C. Inconel X is also oxidized internally by carbon monoxide impurity in the helium. Inconel 702 is especially vulnerable to internal oxidation, probably because of the 3.3 per cent addition of aluminum; the internal oxidation is most extensive at 705°C. Incoloy and Hastelloy B resist internal oxidation but carburize rapidly at 815°C.

(e) *Austenitic Steel.* The coefficients of expansion of alloys of the austenitic steels are very much higher than those of graphite; consequently they are less attractive as graphite cladding materials than alloys of the preceding groups. As might be expected from the high solubility of carbon in austenite, this group of alloys exhibits relatively low resistance to carburization. In most cases carburization occurs²³ in contact with graphite

in helium at 705°C, and all alloys except the silicon-modified 25-20 alloy and type 314 stainless steel carburize at 815°C. The test results are quite erratic, sometimes showing carburization and sometimes showing no carburization for the same alloy exposed at the same temperature. This behavior is evidently caused by a surface effect since the carburization was observed to be sensitive to impurities in the helium. For example, type 314 stainless steel carburizes rapidly at 870°C in zirconium-gettered helium but carburizes very little, if at all, at 930°C in impure helium. Also type 310 stainless steel carburizes at 705°C in areas where it is welded to "A" nickel saturated with carbon, but it does not carburize across the steel-graphite interface. Type 304 stainless steel is particularly susceptible to carburization, whereas stainless steels with higher chromium content are somewhat more resistant to carburization. The alloy containing 17 wt.% chromium and 14 wt.% nickel with small amounts of copper and molybdenum and the alloy with 15 wt.% chromium and 15 wt.% nickel with some nitrogen show no carburization after 2000 hr at 705°C but undergo considerable carburization^{23,24} at 815 and 930°C.

The effects of irradiation³⁸ on the carburization of types 310, 316, 430, and 446 stainless steels and of Inconel indicate that irradiation has no significant effect on the carburization rate of these alloys up to 815°C.

(f) *Protective Coatings.* It has been reported²³ that copper plate 1.5 and 8.0 mils thick reduces, but does not eliminate, carburization of type 316 stainless steel at 1010°C. At 900°C the protection is more complete, although some absorption of carbon is observed through a 1.5-mil plate. At 705 and 815°C, under a 2000-psi contact pressure in helium, a 1.0-mil copper plate on type 304 stainless steel does not retain its integrity²³ for 1000 hr. On the other hand, creep tests of type 304 stainless steel plated with 1.0 mil of copper have been conducted for 1000 hr at 815°C in 1 atm of flowing carbon monoxide with no carbon pickup.³⁹ Apparently copper plating is only effective when the graphite and copper surfaces are not in intimate physical contact.

One mil of chromium plate on type 304 stainless steel has proven effective against carburization at 816°C. This is illustrated by the hardness vs. exposure-time curves²³ shown in Fig. 15.5 for plated and unplated type 304 stainless steel exposed to graphite in helium at 704, 816, and 927°C. The plating is effective to 1750 hr at 816°C but diffuses excessively into types 304 and 430 stainless steel in 1000 hr at 927°C. It has been found²² that 2 to 6 mils of chromium on type 316 stainless steel does not prevent carburization at 1010°C but is quite effective at 900°C.

Diffused aluminum coatings, 2 to 3 mils thick, on type 304 stainless steel protect against carburization. However, at 815°C the coating diffuses, the rate being more than 2 mils in 350 hr and 4.5 mils in 2000 hr. At 930°C the coating diffuses²³ more than 10 mils in 2000 hr.

It has been reported²³ that an aluminized coating on Inconel diffuses

more slowly than it does on type 304 stainless steel. The coating on a specimen exposed at 870°C for 2700 hr diffused about 3.5 mils, making it unsatisfactory for use as a protective coating on thin-walled Inconel tubing for long periods of time at this temperature, but indicating that it might be

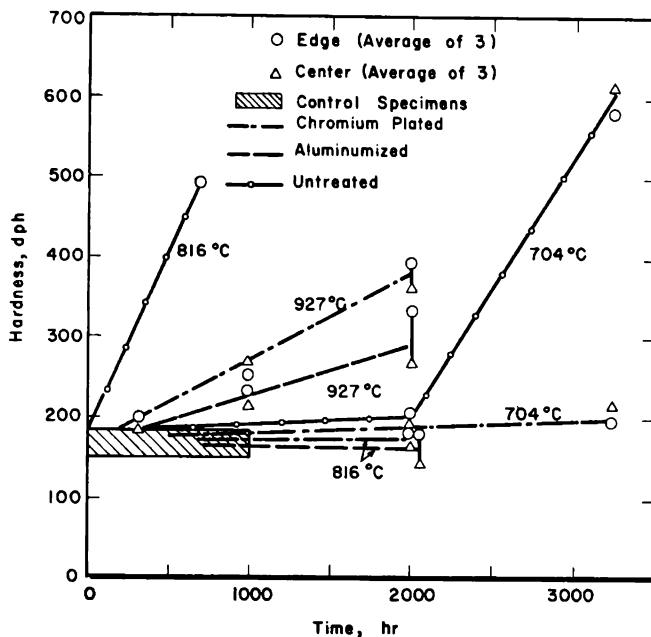


FIG. 15.5 The effect of coatings on the carburization of type 304 stainless steel held in contact with graphite in a helium atmosphere. (From Bokros, *Journal of Nuclear Materials*, Ref. 23.)

useful on heavier walled sections. However, Pessel⁴⁰ has found that a rapid diffusion of aluminum into Inconel occurs during aluminizing at 710°C. Following rapid cooling a diffusion layer about 30 mils thick spalls away. A low-melting (640°C) eutectic of 5.7 wt.% nickel-94.3 wt.% aluminum may account for this behavior.

A diffused chromium coating on Inconel and type 316 stainless steel did not prevent carburization²³ at 870°C.

A 5-mil molybdenum foil placed between type 316 stainless steel and graphite affords some protection against carburization at 870°C. However, carburization from the unprotected edges of the specimens made it impossible to determine whether or not the protection was complete.²³

15-3 Compatibility of Molten Salts and Graphite

The Molten Salt Reactor, conceived some years ago at Oak Ridge National Laboratory, is another concept in which the fluid flowing through the graphite moderator serves both as a heat-transfer medium and a carrier of the fuel. A typical salt is composed of uranium fluoride, thorium fluoride

with alkali metals, and beryllium or zirconium. The graphite in the molten-salt-system is unclad and must have the ability to resist corrosion and spallation. Evaluation tests have been made on the graphite to determine the degree of salt penetration, the compatibility with the fluoride-salt mixtures, and the effect on other container materials such as metal or nickel-base alloys. None of the foregoing has proved to limit severely the reactor concept.

A number of static tests have been conducted with graphite submerged in a mixture of $\text{LiF}-\text{BeF}_2-\text{UF}_4$ (62-37-1 mole %). At a temperature of 705°C , which is slightly above the expected reactor operating temperature, some UO_2 precipitate forms.^{41,42} Most of the precipitation occurs during the first 5 hr. The amount of precipitate obtained is a function of the volume of the graphite and therefore is believed to be due to oxygen absorbed from the graphite. Several methods can be successfully employed to remove the oxygen. One method is to expose the graphite to a fuel mixture at 700°C for 20 hr, discard this charge, and add a new one.⁴³ The oxygen can also be removed by the thermal decomposition of crystals of ammonium bifluoride.⁴⁴ Either method prevents the precipitation of UO_2 from a new charge of fuel for at least 1000 hr at 700°C .

Table 15.5 — PERMEATION OF VARIOUS GRADES OF GRAPHITE⁴³
BY $\text{LiF}-\text{BeF}_2-\text{ThF}_4-\text{UF}_4$ (67-18.5-14-0.5 mole %)

Test conditions:		Temperature:	705°C
		Pressure:	150 psig
		Exposure period:	100 hr
Graphite grade	Fabrication shape	Apparent density,† g/cm^3	Bulk volume of graphite permeated,† %
B-1	Rod	1.91	0.0
S-4-B	Bar	1.90 ⁽⁴⁾	0.2 ⁽⁴⁾
GT-123-82	Rod	1.91 ⁽⁵⁾	0.3 ⁽⁵⁾
CS-112-S	Rod	1.89 ⁽⁴⁾	0.5 ⁽⁴⁾
RH-1	Rod	1.89 ⁽⁵⁾	0.6
CEY-1350	Pipe	1.90	0.7
CEY-G	Pipe	1.88	0.9
S-4-A	Bar	1.89 ⁽⁴⁾	1.0 ⁽⁴⁾
CEY	Pipe	1.91 ⁽⁵⁾	1.0 ⁽⁵⁾

† Experimental graphites manufactured by the National Carbon Company. All values are averages of three measurements, with the exception of those with superscripts in parenthesis; the numbers in parenthesis are the number of values averaged.

The absorption of molten salts at 700°C has been measured for more than thirty different graphites.⁴³ It was found that the penetration of the salt into the graphite is independent of the type of salt used. The apparent densities and permeation values for some of the graphites tested are given in Table 15.5. The first three graphites listed satisfy the reactor design criterion that the maximum salt absorption be less than 0.5 per cent of the bulk volume of the graphite.

The metallic container materials in the liquid-salt reactor seem to be influenced by the graphite. Carburization of nickel-base container materials occurs when graphite is placed in circulating loops. Evidence of graphite in the salt has been observed after 500 hr at 815°C. Apparently it is dispersed in the liquid and then interacts with the metal.^{42, 44, 45}

References

1. W. P. Eatherly et al., Physical Properties of Graphite Materials for Special Nuclear Applications, in *Proceedings of the Second United Nations International Conference on the Peaceful Uses of Atomic Energy, Geneva, 1958*, Vol. 7, pp. 389-401, United Nations, New York, 1959.
2. C. J. Klamut et al., Material and Fuel Technology for an LMFR, in *Proceedings of the Second United Nations International Conference on the Peaceful Uses of Atomic Energy, Geneva, 1958*, Vol. 7, pp. 173-195, United Nations, New York, 1959.
3. M. W. Mallett et al., The Uranium-Carbon System, *J. Electrochem. Soc.*, **99**: 197-204 (1952).
4. W. G. Stroud, *The Penetration of Graphites of Different Purities by Lead-Bismuth Eutectic*, USAEC Report CP-2242, University of Chicago, Sept. 25, 1944.
5. R. Keen and R. Cygan, *High-temperature Materials Studies Semi-Annual Progress Report, July-December 1952*, USAEC Report NAA-SR-231, North American Aviation, Inc., May 1953.
6. S. C. Carniglia, North American Aviation, Inc., Interactions of Graphite with Liquid Sodium, in *Proceedings of the French-American Conference on Graphite Reactors, Brookhaven National Laboratory, November 12-15, 1957*, USAEC Report BNL-489, pp. 159-167, 1957.
7. V. K. Fredenhagen and H. Suck, Über die Bindung der Alkalimetalle durch Kohlenstoff, II, *Z. anorg. u. allgem. Chem.*, **178**: 353-365 (1929).
8. M. Dzurus et al., Argonne National Laboratory, Chemical Reactions of Graphite, in *Proceedings of the French-American Conference on Graphite Reactors, Brookhaven National Laboratory, November 12-15, 1957*, USAEC Report BNL-489, pp. 156-158, 1957.
9. R. C. Asher, A Lamellar Compound of Sodium and Graphite, *J. Inorg. and Nuclear Chem.*, **10**: 238-249 (1959).
10. R. C. Asher and S. A. Wilson, Lamellar Compound of Sodium with Graphite, *Nature*, **181**: 409-410 (1958).
11. C. Starr and R. W. Dickinson, *Sodium-Graphite Reactors*, Addison-Wesley Publishing Co., Inc., Reading, Mass., 1958.
12. R. L. Loftness et al., *The Corrosion of Refractory Materials in Sodium*, USAEC Report AECD-3472, North American Aviation, Inc., Nov. 20, 1951.
13. R. N. Lyon (Ed.), *Liquid-Metals Handbook*, 2nd ed., Superintendent of Documents, U. S. Government Printing Office, Washington 25, D. C., 1952.

14. M. M. Moyle, Pumping Molten Magnesium, *Metals & Alloys*, **22**(3): 716-720 (1945).
15. D. W. Mitchell, Solubility of Iron in Liquid Magnesium, *Metals Technol.*, **15**: T.P. No. 2309 (January 1948).
16. L. R. Kelman et al., *Resistance of Materials to Attack by Liquid Metals*, USAEC Report ANL-4417, Argonne National Laboratory, July 1950.
17. F. R. Morral, Corrosion by Molten Materials, *Wire and Wire Products*, **23**: 484-489, 571-579 (1948).
18. M. Simnad, General Atomic Div., General Dynamics Corp., personal communication, 1960.
19. T. A. Coultas, *Corrosion of Refractories by Tin and Bismuth*, USAEC Report NAA-SR-192, North American Aviation, Inc., September 1952.
20. E. L. Swarts, *The Action of Molten Uranium on Graphite*, USAEC Report KAPL-1765, Knolls Atomic Power Laboratory, April 1957.
21. L. D. Loch et al., Diffusion of Uranium Through Graphite, *A.I.Ch.E. Journal*, **2**: 195-198 (1956).
22. A. F. Gerds and M. W. Mallett, Compatibility of a Number of Metals and Alloys with Graphite, *Trans. Am. Soc. Metals*, **52**: 1027-1045 (1960).
23. J. C. Bokros, Graphite-Metal Compatibility at Elevated Temperatures, *J. Nuclear Materials*, **3**(1): 89-100 (1961).
24. J. C. Bokros, *Graphite Metal Compatibility at Elevated Temperatures*, USAEC Report GA-687, General Atomic Div., General Dynamics Corp. 1959.
25. M. Pirani and J. Sandor, Diffusion of Carbon into Tungsten, *J. Inst. Metals*, **73**: 385-395 (1947).
26. W. V. Green, Los Alamos Scientific Laboratory, personal communication, 1960.
27. I. E. Campbell et al., The Vapor Phase Deposition of Refractory Materials, *J. Electrochem. Soc.*, **96**: 318-333 (1949).
28. K. Becker and H. Ewest, Die physikalischen und strahlungstechnischen Eigenschaften des Tantalkarbid, *Z. tech. Physik*, **11**: 148-150, 216-220 (1930).
29. L. P. Mol'kov and A. V. Khokhlova, Tantalum Carbide in Hard Alloys, *Redkie Met.*, **4**: 10-23 (1935).
30. F. C. Kelley, Cemented Tantalum Carbide Tools, *Trans. Am. Soc. Steel Treating*, **19**: 233-246 (1932).
31. G. J. Trapp et al., *The German Hard Metal Industry*, British Intelligence Objectives Subcommittee Final Report 1385, Item 21, 1945 (p. 63); also issued as U. S. Publication Board Report PB-81624.
32. P. Schwarzkopf and R. Kieffer, *Refractory Hard Metals*, The Macmillan Co., New York, 1953.
33. W. Godsin, General Atomic Div., General Dynamics Corp., unpublished data, 1960.
34. C. Herrick, Los Alamos Scientific Laboratory, personal communication, 1960.
35. G. Tammann and K. Schönert, Über die Diffusion des Kohlenstoffs in Metalle und in die Mischkristalle des Eisens, *Z. anorg. u. allgem. Chem.*, **122**: 27-43 (1922).
36. F. Bowman, Atomics International, unpublished data, 1956.
37. J. C. Bokros, *An Evaluation of Nickel-Copper Alloys for Use as Graphite-Cladding Materials at Elevated Temperatures*, USAEC Report GA-1281, General Atomic Div., General Dynamics Corp., Apr. 30, 1960.
38. W. L. Kosiba, *Effect of Radiation on Metal-Clad Graphite in High Temperature, High Pressure CO₂*, USAEC Report GA-914, General Atomic Div., General Dynamics Corp., November 1959.
39. W. McCoy, Oak Ridge National Laboratory, unpublished data, 1960.
40. J. H. Pessel, Hanford Atomic Products Operation, unpublished data, July 1960.
41. J. A. Lane et al., *Fluid Fuel Reactors*, Addison-Wesley Publishing Company, Inc., Reading, Mass., June 1958.

42. W. H. Cook and D. H. Jansen, *A Preliminary Summary of Studies of INOR 8, Inconel, Graphite and Fluoride Systems, for the Period May 1, 1958 to December 31, 1958*, USAEC Report CF-59-1-4, Oak Ridge National Laboratory, Jan. 30, 1959.
43. *Molten-Salt Reactor Program, Quarterly Progress Report for Period Ending October 31, 1959*, USAEC Report ORNL-2890, Oak Ridge National Laboratory, Mar. 8, 1960.
44. *Molten-Salt Reactor Program, Quarterly Progress Report for Periods Ending January 31, 1960 and April 30, 1960*, USAEC Report ORNL-2973, Oak Ridge National Laboratory, Sept. 8, 1960.
45. *Molten-Salt Reactor Program, Quarterly Progress Report for Period Ending June 30, 1958*, USAEC Report ORNL-2551, Oak Ridge National Laboratory, Sept. 24, 1958.

Graphite-matrix Fuels

W. C. RILEY and J. KORETZKY†

16-1 Advanced Fuel-element Concepts

Since the study of reactors as a source of power began some 15 years ago, many different reactor concepts have attracted attention. The evolution of reactor concepts has been consistent in at least one respect: outlet coolant temperatures have increased continuously. As outlet coolant temperatures have increased, so have fuel-element temperatures. At present many advanced reactor designs require fuel-element temperatures so high that the use of metallic uranium fuel is prohibited; this has caused an increased interest in ceramics. Ceramic fuels, in general, and uranium dioxide, in particular, have poor thermal and mechanical properties. These problems can be lessened, however, by dispersing the ceramic fuel in an inert matrix that has more suitable thermal and mechanical properties.

16-2 Graphite as a Fuel Matrix

High strength at elevated temperatures, exceedingly high melting and sublimation points, excellent resistance to thermally induced stresses, and good moderating ability make graphite particularly attractive as a matrix material for high-temperature fuel elements. The major causes for concern about graphite as a matrix involve qualities that have not been studied extensively: the effects of fission-fragment irradiation and the ability to retain fission products. In addition, the poor resistance of graphite to oxidizing gases and to chemical reaction with uranium dioxide may limit its usefulness in some systems.

Although extensive development programs are now in progress in the United States and in Europe, actual experience in the fabrication and testing of graphite-matrix fuels has been quite limited. Hence the fabrication methods discussed in this chapter are based on experience with small volumes of materials processed in the laboratory.

Irradiation testing of graphite-matrix fuels has only just begun. However, most of the problem areas have been identified, and further testing is proceeding rapidly along the lines indicated in the subsequent sections.

Although graphite-matrix fuels containing plutonium and thorium oxides and carbides are under study, even less has been published on these fuels than on uranium-containing fuels. Because of differences in chemical and physical properties, fabrication methods will differ in some details. However, the problems associated with the graphite are similar. Therefore,

† Battelle Memorial Institute, Columbus, Ohio.

although uranium fuels are discussed exclusively in this chapter, some of the fabrication technology and most of the effects of irradiation apply also to thorium and plutonium fuels.

16-3 Fuel-Graphite Geometries

Graphite-matrix fuel elements have been prepared in various basic geometries, which have been classified as impregnated, admixed, or lumped. Impregnated bodies are formed by the introduction of fuel into the graphite by impregnation with a solution containing uranium. The fuel is converted to oxide or carbide by heat. Admixed bodies are formed by adding particles of fuel directly to the raw material mixture of binder and filler. Lumped specimens are those in which the fuel is in the form of a single piece, surrounded by unfueled graphite.

16-3.1 IMPREGNATED BODIES

An outstanding advantage of impregnation is that the graphite can be machined to size before fuel is added, thereby eliminating problems of contamination of graphite processing equipment and of fuel loss during processing and machining. The impregnation process appears to be the most easily adaptable to the remote handling required by fuel recycle. In addition, there are no restrictions on the graphite processing because of reaction between fuel and graphite. A major disadvantage is that the amount of fuel that can be introduced is limited by the pore characteristics of the graphite. Some difficulties have been encountered in obtaining uniform fuel distributions, although recent work¹ with thorium oxide indicates that this problem can be solved. Another disadvantage is that the fuel-particle size is inherently very small. As the size of fuel particles decreases, the percentage of fission fragments attenuated in the matrix increases, resulting in radiation damage to the matrix by fission fragments. Also, because diffusion of radioactive fission gases probably will be greater in graphite than in the fuel particle, the problem of fission-gas retention may become more serious as the fuel-particle size is decreased.

16-3.2 ADMIXED BODIES

The major advantages of admixed bodies are that a uniform fuel distribution can be obtained and the fuel-particle size can be controlled. Much higher fuel loadings can be obtained than by impregnation. However, the admixture process is not readily adaptable to remote handling, and some fuel loss and equipment contamination in each step of the process are inherent. Also, if uranium dioxide is the desired fuel, the reaction between uranium dioxide and graphite will limit the maximum heat-treatment temperature. It would not be possible, for example, to graphitize the binder carbon.

16-3.3 LUMPED BODIES

The advantages and disadvantages of lumped fuel elements are similar to those of admixed elements. The unfueled graphite will prevent fission products from recoiling out of the fuel element. Also it would be expected that contamination and fuel loss during processing could be minimized. The concentration of fuel in the core of the element will result in higher maximum fuel temperatures for a given power output.

Attempts have been made to combine the advantages of the admixed and lumped elements by placing an unfueled graphite shell around an admixed element. The major disadvantage is difficulty in fabrication.

16-4 Fuel-element Fabrication

16-4.1 IMPREGNATED FUEL ELEMENTS

The amount of fuel that can be added by impregnation and the properties of the fueled body depend on the pore structure of the graphite. The fuel loading that can be achieved is a function of the open porosity of the graphite body. If the pores of a graphite with a bulk density of 1.65 g/cm^3 were completely filled with uranium dioxide, the fuel body would contain about 60 wt.% uranium dioxide. Since a fraction of the pore volume is not available to the impregnating solution and since decomposition of the impregnating solution leaves the pores only partially filled, it is not possible to completely fill the pores with uranium dioxide. A typical value of fuel loading by a single impregnation is about 20 wt.% uranium dioxide.

Three general processes have been used to impregnate graphites with a uranyl solution:² vacuum impregnation, ammonia precipitation, and freeze drying. A brief description of each laboratory process is given below.

(a) *Vacuum Impregnation.*³ Machined graphite specimens are boiled in distilled water for 30 min to remove surface dust and then are placed in a furnace and heated at 800°C for 30 min in a helium atmosphere to remove water and other volatile substances present. The specimens then are placed in the impregnation apparatus and evacuated for 15 min, and a water solution of uranyl nitrate is introduced until the solution just covers the specimen. After the specimen has soaked for 5 min, the apparatus is opened to the atmosphere through a reflux condenser, and the specimens are allowed to remain in the solution for an additional 10 min to allow the atmospheric pressure to drive the solution into the pores.

The specimens are dried by allowing them to stand over a desiccant such as calcium sulfate for 40 to 80 hr, or, alternatively, by passing helium over them at room temperature for 4 to 5 hr. The uranyl nitrate is converted to uranium oxide by heating for 30 min at 800°C in helium.

Bodies containing up to 53 mg of uranium per cubic centimeter have

been prepared by this method. The uniformity of the uranium oxide concentration depends strongly upon the drying step. If the rate of drying is not carefully controlled, the concentration of uranium oxide builds up at the surface.

A similar method has been employed to infiltrate thorium oxide. Starting with 1.5-in.-diameter graphite spheres with a density of 1.25 g/cm^3 , uniform fuel loadings up to 1.4 g of thorium oxide per cubic centimeter have been achieved.¹

(b) *Ammonia Precipitation*. In an effort to achieve a more-uniform distribution of uranium, Steele⁴ precipitated the uranium as ammonium diuranate before drying the sample. This was accomplished by soaking the impregnated sample in ammonia for 24 hr. After the specimen had been dried, it was desiccated for four days and then gradually heated in helium to 800°C to form uranium dioxide. Uranium concentrations up to 35 mg/cm^3 have been prepared by this method.

Precipitation of the diuranate reduced the surface-to-average ratio concentration from 8 to 2. However, it is possible that careful control of the drying operation would result in a uniform distribution and obviate the need for this additional step.

(c) *Freeze Drying*. A uniform distribution of uranium by impregnation methods is obtained by freeze drying.⁵ This is achieved by impregnating a block of graphite with a solution of uranyl nitrate dihydrate in tertiary butyl alcohol and then quickly freezing the impregnated block in liquid nitrogen. The solvent is removed by sublimation, and the block is heated at 725°C to convert to uranium oxide.

16-4.2 ADMIXED ELEMENTS

The properties of fuel elements prepared by the admixture process are governed by the selection of the graphite raw materials and the processing methods. It is advantageous to bake the specimens at as high a temperature as practical to increase the bulk density and thermal conductivity of the fuel element. The highest temperature that can be employed in baking, without appreciable reduction of the uranium dioxide, will depend upon such factors as the fuel-particle size, particle density of the oxide, and the baking atmosphere.

A typical laboratory process for preparing admixed fuel elements is given in Fig. 16.1. Uranium dioxide powder is mixed with 10 wt.% shellac dissolved in ethyl alcohol for 4 hr in a propeller type mixer. During mixing the temperature is raised to about 65°C to vaporize the alcohol. The remaining alcohol is removed by subjecting the mixture to high vacuum. Pellets of uranium dioxide are pressed at 12,500 psi in a steel die. The compacts are crushed, and nodules with the desired size range are retained.

The graphite molding mix is composed of equal parts by weight of

graphite flour and a phenol formaldehyde resin. The graphite and resin are mixed for 15 min in a Muller type mixer and are blended on rolls for 15 min. The mixture is then pulverized in a Muller type mixer for 3 hr.

The uranium dioxide nodules and graphite mix are blended with a spatula to ensure homogeneity. Pellets are pressed at 20,000 psi in a steel

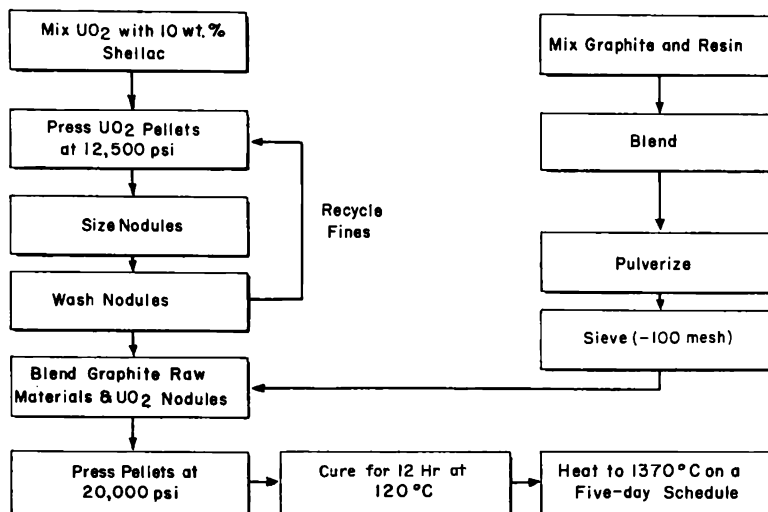


Fig. 16.1 Flow diagram for fabrication of admixed graphite-matrix fuel bodies.⁶

die. The pellets are heated for 12 hr at 120°C in a circulating-air oven to set the resin. Compacts then are packed in graphite tubes, and the tubes are filled with graphite powder and heated in a direct-fired gas furnace on the following five-day schedule:

Temperature range, °C	Heating rate, °C/hr
15–280	17
280–760	8
760–1370	16
4-hr soak at 1370	

Bodies containing uranium in concentrations up to 3100 mg/cm³ have been prepared by this process. The maximum amount of fuel that can be added has not been determined. However, physical properties change with increasing fuel content (Sec. 16-5).

Admixed elements have been made in tubular, cylindrical, rectangular parallelepiped, and spherical geometries. Large blocks, 7 by 7 by 4½ in., and cylinders, 6 in. in diameter and 12 in. high, have been made commercially.

16-4.3 LUMPED ELEMENTS

Like admixed elements, the properties of the lumped element are governed by the selection of the graphite raw materials and by processing conditions.

Several methods of fuel addition are presently being investigated. A brief description of each process is given below. All are in a preliminary stage of development.

(a) *Extrusion of Graphite Around a Uranium Dioxide Cylinder.*⁷ A uranium dioxide extrusion batch is made containing uranium dioxide powder, Carbopol, plasticizer, and sufficient water to make the mixture plastic. Solid cylinders of uranium dioxide are extruded. The cylinders are first air dried and then are dried overnight at 90°C to partially cure the binder. A graphite extrusion mix, containing 65 wt.% graphite and 35 wt.% resin binder, is mixed in a Muller type mixer for 30 min and then blended on sheeting rolls for 15 min. The graphite mixture is extruded around the uranium dioxide cylinder as it moves through the die throat. The composite bodies are cured in air at 200°C overnight, packed in graphite tubes, and baked on a schedule described previously for admixed elements.

(b) *Pressing Graphite Shell on Sphere of Uranium Dioxide.*⁸ A lump of uranium dioxide is placed between a preformed half shell composed of a mixture of graphite and a suitable binder. The composite body is pressed at 10,000 psi. The specimens are then packed in graphite powder and baked in a gas-fired furnace as described in Sec. 16-4.2.

(c) *Inserting Fuel in Preformed Graphite Body.*⁹ A hole is bored in a graphite body, and the desired amount of fuel is inserted. The fuel is held in place by a graphite plug, which is screwed into the bore.

16-4.4 ADMIXED ELEMENT WITH UNFUELED SHELL

Techniques for making elements of this type are similar to those used for admixed and lumped elements.⁸ Spheres with outside diameters up to 1½ in., and with unfueled shell thicknesses ranging from ⅛ to ¼ in., have been made. These spheres contain about 88 mg of uranium per cubic centimeter. This process is in a preliminary stage of development.

16-4.5 URANIUM CARBIDE-MATRIX ELEMENTS

Uranium dicarbide has two definite advantages over uranium dioxide for use as fuel in a graphite matrix. It does not react with graphite,¹⁰ and its thermal conductivity is several times greater than that of the oxide.¹¹ Uranium dicarbide, however, reacts with humid air at room temperature, which introduces problems in handling during processing.

The most extensively used method for the preparation of graphite containing uranium dicarbide involves the addition of the fuel as uranium dioxide and the subsequent conversion to carbide *in situ* by suitable heat-

treatment.¹⁰ In this manner problems encountered in handling the carbides are reduced.

The reaction between uranium dioxide and graphite has been studied by several laboratories with conflicting results (see also Sec. 6-5.2). Some investigators¹² have reported a reaction between these materials at temperatures as low as 800°C; whereas others² have reported no reaction at temperatures up to about 1820°C. It appears that the varying results are caused by differences in the chemical reactivity of different sources of uranium dioxide and graphite and differences in the degree of contact between the graphite and the oxide. Of course, this contact will depend, to a large extent, on the forming conditions.

The major disadvantage in the method of preparing uranium carbide from uranium oxide *in situ* is that the quantity of fuel that can be converted to carbide is limited. When large fuel particles, 100 μ or greater, and high fuel loadings, 2000 mg of uranium per cubic centimeter, are required, an excessive amount of carbon is removed from the graphite in the immediate vicinity of the fuel particles during conversion. Such bodies crumble during handling.¹³

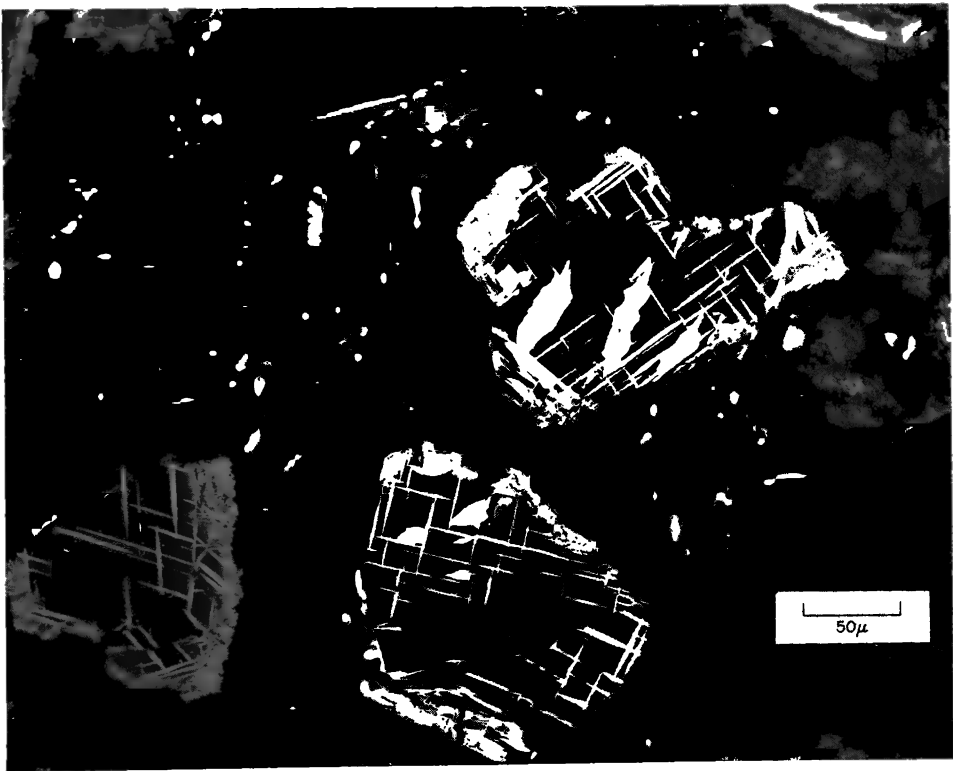


FIG. 16.2 Dispersion of UC in graphite heat-treated at 1260°C for 4 hr. Black portions of fuel particles are UC, white hairlines are UC₂, and large white areas are U₂C₃. (From Riley, *American Society for Testing Materials*, Ref. 13.)

Fabrication of elements with high fuel loadings can be accomplished by incorporation of UC or UC₂ as the starting fuel compound. In this case oxidation of the carbides can be a severe problem during mixing and baking. However, it can be greatly minimized if the following precautions¹³ are taken:

1. Use a coal-tar pitch as a binder. Oxygen released from synthetic resins oxidizes the uranium carbide.
2. Dissolve the binder material in benzene, thereby permitting the mixing operations to be performed under liquid.
3. Bake in a purified argon atmosphere.

Sound bodies with uranium loadings up to 3100 mg/cm³ have been prepared by this method.

Recent experiments¹³ on the chemical stability of UC in a graphite matrix indicate that conversion of the UC to U₂C₃ and finally to UC₂ occurs between 1260 and 1490°C. After graphite containing UC has been baked for 4 hr at 1260°C, three compounds (UC, U₂C₃, and UC₂) can be detected¹³ in the fuel particles, as indicated in Fig. 16.2. Further heating to 1490°C completely converts the carbides to UC₂.

16-5 Effect of Fuel Loading and Particle Size on Physical Properties

The physical properties of admixed fuel elements baked to 1425°C have been studied^{10,14} as a function of fuel content for several uranium oxide loadings. The strength and thermal conductivity decrease with in-

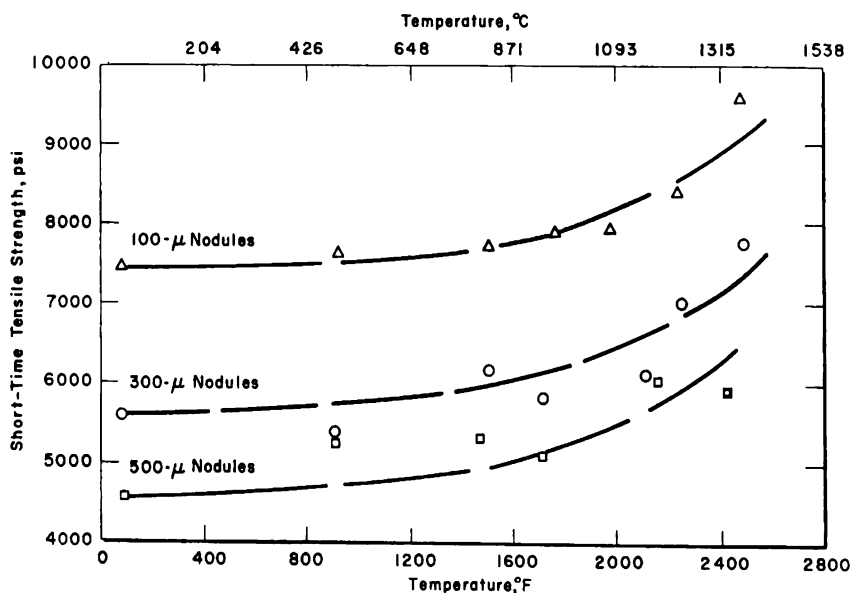


Fig. 16.3 Tensile strengths of extruded bodies containing uranium dioxide nodules.¹⁵

creasing fuel content. A uranium loading of 1.2 g/cm^3 reduces the thermal conductivity to about one-half and the modulus of rupture to about two-thirds of the values for unfueled graphite. Thermal expansion is reduced about 15 per cent.

The physical properties were measured on the same series of samples after heating at 2800°C for 30 min. X-ray diffraction studies indicate that conversion to the carbide is essentially complete after this treatment. At high uranium content (1.26 g/cm^3), the strength is reduced to about 30 per cent of the value for the unfueled graphite. The thermal and electrical conductivities increase significantly with increasing carbide content.

The effect on the tensile strength of increasing the uranium dioxide particle size of extruded uranium dioxide-graphite elements is presented in Fig. 16.3. Stronger bodies are obtained with small fuel particles. The tensile strength increases with temperature for each particle size.

16-6 Radiation Effects in Fueled Graphite

16-6.1 RADIATION-INDUCED PHYSICAL-PROPERTY CHANGES IN FUELED GRAPHITE

Radiation-induced property changes in fueled graphite result from bombardment by neutrons and fission fragments and from the presence of fission fragments lodged in the graphite lattice (Chap. 7). It has been estimated that a light fission fragment dissipates about 6 Mev of its energy in the production of primary lattice-atom displacements before coming to the end of its range (about 17μ in graphite), whereas a heavy fragment with a range of about 12μ loses about 9 Mev in the same manner. For the same fission, neutrons dissipate about 0.6 Mev in the production of atomic displacements in the graphite. Therefore fission fragments produce about 25 times more displacements in graphite than do neutrons. Since the range of fission fragments in graphite is several orders of magnitude smaller than that of neutrons, the fission damage is much more highly localized around fuel particles than is neutron damage.

16-6.2 DEPENDENCE OF EFFECTS OF FISSION FRAGMENTS ON FUEL-PARTICLE SIZE

The percentage of fission fragments attenuated in the graphite matrix decreases with increasing fuel-particle size,¹³ as shown in Fig. 16.4. Therefore radiation damage to the matrix caused by fission fragments decreases with increasing size of the fuel particles. If fuel loadings are not excessive, the use of large fuel particles can provide a continuous portion of the matrix in which no fission fragments are attenuated.¹⁶ Consequently the body would be expected to retain the desirable properties of the graphite up to high exposures.

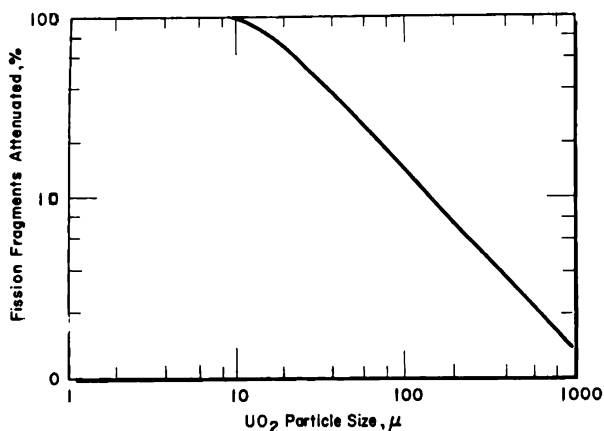


FIG. 16.4 Variation in the percentage of fission fragments attenuated in the matrix with the uranium dioxide particle size. (From Riley, *American Society for Testing Materials*, Ref. 13.)

16-6.3 EXPERIMENTAL WORK

The effect of high-temperature irradiation on the dimensions of various types of fueled graphite is shown in Table 16.1. The raw materials, fuel loading, and geometry of the fuel elements were controlled variables. With the exception of the uranium dicarbide samples, the combined effects of neutrons and fission fragments led to a decrease in dimensions. In no case did irradiation cause structural failure of the fuel body, although it should

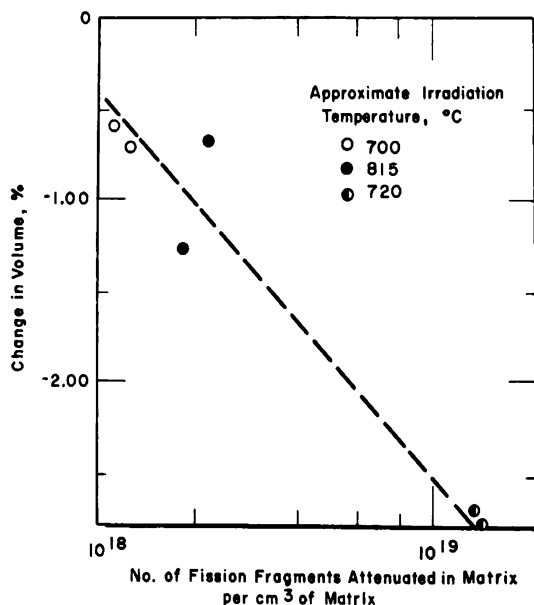


FIG. 16.5 Radiation-induced volume changes in uranium dioxide-graphite fuel elements. (From Riley, *American Society for Testing Materials*, Ref. 13.)

Table 16.1— FABRICATION AND IRRADIATION HISTORY OF FUELED GRAPHITE SPECIMENS^{13, 18}

Sample No.	Raw materials	Fuel	Uranium loading, mg/cm ³	Av. fuel-particle size, μ	Laboratory heat-treating temp. (max.), °C	Approximate irradiation temp., °C	U ²³⁵ burn-up, at. %	Change in volume, % [†]
1	Texas 55 coke bonded with standard pitch (admixed)	UC ₂	43	18	2480	815	5	+1.68 [‡]
2	AGOT graphite bonded with BV-1600 resin (admixed)	UO ₂	45	66	1370	815	5	-1.01
3	AGOT graphite (impregnated [§])	UO ₂	130	~1	800 ^{§§}	720	1.9	-2.74
4	NC-2301 graphite bonded with standard pitch (admixed)	UO ₂	150	150	1400	700	1.6	-0.68
5	AGOT graphite bonded with BV-1600 resin (admixed)	UC	2600	61	1200	780	1.2	-3.44

[†] Average of two specimens, except where noted.[‡] Average of three specimens.[§] Desired shapes were machined from fully graphitized AGOT graphite and impregnated with boiling uranium nitrate. The specimen was heated to convert the nitrate to oxide.^{§§} After impregnation.

be noted that the burn-ups are well below those required by most reactor concepts.

In Fig. 16.5 the per cent change in volume for samples containing uranium dioxide is plotted against the number of fission fragments attenuated in the matrix per cubic centimeter of matrix.¹³ A continuous decrease in volume with increasing exposure is indicated.

As in the case of unfueled graphite, irradiation of graphite fuel elements results in a reduction of the thermal conductivity. The effect of irradiation temperature has been measured¹⁷ from room temperature to 1300°C. As might be expected the change decreases continuously with increasing irradiation temperature.

The effect of irradiation at 700°C on the mechanical properties of spherical graphite fuel elements has been reported¹³ on two samples in which a burn-up of about 1.7 at.% of U²³⁵ atoms was achieved. The combined neutron and fission-fragment irradiation caused an increase in compressive strength, a decrease in impact resistance, and an increase in abrasiveness.

16-6.4 STRUCTURAL CHANGES IN THE GRAPHITE MATRIX

The irradiation of fueled graphite tends to change the graphite to a disordered carbon structure. With respect to mechanical properties, the decrease in impact resistance, the increase in compressive strength and abrasiveness, and the decrease in thermal conductivity are indicative of a change to a disorganized carbon structure. However, it would be expected that the disordering process would be accompanied by a decrease in density. For this reason the observed dimensional contraction of graphite-uranium dioxide elements is somewhat surprising. Some decrease in density in experiments on admixture type graphite fuel elements has also been noted by British workers.¹¹

In the case of dimensional changes, it is possible to separate the effects of neutrons and fission fragments, at least qualitatively, by comparison of measurements on unfueled graphite with those on impregnated and admixed fuel elements.¹³ At temperatures above 300°C the neutron bombardment of unfueled graphite results in dimensional contraction.¹⁹ The amount of contraction depends on exposure, irradiation temperature, and the microstructure of the graphite, as determined by raw materials and fabrication conditions (Sec. 9-4). In general, the amount of contraction appears to be much greater for less-ordered carbon structures than for highly graphitic structures. Now consider fuel elements with different fuel particle sizes and exposed to the same irradiation conditions. The impregnated elements (sample 3, Table 16.1) had a more highly graphitic structure than did the admixed elements (sample 4, Table 16.1) because both binder and filler of the former were graphitized at about 2750°C. It would be expected, then, that neutrons alone would cause less contraction in these elements than in

the admixed elements. However, the amount of contraction induced by neutrons plus fission fragments in the impregnated elements was greater by a factor of 4 than that induced in admixed or lumped elements. Therefore these data strongly suggest that fission-fragment irradiation as well as neutron irradiation caused dimensional contraction.

16-6.5 ANNEALING OF RADIATION EFFECTS

It is possible to anneal radiation effects induced at low temperature in graphite fuel elements.²⁰ However, it appears to be more difficult to anneal radiation damage caused by fission fragments than that caused by neutrons.

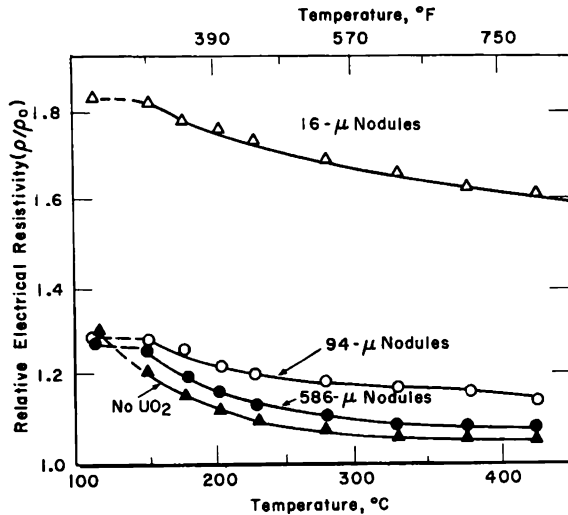


FIG. 16.6 Radiation-damage annealing in uranium dioxide-graphite bodies. The irradiation temperature ranged from 30 to 88°C. Samples were heated for 1 hr at each temperature.¹⁵

Figure 16.6 shows the change in the electrical resistivity ratio, ρ/ρ_0 , during pulse annealing for 1 hr at successive 25°C intervals. The major portion of neutron damage is annealed at 425°C. By contrast, fission-fragment damage¹⁰ for 16-μ fuel particles does not anneal appreciably after 12 hr at 725°C.

16-7 Fission-product Release from Fueled Graphite

Fission-product release is perhaps the major unresolved question concerning the performance of graphite-matrix fuels. In a number of reactor concepts, the reactor coolant flows directly over the graphite-matrix fuel element. No limit has been established on the maximum fractional release (ratio of fission-gas atoms released from graphite to fission-gas atoms created) of fission products that can be tolerated if direct maintenance is to be done on equipment in the primary coolant loop. However, a fractional release of 10^{-7} is generally considered to be satisfactory.

16-7.1 EXPERIMENTAL WORK

Two types of experiments have been used to measure the release of fission products from fueled graphite. Annealing experiments have been conducted by performing irradiations at low exposure and low temperature followed by measurement of the fission gas released by subsequent heat treatment.²¹ In-pile experiments have also been performed²² in which helium gas was passed over the specimens during high-temperature (540 to 815°C) irradiation. The sweep gas was conducted out of the reactor, and the fission products were trapped and measured.

Table 16.2 — FISSION-GAS RELEASE FROM SPHERICAL FUEL ELEMENTS CAUSED BY A 6-HR HEAT-TREATMENT²² at 815°C

Type of fuel element [†]	Fuel particle size, μ	Available Xe ¹³³ released, %
Admixed	150	2.9
Impregnated	1	7.6
Admixed-lumped	150	1.0

[†]Spheres were about 1.5 in. in diameter and contained about 5.1 g of UO₂. Irradiation, prior to laboratory heat-treatment, was about 10^{12} neutrons/cm². The uranium was about 93 per cent enriched.

Some results of the laboratory annealing experiments are presented in Table 16.2 for admixed, impregnated, and admixed-lumped fuel elements of spherical geometry. The relatively high release from the impregnated sphere resulted from the large fraction of fission fragments which escaped from the fuel particle into the graphite matrix.

During the in-reactor experiment on an admixed sphere at 700°C, the ratio of release rate to equilibrium production rate was about 0.01 for Xe¹³³ and about 0.06 for Kr^{85m}. The activity in the gas stream flowing over an impregnated element was too great to be handled by the available equipment.

The results of the above experiments indicate that fission-product release from these elements is undesirably high for a reactor system in which the coolant comes in contact with the fuel elements. However, at these temperatures the total quantity of fission gas released is smaller than that calculated to have recoiled into the graphite matrix, indicating that graphite retains at least a portion of the recoiled fission gases.

16-7.2 METHODS OF REDUCING FISSION-PRODUCT RELEASE

Three methods of reducing fission-product release from graphite appear to merit consideration: the application of surface coatings, the use of an

impervious graphite, and the development of an impervious coating on fuel particles.

Results of recent experiments indicate that surface coatings on graphite can materially reduce fission-product release at high temperature (see also Sec. 14-7). A number of coatings were subjected to screening tests, and two types of silicon-silicon carbide coatings merited further evaluation. Graphite-matrix fuel elements with these coatings were irradiated and subjected to laboratory annealing tests.²¹ At the maximum temperature of testing (815°C), no fission-product release was detected. However, in other tests²² conducted during irradiation, silicon-silicon carbide coatings did not prevent the release of fission gases. The reason for failure of the coatings in this second experiment was not determined.

The development of impervious graphites for use as fuel containers is another approach to the retention of fission gases. This work is in an early stage of development, but the results appear promising. Several experimental materials have been developed with very low permeability (Sec. 6-9.5). The effects of long-term reactor radiation on the permeability are, as yet, relatively unknown, and much more testing is necessary.

Two techniques for applying a ceramic cladding to the individual uranium dioxide particles have been studied recently. In one, a highly sinterable alumina powder was applied to unsintered uranium dioxide particles by a spraying-tumbling technique.²³ The composite pellets were then pressed isostatically and sintered in hydrogen. The other involved vapor deposition of aluminum oxide on uranium dioxide particles in a fluidized bed.²⁴ Clad fuel particles can be dispersed in graphite by admixture methods.

The results of a preliminary evaluation show that the aluminum oxide protected the uranium dioxide from oxidation when the pellets were heated in air for 100 hr at 650 and 980°C. After an exposure of 3.6×10^{14} thermal neutrons/cm² at room temperature, there was no measurable release of fission products from uranium dioxide particles clad with aluminum oxide by spray tumbling when heated to 925°C in vacuum for seven days. Under similar treatment, bare uranium dioxide of 85 per cent theoretical density released about 1.5 per cent of the fission gases. The uranium dioxide particles clad with vapor-deposited aluminum oxide released 3.7×10^{-3} per cent of the available Xe¹³³ during a 4-hr heat-treatment at 1090°C following an exposure of 5.2×10^{14} thermal neutrons/cm² at room temperature.

16-8 Future Research Effort

There are several problems associated with the preparation and evaluation of graphite fuel elements which require intensive research. By far the most important problem is fission-product release. Certainly the preliminary experiments on coatings for both fuel particles and graphite are encouraging. However, the effect of irradiation on the permeability of these

materials is not known. Radiation effects on these materials must be investigated at reactor design exposures.

Present data on radiation effects have been obtained from experiments in which the fuel burn-up is low compared with that required for most reactor applications. In addition, the effect of irradiation temperature on physical-property changes has not been defined over the temperature range now being considered in advanced reactor design. Additional information on radiation effects, both as a function of temperature and exposure, is needed.

Many reactor concepts now require fuel recycle. Some of these concepts employ either thorium carbide in graphite or plutonium oxide or carbide in graphite. A great deal of fabrication development is needed in these areas.

References

1. W. E. Parker and F. Rusinko, Jr., *Thorium Oxide Infiltration of Graphite Spheres*, USAEC Report NYO-9059, Speer Carbon Co., June 15, 1960.
2. *Design and Feasibility Study of a Pebble Bed Reactor-Steam Power Plant*, USAEC Report NYO-8753 (Vol. II), Sanderson & Porter, May 1, 1958. (Classified)
3. M. A. Kanter, *Impregnation of Graphite with Uranium Compounds for Use as Fuel Rod Material*, USAEC Report ANL-4118, Argonne National Laboratory, Feb. 6, 1948.
4. G. N. Steele, *Studies in the Impregnation of Graphite with Uranium*, USAEC Report NAA-SR-36, North American Aviation, Inc., June 23, 1950.
5. D. J. Zigrang and G. A. Bennett, *Preparation of Fuel Elements for the NAA Homogeneous Graphite Research Reactor*, USAEC Report NAA-SR-240, North American Aviation, Inc., Aug. 12, 1953.
6. H. Z. Schofield et al., *Fabrication of Urania-Bearing Graphite*, USAEC Report BMI-T-26, Battelle Memorial Institute, May 15, 1950.
7. L. D. Loch, Battelle Memorial Institute, unpublished data, 1956.
8. *Progress Report, Pebble Bed Reactor Program, June 1, 1958-May 31, 1959*, USAEC Report NYO-2373, Sanderson & Porter, May 31, 1959.
9. R. Schulten, The Development of High Temperature Reactors, in Symposium on Gas-Cooled Reactors, *Franklin Inst., Monograph No. 7*, May 1960.
10. W. P. Eatherly et al., Physical Properties of Graphite Materials for Special Nuclear Applications, in *Proceedings of the Second United Nations International Conference on the Peaceful Uses of Atomic Energy, Geneva, 1958*, Vol. 7, pp. 389-401, United Nations, New York, 1959.
11. P. Murray, The Future of Ceramics as Nuclear Fuel. 2. Development of the New Fuels, *Nuclear Power*, 4(37): 89-94 (May 1959).
12. W. J. Kroll and A. W. Schlechton, Reactions of Carbon and Metal Oxides in a Vacuum, *J. Electrochem. Soc.*, 93: 247-258 (1948).
13. W. C. Riley, Graphite as a Fuel Matrix, *Am. Soc. Testing Materials, Spec. Tech. Publ. No. 276*, pp. 324-335, 1960.
14. M. Janes, National Carbon Company, Graphite-Matrix Fuel Element Research by National Carbon Company, in *Progress in Carbide Fuels*, pp. 34-35, USAEC Report TID-7589, Apr. 20, 1960.
15. L. D. Loch et al., *Studies of Graphite for Fuel Elements*, USAEC Report TID-10001, Battelle Memorial Institute, Oct. 13, 1954.
16. D. W. White et al., General Electric Company, Irradiation Behavior of Dispersion

- Fuels, in *Fuel Elements Conference, Paris, November 18-23, 1957*, pp. 717-747, USAEC Report TID-7546 (Bk. 2), 1958.
17. C. R. Tipton, Jr. (Ed.), *Reactor Handbook, Vol. 1, Materials*, 2nd ed., p. 301, Interscience Publishers, Inc., New York, 1960.
 18. R. W. Dayton and C. R. Tipton, Jr., *Progress Relating to Civilian Applications During July 1959*, USAEC Report BMI-1366, Battelle Memorial Institute, Aug. 1, 1959.
 19. R. E. Nightingale et al., Damage Effects to Graphite Irradiated Up to 1000°C, in *Proceedings of the Second United Nations International Conference on the Peaceful Uses of Atomic Energy, Geneva, 1958*, Vol. 7, pp. 295-300, United Nations, New York, 1959.
 20. R. H. Kernohan, The Effect of Fissionable Particle Size on Fission Damage in Graphite, in *Proceedings of the French-American Conference on Graphite Reactors Held at Brookhaven National Laboratory November 12-15, 1957*, pp. 10-15, USAEC Report BNL-489, September 1958.
 21. H. S. Rosenberg et al., *Apparatus for the Study of Fission-gas Release From Neutron-activated Fueled Graphite*, USAEC Report BMI-1444, Battelle Memorial Institute, June 7, 1960.
 22. W. C. Riley et al., Release of Fission Products from Fueled Graphite, in *Nuclear Metallurgy*, Vol. VI, pp. 87-94, McGraw-Hill Book Company, Inc., New York, 1959.
 23. A. K. Smalley et al., *Alumina-Clad UO₂ for Fuel Applications*, USAEC Report BMI-1321, Battelle Memorial Institute, Feb. 18, 1959.
 24. R. W. Dayton and C. R. Tipton, Jr., *Progress Relating to Civilian Applications During February 1960*, USAEC Report BMI-1423, Battelle Memorial Institute, Mar. 1, 1960.

Graphite Moderator Design

J. C. FOX†

17-1 Advantages and Limitations of Graphite as a Structural Moderator

In the design of graphite-moderated reactors, many unique features have been devised to take advantage of the desirable properties of graphite or to minimize or compensate for undesirable characteristics. The general principles of moderator design will be illustrated in this chapter by descriptions of design features and operating experience of many graphite-moderated reactors of all types. A listing of the principal graphite-moderated reactors can be found in Table 1.2.

17-1.1 ADVANTAGES

When the first nuclear reactors were built in 1942, graphite was chosen for the moderator primarily because it was readily available. Today it is still one of the most widely available moderator materials, produced in volume in many countries for other industrial uses. Graphite is also an economical moderator because it is easily manufactured, shaped, and purified to meet nuclear standards and because it does not normally require repurification, replenishment, or replacement.

Certain properties of graphite make it singularly attractive for high-temperature reactors. It is the only commonly employed structural material whose strength increases with temperature. Graphite can withstand high-temperature gradients, has good shock resistance, and is normally inert to other structural materials.

17-1.2 LIMITATIONS

Early reactors were constructed with little knowledge of the remarkable changes in the properties of graphite caused by neutron bombardment. Dimensional changes and the storage and release of energy have caused problems in some reactors designed without foreknowledge of such phenomena. Today, although the effects of irradiation on the properties of graphite are more thoroughly understood, there are not sufficient data available, particularly for high temperatures, to enable rigorous analytical design of moderator structures. Despite considerable experience with moderator structures of differing design, it is still difficult to predict the behavior of an entire structure.

Other limitations of graphite, such as low tensile strength, porosity,

† Hanford Laboratories, General Electric Company, Richland, Wash.

chemical reactivity with some coolants, galvanic corrosion with some structural materials, and lack of homogeneity, are better understood, although for many applications existing data are inadequate.

17-2 Structural Design Considerations

A sound graphite structural design is based on the evaluation of many factors. These include objectives of the design, graphite temperature, mechanical loads, properties of graphite, reactor operating requirements, manufacture, and construction. Also pertinent to moderator design is the development and testing work conducted to ascertain the behavior of the moderator in service.

17-2.1 OBJECTIVES

The purposes for which a reactor is built establish the relative importance of the moderator in the whole design. In a materials-testing reactor operating at modest service conditions, the moderator design may be subordinate to that of other components. When reactors are built to advance a technology (e.g., a liquid-metal-fuel reactor), extensive development and testing and generous provision for monitoring and inspection may be justified. In large power or production reactors, considerable attention to design detail is warranted to effect economies in fabrication and erection and to assure a long useful life for the reactors.

17-2.2 TEMPERATURE

Changes in the properties of graphite during irradiation depend greatly on temperature, as do the amount of thermal expansion, rate of chemical reactions, core reactivity, and the nature of accidents that can occur in the reactor core. Correct evaluation of these factors, vital to a sound design, is possible only if the temperature distribution in the graphite is well known.

Unfortunately, it is difficult to determine accurately the temperature patterns in many graphite structures. The rate of heat generation in the graphite is usually 5 to 6 per cent of the reactor thermal power. For simplicity it is commonly assumed that this heat is generated uniformly in the graphite in proportion to the specific power in the adjacent fuel. Although conventional heat-transfer equations apply, significant errors can be introduced in evaluating the power distribution in the reactor by the effect of surface contacts or clearances (especially after long service) or by the thermal conductivity of the graphite.

Heat generated in the moderator is ordinarily removed by coolant flowing through the fuel channels (Fig. 17.1). Temperature gradients are therefore steeper near those channels. In gas-cooled reactors having a low specific power, clearance spaces containing gas are the chief resistance to heat flow, and the graphite temperature across a lattice cell is relatively uniform. Water-cooled reactors usually have higher specific powers and

higher thermal gradients in the graphite than gas-cooled reactors. The temperature distribution throughout the moderator depends on the power distribution in the reactor and the coolant flow arrangements, as illustrated

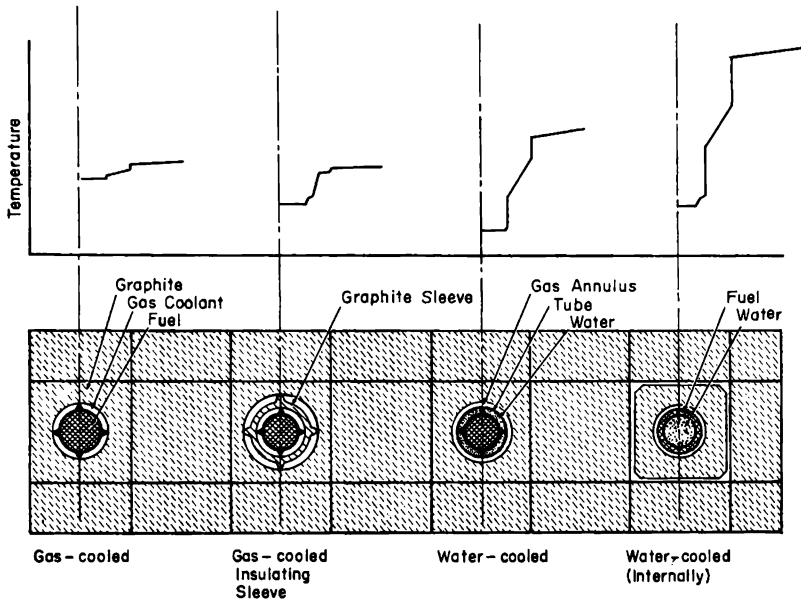


Fig. 17.1 Temperature distribution in some representative graphite lattices.

by a comparison of the Oak Ridge X-10 Reactor and the Brookhaven Graphite Research Reactor (BGRR) (Fig. 17.2).

At a given point in a reactor, the graphite is subjected to significant

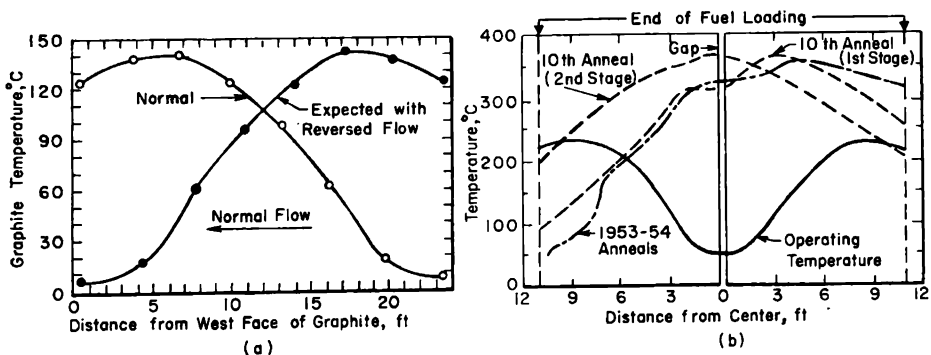


Fig. 17.2 Temperature distribution on the longitudinal axis of (a) the Oak Ridge X-10 Reactor and (b) the Brookhaven Graphite Research Reactor, showing the effect of coolant flow direction.^{1,2}

variations in temperature because of fluctuations in power distribution. These changes are caused by control-rod manipulation, fuel burn-up, or loading of fresh fuel. Changes can also be caused by accidents, such as the flooding of a portion of the moderator with sodium or water.

In the face of these uncertainties, it is difficult to assign an exact temperature to a particular region of a graphite structure. Moreover, the effect of the temperature of the structure depends on such design features as the manner in which graphite pieces are supported, aligned, and restrained with respect to each other; on clearances; and on mechanical loads. All factors considered, the behavior of a moderator structure is predictable only within a broad range of values. Ordinarily, then, temperature effects require that a design either accommodate a wide range of behavior or allow corrective measures to be taken.

17-2.3 MECHANICAL LOADS

Among the mechanical loads that a moderator may bear are the weight of the graphite, fuel, coolant, and other structural materials; gas pressure or differential pressure; restraining forces; earthquake loads; and forces imposed by operating or maintenance procedures. Supporting and restraining structures must act to transmit and limit moderator loads, to maintain accurate alignment of the moderator and its supports, and to control movements under both equilibrium and transient conditions. Thermal-expansion effects are often most important during transient conditions, when the large heat capacity of the moderator can cause it to lag behind other components in heating or cooling. Mechanical loads largely determine the manner in which individual pieces or groups of pieces are supported or interlocked.

Internal pressure loads are exerted on moderator blocks and on the structure in gas-cooled reactors by the pressure differential required to force gas through the cooling channels, as in the French G-2 Reactor (see Sec. 17-3.3). Pressure loads can also occur in pressurized-water-cooled reactors if large quantities of steam issue from a leaking tube.

Earthquake loads, which depend on the geographical location of the reactor, have received greater attention in recent designs. An example of a reactor designed for a region of high seismic intensity is the Japanese Tokai Mura Reactor. Earthquake loads to be assumed in design are usually fixed by government agencies or by local building codes and standards.

High forces may be exerted on portions of the moderator by extraordinary operating or maintenance procedures, such as removal of swollen fuel elements and damaged tubes or removal of a safety rod from a crooked channel. Such forces can be confined to a small region of a structure by careful design of the support and interlocking of pieces.

17-2.4 GRAPHITE PROPERTIES

Properties that have been most important in past moderator designs are dimensional changes, stored energy, and chemical reactivity. In more recent designs increasing attention is being directed to permeability, strength, and thermal conductivity.

The well-known expansion of graphite during low-temperature irradiation has received considerable attention in reactor design. Recently, contraction of graphite during high-temperature irradiation has become an equally important consideration. This reversal of behavior at elevated temperature emphasizes the dependence of a design on the operating temperature.

Stored energy has been a formidable problem in some low-temperature gas-cooled reactors, primarily because this phenomenon was not anticipated and the early designs do not always lend themselves to alleviating its effects. Removal of part of the stored energy can be accomplished if proper instrumentation and equipment are provided to enable controlled release of the energy. Stored energy is expected to be of less concern as reactor temperatures are increased.

Chemical reactions, however, are of vital importance to high-temperature reactors. Interest has centered on graphite-air, graphite-carbon dioxide, and related reactions, but others have also received study, e.g., reactions with water, molten metals and salts, and galvanic cells formed with other structural materials.

17-2.5 REACTOR OPERATING REQUIREMENTS

Some important moderator design considerations are imposed by the operating conditions and characteristics of the reactor. The examples that follow illustrate the need for a careful examination of reactor design under all equilibrium and transient conditions to elucidate every factor pertinent to the design.

In many reactors the specific power and graphite temperature are highest at the center of the core and are lowest nearer the core boundary. A more uniform temperature can be achieved if the graphite is insulated from the coolant channels in regions of lower power by a semistagnant gas layer between the moderator and the coolant (Fig. 17.1). The effect of insulating spaces on the temperature coefficient of reactivity of local regions of the reactor should be carefully analyzed and related to control-systems design.

Extraordinary incidents must always be anticipated in a reactor design. Examples of such incidents include coolant-tube leakage and fuel-element or moderator-can failure. A moderator soaked with either water or sodium will be seriously poisoned; this poisoning can result in a distorted power distribution or inability to operate the reactor. In water-cooled reactors the possibility of a coolant-tube leak makes it necessary to incorporate means for draining and drying the graphite. With a pressurized hot-water system, where large quantities of steam can escape into the graphite structure, adequate venting must be provided to avoid excessive pressure loads on the structure. In sodium-cooled reactors moderator cans must be replaceable in anticipation of a possible sodium leak into a can.

17-2.6 MANUFACTURE AND CONSTRUCTION

Achieving economy and simplicity without sacrificing accuracy or quality is a prime goal in the fabrication of a moderator structure. A large reactor may use as many as 100,000 pieces, variously called bars, blocks, bricks, logs, or tiles, according to local custom. Proper design can achieve production economy by requiring as few different types of block as possible, by simplifying each block design, and by minimizing the number of machining steps and setups. Fabrication and erection dimensions and tolerances must take into account the required accuracy of alignment at assembly, settlement or cumulative errors in assembly, and the accuracy of fabrication of other reactor components.

17-2.7 DEVELOPMENT AND TESTING

Although most information on the physical and chemical properties of graphite is obtained from continuing research programs, unique design problems requiring specific development and testing programs are usually encountered in each reactor design. For example, a liquid-metal-fuel reactor project would require the development of low-porosity graphites, fabrication techniques for large complex blocks, and methods of forming cemented joints.

Graphite stack mock-ups are useful to verify the accuracy of design, manufacture, and erection. Moderator mock-ups are also used to determine the effect of dimensional changes and as practice beds for mechanical equipment and procedures used in fuel handling, control, maintenance, and inspection. Some moderator structures have been prestacked in sections to assure proper final assembly.

More-complex equipment may be required for certain tests such as determining the effect of sodium flooding of a moderator can or coolant-tube failure in a pressurized-water reactor. In the latter case a full-scale test is necessary because of the difficulty of making an analytical evaluation of the incident and the difficulty of extrapolating from model tests. The test equipment includes a portion of the moderator enclosed in a pressure vessel for safety, a tube supplied from a hot pressurized-water reservoir, and a mechanism to initiate a complete parting of the tube. A series of tests with different moderator structural designs establishes the optimum design for confining graphite damage to a small region.

17-2.8 MONITORING AND INSTRUMENTATION

Regardless of calculations, analyses, and predictions, the behavior of a graphite-moderator structure in service can be determined with certainty only by observation. This may take the form of continuous monitoring, as for temperature or position of components; periodic inspection, as for move-

ment or oxidation; or sampling to assess cumulative physical and chemical effects.

Temperature monitoring is of particular value because so many effects depend on temperature; thus it is wise to distribute a large number of temperature monitors through representative temperature regions of the reactor.

Monitoring the movement of a moderator is commonly accomplished by continuous indication of the position of the extremities of the stack or by periodic measurement of the alignment of channels (Sec. 8-5.1). These methods do not distinguish between thermal expansion and the contraction or expansion caused by irradiation, but they can be useful for predicting long-range trends and for determining the need for corrective measures.

Monitoring for chemical reactions and irradiation effects utilizes both irradiation of test specimens and sampling of the moderator, but only the latter technique provides a clear idea of the variations that occur in the moderator. Clever remote-operation trepanning tools have been used successfully at the British Experimental Pile Zero (BEPO), Windscale, Hanford, Brookhaven, and Oak Ridge reactors to cut small cylindrical samples from the moderator blocks (see Fig. 8.11).

17-3 Reactor Moderator Designs and Operating Experience

17-3.1 UNCOOLED REACTORS

In 1942 the world's first nuclear reactor (built under the football stands at the University of Chicago) was candidly dubbed "Chicago Pile No. 1" because it was simply a pile of graphite blocks interspersed with chunks of fuel. Although the word "pile" effectively described the unsophisticated design of the first reactors, it is now considered an obsolete term, relegated to history. Similarly, the early reactors are important more for their role in laying the foundation for nuclear science than for the significance of their designs.

Several uncooled graphite-moderated reactors have been built, chiefly for physics experiments. These reactors include CP-1 (later restacked as CP-2), Hanford 305 Test Reactor, Savannah River 305 Test Pile, Graphite Low Energy Experimental Pile (GLEEP), Physical Constants Test Reactor (PCTR), and the first Soviet reactor (see Table 1.2). Reactors of this type operate at low power, i.e., in the range of watts to kilowatts, and at approximately room temperature. Since neutron-flux levels are very low, radiation effects on the graphite are insignificant.

17-3.2 LOW-TEMPERATURE GAS-COOLED REACTORS

Air-cooled reactors comprise the category of gas-cooled reactors operating at graphite temperatures of 200°C or less. Restricted to low operating temperatures to avoid excessive oxidation of the graphite, air-cooled reac-

tors are susceptible to radiation damage that is manifested chiefly as growth in dimensions and in the storage of energy.

Reactors in this group include the Oak Ridge X-10, the BEPO, the Belgian BR-1, the BGRR, the French G-1, and the two Windscale reactors. Power ratings range from several megawatts to as high as 160 Mw. Their moderator designs generally do not incorporate features that mitigate radiation effects. The lower power reactors, X-10, BEPO, and BR-1, are quite similar in design. Slow accumulation of radiation damage has not impaired their operation, although stored-energy releases have been conducted in BEPO and X-10. Radiation effects in higher power reactors may lead to serious indirect effects, as illustrated by the Windscale incident, which occurred during a stored-energy release [see Sec. 17-3.2(e)].

(a) *Oak Ridge Graphite Reactor (X-10)*. The X-10 Reactor was built in 1943 at the Oak Ridge National Laboratory as a forerunner of the Hanford water-cooled production reactors; it is now utilized as a research and isotope-production facility. From early irradiations made in X-10, the strange physical effects of reactor radiation on graphite were first observed. The X-10 Reactor³ is a simple 24-ft cubical pile of horizontal layers of 4-in.-square graphite blocks up to 50 in. long. The blocks are parallel except for occasional transverse stringers, and the structure is keyed for stability. The 1248 fuel channels are formed by V cuts in the sides of adjoining blocks. Air is drawn into the reactor at atmospheric pressure and temperature and is discharged 60°C higher in temperature; air leaving some channels may reach 225°C. The maximum measured graphite temperature is normally 145°C.

Having been in operation over 16 years, the X-10 Reactor has accumulated some radiation damage despite the modest neutron flux. In this period the height of the graphite stack has increased slightly more than $\frac{1}{4}$ in. at a distance of 8 ft from the front of the 24-ft cube. A stored-energy region was found to exist generally in the forward portion of the moderator, skewed slightly to the side where the cool air enters.¹ In 1960 it was estimated that 4 per cent of the stack volume contained energy that could be released spontaneously; maximum stored energy releasable at 250°C was 35 cal/g. Although this condition was not considered hazardous and did not jeopardize continued operation of the reactor, a low-temperature stored-energy release was conducted in 1960. The release was accomplished by operating the reactor with reversed air flow, holding the graphite temperature for soaking periods at 140 and 160°C, then shutting down the reactor and blocking air flow to increase temperature during the release. A maximum graphite temperature of 236°C was reached in the final stage. Annealing was accomplished except in peripheral regions, including the three outer rings of fuel channels. Similar anneals may be conducted in the future, possibly incorporating reduced flow in fringe channels and a longer final baking period to increase annealing in peripheral regions.

(b) *British Experimental Pile Zero*. BEPO has been in operation at Harwell since 1948 as a research facility. It is generally similar in construction to the X-10 Reactor, having a slightly larger (26 ft) cubical graphite stack.⁴ Fuel channels are five sided and have a V-trough bottom and a rectangular top. With the forced-exhaust cooling system, air enters at atmospheric temperature and leaves at approximately 80°C. The maximum graphite temperature is normally 110°C.

Two stored-energy releases have been performed in BEPO, the first in 1954 and the second in 1958. Their purpose was to avoid the accumulation of what could be considered a hazardous amount of stored energy. The first release was accomplished by operating the reactor at low power without cooling until, at a temperature of 120°C, a spontaneous release was triggered. This release, which gradually spread through the reactor, raised the maximum observed temperature to 325°C, although it failed to anneal a considerable volume of the reactor.⁵

Following the accident at Windscale during a stored-energy release (see below), it was clear that, despite voluminous laboratory data on adiabatic stored-energy release, there was insufficient understanding of the more complex process of release in an actual reactor structure. Planning and execution of the second BEPO release was therefore quite elaborate. An extensive sampling program was carried out prior to the release, and the sequence of the release was predicted in some detail. Some 476 thermocouples were installed in the reactor, 411 in graphite and 65 in fuel. The second release was initiated by drawing preheated air into the reactor while the reactor was operating at a power just sufficient to make the burst-cartridge detection system useful. The maximum graphite temperature achieved during the release was slightly in excess of 300°C. A more thorough anneal was accomplished on this second anneal, and much information was gained on the propagation of energy release in graphite structures.⁵

(c) *Brookhaven Graphite Research Reactor (BGR)*. Because this reactor was designed for a much higher operating power than BEPO, expansion of the graphite received greater attention in its planning. Since some data were available at the time of design, it was possible to allow for expansion of the moderator stack and to provide means of periodic measurement of movement.

The graphite stack is a 25-ft cube, split into two separate stacks with a 3-in. gap at the mid-plane (Fig. 17.3). Round fuel channels bored in the graphite bars are perpendicular to the central gap, which serves as the inlet plenum for cooling air.⁶ Air flows outward to either end of the stack from the center, an arrangement that achieves a high power level in a cubical moderator with modest outlet air temperature.

The moderator design was based on the expectation that graphite blocks would remain essentially stable parallel to the extrusion axis but would expand in the transverse directions; the blocks are parallel to the fuel

channels and are interlocked with transverse graphite keys. It was anticipated this design would allow sufficient freedom for transverse expansion but would prevent obstruction of the central air gap. The stack is supported on steel base plates to allow thermal movement. Coil springs are placed between the side shields and the moderator to furnish some restraint to lateral expansion. The top shield, which rests on the moderator, is built in 25 sections so that it can move with the graphite.

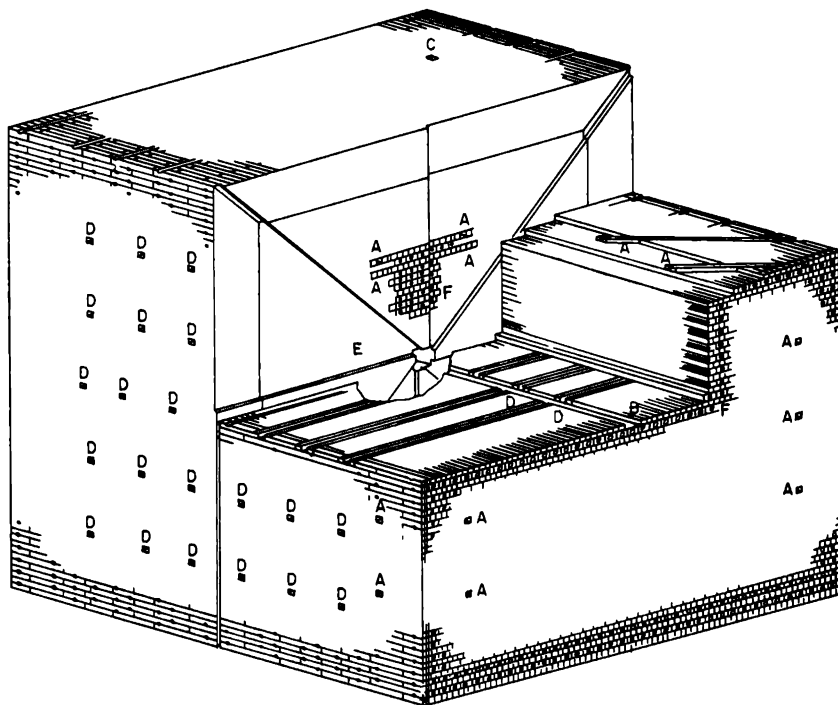


FIG. 17.3 Graphite structure of the Brookhaven Graphite Research Reactor.¹ A, diagonal control-rod channels. B, central core opening. C, shot wells. D, experimental channels. E, central gap. F, fuel channels.

With cooling air entering at the mid-plane, graphite temperatures are lowest (50°C) in the high-neutron-flux region (see Fig. 17.2), making the structure relatively vulnerable to irradiation effects. After three years of operation, the graphite had expanded $\frac{3}{32}$ in. vertically and $\frac{9}{16}$ in. horizontally at the mid-plane, and stored energy was estimated to be reaching potentially hazardous values.²

Anneals were performed in 1953, 1954, and 1955 and have been performed several times since then. For the first three anneals, the cooling system was converted to unidirectional flow through the reactor toward the diagonal control-rod banks so that fission heating would be more concentrated near the temporary inlet side of the reactor. The reactor was oper-

ated at approximately 1 Mw power and 10 per cent air flow to induce graphite temperatures of 320 to 350°C in 24 to 36 hr; then power and air flow were reduced to zero for several hours before air flow was restored to cool the stack. No unexpected rapid heating was observed with this controlled-heating method. Procedures have been revised in subsequent anneals. The most satisfactory procedure yet reported⁷ was that used in the tenth anneal of May 30–31, 1959 (see Fig. 17.2). The reactor was operated at $\frac{3}{4}$ Mw for a period of 22½ hr with single-pass air flow at a very low rate. During this time the graphite temperature increased to a maximum of 370°C. The reactor was then scrammed, air flow was reversed in a few minutes, and the reactor was again operated at approximately the same power for 3½ hr. The power and air flow were then reduced over a 4-hr period.

Growth in 1958 had reached approximately $\frac{3}{4}$ in. vertically and $1\frac{3}{16}$ in. horizontally at the mid-plane but was only slightly more than half that which would have occurred without annealing. No movement of the two outlet faces of the stack has been observed. An unexpected trend has been the decrease of the central air gap by about $\frac{7}{8}$ in. This is attributed to a fanlike bulging of each half-stack resulting from the weight of the top shield and the cyclic thermal stresses on the distorted stack.²

(d) *French Reactor G-1*. The first French plutonium-production reactor at Marcoule is generally similar to the BGRR. The moderator is approximately a horizontal cylinder nearly 27 ft in diameter and $27\frac{1}{2}$ ft long and is bisected by a cooling-air inlet plenum like the BGRR. The graphite blocks lie parallel to the horizontal fuel channels, which are formed by cutouts at the edges of the bars. The stack is restrained around the periphery by a structural-steel framework. Air enters at atmospheric temperature⁸ and leaves at about 220°C. The average graphite temperature is 125°C.

(e) *Windscale Reactors*. Two identical large air-cooled reactors were built at Windscale by the United Kingdom as plutonium-production units. They began operation in 1950 and 1951 but were abandoned in 1957 following the fire and contamination incident in Reactor No. 1 during a stored-energy release.

The graphite stack has the form of an octagon 50 ft across flats and 25 ft thick along the horizontal axis; it is held in compression by spring-loaded structural-steel members.⁹ Fuel channels are parallel to the axis of the stack. The horizontal control rods are perpendicular to them, and the safety rods are vertical. Cooling-air plenums are located between the shield and the graphite at the front and rear. Air was forced through the core under pressure and exhausted through a stack and filter. Since these reactors were used for production, little has been published about them in the unclassified literature, although the moderator stack design has been described as being more "open" than BEPO, apparently having some clearances between blocks.¹⁰ It may be presumed that operating conditions were not

radically different from those of the similar BGRR or G-1 reactors, although power was approximately 160 Mw in the larger Windscale reactors.

Owing to the rate of accumulation of stored energy in these reactors, it was the practice to conduct periodic releases in a manner similar to the initial BEPO release, i.e., by operating the reactor at low power without cooling. In the course of such a release in Windscale No. 1 on the morning of Oct. 8, 1957, it was surmised that the graphite temperature was beginning to decrease too soon, and the reactor, having been shut down after the release began, was restarted to increase the temperature.¹¹ Unfortunately the temperature of reference was not representative, and, unknown to the staff, further operation of the reactor served to increase the fuel and graphite temperature to the point of initiating self-sustaining graphite combustion. During the following days it became apparent that the graphite temperature could not be reduced, even by repeated attempts at air cooling by convection or forced flow. From sharp increases of radioactivity in the exhaust air during the cooling trials, it was concluded that some fuel cans had burst. Inspection revealed that the graphite was indeed burning in a region encompassing 150 channels. Various stratagems to control the reaction during the evening of October 10 were unsuccessful. It was finally extinguished the next morning by flooding the reactor with water. By this time, however, substantial quantities of gaseous fission products had escaped from the reactor stack.

Investigation of the incident led to the conclusion that monitoring of reactor power and temperatures of both graphite and fuel was inadequate because the heating pattern in the large reactor during stored-energy releases was different from that during normal operation. In addition it was evident that the release procedure was based on inadequate information on the temperature of the graphite and on the process of propagation of energy release in a moderator structure. The second BEPO release was planned to elucidate these factors.

Recommendations were made for modification of both Windscale reactors to ensure their safety in future releases; however, the capital investment required was not deemed worth while since the Calder Hall reactors were already on line and producing plutonium. The reactors were consequently abandoned.

17-3.3 INTERMEDIATE-TEMPERATURE GAS-COOLED REACTORS

The intermediate-temperature range in today's technology may be defined as lying generally between the temperature of the peak stored-energy release (approximately 200°C) and an upper temperature (roughly 400°C) which has been considered a limiting temperature for both fuel cladding and chemical reactions between graphite and carbon dioxide. The carbon dioxide-cooled British and French power reactors operate in this temperature range.

Gas cooling was originally favored in Britain for graphite-moderated reactors because of a hazardous characteristic of most water-cooled graphite-moderated designs: loss of cooling water (e.g., by boiling) can cause a sudden reactivity increase and a power excursion that could result in an accident of disastrous consequences. Such an incident is impossible in a gas-cooled reactor, although other severe accidents can occur.

By concentrating on carbon dioxide-cooled reactors, the British have developed a family of installations based on the original Calder Hall design, each successive design incorporating refinements and improvements or occasional unique departures. Reactors in this family are: Calder Hall, Chapel Cross, Berkeley, Bradwell, Hinkley Point, Hunterston, Latina, Tokai Mura, Trawsfynydd, and Dungeness (see Table 1.2). In the French program, however, the G-2 and G-3 production reactors were patterned after the air-cooled G-1, but a design generally similar to the British type was adopted for a newer series of power reactors, EDF-1, EDF-2, and EDF-3.

(a) *Calder Hall Reactors.* The general arrangement of the Calder Hall graphite stack was influenced largely by the necessity of fitting it inside a pressure vessel, providing for thermal movement and irradiation effects, and establishing a sound basic design amenable to development and refinement. Balancing these factors led to the choice of a cylindrical pressure vessel enclosing a graphite stack having vertical fuel channels. The stack is 24-sided, 36 ft across at the corners, and 27 ft high. It occupies approximately 30 per cent of the vessel volume and is supported on a steel grid inside the vessel.¹²

Structural design of the graphite stack is based on the expectation that graphite would remain dimensionally stable parallel to its extrusion axis but would expand in the perpendicular directions. Maximum growth was anticipated just below the center of the core because of the power and temperature distribution (coolant flows upward, entering at 135°C and leaving at 333°C). Since expansion was expected, a solid stack with all bricks touching was considered impractical. Instead, a brick-and-tile construction was adopted, which is essentially a forest of columns 8 in. square by 27 ft high (Fig. 17.4). Each column is composed of alternate brick and tile layers. The bricks are 32 in. tall, with the extrusion axes vertical; the tile layers are composed of two thin tiles laid with the extrusion axes horizontal but perpendicular to each other (Fig. 17.5). Bricks have clearance for growth, whereas the tiles are intended to preserve constant spacing between columns. Bricks and tiles are keyed together in cruciform pattern, which minimizes clearances at the keys.

Since a columnar structure lacks stability, the stack has peripheral elastic garters at the tile layers. Each garter is composed of 24 members connected by pin joints at the stack corners, where bearing plates transmit restraining loads to the solid reflector blocks. The upper and lower garter members encircling the top and bottom reflectors are composed of a rod and

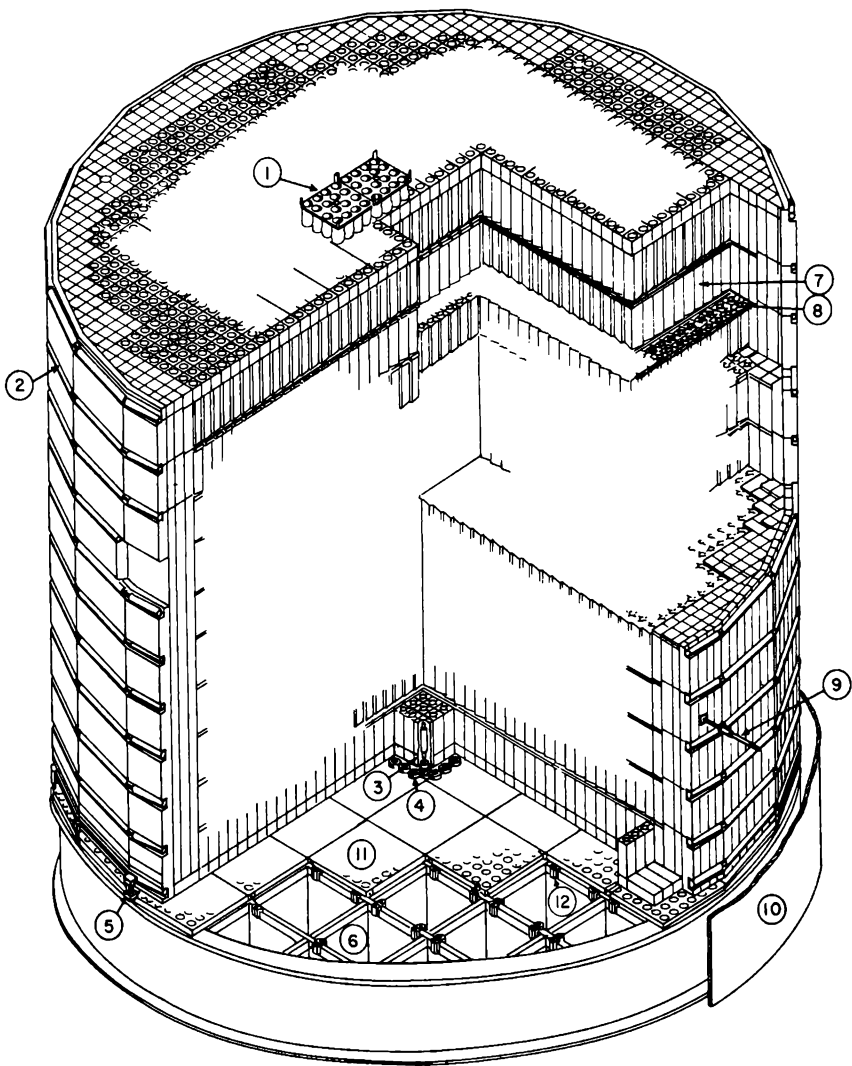


FIG. 17.4 Calder Hall moderator structure. (1) Charge pan. (2) Side restraint garters. (3) Fuel-element support boss. (4) Graphite support bearing. (5) Bottom side restraint and radial keys. (6) Support grid. (7) Moderator bricks. (8) Moderator tiles. (9) Wigner probe. (10) Pressure vessel. (11) Base support plates. (12) Levelling screws. (From Long, *Nuclear Power*, Ref. 12.)

four tubes of steel and stainless steel having a net thermal-expansion coefficient equal to that of graphite. All other garter members are nine-piece steel units, which allow greater expansion. Garters thus allow freedom for thermal expansion and growth yet bind the stack for stability unless shrinkage predominates.

Each graphite column is supported by a strut that rests on a ball bearing on the base plate (Fig. 17.6). The bearings allow for differential thermal

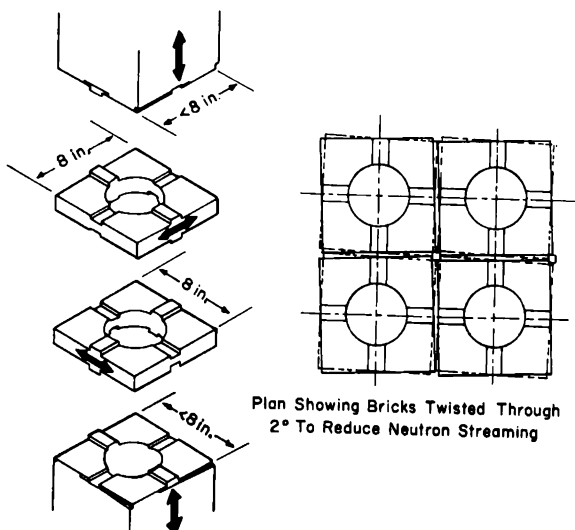


FIG. 17.5 Calder Hall brick and tile arrangement. Arrow shows direction of graphite extrusion. Sides of bricks are angled in opposite directions in alternate layers to reduce vertical streaming of neutrons. (From Long, *Nuclear Power*, Ref. 12.)

expansion between steel and graphite. Angle brackets on the stack garters are keyed at the 24 corners to the supporting steel to maintain orientation of the stack.

It was desirable to enhance performance by employing the highest practical density of the graphite structure and by minimizing leakage of coolant and neutrons. Fuel channels were bored through the bricks and

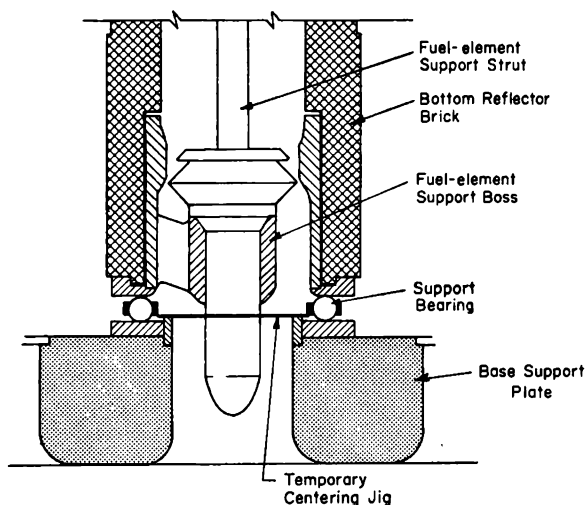


FIG. 17.6 Calder Hall graphite-column support. The ball bearing allows relative motion of the graphite and the steel bedplates to accommodate differential thermal expansion.¹⁴

tiles rather than cut from the sides or corners where they would be open to the gaps between blocks. There are four sizes of clearance space in the moderator, placed according to the amount of expansion predicted; no clearance is allowed between bricks in the side reflector. Bricks are rotated 2° from the lattice grid to opposite directions in adjacent layers to reduce neutron streaming.

Stored energy is not generally considered to be a serious problem in the Calder Hall family of reactors because of their operating temperature, although consideration has been given to techniques for conducting stored-energy releases at infrequent intervals (see also Chap. 13).

(b) *Bradwell Reactors*. These two reactors were originally designed with graphite sleeves surrounding the fuel elements to increase the moderator temperature and to reduce the amount of radiation-induced expansion. During construction of the reactors, it became known that radiation-induced graphite contraction would occur. The stack was redesigned to allow for contraction, the final version omitting the graphite sleeves and incorporating zirconium spacer pins between bricks to maintain a constant spacing.¹³ This design is not considered desirable for locations of high seismic activity.

(c) *Hinkley Point Reactors*. The two Hinkley Point reactors have spherical pressure vessels, containing graphite stacks 49 ft in equivalent diameter and 25 ft high. The graphite occupies 40 per cent of the vessel volume. Modifications to the Calder Hall design include offset keyways between bricks and tiles to reduce gas leakage and a more elaborate garter design, which maintains tension in event of failure of one member of the garter.¹⁴

(d) *Hunterston Reactors*. A greater number of design refinements are incorporated in the Hunterston reactors. The graphite stack is 28-sided, $50\frac{1}{2}$ ft in equivalent diameter, and 28 ft high.¹⁵ The restraining structure is built in the form of a cage with 56 main vertical members pivoted at the bottom and backed by two garters at the top. The upper garters have the same thermal-expansion coefficient as graphite, whereas the lower pivots will move outward with the supporting steel. Owing to the difference in temperature between the steel and the top graphite layers, their radial thermal expansion is nearly equal. The individual graphite columns are therefore spigotted to the steel support plates rather than being mounted on ball bearings. Top garters are connected to corner beams as in Calder Hall reactors and are linked to radial arms from the pressure vessel.

Graphite support sleeves surrounding the fuel elements insulate the moderator from the coolant gas in cooler regions of the reactor. This design was originally intended to reduce the stored-energy content of the moderator. Although this precaution was later found to be unnecessary, the design was not altered. Tile layers are composed of a single thickness of tiles each having circular spigots for alignment with adjacent bricks and eight radial

keyways. The four keys that fit in the sides of the square tiles are straight, but those at the corners are cruciform. Extensive model tests were conducted to prove the stability of this stack design and demonstrate its ability to accommodate both expansion and contraction of the graphite.

(e) *Tokai Mura Reactor*. This reactor is being built by a British consortium for the Japanese government. Originally intended as a refinement of the Hunterston design, Tokai Mura was revised to incorporate an entirely new moderator and support structure based on two important factors: (1) high earthquake-imposed forces and (2) radiation-induced graphite contraction at elevated temperature. Brick-and-tile construction with a square lattice was abandoned in favor of an interlocking hexagonal-brick arrangement with a triangular lattice similar to EDF-2. The cage-and-garter restraint design was replaced by a reinforced cylinder with tie bars placed in the graphite stack.¹⁶

Bricks are hexagonal prisms 9 in. across flats and 37 in. tall, with three ribs and three slots to fit the ribs of adjacent bricks (Fig. 17.7). Alternate

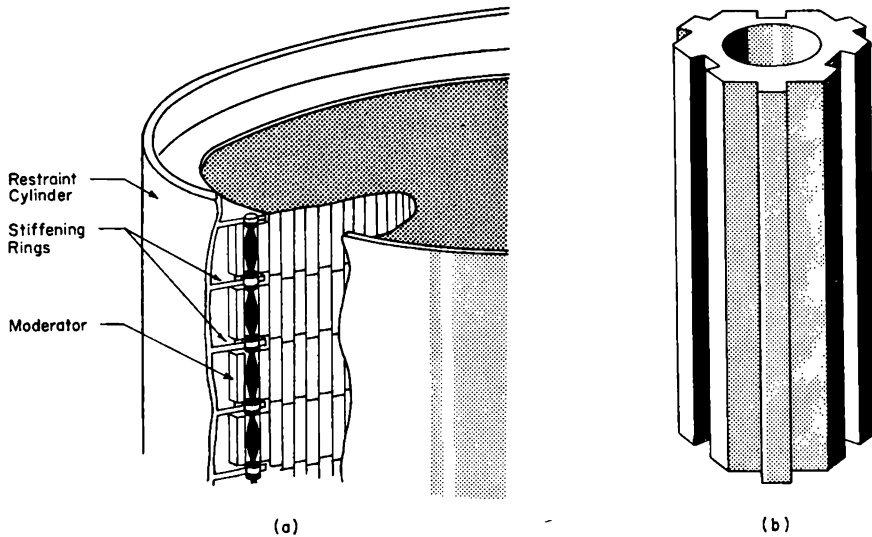


FIG. 17.7 Tokai Mura Reactor.¹⁶ (a) Core restraint. (b) Brick design.

bricks are staggered in elevation for complete interlocking. Bricks are keyed throughout the graphite stack; control rods are located in empty fuel channels to avoid weakening bricks by cutting away the corners for separate channels. This design allows each brick to expand or contract freely about its extrusion axis without distorting the stack, at the same time permitting symmetrical expansion or contraction of the entire core without restraint. Keying of the blocks will offer restraint to nonsymmetrical distortion of the stack.

The restraining cylinder is lined with internal stiffening rings, which

are connected to rods inserted in channels in the outer ring of graphite bricks. Columns of bricks are spigotted to the supporting structure by relatively flexible members.

With shrinkage now expected in the graphite (Sec. 9-4), bars are machined without clearance gaps, except for those required for assembly of the stack. It is predicted that clearance between bricks will reach $\frac{1}{10}$ in. in 20 years. Differential thermal expansion between the steel support and the graphite during start-ups will cause an initial clearance of 0.023 in. A mock-up of part of the stack was used to verify that the interlocking design would preserve channel alignment and resist stack distortion even with large clearances between bricks.

A conservative approach was taken in designing to resist earthquake loads; requirements of the Japanese building codes were increased by factors of $1\frac{1}{2}$ to 3 in determining forces imposed. In addition to strengthening the supporting and restraining structures, care was taken to make connections to the graphite elastic so that accelerating forces would be transmitted smoothly. It is difficult to assess the consequences of large clearances between bricks at the time of an earthquake, but the interlocked and staggered layer construction is considered superior in shock resistance to the brick-and-tile arrangement.

(f) *Trawsfynydd Reactors*. These reactors utilize a brick-and-tile stack design modified to accommodate contraction of graphite. The tiles have vertical keys on each side and vertical keyways at the corners. Separate cruciform key pieces are placed at the intersection of the tile corners to maintain spacing of the columns of bricks and tiles.

(g) *Dungeness Reactors*. The Dungeness design is the latest refinement of the Berkeley-Bradwell-Latina series constructed by two British consortia. The temperature has been increased to the point that stored energy is dismissed as a problem. However, the potential for graphite shrinkage has led to the adoption of a design that intersperses square and octagonal bricks, keying them at the sides by T sections. Solid spigotted supports are used.

(h) *French Reactors G-2 and G-3*. These reactors, like G-1, have horizontal fuel channels.¹⁷ The graphite stack, only slightly larger than the 47-ft cylinder of G-1, resembles a barn (Fig. 17.8). A separate graphite-reflector wall is mounted inside the rear shield. This arrangement is dictated by placement of fuel-discharge chutes between the moderator and rear reflector. Fuel channels are cut from the sides of adjacent graphite bars, which are staggered as illustrated in Fig. 17.8.

The graphite stack rests on a heat shield supported by 140 jacks standing on five T-shaped beams. The beams are supported at their three extremities. Restraint is furnished by 18 straps, which girdle the top and sides of the stack. Each strap is composed of five articulated beams and each beam

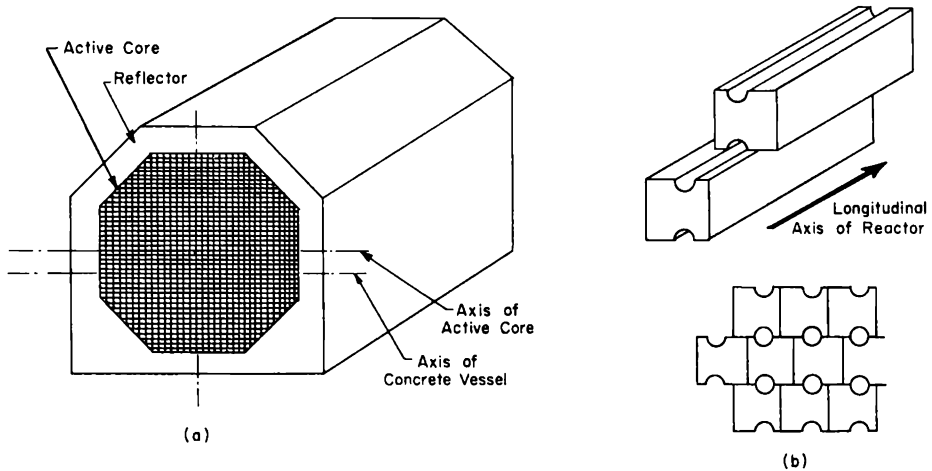


FIG. 17.8 The G-2 Reactor moderator.¹⁷ (a) Perspective of stack. (b) Graphite blocks.

holds sets of coil springs against thrust-distribution plates to restrain the graphite (Fig. 17.9).

The friction of gas being forced through the fuel channels creates a high thrust load, which must be borne by the front (fuel loading) face of

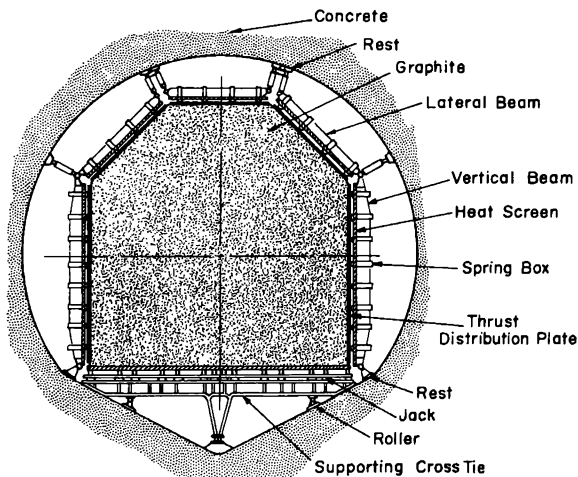


FIG. 17.9 The G-2 moderator stack support.¹⁷ The stack stands on 140 jacks supported by five T-shaped beams and is restrained by spring-loaded thrust plates held by 18 sets of articulated beams.

the reactor since gas enters at the discharge face. All thrust loads are taken by the fuel-loading liner tubes bridging the gas plenums between the front shield and the graphite. To hold the stack in a fixed position and yet allow for its horizontal thermal expansion, springs are located in liner tubes in

part of the core region (Fig. 17.10). Peripheral tubes are fixed. This arrangement holds the stack in place within acceptable limits. Spring loading is applied over the entire rear (gas inlet) face to maintain proper stack position on heating and cooling. The spring loading is transferred to the rear shield by a more elaborate articulated system owing to the separate reflector mounting at this end.

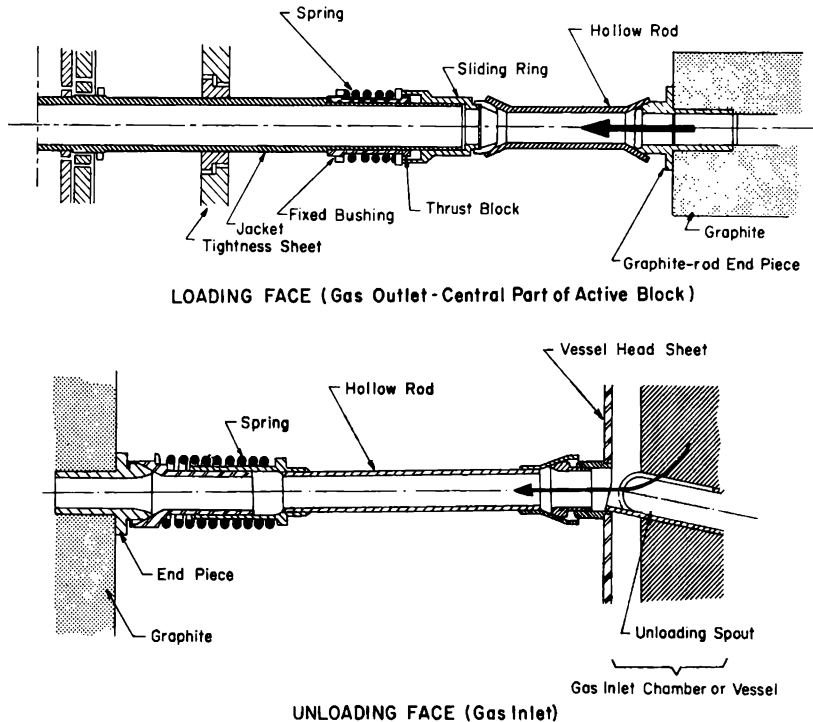


FIG. 17.10 The G-2 moderator holding system.¹⁷ Spring-loaded sleeves at the fuel channels hold the graphite in place against force exerted by friction of gas flowing through the reactor.

(i) *Electricité de France Reactor-1 (EDF-1)*. The first French reactor (EDF-1) to adopt the vertical channel configuration has a tall (10.2 m) graphite stack 9.5 m in diameter in a cylindrical pressure vessel.¹⁸ A novelty of the design is the division of the active core into three zones through the use of two lattice spacings and two channel sizes. Channels are bored in the graphite blocks, and space is allowed between blocks for expansion. Blocks are spigotted to curved tubes that transmit the weight of the stack to a steel dome under the stack inside the pressure vessel. The dome is suspended from an internal ledge and is reinforced by a large ring so that only vertical loads are transmitted to the pressure-vessel wall. This novel support design allows access to all tubes with a single pivoted fuel-handling boom.

(j) *Electricité de France Reactor-2 (EDF-2)*. With a graphite stack of

proportions similar to British practice (24 ft high, 40 ft in diameter), EDF-2 has a considerably higher power than EDF-1. A two-zone lattice is used, with larger spacing in the outer zone but with the same channel size. The pressure vessel is spherical.¹⁹

Hexagonal graphite blocks are used in a manner resembling the revised Tokai Mura design. Each block has three vertical keyways; separate keys are inserted between the blocks. This design was adopted because it could accommodate both expansion and contraction of graphite bars without distortion of the stack. It is possible for expansion to occur at the base of the columns while shrinkage occurs at the top.

A supporting structure traverses the outer graphite blocks. This structure is composed of steel columns connected at the top by low-expansion steel chains to equalize expansion of the upper and lower parts of the stack.

17-3.4 HIGH-TEMPERATURE GAS-COOLED REACTORS

We may consider as high-temperature gas-cooled reactors both those being built to determine the maximum practical operating temperature with carbon dioxide cooling and those which will introduce the use of helium cooling to increase operating temperatures further. In this group are the British Advanced Gas Cooled Reactor (AGR), intended to pilot the ultimate designs for carbon dioxide-cooled reactors; the American Experimental Gas Cooled Reactor (EGCR), a somewhat conventional design with helium cooling; and the more radical quasi-homogeneous Dragon Reactor and the High Temperature Gas Cooled Reactor.

These reactors impose varied and stringent requirements on the graphite. At higher temperatures chemical reaction rates become more rapid, and thermal gradients and thermal shock are also of greater importance. In some designs graphite serves additional functions as a fuel matrix, diffusion barrier, and flow barrier, as well as being employed to a larger extent as a structural material.

(a) *Advanced Gas Cooled Reactor (AGR)*. The AGR, on which a second generation of higher efficiency nuclear power plants in Britain may be based, is intended to establish the maximum practical operating temperatures for a carbon dioxide-cooled graphite reactor. The exit gas temperature is expected to be 500°C initially, later increasing to 575°C. Beryllium and stainless steel will supplant Magnox as the fuel-can material, and uranium oxide will be the fuel.

The graphite stack, encased in a double-shell cylindrical pressure vessel, is 18 ft high and slightly over 18 ft in diameter.²⁰ The 253 vertical fuel channels are spaced 10¾ in. apart in a triangular lattice, but the graphite bricks are rectangular. A reentrant gas flow pattern is used; cooling gas enters near the top of the vessel, flows downward through tapered passages formed by machined recesses in the sides of the graphite bricks and in the annulus between the vessel and the stack, then passes upward

through the fuel channels. A piping manifold connects the outlet of each channel to the main exhaust. Each channel is equipped with an adjustable sleeve valve to regulate gas flow, thereby affording flexibility for experimental use of the reactor. A neutron shield of graphite and boron steel is placed above the core to enable future access inside the vessel when fuel is discharged, making it possible to alter or replace the core. Fuel elements are clusters of rods mounted in graphite sleeves; assemblies are linked into a single chain per fuel channel.

A zero-energy prototype of the AGR, called HERO, is equipped with removable graphite blocks to enable a change in the lattice spacing.²¹

(b) *Experimental Gas Cooled Reactor (EGCR)*. The EGCR, first American power reactor of its type, bears an outward resemblance to the AGR and is approximately the same size. Although designed for nearly the same temperature range (565°C gas outlet), the EGCR will be cooled by helium rather than by carbon dioxide, thereby averting most problems arising from chemical reactions. The uranium oxide fuel elements will be canned in stainless steel.

The graphite stack is tall when compared to British practice, being 19½ ft high and 16 ft in diameter.²² It is composed of 120 monolithic graphite columns 16 in. square, except for specially shaped blocks at the periphery (Fig. 17.11). Each of the 68 core columns contains 4 channels spaced on an 8-in.-square lattice. These channels contain the fuel, control rods, and instrumentation. Six additional experimental-loop passages are provided. Gas-seal slats key the peripheral blocks. Graphite sleeves are used to support the six seven-rod cluster fuel elements in each channel.

The stack rests on a bottom plate that is bolted to a grid structure inside the pressure vessel. Bottom blocks in each column are keyed to the bottom plates. A gas-seal bellows is fitted into the bottom plate at each coolant channel to seal against the surface of the bottom graphite block and achieve maximum coolant effectiveness. A stainless-steel core-restraint lattice assembly is recessed into the top of the core to maintain alignment of the graphite columns and allow for thermal expansion and radiation-induced contraction. A top grid structure positions the restraint lattice in the pressure vessel, transmits earthquake loads, and supports the various channel extension pipes. It also holds the fuel in place in event of a depressurization that causes fuel levitation. Three steel restraint bands encircle the core near the mid-plane. These limit deflection from column bowing to 1 in.

It is expected that slight radiation-induced expansion may occur in the lower regions of the graphite stack and that considerable contraction will occur in the remainder. Since the EGCR core consists of independent columns keyed into end plates that determine the position of the columns, stack distortion by irradiation effects in the graphite should be minimized.

(c) *Dragon Reactor*. With graphite boldly used throughout its core as

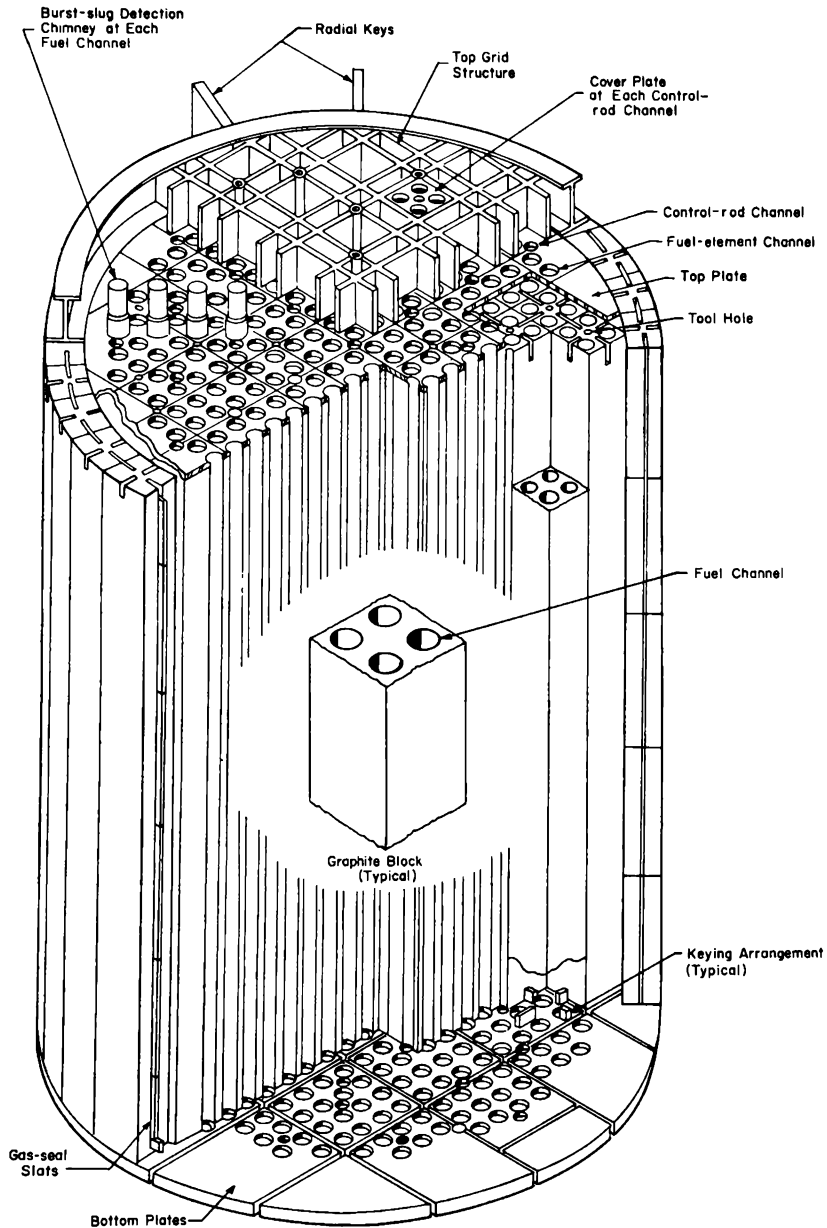


FIG. 17.11 The EGCR graphite core structure.²²

structure, cladding, diffusion barrier, and as fuel matrix, Dragon is a quasi-homogeneous reactor resembling a pressurized-water design more than a graphite type. The chief objective of the project (a joint effort of 12 European countries) is to achieve the high temperatures needed in nuclear power plants to compete with modern conventional stations.²³ In Dragon the high temperature of the helium cooling gas (350°C inlet, 750°C

outlet) resulted in a core having no moderator structure as such; instead, 259 hexagonal fuel-moderator rods, bundled in 37 vertical seven-rod clusters, are surrounded by two rings of reflector bricks (Fig. 17.12). The core is enclosed in the reactor vessel; top and bottom reflectors are incorporated in the fuel clusters. Utilization of graphite in such varied applica-

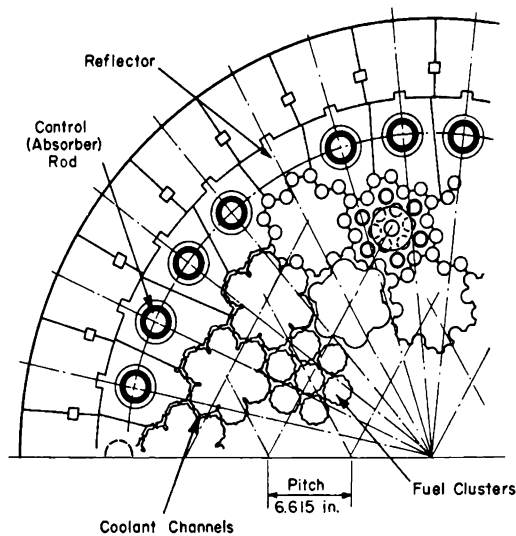


FIG. 17.12 The Dragon core arrangement. Partial plan view showing the relative positions of fuel clusters, reflector, and coolant channels. (From *Nuclear Engineering*, Ref. 23.)

tions and under an extreme range of service conditions imposes perhaps the greatest diversity of material requirements yet encountered in designing a graphite-moderated reactor. A mitigating factor is the fact that it is necessary for the graphite in the core to serve only for the life of the fuel element rather than for the life of the reactor.

The fuel clusters and stacked reflector rest on reinforced plates suspended from the pressure-vessel wall. These bedplates are connected by skirt rings, which allow symmetrical thermal expansion about the core axis. Each stacked column in the two reflector rings is pivoted at the base and is keyed to adjacent columns. Cooling gas enters from the top of the pressure vessel, flows downward outside the reflector, then passes upward through the core. Peripheral restraint for the reflector bricks is contributed by the pressure differential existing across the reflector. Outer-ring bricks have vertical sealing members to prevent gas leakage from bypassing the core. The inner-ring bricks contain holes for control rods and instrumentation. Fuel-moderator clusters are supported on pins in the bedplates. Fuel rods are clustered in groups of seven to facilitate fuel handling and simplify the gas scavenge system. The choice of $2\frac{1}{2}$ in. for the fuel-rod pitch is somewhat arbitrary. The coolant-channel shape was selected so that dimensional

changes in the core would not cause undue effects on heat transfer. Extended surfaces were not considered because of lack of restrictive operating limits on the fuel temperature and the desire not to weaken the graphite, which is employed as a structural member.

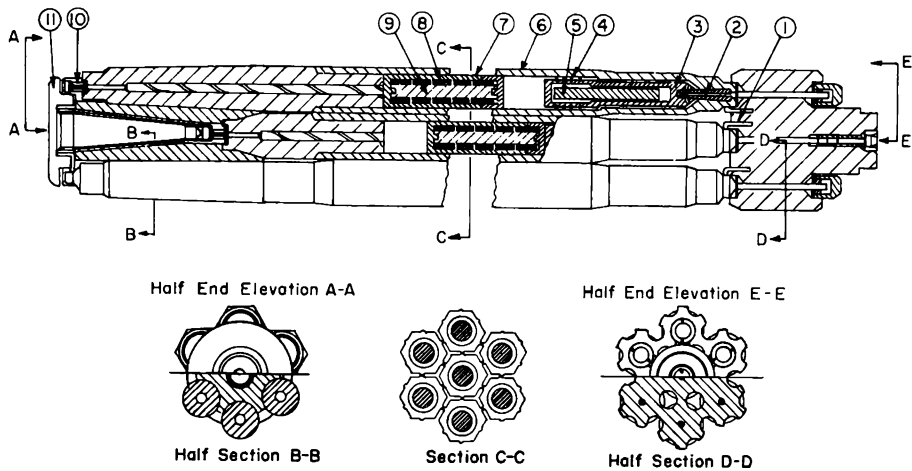


Fig. 17.13 The Dragon fuel-moderator cluster. Each of the hexagonal fuel rods incorporates the following components: (1) orientation dowels, (2) scavenge-gas inlet, (3) porous plug, (4) expansion washers, (5) filled piece, (6) fuel-rod tube, (7) fuel boxes (10 per tube), (8) fuel inserts (6 per fuel box), (9) graphite center piece (1 per box), (10) cap nut and compensating bellows, and (11) scavenge-gas outlet. (From *Nuclear Engineering*, Ref. 23.)

Design of the fuel cluster is shown in Fig. 17.13. Fuel rods are bolted to the top graphite spider; a diaphragm washer is placed between the fuel rods and the spider to allow for differential expansion among rods. Gross differences of expansion can be accommodated by yielding of the washers. Fuel-rod orientation is fixed by doweling between the rods and the top spider.

The porous plug and its hollow retaining screw admit gas from the main coolant stream to the gap between fuel boxes and fuel tube for scavenging fission products from the reactor. A group of safety washers below the porous plug will fracture progressively to limit the force transmitted to the fuel tube if expansion of the fuel box should exceed the allotted clearance. Graphite filler plugs at each end of the fuel rod serve as part of the top and bottom reflector.

At the bottom each rod is attached to a steel header by a cap nut with integral expansion bellows, the latter being required both during operation and during brazing of the cap nut to the graphite end plug. The gastight steel header serves also to duct scavenge gas to the exit at the support pin.

Fuel inserts are mixtures of uranium, thorium, and graphite powders cold-compacted into tubular pieces. These are threaded onto a high-density graphite spine for insertion into the fuel boxes. Clearance is allowed for growth of the insert and shrinkage of the box. Fuel-box end caps are

zirconium brazed. The uranium and thorium are expected to react and form carbides at the estimated operating temperature of 1700°C.

Since it is not now possible to produce completely impermeable graphite fuel boxes or fuel tubes, excessive contamination of the main-stream coolant gas is avoided by the scavenging arrangement. Fuel boxes are impregnated so that diffusion of gases through the wall is delayed for 1 hr, thereby limiting the activity in the scavenge-gas system. Fuel tubes are also impregnated, although the permeability is much higher, since it is necessary only to prevent back diffusion counter to the pressure gradient. Two future possibilities are: (1) the development of impermeable graphites that would eliminate contamination of the coolant gas or (2) an increase in the permeability of graphite to accelerate escape of fission products while operating with a highly contaminated coolant.

(d) *Zenith Reactor*. Zenith, a high-temperature zero-energy companion reactor to the Dragon, is designed to explore reactor characteristics at temperatures up to 950°C. The core is similar to that of the Dragon reactor. A heated-gas circulating system is incorporated.²⁴

It is necessary to insulate the side reflector from the active core to simulate the temperature distribution of a power reactor. An insulating layer is formed by pelletized lampblack packed in a 2-in. space between the reflector and a 1½-in. graphite barrier wall adjacent to the active core. A skirt mounted inside the pressure vessel below the insulating wall provides support for both core and reflector.

(e) *High-temperature Gas-cooled Reactor (HTGR)*. This American power reactor, although larger than the Dragon Reactor, is similar in many design concepts and proposed operating conditions. The core is 9 ft in diameter and 7½ ft high and is surrounded by 2 ft of reflector.²⁵ The active core is composed of 810 fuel rods, which incorporate the top and bottom reflector; the side reflector comprises one ring of graphite dummy fuel elements and a ring of graphite bricks.

The fuel elements differ somewhat from those of the Dragon in size, shape, and construction. They are 2¾-in.-OD annular fuel compacts mounted individually on a 1¾-in.-diameter graphite spine. In the HTGR no graphite fuel boxes are used to enclose the uranium-thorium carbide fuel compacts. Instead, the compacts are stacked in core-length low-permeability graphite tubes, and a scavenge-gas system is used to remove fission products from the space between. Spacing of the fuel elements is accomplished by enlarging the outer graphite tubes slightly near the upper end. Differential pressure from the reentrant gas flow path forces the reflector inward to preserve the proper spacing of fuel.

17-3.5 WATER-COOLED REACTORS

Interest in water-cooled graphite-moderated reactors has centered in the United States and in the U.S.S.R. Water cooling has the advantage of

permitting high specific powers because of its excellent heat-transfer properties. Although graphite-moderated reactors are characteristically bulky, water cooling effects substantial savings in size but introduces piping complexity and unique safety hazards.

The United States has built eight water-cooled reactors at its Hanford plant for plutonium production. A ninth now being built there, the N Production Reactor (NPR), is the first reported as capable of producing electric power. In the U.S.S.R. two research reactors and two power reactors employ water cooling. This type reactor has been investigated more vigorously for power production in the U.S.S.R. than elsewhere. It is noteworthy that the graphite in one Soviet reactor operates at a higher temperature than has been reported for any other reactor in the world. No information is available on Soviet plutonium-production reactors, although it is generally presumed that they are graphite-moderated and water-cooled.

(a) *Reactor for Physical and Technical Investigation (RPT)*. The 20-Mw reactor for physical and technical investigations is at the Institute of Physics in Moscow. Although originally intended as a water-moderated reactor, it was built with a graphite moderator to afford a larger lattice for convenient installation of experimental loops.

The core and reflector form a vertical cylinder 2.6 m in diameter and 2.4 m high, the core being slightly taller than the side reflector.²⁶ Horizontal layers of graphite brickwork are used in the reflector, but the core, 1 m in diameter, is composed of vertical blocks stacked in five layers. Core blocks are 14 cm square, with axial channels in which bayonet type coolant tubes are inserted. There are 37 channels in the core and several additional channels in the reflector for loops. A gastight steel vessel encloses the core. Helium is circulated in the vessel to cool the graphite and to dry it if a coolant tube should leak. When moisture in the helium is excessive, the reactor is shut down and cooled, the vessel is drained, and the leaky tube is replaced.

The RPT began operation in 1952 at a power of 10 Mw. It was later reconstructed to increase the power and to provide space in the core for loops (fewer fuel elements of higher enrichment were used). Core channels were enlarged from 55 to 75 mm for the new fuel, making the RPT a more truly water- and graphite-moderated reactor. The graphite temperature was 470°C at 10 Mw power; it now reaches 1000°C near high-temperature loops in the core, the highest temperature reported in a graphite-moderated reactor. Maximum power in a 1-m-long channel is 1000 kw.

(b) *Experimental Uranium-Graphite Isotope Reactor (IR)*. This Soviet reactor, used for radioisotope production, was dismantled and rebuilt following damage to the core from destruction of two fuel elements.²⁷ Provisions for disassembly were incorporated in the original core design. The graphite structure, a vertical cylinder 5.8 m high and 4.4 m in diameter, is built of vertical columns of bricks. Each column has 10 bricks, which

are square with axial cylindrical channels. There are 248 channels, 140 of which are loaded with fuel placed in coolant tubes. A cadmium sheet and a layer of aluminum bricks rest on top of the stack. The stack is girdled by 10 spring-loaded steel bands. Maximum graphite temperature during operation is 400 to 500°C.

When the reactor was dismantled, the top shield and cooling tubes were removed, and the graphite bricks were retrieved with an expanding mandrel inserted in the channels.²⁷ It was possible to remove an entire column of bricks at one time if the bricks were not highly radioactive. Approximately 400 bricks were removed. Of these, 21 were seriously damaged from the previous fuel-element failures. Examination of the graphite removed from the reactor revealed clearly that the extent of radiation damage to graphite depended on the operating temperature. Damage in the central part of the reactor was much less than in the periphery and was less at the outer edge of a brick than at the cooler central channel (Fig. 17.14). The data reported

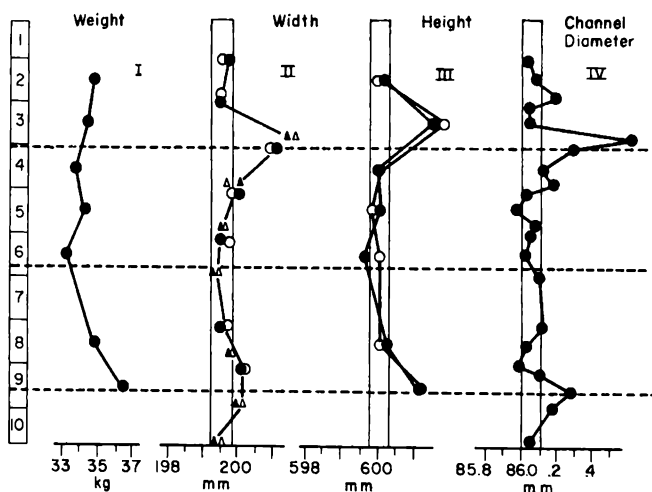


FIG. 17.14 Changes in graphite bricks of the Soviet IR. The changes in weight and size of the bricks are along the vertical line of the block recovered from the brickwork. The dotted lines show the boundaries and the center of the active zone.²⁷

for IR are characteristic of water-cooled reactors of similar lattice construction. Substantial swelling of the graphite occurred only near the upper and lower extremities of the active core. Some cracking of the graphite is attributed to swelling. Although thermal conductivity decreased by as much as a factor of 40, it had little effect on graphite temperature because the thermal resistance that chiefly determines the graphite temperature is the clearance between the tube and channel.

(c) *Atomic Power Station Reactor (APS)*. In 1954 the 30-Mw pressurized-water graphite-moderated reactor APS was placed in operation at Obninsk, U.S.S.R. This reactor is of particular interest because of its

unusual design: part of the moderator is integral with the fuel-element assemblies.

The graphite assembly is 3 m in diameter and 4.6 m high.²⁸ In the active core region, 128 vertical hexagonal blocks are spaced on a 12 cm triangular pitch. Each hexagonal block has a central cylindrical fuel channel. Fuel-element assemblies are bayonet type units, each composed of four internally cooled fuel tubes clustered around a single water inlet tube (Fig. 17.15). Graphite pieces are fitted on the fuel and tubing manifold to

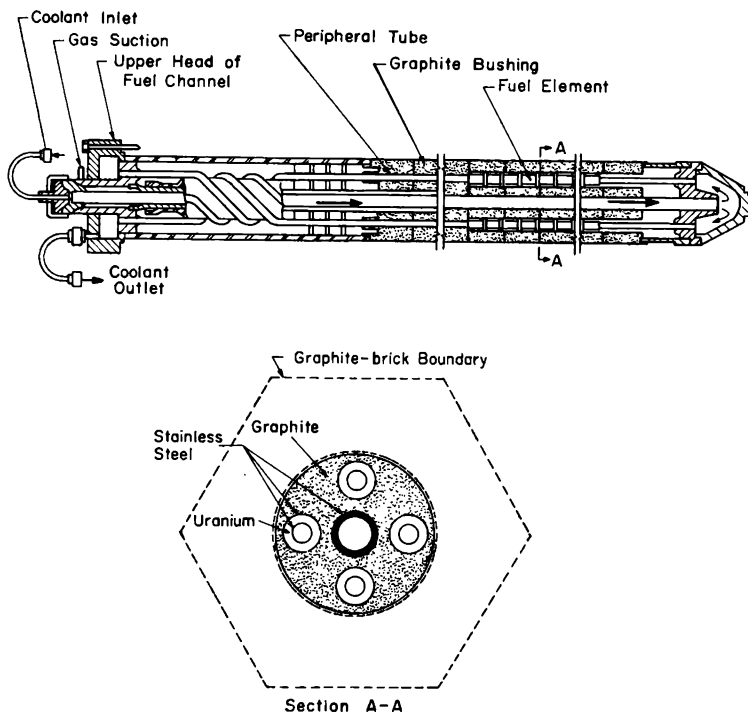


Fig. 17.15 Fuel-element sections of the Soviet APS reactor.²⁰

form a smooth cylindrical unit 6.5 cm in diameter. Clearance between the fuel and the channel is based on a compromise between allowing for graphite expansion and minimizing resistance to heat transfer. A nitrogen atmosphere is used, although initial operation was with helium. The maximum graphite temperature is approximately 800°C.

(d) *Urals Power Station Reactors.* Design of the 285-Mw reactors for this large power station is based on that of the APS. Apparently one reactor is being built at Beloyarsk and the construction of three similar units is planned. The chief innovation in the Urals reactor is a two-pass two-fluid cooling system. Primary water is boiled in one pass through the reactor and is then used in a boiler to generate steam in the secondary system; the steam is superheated in a second pass through the reactor.

The graphite assembly, including reflector, is 9 m high and 9.6 m in diameter; it rests on a water-cooled steel bedplate.³⁰ Outer reflector blocks are pierced by steel uprights connected by horizontal crosspieces. A top plate with standpipes at the fuel channels is connected to the steel reactor vessel by a compensator, which allows for elongation of the vessel and expansion of the graphite stack.

Channels for 1134 fuel, control, or safety rods and instrument assemblies are spaced 20 cm apart in a square lattice pattern. Of the 998 fuel elements, 730 are used for boiling and 268 for superheating. Fuel elements are similar to those of the APS, except that six fuel tubes are clustered around the inlet tube of each assembly rather than four. The graphite temperature is expected to be 660°C in the boiling zone and 775°C in the superheating region.

(e) *Hanford Production Reactors.* The world's first large reactors are the three production units constructed at Hanford in 1943 and 1944: B, D, and F Reactors. Although patterned after the small X-10 at Oak Ridge, the Hanford reactors employ water cooling. The graphite stack is approximately cubical in shape and of sufficient size to accommodate about 2000 horizontal aluminum tubes spaced $8\frac{3}{8}$ in. apart in a square lattice pattern³¹ (Fig. 17.16). Control rods are horizontal but perpendicular to the tubes;

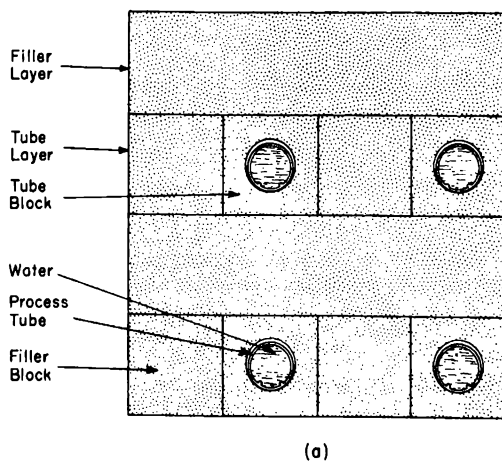
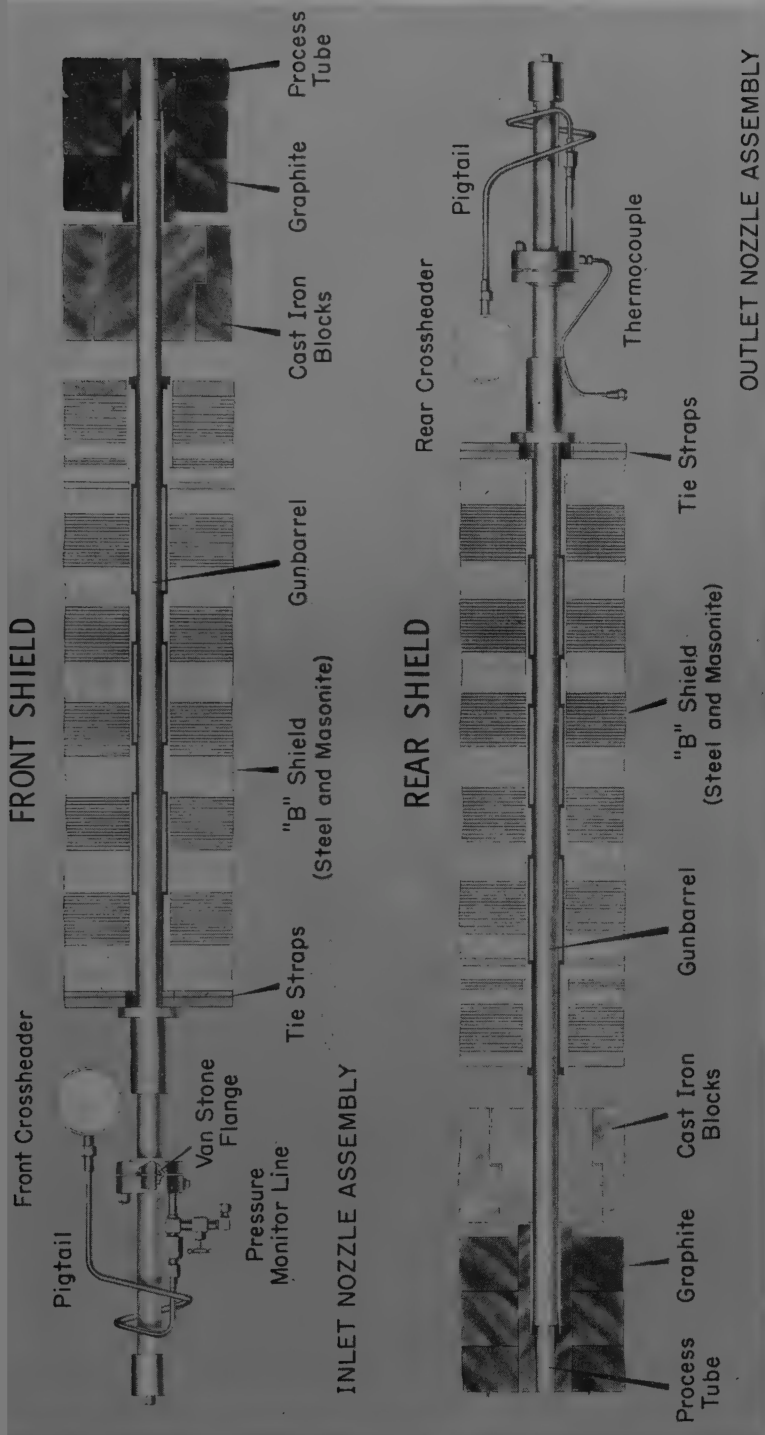


FIG. 17.16 Cross sections through fuel channels of a Hanford production reactor.¹¹
 (a) Perpendicular cross section showing empty tubes. (b) Longitudinal cross section showing moderator, shields, and piping. (See facing page for part b.)

safety rods are vertical. The graphite bars are $4\frac{3}{16}$ in. square and several feet long. Bars in alternate layers (called "tube block" layers and "filler block" layers) are crisscrossed. Tube channels are bored along the axis of alternate blocks in the tube layers. At the front and rear of the reactors, steel sleeves (called "gun barrels") bridge the gap between the graphite and



(See facing page for legend)

(b)

shields. The gun barrels support cast-iron thermal-shield blocks and guard the aluminum process tubes against misalignment of channels in the graphite and shield (Fig. 17.16). No external restraint is imposed on the stack. Helium and carbon dioxide are used in the reactor atmosphere.

Like the Brookhaven and Windscale reactors, such a design is vulnerable to expansion of the graphite; it is possible that tube and control-rod channels could become crooked enough to interfere with fuel-element cooling, fuel charging and discharging, tube replacement, or control-rod operation.

At first, before the dimensional behavior of graphite was known, it was feared that continued expansion could ultimately render the reactors inoperable. However, dimensional changes in the graphite have not presented insurmountable operating problems, and the original reactors continue in operation.

Stored energy, although appreciable in magnitude in the cooler regions of the graphite, has not been considered a threat to the safety of the Hanford reactors. The water-cooling system presents such a large heat sink that a serious temperature excursion is unlikely. Water cooling protects the fuel element for any probable graphite temperature.

As illustrated by Soviet experience with the IR, a problem in water-cooled reactors is flooding of the graphite from tube leaks. It is especially necessary in larger reactors to develop sensitive means of detecting leaks before they become serious enough to render a portion of the reactor inoperable and affect the integrity of other tubes. If the graphite becomes flooded, considerable time may be required to dry it regardless of the technique used.

(f) *N Production Reactor (NPR)*. The NPR is the first Hanford reactor to be fitted with a recirculating pressurized-water cooling system designed to permit power recovery.³² Like the previous Hanford reactors, it has horizontal tubes and an unrestrained graphite stack. The graphite stack is

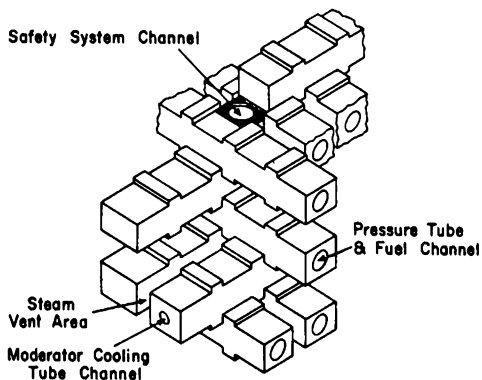


Fig. 17.17 Isometric sketch of NPR moderator-block stacking.

over 30 ft square and nearly 40 ft long, accommodating approximately 1000 tubes on an 8- by 9-in. rectangular lattice. It has been reported that 300 to 900 Mw of electrical power could be produced by the NPR.

The graphite stack is superficially similar to those of other Hanford reactors, but the crisscrossed layers are interlocked in the manner illustrated in Fig. 17.17. A separate cooling system limits the operating temperature of structural moderator blocks to prevent excessive distortion of the stack from contraction of the graphite. Steam-venting passages are provided throughout the stack to allow for dissipation of steam that would be ejected if a pressure tube should burst.

17-3.6 LIQUID-METAL-COOLED REACTORS

Much development work has been performed on liquid-metal-cooled graphite-moderated reactors, but only two such reactors have been built, the Sodium Reactor Experiment and Hallam sodium graphite reactors in the United States. Formidable problems associated with the use of materials and equipment at high temperatures and in contact with molten metals have required much emphasis on development of engineering technology.

(a) *Sodium Reactor Experiment (SRE)*. The SRE was conceived as a promising approach to better thermal efficiencies in nuclear power plants through higher operating temperatures. In the SRE sodium enters the reactor at 285°C and leaves at 510°C, a temperature range comparable to that of recent advanced gas-cooled designs.³³

The SRE core, including reflector, is 10 ft high and 10 ft in diameter and is immersed in the sodium coolant inside a steel tank. If losses in neutron economy and swelling of the moderator are to be prevented, the graphite must be protected from the sodium (see Chap. 15). The core therefore is constructed as a close-packed array of hexagonal zirconium cans containing graphite logs (the outer row of reflector logs is canned in stainless steel). There are 43 moderator and 76 reflector cans, each 11 in. across flats, except for irregular peripheral units. Three graphite logs are stacked vertically in each can and are keyed together with cylindrical graphite plugs (Fig. 17.18, part a). Each moderator can has a central tube for a fuel channel; additional channels for control, safety, and experimental units are formed by cutouts at corners of the cans. A small clearance allows some coolant flow between the flats of the cans.

The sides of the zirconium cans are 0.035 in. thick; the end plates are thicker. Moderator and reflector assemblies are bolted to supporting pedestals at the bottom and to spacer plates at the top. The stainless-steel pedestals fix the position of the cans in the lattice pattern of the bottom grid plate. Top spacers on adjacent cans nest together and are maintained in place by a clamping band around the periphery of the core.

A snorkel vent tube extends 7 ft above each can to the gas blanket above the reactor sodium pool to allow for possible outgassing of heated

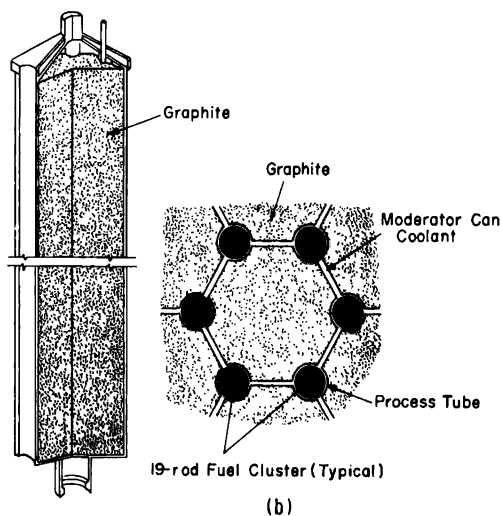
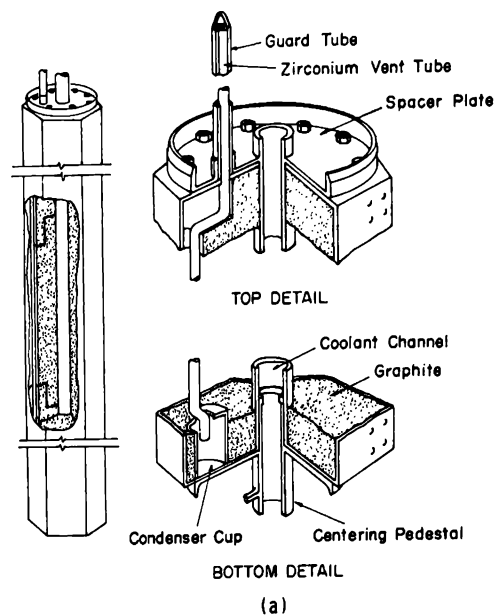


FIG. 17.18 (a) SRE moderator unit. (From Starr and Dickinson, *Sodium Graphite Reactors*, Addison-Wesley Publishing Company, Inc., Ref. 33.) (b) Hallam reactor moderator unit.³⁴

graphite. Inside the can the tube extends to a cup at the base which is designed to collect condensed sodium vapor from the gas atmosphere.

No significant carburization of the zirconium cans has occurred. Sixteen SRE moderator cans have recently been replaced because a region of the core overheated when Tetralin leaked from the auxiliary-components cooling system into the sodium system and obstructed the flow of the sodium in

the reactor core. For future installations in the SRE, a calandria type core similar to those used in heavy-water reactors is considered promising primarily because of its better neutron economy. The graphite would be roofed with stainless steel for protection from leakage at the top of the calandria, and a pump-out system would be provided to eliminate accumulation of sodium from leakage.

(b) *Sodium Graphite Reactor (SGR)*. As a result of experience with the SRE, several refinements were incorporated into the core design of the SGR at Hallam, Neb. (Fig. 17.18, part b). The core, 18 ft high and 18 ft in diameter, is larger than the SRE core. Channels are provided for 243 fuel elements and 40 control and safety rods.³⁴ These channels are located at the corners of the 225 hexagonal moderator cans rather than at the axis, a design that simplifies fabrication and handling of the canned moderator elements and improves their reliability. In the fuel channels separate tubes direct flow over the fuel elements; control and safety rods occupy sealed thimbles. Moderator blocks, 14 in. across flats and 18 ft high, are canned in 0.016-in.-thick stainless steel rather than zirconium (Fig. 17.18). Stainless steel was chosen because it was considered at the time of design to be more reliable for the reactor lifetime. Vents are connected to a chamber under the can lids, and the lids are reinforced for lifting the heavy pieces. In other respects the design is similar to the SRE.

(c) *Liquid-metal-fuel Reactor*. Although no liquid-metal-fuel reactor with graphite moderator has been built, enough development effort has been expended in the United States to warrant mention of the concept. A preliminary design for a 5-Mw Liquid Metal Fuel Reactor Experiment (LMFRE) utilizes a graphite moderator and reflector structure encased within a double pressure vessel.³⁵ The graphite assembly, a rounded cylinder 8½ ft high and nearly 9 ft in diameter, is composed of only 46 pieces, 30 of which are side reflector blocks, 8 are core blocks, and 8 are top and bottom reflector pieces (Fig. 17.19). Reflector blocks are suspended from the vessel head by molybdenum rods and are bound around the periphery by four temperature-compensated clamps. Quadrant blocks with bored fuel channels are used in the core. Distribution plenums are formed at the end of the core blocks. The largest practical block size is proposed to reduce the surface area exposed to fuel solution, thereby lessening the problem of fuel penetration into the moderator.

The average core temperature anticipated is 450°C, but this temperature can rise to 470°C with fuel penetration into core graphite and to 560°C if fuel penetrates the reflector. Since the graphite proposed for this use has a void volume of 20 per cent, much of which is accessible to the fuel solution, it is necessary to develop a means of reducing or preventing absorption of the fuel solution by the graphite. Proposed methods include cemented joints between blocks, metallic carbide coatings, metal impregnation followed by oxidization or carburization of the metal, and impregnation

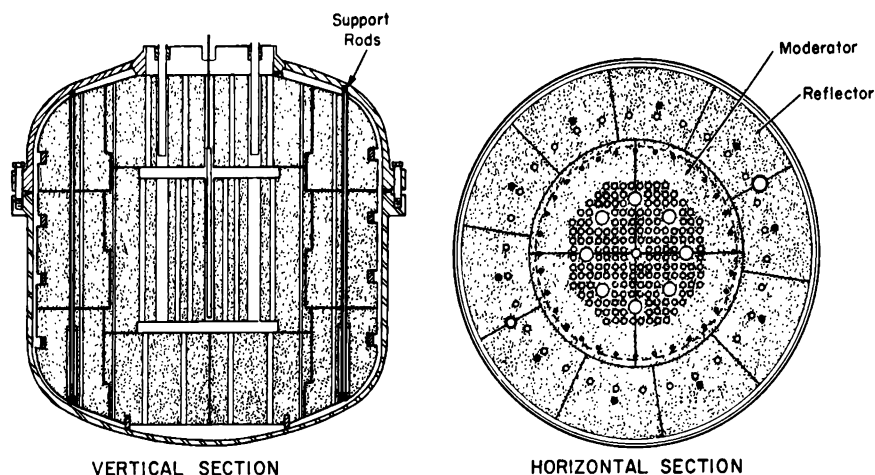


FIG. 17.19 LMFRE core cross sections.³⁵

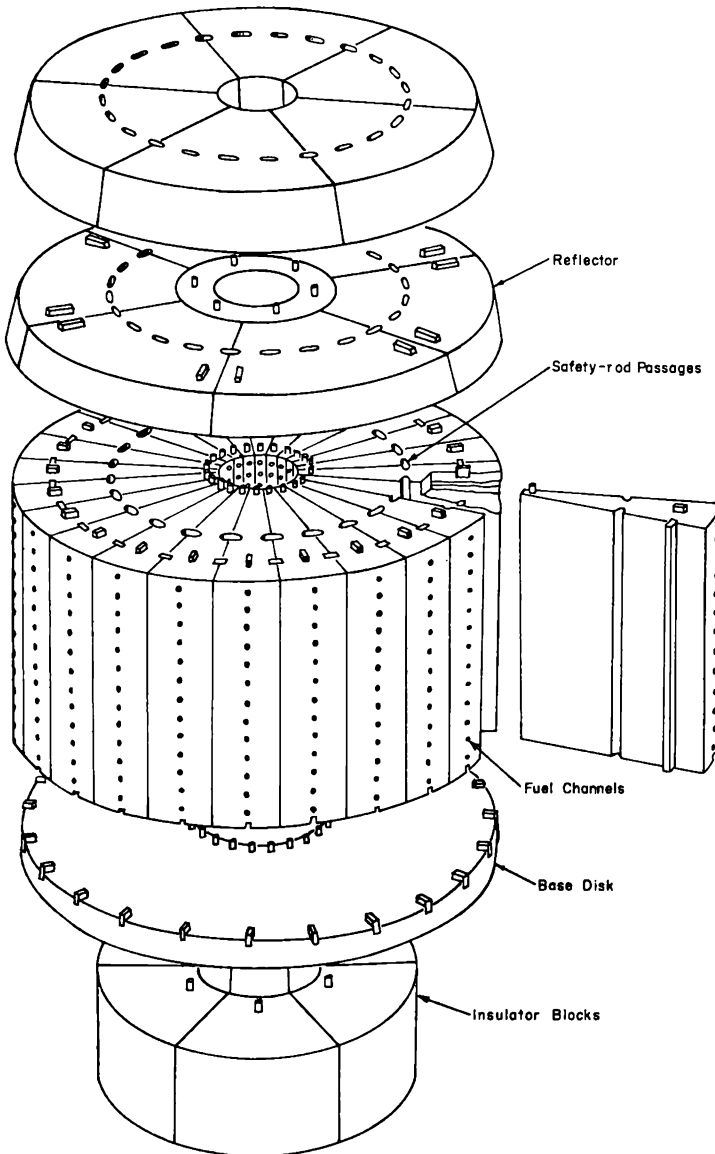
with a metallic salt followed by decomposition to an oxide. A problem encountered because of the use of large blocks is nonuniformity of the graphite.

17-3.7 UNUSUAL REACTORS

(a) *Transient Reactor Test Facility (TREAT)*. This reactor has the unusual purpose of generating safely a very large transient thermal-neutron flux of short duration. This condition is needed for studies on the meltdown behavior of fast-reactor fuel elements.³⁶ The reactor has a low fuel loading of enriched uranium oxide dispersed in graphite to provide the greatest margin of safety when metallic fuel elements are melted. The graphite serves as an effective sink for heat generated during the brief operating bursts as short as 40 msec. A significant safety factor is the strongly negative temperature coefficient of reactivity of this reactor. The maximum graphite temperature is 460°C.

(b) *Ultrahigh Temperature Reactor Experiment (UHTREX)*. Certainly one of the most radical graphite reactors yet conceived is UHTREX (formerly called "Turret"). Its primary purpose is the study of unclad fuel elements and their effect on reactor operation. The first name given to this reactor, Turret, reflected its unique rotating core, which is designed to simplify fuel handling. So that the potential of unclad fuel in a gas-cooled reactor can be fully exploited, the intended helium temperatures are the highest ever proposed: 870°C inlet and 1315°C outlet.³⁷

A spherical steel pressure vessel, 12 ft in diameter, encloses the reactor. The rotating core is a cylinder 74 in. in diameter and 40 in. high, with an axial hole 12 in. in diameter (Fig. 17.20). Between the core and the vessel, graphite bricks, carbon bricks, and porous carbon are used as reflector and

FIG. 17.20 UHTREX core.⁸⁷

insulation. The core consists of 24 pie-shaped graphite blocks keyed and pinned to a graphite base disk to prevent radial ratcheting movement. The disk, in turn, rests on insulator blocks mounted on the core turntable. Each core block has 13 radial fuel channels and vertical slots for safety rods. Fuel is charged from the periphery of the core into the channels and is discharged from the channels through the central hole to a discharge chute. Helium flows outward through the channels.

The fuel elements are graphite tubes impregnated with uranium oxide. They are 1 in. in diameter and about 6 in. long, with a $\frac{1}{2}$ -in. hole. Maximum fuel temperature is expected to be 1820°C.

A regenerative heat exchanger is incorporated in the gas-cooling system to permit operation of the circulating blowers at a more moderate temperature. Because of the high operating temperatures, the heat exchanger is a graphite cylinder 35 in. in diameter and 54 in. long, with 480 holes. Alternate holes are used for the heating and cooling passes in this counterflow unit. The header construction at each end is of graphite. Porous carbon brick is used for insulation between the core and the steel vessel.

(c) *Pebble-Bed Reactor (PBR)*. A small power reactor is being constructed in West Germany to test the feasibility of uncanned fuel elements. Its novel core is a bed of graphite spheres, called "potatoes," through which the helium cooling gas flows.³⁸ Surrounding the core is a graphite reflector from which four vertical fins project into the core to serve as control-rod guides. Fuel spheres are fed through apertures at the top of the reactor, distributed in the core, and discharged through a funnel at the bottom. At the expected inlet gas temperature of 200°C and outlet temperature of 850°C, the maximum sphere surface temperature is estimated³⁹ to be 900°C, and the maximum fuel temperature, 1400°C.

The potatoes are 6 cm in diameter, each having a drilled hole in which a small cylinder of uranium carbide or thorium carbide is inserted. Graphite plugs are inserted into the holes prior to final impregnation and baking. These fuel elements are resistant to thermal and mechanical shock, a quality that is necessary to limit breakage in service and reduce contamination of the cooling gases.

(d) *Pebble-Bed Reactor Experiment (PBRE)*. The PBRE is a design proposed for construction at Oak Ridge.⁴⁰ It would utilize helium entering at 675°C to cool a bed of spherical fuel elements. The pebble bed would be 11½ ft in diameter and 8 ft high, surrounded by a 3-ft-thick reflector. Three regions would form the reflector; a set of four concentric graphite tubes to line the core cavity, horizontal layers of wedge-shaped bricks, and an outer row of borated graphite bricks. The inner reflector would be supported in threaded sockets at the base to minimize thermal-expansion problems and would be tapered to prevent bridging of fuel balls in the core.

Fuel balls would be graphite containing a fuel-particle dispersion of UO_2 , UC_2 , or UC. Several types of coating techniques are being considered, including siliconized-silicon carbide and pyrolytically deposited carbon (see Sec. 14-7). The proposed ball diameter is 1½ in.

(e) *Molten Salt Reactor Experiment (MSRE)*. A small experimental molten-salt reactor is being constructed at Oak Ridge to test molten-salt circulating fuels.⁴¹ The moderator is a cylinder approximately 4½ ft in diameter and 5½ ft high. Vertical columns of graphite contain 600 fuel

channels. Fuel is a solution of fluorides of uranium, thorium, Li^7 , beryllium, and zirconium.

References

1. L. E. Stanford et al., *Safeguard Report on the Proposed Method of Annealing Graphite in the X-10 Reactor*, USAEC Report ORNL-2725(Rev.), Oak Ridge National Laboratory, May 18, 1960.
2. R. W. Powell et al., Control of Radiation Effects in a Graphite Reactor Structure, in *Proceedings of the Second United Nations International Conference on the Peaceful Uses of Atomic Energy, Geneva, 1958*, Vol. 7, pp. 282-294, United Nations, New York, 1959.
3. J. F. Hogerton and R. C. Grass (Eds.), *The Reactor Handbook, Vol. 2, Engineering*, USAEC Report AECD-3656, pp. 994-997, 1955.
4. BEPO-British Experimental Pile, *Nuclear Eng.*, 1: opposite page 14 (April 1956).
5. J. L. Dickson et al., BEPO Wigner Energy Release, in *Proceedings of the Second United Nations International Conference on the Peaceful Uses of Atomic Energy, Geneva, 1958*, Vol. 7, pp. 250-281, United Nations, New York, 1959.
6. J. F. Hogerton and R. C. Grass (Eds.), *The Reactor Handbook, Vol. 2, Engineering*, USAEC Report AECD-3646, pp. 997-1000, 1955.
7. R. W. Powell and C. L. Osborne, *The Ninth and Tenth Anneals of the Graphite Moderator Structure in the BNL Reactor*, USAEC Report BNL-570, Brookhaven National Laboratory, Jan. 7, 1960.
8. Reactor G-1 at Marcoule, *Nuclear Eng.*, 3: 258 (June 1958).
9. Sir Christopher Hinton, The Graphite-Moderated, Gas-Cooled Pile and Its Place in Power Production, in *Proceedings of the First United Nations International Conference on the Peaceful Uses of Atomic Energy, Geneva, 1955*, Vol. 3, pp. 322-329, United Nations, New York, 1956.
10. A. H. Cottrell et al., Theory of Annealing Kinetics Applied to the Release of Stored Energy from Irradiated Graphite in Air-cooled Reactors, in *Proceedings of the Second United Nations International Conference on the Peaceful Uses of Atomic Energy, Geneva, 1958*, Vol. 7, pp. 315-327, United Nations, New York, 1959.
11. *Accident at Windscale No. 1 Pile on 10th October, 1957*, Her Majesty's Stationery Office (White Paper), Command 302, 1957.
12. E. Long, The Calder Hall Graphite Structure, *Nuclear Power*, 3: 58-63 (February 1958).
13. R. D. Vaughan et al., Bradwell—Construction and Design Changes, *Nuclear Power*, 5: 77-79 (November 1960).
14. H. S. Arms et al., The Hinkley Point Power Station, in *Proceedings of the Second United Nations International Conference on the Peaceful Uses of Atomic Energy, Geneva, 1958*, Vol. 8, pp. 434-449, United Nations, New York, 1959.
15. R. N. Millar, The Hunterston Power Station, in *Proceedings of the Second United Nations International Conference on the Peaceful Uses of Atomic Energy, Geneva, 1958*, Vol. 8, pp. 424-433, United Nations, New York, 1959.
16. Japan's First Nuclear Power Station, *Nuclear Power*, 5: 104-118 (March 1960).
17. France Atome, Description of Reactors G2 and G3, in *Proceedings of the Second United Nations International Conference on the Peaceful Uses of Atomic Energy, Geneva, 1958*, Vol. 8, pp. 334-355, United Nations, New York, 1959.
18. M. Roux and M. Bienvenu, The Chinon Nuclear Power Plant EDF 1 and EDF 2, in *Proceedings of the Second United Nations International Conference on the Peaceful Uses of Atomic Energy, Geneva, 1958*, Vol. 8, pp. 356-379, United Nations, New York, 1959.

19. M. Bienvenu et al., The Second Nuclear Power Station, *Nuclear Power*, **5**: 118-123 (April 1960).
20. D. Iggulden, Building the AGR, *Nuclear Power*, **5**: 84-87 (July 1960).
21. HERO—Design and Construction, *Nuclear Eng.*, **5**: 150-153 (April 1960).
22. *Experimental Gas-Cooled Reactor: Preliminary Hazards Summary Report*, USAEC Report ORO-196, Kaiser Engineers Div. and Allis-Chalmers Mfg. Co., May 1959.
23. DRAGON, *Nuclear Eng.*, **5**: 302-315 (July 1960).
24. K. J. Mitchell and R. A. Geary, The High Temperature Zero Energy Reactor "Zenith," in *Proceedings of the Second United Nations International Conference on the Peaceful Uses of Atomic Energy, Geneva, 1958*, Vol. 9, pp. 310-315, United Nations, New York, 1959.
25. P. Fortescue et al., HTGR—Underlying Principles and Design, *Nucleonics* **18**(1): 86-90 (January 1960).
26. V. V. Goncharov et al., Some New and Rebuilt Thermal Research Reactors, in *Proceedings of the Second United Nations International Conference on the Peaceful Uses of Atomic Energy, Geneva, 1958*, Vol. 10, pp. 321-367, United Nations, New York, 1959.
27. B. B. Brohovich et al., Disassembly of Experimental Uranium-Graphite Isotope Reactor After Four Years of Operation, in *Proceedings of the Second United Nations International Conference on the Peaceful Uses of Atomic Energy, Geneva, 1958*, Vol. 7, pp. 241-249, United Nations, New York, 1959.
28. D. I. Blokhintsev and N. A. Nikolaev, The First Atomic Power Station of the U.S.S.R. and the Prospects of Atomic Power Development, in *Proceedings of the First United Nations International Conference on the Peaceful Uses of Atomic Energy, Geneva, 1955*, Vol. 3, pp. 35-55, United Nations, New York, 1956.
29. *Directory of Nuclear Reactors, Vol. 1, Power Reactors*, International Atomic Energy Agency, Vienna, 1959.
30. N. A. Dollezhal et al., Uranium-Graphite Reactor with Superheated High Pressure Steam, in *Proceedings of the Second United Nations International Conference on the Peaceful Uses of Atomic Energy, Geneva, 1958*, Vol. 8, pp. 398-414, United Nations, New York, 1959.
31. John R. Young, Operational Problems of the Original Hanford Production Reactors, *Nuclear Engineering and Science Conference*, Preprint V-117, Engineers Joint Council, 1959.
32. *Hanford's New Production Reactor*, USAEC Report HW-SA-1965, General Electric Company, Aug. 9, 1960.
33. C. Starr and R. W. Dickinson, *Sodium Graphite Reactors*, Addison-Wesley Publishing Co., Reading, Mass., 1958.
34. R. L. Olson et al., The Sodium Graphite Reactor Power Plant for CPPD, in *Proceedings of the Second United Nations International Conference on the Peaceful Uses of Atomic Energy, Geneva, 1958*, Vol. 9, pp. 161-179, United Nations, New York, 1959.
35. *Liquid Metal Fuel Reactor Experiment, Annual Technical Report*. USAEC Report BAW-1136, Babcock and Wilcox Co., Atomic Energy Div., Mar. 25, 1959.
36. G. A. Freund et al., TREAT, A Pulsed Graphite-Moderated Reactor for Kinetic Experiments, in *Proceedings of the Second United Nations International Conference on the Peaceful Uses of Atomic Energy, Geneva, 1958*, Vol. 10, pp. 461-475, United Nations, New York, 1959.
37. R. P. Hammond and J. P. Cody (Eds.), *A Preliminary Study of the Turret Experiment—An Operating Test of Unclad Fuels at High Temperature*, USAEC Report LA-2303, Los Alamos Scientific Laboratory, March 1959.
38. R. Schulten, A 15 Mw High-Temperature Pebble-Bed Reactor, in *Proceedings of the*

Second United Nations International Conference on the Peaceful Uses of Atomic Energy, Geneva, 1958, Vol. 9, pp. 306-309, United Nations, New York, 1959.

39. O. Machnig et al., Special Features of the Brown Boveri-Krupp Reactor, *Nuclear Power*, 6: 63-66 (March 1961).
40. A. P. Fraas et al., *Preliminary Design of a 10 Mw(t) Pebble-Bed Reactor Experiment*, USAEC Report CF-60-10-63(Rev.), Oak Ridge National Laboratory, May 8, 1961.
41. USAEC Press Release No. C-213, Oct. 28, 1960.

Author Index

Numbers in parentheses are reference numbers and are inserted to assist in locating a reference when the author's name is not cited at the point of reference in the text. Numbers in *italic* indicate the page on which the complete reference is listed.

A

- Acheson, E. G., 42, *50*
 Ajzenberg, F., 72(7), *84*
 Akamatu, H., 98, 109, 110, 111, 112, 113
 (36), *114*, *115*
 Albaugh, F. W., 278(56), *292*, 370(19),
 385
 Aleksenko, Yu. N., 261(10), *290*, 298(15),
 311, 313(6), 321(6), *323*, 372, *385*
 Alexander, L. E., 92(7), 98, *113*
 Allen, A. O., 420(91, 92, 93), *441*
 Allison, S. K., 1(1), *17*, 182(168), *194*,
 276(34), *291*, 348(44), *353*
 Amelinckx, S., 233(36), *238*, 273(28), *291*
 Amorosi, A., 147(95), *190*
 Anderson, A. R., 251(26), 252(26), 256
 (26), *258*, 391, 399(5), 407(38), 408
 (5), 410(5), 411(5), 412(5), 430(5),
 431(5), *437*, *439*
 Anderson, E., 14(63), *20*
 Anderson, H. L., 72(9), 73(9), 74(9), *84*
 Andrew, J. F., 318(10), *323*
 Antal, J. J., 271(24), 272, *291*
 Antill, J. E., 420, *441*
 Apker, L., 142(65), *189*
 Arms, H. S., 498(14), *521*
 Arnold, R., 149(103), 152(103), *191*
 Arragon, P., 149, 151(102), *191*
 Arthur, J. R., 413(53, 55), 431(55), *439*
 Asher, R. C., 143(75), 172(149), 173(149),
 174(149), 175(149), *189*, *193*, 450(9,
 10), *461*
 Attree, R. W., 332(21), 350(21), *352*
 Aubeau, R., 416(74), *440*
 Austerman, S. B., 184(179), *194*, 240(9,
 10), *257*, 267(19), *291*, 295(7), *310*,
 339(29), 340, 342(29), *352*, 370(20, 21),
 385
 Austin, A. E., 99(19), 101, 102(24), 113
 (19), *114*, 261(11), *290*, 365(15), 366
 385
 Axtmann, R. C., 10(23), *18*

B

- Bacon, G. E., 93, 99, 106, *113*, *114*, *115*, 259(3), 260, 261, 264, 265(3), 266, 271,
 290, *291*, 310, *312*
 Bailey, R. W., 15(72), *20*, 290(75), *293*
 Baker, C., 273(29), *291*
 Baker, D. E., 251(27), 252(27), 253(27),
 258, 306(35), *312*
 Ballinger, J. C., 161(127), *192*, 332(22),
 338, 340(22), 341(22, 34), 342(34), 348
 (45), *352*, *353*
 Bangham, D. H., 425(112), *442*
 Banks, W. F., 11(38), *18*
 Bardwell, D. C., 407(30), 426(117), *438*,
 442
 Barnes, R. S., 376(32), *386*
 Barnett, E. de B., 143(67), *189*
 Barrer, R. M., 423(104), 424(104), *442*
 Barrett, E. P., 100, 101(22), *114*
 Bartell, F. E., 169(142), *193*
 Baskin, Y., 95(13), 96, *114*, 147(101), *191*
 Basset, J., 147, *190*
 Bassett, J., 117(1), 118(1), *186*
 Becker, K., 454(28), *462*
 Bell, J. C., 184(173), *194*, 231(35), *238*,
 329(33), 330(33), 337(27), 341(33),
 352
 Bennett, G. A., 468(5), *480*
 Bennett, R. A., 73(15), *84*
 Berenbaum, R., 152(109), *191*
 Bergenlid, U., 119(9), *187*
 Berlincourt, T. G., 133(46), 134(46), *188*
 Berman, R., 123(20), *187*
 Bernal, J. D., 89, *113*
 Berthier, R. M., 149, 151(102), *191*
 Bethe, H. A., 209, *237*
 Bienvenu, M., 13(58), *19*, 290(76), *293*,
 502(18), 503(19), *521*, *522*
 Bierlein, T. K., 104(30), *115*
 Binford, J. S., Jr., 419(85), *441*
 Binner, C. R., 59(3), *65*
 Blacet, F. E., 249(25), *258*
 Blackman, L. C. F., 141(64), *189*, 429
 (140), *444*
 Blakely, J. P., 172(148), 173, 174(148),
 175(148), *193*
 Blocher, J. M., 432(148, 149), *444*

- Blokhintsev, D. I., 10(25), 18, 511(28),
 522
 Blyholder, G., 413(64), 414(64), 440
 Bokros, J. C., 143(74), 189, 453(23, 24),
 455(23), 456, 457, 458(23, 24), 459,
 462
 Bollmann, W., 272, 291
 Bond, R. L., 162(129), 163(129), 192
 Bonner, F., 399-400, 438
 Born, G. I., 81(26), 82(26), 85
 Bortz, S. A., 152(110), 191
 Bourdeau, R. G., 316, 323
 Bovenkerk, H. P., 117(3), 118(3), 186
 Bowman, F., 455(36), 462
 Bowman, J. C., 46(24), 47(24), 50, 119
 (11), 120(12), 122(11), 182(12), 187,
 315(8), 323
 Bowring, J. R., 431(144), 444
 Boyd, G. E., 81(28, 29), 82(28, 29), 85
 Boyland, D. A., 176(156), 180(156), 181
 (156), 193
 Boyle, W. S., 130(37), 188
 Bradstreet, S. W., 33(20), 50
 Branch, G. M., 73(14), 84
 Brickwedde, F. G., 422(101), 442
 Bridger, G. W., 413(54), 439
 Brinkman, J. A., 212, 237
 Brodie, I., 152(109), 191
 Brohovich, B. B., 10(22), 18, 509(27),
 510(27), 522
 Brooks, H., 120(14), 187, 299(21), 311
 Brooks, L., 47(26), 50, 83(38), 85
 Brown, A. R. G., 433(154), 435, 444
 Brown, C., 169(144), 193
 Brown, F. W., 209, 215, 237
 Brown, G., 349(48), 353
 Browning, L. C., 424, 442
 Brunauer, S., 168(137, 140), 192, 193
 Buck, J. H., 239(3), 257
 Bunney, L. R., 81(25), 82(25), 85
 Burton, H. H., 413(60), 440
 Burton, M., 5(8), 17, 230(28), 237, 276
 (35, 37), 291, 292, 347(42)
 Bush, P. D., 239(4), 257
- C
- Cameron, A. T., 407(34), 417(34), 428
 (34), 438
 Camp, I. McI., 29(10), 50
 Campbell, I. E., 454(27), 462
 Carleton, J. T., 276(45, 46), 292
 Carman, P. C., 176(157), 178, 193
- Carniglia, S. C., 449(6), 450, 461
 Carter, R. L., 305, 306(32), 312, 383, 386
 Carter, R. S., 198(2), 236
 Castle, J. G., 136(57), 189
 Chambadal, P., 13(49), 19
 Charraut, J. C., 383, 386
 Chikalla, T. D., 144(78), 145(78), 190
 Chipman, D. R., 100(21), 114
 Chukhanov, Z. F., 413(50, 51), 439
 Clark, T. J., 254, 258
 Clayton, J. O., 427(122, 123), 443
 Clementi, E., 117(4), 118(4), 186
 Cockcroft, J., 271(22), 291
 Cody, J. P., 11(36), 18, 518(37), 519(37),
 522
 Cohen, E. R., 73, 84
 Collins, F. M., 125(23, 24), 126(23), 187
 Coltman, R. R., 241(14), 257
 Cook, W. H., 460(42), 461(42), 463
 Copeland, L. C., 416(77), 441
 Copestake, T. B., 397(10), 409(10), 410
 (10), 437
 Cordall, D., 327(4), 351
 Corlett, R. F., 276(53), 292
 Corners, A. M., 82(36), 85
 Corney, N. S., 249(24), 258, 397(10), 400
 (18), 409(10), 410(10), 420(97), 423
 (97), 424, 426(97), 437, 438, 441
 Cottrell, A. H., 332(16), 333, 334(16),
 341(16), 351, 360(6), 362, 384, 493(10),
 521
 Coucoulas, A., 145(83), 190
 Coulson, C. A., 90(4), 113
 Coultas, T. A., 451(19), 462
 Coveyou, R. R., 73, 84
 Cowen, H. C., 255(29), 258, 409(42), 414,
 439, 440
 Craven, B., 145(86), 190
 Croft, R. C., 146(89), 190
 Crone, H. G., 431(144), 444
 Cunningham, J. B. W., 13(54), 19
 Currie, L. M., 24(5), 50, 109(35), 115, 151
 (108), 152(108), 154(108), 163(108),
 164(108), 191
 Curtiss, D. H., 276(52), 289(72), 292, 293
 Cygan, R., 449(5), 451(5), 461
- D
- Dahl, R. E., 368(16), 385, 414(59), 416
 (73), 431(146), 432(146), 440, 444
 Dalmasso, C., 331(13), 351
 Damask, A. C., 231(34), 238

Davey, H. G., 13(53), 19

Davidge, P. C., 249(22), 250(22), 258,
388(2), 407(33), 408(33), 409, 411(33),
417(80), 437, 438, 441

Davidson, H. W., 88, 113, 154, 156(115),
157(115, 117), 158, 159(125), 191, 192,
313(5), 315(7), 317, 318(7), 320(5),
323, 370, 385

Davidson, J. M., 225(19), 237, 243(17),
246(21), 247(17), 255(32), 256(32), 257,
258, 277, 285(54), 286(66), 287(67, 68),
292, 293, 329(10), 330, 331(14), 338(10),
351

Day, R. J., 413(49), 414(65), 439, 440

Dayton, R. W., 475(18), 479(24), 481

deBoer, J. H., 167(134), 168(138), 192

Deegan, G. E., 295(2), 301(2), 310, 371(22),
382(22), 385

de Halas, D. R., 288(70), 293

Deitz, V. R., 425(114), 442

Delavignette, P., 233(36), 238, 273(28),
291

Delbeq, C. J., 299(20), 311

de Rouville, M., 13(48), 19

Desorbo, W., 119, 120(15), 121(15), 123(7),
187, 309, 312

Dickinson, H. C., 327(3), 351

Dickinson, R. W., 450(11), 461, 515(33),
516, 522

Dickson, J. L., 332(24), 334(24), 336(24),
352, 491(5), 521

Dienes, G. J., 127(26), 187, 198, 200(4),
207(4), 208(4), 213(4), 231(34), 234,
236, 238, 288(71), 293, 344, 352, 415(68,
69), 417(68), 440

Dmitriev, M. T., 416(76), 420(76), 440

Dodd, C. G., 169(142), 193

Dodson, J. A., 419(89), 441

Dodson, M. H., 178(160), 193

Dollezhal, N. A., 10(26), 14(59), 18, 19,
512(30), 522

Dondes, S., 407, 417(81), 428(81), 438, 441

Donoghue, J. J., 299(17), 300(17), 302(27),
303(27), 311, 312

Drake, L. C., 102(25), 114

Dressl, E. M., 162(130), 192

Drowart, U., 118(5), 186

Durand, R. E., 228(21), 237

Duval, X., 413(48), 439

Dyson, F. J., 136(55), 189

Dzurus, M., 425, 442, 450(8), 461

E

Earp, F. K., 430(142), 444

Eatherly, W. P., 102(26), 103(26), 114,
150(106), 151(106), 155(106), 166(106),
178, 179(106, 163), 181(106), 182(106),
183(106), 184(106), 191, 194, 299(17),
300(17), 301(25), 306(34), 311, 312,
373(27), 386, 446(1), 447(1), 448(1),
461, 470(10), 471(10), 472(10), 477(10),
480

Edlund, M. C., 68(3), 84

Edstrom, T., 31(13), 50

Eggen, D. T., 196(1), 236, 295(5, 6), 310

Eggleston, R. R., 172(150), 193

Elliott, R. J., 136(54), 189

Elston, W. T., 184(172), 194

Emmett, P. H., 169(143), 183(143),
184(143), 193, 424, 442

Ergun, S., 399, 400, 437

Etherington, H., 9(17), 10(17), 17

Evans, R. M., 276(39), 292

Ewest, A., 454(28), 462

Eyring, H., 413(64), 414(64), 419(85), 440,
441

F

Faris, F. E., 154(116), 155(116), 156(116),
191, 228(21), 237, 295(4), 310

Fast, E., 230(30), 238

Feldman, M. H., 128(29), 188

Fermi, E., 1(2), 3(3, 4), 5(4), 9(2), 17,
276(33), 291

Filon, L. N. G., 153, 191

Finniston, H. M., 310

Firestone, R. F., 420(95), 441

Fischbach, D. B., 159(126), 192

Fletcher, J. F., 246(19), 257, 259(4),
264(14), 267(20), 268(4), 281, 284(20),
290, 291, 298(16), 304(30), 305(16), 311,
312, 341(32), 352

Flubacher, P., 120(13), 187

Fortescue, P., 12(42), 19, 508(25), 522

Fowler, A., 9(12), 10(12), 17

Fox, J. C., 242(15), 257

Fraas, A. P., 520(40), 523

Franck, H. G., 31(12), 50

Franck, J., 5(8), 17, 276(35, 37), 291, 292

Franklin, R. E., 91(6), 93(9), 113(38), 113,
114, 115

Fredenhagen, V. K., 450(7), 461

Freund, G. A., 11(31), 18, 518(36), 522

Fuchs, L. H., 138(59, 61), 140(59), 142(59),
189, 230(29), 238, 295(1), 298(14), 310,
311

Fujita, F. E., 273(30), 291

Fulkerson, S. D., 179(162), 194

Fursov, V. S., 4, 17

G

Gadsby, J., 399, 418, 437, 441

Galt, J. K., 136(52), 188

Gangler, J. J., 144(77), 189

Ganguli, N., 132(41), 188

Gavin, G. B., 73(12), 84

Gaylord, W. M., 176(155), 193

Gazza, G. E., 104(29), 114

Geary, R. A., 11(35), 18, 508(24), 522

Gendron, N. J., 104, 115

Gerds, A. F., 143(71), 189, 453, 458(22), 462

Gershinowitz, H., 428(130), 443

Ghalib, S. A., 14(61), 19

Giaugue, W. F., 427(122, 123), 443

Giberson, R. C., 428, 443

Gigon, J., 228(26), 237

Gilbreath, J. R., 328(6), 332(6), 351,
379(35), 386

Girifalco, L. A., 91(5), 113

Glasstone, S., 68(3), 71(4), 84

Glockler, G., 345(40), 353

Godsin, W., 454(33), 462

Goggin, P. R., 371, 385

Goldthwaite, W. H., 433(152), 444

Goncharov, V. V., 10(21), 18, 509(26), 522

Goodman, B. B., 309, 312

Gordon, S., 421(96), 441

Gorin, E., 423(105), 424(105), 442

Goring, G. E., 424(106), 442

Gorton, A. F., 157(122)

Gow, H. B. F., 249(23), 253, 408(40, 41),
439

Grant, P. J., 349(49), 353

Grass, R. C., 143(69), 144(69), 189, 490(3),
491(6), 492(6), 521

Greaves, J. C., 416(78), 441

Green, L., Jr., 127(25), 187, 427(121), 443

Green, W. V., 454(26), 462

Greenough, G. B., 328(9), 329(9), 330(9),
337(27), 341(9), 351, 352

Griggs, B., 406(29), 438

Grodzovskii, M. K., 413(51), 439

Gunnill, G., 11(34), 18

H

Haering, R. R., 129(30, 31), 130(39), 131,
138

Hales, R. L., 104(31), 115

Hamister, V. C., 29(9), 31(16), 50

Hammond, R. P., 11(36, 37), 18, 518(37),
519(37), 522

Harris, G. M., 426(116), 442

Harris, P. M., 45(23), 50

Harrison, R. J., 261(11), 290, 365(15), 366,
385

Hart, E. J., 420(94), 421(96), 441

Harteck, P., 407, 417(81), 428(81), 438, 441

Hatfield, M. R., 27(6), 50

Head, J. L., 15(72), 20, 290(75), 293

Healy, F. J., 27(7), 50

Hedden, K., 431(145), 444

Hedden, W. A., 33(19), 50, 99, 113(19),
114, 164(131), 165(131), 183(131), 192,
276(49), 279(49), 292

Hedges, J. D., 49(33), 51

Heineman, R. E., 73(15), 84

Helm, J. W., 225(19), 237, 243(17), 247(17),
257, 286(66), 287(68), 293

Hennig, G. R., 136(58), 143(70), 144(70),
146(70, 93), 189, 190, 208(9), 222, 223,
232(9), 233(9), 237, 239(1), 257, 266,
268, 291, 296, 297(9), 299(20), 300(23),
301(23), 303(9, 29), 310, 311, 312, 344,
345(39), 352, 353, 363, 371, 385, 403(20),
415(20), 438

Henson, R. W., 334(26), 335, 352

Hering, H., 76(19), 82(33), 84, 85, 279(61),
293

Herold, A., 143(72), 189, 429(139), 444

Herrick, C., 454(34), 462

Hill, M. W., 430(142), 444

Hilsenrath, J., 388(1), 437

Hilton, H. B., 350(51), 353

Hincke, W. B., 145(87), 190

Hinton, Sir Christopher, 493(9), 521

Hirschfelder, J. O., 407(31), 408(31), 438

Hogerton, J. F., 143(69), 144(69), 189,
490(3), 491(6), 492(6), 521

Honig, R. E., 426(118), 443

Horton, C. C., 170, 171(146), 193

Hove, J. E., 119(6), 122(18), 123(18), 186,
187, 208(9), 232(9), 233(9), 237, 240(9),
257, 266, 268, 291, 295, 296, 297(9),
301(26), 302(26), 303(9, 28), 307(36),
308, 309(36), 310, 311, 339(30), 340,

352, 363(10), 370(21), 371, 373(28),
374, 375, 385, 386
Hughes, D. J., 80, 84, 198(2), 236
Hunt, B. E., 419(88), 441
Hutcheon, J. M., 156(119), 157(119), 177,
192, 193
Hyder, H. R. McK., 208(11), 220 to 221,
237

I

Ichikawa, Y. H., 142(66), 189
Iggulden, D., 503(20), 522
Ikegawa, T., 139, 189
Isbin, H. S., 9(16), 13(16), 14(16), 17
Izui, K., 273(30), 291

J

Jackson, G. F., 327(4), 351
Jackson, J. L., 433(153), 436(153), 444
James, R. W., 266(17), 291
Janes, M., 472(14), 480
Jansen, D. H., 460(42), 461(42), 463
Jefferson-Loveday, D. W., 241(12), 257
Jeffrey, J. O., 155(118), 156(118), 191
Johnson, A. A., 276(46, 47), 292
Johnson, P. D., 144(80), 145(80), 190
Johnston, D. F., 299(22), 311
Johnston, W. H., 82(30), 85
Johnstone, H. F., 418, 441
Jones, F. W., 97, 98, 114, 262, 290
Jones, M. T., 117(2), 118(2), 186
Jones, S. S., 239(5), 257
Joyner, L. G., 103(27), 104(27), 114,
169(143), 183(143), 184(143), 193
Juel, L. H., 47(28), 51, 183(175), 194

K

Kanter, M. A., 127(27), 128, 187, 188, 344,
352, 467(3), 480
Karzharina, N., 413(50), 439
Kaufman, F., 417 (79), 441
Keating, D. T., 267(18), 291
Keen, R. D., 180(166), 194, 449(5), 451(5),
461
Keesom, P. H., 119(8), 187
Kelley, F. C., 454(30), 462
Kelley, K. K., 390, 437
Kelman, L. R., 451(16), 462
Kelso, J. R., 417(79), 441
Kenward, C. J., 208(11), 220 to 221, 237
Kernohan, R. H., 477(20), 481
Kerr, G. P., 332(20), 352

Key, A., 399(15), 437
Khokhlova, A. V., 454(29), 462
Kieffer, R., 454, 462
Kiive, P., 132(43, 44), 146(44), 188
Kinchin, G. H., 11(34), 18, 133(49),
134(49), 135(49), 153(114), 155(114),
188, 191, 207, 213, 214, 236, 278(59, 60),
293, 297(12), 298(12), 299(19), 311,
313(3), 323, 328, 345(11), 351, 365(13),
369(13), 372, 385
Kistiakowsky, G. B., 428(130), 443
Kitano, Y., 211(14), 237
Klamut, C. J., 449(2), 461
Klimenkov, V. I., 261(10), 290, 298(15),
311, 313(6), 321(6), 323, 372, 385
Klinger, N., 145(84), 190
Klug, H. P., 92(7), 98, 113
Kmetko, E. A., 111, 113(37), 116, 146(91),
190
Knott, D. M., 183(171), 184(171), 185(171),
194
Ko, R., 82(35), 85
Koehler, J. S., 201(5), 202(5), 203(5),
205(5), 208(5), 209(5), 211, 213(5), 236
Komarek, K. L., 145(83, 84), 190
Kondo, M., 428(131), 443
Kosiba, W. L., 415(68, 69), 417(68),
427(120), 440, 443, 458(38), 462
Koyama, K., 245(20), 246(20), 253, 332(25),
333, 352
Krishnan, K. S., 132(41, 42), 188
Kroll, W. J., 145(81), 190, 471(12), 480
Kruber, O., 30(11), 50
Krumhansl, J. A., 120(12, 14), 182(12), 187
Kruyer, S., 167(134), 192
Kruzhilin, G. N., 10(20), 17
Kuchta, J. M., 414(66), 440
Küchle, M., 73(13), 84
Kuroda, H., 109, 110, 111, 112, 113(36), 116

L

Lad, R. A., 91(5), 113
Lambert, F. J., 179(162), 194
Lane, J. A., 460(41), 462
Lane, R. O., 198(3), 236
Langdon, W. R., 239(5), 257
Langmuir, I., 413(44), 439
Larson, E. A. G., 350(51), 353
Laves, F., 147(101), 191
Lauritsen, T., 72(7), 84
Lees, R. B., 332(19), 337, 341(19), 344,
345(19), 347(19), 352, 360(5), 378, 384

- Legendre, A., 48(30), 51, 183(174), 194
 Legendre, P., 48(29), 51
 Leighton, P. A., 249(25), 258
 Leppla, P. W., 82(31), 85
 Lewis, W. K., 413(58), 439
 Lewis, W. R., 276(43, 47, 48), 292
 Leyse, C. F., 239(3), 257
 Lind, R., 255(29), 258, 409(42), 439
 Lind, S. C., 407(30, 37), 426(117), 438, 439, 442
 Linnett, J. W., 416(78), 441
 Livingston, M. S., 209, 237
 Lloyd, R. C., 74, 84
 Loch, L. D., 101, 102(24), 114, 264(15), 276(15), 279(15), 280(15), 291, 452(21), 462, 470(7), 472(15), 477(15), 480
 Loebenstein, W. V., 425(114), 442
 Loebner, E. E., 131(40), 141(40), 188
 Loftness, R. L., 450(12), 461
 Lomer, W. M., 360(7), 385
 Long, E., 290(74), 293, 495(12), 496, 497, 521
 Long, F. J., 392(6, 7), 396, 418(7), 437
 Losty, H. H. W., 88, 113, 149(104), 154(117), 156, 157(104, 117, 121), 158(124, 125), 159(121, 125), 191, 192, 313(5), 315(7), 317, 318(7, 11), 319, 320(5), 323, 370, 385
 Love, C. E., 58(1), 59(1), 65
 Lund, C. A., 261(6), 262, 267(6), 290
 Lund, H. H., 152(110), 191
 Lynch, J. F., 433(150), 444
 Lyon, R. N., 143(73), 179(161), 189, 193, 450(13), 451(13), 461
- M**
- McCartney, E. R., 145(86), 190
 McClelland, J. D., 122(17), 184(176), 187, 194, 298(13), 300(13), 301(13), 302(27), 303(27, 28), 311, 312, 373(29), 379(36), 386
 McClure, J. W., 130(34, 35, 38), 132(38), 133(48), 137(48), 188
 McCoy, W., 458(39), 462
 Machnig, O., 520(39), 523
 McIntosh, A. B., 150(105), 151(105), 152(105), 155(105), 191, 430(143), 444
 McNeil, D., 32(18), 50
 McReynolds, A. W., 240(11), 257
 Madley, D. G., 428(133), 443
 Maimoni, A., 427(126), 443
 Maire, J., 146(92), 190
 Makin, M. J., 376(32), 386
 Mallett, M. W., 143(71), 189, 449(3), 451(3), 453, 458(22), 461, 462
 Mallison, H., 31(15), 50
 Malmstrom, C. R., 152, 153(111), 154(111), 157(122), 158(111), 159(111), 182(111), 191, 192, 295(3), 310
 Mansius, C. A., 68(1), 84
 Mantell, C. L., 147(96), 184(181), 190, 194
 Markel, R. F., 82(31), 85
 Marsh, W. R., 249(22, 23), 250(22), 258, 407(33), 408(33, 40, 41), 409, 411(33), 438, 439
 Martens, H. E., 153(112), 158(112), 183(112), 184(112), 191
 Martin, D. G., 228(25), 237
 Martin, S. W., 104(28), 114
 Mason, I. B., 140(63), 141, 189
 Maurer, R. J., 299(18), 311
 Mayer, G., 228(26), 237, 332(23), 352
 Mayers, M. A., 419(87), 441
 Mering, J., 146(92), 190
 Metcalf, H. E., 9(10), 17
 Meyer, L., 95(13), 96, 114, 413(46, 63), 439, 440
 Meyer, R. A., 316, 323
 Millar, R. N., 14(64), 20, 498(15), 521
 Mitchell, C. V., 28(8), 50
 Mitchell, D. W., 451(15), 462
 Mitchell, K. J., 11(35), 18, 508(24), 522
 Mol'kov, L. P., 454(29), 462
 Montet, G. L., 300(24), 311, 363(11), 364, 365(11), 385
 Moore, R. V., 11(33), 18
 Morral, F. R., 451(17), 462
 Moyle, M. M., 451(14), 462
 Mrozowski, S., 129(30), 131, 132(43), 146(90), 157(120, 123), 188, 190, 192, 318(12), 323
 Murray, P., 470(11), 476(11), 480
 Music, J. F., 276(50), 292
- N**
- Nairn, J. S., 228(27), 237, 415(70), 416(72), 440
 Nardelli, G. F., 331(13), 351
 Nathans, M. W., 164(132), 165(132), 192
 Naydon, T. T., 239(5), 257
 Nelson, J. B., 95(12), 96, 114
 Neubert, T. J., 5(9), 17, 230(28), 237, 332(19), 337, 341(19), 344, 345(19),

347(19, 42), 352, 353, 360(5), 368, 372,
376(30), 378, 384, 385, 386
Newgard, J. J., 329, 351
Nichols, G. E., 119, 123(7), 187
Nichols, P. F., 71(5), 75(5), 76(5), 77(5),
81(23), 84
Nightingale, R. E., 259(4, 5), 267(5),
268(4, 5), 275(5), 276(5), 285(5),
287(5), 290, 305(31), 312, 329(8),
331(8), 351, 359(4), 365, 366(14), 367,
377(33), 378(33, 34), 379(37), 380(37),
384, 385, 386, 476(19), 481
Nikolaev, N. A., 10(25), 18, 511(28), 522
Nozieres, P., 130(36, 37), 136(53), 188

O

Oaks, H. P., 58(2), 65
O'Conner, J. J., 332(15), 351, 376(31), 386
Odening, C. A., 46(24), 47(24), 50
O'Driscoll, W. G., 184(173), 194
Okada, J., 139, 189
Olson, R. L., 14(67), 20, 516(34), 517(34),
522
Onslow MacAulay, I. N., 255(30), 258,
427(119), 443
Osborne, C. L., 493(7), 521
Overholser, L. G., 172(148), 173, 174(148),
175(148), 193

P

Parker, W. E., 466(1), 468(1), 480
Parkins, W. E., 11(30), 18, 295(5), 310,
362(9), 372(26), 373(9), 385, 386
Pascal, M., 13(49), 19
Pattenden, N. J., 278(58), 279(58), 293
Pattin, H. S., 24(3), 50
Pavlov, Ya. A., 145(82), 190
Peakall, K. A., 420, 441
Pearlman, N., 119(8), 187
Pease, R. S., 207, 213, 214, 236
Penneman, R. A., 179(164), 194
Pessl, H. J., 459, 462
Petersen, E. E., 393(8), 402(8), 403, 404,
437, 438
Phillips, G., 31(14), 50
Pierce, C., 168(139), 171(147), 193
Pilcher, J. M., 419(86), 441
Pincus, I., 104, 115
Pinnick, H. T., 132(44), 146(44), 188
Piper, E. L., 31(16), 50
Pirani, M., 454, 462
Pitzer, K. S., 117(4), 118(4), 186

Powell, R. W., 10(19), 17, 124(22), 187,
255(31), 258, 289(73), 293, 306(33),
312, 485(2), 492(2), 493(2, 7), 521
Prater, C. D., 406(27), 438
Prescott, C. H., Jr., 145(87), 190
Preskitt, C. A., 220(16), 237, 243(16), 257
Price, M. S. T., 49(32), 51, 156(119),
157(119), 192
Primak, W., 138(59, 60, 61), 140(59),
142(59), 189, 208(10), 214(10), 222,
230(29), 237, 238, 295, 298(14), 310,
311, 328(7), 345(41), 351, 353, 356,
357, 358, 359, 360(1), 384
Prosen, E. J., 327(1, 2, 5), 351
Pshezhetskii, S. Ya., 416(76), 420(76), 440

Q

Quarterman, L. A., 328(7), 351

R

Raines, C. E., 433(152), 444
Ramachandra Rao, P. V. N., 404(22), 438
Ramsey, W., 407(34), 417(34), 428(34),
438
Rasor, N. S., 122(17), 123(21), 182(177),
184(177), 187, 194, 301(25), 311
Redding, V. L., 83(37), 85
Redmond, J. P., 173, 193, 425(110), 442
Reif, A. E., 399(14), 418(14), 437
Reinker, P. H., 276(47), 292, 413(62), 440
Reynolds, W. N., 273(27), 291, 371, 385
Rhead, T. F. E., 413(52), 439
Riedinger, A. B., 180(167), 194
Riley, D. P., 95(12), 96, 114, 147, 190
Riley, H. J., 24(4), 50
Riley, W. C., 82(36), 85, 278(57), 279(62),
283(64), 292, 293, 471, 472(13), 473(13),
474, 475(13), 476(13), 478(22), 479(22),
480, 481
Rimmer, D. E., 360(7), 361(8), 362(8), 385
Ritter, H. L., 102(25), 114
Roberts, L. E. J., 162(130), 170, 171(146),
192, 193
Robertson, D. M., 82(34), 85
Robinson, P. J., 415(70), 416(71, 75), 440
Rosenberg, H. S., 478(21), 479(21), 481
Ross, A. M., 81(27), 82(27), 85
Rossberg, M., 413(57), 419(57), 439
Rossini, F. D., 122(16), 187, 327(1, 2), 351
Roux, M., 13(58), 19, 290(76), 293, 502(18),
521
Roy, J. C., 228(23), 237

Ruder, R. C., 299(18), 311
 Rudorff, W., 146(88), 190, 429(137), 444
 Ruff, O., 429(141), 444
 Runck, R. J., 143(68), 144(68), 145(68),
 189
 Rusinko, F., Jr., 404(21), 438, 466(1),
 468(1), 480
 Rutner, E., 427(124), 443
 Ryan, B. A., 173, 175(153), 193

S

Sachanen, A. N., 23(2), 50
 Sandor, J., 454, 462
 Sartain, C. C., 241(13), 257
 Savage, R. H., 169(144), 193
 Sawai, T., 164(133), 192
 Scheidegger, A. E., 176(158), 177(158), 193
 Schlechton, A. W., 145(81), 190, 471(12),
 480
 Schönert, K., 454, 462
 Schofield, F. H., 124(22), 187, 306(33), 312
 Schofield, H. Z., 469(6), 480
 Schulten, R., 12(45), 19, 470(9), 480,
 520(38), 522
 Schwartz, R. B., 80(22), 84
 Schwarz, H. A., 420(93), 441
 Schwarzkopf, P., 454, 462
 Schweinler, H. C., 75(18), 84
 Seeley, S. B., 99(20), 114
 Seitz, F., 5(6), 17, 201(5), 202(5), 203(5),
 205(5), 208, 209(5), 211, 213, 214, 236,
 237, 271, 291
 Sermon, G. T., 47(25, 26), 50
 Shannon, D. W., 418(82), 441
 Shea, F. L., Jr., 104(28, 33), 113(33), 114,
 115
 Sheard, H., 278(58), 279(58), 293
 Shepline, V. M., 143(68), 144(68), 145(68),
 189
 Shepherd, L. R., 12(39), 19
 Sheppard, C. W., 426(118), 443
 Shoenberg, D., 133(45), 188
 Siegel, S., 173(151), 193
 Sihvonen, V., 413(45), 439
 Simmons, J. H. W., 148, 190, 228(24),
 230(24, 31, 32), 231(33), 237, 238,
 313(1, 2), 323, 334(26), 335, 352
 Simnad, M., 451(18), 462
 Simons, E. M., 147(97), 190
 Simpson, O. C., 328(6), 332(6), 351,
 379(35), 386
 Slonczewski, J. C., 130(33), 188
 Smaller, B., 136(58), 189, 303(29), 312

Smalley, A. K., 479(23), 481
 Smith, A. W., 122(18), 123(18, 21),
 182(177), 184(176, 177), 187, 194,
 298(13), 300(13), 301(13), 307(36), 308,
 309(36), 311, 312
 Smith, R. N., 146(94), 168(139), 171(147),
 183(178), 190, 193, 194, 425(115),
 428(134), 442, 443
 Snyder, W. A., 264(14), 276(51), 278(57),
 281, 291, 292, 304(30), 312, 365,
 366(14), 367, 385
 Soule, D. E., 130(34), 133(47), 135(51), 188
 Southwood, J. R. M., 14(61), 19
 Spalaris, C. N., 100(23), 114, 167, 168, 169,
 171(136), 192, 193, 273(31), 274, 291,
 396(9), 403(19), 405(19, 24), 437, 438
 Stafford, J., 425(112), 442
 Stanford, L. E., 485(1), 490(1), 521
 Stanwix, P. R., 228(25), 237
 Starr, C., 450(11), 461, 515(33), 516, 522
 Steel, M. C., 133(46), 134(46), 188
 Steele, G. N., 468
 Stiennon, G., 11(28), 18
 Stover, E., 435(156), 444
 Strickland-Constable, R. F., 399(16),
 413(47), 428(132, 133), 437, 439, 443
 Strocchi, P. M., 77, 80, 81(20), 84
 Stroud, W. G., 449(4), 451(4), 461
 Strutt, R. J., 428, 443
 Suck, H., 450(7), 461
 Swarts, E. L., 144(79), 190, 451(20), 462
 Sykes, C., 332, 352
 Sykes, K. W., 392(6, 7), 396, 418(7), 437
 Szabó, Z., 423(103), 442

T

Taft, E., 142(65), 189
 Tammann, G., 454, 462
 Tarpinian, A., 104(29), 114
 Tate, R. E., 82(32), 85
 Taylor, H. S., 407(31), 408(31), 438
 Taylor, J. C., 416(71), 440
 Temkin, M. I., 425, 442
 Thomas, R. B., 421(97), 423(97), 424,
 426(97), 441
 Thomas, W. J., 425(109), 442
 Thompson, M. W., 241(12), 257, 427(125),
 443
 Tickner, A. W., 426(116), 442
 Tipton, C. R., Jr., 475(18), 476(17),
 479(24), 481
 Tomlinson, M., 255(30), 258, 427(119), 443
 Touloukian, Y. S., 388(1), 437

Townsend, J. R., 261(6, 9), 262, 263(13),
267(6), 290, 291, 379(37), 380(37), 386
Trapp, G. J., 454(31), 462
Travers, M. W., 422, 424(102), 442
Trice, J. B., 228(22), 237
Troesch, A., 424, 442
Trumble, R. E., 276(52), 292
Turkevich, J., 399-400, 438
Tyler, W. W., 120(15), 121(15), 187, 309,
312

V

Valent, D. R., 327(5), 351
Vand, V., 358, 384
Van Der Ley, P. H., 429(136), 443
Vastola, F. J., 398(11), 437
Vaughan, R. D., 14(62, 63), 20, 498(13), 521
Vineyard, G. H., 198, 200(4), 207(4),
208(4), 213(4), 234, 236, 288(71), 293

W

Wagman, D. D., 422(98, 100), 442
Wagner, P., 149(107), 150(107), 151(107),
153(107), 158(107), 159(107), 160(107),
182(107), 183(107), 191, 322(16), 324
Wagoner, G., 136(56); 189
Waite, R. J., 407(38), 439
Walker, P. L., Jr., 95(14), 96, 99(20), 114,
169(145), 173, 193, 388, 389(3), 390,
391(3), 394, 395, 396(3), 397(3), 398(3),
401(3), 402(3), 404(21, 23), 405(23),
406(21), 413, 419, 425(110), 437, 438,
442
Wallace, P. R., 129(32), 130(39), 188
Warekois, E. P., 261(8), 290
Warner, P. C., 290(77), 293
Warren, B. E., 98, 100, 114, 259(3), 260,
261, 263, 264, 265(3), 266, 290, 310, 312
Watanabe, H., 207, 237
Watt, W., 180(165), 181(165), 194, 433
(154), 435, 444
Watts, H., 428(135), 443
Webb, F. J., 119(10), 187
Wechsler, M. S., 332, 352
Wehrman, R., 432(147), 444
Weinberg, A. M., 68(2), 72(2), 73(16),
75(18), 84
Weiss, P. R., 130(33), 188
Weisz, P. B., 406(27), 438
Weltner, W., Jr., 117(2), 118(2), 186
Werking, L. C., 429(138), 444
West, J. M., 47(27), 51, 81, 82(24), 86
Wheeler, A., 406(26), 438

Wheeler, J. A., 332(15), 351, 376(31), 386
Wheeler, R. V., 413(52), 439
Whelan, P. T., 433(151), 444
White, D. W., 473(16), 480
Wibaut, J. P., 443
Wicke, E., 413(56), 431(145), 439, 444
Wieland, K., 422(99), 442
Wigner, E. P., 68(2), 72(2), 73(16), 84
Wilkinson, V. J., 416(72), 440
Wilks, J., 119(10), 187
Williamson, G. K., 273(29), 291
Wills, J. E., Jr., 72(6), 84
Wilson, A. J. C., 90(3), 93(11), 113, 114
Wilson, C. L., 143(67), 189
Wilson, S. A., 143(75), 189, 450(10), 461
Winder, D. R., 134(50), 135(50), 188
Wittels, M. C., 9(11), 17
Wood, L. J., 31(14), 32(18), 50
Woodfield, F. W., 287(69), 293
Woodley, R. E., 239(2), 257, 275, 291,
405(25), 408(39), 410(39, 43), 413(61),
420(43), 438, 439, 440
Woodruff, E. M., 104(31), 115, 161(128),
185(180), 192, 194, 267(21), 278(21),
280(21), 281(63), 283(64), 285(21), 291,
293, 297(11), 304(11), 311, 321(14, 15),
322(15), 324, 382(38), 386
Woods, W. K., 276(38, 40, 41, 42, 44),
277(55), 278(40), 292, 297(10), 302(10),
304(10), 311, 313(4), 314(4), 316(4),
317(4), 321(4), 323, 337, 339, 352,
365(12), 367, 369, 373(12), 376, 385
Wright, C. C., 393(8), 402(8), 403, 404, 437
Wright, J., 407(35), 408(35), 438
Wuschke, D., 228(23), 237

Y

Yeats, F. W., 49(32), 51
Yockey, H. P., 239(7, 8), 240(7), 241(13),
257
Yoshikawa, H. H., 228(20), 237, 243(18),
257, 285(65), 288(70), 293
Yoshimori, A., 211(14), 237
Young, J. R., 512(31), 522

Z

Zachariasen, W. H., 259, 266, 290
Zigrang, D. J., 468(5), 480
Zielke, C. W., 423(105), 424(105), 442
Zinman, W. G., 428, 443
Zinn, W. H., 72(8), 84
Zuhr, H. F., 276(50), 292
Zumwalt, L. R., 180(167), 194

Subject Index

A

- A graphite, 447-448
- "A" nickel and monel, effects of carburization on, 457
- a* spacing, 92-94
 - contraction from irradiation, 259, 264, 266
 - decrease in, annealing of, 366-367
 - effect of temperature on, 96
 - measurement of, 92-94
- Absorption cross section, 69, 73-75, 81-83
 - comparison of measurements, 76-77
 - from DIH measurements, 75
 - effect of impurities on, 77-80
 - of elements, 78-79
 - of gases, 389
 - measurement in HTR, GLEEP, and ZOE, 76-77
- Accidents in reactors, 487
- Acheson furnace, 42-44
- Activation, of gases, 397
 - by "hot atoms," 381
- Activation energy, for carbon dioxide-graphite reaction, 402
 - for creep, 159
 - of discrete annealing process, 362-363
 - for gas-graphite reactions, 394-395
 - for hydrogen-graphite reaction, 424
 - for self-diffusion, 128
- Activation-energy spectra, 357-360, 378-379
- Active sites, 401-405
 - in gas-graphite reactions, 391-393, 401
 - produced by neutron irradiation, 415
- Additives, 33
- Admixed fuel bodies, 466, 468-470
- Adsorption, of molecules, 166-167
 - physical, 166
 - of water, 170-171
- Advanced Gas Cooled Reactor (AGR), 11, 503-504
 - coolant temperature, 387
 - design, 503-504
- Age-diffusion theory, 69
- AGOT graphite, 15, 182
 - coefficient of friction, 159-160
 - compressive strength, 150
 - in CP-1 Pile, 4, 9
 - crushing strength, 448
 - flexural strength, 154
 - gas desorption from, 171-175
 - magnetoresistance of, 134-135
 - pore volume, 102-103
 - purification, 46
- AGR (see Advanced Gas Cooled Reactor)
- AGR graphite, tensile strength, 153
- AGSR graphite, impact strength, 156
- AGX graphite, 182
 - in CP-1 Pile, 1, 4
 - Hall coefficient, 133-134
 - tensile strength, 153
- AGXP graphite, 182
 - adsorption of water by, 170-171
 - growth in, 278
- Alkali hydroxides, reaction with graphite, 147
- Alloy-graphite systems, 455-459
- Aluminum carbide, 451
- Aluminum-graphite system, 451
- Ammonia, reaction with carbon, 429
- Anisotropy, of coke particles, 109
 - of electrical resistivity, 137
 - of electrographites, 106
 - of electron-spin resonance, 136
 - in extruded graphites, 35-36
 - of knock-on atom, 203
 - of nuclear graphites, 106-108
- Annealing, adiabatic, 334-336, 362
 - analysis by Vand method, 356-360
 - of *c* spacing, 359, 365, 368, 377
 - concentration of the participating species, 356
 - constant-frequency factor model, 356-360
 - in diamond, 365
 - of electrical resistivity, 371-373
 - by ionizing radiation, 379
 - isothermal, 355, 357-358, 361-362
 - kinetic order, 356
 - of length, 367-368, 377, 382
 - by linear temperature rise, 332-334, 355, 360-362
 - at low temperature, 370-371
 - by radiation, 374-383
 - reduced time in, 361-362, 370
 - of stored energy, 331-342, 376-379
 - of thermal conductivity, 373, 376-379
 - (See also Stored energy)
- Annealing function, isothermal, 357

- Annealing kinetics, 356
 Applications of nuclear graphite, future, 16-17, 48-49
 APS Reactor (see Atomic Power Station Reactor)
 Artificial graphite, 88
 ATJ graphite, 182
 coefficient of friction, 160
 compressive strength, 150
 flexural strength, 154
 ATJ-82 graphite, 182
 compressive strength, 150
 flexural strength, 154
 ATL-82 graphite, 182
 compressive strength, 150
 flexural strength, 154
 thermal conductivity, 306
 Atomic Power Station Reactor (USSR), 10, 510-511
 AUF graphite, 182
 permeability of, 180
 Autoclave for pitch impregnation, 41-42
 AWG graphite, 182
 annealing at low temperature, 371
 stored-energy release in, 339-341
 thermal conductivity, radiation effects on, 308-309
- B**
- Baked carbon, 39-40
 Baking, of carbon, 37-40
 gases formed in, 164
 Baking furnace, 38-39
 Belgian Reactor (BR-1), 11, 490
 BEPO (see British Experimental Pile Zero)
 Berkeley reactors, 14
 Bernal crystal structure, 89-90, 129
 Beryllium, moderating properties of, 71
 Beryllium oxide, moderating properties of, 71
 BET surface area, 167-169
 effect of oxidation on, 405
 effect of radiation on, 273-275
 equations for, 168
 BGRR (see Brookhaven Graphite Research Reactor)
 Binder, coal-tar pitch as, 28-29
 Binders, chemical constituents of, 31
 physical properties of, 31-32
 Bismuth, absorption by graphite, 446-449
 surface tension of, 446-447
 Bismuth-graphite surface, 446-447
 Bisulfate doping, 132-133
 Body, definition, 88
 Bond strengths, 91, 127-128
 Boronated graphite, 7
 Boron, in coal-tar pitch, 31
 cross section of, 80-81
 Boron carbide impurity, 46-47
 Boron doping, 119-120, 122, 136
 Bradwell reactors, 14, 498
 Bravais-Miller indices, 91-92
 Breaking strain, radiation effects on, 316-318
 Brillouin zone, energy band structure of, 130-131
 form of for Bernal structure, 129
 Brillouin zone and charge carriers, 137
 Brillouin zone and diamagnetism, 302-303
 British Experimental Pile Zero (BEPO), 9, 490-491, 493-494
 cryostat in, 241
 equivalent dose, 241
 equivalent flux, 241
 loop in, 249-251
 Bromine, as inhibitor of oxidation, 431
 reaction with graphite, 429
 Brookhaven Graphite Research Reactor (BGRR), 10, 490-494
 graphite structure of, 492
 growth in, 289, 493
 temperature distribution, 485
 Bulk density, 163-166, 406
 (See also Density)
 Bulk packing during baking, 39
 Burning of graphite in air, 415-416
- C**
- c* spacing, 89, 92-93
 annealing of, 359, 365, 368, 377
 effects of irradiation temperature on, 267-268
 effects of radiation on, 259-268, 282-283, 287, 315-316
 effects of temperature on, 96
 measurement of, 92-93
c spacing and stored energy, 347
c spacing and transverse length change, 282
 C-18 graphite, 182
 tensile strength, 153
 Calder equivalent dose (Mwd/At.), 231

- Calder Hall reactors, 13, 495-498
 design, 495-498
 graphite-column support, 497
 moderator structure, 496-497
 operating temperature, 387
 stored energy in, 349
Calorimeter, 333, 335
Carbides (see Metals)
Carbides as coatings, 432-434
Carbides in liquid-metal system, 449
Carbon, amorphous, 87
Carbon dioxide, diffusion in graphite, 402-403
 effects of radiation on, 406-407
Carbon dioxide-carbon monoxide equilibrium, 398
Carbon dioxide-cooled reactors, 495
Carbon dioxide-graphite reaction, 387, 397-411
 activation energy of, 402
 effects of flow rate on, 409-411
 effects of pressure on, 408-409
 effects of temperature on, 408-409
 equilibrium constant for, 400
 radiation-induced, 407-411
 rate equation for, 393, 401
 reaction kinetics, 408
Carbon dioxide-graphite system, 397-412
Carbon monoxide, in Calder-2 Reactor, 411
 effects of radiation on, 407
Carbon tetrachloride as inhibitor of oxidation, 431
Carburization of metals, 452
Catalytic cracking of petroleum crudes, 22-23
CCN graphite, 182
 compressive strength, 150
 flexural strength, 154
Cemented joints, strength, 64-65
Cementing techniques, 62-65
Cements, 62-63
 oxidation of, 65
CEQ graphite, flexural strength, 154
 impact strength, 156
 modulus of rigidity, 155-156
 tensile strength, 153
Cesium in liquid-metal system, 449
Chapel Cross reactors, 13, 495
Charge carriers, electrons as, 136
 number of, 133
 properties of, 137
 sign of, 131-132
Chemical properties of graphite, 142-147
Chemisorption, 166-167
Chlorine, absorption cross section, 81
 impurity in graphite, 83
 as inhibitor of oxidation, 431-432
 purification with, 47
Chlorine-graphite reaction, 429
CK graphite, 182
 compressive strength, 150
 tensile strength, 153
Cleves coke, 94, 109, Plate II
CNG graphite, 182
 specific heat, 119-120
CNGB graphite, 182
 specific heat, 119-120
Coal distillation, 29-30
Coal-tar distillation, 30
Coal-tar pitch, 28-32
Coefficient of friction, 159-161
 effect of radiation on, 321-322
Coefficient of thermal expansion, 35, 40, 45, 124-126
 relation to dimensional changes, 283
 (See also Thermal expansion)
Coke, calcination of, 24-27
 impurities in, 25, 28
 properties of, 24, 27-28
Coke flour, 32
Coke particles, 88
Cokes, needle, 36, 109, Plate II
Coking process, 23-24
 effect on graphite, 113
Coking values, 164-165
Collisions, elastic, 201
 hard-sphere, 202-204
 inelastic, 200-201, 207-208
 Rutherford (see Rutherford collisions)
Compressive strength, 45
 effects of oxidation on, 406
 effects of radiation on, 316-317
 effects of temperature on, 150
 measurements of, 149-151
Conduction electrons, energy dissipation of, 209
Contamination from machining, 56-57
Contraction, annealing of, 288, 368
 caused by radiation, 286-287
Copper-graphite system, 452-453
Cost of graphite, 8
Coulomb interaction potential, 201

- CP-1 Pile, 1-5, 9
 graphite in, 4
CP-2 Pile, 3-4, 9, 489
Creep, 158-159
 effects of radiation, 319-320
 from radiation, beneficial effect of, 322-323
Cross section (see Absorption cross section)
Crystal density, 163
 of diamonds, 87
 of graphite, 87
Crystal growth, 42, 108-113
Crystal structure, of graphite, 89-90
 effects of radiation, 259-273
Critical point, 117
Cryostats in reactors, 240-241
Crystallinity, 108-111
Crystallite, chemical forces, 90
 definition, 87
 dimensions, 89, 94, 98-99
 annealing of, 365-367
 effect on thermal conductivity, 123-124
 effect of radiation on, 261-263, 268
 electrical conductivity, 90, 138
 grinding of, 99
 properties of, 94, 97-99
CS graphite, 10, 182
 compressive strength, 150
 flexural strength, 154
CSF graphite, 182
 adsorption-desorption isotherm, 167
 annealing dimensional changes in, 367
 annealing thermal conductivity of, 373
 burning in air, 416
 c spacing, 94
 effect of radiation on, 263-264, 268, 282
 contraction rate, 286
 crystallite properties of, 94
 desorption of gases from, 172-173
 effect of radiation on crystal dimensions of, 263-264, 268
 effect of radiation on dimensions of, 277-280, 284-286
 effect of radiation on electrical resistivity of, 297-298
 effect of radiation on surface area of, 275
 effect of radiation on thermal resistivity of, 304-305
 electron photomicrograph, 105
 expansion rates, 277-280
 graphitization, 94
 graphitizing temperature, 278-279
 Hall coefficient, 134
 heat of adsorption, 171
 machinability, 321
 micropores in, effect of oxidation on, 405-406
 pore-size distribution, 275, 405
 pore volume, 103
 reaction with air, 414
 reaction with oxygen, 413
 stored energy in, 337, 340-342, 347
 surface area, 168-169
 thermal conductivity, 304-306
 thermal expansion, 278-279
 X-ray line broadening, 261-263
CSGBF graphite, 10, 183
 effect of radiation on dimensions of, 285-286
 stored energy in, 331
 surface area of, 169
 thermal conductivity of, 307
CSO graphite, 10, 183
 thermal conductivity of, 307-309
Cyclotron for irradiations, 239-240
Cyclotron resonance, 136
- D**
- Danger coefficient, measurement of, 74-75
Darcy's law, 177, 181
Defects, annealing of, 233-234, 296
de Haas-van Alphen effect, 133
Delta in-hours (DIH), 74-75
Density, 161-166
 of baked carbon, 40
 bulk, 163
 effect of oxidation on, 403
 definition, 163
 effect on neutron moderation, 67-68
 effect on radiation-induced expansion, 280
 effect on Young's modulus, 156-157
 of graphites, 162
 real, 163
Desorption of gases, 171-175
Diamagnetic susceptibility (see Magnetic susceptibility)
Diamond, 117
 annealing of damage in, 365

- Diffraction lines (see X-ray diffraction lines)
 Diffusion coefficient for electrons, 211
 Diffusion-controlled gas reactions, 395
 Diffusion length of neutrons, 73-74
 Dimensional changes caused by radiation, 276-288
 monitoring of, 255
 in reactors, 276, 288-290, 487
 Dislocation loops, 273
 Displaced atoms, calculated vs. experimental rates, 222-223
 number produced by neutrons, 199, 200-217, 221, 271, 379-381
 by radiation, 195
 range of, 210-211
 rates of formation, 218
 reintegration of, 364-365
 Displaced atoms and stored energy, 345
 Displacement cross section, 205
 Displacement energy, 196-197
 Displacement process, 197-200, 213
 Displacement spikes, 212
 Displacements produced in various irradiated facilities, 227
 Doping, boron, 119-120, 122, 136
 bisulfate, 132-133
 Dragon Reactor, 12, 504-508
 core design, 506
 fuel-moderator cluster, 503, 507
 helium cooling, 387
 Dungeness reactors, 15, 500
 Dust collection during machining, 56
 Dust, wear, surface area of, 169
- E**
- Earthquake loads, 486
 EBP graphite, 182
 tensile strength, 153
 ECA graphite, 183
 Hall coefficient, 134
 modulus of rigidity, 155-156
 tensile strength, 153
 Young's modulus, 154
 EDF-1 (see Electricité de France Reactor-1)
 EDF-2 (see Electricité de France Reactor-2)
 Effective radius for a knock-on atom, 204
 EGCR (see Experimental Gas Cooled Reactor)
 Elastic collisions, 201
 Elastic constants, 147
 Elastic deformation, 315, 318
 Elastic modulus, of baked carbon, 40
 effects of radiation on, 313-316, 318-319
 in compression, 148-151
 in flexure, 153
 in tension, 151-152
 (See also Young's modulus)
 Elastic scattering of neutrons, 216
 Electrical resistivity, annealing of radiation effects, 371-373
 of baked carbon, 40
 effects of radiation on, 196, 295-298
 of joints, 64
 of polycrystalline graphite, 45, 138-141
 of single crystals, 138
 theory of, 90-91, 137
 Electricité de France, Reactor-1 (EDF-1), 13, 502
 Reactor-2 (EDF-2), 13, 502-503
 keyed blocks in, 290
 Electrographite, definition, 88
 grades, 186
 lattice dimensions, 93-94
 machinability, 53
 cutting tools for, 54-55
 manufacture of, 21-51
 Electron diffraction in petroleum coke, 110
 Electron excitation by moving ions, 207-210
 Electron microscopy, 104-105
 of irradiated graphite, 272-273
 Electron spikes, 211-212
 Electron traps, 302-303
 Electron-spin resonance, 136-137
 Electronic band structure, 129-132
 effects of radiation on, 300-302
 of polycrystalline graphite, 131-132
 three dimensional, 130, 136
 two dimensional, 129
 Energy of formation, of interstitial carbon atoms, 344
 of interstitial-vacancy pairs, 343-345
 Energy loss per collision for neutrons in graphite, 198
 Energy transfer from moving particles, 195-196
 Enthalpy, 120-122
 Entropy, 120-122
 effect of lattice disorders on, 391
 Epithermal neutrons, 219

Erosion by liquid bismuth, 449
 Etching of polished surfaces, 104
 ETR X-basket irradiations, 243-244
 Experimental Gas Cooled Reactor (EGCR), 11, 503-505
 design, 503-505
 Experimental graphites, expansion behavior, 279-281
 Experimental Uranium-Graphite Isotope Reactor, 10, 509-510
 Extruded bodies, tensile strengths, 472
 Extrusion of coke mix, 33-36
 Extrusion press, 34
 EY9 graphite, 183
 pore size, 448
 reaction rates with water, 420

F

F purification process, 46-47, 83
 Fermi energy, 207
 Fermi level, displacement of, 140
 Fermi level and Brillouin zone, 129, 131
 Fermi level and density of states, 142
 Fermi level and free electrons, 131-132
 Fermi surface, anisotropy of, 134-135
 Finishes, grades of, 53-54
 Fission-neutron spectrum, 211
 Fission-product release, 478-479
 Fission recoils, effects on graphite, 200, 272-273, 449, 473-477
 Flexural strength, 153-154
 of baked carbon, 40
 effects of radiation on, 317
 of graphites, 45, 154
 Fluid densities of graphites, 163
 Fluorine-graphite reaction, 429
 Forming, 32-37
 Free energy, 120-122
 French nuclear graphite, 13, 76-77, 183
 crystallite properties, 94
 French reactors (G-1, G-2, G-3), 13, 490, 493-494, 500-502
 Freon, purification with, 47
 Friction (see Coefficient of friction)
 Fueled graphite, effects of radiation on, 473-477
 fission-product release from, 477-479

G

G graphite, 447-448
 G-1 Reactor, 13, 490, 493-494, 500-502

G-2 Reactor, 13, 500-502
 moderator, 501-502
 G-3 Reactor, 13, 500-502
 Gamma heating in graphite irradiations, 246-248
 Gamma irradiation facility, 250-251
 Gas-cooled reactors, graphite reactions in, 387, 445
 high temperature, 503-508
 low temperature, 489-494
 Gas desorption, from AGOT graphite, 174
 from PGA graphite, 174
 from TSF graphite, 175
 Gas-graphite reactions, effects of impurities on, 396-397
 effects of radiation on, 391
 effects of temperature on, 394-395, 397
 equilibrium constants, 390
 heat of reaction, 389
 inhibitors, 429-432
 kinetics, 395-396
 relative reaction rates, 388
 Gas-graphite systems, 387-397
 Gas loop in Plutonium Recycle Test Reactor (PRTR), 252-254
 Gas loops, glass, 251
 high pressure, 251-254
 low pressure, 249-251
 GL-10 graphite, 183
 GLEEP (see Graphite Low Energy Experimental Pile)
 Grain, definition, 88
 Grain structure, determination, 104-108
 of needle-coke graphite, 104-105, Plate I
 preferred orientation, 106-108
 Graphite, properties as moderator, 483-484
 Graphite as a container, 7, 245
 Graphite core borer, 256
 Graphite dust, oxidized, density of, 162
 Graphite fabrics, 16-17
 Graphite Low Energy Experimental Pile (GLEEP), 9, 489
 Graphite-metal systems, 445-461
 Graphite sleeves in Calder type reactors, 349
 Graphite wear dust, surface area, 169
 Graphitic oxide, 146-147
 Graph-i-tite A, 183

- compressive strength, 150
- flexural strength, 154
- Graph-i-tite G, 183
 - coefficient of friction, 160
 - compressive strength, 150
 - flexural strength, 154
- Graphitization, 42-45
 - of carbon blacks, 111-113
 - catalysts for, 49
 - cycle, 43
 - effects on structure, 108-113
 - mechanism of, 111
 - of metals, 452-459
 - of petroleum cokes, 108-111
- Graphitization temperature, effects on radiation-induced expansion, 281, 286-287
- Graphitized lampblack, coefficient of friction, 160
- Graphitized particle, definition, 88
- Graphon, 183
- Grinding, surface finish, 55
 - (See also Finishes)
- deformation of crystallites, 99

H

- H3LM graphite, 184
 - tensile strength, 153
- H4LM graphite, 184
 - coefficient of friction, 160
 - compressive strength, 149-150
 - tensile strength, 153
- Hall coefficient, of carbons, 134
 - change in sign, 131-132
 - effects of radiation on, 299-300
 - pulse annealing of, 374
- Hall effect, 133-134
- Hallam Reactor [see Sodium Graphite (Hallam) Reactor (SGR)]
- Hanford production reactors, 5-6, 12
 - design, 512-514
 - fuel channels in, 513
- Hanford 305 Test Reactor (HTR), 9, 75, 489
 - DIH measurements in, 74-75
- Hanford test holes, 242-244
- Hardness, 161, 321
- Hard-sphere scattering, 206
- Heat of adsorption, 171
- Heat of combustion, 326-327
- Heat of formation of irradiated graphite, 390

- Heat of reaction with potassium, 328
- Heat of sublimation, 118
- Heat transfer (see Thermal conductivity)
- Heats of reaction in gas-graphite systems, 389
- Heat-treatment, effect on elastic modulus, 157-158
 - (See also Graphitization)
- Helium density of graphite, reduction by radiation, 273-275
- Helium as reactor coolant, 427, 504-508
- HERO reactor, 504
- Hexagonal crystal structure, 90, 147
- High-density graphite, 163-166
- High Temperature Gas-cooled Reactor (HTGR), 12, 387, 508
- Hinkley Point reactors, 14, 498
- Hot-working process, 49
- Hunterston reactors, 14, 498-499
- Hydrogen, adsorption on graphite, 425-426
 - cross section, 80
 - desorption, 173-175
 - as reactor coolant, 426-427
- Hydrogen-graphite reaction, 421-427

I

- Impact strength, 156
 - effects of radiation on, 317
- Impermeable graphite, 179-181, 445, 479
- Impregnation, 40-42, 49
 - effect on density, 165-166
 - effect on Young's modulus, 156-157
 - of fuel bodies, 467-468
- Impurities, cross sections, 77-81
 - determination by chemical analysis, 77-80
 - effect on moderating properties, 74
 - effect on plutonium production, 67-68
 - in enriched reactors, 67-68
 - in natural-uranium reactors, 67-68
 - in nuclear graphite, 47, 77-83
 - radioactivation of, 83
- Inelastic collisions, 200-201, 207-208
- Infrared absorption, 142
- Intercalation compounds, 146
- Interlayer binding energy, 91
- Interplanar spacings, 92-95
 - change with temperature, 95-96
- Interstitial compounds, 146
- Interstitial diffusion, 269
- Interstitial groups, 364-365

Interstitial-vacancy pairs, 212, 233, 343-345
 Interstitials, annealing, 268-271, 359-360
 clustering of, 269-271, 345
 increase in layer spacing by, 266
 rate of production, 223
 trapping of, 342
 Iodine-graphite reaction, 429
 Irradiations, in controlled atmospheres, 244-246, 248-255
 by electrons at low temperatures, 240
 at high temperatures, 246-248
 at intermediate temperatures, 245
 at low temperatures, 240-241
 at room temperature, 242
 Isotropic neutron scattering, 198

J

Japanese Tokai Mura reactor, 15, 499-500
 keyed blocks in, 290, 499-500
 Joints, 62-63
 properties of, 64-65

K

k_{err} , 68
 KC graphite, 10, 94, 183
 contraction rate, 286
 crystallite properties, 94
 effects of radiation on, 261
 expansion rate, 278-281
 graphitizing temperature, 278
 growth rate, 277-279
 magnetic susceptibility, 302-303
 surface area, 169
 thermal conductivity, 306-308
 effects of radiation on, 306-308
 thermal expansion, 278
 thermoelectric power, 301
 KCF graphite, 183
 Kendall coke, 26, 35-36
 graphitization of, 94
 thermal expansion of graphite prepared from, 126
 Keying of blocks, 290
 Knock-on atoms, average charge, 208
 collisions, 200-202, 213-214
 energy of, 197-200
 production of, 195-196
 rate of energy loss, 209
 residual range, 210
 Knudsen flow, 177

Korite graphite, 183
 c spacing of, 264
 crystallite properties, 94
 crystallite size, 98-99
 stored energy, 342
 thermal resistivity, effects of radiation on, 304
 Kraftwerk Pebble Bed Reactor (AVK), 12, 520
 KS graphite, 183
 Young's modulus, 369

L

L unit of exposure, 230
 Lamellar compounds, 146
 Lampblack, 134
 graphitized, coefficient of friction, 160
 Latina Reactor, 14, 495
 Lattice dimensions, 92-95
 effects of radiation on, 263-267, 365-367
 Lattice distortion, 96-99
 from irradiation, 232-233, 259-263
 Lattice temperature, 211-212
 Lead-bismuth eutectic, 449
 Length, effects of radiation (see Dimensional changes)
 Line broadening (see X-ray diffraction lines, broadening of)
 Linear-rise annealing, 360-362
 Linear-rise calorimeter, 333
 Liquid-metal-cooled reactors, 515-518
 Liquid Metal Fuel Reactor Experiment (LMFRE), 445, 517-518
 LITR cryostat, 241
 LMFRE (see Liquid Metal Fuel Reactor Experiment)
 Load deflection, single crystals, 313
 Lubricating oil for extrusion, 33
 Lumped fuel bodies, 467, 470

M

Machinability, 161
 effects of radiation on, 321
 Machine shop layout, 59
 Machining, at Brookhaven, 59-60
 at Hanford, 58-59
 speeds and feeds, 55-56
 tolerances, 60
 of trunnion blocks, 58-59
 in United Kingdom, 60-62
 Macropore volume, 102-104, 406

- Magnesium in bismuth reactor system, 446-447
 Magnesium-graphite system, 451
 Magnetic susceptibility, 132-133
 annealing of, 375
 effect of radiation on, 302-303
 Magnetoresistance, 134-135
 effect of radiation on, 299
 pulse annealing, 375
 Manufacture of graphite, 21-49
 Materials Testing Reactor (MTR), 239
 Matrix fuels, 6-7, 465-480
 annealing of radiation damage, 477
 attenuation of fission fragments in, 474
 effects of radiation on, 474
 by impregnation, 466
 preparation, 466
 structural changes in, 476-477
 Mean free path, for knock-on atoms, 204
 of neutrons, 199
 Mechanical loads, relation to reactor design, 486
 Mechanical properties, 147-161
 effects of radiation on, 313-323
 Melting point, 117
 Mercury porosimetry, 102-104
 Metal oxides, reactions, 144-145
 Metallographic polishing, 104
 Metals, reactions, 142-144
 Methane from hydrogen and graphite, 175, 421-426
 MH4LM-90 graphite, 184
 compressive strength, 150
 flexural strength, 154
 thermal annealing, 306
 Micropores (see Pores)
 Microwave glow discharge, 254-255
 Miller indices, 91-92
 Mix formulation, 32
 Mixing coke and pitch, 33
 Mobility, of displaced carbon atoms, 268-270, 363-365
 of electrons, 133
 of holes, 133
 Mock-ups of moderator stacking, 58, 488
 Model-channel loop in BEPO, 251-252
 Moderating ratio, 71-72
 Moderation of neutrons, 68-74
 Moderator, design and assembly, 488
 diffusion area, 69
 graphite as, 67-68
 parameters, 71-72
 sampling, 255-256
 Moderator physics, 68-74
 Moderator structures, dimensional changes in, 288-290
 Modulus of rigidity, 154-156
 annealing of, 370
 effect of heat-treatment on, 158
 effects of radiation on, 313-314
 of ungraphitized carbon, 315
 Molding, 36-37
 Molecular orbitals, in diamond, 90
 in graphite, 90-91
 Molten salt-graphite systems, 445-461
 Molten Salt Reactor Experiment (MSRE), 12, 520-521
 Molten-salt reactors, 459-461
 Molybdenum disilicide as a coating, 433
 Molybdenum-graphite reaction, 453
 Monitoring of a reactor moderator, 256-257, 488-489
 MSRE (see Molten Salt Reactor Experiment)
 MTR X-basket irradiations, 243-244
 Multiplication factor, 68
 Mwd/At, definition, 229
- ## N
- N Production Reactor (NPR), 15, 509, 514-515
 Natural flake graphite, *c* expansion, 267
 crystallite properties, 94
 density, 162
 electrical resistivity, 298
 magnetic susceptibility, 302-303
 Needle-coke graphite, grain structure, 35-36, 104, Plate I
 Needle cokes, 26-27, 109, Plate II
 Neutron cycle, 68-70
 Neutron diffraction, 271
 Neutron exposure as a dosage unit, 225-227
 Neutron exposure level, measurement of, 224-225
 Neutron flux, comparison in various reactors, 228
 effect of intensity on properties, 231-232
 Neutron-flux monitors, 224-225
 Neutron spectrum in reactors, 218-219
 Neutrons, absorption by moderator, 67
 anisotropic scattering, 72

collisions with moderator atoms, 67
 diffusion length, 73-74
 escape probability, 68
 inelastic scattering, 72
 leakage, 68-70
 logarithmic energy decrement, 69-71
 moderation of, 68-74
 multiplication factor, 68
 rethermalization, 73
 temperature of, 72-73
 thermal utilization, 68
 transmission at long wave length, 271-272
 Nickel-graphite system, 453
 Niobium-graphite system, 454-455
 Nitric oxide reaction with carbon, 428
 Nitrogen adsorption-desorption isotherm, 167
 Nitrogen compounds, reactions with graphite, 428
 Nitrogen cross section, 81
 Nitrogen-graphite system, 427-428
 Nitrogen as reactor coolant, 427-428
 Nitrous oxide, 428
 Notch sensitivity, 156
 NRX reflector, stored energy in, 350-351
 Nuclear graphite, 44-45
 costs, 8
 definition, 88
 Nuclear-1 graphite, 185
 Nuclear-2 graphite, 182

O

Oak Ridge Graphite Reactor (X-10), 9, 490
 Optical microscopy, 104-105
 Orientation, of coke particles, 35-37
 in graphite, 106-108
 Outgassing (see Gas desorption)
 Overlap electron band model, 130-132
 Oxidation, effects on physical properties, 405-406
 in graphite moderators, 411-412
 of irradiated graphite, 415
 (See also individual oxidants)
 Oxygen, effects of radiation on, 416-417
 Oxygen-graphite reaction, 412-418
 activation energy, 413
 effect of radiation on, 417-418
 effects of temperature on, 413
 Ozone, formation by radiation, 416

P

Paramagnetic centers, 303
 Particle size, effect on density, 164
 PBNG-G graphite, 184
 stored-energy release, 339
 PBRE (see Pebble-Bed Reactor Experiment)
 Pebble-Bed Reactor, West Germany, 12, 520
 Pebble-Bed Reactor Experiment, 520
 Permanent set, 149, 314, 370
 Permeability, 45, 176-186
 effect of impregnation, 180-181
 equations, 177-178
 of joints, 64-65
 to liquids, 181-186
 measurement of, 179
 to molten salt, 460
 units, 179
 Permeability and pore structure, 103
 Petroleum cokes, Hall coefficient, 134
 layer diameter, 109
 manufacture, 22
 texture, 109, Plate II
 (See also Graphitization)
 PGA graphite, 184
 compressive strength, 150
 crystallite properties, 94
 density of rods, 162
 flexural strength, 154
 gas desorption from, 172-174
 permeability, 180
 purification, 46
 reaction with hydrogen, 424
 reaction rates with water, 420
 stored energy in, 347
 stress-strain diagram, 148, 151
 surface and in-pore reactions, 410
 use in reactors, 13-15
 PGB graphite, use in reactors, 13-14
 Phase diagram of carbon, 117-118
 Phonon conduction, 123-124
 Phosphate treatment of graphite, 430-431
 Photoelectric emission, 142
 Physical Constants Test Reactor (PCTR), 10, 489
 Pie oscillator, 75-76
 Pitch, coking value, 32
 Pitch impregnation, effect on density, 165
 Poisoning factors for elements, 78-80
 Poisson ratio, 155

Pole figures, 106
 Pore-size distribution, 100-104
 effect of grinding on, 101
 effect of oxidation on, 405-406
 effect of radiation on, 274-275
 from X-ray scattering, 100
 Pore volume, 102
 by mercury porosimetry, 102-104
 Pores, definition, 88
 Porosity of baked carbon, 40
 Porosity and permeability, 177
 Preferred orientation, production during
 manufacture, 107-108
 (See also Grain structure)
 Pressure baking, 49, 165
 Primary recoil energy, 380-381
 Proton irradiations, 295-296
 Pulse annealing, 373-375
 Purification, 45-48
 Purification furnace, 48
 Pyrolytic graphite, as a coating, 434
 permeability, 180
 properties, 435-437
 structure, 436

R

R-1 graphite, 182
 R-3 graphite, 185
 R-4 graphite, 184
 compressive strength, 150
 flexural strength, 154
 R-0013 graphite, 184
 compressive strength, 150
 differential accessible volume, 103
 flexural strength, 154
 R-0018 graphite, 184
 compressive strength, 150
 differential accessible volume, 103
 flexural strength, 154
 R-0020 graphite, 184
 compressive strength, 150
 flexural strength, 154
 R-0025 graphite, 184
 compressive strength, 150
 flexural strength, 154
 thermal conductivity, 306
 water permeability, 181
 Radiation damage, to graphite, 6
 self-limitation of, 383
 (See also individual properties)
 Radiation damage rates, 223
 Radiation dosage units, 223-232

Radiolytic decomposition of water, 420-421
 Rare earths, neutron-absorption cross section, 81
 Reactor operation, 487
 Reactor for Physical and Technical Investigation (RPT), 10, 509
 Reactors, graphite moderated, 8-16
 Reintegration of displaced atoms, 365
 Resin binders, 165
 Resin impregnation, 181
 Rhombohedral structure, 90, 129, 147
 RPT (see Reactor for Physical and Technical Investigation)
 Rutherford scattering, 201-210, 215

S

SA-25 graphite, 184
 effects of radiation on Hall coefficient, 300
 effects of radiation on thermal conductivity of, 308-309
 Hall coefficient, 134
 magnetic susceptibility, 302-303
 specific heat, 120
 stored-energy release, 339
 thermoelectric power, 301
 Sagger furnace, 39
 Savannah River 305 Test Pile, 10, 489
 Self-diffusion, activation energy, 127-128, 344
 SGR (see Sodium Graphite Reactor)
 Shear strength, 154-156
 Siberian power station reactors, 13
 Sigma piles, 4-5
 Silicon carbide as a coating, 432-434
 Silicon coatings, 432
 Sizewell reactors, 15
 Slow-neutron intensity, 272
 Slowing down power, 71
 Sodium fluoride, purification with, 48
 Sodium Graphite (Hallam) Reactor (SGR), 14, 517
 Sodium-graphite reaction, 449-450
 Sodium Reactor Experiment (SRE), 11, 515-517
 moderator, 516
 Soviet graphite pile, 9
 Soviet Isotope Reactor (IR), 10, 509-510
 Soviet reactors, 509-512
 SP7B graphite, 184
 analysis, 82

- SP24B graphite, 184
 analysis, 82
Specific heat, 118-120
 effect of radiation on, 309-310
 at low temperatures, 119
Speer gas-purified graphite, 10, 184
 crystallite properties, 94-95
 effect of radiation on, 286
Speer-3499 graphite, 184
 tensile strength, 153
Spheron-6 graphite, 184
 surface area, 169
Springs of graphite, 319-320
SRE (see Sodium Reactor Experiment)
Stacking of layer planes, 90
Steam-graphite reaction, 418-421
 equilibria in, 419
 kinetics of, 419-420
Steel, reaction with graphite, 457-459
Stored energy, in air-cooled reactors, 348-349
 annealing of, 376
 in BEPO, 491
 in Brookhaven Graphite Research Reactor, 491-493
 in Calder reactors, 349, 498
 effect of radiation temperature on, 329-331
 in gas-cooled reactors, 487
 in graphite reflectors, 350-351
 in Hanford reactors, 347-348
 in high-temperature reactors, 350
 measurement of, 326-328, 331-336
 origin, 325-326
 release curve, 325-326, 336-342
 in special carbons, 342
 theory, 343-345
 in X-10 Reactor, 490
Stored energy and physical properties, 345-347
Stored-energy release, adiabatic, 334-336
 analysis of, 360-362
 isothermal, 331-332
 linear-rise method, 332-334
Stored-energy release curve, 325-326, 336-342
 effect of irradiation temperature on, 341
 measurement, 331-336
Stress relaxation, radiation-induced, 319
Stress-strain behavior, effects of radiation on, 315
Stress-strain diagram, 148, 151
Structure, of carbons, 87-89
 of diamond, 87
 effects of radiation on, 259-275
 of graphite, 87-90
Sublimation temperature, 117-118
Surface activity of carbons, 166-167
Surface activity and rate equations, 392-393
Surface area, 167-170
Surface enrichment of C^{14} , 363-364
Surface finishes on graphite, 54
Szilard complication, 5-6
- T
- Tantalum-graphite system, 454
Temperature distribution in graphite moderator, 484-485
Tensile strength, anisotropy of, 45
 effects of radiation on, 317
 effects of temperature on, 153
 measurement of, 152-153
Texas coke, 26-27
 thermal expansion of graphite prepared from, 35-36, 125
Thermal conductivity, 120-124, 304-309
 anisotropy of, 45
 annealing of, 371, 373, 378, 382-383
 of baked carbon, 40
 of CSF graphite, 305-306
 effects of radiation on, 304-309
 effects of temperature on, 306-307
 of joints, 64
 measurement of, 124
Thermal conductivity vs. stored energy, 347
Thermal expansion, 124-126
 dependence on structure, 107
 change with heat-treatment, 126
 of crystals, 95-96
 extrapolation of, to high temperatures, 125
 (See also Coefficient of thermal expansion)
Thermal ratcheting, 288
Thermal resistivity (see Thermal conductivity)
Thermal-shock resistance of materials, 126-127
Thermal spike, 212
Thermal Test Reactor (TTR), 10
Thermax, 184
 as additive, 33, 164

crystallite properties, 94
 effects of radiation on, 280
 electron micrograph of, 111-113
 structure, 111-113
 Thermodynamic properties, 120-122
 Thermoelectric power, 141-142
 effect of radiation on, 300-302
 Thermoelectric-power ratio, pulse annealing of, 374
 Threshold energies for displacements, 197
 Tin-graphite system, 451
 Titanium, cross section, 81
 Tokai Mura Japanese Reactor, 15, 499-500
 keyed blocks in, 290, 499-500
 Transient Reactor Test Facility (TREAT), 11, 518
 Transport cross section for neutrons, 69
 Trawsfynydd reactors, 15, 500
 keyed blocks in, 290, 500
 TREAT (see Transient Reactor Test Facility)
 Triple point of carbon, 117
 TS graphite, surface area, 169
 TSF graphite, 185
 gas desorption from, 172-175
 TSGBF graphite, 185
 coefficient of friction, 321-322
 crystallite damage, 268
 crystallite properties, 94
 effect of radiation on, 277-279, 297-298
 electrical resistivity, 297-298
 gas desorption from, 173, 175
 graphitization temperature, 94, 278-279
 pore-size distribution in powdered, 274
 stored energy in, 338, 347
 thermal conductivity, 304
 thermal expansion, 278
 TSP graphite, gas desorption from, 173
 use in reactors, 11
 TSX graphite, 185
 use in reactors, 15
 Tungsten-graphite system, 454

U

UHTREX (see Ultrahigh Temperature Reactor Experiment)
 Ultrahigh Temperature Reactor Experiment (UHTREX), 11, 518-520
 Urals power station reactors, 14, 511-512
 Uranium, in bismuth reactor system, 446-447

diffusion through graphite, 452
 Uranium carbides, dispersion in graphite, 471
 formation, 451-452
 as fuels, 470-472
 in liquid-metal system, 445-449
 Uranium dioxide, from ammonium diuranate, 468
 cladding with aluminum oxide, 479
 by freeze drying, 468
 reaction with graphite, 471
 Uranium-graphite system, 451-452

V

Vacancies, activation energy for annealing, 343-344
 activation energy for formation, 344
 annealing, 269-273, 372
 clustering of, 269-271
 effect of irradiation temperature, 270
 energy of formation, 343-345
 formation of, 232, 272-273, 364-365
 Vanadium, cross section, 81
 Vanadium carbide, 46-47
 Vanadium in coal-tar pitch, 31
 Vanadium-graphite system, 454
 Vapor pressure of carbon, 117
 Volga Reactor, 13

W

Water, adsorption by graphite, 170-171
 moderating properties of, 71
 permeability through graphite, 181
 Water-cooled reactors, 508-515
 Water-graphite reaction, 418-421
 (See also Steam-graphite reaction)
 Weight loss of graphite, in Calder-2 Reactor, 412
 Welding graphite, 62
 Wiedemann-Franz ratio, 122, 304
 Wigner effect, prediction of, 5-6
 Wigner energy (see Stored energy)
 Windscale reactors, 12, 387-388, 493-494
 WSF graphite, 185
 surface area, 169

X

X-ray diffraction lines, of baked carbon, 42
 broadening of, 96-99
 by radiation, 259-267

SUBJECT INDEX

547

effect of annealing on, 262-263, 365-367
 effect of grinding on, 99
 of graphites, 91-93
 Scherrer shape factor, 98
 X-10 Reactor, 9, 490
 temperature distribution in, 485
 cryostat in, 241

Y

Young's modulus, anisotropy of, 45
 effect of annealing on, 368-370, 372-373

effect of density on, 156-157
 effect of radiation on, 313-316
 effect of temperature on, 154
 (See also Elastic modulus)

Z

Zenith Reactor, 11, 508
 Zirconium, in bismuth reactor system,
 446-447
 gettering by, 454-455
 Zirconium-graphite system, 454-455

DATE DUE

A fine of TEN CENTS will be charged for each day the book is kept overtime.

[illegible]

TK

9202.

199668

N5

Nightingale, R.E.

Nuclear graphite.

SAINT JOHN'S, COLLEGEVILLE, MN
TK9202 .N5

Nightingale, Ri - Nuclear graphite / contributors:



3 0502 00347 4276



W7-CWT-573



